Proceedings of the 36th European and the 12th International Peptide Symposium

28th August-2nd September 2022 | Sitges, Spain

Edited by:

Michal Lebl

Spyder Institute Prague, Czech Republic

Contents

Welcome

On behalf of the organizing committee, we welcomed you to the 36th European and 12th International Peptide Symposium in Sitges (Barcelona), Spain, from August 28 to September 2, 2022. This was a great occasion to rejoin the international peptide family again after these uncertain times.

The meeting. themed "From Peptides to the World", was an ideal occasion for academia and industry scientists from all over the world. It provided an opportunity to learn and discuss about the thriving field of peptide science, exchange ideas, create new alliances as well as to meet old friends-and make new friends.

The 36th EPS scientific committee had set out to assemble an exciting program with a broad range of topics covering, among others, advances in peptide chemistry and structure, bioactive peptides and their therapeutic applications, peptide biomaterials, and nanotechnology and delivery. In addition. more than 475 posters was the perfect environment to move peptide science ahead.

The conference venue (Melia Sitges) was a pleasant setting for commercial exhibition, poster sessions and coffee breaks surrounded by outdoor pool gardens and terraces overlooking the Mediterranean Sea. Sitges, 40 km south of Barcelona, is a trendy resort with a privileged location and mild Mediterranean climate. Four kilometers of beach, fringed by a sea-front promenade dotted with artful colonial mansions facing the sea, provided a perfect excuse for strolling in this convivial town well-known for its open, inclusive, relaxed atmosphere.

The scientific and local organizing committees, supported by the E P S executive committee, were keen to make the 36EPS/12IPS a memorable and successful scientific event. Convinced that your presence contributed to that we like to take the opportunity to thank you for your presence, continuing support and understanding during these difficult times.

Dr. Meritxell Teixidó	**Prof. David Andreu**	**Prof. Fernando Albericio**
36EPS Symposium Chair	Vice-Chair	Vice-Chair

Dear colleagues, friends, and dear peptide scientists from all over the world:

It is my privilege to address a few words to you on the occasion of the 36th European and 12th International Peptide Symposium that took place in Sitges, Catalonia. The international peptide community thus returned to the Barcelona area after 22 years, as the 21st EPS took place in 1980 in Barcelona.

After more than *2* years of pandemic restrictions, the symposium was one more step back to "normality" as we knew it before 2020. You may agree that virtual meetings became a viable alternative in lockdown times, but they will never replace a life symposium, which provides, besides excellent science, the opportunity to interact and discuss personally, and to build or intensify productive professional and personal ties with colleagues from all over the world.

The 36th European and 12th International Peptide Symposium had to be postponed from 2020 to 2022 because of the pandemic-related travel restrictions. I am confident that you were excited to listen to the latest scientific results, discuss in front of a poster, and dive into the multifaceted world of peptide science.

I take the pleasure to thank the Symposium Chair Meritxell Teixido and the Co-chairs David Andreu and Fernando Albericio for organizing this wonderful symposium in a splendid location, for putting together an inspiring programme, and for the tireless engagement.

Norbert Sewald
President European Peptide Society

Editor's Comments

This year's proceedings production was quite different from all previous years. Since many Symposium participants were experiencing this type of meeting for the first time, many of them had no idea that the production of symposium proceedings has a long tradition, starting with the first peptide symposium in Prague in 1958, organized by Professors Rudinger and Šorm. Every word presented at that meeting, including the discussion after each lecture was transcribed and published in the special issue of Collection of Czechoslovak Chemical Communication, which became the first book of proceedings. Today, understandably, not everything presented at the symposium makes it into the book since it is up to the authors whether they would submit their work or not. In this book of proceedings only 96 out of more than 500 presentations were submitted to this collection. And it actually goes against the original idea of Rudinger and Šorm that the peptide symposium should bring together scientists working in this area to share their ideas and "cross-pollinate" their thinking.

I remember the times when it was a thing of high prestige to have the presentation accepted for a plenary lecture and therefore automatically for the book of proceedings. There were no poster presentations, and when the posters were introduced, not every poster was accepted for publication. Yes, there were not as many participants as today, but the idea of sharing the knowledge beyond the weeklong meeting should be revisited again.

And this year's Nobel prize in chemistry best illustrated the importance of publishing your work in the Proceedings. The priority of Meldal's work was unambiguously established by his article in the proceedings of the American peptide symposium (Tornoe W.T. and Meldal M., in "Peptides, The Wave of the Future; Proceedings of the Second International and the Seventeenth American Peptide Symposium" (Lebl M. and Houghten R.A., Eds.), American Peptide Society, 2001, p. 263).

So, let me make a proposal, which was briefly floated at the EPS committee meeting in Sitges.

Let us change the format of the proceedings book:
- Every lecture or poster is available electronic form – usually the Powerpoint presentation or pdf file.
- Once the lecture or poster is presented at the symposium, everything in it is legally public knowledge.
- Presentation at the meeting is considered preliminary publication and should not prevent publication of the full version of the particular paper in Science or Nature.
- Every presentation will receive the doi identifier.
- Every symposium will receive a dedicated web site in which all presentation will be collected.
- The name of that site will be http://......../ProceedingsOfTheXXthEuropeanPeptide Symposium

In this way we will revive the original idea of the founders utilizing the technologies which were not available at their time. (Personally, I believe that Prof. Rudinger would approve this without hesitation.)

Some observation from this year's book production. Many authors did not realize that book will not be printed in color and did not provide appropriate monochromatic versions of their figures and graphs, as well as they did not pay attention to the size of their pictures. There was no way to redo their work and keep the timeline of the book production. However, the editor's reasoning for accepting these papers was based on the experience with publishing many proceedings books for EPS and APS – printed book is purchased only in single digit number of copies and pdf of the book with color graphics is downloaded more than thousand times. So, once more, thanks go to all authors who followed the format and responded quickly to our requests for changes and who read the galley proofs in timely manner.

Michal Lebl and Polly Story-Lebl

Organization

Organizing Committee
Chairman
  Dr. Merixell Teixidó

Co-Chairs
  Prof. David Andreu
  Prof. Fernando Albericio

Committee Members
  Prof. Florine Cavelier
  Dr. Sira Defaus
  Prof. Ernest Giralt

EPS Council

EPS National Representatives
  Christian Becker, Austria
  Steven Ballet, Belgium
  Dancho Danalev, Bulgaria
  Ruža Frkanek, Croatia
  Michal Lebl, Czech Republic
  Tomas Eiland Nielsen, Denmark
  David Fewer, Finland
  Oleg Melnyk, France
  Roderich Süßmuth, Germany
  Andreas Tzakos, Greece
  Gábor Tóth, Hungary
  Mark Devocelle, Ireland
  Norman Metanis, Israel
  Paolo Rovero, Italy
  Ingrid Dijkgraaf, The Netherlands
  Markus Baumann, Norway
  Aleksandra Kesik-Misicka, Poland
  Nuno Correia Santos, Portugal
  Ekaterina Kolesanova, Russia
  Jan Bakos, Slovakia
  Tomaž Bratkovič, Slovenia
  Rosario Gonzalez-Muňiz, Spain
  Alesia A. Tietze, Sweden
  Jeffrey W. Bode, Switzerland
  Steven Cobb, United Kingdom

Awards

Josef Rudinger Memorial Award 2020

The Josef Rudinger Memorial Lecture Award is presented "in commemoral:ion of Josef Rudingers role in the foundation of the European Peptide Symposia and of diverse contributions he made to peptide chemistry". The Award is presented during the EPS Symposium and is sponsored by PolyPeptide Group.

Awardee:

Herbert Waldmann, *Max Planck Institute Of Molecular Physiology. Germany*

Leonidas Zervas Award 2020

The Leonidas Zervas Award is presented in commemoration of his outstanding contributions to peptide science. The award is given to the scientist who has made the most outstanding contributions to the chemistry, biochemistry and/or biology of peptides in the five years preceding the date of selection. and is sponsored by the donation of Dr. Rao Makineni.

Awardees:

Gilles Subra, *IBMM. Universite de Montpellier, France*

Ali Tavassoli, *University of Southampton.United Kingdom*

Miklos Bodanszky Award 2020

The Miklos Bodanszky Award is presented every two years. during the European Peptide Symposium, in commemoration of Miklos Bodanszky's contributions to peptide research, to a young scientist who has in the opinion of the General Assemb1y of the Society made the most outstanding contribution to peptide research in the period of maximum ten years after obtaining the PhD degree. The·Award is presented during the EPS Symposium and is sponsored by BCN Peptides.

Awardee:

Kathrin Lang, *ETH Switzerland*

Dr. Bert and Dr. Elizabeth Schram Awards

36EPS is pleased to announce the Young Investigators' Mini Symposium (YIMS) awards

Oral Presentation Awards

1st place:
Development of G protein peptidomimetics able to stabilize active state G protein-coupled receptors for application in drug discovery

Morgane Mannes
Vrije Universiteit Brussel (VUB), Brussels, Belgium

2nd place:
Ligation of mu-conotoxin KIIIA and Na$_V$1.7-selective spider toxin Pn3a: Effects on target selectivity and conformational isomerization

Poanna Tran
Institute for Molecular Bioscience, University of Queensland, St Lucia, Australia,

Poster Presentation Awards

1st place:
Quorum Sensing Peptides as a novel influencing factor unravelling the microbiome associations in sarcopenia

Amélie Descamps
Ghent University, Ghent, Belgium

Thiol-Ene Mediated Peptide Macrocyclisation for the Synthesis of Neuropeptide Analogues

Mark Nolan
Trinity College Dublin, Ireland

2nd place:
Impact of peptide length on in vivo hydrogel stability and sustained drug release

Julie Heremans
Research Group of Organic Chemistry, Vrije Universiteit Brussel, Elsene, Belgium

A Radical Approach to Unnatural Amino Acids

Joshua Hammond
The Australian National University, Canberra, Australia

Targeting Gαi/s Proteins With Peptidyl Nucleotide Exchange Modulators

Anna Pepanian
Pharmaceutical Institute, University of Bonn, Bonn, Germany

Effect of Conformational Restriction of 3-epi-Deoxynegamycin on Readthrough Activity

Noriko Omura
Department of Medicinal Chemistry, Tokyo University of Pharmacy and Life Sciences, Hachioji, Japan

3rd place:
Molecular Basis of Antibiotic Self-Resistance in a Bee Larvae Pathogen

Tam Dang
Technische Universität Berlin, Berlin, Germany

Hydrolase-inspired design of short catalytic linear and cyclic peptides

Patrizia Janković
University of Rijeka, Department of Biotechnology, Rijeka, Croatia

Acceleration of Bio-orthogonal Suzuki-Miyaura Cross-Coupling by In-Situ Formation of Peptidic Palladacycles

Steffen Dachwitz
Bielefeld University, Bielefeld, Germany

Sponsors, Exhibitors and Supporters

Platinum Sponsors
CEM
BCN PEPTIDES SA

Gold Sponsors
Gyros Protein Technologies

Silver Sponsors
Iris Biotech GmbH
PolyPeptide Group

Sponsors
ESCOM Science Foundation
EPS
BACHEM

Awards
BCN PEPTIDES
Dr. Rao Makineni
PolyPeptide Group
ESCOM Science Foundation

Collaborators
ChemPep
Novo Nordisk

Exhibitors
aapptec
Activotec
Advion Interchim | Chromlab
ALMAC
BACHEM
BCN Peptides
Biosynth Carbosynth
Biotage
Biotide Core
C.A.T. GmbH & Co KG
CEM
Chempartner
Christoff Senn Laboratories AG
CSBIO
Curia
Gate 2Brain
GL BIOCHEM (SHANGHAI) LTD
HECHENG
Iris Biotech
Luxembourg Biotechnologies
Merck
Mimotopes
Pepscan
PolyPeptide
Polypure
Purolite
Rapp Polymere GmbH
SB Peptide
Spyder Institute Praha
STA Pharmaceutical
WuXi Aaptec
Teledyne ISCO
Vapourtec

List of Articles

Synthetic Collagen Peptides

Helma Wennemers

Laboratory of Organic Chemistry, ETH Zurich, D-CHAB, 8093 Zurich, Switzerland

Introduction

Collagen, the most abundant protein in mammals, is a key contributor for the strength and stability of skin, bones, and connective tissue [1]. Collagen formation is thus vital for the integrity of skin, tendons, and the tissue in essentially any organ. Excessive collagen formation is, however, characteristic of fibrotic and malignant diseases, which include major global health issues.

The Wennemers group has used collagen model peptides (CMPs) to understand the stability of collagen at the molecular level and to establish functional synthetic collagen triple helices [2]. These include pH-responsive synthetic collagen [3-6], hyperstable triple helices [7-9], and heterotrimeric collagen [10]. Building on these data, we designed and synthesized a chemical probe for the simultaneous monitoring and targeting of lysyl oxidase (LOX)-mediated collagen cross-linking [11]. The probe allows for the detection of LOX activity *in vivo* and in tissue sections.

Results and Discussion

Functionalizable and pH responsive collagen triple helices. C^γ-substituted proline derivatives are valuable tools for developing functionalized collagen peptides for biological and materials investigations [1,2], yet the stereochemistry at C^γ can produce undesired steric or stereoelectronic constraints. We mitigated this drawback by using γ-azaproline (γ-azPro) as a proline mimetic that lacks a stereogenic center at the γ-position of the ring and can thus utilize the invertibility of nitrogen to adapt its conformation (Figure 1) [5,6]. NMR spectroscopic analyses and DFT calculations highlight how alkylated γ-azPro and alkylated derivatives thereof are conformationally dynamic and adopt conformational preferences through ring pucker flip along with nitrogen inversion. Incorporation of alkylated γ-azPro into collagen peptides produced functionalized pH-responsive triple helices with similar thermal stabilities, regardless of their placement in the Xaa or Yaa position within the characteristic Xaa-Yaa-Gly repeating unit of collagen peptides.
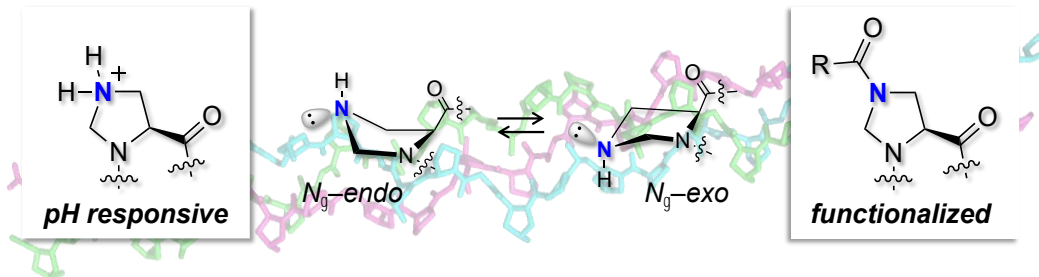
Fig. 1. pH-responsive and functionalized collagen triple helices using γ-azaPro

Lipidation bestows hyperstability and fast-folding on collagen triple helices. Cross-linking of collagen single strands by oxime ligation creates hyperstable collagen triple helices [7]. Through the study of the *trans/cis* ratio of Xaa-Pro amide bonds and their *trans/cis* isomerization speed in different solvents [12] we hypothesized that a hydrophobic environment should bestow collagen triple helices with hyperstability and fast-folding. Indeed, pendant hydrophobic moieties endow triple helical collagen with hyperstability and accelerate the *cis-trans* isomerization to an extent that thermally induced unfolding and folding of collagen triple helices take place at the same speed (Figure 2a) [8,9]. A systematic study with CMPs bearing different hydrophobic moieties even revealed a direct correlation between the length of the fatty acid and the stability and the folding speed of the triple helix (Figure 2b) [9]. Our experimental data and MD simulations revealed that lipidation enhances the

thermal stability and folding rate of triple-helical collagen by: *(i)* an increase of the *trans/cis* ratio of Xaa-Pro bonds, *(ii)* an acceleration of *trans-cis* isomerization, and *(iii)* van der Waals interactions with the grooves of the collagen triple helix [9].
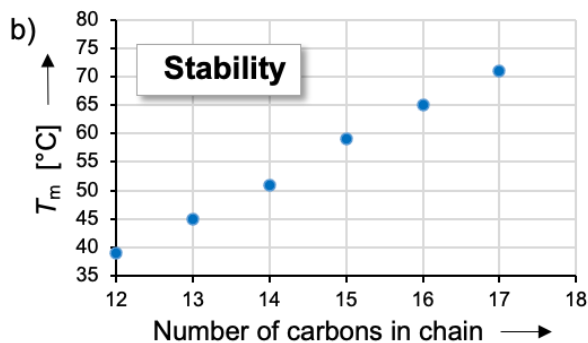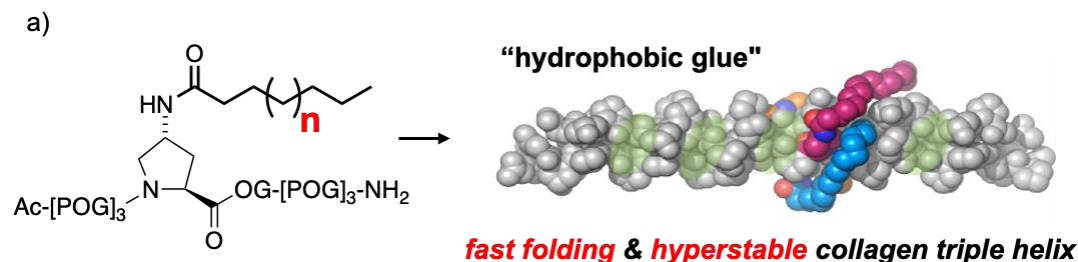
Fig. 2. a) Example of lipidated collagen triple helices. b) Correlation between lipid chain lengths and T_m values.

Heterotrimeric collagen triple helices. Heterotrimeric collagen triple helices are most common in nature. Synthetic heterotrimeric ABC-type collagen triple helices are difficult to access since a total of $3^3 = 27$ trimers that differ in their composition and register can form in a mixture of three different strands. We used our knowledge from pH-responsive (4*S*)-aminoproline (Amp) containing collagen model peptides (CMPs) [3,4] and covalently cross-linked CMPs [7] to create synthetic collagen hetero-trimers by placing (4*S*)-aminoproline (Amp) and aspartic acid (Asp) residues in coplanar Xaa and Yaa positions of neighboring strands (Figure 3a) [10]. This geometrically well-defined Amp–Asp salt bridge enabled the design of strands that assemble exclusively into the target heterotrimers. An important feature for this selective assembly is that unpaired (4*S*)Amp and Asp residues disfavor triple helix formation and preclude undesired assemblies [10]. Thus, specific heterotrimer formation only occurs when the Amp and Asp residues are paired in coplanar Xaa and Yaa positions. As little as three of the lateral Amp–Asp salt bridges sufficed to assemble 24-mers into tailored AB_2 or ABC-type heterotrimers with control over their composition and register (Figure 3b).
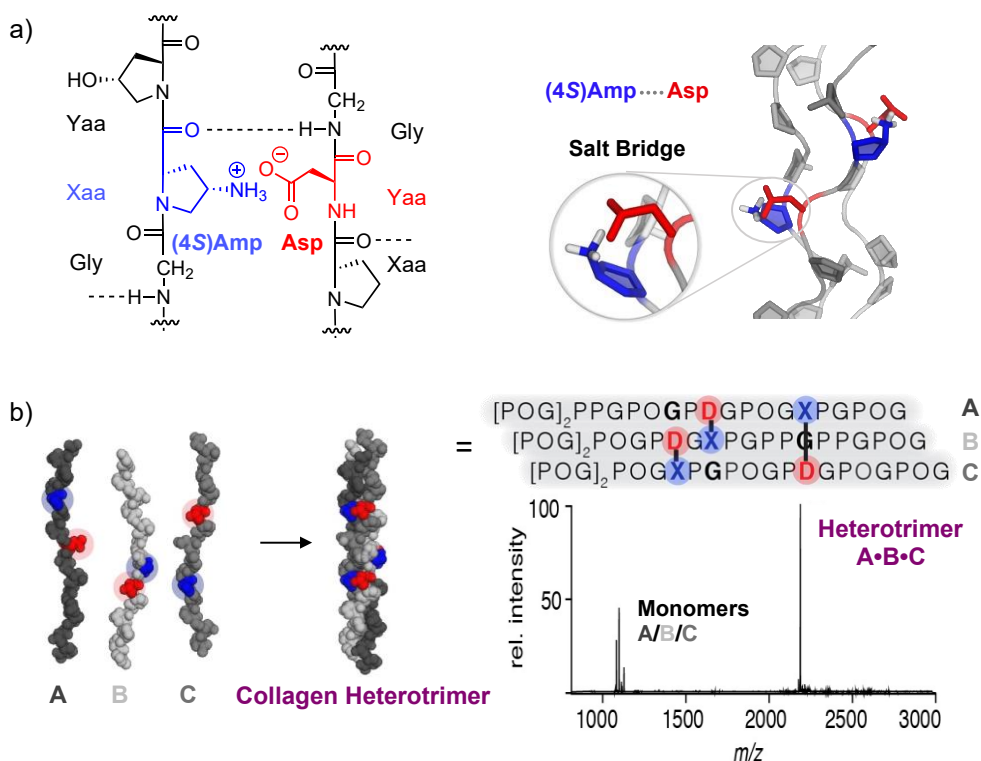
Fig. 3. Collagen heterotrimer formed by the Amp–Asp salt bridge.

For studying collagen heterotrimer formation, we established a native ESI-MS method [13]. This powerful tool allows for simultaneously monitoring the composition and thermal stability of non-covalently assembled triple helices. In contrast to CD-spectroscopy, an analysis tool that only provides data averaged over all species in a mixture, native ESI-MS allows for distinguishing different triple helices in a mixture of CMPs. A temperature-controlled native ESI source enabled the measurement of their thermal denaturation profiles in a single experiment.

Acknowledgments

References

1. Shoulders, M.D., Raines, R.T. *Annu. Rev. Biochem*. **78**, 929 (2009),
   https://doi.org/10.1146/annurev.biochem.77.032207.120833
2. Wennemers, H. *Chimia* **75**, 525 (2021), https://doi.org/10.2533/chimia.2021.525
3. Siebler, C., Erdmann, R.S., Wennemers, H. *Angew. Chem. Int. Ed*. **53**, 10340 (2014)
   https://doi.org/10.1002/anie.201404935
4. Egli, J., Siebler, C., Maryasin, B., Erdmann, R.S., Bergande, C., Ochsenfeld, C., Wennemers, H. *Chem. Eur. J*. **23**, 7938 (2017), https://doi.org/10.1002/chem.201701134
5. Aronoff, M.R., Egli, J., Menichelli, M., Wennemers, H. *Angew. Chem. Int. Ed*. **58**, 3143 (2019),
   https://doi.org/10.1002/anie.201813048
6. Aronoff, M.R., Egli, J., Schmitt, A., Wennemers, H. *Chem. Eur. J*. **26**, 5070 (2020)
   https://doi.org/10.1002/chem.201905768

7. Hentzen, N.B., Smeenk, L.E.J., Witek, J., Riniker, S., Wennemers, H. *J. Am. Chem. Soc*. **139**, 12815 (2017), https://doi.org/10.1021/jacs.7b07498
8. Egli, J., Siebler, C., Köhler, M., Zenobi, Rennemers, H. *J. Am. Chem. Soc*. **141**, 5607-5611 (2019), https://doi.org/10.1021/jacs.1c01512
9. Egli, J., Esposito, C., Müri, M., Riniker, S., Wennemers, H. *J. Am. Chem. Soc*. **143**, 5937 (2021), https://doi.org/10.1021/jacs.1c01512
10. Hentzen, N.B., Islami, V., Köhler, M., Zenobi, R., Wennemers, H. *J. Am. Chem. Soc*. **142**, 2208 (2020), https://doi.org/10.1021/jacs.9b13037
11. Aronoff, M.R., Hiebert, P., Hentzen, N.B., Werner, S., Wennemers, H. *Nat. Chem. Biol*. **17**, 865 (2021), https://doi.org/10.1038/s41589-021-00830-6
12. Siebler, C., Maryasin, B., Kuemin, M., Erdmann, R.S., Rigling, C., Grünenfelder, C., Ochsenfeld, C., Wennemers, H. *Chem. Sci*. **6**, 6725 (2015), https://doi.org/10.1039/C5SC02211H
13. Köhler, M., Marchand, A., Hentzen, N.B., Egli, J., Begley, A.I., Wennemers, H., Zenobi, R. *Chem. Sci*. **10**, 9829 (2019), https://doi.org/10.1039/C9SC03248G

Esculentin-1a Derived Peptide Diastereomers to Target *Pseudomonas aeruginosa* Lung Infection in Cystic Fibrosis: From Nature to Bench towards Therapeutic Application

Maria Luisa Mangoni[1], Bruno Casciaro[1], Floriana Cappiello[1], Maria Rosa Loffredo[1], Elena Puglisi[1], Francesca Ungaro[2], Ivana d'Angelo[3], Mattia Mori[4], Loretta Ferrera[5], Luis Galietta[6,7], and Y. Peter Di[8]

[1]Laboratory affiliated to Istituto Pasteur Italia-Fondazione Cenci Bolognetti-Department of Biochemical Sciences, Sapienza University of Rome, Rome, 00185, Italy; [2]Department of Pharmacy, University of Naples, Federico II, Naples, 80131, Italy; [3]DiSTABiF, University of Campania Luigi Vanvitelli, Caserta, 81100, Italy, [4]Department of Biotechnology, Chemistry and Pharmacy, University of Siena, 53100, Siena, Italy; [5]Genetica Medica, Istituto di Ricovero e Cura a Carattere Scientifico (IRCCS), Istituto Giannina Gaslini, Genoa, 16147, Italy; [6]Telethon Institute of Genetics and Medicine (TIGEM), Pozzuoli, Italy; [7]Department of Translational Medical Sciences, University of Napoli "Federico II", Napoli, Italy, [8]Department of Environmental and Occupational Health, University of Pittsburgh, 15260, Pittsburgh, USA

Introduction

The alarming rise of "superbugs" resistant to the available antibiotics poses a serious threat to global human health and has been predicted as the next pandemic. Experts in the field have estimated that if these pathogens are left untreated, they could lead to a significant increase in the number of infection-related deaths, with about 10 million deaths per year, worldwide, by 2050 [1,2]. Among superbugs, there is *Pseudomonas aeruginosa*, a highly virulent opportunistic Gram-negative bacterium that is very difficult to eradicate, especially because of its capability to form biofilm, where bacterial cells are embedded into an extracellular matrix which confers protection from the host immune response and from traditional antibiotics. This microorganism provokes a large variety of infections, including those found in the lungs of cystic fibrosis (CF) patients [3]. The disease of CF is caused by mutations in the gene encoding the CFTR transmembrane channel, which controls the passage of chloride ions [4,5]. The most common mutation consists in the deletion of phenylalanine 508 (F508del-CFTR), which is associated with misfolding and premature degradation of the mutated protein which also has a gating defect. Therefore, a decreased amount of the defective protein reaches the cell membrane. The impaired function of CFTR leads to the formation of sticky and dehydrated mucus lying in the respiratory tract. This favors the entrapment of inhaled microbes, including *P. aeruginosa,* that rapidly colonizes the lung with deterioration of lung tissue and final failure of respiratory functions. Therefore, treatment of *P. aeruginosa* lung infections in CF may benefit from compound(s) endowed with multiple biological properties, such as antimicrobial peptides (AMPs) [6,7]. We demonstrated how derivatives of the frog skin AMP esculentin-1a hold promise for the development of such new therapeutic agents.

Results and Discussion

We previously demonstrated that the frog skin-derived AMP Esc(1-21) has a rapid killing kinetics against both free-living and biofilm forms of *P. aeruginosa*, with a membrane-perturbing mechanism that reduces resistance, in contrast with traditional antibiotics [8]. Furthermore, it was found to promote re-epithelialization in bronchial cell monolayers, and presumably to accelerate the healing of damaged airway epithelium. This property is not displayed by conventional antibiotics [9,10]. However, before bringing AMPs from the bench to the bedside, we need to overcome some relevant challenges, such as cytotoxicity towards host cells, poor biostability, and limited targeted delivery [11]. We found out that by changing the stereochemistry of two selective L amino acids to the corresponding D-enantiomers, the resulting diastereomer Esc(1-21)-1c carrying D-Leu[14] and D-Ser[17] (Figure 1) displays the following enhanced properties.

(i) Lower cytotoxic towards mammalian cells, likely due to its decreased alpha-helical content.

(ii) Higher stability in the presence of proteolytic enzymes abundant in the lungs of CF patients, such as elastase from human neutrophils and from *P. aeruginosa* [9].

(iii) Higher efficacy in eradicating *Pseudomonas* biofilm.
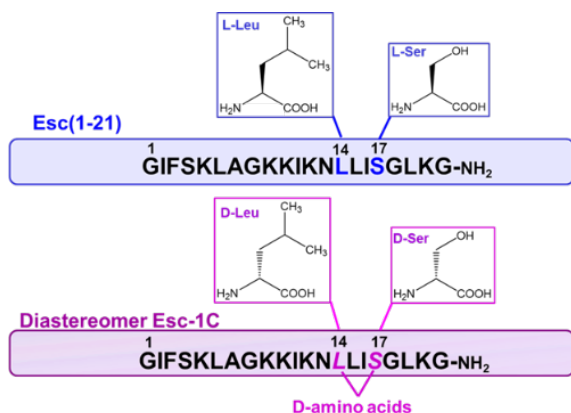
Fig. 1. Primary structure of Esc peptides. The L to D-amino acid changes at positions 14 and 17 are highlighted.

These properties make Esc(1-21)-1c, rather than the corresponding all-L isoform, the more appropriate molecule for *in vivo* studies. By using a mouse model of acute *P. aeruginosa* lung infection, we demonstrated that a single intratracheal instillation of Esc(1-21)-1c, at 0.1 mg/kg, can yield a 2-log reduction in the number of lung bacterial cells 24 h after infection, comparable to the clinically-used lipopeptide colistin [12]. However, colistin quickly generates resistance and, unlike Esc peptides, does not possess any airway wound healing activity, which is relevant to restoring tissue integrity and respiratory function while preventing pathogen penetration.

Considering the role of airway epithelium and CFTR in maintaining lung function and wound repair [13,14], we then evaluated the effect of these peptides on the ion current controlled by the protein channel. Notably, activation of CFTR requires (i) phosphorylation of its R domain by protein kinase A [15] and (ii) binding of ATP to the nucleotides binding domains (NBDs) to elicit their dimerization with the consequent opening of the gate at the level of the transmembrane domains.

Electrophysiological experiments, including measurements of transepithelial conductance across epithelia expressing F508del-CFTR as well as measurements of membrane currents in single cells expressing F508del-CFTR (patch-clamp technique) after correction with lumacaftor (which acts as a protein-folding chaperone to assist the delivery of the mutated protein to the plasma membrane) were performed. Our results demonstrated the ability of these two Esc peptides to restore the activity of F508del-CFTR, likely upon direct interaction with the channel [16]. This effect was more pronounced for the peptide analog carrying a D-phosphoserine at position 17 [16]. Computational studies indicated its interaction with the cytosolic side of the complex made by the two NBDs bound to ATP [16]. The peptide bridges the two NBD domains, thanks to a network of hydrophobic and electrostatic interactions reinforced by hydrogen bonds with Glu[632] and Arg[1386]. This is expected to stabilize the heterodimer and presumably the open state of the channel [16].

Based on the antimicrobial activity of Esc peptides, their airway wound healing properties, and CFTR rescue activity, we believe these peptides represent promising candidates for treating lung pathology in CF. However, as mentioned above, before bringing AMPs from the bench to the bedside, we must consider their limited diffusion through biological barriers (such as bronchial mucus) and therefore limited delivery to the target site. To this aim, the peptides were incorporated into biodegradable polymeric nanoparticles (NPs) made of poly(lactide-co-glycolide) (PLGA), coated with polyvinyl alcohol (PVA) to stabilize them [17]. They resulted in having a spherical shape with a hydrodynamic diameter lower than 300 nm, a suitable size for pulmonary administration, and reaching the deepest part of the lungs. Such NPs were found to facilitate the diffusion of the encapsulated peptide through an artificial mucus layer and to prolong the *in vitro* antipseudomonal activity compared to the corresponding free counterpart (Table 1).

Furthermore, NPs were found to significantly potentiate the *in vivo* antibacterial activity of the peptides at the lung level upon delivery in the conductive airways. Overall, these findings have contributed to highlighting the potential of these peptides as new multi-functional drugs for topical treatment of lung pathology, especially in CF patients, and to suggest the engineered PLGA NPs as attractive nanocarriers for delivery of AMPs in the conductive airways and to improve their antimicrobial efficacy compared to the corresponding soluble free counterparts (Figure 2).

6

Table 1. Antibacterial activity of Esc peptides in the free or encapsulated form, expressed as optical density at 590 nm ±standard deviation (S.D.) after 24 and 72 h treatment. The absorbance values were taken from ref [17].

Treatment	Absorbance of samples at 590 nm	
	After 24 h	After 72 h
PVA-PLGA NPs*	0.6823 ± 0.075	0.7415 ± 0.065
Esc(1-21)	0.0121 ±0.007	0.5400 ±0.06
Esc(1-21)_PVA-PLGA NPs	0.2785 ±0.031	0.2653 ±0.044
Esc(1-21)-1c	0.0400± 0.008	0.5353 ±0.022
Esc(1-21)-1c_PVA-PLGA NPs	0.3781 ±0.037	0.3448 ±0.05
Untreated control cells	0.6545±0.012	0.7802 ±0.059

*Bare PVA-PLGA NPs were included for comparison as well as untreated control cells
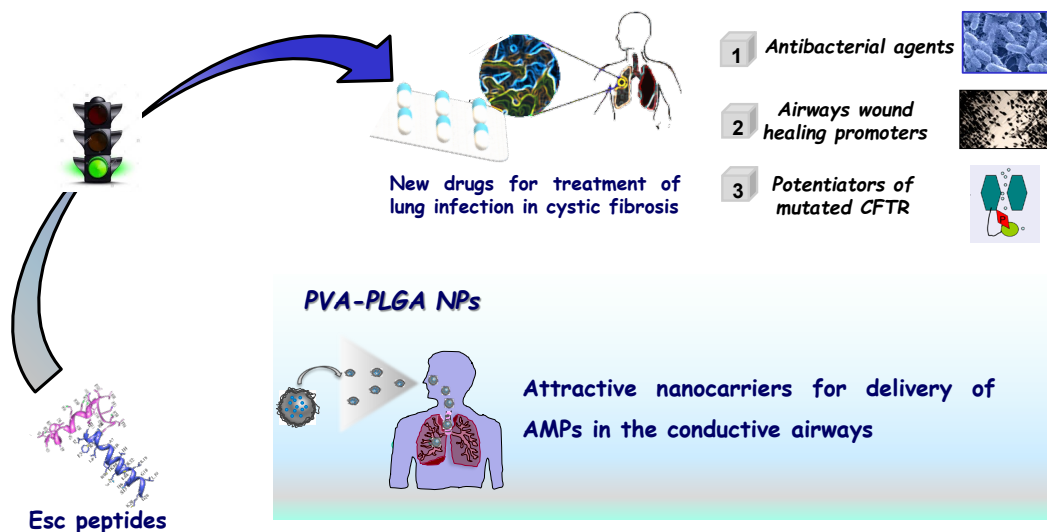
Fig. 2. Schematic representation of the main advantageous properties of Esc peptides and PVA-PLGA NPs for treatment of lung pathology in CF.

Acknowledgments

References

1. https://www.ecdc.europa.eu/sites/default/files/documents/surveillance-antimicrobial-resistance-Europe-2019.pdf
2. Lepape, A., Jean, A., De Waele, J., Friggeri, A., Savey, A., Vanhems, P., Gustin, M.P., Monnet, D.L., Garnacho-Montero, J.,Kohlenberg, A. *Antimicrob Resist Infect Control* **9,** 1 (2020), https://doi.org/10.1186/s13756-019-0662-8
3. Hoiby, N., Ciofu, O.,Bjarnsholt, T. *Future Microbiol.* **5**, 1663-1674 (2010), https://doi.org/10.2217/fmb.10.125

4. Sheppard, D.N.,Welsh, M.J. *Physiol Rev*. **79**, S23-45 (1999), https://doi.10.1152/physrev.1999.79.1.S23
5. Turcios, N.L. *Respir Care* **65**, 233-251 (2020), https://doi.org/10.4187/respcare.06697
6. Mahlapuu, M., Bjorn, C., Ekblom, J. *Crit Rev Biotechnol*. **40**, 978-992 (2020), https://doi.org/10.1080/07388551.2020.1796576
7. Zhang, L., Parente, J., Harris, S.M., Woods, D.E., Hancock, R.E.,Falla, T.J. *Antimicrob Agents Chemother*. **49**, 2921-2927 (2005), https://doi.org/10.1128/AAC.49.7.2921-2927.2005
8. Luca, V., Stringaro, A., Colone, M., Pini, A.,Mangoni, M.L. *Cell Mol Life Sci*. **70**, 2773-2786 (2013), https://doi.org/10.1007/s00018-013-1291-7
9. Cappiello, F., Di Grazia, A., Segev-Zarko, L.A., Scali, S., Ferrera, L., Galietta, L., Pini, A., Shai, Y., Di, Y.P.,Mangoni, M.L. *Antimicrob Agents Chemother*. **60**, 7252-7262 (2016), https://doi.org/10.1128/AAC.00904-16
10. Cappiello, F., Ranieri, D., Carnicelli, V., Casciaro, B., Chen, H.T., Ferrera, L., Di, Y.P.,Mangoni, M.L. *Sci Rep*. **9**, 18988 (2019), https://doi.org/10.1038/s41598-019-55426-x
11. Casciaro, B., Cappiello, F., Loffredo, M.R., Ghirga, F.,Mangoni, M.L. *Curr Med Chem*. **27**, 1405-1419; (2020), https://doi.org/10.2174/0929867326666190722095408
12. Chen, C., Mangoni, M.L.,Di, Y.P. *Sci Rep*. **7**, 8548 (2017), https://doi.org/10.1038/s41598-017-08361-8
13. Wine, J.J., Hansson, G.C., Konig, P., Joo, N.S., Ermund, A.,Pieper, M. *J Cyst Fibros*. **17**, S35-S39 (2018), https://doi.10.1016/j.jcf.2017.09.003
14. Progress in Understanding Cystic Fibrosis. (Sriramulu, D. Ed.). *IntechOpen*. **2017**, ISBN 978-953-51-3292-9, https://doi.10.5772/63263
15. Cheng, S.H., Rich, D.P., Marshall, J., Gregory, R.J., Welsh, M.J., Smith, A.E. *Cell*. **66**, 1027-1036 (1991), https://doi.org/10.1016/0092-8674(91)90446-6
16. Ferrera, L., Cappiello, F., Loffredo, M.R., Puglisi, E., Casciaro, B., Botta, B., Galietta, L.J.V., Mori, M.,Mangoni, M.L. *Cell Mol Life Sci*. **79**, 67 (2021), https://doi.org/10.1007/s00018-021-04030-2
17. Casciaro, B., d'Angelo, I., Zhang, X., Loffredo, M.R., Conte, G., Cappiello, F., Quaglia, F., Di, Y.P., Ungaro, F., Mangoni, M.L. *Biomacromolecules* 20, 1876-1888 (2019), https://doi.org/10.1021/acs.biomac.8b01829

Therapeutic Peptides: Regulatory Challenges and Future Direction

Ved Srivastava

Aktis Oncology, vedsrivastava1@yahoo.com

Introduction

Peptide therapeutics have continued to be an innovative strategy for developing biopharmaceutical pipelines and diagnostics tools. Peptide therapeutic is still an untapped innovative area because of the challenges associated with lack of oral bioavailability, cell permeability; and lack of regulatory guidance for manufacturing. This article covers (a) regulatory challenges in peptide-based drug discovery and development, and (b) future direction for peptide-based drugs.

Discussion

Therapeutic peptides are endogenous ligands that are efficacious and safe. Because of the safety and efficacy advantage, the attrition rate of peptides over small molecules are exceptionally low. Twenty-five percent of peptide-based clinical candidate that enters the clinical trial make it to market. This is more than two times higher than small molecules because of its unpredictable safety profile. The Food and Drug Administration (FDA) has approved more than one hundred peptides including peptidomimetics based drugs for marketing. The commercial successes of peptide therapeutics have been seen in metabolic diseases and for peptide drugs acting on extracellular targets such as GPCR.

Symlin™: a Amylin analogs with three modifications

Reduces:
Glucose fluctuations
Gastric emptying
Food intake

Fig. 1. Amylin is a 37 amino acid peptide co-secreted with Insulin.

Approximately thirty plus peptides are in Phase 2 and Phase 3 clinical studies; and those have commercially potential for sale for billions of dollars. Even with the successful Phase 2 and Phase 3 clinical studies results, the regulatory approval process for peptides is not straight forward as we may think. For example, regulatory process for approval of SymlinPen® (Figure 1) for treatment of Type I and Type 2 diabetes took almost 3-5 years. After the first review of Symlin New Drug Application (NDA), FDA responded as 'Not Approved' for concern that it may cause hypoglycemia when taken with Insulin. Amylin pharmaceutical addressed the regulatory concern by careful statistical analysis of the data and resubmitted the application. The FDA responded as "Approvable" and asked to provide the dose titration in combination with Insulin at multiple time points. Amylin pahrmaceuticals performed the studies and resubmitted the application, and this time (in 2005) FDA approved the SymylinPen™ for both Type 1 and Type 2 diabetic patients.

Persistence, hard work, and belief in science ultimately paid off

In recent years, the FDA has denied the approval of drugs because of Manufacturing issues. The FDA and the EMA are paying close attention to Chemistry, Manufacturing and Control (CMC). The FDA recently provided CMC guidance that covers five peptide drug products: glucagon, liraglutide,
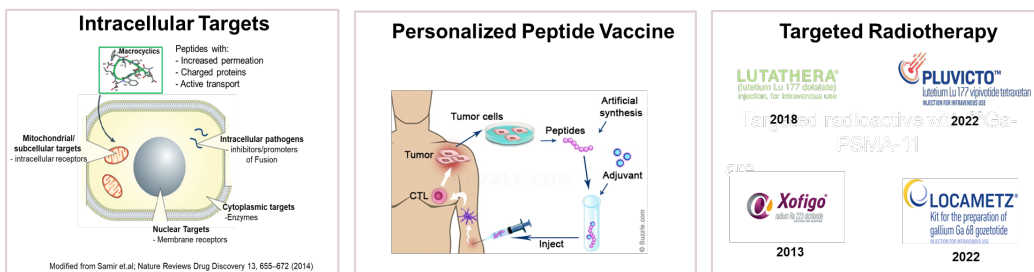
Fig 2. Foresight for therapeutic peptide for oncology.

nesiritide, teriparatide, and teduglutide. The regulators recommend identifying and characterizing all impurities present at levels between 0.10% and 0.5%, including their potential immunogenicity. In-silico and cell-based immunogenicity assessments are good enough. The ICH guideline suggests the process-related impurities or product-related impurities must be differentiated. The development of accelerated stability indicating analytical methods are critical to analyze impurity profiling. In addition, regulators require to evaluate extractable and leachable impurities and sterility testing for the Container Closure system. A total quality system management is required.

The assessment of quality risk in manufacturing is required, early in the process development, by Quality by Design (QbD) and Failure Modes and Effects Analysis (FMEA) for the smooth approval of the peptide-based drug [1].

There are two key areas in peptide therapeutics that need immediate attention to make a significant impact on the commercial scale. One is the development of technology for alternative peptide drug delivery routes, and the other is discovery and development focused on the oncology therapeutic areas.

Delivery Routes for Peptides: Peptides are being delivered via the invasive parenteral route; however, several non-invasive delivery routes, such as nasal, buccal, transdermal, and pulmonary, have been investigated, particularly for chronically administered drugs [2]. Peptide drug molecules are not delivered orally because of its poor aqueous solubility and poor membrane permeability in the gastrointestinal (G.I.) tract, leading to unacceptably low oral bioavailability. The oral route is a better option because of its patient-friendly delivery and increase in the drug's therapeutic value. However, a few peptide drugs are approved for oral delivery, but they are intended for the G.I. restricted therapeutic targets, e.g., Linaclotide (Linzess®). Several biotech and large pharma are investing in developing the technologies for oral delivery of peptides, and most recently Semaglutide, RYBELSUS®) for lowered blood sugar and body weight. Implantable technologies can facilitate the delivery of a controlled drug concentration to a patient by controlling the rate of drug release. Considerable progress has been made toward developing various implantable technologies to deliver drugs via intracranial, intrathecal, or intravaginal routes [3]. However, the most promising developments have been in intraocular and subcutaneous implants. These implantable technologies may contain therapeutic agents in nanomaterial formulations of non-bioabsorbable and biodegradable polymers.

Therapeutic Peptides for Oncology: On the discovery front, understanding and exploration of intracellular targets are critical for the next wave of peptide therapeutics for cancer treatment. For example, modulation of protein-protein interaction by peptides MDM2/p53 for HCV, cytoplasmic targets such as kinases involved in pathways like JNK1 for inflammation, nuclear targets receptors such as transcription factors, AP-1, mitochondrial and subcellular targets, heat shock proteins. Macrocyclic peptides of 10-15 aa possess cell-penetrating properties and could be a good modality to achieve the goals. Target specificity for these peptides is still a challenge though.

Personalized neoantigen vaccines came into play very recently; after diagnosis, biopsies are done on the patient's tumor on both cancerous and normal tissues. A set of most immunogenic antigen sequences are then identified using differential bioinformatics tools and AI approaches. These peptides are then manufactured and formulated with immunoadjuvant before administering to the patient, and immune responses are monitored. GAPVAC, a consortium of eight organizations in Europe, is developing GAPVC-101, a mixture of four peptides for newly diagnosed patients with glioblastoma.

Targeted Radiopharmaceuticals drugs raise hopes for treating cancer [4]. In 2018, Lutathera®, a radioactive ^{177}Lu-DOTATATE was approved for neuroendocrine tumor treatment. It is a Somatostatin-targeted theragnostic. In 2022, the FDA approved, Pluvicto™, ^{177}Lu PSMA-617 to treat metastatic castration-resistant prostate cancer. LOCAMETZ®, Ga 68 Gozetotide, a kit for preparing PET Imaging in PSMA, Prostate Cancer. The FDA designates Pluvicto as brake through therapy. Both these drugs were conjugated to the beta-emitting radioisotope Lutetium-177. Bayer received approval for Xofigo® (radium Ra 223 dichloride) in 2013 as a new treatment for Castration-Resistant Prostate Cancer with Bone Metastases. Xofigo is not a radioconjugate but a straight ^{223}Radium dichloride for prostate cancer. ^{223}Ra – Radium dichloride is a calcium mimic, localizes in areas of bone mineralization (i.e., bone metastases). Xofigo is an alpha-emitting radiopharmaceuticals.

It is believed alpha-targeted radiopharmaceuticals can provide a powerful new treatment option for all stages of solid tumor cancers, including breast, lung, liver, ovarian, bladder, and colorectal

cancer. Alpha particle therapy includes a highly localized large particle, He nuclei and tissue exposure are very narrow100 μm range and covers only a 2-10 cell radius thus killing only tumor cells and irreversibly brakes both double-strand DNA. In clinical use, patients are shielded by just a paper, with limited risk of exposure to family and doctors. On the other hand, current beta particle therapy, beta particle radiates energy to ~1 cm radius, with Linear Energy Transfer LET of 0.2keV/mm, covering 10-1200 cells thus killing healthy cells and immune cells in addition to tumor cells and brakes only a single strand of the DNA. This requires extensive lead shielding and patient sequestration. Often requires an in-patient stay in the hospital for several days (Figure 2).

References

1. *Peptide Therapeutics: Strategy for Chemistry Manufacturing and Control* (Srivastava, V., Eds), Royal Society of Chemistry, (2019), https://doi.org/10.1039/9781788016445
2. *Peptide-based Drug Discovery: Challenges and New Therapeutics* (Srivastava, V., Eds), Royal Society of Chemistry, (2017), https://doi.org/10.1039/9781788011532
3. *Implantable Technologies: Peptides and Small Molecules Drug Delivery* (Srivastava, V., Eds), Royal Society of Chemistry, (2022), https://doi.org/10.1039/9781839164958
4. Boerner, L.K. *Chemical Engineering News* **100**, (13), (2022), https://cen.acs.org/pharmaceuticals/oncology/Targeted-radioactive-drugs-raise-hopes-cancer/100/i13

Numaswitch – The First Viable Alternative for Chemical Synthesis of Peptides and Pepteins

Bach-Ngan Nguyen, Florian G. Neusius, Florian Tieves, and Christian Schwarz

NUMAFERM GmbH, Düsseldorf, 40225, Germany

Introduction

Progress in peptide and protein therapeutics increased the need for rapid and cost-effective production platforms. Yet, the high cost of production remains the major obstacle to the broader use of polypeptide therapeutics. Especially, pepteins of 30-300 amino acids length, covering such important families as long-chained peptides, disulfide-rich peptides, growth factors, peptide fusions and antibody fragments are of high interest and neither chemical synthesis nor traditional recombinant approaches are a reliable and cost-efficient production platform. To this end, we developed such a production platform called Numaswitch [1]. Here, bifunctional Switchtag proteins were developed combining two essential functions (Figure 1). In the first step, Switchtags allow the high titer expression with the accuracy of ribosomal biosynthesis ($> 99.99\%$) as inclusion bodies (IB) protecting the target and cells by aggregation and facilitating easy upscaling of the processes. In the second step, Switchtags act as solubility tags that convert targets quantitatively in water-soluble, functional molecules.
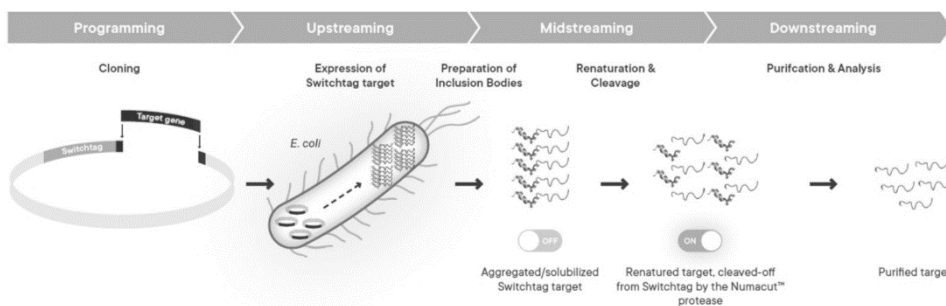
Fig. 1. Numaswitch approach enabling high-titer peptein expression. Adapted from [1].

The development of Switchtags was possible by the application of Ca^{2+} binding domains, so called GG repeats. Being unfolded proteins at the stage of solubilized IBs, the binding of Ca^{2+} to Switchtags (and fusion proteins including target molecules of 2-500 amino acids) enables the quantitative refolding into the native conformation. Inside the cytoplasm of *Escherichia coli* (*E. coli*) and in the absence of Ca^{2+}, Switchtags are unstructured and aggregation-prone proteins. Obviously, Ca^{2+} is acting chaperon-like preventing intermolecular interactions (and thereby aggregation and/or precipitation) of unfolded proteins increasing the overall refolding efficiencies significantly.

Our data show that Switchtags are also applicable for the efficient production of complex, antimicrobial and aggregation-prone targets being fused to Switchtags, like disulfide-rich pepteins, antimicrobials or growth factors. Additional limitations with recombinant approaches are the production of pepteins containing unnatural amino acids [2]. With Numaswitch many of such obstacles can be overcome and many non-natural amino acids can be inserted either during the biosynthesis (via amber stop codon strategy) or by developed protocols (*C*-terminal amidation, *N*-terminal acetylation, side-chain elongations, etc.) [3,4].

As case study (Figure 2), we introduced an unnatural amino acid in Liraglutide (Lira-Bpa), produced the disulfide bridge containing LaM2 light chain antibody fragment and the antimicrobial bifunctional dipeptide conjugate Dermaseptin-Thanatin (DS-THA).

Results and Discussion

To address the current challenges, we generated Switchtag screening libraries of all three above mentioned pepteins and performed expression studies in *E. coli* cells. In agreement with our aim to provide a generally applicable expression platform, we found high-titer expression of the Switchtag target fusion proteins as inclusion bodies. This although hold true for pro-Liraglutide, where an alanine was replaced with the non-canonical amino acid *p*-Benzoyl-L-Phenylalanine (Bpa) by genetic code expansion. Interestingly, the co-expressing of Bpa-tRNA synthetase and the corresponding tRNA had only minor influence on the Switchtag expression level (~ 90%). Refolding from inclusion bodies normally comes along with complex denaturing/refolding procedures and high dilutions (µg/ml). The high renaturation rates observed of up 94% indicate that the Switchtag for the first-time grants access to the advantage of inclusion bodies while acting as a solubility-tag in aqueous solution after execution its molecular switch function by the addition of Ca^{2+}. After renaturation, the pepteins were cleaved-off from the Switchtag, natively and without any traces, using our highly active and specific Numacut TEV protease platfrom (https://numaferm.com/product/). Purification was carried out by state-of-the-art chromatography methods.
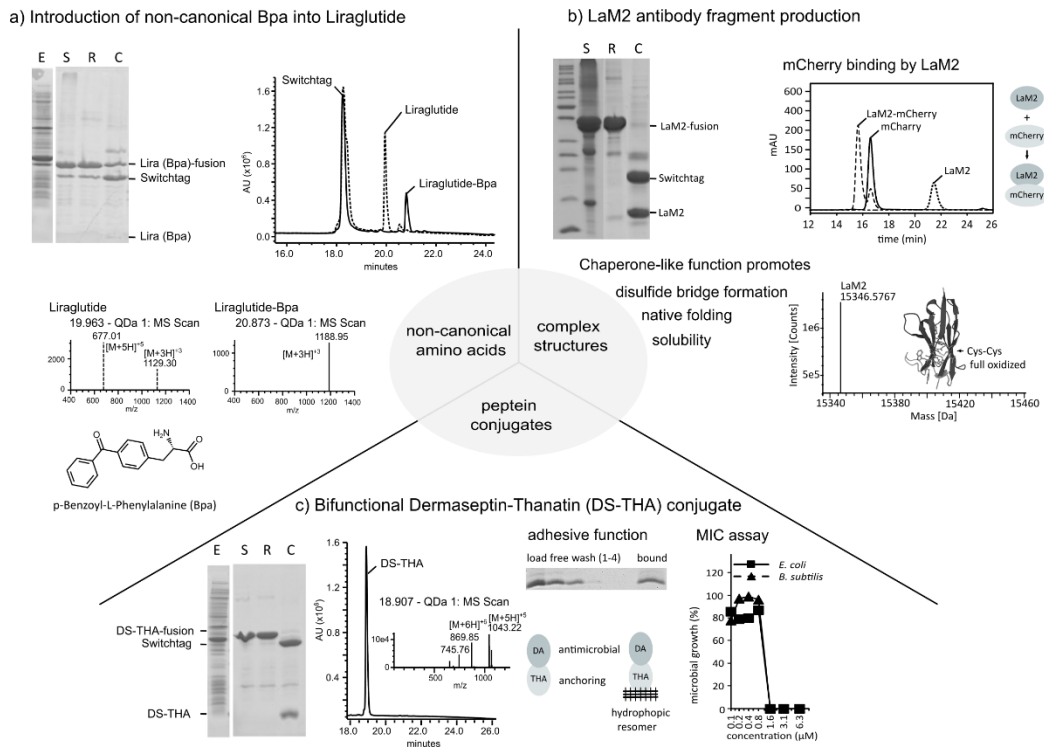
Fig. 2. Application of Numaswitch approach. a) Introduction of the non-canonical amino acid Bpa into pro-Liraglutide. b) Production of complex, disulfide-bridge containing LaM2 light chain antibody fragment. c) Production of the antimicrobial bifunctional peptein conjugate DS-THA. SDS-PAGE illustrated show the expressed (E), the solubilized (S), renatured (R) and by Numacut TEV protease cleaved (C) Switchtag fusion proteins. Introduction of Bpa was confirmed by HPLC/MS, functionality of LaM2 was verified by SEC analysis via binding assay with mCherry. The adhesive function of DS-THA was confirmed by pull down assays and its antimicrobial activity was determined for E. coli and B. subtilis (MIC 1.6 µM).

13

Table 1. Characteristics of Switchtag-based Liraglutide-Bpa, LaM2 and Dermaseptin-Thanatin production.

Peptein	Liraglutide-Bpa	LaM2	Dermaseptin-Thanatin
Type	non-canonical amino acid	Cys-Cys bridge(s)	antimicrobial peptein conjugate
Size (kDa)	2.7	15.4	5.2
Cys residues	-	2	2
Renaturation (%)	92	83	94
Purity (%)	> 99[a]	> 98[b]	> 99[a]
Titer (g/L)	≥ 2.0[c]	4.5[d]	2.5[d]

[a]determined by RP-HPLC; [b]determined by UV/VIS spectrometry; [c]expected or [d]obtained titer of purified peptein per liter fermentation broth

Mass spectrometry analysis of pro-Liraglutide-Bpa revealed that Bpa was successfully introduced by genetic code expansion, suggesting that the Switchtag approach can act as a promising platform for generation of pepteins harboring non-canonical amino acids. Furthermore, mass spectrometry analysis confirmed that the LaM2 antibody fragment was obtained in the full oxidized state; meaning, that the cysteine-bridge was formed. In addition, functionality of the LaM2 antibody fragment was confirmed by mCherry binding via size exclusion chromatography [5]. Although pepteins are expected to fold correct to the native conformation under thermodynamic control, the folding is very inefficient and dominated by intermolecular interactions yielding to aggregated and/or precipitated targets, especially for cysteine-containing pepteins [6]. The Switchtags act as solubility tags keeping the target in solution and preventing premature aggregation/precipitation. Hereby, the Switchtags gives the peptein more time to form the correct fold and even the right isomers for disulfide-rich candidates (sometimes in the presence of redox shuffle systems).

We also produced, purified, and analyzed the bifunctional antimicrobial peptide DS-THA. DS-THA consist of a hydrophobic, antimicrobial, anchoring domain Thanatin (THA) and an antimicrobial peptide Dermaseptin (DS) [7]. Expression of such a combination is difficult to realize in recombinant systems without the loss of productivity due to the tendency of aggregation and the target toxicity towards the expression host. Although the produced DS-THA is toxic towards *E. coli* with a minimal inhibitory concentration (MIC) of 1.6 µM, growth was not affected and high amount of Switchtag fusion proteins were formed.

Switchtag fusion proteins are expressed in high titers and refolded up to quantitatively, even for complex pepteins. In addition, due to the highly pure refolded Switchtag proteins, process-related impurities (host cell DNA, proteins, and endotoxins) are easily removed before, after or during the refolding step allowing high production titers and purities (Table 1).

Overall, our data show that Numaswitch serves as high-titer expression platform for peptides and pepteins independently of the length, functionality and physicochemical properties.

References

1. Nguyen, B.-N., et al. *AMB Expr* **11**, 48 (2021), https://doi.org/10.1186/s13568-021-01204-w
2. Wang, L., et al. *Signal Transduct Target Ther* **7**, 48 (2022), https://doi.org/10.1038/s41392-022-00904-4
3. Marino, G., et al. *ACS Chemical Biology* **10**, 8 (2015), https://doi.org/10.1021/acschembio.5b00189
4. Erak, M., et al. *Bioorganic & Medicinal Chemistry* **26**, 10 (2018), https://doi.org/10.1016/j.bmc.2018.01.012
5. Wang, Z., et al. *Protein Science* **30** (2021), https://doi.org/10.1002/pro.4194
6. Hidaka, Y., et al. *BioMolecular Concepts* **4**, 6 (2013), https://doi.org/10.1515/bmc-2013-0022
7. Schwinges, P., et al. *Green Chemistry* **21**, 9 (2019), https://doi.org/10.1039/C9GC00457B

Attenuated Cationic Lytic Peptides for Intracellular Delivery

Shiroh Futaki

Institute for Chemical Research, Kyoto University, Uji, Kyoto 611-0011, Japan

Introduction

Intracellular delivery of biomacromolecules is one of the most important topics in current peptide research. Although many approaches have been developed, more efficient methods for the delivery of high molecular weight proteins, including immunoglobulin G (IgG), are still awaited. Cationic amphiphilic peptides often have potent membranolytic activity. If the lytic activity of these peptides can be properly controlled, they could be used as a novel means of intracellular delivery. Since the hydrophobic interaction of peptides with the membrane is very important for membrane lysis, the placement of negatively charged Glu residues in the potential hydrophobic region of the peptides could be used as a switching device to modulate membrane lysis. This simple idea was the impetus for our efforts to develop a new class of delivery peptides, i.e., attenuated cationic lytic (ACAL) peptides.

Results and Discussion

First, we investigated the lytic activity of various amphiphilic peptides, and California wolf spider toxin-derived M-lycotoxin was chosen as the design platform. The mutant peptide L17E, in which the leucine at position 17 was replaced by glutamic acid (IWLTALKFLGKHAAKHEAKQQLSKL amide), was designed [1]. The EC_{50} value (concentration at which 50% of cells die) of L17E was reduced to >40 µM compared to that of M-lycotoxin (1.36 µM). Treatment of cells with model macromolecules, polydextran (10 kDa) and IgG (~150 kDa), in the presence of L17E resulted in marked cytosolic translocation of these molecules in 50% of cells. Efficient intracellular delivery of a ribosome-inactivation protein (saporin), Cre recombinase and IgG delivery was thus achieved, resulting in a specific recognition of cytosolic proteins and subsequent suppression of the glucocorticoid receptor-mediated transcription. The increased hydrophobicity of L17E improved the low pH helical structure and cytosolic delivery efficiency (HAad: IWLTALKFLGKAAAKA-XAKQXLSKL amide; X = L-2-aminoadipic acid (Aad)), resulting in cytosolic translocation of IgG in 75% of cells, an increase of approximately 25% over L17E [2] (Figure 1).
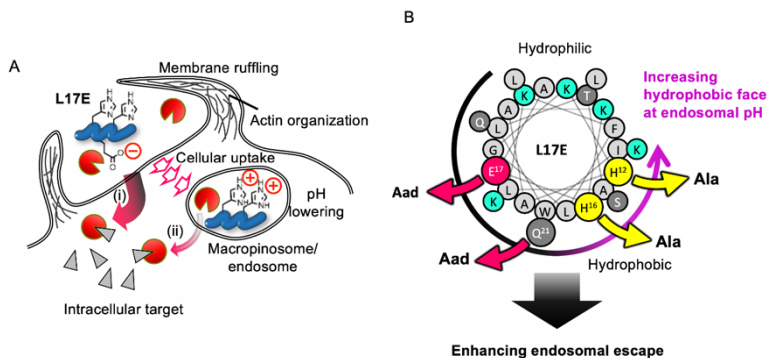
Fig. 1. (A) Schematic representation of the mode of intracellular delivery by L17E. L17E was found to have an ability to induce membrane ruffling, leading to transient permeabilization of membranes at early stages of endocytosis and cytosolic translocation of biomacromolecules (route (i)). However, endosomal escape (route (ii)) did not play a significant role in attaining cytosolic translocation as originally intended [3]. (B) Helical wheel projection of L17E showing substitutions of His[12] and His[16] to Ala, and Glu[17] and Gln[21] to Aad, yielding HAad. Substitutions led to the enlargement of the potential hydrophobic face in endosomes and enhanced delivery using both routes (i) and (ii). Reprinted with permission from ref. [2].

Conjugation of HAad with pyrene butyric acid as a membrane anchoring moiety (pBu-HAad) further improved the release efficiency. pBu-HAad achieved a comparable level of protein release efficiency into cells with only 1/20 of the HAad concentration [4]. In contrast, conjugates with cholesteryl hemisuccinate and aliphatic fatty acids did not yield a marked improvement. The results of the time-laps microscopic observation and inhibitor studies indicate that membrane anchoring of HAad by a pyrene moiety results in enhanced peptide-membrane interaction and loosening of the lipid packing, which facilitates cytosolic translocation of proteins.

More sophisticated IgG delivery systems based on L17E and other ACAL peptides can be created by appropriate means of complexation or packaging, since IgG must be localized with membrane-permeabilizing ACAL peptides to achieve cytosolic translocation. We therefore sought to formulate IgG with the ACAL peptide L17E to facilitate more efficient permeation of IgG across membranes, using a trimer of L17E. To facilitate complex formation with IgG, the trimer was tagged with an Fc binding peptide. To assess cytosolic translocation, IgG was fluorescently labeled with Alexa Fluor 488 (IgG-Alexa488). Notably, mixing FcB(L17E)$_3$ with IgG-Alexa488 resulted in the formation of liquid droplets or coacervate, which allowed efficient cytosolic translocation of IgG [5] (Figure 2). The addition of negative charges on IgG by modification with Alexa Fluor 488 was crucial for liquid droplet formation. This liquid droplet-mediated intracellular translocation of IgG was not achieved by simple pore formation in the cell membrane. The need for energy-dependent, actin-driven membrane dynamics triggered by the liquid droplet was suggested by pharmacological inhibition experiments. The potential applicability of this approach to other proteins modified with negatively charged molecules was illustrated by the successful delivery of an antibody to the nuclear pore complex (modified with Alexa Fluor 594) and an antibody to mCherry nanobody (labeled with a supernegatively charged green fluorescent protein ((-30)GFP).
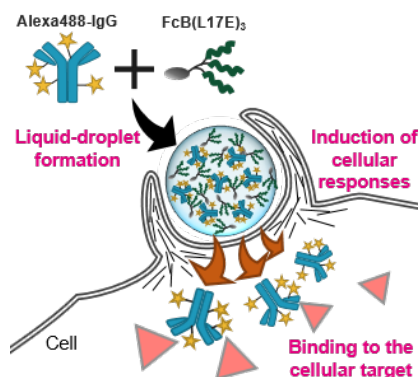
Fig. 2. Possible mechanism of liquid droplet formation and facile cytosolic translocation of IgG in the presence of the trimer of L17E. Reprinted with permission from ref. [5].

Acknowledgments

References

1. Akishiba, M., et al. *Nature Chem*. **9**, 751-761 (2017), https://doi.org/10.1038/nchem.2779
2. Sakamoto, K., et al. *Angew. Chem. Int. Ed. Engl*. **59**, 19990-19998 (2020), https://doi.org/10.1002/anie.202005887
3. Akishiba, M. and Futaki, S. *Mol. Pharm*. **17**, 2175-2185 (2021), https://doi.org/10.1021/acs.molpharmaceut.0c00312
4. Sakamoto, K., et al. *Bioconjug. Chem*. **32**, 950-957 (2021). https://doi.org/10.1021/acs.bioconjchem.1c00101
5. Iwata, T., et al. *Angew. Chem. Int. Ed. Engl*. **60**, 19804-19812 (2021), https://doi.org/10.1002/anie.202105527

SARS Coronavirus 3CL Protease Inhibitors with an Electrophilic Aryl-Ketone Warhead

Sho Konno[1], Kiyotaka Kobayashi[1], Miki Senda[2], Yuta Funai[3], Yuki Seki[3], Ikumi Tamai[3], Laura Schakel[4], Kyousuke Sakata[1], Thanigaimalai Pillaiyar[5], Akihiro Taguchi[1], Atsuhiko Taniguchi[1], Michael Gutschow[4], Christa Muller[4], Koh Takeuchi[6], Mikako Hirohama[7], Atsushi Kawaguchi[7], Masaki Kojima[1], Toshiya Senda[2], Yoshiyuki Shirasaka[3], Wataru Kamitani[8], and Yoshio Hayashi[1]

[1]*Tokyo University of Pharmacy and Life Sciences, Tokyo, Japan;* [2]*Structural Biology Research Center, Institute of Materials Structure Science, High Energy Accelerator Research Organization, Tsukuba, Japan;* [3]*Faculty of Pharmacy, Institute of Medical, Pharmaceutical and Health Sciences, Kanazawa University, Kanazawa, Japan;* [4]*Pharmaceutical Institute, Pharmaceutical & Medicinal Chemistry, University of Bonn, Bonn, Germany;* [5]*Pharmaceutical Institute, Pharmaceutical/Medicinal Chemistry, University of Tübingen, Tübingen, Germany;* [6]*Cellular and Molecular Biotechnology Research Institute, National Institute of Advanced Industrial Science and Technology, Tokyo, Japan;* [7]*Faculty of Medicine, Transborder Medical Research Center, University of Tsukuba, Tsukuba, Japan;* [8]*Department of Infectious Diseases and Host Defense, Graduate School of Medicine, Gunma University, Maebashi, Japan*

Introduction

The novel coronavirus, SARS-CoV-2, has been identified as the pathogen for the current coronavirus disease (COVID-19) outbreak. 3CL protease (3CLpro), a viral cysteine protease, plays a pivotal role in the SARS-CoV-2 replication, which is therefore the imperative target for the development of therapeutic agents. Since the outbreak of SARS in 2002, we have been studying 3CLpro inhibitors based on its substrate sequence (Figure 1) [1, 2] and develo-ped a potent tripeptide-type inhibitor, Z-Val-Leu-Ala(oxopyrrolidin-3-yl)-2-benzothiazole (**SH-5**, Ki = 4 nM) [3] via early designed inhibitor **1**. **SH-5** contains an electron-withdrawing reactive warhead, benzothiazolyl-2-ketone (P1'-moiety), to capture the SH group at the catalytic center of 3CLpro. Then, based on **SH-5**, a series of low-molecular-weight dipeptidomimetics were also developed by truncating the P3-Val unit, and the 4-methoxy-indole-2-carbonyl unit was identified

*Fig. 1. Development of SARS-CoV 3CL protease inhibitor **YH-53** with an electrophilic aryl-ketone warhead.*

as one of the best P3-scaffolds, resulting in the development of a potent dipeptide-type inhibitor, 4-methoxyindole-2-carbonyl-Leu-Ala((S)-2-oxopyrrolidin-3-yl)-2-benzothiazole (**YH-53**, Ki = 6 nM) in 2013 [4, 5].

Results and Discussion

Our substrate-derived SARS-CoV-1 3CLpro inhibitor **YH-53** showed a potent inhibitory activity against SARS-CoV-2 3CLpro with a Ki value of 34.7 nM, and the inhibition mode was competitive [6]. This suggests that aryl ketone-type 3CLpro inhibitors developed for SARS-CoV-1 are effective

against that of SARS-CoV-2 with a clear mechanism of action. This result is largely attributed to the quite high similarity in the entire amino acid sequence and three-dimensional structure, particularly 100% identity at the active site in 3CLpro between SARS-CoV-1 and SARS-CoV-2. The reversible mode of action is enzymologically supported by the analysis of progress curves which did not show time-dependent inhibition. We also carried out an NMR titration experiment, which confirmed that **YH-53** binds to SARS-CoV-2 3CLpro in 1:1 stoichiometry and with slow exchange kinetics [6]. Then, crystal structures of the SARS-CoV-2 3CLpro-**YH-53** at 1.65 Å resolutions was determined. It revealed the binding mode of **YH-53** with multiple hydrogen bond interactions to backbone amino acids (Figure 2A) and a covalent bond to the active site thiol group of 3CLpro (Figure 2B). These data confirm the predicted mechanism of action, a tight and reversible binding, and interaction with the active site in the S4-S1'-pockets.

YH-53 completely blocked the viral proliferation *in vitro* (Vero cells) and the $TCID_{50}$ value was ~5 μM. This antiviral activity of **YH-53** was enhanced by adding CP-100356, which is a potent inhibitor of MDR-1 efflux transporter, suggesting that **YH-53** acts as a substrate of the p-glycoprotein efflux pump. Safety and toxicological evaluations suggested that **YH-53** has a high safety index with low cytotoxicity, no or moderate but tolerable CYP inhibition, no mutagenicity and no cardiotoxicity. By means of the simultaneous analysis of intravenous and oral pharmacokinetic data, the bioavailability of **YH-53** in rats was estimated to be approximately 3.6%. This low bioavailability is generally caused by poor absorption and/or significant first-pass metabolism. Interestingly, *in vitro* assessment of intestinal permeability of **YH-53** using a Caco-2 cell monolayer system exhibited excellent cell permeability, close to that of metoprolol, a completely absorbed drug (Fa ≥ 90%). Moreover, an *in vitro* metabolism study using cryopreserved hepatocytes revealed that **YH-53** is mainly metabolized by hydrolytic enzymes that cleave it at the *C*-terminal of Leu (P2-moiety). Taking these results into account, it is reasonable to consider that the low bioavailability of **YH-53** in rats may be mainly due to the first-pass metabolism catalyzed by hydrolytic enzymes in the intestine and/or liver. These results suggest that **YH-53** has high potential as a lead compound for the development of COVID-19 therapeutics.

*Fig. 2. Crystal structures of the SARS-CoV-2 3CLpro-**YH-53**.*

Acknowledgments

References

1. Sydnes, O.M., Kiso, Y., et al. *Tetrahedron* **62**, 8601-8609 (2006), https://doi.org/10.1016/j.tet.2006.06.052
2. Regnier, T., Kiso, Y., et al. *Bioorg. Med. Chem. Lett.* **19**, 2722-2727 (2009), https://doi.org/10.1016/j.bmcl.2009.03.118
3. Konno, S., Hayashi, Y., et al. *Bioorg. Med. Chem.* **21**, 412-424 (2013), https://doi.org/10.1016/j.bmc.2012.11.017
4. Thanigaimalai, P., Hayashi, Y., et al. *Eur. J. Med. Chem.* **65**, 436-447 (2013), https://doi.org/10.1016/j.ejmech.2013.05.005
5. Thanigaimalai, P., Hayashi, Y., et al. *Eur. J. Med. Chem.* **68**, 372-384 (2013), https://doi.org/10.1016/j.ejmech.2013.07.037
6. Konno, S., et al. *J. Med. Chem.* **65**, 2926-2939 (2022), https://doi.org/10.1021/acs.jmedchem.1c00665
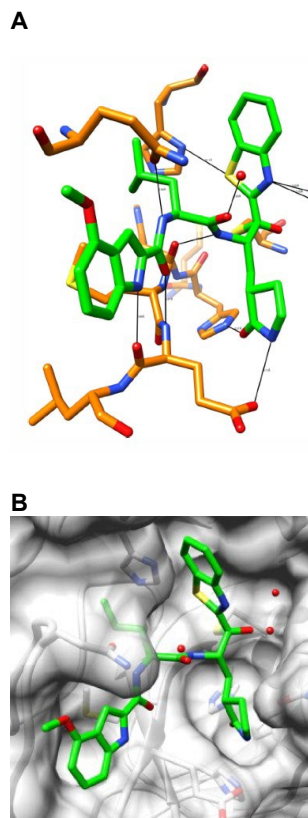
How to Tackle Aspartimide Formation - A Systematic Comparison of Different Methods

Kai Holland-Nell[1], Jacqueline Dalski[1], Thomas Bruckdorfer[2], Raimund Maier[2], Karin Rustler[2], Markus Weishaupt[2], Rudolf Dölling[1], and Stephan Pritz[1]

[1]Biosyntan Gesellschaft für bioorganische Synthese mbH, 13125 Berlin, Germany; [2]Iris Biotech GmbH, 95615 Marktredwitz, Germany

Introduction

Aspartimide formation is still a serious challenge in peptide synthesis. This side reaction is strongly sequence dependent and preferably occurs at Asp-Aaa motifs (Aaa = Gly, Asp, Asn, Gln or Arg). In a first step, the cyclic aspartimide is formed, which can re-open in a second reaction leading to (epimerized) α- and β-Asp peptides and corresponding piperidides. Thus, all in all ten different products can be formed. Over the last decades, several approaches to solve this problem have been developed.

In this work, we systematically compared the combination of various strategies on different model peptides. The steric effect of Asp side chain protecting groups was investigated (OtBu, OEpe, OBno) [1]. The influence of various Fmoc cleaving reagents was studied, including acidic additives [2]. Furthermore, these results were compared to the application of dimethoxybenzyl (Dmb) as backbone protection and cyanosulfurylide (CSY) [3] as side chain protection. Finally, our identified optimal conditions were tested in the synthesis of other peptide sequences prone to aspartimide formation.

Results and Discussion

Three short aspartimide-prone model peptides: VKDGYI-OH, VKDDYI-OH and VKDRYI-OH were synthesized to investigate the sequence dependency of aspartimide formation. The standard protection Asp(OtBu) was applied. In order to minimize aspartimide formation during synthesis, the very mild Fmoc cleaving reagent 50% morpholine/0.1 M formic acid (FA) was used.

Comparing different strategies, repeated Fmoc cleaving steps were simulated by applying various cleavage cocktails to the resin-bound peptide for 18 h. Incubation with pure DMF served as negative control. The released peptides were analyzed by HPLC and the formation of aspartimide/piperidides was quantified.

We observed a strong sequence dependency already with the standard cleaving reagent 30% piperidine - with DG being the most sensitive motif. Aspartimide/piperidide formation was less pronounced for the DR and DD motif.
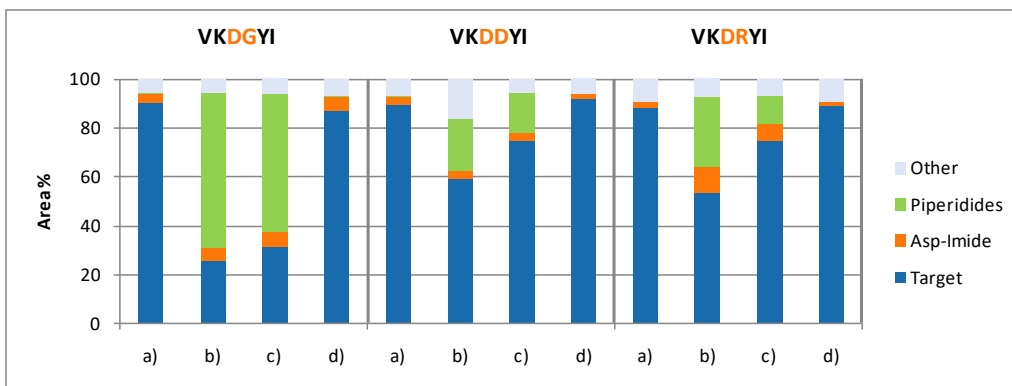
Fig. 1. Product composition after incubation of peptide resin with respective reagent for 18 h. a) DMF only, b) 30% piperidine, c) 30% piperidine/0.1 M FA, d) 50% morpholine.
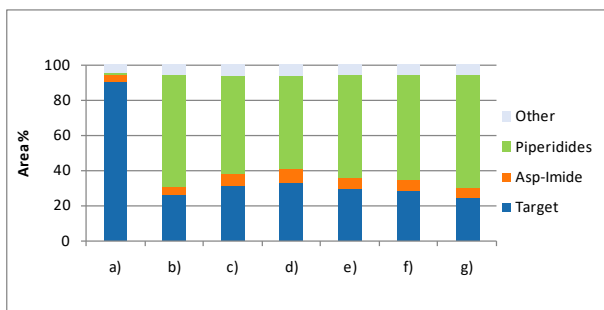
Fig. 2. Effect of acidic additives. a) DMF only, b) 30% piperidine, c) 30% piperidine/0.1 M FA, d) 30% piperidine/0.5 M FA, e) 30% piperidine/0.1 M NH₄OAc, f) 30% piperidine/0.1 M HOBt, g) 30% piperidine/0.1 M trifluoroethanol.
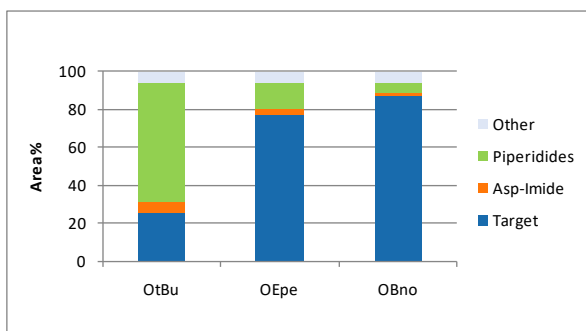
Fig. 3. Effect of different side chain protection groups.
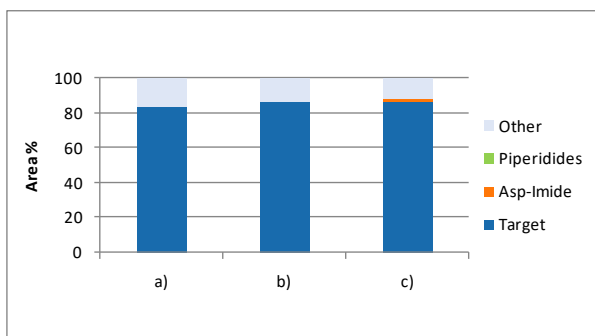
Fig. 4. Effect of Dmb backbone protection. a) DMF only, b) 30% piperidine, c) 2% DBU/2% piperidine.

In a next step we investigated the basicity of the cleavage reagent. The three model peptides were treated either with 30% piperidine, 30% piperidine/0.1 M formic acid or 50% morpholine (Figure 1). When using piperidine, a considerate amount of aspartimide/piperidides was observed, while morpholine showed almost no aspartimide formation. This effect correlates with the lower basicity of morpholine (pK_a piperidine = 11.2; pK_a morpholine = 8.4). Although morpholine reduces the aspartimide formation tremendously, it is often not sufficient for a complete Fmoc cleavage and stronger bases are necessary.

We also studied the influence of acidic additives. Addition of 0.1 M FA to piperidine significantly reduced the occurrence of byproducts for the DR and DD sequences. The effect was less pronounced for the most sensitive DG sequence. Various other acidic additives show similar results. Addition of formic acid, ammonium acetate, HOBt, or trifluoroethanol reduced the formation of aspartimide/piperidides in case of the most sensitive DG sequence only slightly (Figure 2).

Therefore, the steric effect of different Asp side chain protecting groups (OtBu, OEpe, OBno) was investigated (Figure 3). The bulkiness of the Asp protective groups has a large influence on aspartimide formation [1]. With increasing steric demand of the protecting group, aspartimide formation is diminished. OBno suppresses aspartimide/piperidide formation to a great extent even at DG sequences (Figure 3).

Dmb backbone protection offers a different strategy that completely prevents aspartimide formation (Figure 4). Even the very strong combination of DBU/piperidine produced almost no apartimide. Introducing Fmoc-Asp(OtBu)-(Dmb)Gly-OH however, needs sometimes more elaborated conditions due to the low coupling efficiency of such dipeptide building blocks at difficult positions. The formation of other byproducts during the synthesis lowered the yield of the target peptide additionally, e.g. we observed that tryptophane residues act as scavenger for Dmb upon TFA cleavage (data not shown).

Table 1. Analysis of naturally occurring peptide sequences.

Sequence[a]	Asp-PG	Cleavage conditions	Crude/ area %	Isolated yield/%
ASYKVTLKTPDGDNVITVPD [5]	OtBu (3x)	30% piperidine	66	29
	OtBu (3x)	30% piperidine/0.1 M FA	71	33
	OBno (3x)	30% piperidine	76	42
	CSY (3x)	30% piperidine	73	37
NPLGFFPDHQLDPAFRANTANPDWDy [2]	OtBu (3x)	30% piperidine	53	23
	OtBu (3x)	30% piperidine/0.1 M FA	58	24
	OBno (3x)	30% piperidine	63	27
	CSY (3x)	30% piperidine	64	14

[a]*All peptides were synthesized as C-terminal amides*

The Asp(CSY) protection recently introduced by Bode *et al.* shows complete suppression of aspartimide formation. However, other undefined side products were observed, even when applying morpholine (Figure 5). In contrast to other protecting schemes, the stable C-C-bond of the sulfur ylide allows the use of DBU as Fmoc cleaving reagent. Only in case of the DD motif, a significant drop of target yield was detected. We attribute this to the (expected) formation of aspartimide at DY, since regular Asp(OtBu) was used in this position. The cleavage of the CSY group in a second step went smoothly with approximately two equivalents of *N*-chlorosuccinimide (NCS). A larger excess of NCS led to multiple chlorinated products at the tyrosine residue.

Finally, our identified optimal conditions were tested in the synthesis of longer, naturally occurring peptide sequences prone to aspartimide formation. Synthesis was performed with different Asp protecting groups and Fmoc cleaving reagents (Table 1). In these cases, no additional incubation of the resin bound peptides with Fmoc cleaving reagents was performed. Application of CSY requires an additional cleavage step with NCS after final deprotection. All peptides were purified by preparative HPLC and isolated yields were determined. Using OBno or CSY protection resulted in increased crude yields for both sequences compared to standard OtBu protection. Addition of FA to the Fmoc cleaving cocktail improved the yields to a certain degree. Overall yields improved in the order OtBu, OtBu/FA, OBno similar to the model peptides. CSY showed comparable yields to OBno only for the first peptide.
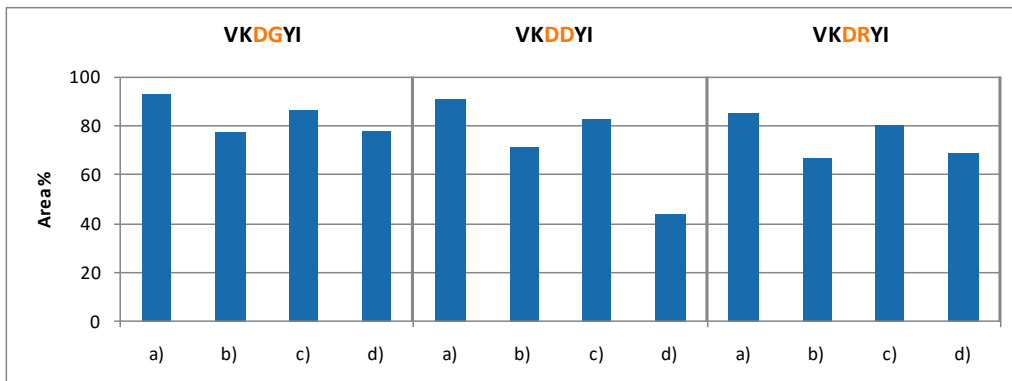
Fig. 5. Amount of target sequence after incubation of Asp(CSY)-peptide resins with respective reagent for 18 h. a) DMF only, b) 30% piperidine, c) 50% morpholine, d) 2% DBU.

In the second sequence we observed a byproduct with a Trp oxidation (confirmed by LC-MS/MS analysis), which was very difficult to separate by HPLC resulting in lower yield. Chlorination of Tyr was avoided by careful titration of NCS and monitoring by LC-MS. We could not prevent oxidation of Trp by this approach. Other literature known side reactions with NCS [4] can be circumvented by simple alterations: oxidation of Cys by disulfide protective groups (e.g. StBu or SIT) and oxidation of Met by substitution by norleucine.

Although aspartimide formation has been studied for decades, a universal low-cost method to circumvent this side reaction is still lacking. A simple and inexpensive approach is the standard Asp(OtBu) protection and addition of an acidic additive (e.g. FA) to the Fmoc cleavage cocktail. For the majority of peptides, these conditions reduce aspartimide formation to an acceptable level. In difficult cases, the use of special residues like Asp(OBno), Asp(CSY) or Dmb backbone protection should be considered. These more cost intensive special derivatives guarantee almost complete suppression of aspartimide-related side products.

Acknowledgments

References

1. Behrendt, R., et al. *J. Pept. Sci.* **22**, 92-97 (2016), https://doi.org/10.1002/psc.2844
2. Michels, T., et al. *Org. Lett.* **14**, 5218-5221 (2012), https://doi.org/10.1021/ol3007925
3. Mergler, M., et al. *J. Pept. Sci.* **9,** 518-526 (2003), https://doi.org/10.1002/psc.473
4. Neumann, K., et al. *Nat. Commun.* **11**, 982 (2020), https://doi.org/10.1038/s41467-020-14755-6
5. Packman, L.C. *Tetrahedron Lett.* **36**, 7523-7526 (1995), https://doi.org/10.1016/0040-4039(95)01522-1

Development of Peptide-Photooxygenation Catalyst Conjugates for Myostatin Inactivation

Hideyuki Okamoto[1], Atsuhiko Taniguchi[1], Shoya Usami[1], Masahiro Katsuyama[1], Shuko-Amber Murano[1], Sho Konno[1], Akihiro Taguchi[1], Kentaro Takayama[1,2], and Yoshio Hayashi[1]

[1]*Department of Medicinal Chemistry, Tokyo University of Pharmacy and Life Sciences, Hachioji, Tokyo 192- 0392, Japan;* [2]*Department of Environmental Biochemistry, Kyoto Pharmaceutical University, Yamashina- ku, Kyoto 607-8414, Japan*

Introduction

Myostatin is a protein belonging to transforming growth factor β (TGF-β) superfamily. Since myostatin negatively regulates the growth of skeletal muscle, the inactivation of myostatin activity causes an increase in muscle mass. Hence, the inactivation is expected as a promising therapeutic strategy for muscular atrophic diseases such as muscular dystrophy, cancer cachexia and disused muscular atrophy. Previously, we discovered a 23-residues myostatin-binding peptide **1** (Figure 2) from *N*-terminal sequence of a prodomain protein which forms interactions with myostatin in a latent myostatin complex [1]. This peptide reversibly binds with myostatin and inhibited its activity. To drastically improve the inhibitory effect, we developed peptide-photocatalyst conjugates which inactivate myostatin *via* photooxygenation irreversibly and catalytically (Figure 1).

Results and Discussion

We synthesized conjugate **2** with an on/off switchable photooxygenation catalyst [2] at the position 12 (Figure 2) [3]. The amino acid residue at the position 12 has been reported to show a high tolerance against structural modifications in our previous structure-activity relationship studies [4]. Since Trp is sensitive to oxidation, Trp1 of **1** was also replaced with 3,3-diphenyl propionic acid which was used as a surrogate for Trp1 in our previous study [5]. Myostatin was oxygenated with conjugate **2** under near-infrared light irradiation conditions (wavelength: 730 nm). This
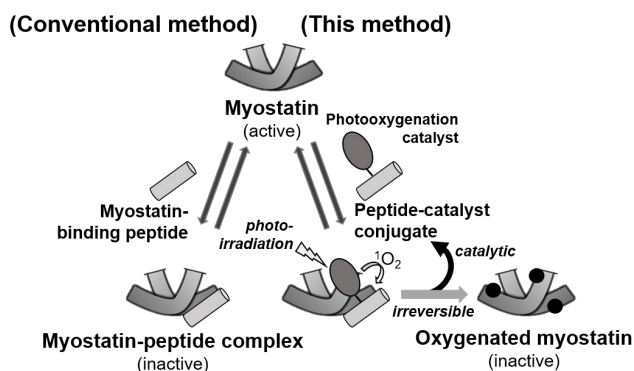
Fig. 1. Inhibition of myostatin using a conjugate of myostatin-binding peptide and photooxygenation catalyst.
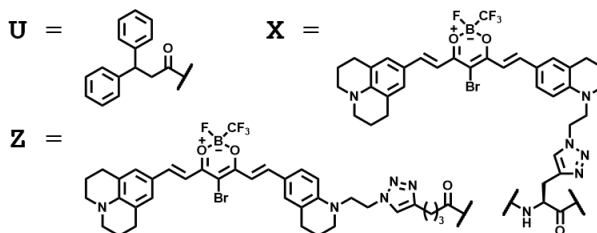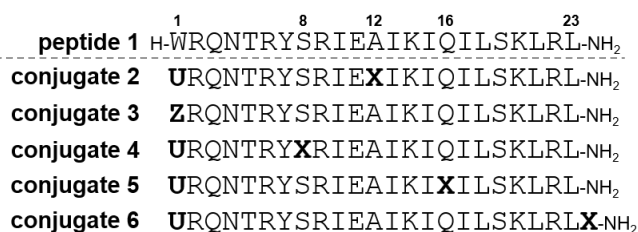
*Fig. 2. Structures of myostatin-binding peptide **1** and peptide-photocatalyst conjugates **2-6**.*

wavelength enables a high light transmission in a living tissue. No oxygenation occurred in the absence of **2** or light irradiation. Moreover, the oxygenation was significantly suppressed under degassing conditions. These results indicated that conjugate **2** induced the photooxygenation of myostatin. Then, to evaluate the inactivation of myostatin by **2**, the myostatin activity was measured by a luciferase reporter assay. As a result, the oxygenated myostatin was significantly less active than native myostatin. No inactivation of myostatin was observed in the absence of **2** or light irradiation. Therefore, myostatin was effectively inactivated by photooxygenation with **2**.

Next, we optimized the position of photooxygenation catalyst on the myostatin-binding peptide. Based on our previous Ala scan study of peptide **1** [6], Ser8 and Gln16 were selected as modification sites. Trp1 and the C-terminus were also selected since they are termini of the peptide chain. Conjugates **3-6** with the photooxygenation catalyst at each position were synthesized (Figure 1) [7]. Comparing the myostatin photooxygenation by conjugates **2-6**, all conjugates exhibited the similar photooxygenation activities. Then, to compare the myostatin selectivity, we examined the photooxygenation of off-target models such as amyloid-β and substance P. As a result, **2-6** induced much less photooxygenation of off-targets than methylene blue which is a nonspecific photosensitizer, while especially **2**, **4** and **5** exhibited a better selectivity than **3** and **6**. Probably because **2**, **4** and **5** have the photooxygenation catalyst in the middle part of the peptide chain, the peptide chain may prevent the catalyst part from approaching off-target molecules. Comparing the myostatin-inhibitory activities of **2-6**, particularly **5** with the photooxygenation catalyst at the position 16 showed the strongest myostatin inhibitory activity among all conjugates. The inhibitory activity of **5** (IC_{50} 2.1 nM) was twice higher than that of **2** (IC_{50} 4.0 nM). In addition, **5** inhibited myostatin more than 1500-fold efficiently compared to original peptide **1** (IC_{50} 3500 nM), suggesting that irreversible and catalytic inactivation of myostatin by photooxygenation is highly effective. Finally, we evaluated the cytotoxicity of the conjugate by a WST-1 assay using HEK293 cells. Conjugate **5** showed no significant cytotoxicity under both non-irradiated and irradiated conditions despite its high concentration of 3 μM, suggesting that **5** has no cytotoxicity and phototoxicity. This could be attributed to the high target selectivity of **5**.

In conclusion, we developed the new conjugates of myostatin-binding peptide and photooxygenation catalyst and optimized the catalyst-attachment position. The conjugates selectively oxygenated myostatin with near-infrared light irradiation, resulting in its efficient inactivation. These findings would contribute to a new photooxygenation-based myostatin-targeting therapy. The protein inactivation based on target-selective photooxygenation would open new therapeutic modalities for diseases.

Acknowledgments

References

1. Takayama, K., et al. *J. Med. Chem.* **58**, 1544-1549 (2015), https://pubs.acs.org/doi/pdf/10.1021/jm501170d
2. Ni, J., et al. *Chem* **4**, 807-820 (2018), https://doi.org/10.1016/j.chempr.2018.02.008
3. Okamoto, H., et al. *Chem. Commun.* **55**, 9108-9111 (2019), https://doi.org/10.1039/C9CC04368C
4. Takayama, K., et al. *ACS Med. Chem. Lett.* **8**, 751-756 (2017), https://pubs.acs.org/doi/10.1021/acsmedchemlett.7b00168
5. Takayama, K., et al. *ChemMedChem*, **11**, 845-849 (2016), https://doi.org/10.1002/cmdc.201500533
6. Asari, T., et al. *ACS Med. Chem. Lett.* **8**, 113-117 (2017), https://pubs.acs.org/doi/10.1021/acsmedchemlett.6b00420
7. Okamoto, H., et al. *Org. Biomol. Chem.* **19**, 199-207 (2021), https://doi.org/10.1039/D0OB02042G

Development of G Protein Peptidomimetics to Stabilize Active State G Protein-Coupled Receptors

Morgane Mannes[1], Charlotte Martin[1], Sarah Triest[2], Toon Laeremans[2], Christel J. Menet[2], and Steven Ballet[1]

[1]Research Group of Organic Chemistry, Vrije Universiteit Brussel, Brussels, 1050, Belgium;
[2]Confo Therapeutics N.V., Ghent, 9052, Belgium

Introduction

G protein-coupled receptors are cell-surface proteins that have been of long-standing interest because of their involvement in various physiological processes. To date, the pharmaceutical industry has more effectively exploited GPCRs than any other target class. However, the vast majority of this large class of targets remains therapeutically untapped [1]. Targeting GPCRs for drug discovery is still challenging because of their intrinsic dynamics and instability when extracted from the cell membrane, making them difficult to isolate and purify for use in screening assays. In past years, Confobodies (Cb, single-chain camelid antibody) were discovered to stabilize GPCRs in their active signaling state and they played an important role in the search for orthosteric GPCR agonist ligands [2,3]. The Confobody strategy is an attractive technology, that enables agonist drug discovery by looking for small molecule fragments that selectively bind to the confobody-constrained signaling conformer of a GPCR. Although Cbs have been recognized to be of extreme value in the search for novel therapeutics and in structural biology, the significant costs and time required for the discovery and development of specific Cbs has sparked our interest to develop a new, potentially more generic, technology to stabilize GPCRs to use in drug discovery. To overcome the drawbacks associated to Cbs, we developed an approach to mimic the G protein, an endogenous allosteric modulator of GPCRs, *via* a peptide mimicry approach [4]. Based on a rational design strategy a set of peptidomimetic ligands, stabilizing the active state conformation of the β_2 adrenergic receptor (β_2AR), was developed [5,6]. Therefore, a previously identified epitope of the G_s protein, the α_5 helix (F^{376}NDCRDIIQRMHLRQYELL^{394}), that is responsible for most interaction with the β_2AR [7], was chosen as template to design the peptidomimetics (Figure 1).
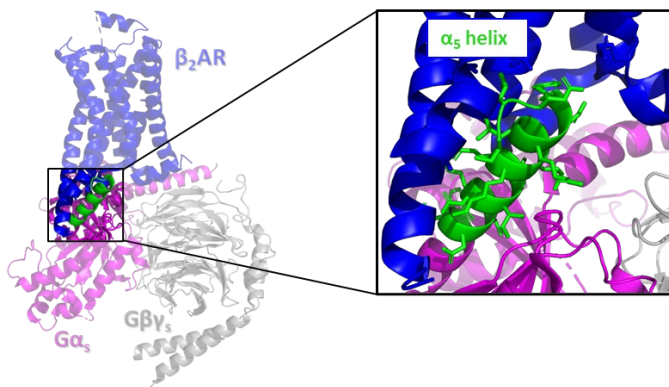
Fig. 1. Crystal structure of the β_2AR bound to the heterotrimeric G_s protein from protein data bank entry (PDB): 3SN6. Zoom on the interaction of the α_5 helix with the receptor.

Results and Discussion

The peptidomimetics were prepared using the Fmoc-based solid phase peptide synthesis (SPPS) and stabilized using 'stapling' strategies to improve binding to the targeted receptor (Figure 2). This was realized by varying the length, the type and the position of the staple that covalently bridges one or

two helical loops, inserted on one side of the helix, where no critical native contacts are made with the receptor. The α-helicity of the stapled peptides was evaluated using CD spectroscopy and the best results were obtained for the peptidomimetics with a triazole bridge near the *N*-terminus, generated through a copper-catalyzed azide-alkyne cycloaddition (**SBL-CM-12,** Ac-FN$_e$**[Pra**CRD**Azk]**IQRMH LRQYELL-OH). In addition, a trilysine (KKK) motif was introduced at the *N*-terminus to ensure solubility of the peptidomimetic. Simultaneously, the functionality of the peptidomimetic was screened using the radioligand displacement assay, to quantify the stabilization of the receptor in the active state conformation. Since the four last *C*-terminal amino acids of the key helix were suggested to be crucial residues for interaction with the receptor, point mutations were introduced in the lead peptide, **SBL- CM-12**. Unexpectedly, the substitution of the penultimate leucine (L^{393}) by a cyclohexylalanine residue (Cha), to give **SBL-CM-51**, resulted in an extraordinary affinity increase of the agonist for the stabilized receptor (Figure 2), comparable to Cb80, a well-studied allosteric modulator of β$_2$AR [2,5,6].
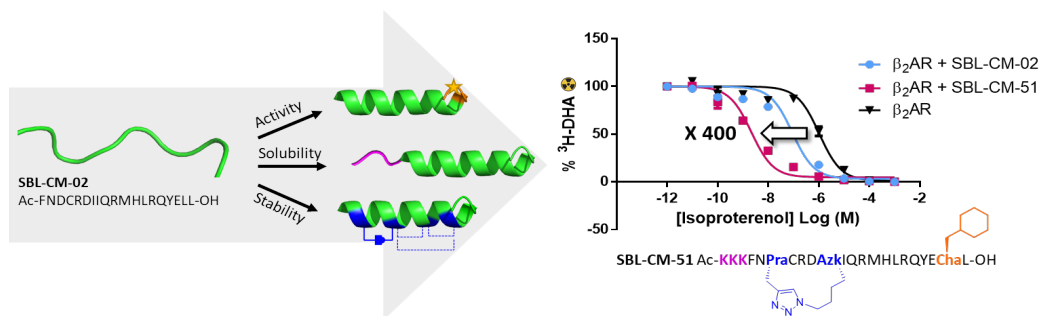
Fig. 2. Design of G$_s$-subunit peptidomimetics to stabilize β$_2$AR in the active signaling conformation. (standard amino acid one letter coding used; Azk: azidolysine; Cha: cyclohexylalanine; Pra: propargylglycine).

Next, the genericity of the identified G$_s$ peptidomimetics was explored by testing other GPCRs, that signal through G$_s$ [5,6]. Selected peptide mimetics were screened to evaluate their ability to bind and stabilize an active conformation of the dopamine 1 receptor (D1R) and similarly to β$_2$AR, the highest affinity shift was obtained for the stapled peptidomimetic containing the Cha point mutation (**SBL- CM-51**). The best-performing peptidomimetic **SBL-CM-51** was used next for fragment-based screenings on conformationally constrained receptors, to challenge the efficiency of the peptidomimetics to pick up fragments, for further design of agonist therapeutics. For both receptors, β$_2$AR and D1R, potential agonist fragments were identified and these could be optimized to design novel conformational-selective drugs targeting GPCRs [5,6].

Acknowledgments

References

1. Hauser, A.S., et al. *Nature Reviews Drug Discovery* **16**, 829-842 (2017), https://doi.org/10.1038/nrd.2017.178
2. Rasmussen, S.G., et al. *Nature* **469**, 175-180 (2011), https://doi.org/10.1038/nature09648
3. Pardon, E., et al. *Angewandte Chemie International Edition* **57**, 5292-5295 (2018), https://doi.org/10.1002/anie.201712581
4. Mannes, M., et al. *Trends in Pharmacological Sciences* **43**, 406-423 (2022), https://doi.org/10.1016/j.tips.2021.10.011
5. Mannes, M., et al. *Angewandte Chemie International Edition* **60**, 10247-10254 (2021), https://doi.org/10.1002/anie.202100180
6. Mannes, M., Martin, C., and Ballet, S. EP4015529 (2022).
7. Rasmussen, S.G., et al. *Nature* **477**, 549-555 (2011), https://doi.org/10.1038/nature10361

A Fluorogenic Peptide-Based Smartprobe for the Detection of Human Neutrophil Elastase in Inflammation

Maria Rodriguez-Rios[1], Gloria Garoffolo[2], Maurizio Pesce[2], and Mark Bradley[1]

[1]EaStCHEM School of Chemistry, University of Edinburgh, David Brewster Road, EH9 3FJ Edinburgh, UK;
[2]Tissue Engineering Research Unit, Centro Cardiologico Monzino, IRCCS, Milan, Italy

Introduction

Neutrophils are one of the most abundant immune cells and are first to be recruited to sites of inflammation where they can fight invading pathogens very effectively [1]. Activation of neutrophils results in the release of proteases, with human neutrophil elastase (hNE) being the most abundant. This protease is involved and implicated in a variety of inflammatory diseases and includes association with so-called Neutrophil Extracellular Traps (NETs). NETs are networks of extracellular fibers, produced by dying neutrophiles, that are primarily composed of extruded DNA, embedded with proteases that effectively kill pathogens. These structures have been associated with a variety of chronic inflammatory diseases such as idiopathic pulmonary fibrosis [2] while the fibrillar nature and excessive development of NETs in SARS-CoV-2 infection has been linked to the development of acute respiratory distress syndrome and blood vessel blockage.

Peptide based "dendritic" or multi-branched fluorogenic probes [3] can provide significantly higher signal amplification and lower background noise when compared to their linear counterparts as well as offering high sensitivity (multiple copies of the fluorophore are released upon cleavage). In this area our group previously reported a self-quenching probe for the detection of hNE [5]. However, this probe, the so-called "Neutrophil Activation Probe" (NAP) suffered from high background signals and showed poor levels of signal amplification, making it unsuitable for *in vivo* application and was also unsuccessful in the visualization of NETs *in vitro* [5].

*Fig. 1. A triple-quenched, super-silent tri-branched probe (**HNE-FQ**), which upon specific cleavage by human neutrophil elastase (hNE) liberates three fluorescent molecules resulting in an increase in fluorescence.*

Herein, we report a highly sensitive fluorogenic probe for the detection of hNE in activated neutrophils and Neutrophil Extracellular Traps (NETs). It was based on the previously reported triple self-quenched, tri-branched probe (NAP), but with amplification of signal dramatically enhanced by the addition of three copies of a traditional FRET quencher (methyl red), and generated a >20 fold increase in fluorescence upon specific cleavage by hNE (Figure 1) [6].

Results and Discussion

The probe contained the highly specific hNE cleavable peptide (Glu-Glu-Ile ¦ Nle-Arg-Arg) and was synthesized on an aminomethyl ChemMatrix resin functionalized with the Fmoc-Rink Amide linker (Figure 2). The starting trivalent isocyanate (**1**) was synthesized following a previously reported procedure [7] and immobilized onto the solid support. Removal of the Dde protecting groups exposed the three terminal amino groups (**2**) that served for the synthesis of the FRET-peptides using Fmoc solid-phase peptide synthesis with DIC/Oxyma as the coupling combination. The quencher was incorporated as an intact Fmoc-Lys(MR)-OH building block to simplify the synthesis and avoid the need for orthogonal deprotection on the resin. A bis-ethylene glycol unit, between the fluorophore and the peptide, was introduced to increase water solubility.
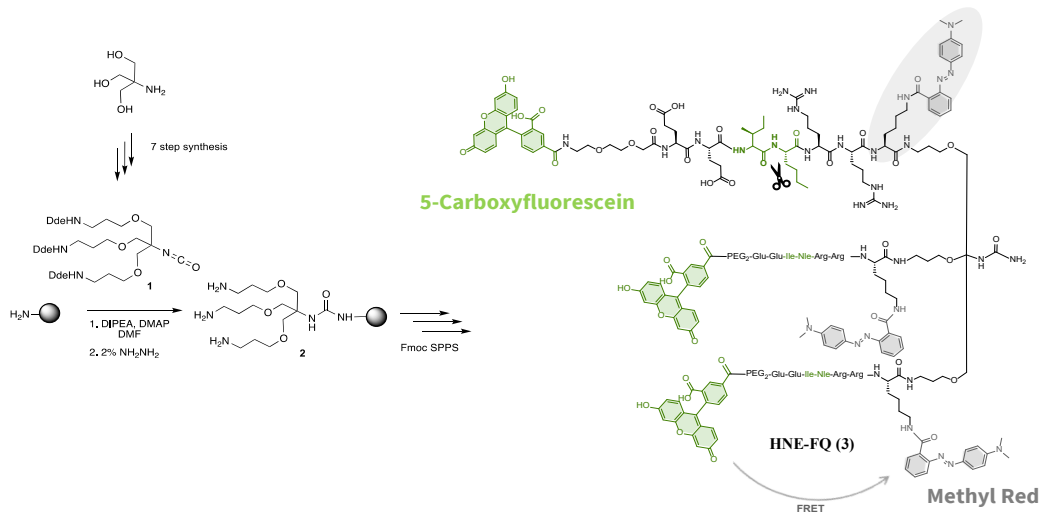
*Fig. 2. Probe synthesis started by attachment of the tribranched scaffold **1** onto a Rink-amide-ChemMatrix resin-linker combination [6]. This was followed by deprotection of the Dde protecting groups, and synthesis of the FRET-peptide using an Fmoc/tBu solid-phase peptide synthesis strategy. The FRET pair consisted of 5-carboxyfluorescein as the fluorophore and methyl red as the dark quencher. Fmoc-Lys(MR)-OH was incorporated as the first amino acid residue (shadowed).*

The probe's maximum excitation was at 490 nm with a maximum emission at 520 nm [6] with activation of **HNE-FQ** in presence of the hNE proving to be rapid, with a 20-fold increase in fluorescence within minutes while *Sivelestat* fully inhibited probe activation (Figure 3a). Specificity of the probe was confirmed by exposure to two closely related neutrophil serine proteases: Cathepsin G and Proteinase 3, with negligible cleavage observed in both cases (Figure 3b).
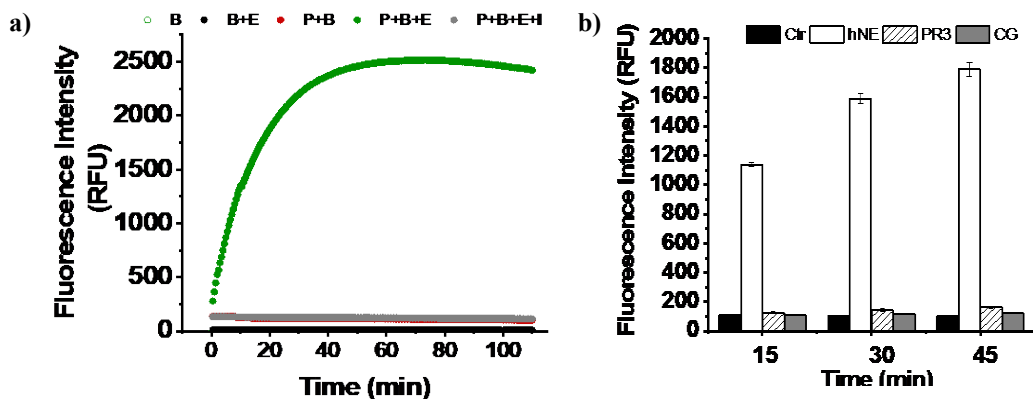
Fig. 3. a) The time-course dequenching of probe (5 µM) following incubation with hNE (100 nM) in the presence or absence of the inhibitor Sivelestat (100 µM) n = 3. B = buffer; E = enzyme; P = probe; I = inhibitor. b) Specificity assessment of probe (5 µM) incubated in the presence of hNE (100 nM) and related serprocidins PR3 (100 nM) and Cathepsin G (300 nM) at different time points at 37ºC, n = 3.

The activity of **HNE-FQ** was compared to the previous probe **NAP (4)** a tribranched compound containing three copies of a hNE cleavable sequence, capped with 5-carboxyfluorescein on its *N*- terminus (Figure 4a). In **NAP** the fluorophores are in close proximity to each other leading to self-quenching. However, **NAP (4)** suffers from high background fluorescence levels and limited signal amplification (3.6-fold) [5]. In addition, **HNE-FQ** activation was compared to another tribranched probe that targets a broader range of serprocidins, the probe **NES (5,** Figure 4a). **NES** uses a different peptide sequence but shares structural similarities, since it also consists of a tribranched scaffold and contains a FRET quencher (Methyl Red) to enhance quenching of carboxyfluorescein. However, in NES, the Methyl Red groups are attached at the *N*-terminus and the carboxyfluorescein fluorophores on the *C*-terminus [4]. Thus, although **NES (5)** provided an improvement in amplification of signal upon activation when compared to **NAP (4),** this was still limited (approximately 7-fold). This can be explained by the effect of self-quenching following cleavage, since, in NES, upon activation, the Methyl Red containing fragments are released, but the three molecules of 5-carboxyfluorescein remain attached to the tribranched "core", leading to self-quenching. The optimised design in **HNE-FQ** tackles the limitations of the two previous designs by reorienting the FRET pair labels on the peptide sequence (5-carboxyfluorescein on the *N*-terminus and Methyl Red on the *C*-terminus), allowing full release of three carboxfluorescein fluorophores. This rearrangement resulted in a significant improvement in the signal amplification upon probe activation, (22-fold). Taken together, optimisation of the first- and second-generation elastase probes lead to probe **HNE-FQ**, which showed a significant improvement in fluorescence signal amplification and a major reduction in background fluorescent levels.

In order to visualize NETs using **HNE-FQ**, neutrophils were differentiated from HL-60 cells by exposure to with all-*trans*-retinoic acid (ATRA) as previously reported [6] and stained with probe (5 µM), 4′,6-Diamidine-2′-phenylindole dihydrochlorideI (DAPI; 0.2 mM) and the extracellular DNA intercalating dye (SYTOX Orange; 5 µM). Morhologically, ATRA/PMA treated cells exhibited four different stages of NETosis, based on nuclear morphology and hNE distribution (Figure 5). Early stages of neutrophil activation exhibited a small and round nucleus with hNE colocalized with condensed chromatin (stage 1; yellow circles). At later stages, chromatin decondensation led to spherical (stage 2; green circles) or more "cloud-like spread" shapes (stage 3; red circles). In the final stage, neutrophils formed extracellular chromatin filaments composed by cytoplasmic granules and hNE (stage 4; Figure 5e).
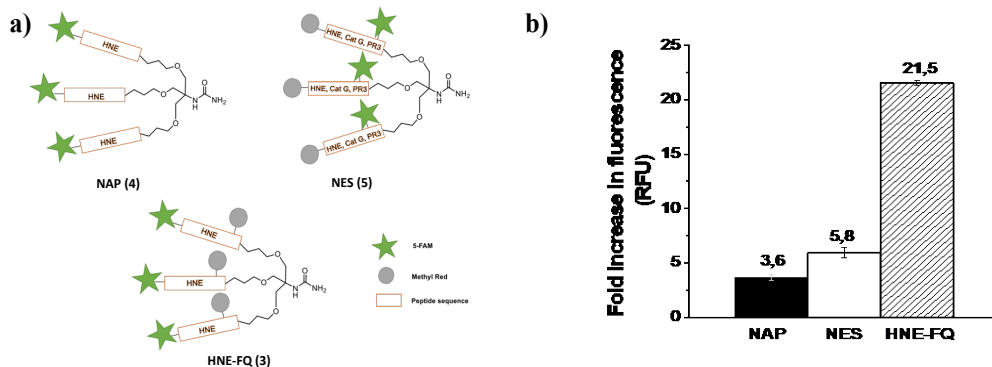
*Fig. 4. a) Structures of **NAP (4), NES (5)** or **HNE-FQ (3)**; b) Probes (5 µM) were exposed to elastase (100 nM) with activation monitored over time. The bar plot shows the maximum fold increase upon activation of all three probes.*
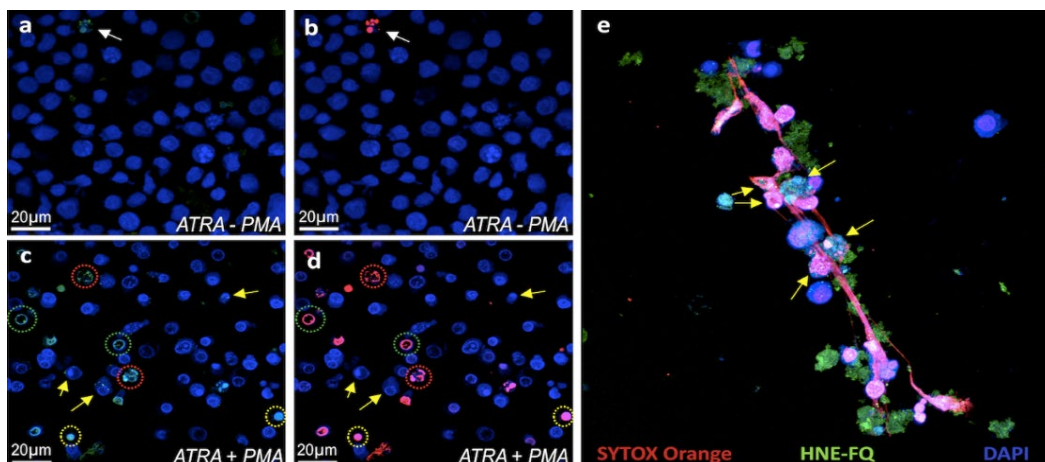
*Fig. 5. Fluorescence microscopy images of HL-60 cells stained with DAPI (blue), **HNE-FQ** (green) and SYTOX Orange (red). Top row left: Control HL-60 neutrophils in absence of PMA a) Blue/Green channels b) Blue/Red channels. Bottom row left: HL-60 neutrophils stimulated with PMA c) Blue/Green channels and d) Blue/Red channels. Yellow arrows indicate cells expressing low hNE (likely at the beginning of NETosis process) while those encircled in green, red and yellow are cells at different stages of NETosis (see text for description). e) 3D image slice of a typical NET stained as in the panels on the left. Arrows indicate chromatin studded with **HNE-FQ**, indicative of chromatin release by activated cells.*

In conclusion, a tri-branched human Neutrophil Elastase activatable fluorescent probe (**HNE-FQ**) was designed and synthesized and allows the rapid, specific, and sensitive detection of hNE in activated neutrophils and NETs. The data shows that **HNE-FQ** was highly specific for the staining of human neutrophil activation and highlights its potential as a diagnostic tool to detect and quantify NETosis and activated neutrophils, with current efforts focused on the synthesis of a near infrared (NIR) variant of the sensor.

Acknowledgments

References

1. Mayadas, T.N., Cullere, X., and Lowell, C.A. *Annu Rev Path*ol **9**, 181-218 (2014), https://doi.org/10.1146/annurev-pathol-020712-164023
2. Brinkmann, V., et al. *Science* **303**(5663), 1532-1535 (2004), https://doi.org/10.1126/science.1092385
3. Rodriguez-Rios, M., et al. *Chemical Society Reviews* **51**(6), 2081-2120 (2022), https://doi.org/10.1039/D1CS00798J
4. Craven, T.H., et al. *Sci. Rep.* **8**(1), 13490 (2018), https://doi.org/10.1038/s41598-018-31391-9
5. Craven, T.H., et al. *Scientific Reports* **11**(1), 76 (2021), https://doi.org/10.1038/s41598-020-80083-w
6. Rios, M.R., et al. *Chem Commun (Camb)* **57**(1), 97-100 (2021), https://doi.org/10.1039/D0CC07028A
7. Lebreton, S., et al. *Tetrahedron* **59**(22), 945-3953 (2003), https://doi.org/10.1016/s0040-4020(03)00463-0

Peptide Dimerization Effect on Bacterial Topoisomerases Activity

Camila Aguiar Rocha, Jonatas Medeiros de Almeida Angelo, Edson Crusca, and Reinaldo Marchetto

UNESP - Institute of Chemistry, Department of Biochemistry and Organic Chemistry, Caixa Postal 355, 14.800-900 - Araraquara, São Paulo, Brazil

Introduction

Bacterial DNA topoisomerases are essential enzymes that play critical roles in many biological processes involving DNA and consequently the cell growth. Type II DNA topoisomerases are attractive targets to antibacterial therapy [1]. The increasing incidence of drug-resistant bacteria emphasizes the urgent need for a new generation of antibacterial drugs. In this context, WRWYCRCK, a peptide conceived as of a positional scanning screen of an L-amino acid synthetic peptide combinatorial library [2], was synthesized, oxidized and investigated regarding the disulfide bonds effect in the inhibition of topoisomerases activity and microorganisms' growth. The dimeric peptides showed best results of inhibition for all tested topoisomerases compared to monomer peptide. The CM3 peptide, the parallel two-disulfide bonds dimer was the most effective. For bacterial growth, the CM1 dimer (BR1020190256524) was the most effective. The dimerization of WRWYCRCK peptide was sufficient to improve its activity on type I topoisomerases and to turn it into a new inhibitor of bacterial type II topoisomerases.

Results and Discussion

One of the main threats to human health are infectious diseases caused by multidrug-resistant microorganisms. In addition, studies show that the number of new antibiotics on the market has decreased significantly [3]. Therefore, it is urgent the development of new antimicrobial drugs, to be more potent and less susceptible to the different mechanisms of drug resistance. A new and important approach for the development of new antimicrobials is through the synthesis of DNA topoisomerases inhibitor peptides [4]. In this context, the octapeptide WRWYCRCK (Lin1) and its linear derivatives were synthesized by solid-phase methodology employing the Fmoc/tBu strategy, considering the usual polymer solvation parameters [5]. Acetamidomethyl and trityl groups were used as cysteine side chain protectors as a way to direct disulfide bonds. Cysteine residue at 5 or 7 position was also replaced by alanine to change the number and position of disulfide bonds in the dimers (Figure 1). The peptides were analyzed and purified by RP-HPLC and the chemical identity was confirmed by mass spectrometry (positive ES-MS): 1240.6, 1311.6, 1208.5 and 1208.5 g/mol (Lin1, Lin2, A^7Lin1 and A^5Lin1, respectively).

$$Ac^1WRWYCRCK^8\text{-}NH_2 \quad \textbf{\textit{Lin1}}$$

$$Ac^1WRWYCRC(Acm)K^8\text{-}NH_2 \quad \textbf{\textit{Lin2}}$$

$$Ac^1WRWYCRAK^8\text{-}NH_2 \quad \textbf{\textit{A}}^7\textbf{\textit{Lin1}}$$

$$Ac^1WRWYARCK^8\text{-}NH_2 \quad \textbf{\textit{A}}^5\textbf{\textit{Lin1}}$$

Fig. 1. Primary structure of synthesized linear peptides.

Lin1 and its linear derivatives were then oxidized with air or iodine to obtain their respective dimeric forms (Table 1), which were obtained with good yield (40 - 50%) and high purity (98 to 99%). The peptides' ability to inhibit the supercoiling reaction of DNA gyrase and the relaxation reaction of topoisomerase IV (Topo IV) and Topo IA was investigated by gel electrophoresis. The assays were performed by titrating Lin1 and its dimeric forms into a fixed concentration of topoisomerase and DNA followed by IC_{100} determination (the minimum concentration that produces complete inhibition of supercoiling or relaxation activity). In the standard supercoiling and relaxation assays at 37°C, an

Table 1. Primary structure and molecular mass characterization of dimers.

Peptide	Primary structure	MW (g.mol^{-1})	ES+	ES m/z (g.mol^{-1})
CM1	Ac^{1}WRWYCRAK^8-NH$_2$ Ac^{1}WRWYCRAK^8-NH$_2$	1,241.49	+2 +3	621.3 414.5
CM2	Ac^{1}WRWYARCK^8-NH$_2$ Ac^{1}WRWYARCK^8-NH$_2$	1,312.56	+2 +3	656.8 438.2
CM3	Ac^{1}WRWYCRCK^8-NH$_2$ Ac^{1}WRWYCRCK^8-NH$_2$	1,209.43	+3 +4	605.3 403.8

initial screening at 100 µmol/L selected CM1, CM2 and CM3 as the better topoisomerases inhibitors (complete inhibition). Lin1 did not inhibit DNA gyrase and Topo IV activities.

Subsequently the IC$_{100}$ for the selected peptides were determined (Figure 2) and showed that CM3 was better, inhibiting 37% of the supercoiling reaction of gyrase and relaxation reaction of Topo IV with IC$_{100}$ values of 25 and 10 µmol/L, respectively (Table 2). CM1 and CM2 showed only partial inhibition at 50 and 75 µmol/L, respectively. The dimers were more efficient in inhibiting DNA gyrase and Topo IV compared to the monomer, which did not inhibit the activity of this enzyme, evidencing the importance of dimerization in the inhibitory activity of Lin1. The two disulfide bonds C^5-C$^{5'}$ and C^7-C$^{7'}$ of CM3 were shown to be important for peptide-enzyme interactions, especially to Topo IV. Topoisomerases inhibitors, as CM3 peptide, which act simultaneously in both DNA gyrase and Topo IV, may greatly contribute to reduce the emergence of target-based resistance.
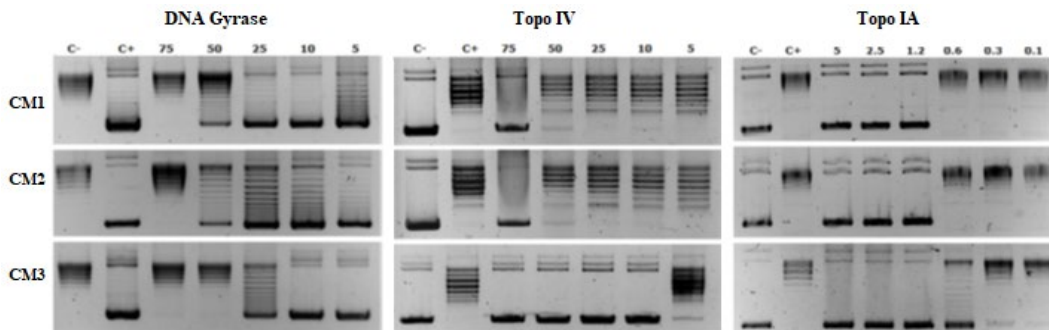
Fig. 2. IC$_{100}$ determination of dimeric peptides CM1, CM2 and CM3 for DNA supercoiling of DNA gyrase and DNA relaxation of TopoIV and Topo IA reactions. Line C-: relaxed plasmid pBR322 for DNA Gyrase and supercoiling DNA for TopoIV and TopoIA. Line C+: relaxed pBR322+DNA gyrase; supercoiling DNA+TopoIV; supercoiling DNA+TopoIA, in the absence of peptide. The indicated values are the peptide in µmol/L. The enzymes are from E. coli.

As bacterial topoisomerase IA is essential for cellular viability of a number of important bacterial pathogens, this enzyme also represents a valid target for novel antibiotics aimed at overcoming antimicrobial resistance [6]. Again, CM3 was the best inhibitor (Table 2). Completely inhibited the Topo IA relaxation reaction with an IC$_{100}$ of 0.6 µmol/L. CM1 and CM2, which differ only in disulfide bond position, inhibited the enzyme identically (1.2 µmol/L) but less efficiently than CM3, which has

two disulfide bonds. Lin1 peptide, which does not contain any disulfide bonds, was the least potent, as observed for type II topoisomerases. The enzymatic assays showed that the presence of two disulfide bonds seems to favor the inhibitory activity of the octapeptide Lin1, regardless of the topoisomerase type. The CM3 dimer, which has two specific and targeted disulfide bonds, was more effective in inhibiting type I and type II topoisomerases when compared to those with only one (CM1 and CM2) or no disulfide bond (Lin1). Probably, the greater structural rigidity of dimers containing two disulfide bonds should favor the inhibition of different topoisomerases involving the formation of a more stable peptide-enzyme complex with lower rotational mobility.

Table 2. Inhibitory activities of monomeric and dimeric peptides on bacterial topoisomerases.

Peptide	IC_{100} (µmol/L)		
	DNA gyrase	Topo IV	Topo IA
Lin1	ND	ND	>10[d]*
CM1	>50[a]*	75	1.2
CM2	>50[b]*	75	1.2
CM3	>25[c]*	10	0.6

*IC_{100} = Concentration of the peptide required for complete inhibition of topoisomerase activity; ND = No detectable inhibitory activity; *estimated by AlphaView software (AlphaImager®EP); [a]83% inhibition of E. coli gyrase at 50 µmol/L; [b]70% inhibition of E. coli gyrase at 50 µmol/L; [c]37% inhibition of E. coli gyrase at 25 µmol/L; [d]42% inhibition of E. coli topo IA at 10 µmol/L*

The antimicrobial activity of peptides was evaluated by analysis the growth of *E. coli* (ATCC 43895), *S. aureus* (ATCC 14458) and *C. albicans* (ATCC 90028), in a microdilution test [7]. The MIC values were considered as the lowest concentration of peptide able to inhibit at least 90% of the strains growth, within 24 hours for the bacteria and 48 hours for the fungus. It was observed that the oxidation of one or two cysteine residues of Lin1 affects differently the growth of the tested microorganisms. CM1 showed the best growth inhibition results of all groups of microorganisms. It was observed that the oxidation of one or two cysteine residues of Lin1 affects differently the growth of the tested microorganisms. Differently of topoisomerases inhibition studies, CM1, CM2 and CM3 showed very similar activities. CM1 was the most effective in inhibiting the growth of the three microorganisms tested (Table 3). Apparently, the C^5-$C^{5'}$ disulfide bond allows CM1 to have greater rotational mobility, compared to CM2 and CM3, probably due the greater molecular symmetry provided by this bond. This characteristic, added to the composition of the intracellular medium and concentration conditions, different from those used in the enzymatic inhibition assays, reflects in a better adjustment of the CM1

Table 3. Antimicrobial activity of monomeric and dimeric peptides.

Peptide	MIC (µmol/L)		
	S. aureus	E.coli	C. albicans
Lin1	5	0.6	1.2
CM1	2.5	0.1	0.2
CM2	2.5	0.3	0.6
CM3	10	0.3	1.2

MIC = Minimal inhibitory concentration

to its binding site with the target enzyme and, consequently, better results in growth inhibition assays. The intracellular environment effect is quite evident when considering the Lin1 activities. Lin1 was the peptide with the lowest inhibitory activity for all topoisomerases, but showed great antimicrobial activity, especially for Gram-negative bacteria and fungi. Unlike the medium used for the enzymatic inhibition assays, the intracellular medium can provide conditions for the natural oxidation of Lin1, favoring their dimerization and consequently improving their inhibitory capacity on topoisomerases and their antimicrobial activity. Furthermore, the microorganism's membrane permeability must also be considered. Molecules with greater rotational freedom such as CM1 can be transported more easily across the biological membrane.

The dimerization of WRWYCRCK was sufficient to improve its activity on type I topoisomerases and to turn it into a new inhibitor of bacterial type II topoisomerases. Dimeric peptides from WRWYCRCK demonstrated a good potential to constitute a new generation of antimicrobial agents.

Acknowledgments

References

1. Delgado, J.L., et al. *Biochem. J.* **475**, 373-398 (2018), https://doi.org/10.1042/BCJ20160583
2. Fujimoto, D.F., et al. *J. Molec. Biol.* **5**, 891-907 (2006), https://doi.org/10.1016/j.peptides.2012.12.025
3. Fernandes, P. Martens, E. *Biochem. Pharmacol.* **133**, 152-163 (2017), https://doi.org/10.1016/j.bcp.2016.09.025
4. Lau, J.L., Dunn, M.K. *Bioorg. Med. Chem.* **26**, 2700-2707 (2018), https://doi.org/10.1016/j.bmc.2017.06.052
5. Marchetto, R., et al. *J. Org. Chem.* **12**, 4561-4568 (2005), https://doi.org/10.1021/jo9611632
6. Yang, R., et al. *Int. J. Mol. Sci.* **20**, 1116 (2019), https://doi.org/10.3390/ijms20051116
7. Almeida, C.V., et al. *BBA Gen. Sub.* **1865**, 129937 (2021), https://doi.org/10.1016/j.bbagen.2021.129937

Peptide VSAK Derived from the *C*-Terminal Region of CETPI Blocks LPS in an Animal Model of SIRS. Evidence Using PET-Imaging

Ismael Luna-Reyes[1], Eréndira G. Pérez-Hernández[1], Blanca Delgado-Coello[1], M.A. Ávila-Rodríguez[2], and Jaime Mas-Oliva[1]

[1]Departamento de Bioquímica y Biología Estructural, Instituto de Fisiología Celular, Universidad Nacional Autónoma de México. Ciudad Universitaria, 04510 Ciudad de México, México;
[2]Unidad Radiofarmacia-Ciclotrón, Facultad de Medicina, Universidad Nacional Autónoma de México. Ciudad Universitaria, 04360 Ciudad de México, México

Introduction

Sepsis and septic shock are considered two of the most important life-threatening conditions worldwide. It is known that an uncontrolled inflammatory response is the main process responsible behind the harmful effects during the development of these conditions. This inflammatory response is well established and defined to be triggered by pathogen-derived molecules such as lipopolysaccharides (LPS) located at the surface of Gram-negative bacteria, known to be released in the early stages of sepsis.

Work carried out in our laboratory has demonstrated both *in vitro* and *in vivo*, that VSAK (VSAKPLSARSPGGRPLSP), a peptide derived from the last eighteen amino acids of the carboxy-end segment of CETPI, an isoform of the cholesteryl-ester transfer protein (CETP), identified by us several years ago [1,2], is able to bind LPS, and therefore also capable to prevent their deleterious effects [3].

The experimentation that is now presented employing Positron Emission Tomography (PET) using 2-[^{18}F] fluoro-2-deoxy-D-glucose (FDG) shows new evidence supporting the fact that the intravenous administration of peptide VSAK in a model of Systemic inflammatory response syndrome (SIRS) established in the rabbit, prevents these animals from developing septic shock after the administration of LPS [4].

Materials and Methods

During the experiment, twelve male Dutch dwarf rabbits were used randomly assigned to four experimental groups: 1) Control, 2) VSAK treatment, 3) LPS treatment, and 4) LPS+VSAK treatment. Rabbits from the different groups were administered FDG as radiotracer and monitored by PET for 90 minutes. Depending on the experimental group, LPS, VSAK, or LPS+VSAK were further administered. For the LPS+VSAK group, the intravenous administration was carried out with 2-minutes interval using different ears. PET data analysis was carried out using spherical areas to define Volume of Interest (VOI) in order to reduce slight variations associated with differences in animal size. In addition, specific tissue activity was measured using 1gm of tissue samples from each animal. Additionally, the level of several pro-inflammatory cytokines was analyzed in the plasma obtained from all experimental animals [5].

Results and Discussion

In this work, we studied the effects of VSAK as a potential peptide with the ability to hamper LPS effects *in vivo*. This study was focused on the metabolic dysfunction of glucose that occurs during the early stages of SIRS after an LPS intravenous challenge, studied by PET technology. Figure 1 shows representative images obtained from the PET data reconstruction analysis. The left panel corresponds to an animal from the control group, only administered with saline buffer, showing a normal distribution FDG pattern in organs such intestine and liver. The organs showing the highest signal correspond to the kidneys showing after 90 min an important rate of FDG elimination. The central panel shows a representative

image from the LPS-treated animals, showing the lack of glucose perfusion in most organs, mainly the liver. In contrast with this result, animals that were administered first with LPS and almost simultaneously with peptide VSAK (LPS+VSAK, right panel), the recovery of FDG uptake in peripheral tissues is observed, showing in the experimental animals from this group an uptake pattern similar to the one observed with the control group. Non-relevant changes in FDG uptake were observed in animals administered only with VSAK (data not shown). These findings suggest that an alteration in the uptake of glucose occurs when animals have LPS present in circulation. That effect is prevented when peptide VSAK is administered in a simultaneous way. Based on these results, the levels of circulating insulin and glucose were also measured in all experimental groups. It was found that an important increase in circulating glucose occurs in animals treated with LPS alone. That effect is prevented in animals also treated with peptide VSAK. Additionally, when insulin was analyzed, an increase was also found in circulation in LPS-treated animals. Circulating levels of insulin were found to be in the normal range when peptide VSAK was administered.
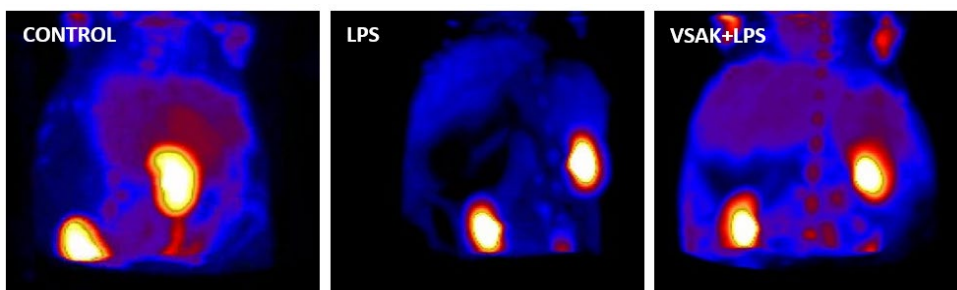
Fig. 1. Representative images obtained from animals of each experimental group. All images were rendered using data obtained from the 90-minute PET scans.

Altogether, the effects observed in FDG uptake, together with the alterations found in insulin and glucose levels in the LPS group, indicate that these experimental animals might be experiencing an insulin-resistant-like state (Figure 2). Since there is evidence that hyperglycemia observed during the course of sepsis and septic shock, can be due in part to the inability for glucose to enter the cell, energy deficiency has been proposed among the mechanisms responsible for cell dysfunction in septic shock, where low ATP levels and phosphocreatine/ATP ratios have been associated to non-surviving cases of septic shock.
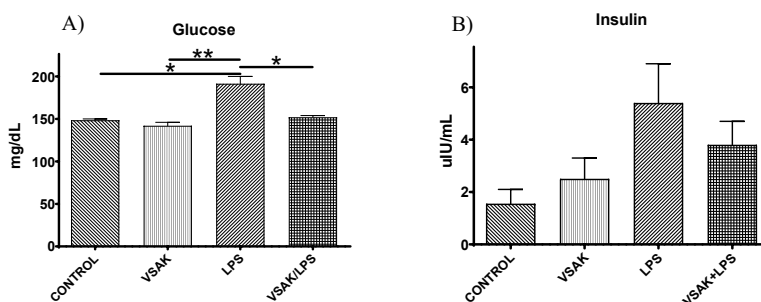
Fig. 2. Circulating levels of Glucose and Insulin. The graph A shows the levels of Glucose observed in the experimental animals. In the panel B the measured levels of Insulin are shown.

It has been previously reported that several cytokines involved in the pro-inflammatory response could cause alterations in the normal glucose uptake of insulin-dependent tissues.

This event does not occur exclusively during infectious processes since it can also be observed in other inflammation-related diseases. In this regard, an analysis of circulating pro-inflammatory cytokines was also performed in all the experimental groups studied (Figure 3). It is shown that not only circulating levels of TNFα, a highly related cytokine with a LPS challenge, but also IL-8 and MIP-1β, two cytokines with chemoattractant properties known to be released during the early stages of LPS-related sepsis, are importantly increased in the LPS treated group. Interestingly, TNFα that presents a central role in the response that leads to sepsis and septic shock, has been directly involved in the host's response mediated by the TLR4 receptor, and also associated to the development of insulin resistance.

Together with IL-1α, and IL-1β (data not shown), TNFα, IL-8, and MIP-1β show an important increase in their plasma level after the infusion of LPS, response shown to be avoided if peptide VSAK is concomitantly administered. Our results support the view that attenuation of the various pro-inflammatory molecules carried out by CETPI itself, or through peptides derived from this protein such as peptide VSAK, might be occurring during the early stages of SIRS.
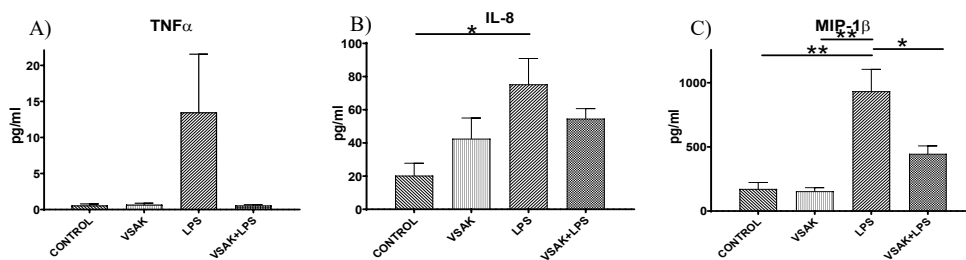
Fig. 3. Circulating pro-inflammatory cytokine levels observed in all experimental groups.

In order to find out and understand the molecular mechanisms that would explain the *in vitro* and *in vivo* association effect observed between LPS and peptide VSAK, it is important to understand the type of interactions that may occur between these two molecules. Therefore, we have employed coarse grain molecular dynamics of peptide VSAK peptide studied in association with LPS/DOPC composite systems (Figure 4). Our results support the possibility that independently of a direct interaction between peptide VSAK and LPS in plasma, an interaction between peptide VSAK and LPS already located in the plasma membrane of cells, might be able to decrease membrane fluidity that in turn interfere with the harmful cascade of cellular events known to be carried out by LPS.
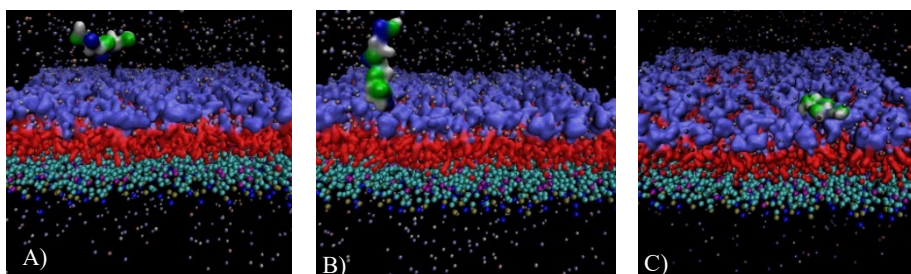
Fig. 4. Molecular Dynamics simulation of peptide VSAK and a LPS membrane. Panel A, the peptide is located in the solute interface. Panel B, the peptide shows a change in the orientation towards the LPS-POPC bilayer. Panel C, the peptide is incorporated into the lipid bilayer. LPS-core (purple), LPS-antigen A (red), POPC (cyan), VSAK hydrophobic aa (white), VSAK hydrophilic aa (green) and VSAK positive aa (blue).

Taken together, our results support that CETPI and peptides derived from its carboxy-end segment, such as peptide VSAK, present important LPS-binding properties associated with the regulation of key regulatory pathways linked to glucose metabolism and inflammation. These results reveal the physiological function of CETPI and support the role peptide VSAK might have in the clinic as a therapeutic LPS-binding peptide during sepsis and septic shock.

Acknowledgements

References

1. Alonso, A.L., Zentella-Dehesa, A., Mas-Oliva, J. *Molecular and Cellular Biochemistry* **245**, 173-182 (2003), https://doi.org/10.1023/A:1022832531473
2. Pérez-Hernández, E.G., Delgado-Coello, B., Luna-Reyes, I., and Mas-Oliva, J. *Biomedicine & Pharmacotherapy* **141**, 111890 (2021), https://doi.org/10.1016/j.biopha.2021.111890
3. García-González, V., Gutiérrez-Quintanar, N., and Mas-Oliva, J. *Scientific Reports* **5**, 16091 (2015), https://doi.org/10.1038/srep16091
4. Mas-Oliva, O., Gutiérrez-Quintanar, N., García-González, V. International Patent. (2014), PCT/MX2014/00087 WO2015190903A1. https://patents.google.com/patent/WO2015190903A1/es
5. Luna-Reyes, I., Pérez-Hernández, E. G., Delgado-Coello, B., Ávila-Rodríguez, M. Á., and Mas-Oliva, J. *Scientific Reports* **11**, 14752 (2021), https://doi.org/10.1038/s41598-021-94224-2

Different Strategies of Antimicrobial Peptides Production for Biomedical Applications

Cristina Cantallops-Vilà[1]*, Laura Colomina-Alfaro[2]*, Pietro Riccio[3]*, Hanieh Ijakipour[3], Edwige Meurice[1], Antonella Bandiera[2], and Artemis Stamboulis[3]

[1]*University Polytechnic Hauts-de-France, Campus Mont Houy - 59313 Valenciennes Cedex 9, FR, France;*
[2]*University of Trieste, Department of Life Sciences, via L. Giorgieri, 1, 34127 Trieste, IT;* [3]*University of Birmingham, School of Metallurgy and Materials, Biomaterials Research Group, Edgbaston, Birmingham B15 2TT, UK*

Introduction

The increase of antibiotic-resistant bacterial infections over the last decades has prompted the search for novel antimicrobial molecules. Antimicrobial peptides (AMPs), such as human defensins and cathelicidins, have become outstanding candidates to fight infection due to their properties and the low risk of developing resistance [1,2]. They can be modified by *in-silico* models to improve their biological activity and selectivity [3]. Many studies have addressed their potential but there are still limitations in the production and their effective delivery to infection sites. The synthesis of peptides can be replicated in the laboratory with techniques such as the Solid Phase Peptide Synthesis (SPPS) which allows excellent results in terms of yield, purity, and structure in a short time and with minimal use of solvents. This technique consists of the synthesis of peptides on a solid support, running from the *C*-terminal to the *N*-terminal contrary to how it occurs in nature.

On the other hand, recombinant technology offers the possibility to produce peptides on a large scale avoiding labor-intensive isolation from natural sources and costly chemical synthesis procedures [4]. This method also allows the fusion of peptides to biopolymers, which can serve as a delivery platform to the site of infection and improve their biocompatibility.

Collagen is the main structural protein of the extracellular matrix. Recent studies have found that some bacterial collagen-like proteins (Bcl) form a stable triple helix similar to mammalian collagen, making it an attractive biopolymer to increase biocompatibility and promote biointegration when used for biomedical applications [5].

Human Elastin-like Polypeptides (HELP) is a biopolymer inspired by elastin characterized by its thermo-responsive properties employed for its purification [6,7,8]. It can be tagged to peptides offering a simple purification strategy with reduced costs and high production yields [9,10].

Here, we aimed to compare different strategies to produce and purify AMPs. A peptide based on human β-defensin (P3) was produced using a chemical synthesis platform. Moreover, the human β-defensin-1 (hBD1) was produced as a fusion partner of HELP, and a cathelicidin-derived peptide, LL25, was produced as a fusion of Bcl, both produced recombinantly in the cytoplasm of *E coli*.

Results and Discussion

AMPs were produced by chemical synthesis followed by RP-HPLC purification, and by recombinant technology fusing the AMPs to either Bcl or HELP followed by purification using IMAC or phase transition properties, respectively.

Chemical synthesis of P3

A human β-defensin modified peptide (P3) was synthesised using SPPS (Rink amide resin) with Fmoc protected amino acids. The synthesis was performed using 20% piperidine in DMF as deprotection, then coupling was performed by adding the next amino acid in a basic environment. Capping was performed using acetic anhydride and DIEA (N,N-diisopropylethylamine) to avoid unwanted reactions. Finally, the cleavage from the resin was performed using 95% TFA (trifluoroacetic acid) as acid and 2.5% TIPS (triisopropylsilane) as scavenger. The mass and retention time analyses were performed using LC-MS system and the purification was done using an RP-HPLC system. Purity control, molecular mass determination, and molecular mass fingerprints were performed by MALDI-TOF mass spectrometry (Figure 1A and 1B).
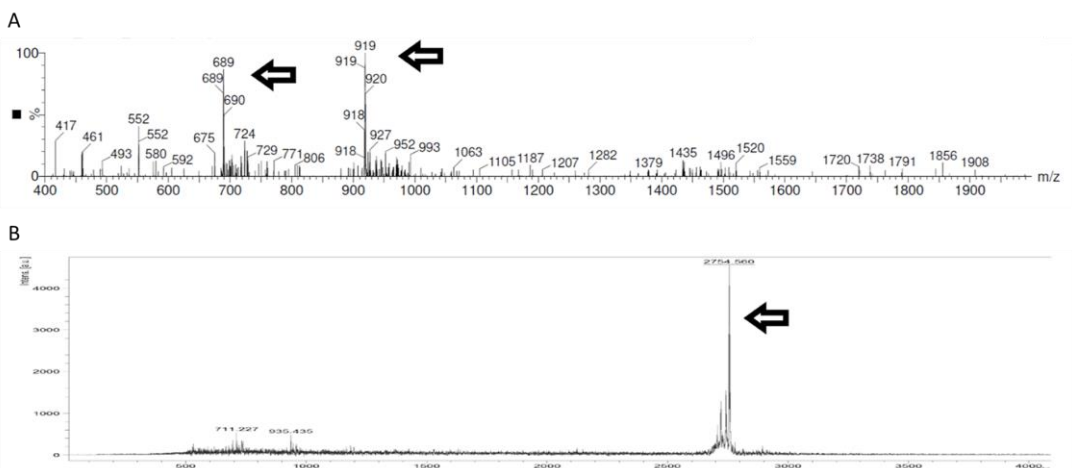
Fig 1. (A) Mass analysis of the purified P3 peptide obtained by LC-MS, that eluted at 28% ACN due to the high temperature of the UPLC coupled with MS; and (B) spectrogram of the molecule with its molecular mass obtained by MALDI-TOF.

Recombinant production of LL25 fused to Bcl

The nucleotide sequence of the cathelicidin-derived LL25 was cloned into a pET100 plasmid fused in-frame to a Bcl protein. *E. coli* BL21(DE3) was transformed with the sequence-verified plasmid and used to express the recombinant fusion protein by induction with IPTG. Cultures were lysed to release the intracellularly produced protein, which was then recovered through IMAC purification. SDS-PAGE and Western Blot were performed to check the purity and concentration of the final product. The Western Blot analysis shown in Figure 2A revealed that, as expected, the induced culture produces significantly more recombinant Bcl protein (at around 18kDa) than the non-induced. As seen in Figure 2B in the purification by IMAC of the cell lysate, the eluted fusion protein Bcl-LL25 appears at around 20kDa in size. The presence of extra bands in the non-induced fraction of the Western Blot and in the eluted fraction of the SDS-PAGE can suggest the formation of aggregates or polymers of the recombinant protein. On the other hand, they could indicate poor efficiency of the method used due to nonspecific binding of histidine-rich proteins native to *E.coli* by the anti-His antibody or to the Nickel-charged columns, respectively [11]. This will be solved in future experiments with further purification steps such as size exclusion and ion exchange chromatographies.

Recombinant production of hBD1 fused to HELP

The coding sequence of the 47 aa domain corresponding to the 22-68 region of the hBD1 (NM_005218.4) was fused in-frame to the *C*-terminus of the HELP synthetic gene. Moreover, specific endoproteinase restriction sites were introduced to precisely release the hBD1 from the fusion protein. The final construct, named HhBD1, was verified by sequencing, and the recombinant product was successfully expressed in the *E. coli* C3037 strain induced by IPTG (Figure 2C, expression lanes). The HhBD1 biopolymer retained the thermo-responsive properties of HELP, therefore, it was purified by exploiting the phase transition properties of the elastin-like domain; the final product was obtained with high purity and the yield of the HhBD1 production was 0.152 g L^{-1} of bacterial culture (Figure 2C, purification lanes).
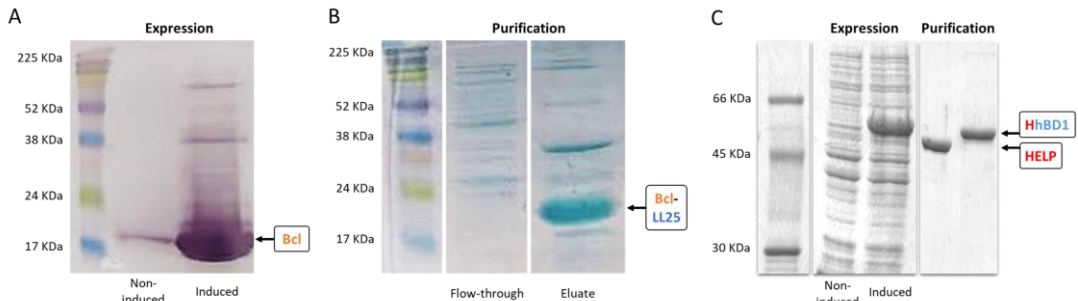
*Fig. 2. (**A**) Western Blot membrane after detection with an anti-His-tag antibody of the Bcl-producing lysed culture; (**B**) 15% SDS-PAGE gel of the lysate of the Bcl-LL25-producing culture after purification through IMAC; (**C**) 9% SDS-PAGE for the visualisation of the expression of the HhBD1 in E.coli C3037 induced by IPTG and the pure HhBD1obtained by phase transition cycling (purification).*

Antimicrobial potency of the free AMP and fusion biopolymers

A broth inhibition assay was performed to evaluate the antimicrobial activity of peptides and biopolymers. This assay allows the determination of the minimum inhibitory concentration (MIC) of each peptide versus the pathogen tested. The pathogens used as targets were chosen among gram-positive and negative bacteria strains such as *Staphylococcus aureus*, *Pseudomonas aeruginosa,* and *E. coli* [12].
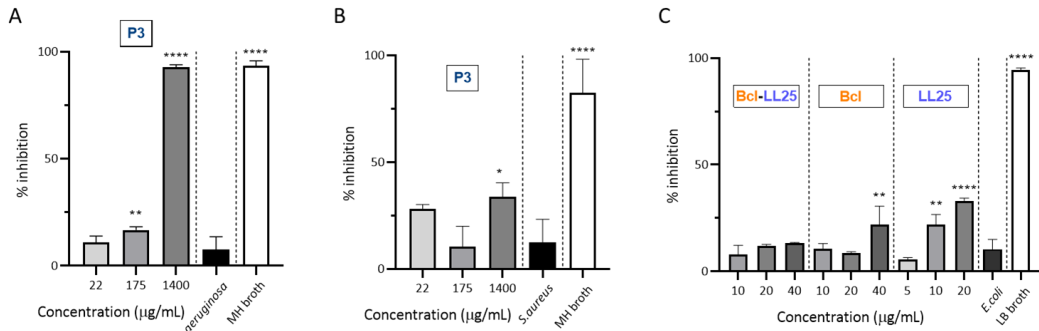
*Fig. 3. (**A**) Broth dilution assays of the peptide P3 against Pseudomonas aeruginosa PAO1, and (**B**) Staphylococcus aureus SH1000, (**C**) as well as the fusion protein Bcl-LL25, Bcl and LL25 alone, against E. coli JM8.*

The antimicrobial activity of the peptide P3 is confirmed only at high concentrations and predominantly against Gram-negative bacterial species such as *Pseudomonas aeruginosa* (Figure 3A and 3B), probably due to differences in membrane composition. Indeed, the thick peptidoglycan layer of Gram-positive bacteria does not allow the peptide to interact efficiently with the cell membrane.

The antimicrobial activity of LL25 is confirmed and concentration-dependent. Bcl-LL25 does not show significant antimicrobial potential, but an increase in growth inhibition can be observed with the concentration (Figure 3C). All in all, higher concentrations and purity of the fusion protein are expected to improve its antimicrobial activity.

MIC assay performed using HhBD1 didn't evidence any antimicrobial potency, even after the digestion with the two specific endoproteinases (data not shown), although the 36 amino acids peptide produced by incubation with Asp-N, is reported to be active towards *S. aureus*, *E. coli,* and *P. aeruginosa* [13]. Many reasons withstand behind these observations, mainly the uncontrolled

oxidation state of the biopolymer and the presence of salts. Thus, the characterization of the antimicrobial properties derived from HhBD1 is still under study.

Here, we present strategies that could successfully lead to the development of highly promising biomaterials that can be incorporated into implants reducing their failure due to bacterial infections and with a low risk of developing bacterial resistance to the material. Their biocompatibility and antimicrobial activity will be further studied to evaluate their suitability for use in biomedical applications.

Acknowledgment

References

1. Riool, M., et al. *Front. Chem.* AUG, 1-13 (2017), https://doi.org/10.3389/fchem.2017.00063
2. Riccio, P., Zare, M., Gomes, D., Green, D. & Stamboulis, A. *Biomaterials Science and Engineering* **17**(4-6) (2022), https://doi.org/10.1007/978-981-16-7435-8_5
3. Hilpert, K., et al. *Front. Microbiol.* **10** (2020), https://doi.org/10.3389/fmicb.2019.03097
4. Li, Y., et al. *Protein Expr Purif* **80**(2), 260-267 (2011), https://doi.org/10.1016/j.pep.2011.08.001
5. Yu, Z., et al. *J Struct Biol* **186**, 451-461 (2014), https://doi.org/10.1016/j.jsb.2014.01.003
6. Bandiera, A., et al. *Biotechnol. Appl. Biochem.* **42**, 247 (2005), https://doi.org/10.1042/BA20050114
7. Urry, D.W. *J. Protein Chem.* **7**, 1-34 (1988), https://doi.org/10.1007/BF01025411
8. Urry, D.W. *J. Phys. Chem. B* **101**, 11007-11028 (1997), https://doi.org/10.1021/jp972167t
9. D'Andrea, P., et al *Biochim. Biophys. Acta - Mol. Cell Res.* **1866**, 504-517 (2019), https://doi.org/10.1016/j.bbamcr.2018.10.012
10. Bandiera, A., et al. *Biotechnol. Bioeng.* **117**, 354-361 (2020), https://doi.org/10.1002/bit.27217
11. Bartlow, P., et al. *Protein expression and purification*, **78**(2), 216-224. (2011), https://doi.org/10.1016/j.pep.2011.04.021
12. Wiegand, I., et al. *Nat Protoc* **3**, 163-175 (2008), https://doi.org/10.1038/nprot.2007.521
13. Bolatchiev, A. *PeerJ* **8**, (2020), https://doi.org/10.7717/peerj.10455

Identification and Synthesis of Immunogenic Peptides to Produce *Tityus* Antivenom

J.A. Rodríguez[1,2], G.R. Barredo-Vacchelli[1,2], L.C. Iglesias-García[1,2], G. Acosta[3,4], F. Albericio[3,4,5], and S.A. Camperi[1,2]

[1]*Universidad de Buenos Aires, Facultad de Farmacia y Bioquímica, Cátedra de Biotecnología, Buenos Aires, Argentina;* [2]*Instituto de Nanobiotecnología (NANOBIOTEC) UBA-CONICET, Buenos Aires, Argentina;* [3]*CIBER-BBN, Networking Centre on Bioengineering, Biomaterials and Nanomedicine, and Dep. of Organic Chemistry, University of Barcelona, Barcelona, Spain;* [4]*Institute of Advanced Chemistry of Catalonia (IQAC-CSIC), Spanish National Research Council (CSIC), Barcelona, Spain;* [5]*School of Chemistry & Physics, University of KwaZulu-Natal, Durban, South Africa*

Introduction

Several endemic scorpions belonging to the genus *Tityus* sp. can cause envenoming in humans in Argentina. The administered antivenoms used for accidental scorpion stinging treatments is produced by immunizing horses repeatedly with captured arachnid venoms extracted by electrostimulation of their telson. This classical antiserum production used since its description by Césaire Auguste Phisalix and Albert Calmette in 1894, depends on an extremely dangerous and low-yielding venom harvest, hampering national demands met. Furthermore, due to the high content of horse proteins injected, adverse reactions such as serum sickness has been reported [1].

Tityus trivittatus is one of the main scorpions of medical importance in South America. Beta-mammal Tt1g neurotoxin, a Cys-rich peptide, has been described as the responsible for the intoxication symptoms caused by its sting to humans [2]. Tt1g, as well as others Cys-rich peptides usually found in arachnids, has low immunogenicity because, its high stability and its digestion is difficult in antigen-presenting cells, a key step to trigger the adaptive immune response [3].

In this work, the epitopes from Tt1g were identified, and immunogenic peptides were designed and chemically synthesized to supplant and/or improve the traditional method of obtaining scorpion venom currently used in South America.

Results and Discussion

The "MHC-II Binding Predictions" tool from "Immune Epitope Database Analysis Resource", was used to identify the Tt1g epitopes [4]. Its most immunogenic fragment, LPNWVKVWERATNRC, corresponding to its *C* terminus, was synthesized by solid phase solid phase peptide synthesis (SPPS) with Fmoc/tBu chemistry using Rink amide-MBHA resin. Cys was replaced by α-aminobutyric acid to avoid Cys bonds formation. To increase the immunogenicity of the selected epitope, the *N*-terminal was palmitoylated and linear and branched peptides, using Fmoc-Lys (Fmoc)-OH, were synthesized. The purity and identity of the synthesized epitopes were assessed by electrospray ionization mass spectrometry (ESI MS) and RP HPLC.

All the peaks obtained in the mass spectra corresponded to the synthesized immunogens (Figures 1A and 2A), demonstrating their high purity. The RP-HPLC analysis of the linear palmitoylated epitope indicated a purity higher than 85% (Figure 1B). On the other hand, the branched palmitoylated peptide chromatogram showed two peaks (Figure 2B), probably due to the presence of two conformations in slow interconversion or the formation of micelle in aqueous medium that disassemble in organic medium. Similar results were obtained with a branched palmitoylated epitope from the spider Tx2-6 neurotoxin, also synthesized in our laboratory.

1A

1B
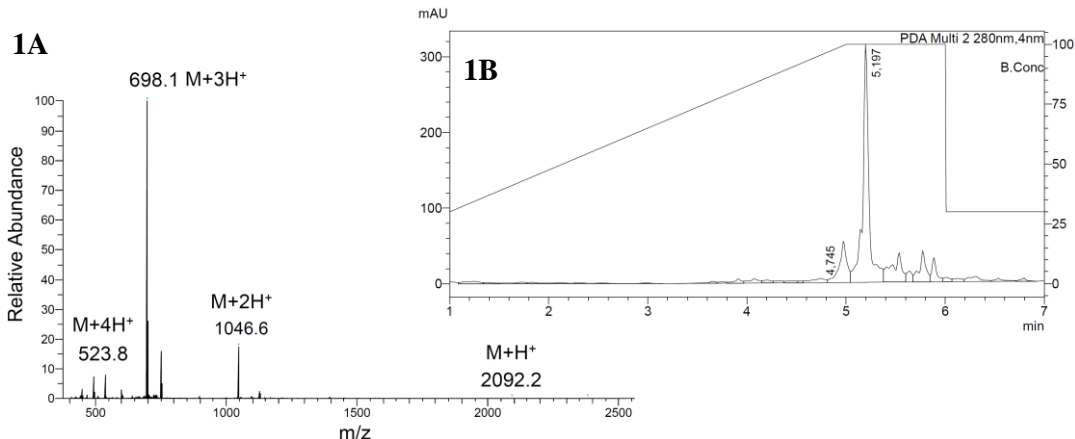
Fig. 1. Palm-LPNWVKVWERATNR-Abu-NH₂ (MW: 2091.58; monoisotopic mass: 2091.26 u). 1A) ESI MS; 1B) RP-HPLC analysis. RP column (C18 3.5μm, 4.6x50mm). Solvent A: 0.045% TFA in H₂O, Solvent B: 0.036% TFA in acetonitrile.

2A

2B
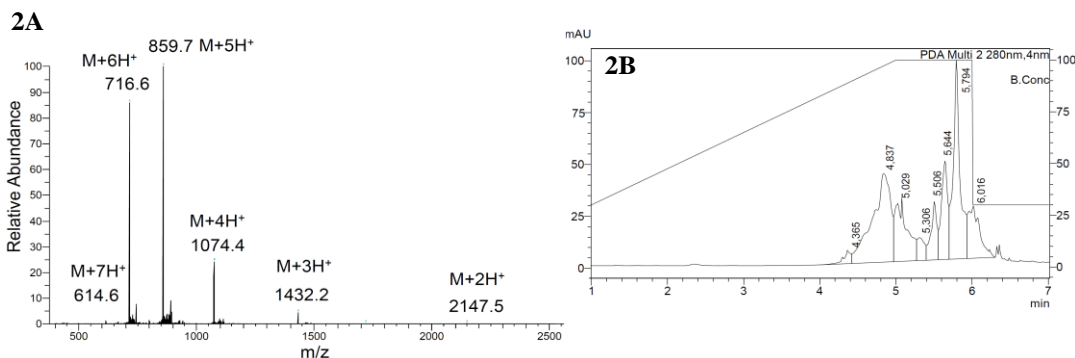
Fig. 2. (Palm-LPNWVKVWERATNR-Abu)₂K-NH₂ (MW: 4294.31; monoisotopic mass: 4292.58 u. 2A) ESI MS; 2B) RP-HPLC analysis. RP column (C18 3.5μm, 4.6x50mm). Solvent A: 0.045% TFA in H₂O, Solvent B: 0.036% TFA in acetonitrile.

Synthesised peptides are currently tested *in vitro* and afterwards they will be assayed in the *Instituto Nacional de Producción de Biológicos, Administración Nacional de Laboratorios e Institutos de Salud Dr. Carlos Malbrán* to assess their capacity to produce *T. trivittatus* antivenom suitable for large-scale production to meet national and regional demands.

Acknowledgments

References

1. Ismail, M. *Int J Antimicrob* **21**, 170-174 (2003), http://doi.org/10.1016/s0924-8579(02)00289-3
2. Coronas, F.I., et al. *Peptides* **68**, 11-16 (2015), http://doi.org/10.1016/j.peptides.2014.05.002
3. Camperi, S.A., et al. *Toxicon X* **6,** 100038 (2020), https://doi.org/10.1016/j.toxcx.2020.100038
4. Jensen, K.K., et al. *Immunology* **154**(3), 394-406 (2018), http://doi.org/10.1111/imm.12889

Identification and Synthesis of Epitopes from a *Phoneutria Nigriventer* Toxin to Produce Immunogens

Lucía C. Iglesias-García[1,2], Jésica A. Rodríguez[1,2], Gabriela R. Barredo- Vacchelli[1,2], Juan M. Minoia[1,2], Gerardo Acosta[3,4], Fernando Albericio[3,4,5], and Silvia A. Camperi[1,2]

[1]*Universidad de Buenos Aires, Facultad de Farmacia y Bioquímica, Cátedra de Biotecnología, Buenos Aires,1113, Argentina;*[2]*Instituto de Nanobiotecnología (NANOBIOTEC) UBA-CONICET, Buenos Aires, 1113, Argentina;*[3]*CIBER-BBN, Networking Centre on Bioengineering, Biomaterials and Nanomedicine and Dep. of Organic Chemistry, University of Barcelona, Barcelona, 08028, Spain;*[4]*Institute of Advanced Chemistry of Catalonia (IQAC-CSIC), Spanish National Research Council (CSIC), 08028, Barcelona, Spain;*[5]*School of Chemistry & Physics, University of KwaZulu-Natal, Durban, 4001, South Africa*

Introduction

The spider *Phoneutria nigriventer*, lives predominantly in Brazil and in the north of Argentina. Envenoming caused by *P. nigriventer* constitutes a medical emergency treatable with suitable antivenoms. The availability of venom, necessary for antivenom production is scarce, mainly because these spiders are difficult to capture and handle in the laboratory. New approaches are necessary for a more efficient and economical antivenom production to satisfy national and regional the demands. *P. nigriventer* venom is composed primarily by cysteine-rich peptide neurotoxins which possess the high stable inhibitor cystine knot (ICK) structural motif [1]. Among them, δ-ctenitoxin-Pn2a (UniProt: P29425), also called PnTx2-6, is one of the most toxic neurotoxins for humans and responsible for envenoming symptoms. Although high toxic, is a poor immunogen due to its high stability, what impairs its degradation in the antigen-presenting cells (APC) necessary to initiate the immune response [2].

The aim of this work was to identify PnTx2-6 epitopes and design and synthesize immunogens to complement the use of crude venoms in the production of antivenom serums in Argentina.

Results and Discussion

Epitopes of the neurotoxin Tx2-6 (δ-ctenitoxin-Pn2a) were identified with the "MHC-II Binding Predictions" tool of the "Immune Epitope Database Analysis Resource" [3,4]. The most antigenic zone, corresponding to the *C*-terminal, GYFWIAWYKLANCKK, was synthesized in solid phase using Fmoc/tBu chemistry and Rink amide-MBHA resin. The Cys was replaced by α-aminobutyric acid to avoid disulphide bonds formation. To increase its immunogenicity palmitic acid was added at the *N*- terminal. Also, branched peptides were synthesized using Fmoc-Lys(Fmoc)-OH. Synthesized peptides were analysed by electrospray ionisation mass spectrometry (ESI-MS). Table 1 shows the monoisotopic masses obtained with the deconvolution function Xtract for each peptide. All the peaks obtained in the mass spectrum corresponded to the synthesized immunogens, demonstrating the high purity of the synthesis. M+44 and M+88 corresponded to the incomplete decarboxylation intermediate $Trp(CO_2H)$ during Trp(Boc) final cleavage which is easily hydrolysed when peptides are dissolved in water.

Table 1. Monoisotopic masses obtained in mass spectra.

Peptide	Monoisotopic mass (M)	Monoisotopic masses obtained by deconvolution		
Palm-GYFWIAWYKLAN-Abu-KKG-NH$_2$	2166.3	M	M+44	
(Palm-GYFWIAWYKLANAbuKK)$_2$-KG-NH$_2$	4500.6	M	M+44	M+88

Also, peptides were analysed by reversed-phase high-performance liquid chromatography (RP-HPLC) (Figure 1). The RP-HPLC analysis of the linear palmitoylated epitope demonstrated a purity higher than 85% while the branched palmitoylated peptide showed two peaks. Probably, the branched palmitoylated peptide exists in two forms that convert very slowly between both conformations.

Similar results were obtained with a branched palmitoylated peptide of the scorpion Tt1g neurotoxin, also synthesized in our laboratory.
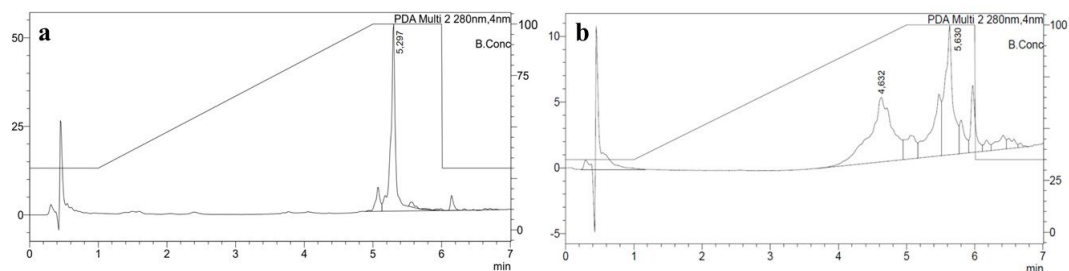
Fig. 1. RP-HPLC chromatograms. RP column (C18 3.5μm, 4.6x50mm). Solvent A: 0.045% TFA in H₂O, Solvent B: 0.036% TFA in acetonitrile: a) Palm-GYFWIAWYKLAN-Abu-KKG-NH₂, b) (Palm-GYFWIAWYKLAN-Abu-KK)₂-K-G-NH₂.

Currently, synthesized peptides are being tested *in vitro* and afterwards they will be assayed in the Instituto Nacional de Producción de Biológicos, Administración Nacional de Laboratorios e Institutos de Salud Dr. Carlos Malbrán, to evaluate their immunogenicity and ability to generate neutralizing antibodies in horses to produce *P. nigriventer* antivenom.

Acknowledgments

References

1. Diniz, M.R.V., et al. *PLoS One*. **1**,13(8), e0200628 (2018), http://doi.org/10.1371/journal.pone.0200628
2. Camperi, S.A., et al. *Toxicon X*. **5**,(6), 100038 (2020), https://doi.org/10.1016/j.toxcx.2020.100038
3. Wang, P., et al. *PLoS Comput Biol*. **4**(4), e1000048 (2008), http://doi.org/10.1371/journal.pcbi.1000048
4. Wang, P., et al. *BMC Bioinfor*. **11**, 568 (2010), http://doi.org/10.1186/1471-2105-11-568

New Antimicrobial Peptides as Potential Candidates in the Control Growth of *Botrytis cinerea*

Alejandra B. Cardillo[1,2]*, Stella M. Romero[3]*, María C. Martínez-Ceron[1,2], Silvia A. Camperi[1,2], and Silvana L. Giudicessi[1,2]

[1]Universidad de Buenos Aires, Facultad de Farmacia y Bioquímica, Cátedra de Biotecnología, Junín 956 (1113), CABA, Argentina; [2]Instituto NANOBIOTEC UBA-CONICET, Junín 956 (1113), CABA, Argentina; [3]Instituto Multidisciplinario de Biología Vegetal (IMBIV), Avenida Vélez Sarsfield 1611, Córdoba, Argentina
*Both authors contributed in the same way in this work

Introduction

Antimicrobial peptides (AMP) are small-polycationic molecules present in the innate immune response [1]. There are currently more than 3000 experimentally reported AMP [2]. Particularly, temporins, a small AMP family present in frogs, have been discovered as potential candidates for antimicrobial activity. These peptides serve to protect the frog against invasion by a variety of pathogenic micro-organisms and represent a component of the innate immunity of these organisms [3,4]. Within this arsenal of defensive peptides, some members of the temporin family have been described [5]. Until now, temporins have only been used in the control of bacteria and some yeasts. In the present work, the inhibition of the phytopathogenic fungus *Botrytis cinerea* growth by temporins for their potential application in the control of crops with agronomic interest.

Results and Discussion

Peptides were synthesized on solid phase using Fmoc/tBu chemistry and the purities afterwards were analyzed by RP-HPLC and MALDI MS. The study was carried out testing different concentrations of the peptides in Petri dishes with potato dextrose agar medium (PDA, Oxoid). PDA plates were inoculated with 1 µL of the spore suspension and incubated in the dark for 3 days. The fungus growth diameter on the plate was measured and the percentage of inhibition was calculated by comparison with a control with pure dimethyl sulfoxide (DMSO). Three peptide concentrations were tested: 10, 50 and 100 µg/mL, and each test was performed in triplicate.

In a first *screening*, 11 AMP were tested. These peptides were chosen from different peptide data bases [6-8], with different amino acid sequence and length (between 4 and 14 amino acids). Best results were obtained with peptides SLLSLIRKLIT and FASLLGKALKALA, with 42% and 50% fungal growth inhibition, respectively. Both peptides had the Ser-Leu-Leu sequence and a high percentage of hydrophobic amino acids in their structure.

From these results, a second screening in databases was carried out searching for AMP with these properties. As a result, we found predominately temporins, with the Ser-Leu-Leu sequence and hydrophobic amino acids. Afterwards, ten simple-to synthesize temporins were selected from the data base, with less than 20 amino acid long and without oxidizable residues (cysteine, tryptophan, methionine). Those temporins were used for the second *screening* using the same conditions. A fungus growth inhibition between 40% and 60% was observed for 7 peptides at a concentration of 100 µg/mL (Table 1). In general, temporins inhibited fungus growth with a high percentage, except for temporin E, that only inhibited in a 31%. The other 3 temporins did not show growth inhibition (data not shown). Particularly, 55% and 57% of inhibition was observed with temporin B and 1CSb respectively. Both peptides were highly hydrophobic peptides with a high content of Leucine and Isoleucine in their structure and with no net charge.

Table 1. Percentage of Botrytis cinerea growth inhibition using temporins at different peptide concentrations.

Peptide	Sequence	Peptide concentration (µg/mL)		
		10	50	100
Temporin E	VLPIIGNLLNSLL	14.4	11.0	31.6
Temporin B	LLPIVGNMMKSLL	25.7	40.2	54.8
Temporin A	FLPLIGRVLSGIL	21.7	38.6	47.8
Temporin1CSb	FLPIIGKLLSGLL	30.9	48.6	57.4
Temporin CGa	FLPILGNLLNGLL	14.5	30.1	42.2
Temporin G	FFPVIGRILNGIL	10.4	44.4	46.4
Temporin PRb	ILPILGNLLNSLL	0.8	23.3	49.4

These results showed that temporins are promising candidates for *Botrytis cinerea* growth control. All peptides that inhibited fungal growth present similar properties as hydrophobicity, amino acid composition, length, and net charge. These findings indicate that other members of temporin family could be potential candidates for fungus growth control. However, only few of these peptides have been proved as antifungal alternatives, so this is an unexplored field. Additional research in temporin activities and efficiency are necessary to incorporate more suitable alternatives in the control of this and other phytopathogenic fungi.

Moreover, synergic activity can be considered for growth control. Temporin B and 1csb could be used as a template to make rational modifications that may eventually improve antifungal activity. Temporins are a large family that have not been fully studied yet and have been gaining importance in antimicrobial studies in recent years [9]. The need for new and more effective antibiotic and antifungal agents makes necessary the discovery and application of new drugs based on natural peptides such as AMP.

Acknowledgments

References

1. Ageitos, J.M., et al. *Biochemical Pharmacology* **133**, 117-138 (2017), http://dx.doi.org/10.1016/j.bcp.2016.09.018
2. de la Torre, B.G., et al. *Molecules* **25**, 2293 (2020), http://dx.doi.org/10.3390/molecules25102293
3. Conlon, J.M. *Peptides* **29**, 1815-1819 (2008), http://dx.doi.org/10.1016/j.peptides.2008.05.029
4. Conlon, J.M., et al. *Biochimica et Biophysica Acta* **1788**, 1556-1563 (2009), http://dx.doi.org/10.1016/j.bbamem.2008.09.018
5. Conlon, J.M. *Cellular and Molecular Life Sciences* **68**, 2303-2315 (2011), http://dx.doi.org/10.1007/s00018-011-0720-8
6. https://aps.unmc.edu/
7. https://dbaasp.org/
8. http://biotechlab.fudan.edu.cn/database/lamp./results.php
9. Romero, S.M., et al. *Surgical Infections* **20**, 309-322 (2020), http://dx.doi.org/10.1089/sur.2019.266

New Thrombospondin-1-Deriving Peptides as TGF-β Activators of Cosmeceutical Interest

Patrycja Ledwoń[1,2], Fosca Errante[2], Feliciana Real Fernández[3], Paolo Rovero[2], and Rafał Latajka[1]

[1]*Department of Bioorganic Chemistry, Faculty of Chemistry, Wroclaw University of Science and Technology, Wrocław, 50 370, Poland;* [2]*Interdepartmental Research Unit of Peptide and Protein Chemistry and Biology, Department of Neurosciences, Psychology, Drug Research and Child Health – Section of Pharmaceutical Sciences and Nutraceutics, University of Florence, Sesto Fiorentino, 50019, Italy;* [3]*CNR – Istituto di Chimica dei Composti Organometallici (CNR-ICCOM), Sesto Fiorentino, 50019, Italy*

Introduction

In recent years, the outward appearance and the health of the skin have become the object of interest of various scientific investigations. Research on new compounds possessing the ability to improve the condition of the skin is no longer required only for the development of new drugs, but also for cosmeceuticals – cosmetic products with scientifically proven and thoroughly tested biological activity, and therefore with higher efficiency and quality compared to traditional cosmetics available in drugstores. Considering the limited possible toxic side-effects, relatively easy synthesis, and several opportunities of further structural modifications, peptides give a fundamental contribution to the cosmeceutical field [1,2]. Collagen turnover regulation is one of the main targets for the design of new compounds relevant in the cosmeceutical arena, with particular attention on peptide-based formulas.

Among the diverse proteins in human body, collagen is one of the most essential and abundant components. Collagen type III acts as the linchpin of type I fibers and supports skin elasticity. Through complicated signaling pathway, Transforming Growth Factors-β (TGFs-β) can facilitate the biosynthesis of fibrillar collagens I and III in fibroblasts. Additionally, TGFs-β downregulate the activity of matrix metalloproteinases (MMPs), highly involved in the collagen fibers degradation [3]. The group of TGFs-β consists of five isoforms, namely TGF-β_{1-5} [4], which function is regulated by their activation, as they exist in active or latent form (LAP-TGF-β). Secreted in the latent type, LAP-TGFs cannot react with the receptor and therefore they are biologically inert. Before the secretion by the cell, TGFs-β undergo various intracellular processes leading to their activation. *N*-terminal part of this dimer protein is called the latency associated peptide (LAP, 390 amino acid length); the *C*- terminal region is called the mature TGF-β (112 amino acid length). Various physiological substances have been found to activate the latent form of TGFs, such as: plasmin, proteases, cathepsins, calpain, and the glycoprotein thrombospondin-1 (TSP-1) (Figure 1) [5,6].
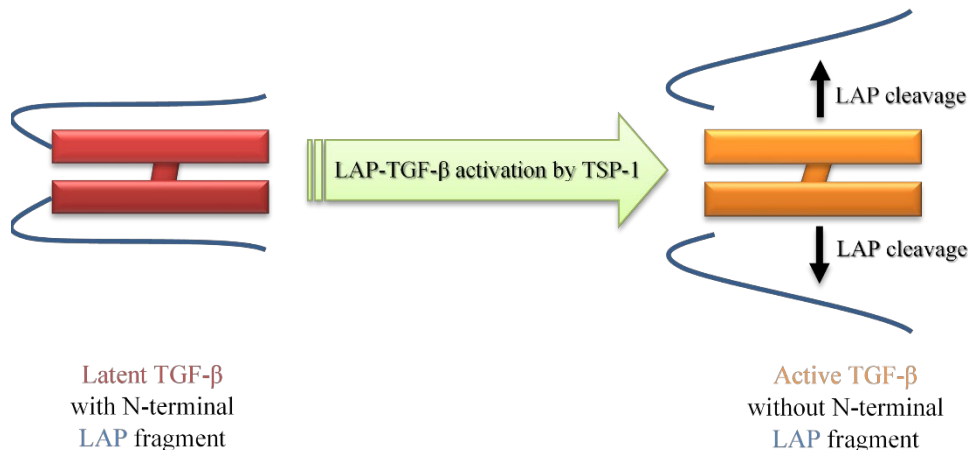
Fig. 1. The process of latent TGF-β activation involving thrombospondin-1 (TSP-1) – its major activator in vivo.

Table 1. Examples of short peptides already applied in the cosmeceutical arena, with collagen synthesis-stimulating properties. They are derivatives of KRFK peptide from TSP-1, based on the initially investigated sequence KRFYVVMWKK.

Sequence	Reference	
	Paper	*Patent*
KRFYVVMWKK	Tolsma et al. 1993 [7] Kanda et al. 1999 [8] Denèfle et al. 2016 [9]	-
KRFK	Ribeiro et al. 1999 [10]	Murphy-Ullrich et al. 2002 [11]
KFK and Elaidyl-KFK	Cauchard et al. 2004 [12]	Bellon et al. 2001 [13]
RFK and KVK and their derivatives	Imfefd et al. 2015 [6]	Ziegler et al. 2007 [14]

Latent TGF-β activation depends on the interaction of the specific TSP-1 portion $K^{412}RFK^{415}$ with LAP-TGF-β$_1$. This complex formation requires the interaction of TSP-1-deriving peptide KRFK and LAP-deriving fragment LSKL, located near the LAP *N*-terminus. Importantly, LAP-TSP-1 association prevents the reformation of LAP-TGF-β$_1$. Sequences already evaluated as activators of LAP-TGF-β$_1$ are summarized in Table 1.

Herein we present the KRFK peptide analogs, which will be further modified aiming at increasing the activity and, most importantly, stability and bioavailability of the original product. Our first goal, reported herein, is to evaluate the applicability of Surface Plasmon Resonance (SPR) technique in the measurements of LAP-TGF-β$_1$ activation process, a method not reported up to now in the literature for this type of assay. To confirm the results of this procedure, standard ELISA, widely applied for this purpose, will be performed simultaneously. Already known analogs will be synthesized as controls. Structure-activity relationship will be investigated for the sequences proving the most significant TSP-1-mimicking activity.

Results and Discussion

Materials and methods. Peptides were synthesized manually *via* solid-phase peptide synthesis (SPPS) according to the Fmoc/*t*Bu strategy. ELISA assays were performed with NUNC® Maxisorp™ microplates. SPR measurements were performed with Biacore™ X100 system, for the antibody immobilization Cytiva Sensor chip CM5 was applied.

ELISA assays. ELISA experiments were performed to confirm the proper activity of anti-TGF-β$_{1,2,3}$ antibody (MAb Clone 1D11, BioTechne) (Figure 2). For this purpose, active TGF-β$_1$ protein was coated on the NUNC® microplate at the concentration of 100ng/mL. After washing with saline solution, wells were blocked with a 5% Bovine Serum Albumin (BSA) in PBS solution (1.5h, room temperature). Then, anti-TGF-β$_{1,2,3}$ antibody was added at the concentration 5μg/mL in 2.5% BSA buffer, and incubated under agitation for 2.5h. After 3 washing cycles with saline solution, the secondary antibody (anti-mouse IgG-AP, Jackson) was added and incubated for 2h under agitation. In order to evaluate the binding of anti-TGF-β$_{1,2,3}$ to the protein, the microplate was developed adding the substrate solution containing 1mg/mL of *p*-NPP. The absorbance in each well was measured at 405 nm. Results of ELISA analyses are presented in Figure 3. It is visible that the

Fig. 2. ELISA assay results confirming the activity of anti-TGF-β$_{1,2,3}$ antibody. Increased signal corresponds to TGF-β$_1$-coated wells, treated then with anti-TGF-β$_{1,2,3}$.

signal corresponding to TGF-β_1-coated wells, and then treated with anti-TGF-$\beta_{1,2,3}$ is the highest among all controls (two protein-coated and two non-coated wells, with and without anti-TGF-$\beta_{1,2,3}$ antibody addition in each group). Therefore, we assumed the right functioning of used antibody.

Immobilization of anti-TGF-$\beta_{1,2,3}$ antibody onto the chip. The standard amine coupling strategy has been chosen for the immobilization of anti-TGF-$\beta_{1,2,3}$ antibody. Sodium acetate buffer (C_M=50mM, pH=5) has been selected as immobilization buffer using the *pH scouting* protocol. Prior to the immobilization, the chip was activated with NHS:EDC (50:50) injection for 480s. Then, the activated chip was treated with a solution of anti-TGF-$\beta_{1,2,3}$ antibody (C_M=10μg/mL in immobilization buffer), by flowing it over the sensor surface for 420s at flow rate 10μL/min. The value of observed signal corresponding to the total amount of immobilized antibody was 5800 RU.

Selectivity of antibody immobilized on the chip. Once anti-TGF-$\beta_{1,2,3}$ antibody was immobilized onto the sensor chip of Biacore™ X100, solutions of latent and active form of TGF-β_1 were flown through the system to prove the selectivity of chosen antibody. All proteins were tested initially at the concentration of 50ng/mL. The signals obtained for LAP-TGF-$\beta_{1,2,3}$ and active TGF-β_1 are presented in Figure 3. Due to the fact that LAP-TGF-$\beta_{1,2,3}$ do not bind to the specific immobilized antibody, and the active TGF-β_1 slightly provided a binding signal, we decided to increase the concentration of active protein solution till 100ng/mL in order to confirm the chip sensibility and selectivity. It is well visible that the signal corresponding to the blank (buffer only) is low and does not contribute significantly to observed signal intensity. Active TGF-β_1 was tested in two concentrations, 50 and 100ng/mL, and both of them were recognized by the immobilized antibody. These results proved the selectivity of used antibody, confirming that this biosensor system can be used to identify active TGF-β_1.

Fig. 3. Binding stability in Resonance Units (RU) observed for different solutions of active TGF-B1 to the immobilized anti-TGF-$\beta_{1,2,3}$ antibody.

Conclusions and prospective

Control sequences with already proven activity as TGF-β_1 activators (based on Table 1) were synthesized, purified, and characterized. It has been shown that inactive (LAP-conjugated) protein is not recognizable, while the signal corresponding to the free form is visible and increases with the protein concentration. ELISA assay was performed and the signal corresponding to the well with active protein and anti-TGF-$\beta_{1,2,3}$ antibody was the highest, confirming the data obtained with the Biacore™ assay.

Ongoing assays include the evaluation of the presence of free LAP, cleaved during the activation, and of the possible reassociation of LAP molecule and the activated TGF-β_1. By now it is known that the activation reaction including the full glycoprotein TSP-1 is not reversible, however there is no data clearly confirming equal behavior of shorter, TSP-1-deriving sequences. In the nearest future we aim to clarify the mechanism of LAP dissociation in the presence of synthesized peptides and to optimize the conditions of the assay involving Surface Plasmon Resonance technique.

The new protocol for Biacore™ measurements of TGF-β_1 activation, once fully optimized, will allow to perform the assay in a robust, rapid, and automated way – as compared to the time-consuming and more complicated ELISA protocols described so far.

Acknowledgments

References

1. Errante, F., et al. *Front. Chem.* **8**, 572923 (2020), http://dx.doi.org/10.3389/fchem.2020.572923
2. Ledwoń, P., et al. *Chem. Biodiversity* **18**, e2000833 (2021), http://dx.doi.org/10.1002/cbdv.202000833
3. Zhong, J., et al. *Medical Hypotheses* **76**, 343-346 (2011), http://dx.doi.org/10.1016/j.mehy.2010.10.035
4. Khalil, N. *Microbes Infect.* **1**, 1255-1263 (1999), http://dx.doi.org/10.1016/s1286-4579(99)00259-2
5. Crawford, S.E., et al. *Cell* **93**, 1159-1170 (1998), http://dx.doi.org/10.1016/s0092-8674(00)81460-9
6. Imfeld, D., et al. *H&PC Today* **10**, 6-11 (2015), no DOI available
7. Tolsma, S., et al. *Int. J. Cell Biol.* **122**, 497-511 (1993), http://dx.doi.org/10.1083/jcb.122.2.497
8. Kanda, S., et al. *Exp Cell Res* **252**, 262-272 (1999), http://dx.doi.org/10.1006/excr.1999.4622
9. Denèfle, T., et al. *J Med Chem* **59**, 8412-8421 (2016), http://dx.doi.org/10.1021/acs.jmedchem.6b00781
10. Ribeiro, S., et al. *J Biol Chem* **274**, 13586-13593 (1999), http://dx.doi.org/10.1074/jbc.274.19.13586
11. Murphy-Ullrich, J.E., et al. US 6,384,189 B1 (2002)
12. Cauchard, J-H., et al. *Biochem Pharmacol* **67**, 2013-2022 (2004), http://dx.doi.org/10.1016/j.bcp.2004.01.028
13. Bellon, P., et al. FR 2810323 A1 (2001)
14. Ziegler, H., et al. US 20070099842 A1 (2007)

The Synthesis and Biological Investigation of New Potent Chimeric Antimicrobial NCR247 Derivatives

János Szolomájer[2], Sándor Jenei[1†], Gabriella Endre[1*], Éva Kondorosi[1*], and Gábor K. Tóth[2,3]

[1]Institute of Plant Biology, Biological Research Centre, Szeged, Hungary; [2]Department of Medical Chemistry, University of Szeged, Szeged, Hungary; [3]MTA-SZTE Biomimetic Systems Research Group, University of Szeged, Szeged, Hungary

Introduction

The worldwide spread of antibiotic-resistant bacteria and the increasing mortality rate by untreatable microbial infections makes the development of new antibiotics with novel modes of action an urgent topic. Plant peptides, produced only in Rhizobium bacterium-legume symbiosis, in the symbiotic cells of root nodules, represent a rich source of so far unexplored biological activities and antimicrobial agents. The infected nodule cells contain thousands of bacteria that are encapsulated by plasma membrane-derived vesicles. In the host cells, the bacteria adapt to the intracellular lifestyle, microaerobic conditions and differentiate progressively into nitrogen-fixing bacteroids. In many legumes, this differentiation process is irreversible and manifested by extreme cell growth, altered morphology and physiology, genome amplifications and definitive loss of cell division.

In *M. truncatula*, 700 genes code for nodule-specific cysteine-rich NCR. The NCR genes usually consist of two exons; the first coding for a relatively conserved signal peptide, while the second one for the mature peptide. The mature NCR peptides exhibit extreme differences in their physicochemical properties due to their highly divergent amino acid compositions and sequence where only the position of 4 or 6 cysteines and a few neighbouring amino acids are conserved. The NCR peptides enter the endoplasmic reticulum during their translation where the signal peptidase complex cleaves the signal peptide, and the mature peptides reach the symbiosomes. By entering the cells, (Figure 1) NCR peptides can interact with the bacterial cell envelope, the bacterial membranes, and specific targets in the bacterial cytosol. NCR247, which is the smallest peptide of the NCR family, is composed of 24 amino acids, four of which are cysteines. This cationic peptide (pI 10.15) is a self-penetrating peptide entering the bacterial cytosol without pore formation, which has exceptionally high protein binding ability and interacts with many bacterial proteins. NCR247 interacting with many ribosomal proteins inhibits translation and downregulates ribosomal gene transcription. Accordingly, treatment of various pathogenic bacteria with synthetic NCR247 provoked the efficient killing of many of them.

Fig. 1. The role and modes of action of AMPs.

Results and Discussion

The antimicrobial peptides (AMPs) listed in Table 1 were synthesized according to the standard procedure of the solid-phase peptide synthesis (SPPS) by using an automatic peptide synthesizer (CEM Liberty Blue) with TentaGel S RAM resin (loading of amino groups 0.23 mmol/g). The applied chemistry utilized the Fmoc amino protecting group and diisopropylcarbodiimide/oxyma coupling with a fivefold excess of reagents. Removal of the fluorenyl-9-methoxycarbonyl (Fmoc) group was carried out with 10% piperazine and 0.1 mol 1-hydroxy-benzotriazole (HOBt) dissolved in 10% ethanol and 90% DMF in two cycles. After completion of the synthesis, peptides were detached from the resin with a 95:5 (v/v) trifluoroacetic acid (TFA)/water mixture containing 3% (w/v) dithiothreitol (DTT) and 3% (w/v) triisopropylsilane (TIS) at room temperature (RT) for 3 h. The resin was removed by filtration and the peptides were precipitated by the addition of ice-cold diethyl ether. Next, the precipitate was filtered, dissolved in water and lyophilized. The identity of

Table 1. *List of antimicrobial peptides.*

Code	Name	Amino acid sequence	pI
A	NCR247	RNGCIVDPRCPYQQCRRPLYCRRR	10.15
B	NCR247C	QQCRRPLYCRRR	11.5
C	NCR247C-StrepII	QQCRRPLYCRRRWSHPQFEK	11.05
D	X1-NCR247C	RPLNFKMLRFWGQQQCRRPLYCRRR	11.99
E	X1-NCR247C-StrepII	RPLNFKMLRFWGQQQCRRPLYCRRRWSHPQFEK	11.8
F	NCR247C-X2	QQCRRPLYCRRRKALAALAKKIL	11.55
G	NCR247C-X2-StrepII	QQCRRPLYCRRRKALAALAKKILWSHPQFEK	11.4
H	X2-NCR247C	KALAALAKKILQQCRRPLYCRRR	11.65
I	X2	KALAALAKKIL	10.98
J	Transportan	GWTLNSAGYLLGKINLKALAALAKKIL	10.77

the peptides was verified by ESI-MS using a Waters SQ detector. The crude peptides were analyzed and purified by reverse-phase high-performance liquid chromatography (RP-HPLC). Peptides were purified using a C18 column with a solvent system of (A) 0.1% (v/v) TFA in water and (B) 80% (v/v) acetonitrile and 0.1% TFA (v/v) in water at a flow rate of 4.0 mL/min. The absorbance was detected at 220 nm. The appropriate fractions were pooled and lyophilized. The purity of the peptides was characterized by analytical RP-HPLC at a flow rate of 1.0 mL/min.

Previously we have shown bactericidal activity of the synthetic NCR247 peptide in PBS on several human and plant pathogen bacteria. Our present work is focused on the activity of NCR247 and its various derivatives (Table 1) on the ESKAPE strains as well as on *L. monocytogenes* and *S. enterica*. Bacterial cultures were treated with 2-fold dilution series of synthetic NCR247 (peptide A, Table 1) starting with 25 mM concentration. The minimal bactericidal concentration (MBC) was the lowest concentration of the tested molecules where no viable bacteria remain after the treatment and therefore the growth of bacteria could not be detected (Table 2). The killing activity of NCR247 was the strongest with an MBC of 3.1 mM on *P. aeruginosa* while the MBC was 6.3 mM in the case of *S. aureus* and *E. coli*, 12.5 mM for *A. baumannii* and 25 mM for *S. enterica*. *K. pneumoniae* and *L. monocytogenes* were resistant at 25 mM to NCR247 (peptide A, Table 2).

Table 2. *Minimal bactericidal concentrations (MBC; in mM) of the studied peptides and antibiotics against different pathogens.*

Peptides/ Antibiotics	E. f.	S. a.	K. p.	A. b.	P. a.	E. c.	L. m.	S. e.
A	>25	6.3	>25	12.5	3.1	6.3	>25	25
B	>25	>25	>25	25	25	6.3	>25	>25
C	>25	6.3	>25	25	6.3	6.3	>25	>25
D	6.3	3.1	12.5	3.1	3.1	3.1	3.1	1.6
E	12.5	3.1	6.3	3.1	3.1	3.1	3.1	3.1
F	25	3.1	6.3	3.1	3.1	1.6	1.6	1.6
G	12.5	1.6	3.1	1.6	3.1	1.6	3.1	1.6
H	3.1	3.1	6.3	3.1	3.1	3.1	3.1	3.1
I	>25	25	>25	25	6.3	>25	25	>25
J	3.1	3.1	3.1	1.6	3.1	3.1	3.1	1.6
Cb	5120	640	>10240	5120	10240	1280	80	640
Lvx	160	2.5	320	20	1.3	5.0	320	1.3

Then we tested which region of NCR247 is responsible for the antimicrobial properties. From the 24 amino acid long NCR247, the 12 amino acid long *N*-terminal and the 12 amino acid long *C*-terminal halves were synthesized. The *N*-terminal part (RNGCIVDPRCPY) was inactive on the tested bacteria, while the *C*-terminal part (peptide B: NCR247C, Table 1) retained the antimicrobial activity of NCR247 on *E. coli* (peptide B, Table 2) but was ineffective to kill the other bacteria at 25 mM concentration. The synthetic, reduced and even oxidized forms of NCR247 seem to be unstructured. However, it cannot be excluded that NCR247 might be properly folded by interacting with the bacterial membranes, which may not be possible if the peptide is only 12 amino acids long. Therefore, we synthesized derivatives of the NCR247C peptide adding either *C*- or *N*-terminal extension. First, the neutral, 8 amino acid long StrepII tag (WSHPQFEK) was added to the *C* terminus (peptide C: NCR247C-StrepII, Table 1). NCR247CStrepII became more active than NCR247C killing in addition to *E. coli*, *S. aureus*, and *P. aeruginosa* (peptide C, Table 2). Then the *N*-terminus of NCR247C was extended with 13 amino acids (X1) deriving from the cationic *N*-terminal part of the unusual double-size NCR335 which part lacks cysteines and characteristics of NCRs but increased the pI from 10.15 to 11.99 (peptide D, Table 1). This chimeric peptide (X1-NCR247C) turned out to be very effective on *S. enterica* (MBC 1.6 mM), *S. aureus*, *A. baumannii*, *P. aeruginosa, E. coli*, and *L. monocytogenes* (MBC 3.1 mM) and became able to kill *E. faecalis* (MBC 6.3 mM) and *K. pneumoniae* (MBC 12.5 mM) (peptide D, Table 2). The addition of StrepII to the *C* terminus of X1-NCR247C (peptide E: X1-NCR247C-StrepII, Table 1) slightly improved the bactericidal property against *K. pneumoniae* but became somewhat less efficient against *E. faecalis* and *S. enterica* (peptide E, Table 2). Thereupon, we investigated how the attachment of another AMP at the *C*- or *N*-terminus of NCR247C could influence the bactericidal efficiency and spectrum. We used the KALAALAKKIL sequence (peptide I: X2, Table 1) from the membranolytic, anti-cancer mastoparan peptide toxin from wasp venom (INLKALAALAKKIL), which is also present in the *C*-terminus of the 27 amino acid long cell-penetrating cationic peptide, transportan (peptide J: Transportan, Table 1) Attachment of KALAALAKKIL to the *C*-terminus Plant Peptides Kill ESKAPE Bacteria of NCR247C (peptide F: NCR247C-X2, Table 1) reduced the MBC to 1.6 mM in the case of *E. coli*, *L. monocytogenes*, and *S. enterica* (peptide F, Table 2). Further elongation of NCR247CX2with StrepII (peptide G: NCR247C-X2-StrepII, Table 1) made this derivative even more effective against *S. aureus* and *A. baumannii* (MBC 1.6 mM) (peptide G, Table 2). The addition of X2 to the *N*-terminal of NCR247C (peptide H: X2-NCR247C, Table 1) drastically increased the killing of *E. faecalis* and was the most active one (MBC 3.1 mM) among all tested peptide derivatives (peptide H, Table 2). X2 alone was incomparably less active on all tested bacteria (peptide I, Table 2). On the other hand, transportan effectively killed all bacteria with MIC in the range of 1.6–3.1 mM (peptide J, Table 2). The antimicrobial activity of cationic peptides is generally attenuated by the presence of divalent cations and higher salt concentrations. Therefore, we determined the MBC and the minimal inhibitory concentration (MIC) values of all peptides (A-J) in MHB used for the cultivation of *S. aureus*, *A. baumannii*, and *E. coli* (Table 3). Peptides A-C, corresponding to NCR247, NCR247C and NCR247C-StrepII were ineffective against the three bacteria cultivated for 3 or 20 h at 25 mM concentration. Growth inhibition was only detectable in the case of A: NCR247 at 25 mM on *E. coli* cultivated for 20 h. Unlike A-C, the D-H peptides retained their activity in MHB. The action of D and E was, however, slowed down, as their MBC values were significantly higher at 3 h than at 20 h. In contrast, the MBC values of peptides F, G and H were identical or almost the same at 3 and 20 h. Moreover, in line with the fast action of these peptides, the MIC and MBC values were practically identical.

In this work, we show that NCR247 is capable of killing several, but not all of the most problematic bacteria causing incurable infections. Therefore, we aimed to further improve its bactericidal properties. Testing the antimicrobial activity of the synthetic *N*-terminal and *C*-terminal halves of NCR247 revealed that antimicrobial activity resided mostly in the *C*-terminal region (NCR247C). While the positive charge of the AMPs is essential for killing, in the case of NCR247C the increased positive charge (pI = 11.50) did not result in the improvement of the antimicrobial activity, or the antimicrobial spectrum compared to NCR247 (pI = 10.15). NCR247C had even a much weaker antimicrobial activity which may be due to the lack of its proper folding as a result of its short length and/or its failure to interact with the bacterial membranes. Adding the neutral StrepII tag to the NCR247C peptide improved slightly the antibacterial properties. Extending the *N*-terminus of NCR247C with the 13 amino acid long cationic peptide from NCR335 (D) increased the pI to

11.99 and resulted in significantly lower MBCs (1.6–12.5 mM) and a broader spectrum, killing all the eight bacterium strains. In summary, we successfully designed and generated several chimeric peptides from the symbiotic antimicrobial plant peptide NCR247 with fast killing action, low MBC values, and numerous bacterial targets without toxicity on human cells. These peptides represent an extremely promising novel generation of highly powerful antimicrobial candidates [1].

Table 3. Minimal bactericidal concentrations (MBC) and minimal inhibitory concentrations (MIC) of the studied peptides in Mueller Hinton Broth on selected pathogens.

	(A)				**(B)**				**(C)**		
	S.a.	*A.b.*	*E.c.*		*S.a.*	*A.b.*	*E.c.*		*S.a.*	*A.b.*	*E.c.*
A	>25	>25	>25	**A**	>25	>25	>25	**A**	>25	>25	>25
B	>25	>25	>25	**B**	>25	>25	>25	**B**	>25	>25	>25
C	>25	>25	>25	**C**	>25	>25	>25	**C**	>25	>25	>25
D	25	6.3	12.5	**D**	3.1	3.1	3.1	**D**	3.1	3.1	3.1
E	25	12.5	25	**E**	6.3	6.3	6.3	**E**	6.3	6.3	6.3
F	3.1	3.1	3.1	**F**	3.1	3.1	3.1	**F**	3.1	3.1	3.1
G	6.3	3.1	3.1	**G**	6.3	3.1	3.1	**G**	3.1	3.1	3.1
H	6.3	6.3	6.3	**H**	3.1	3.1	6.3	**H**	3.1	3.1	6.3
I	>25	>25	>25	**I**	>25	>25	>25	**I**	>25	25	>25
J	6.3	3.1	6.3	**J**	3.1	3.1	6.3	**J**	3.1	3.1	3.1

Acknowledgements

References

1. Jenei, S., Tiricz, H., et al. *Frontiers in Microbiology* **11,** 270 (2020), https://doi.org/10.3389/fmicb.2020.00270

LC-MS Analysis of Various Food Intake Regulating Lipopeptides

David Sýkora[1], Aneta Myšková[1,2], Blanka Železná[2], Veronika Strnadová[2], Anna Němcová[1,2], Miroslava Blechová[2], and Lenka Maletínská[2]

[1]*University of Chemistry and Technology Prague, Department of Analytical Chemistry, 16628 Prague, Czech Republic;* [2]*Institute of Organic Chemistry and Biochemistry, Academy of Science, 16000 Prague, Czech Republic*

Introduction

A number of newly synthesized lipopeptides have demonstrated a great therapeutic potential for obesity treatment. Lipidization of neuropeptides usually brings various advantages including improved stability in plasma, improved ability to bind to plasmatic proteins, increased resistance to proteases, ability to cross blood-brain barrier, and modification of pharmacokinetic/pharmacodynamic profile. Our recently synthesized lipopeptides demonstrate high *in vivo* efficiency; lipidization is a prerequisite for their central effect after peripheral administration.

Plasma stability and pharmacokinetics of lipopeptides in blood plasma can be effectively studied by liquid chromatography-mass spectrometry (LC-MS).

Results and Discussion

Studied lipopeptides

Two groups of lipopeptides were studied; (a) prolactin-releasing peptide (PrRP) analogs, and (b) liver enriched antimicrobial peptide-2 (LEAP2) analogs. Their structures are summarized in Figure 1.

palm: palmitoyl (C16), myr: myristoyl (C14), γE: gamma-glutamic acid,
TTDS: 1,13-diamino-4,7,10-trioxatridecan-succinamic acid, N-Ac: N-acetylatoin at the N-terminus,
F-Cl2: dichlorophenylalanine, Nle: norleucin, βA: beta-alanin.
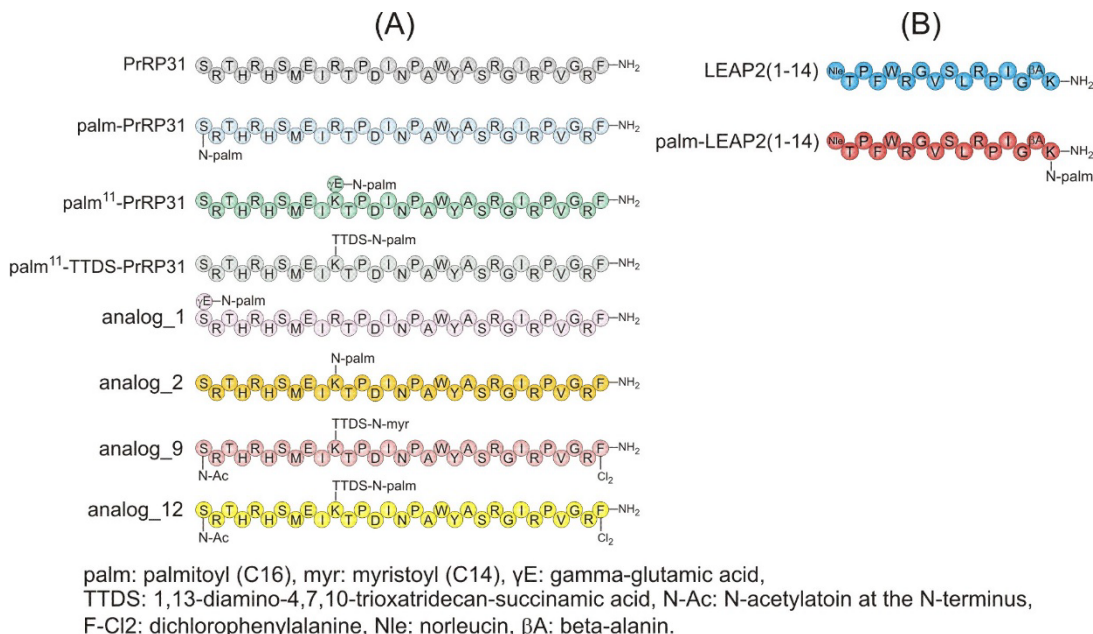
Fig. 1. Chemical structures of (A) PrRP and (B) LEAP2 analogs.

LC-MS instrumentation

For LC an UltiMate 3000 LC system (Thermo, USA) was used. MS was measured with a 3200 Q-TRAP mass spectrometer (AB Sciex, Canada). Separations were carried out with various reversed-phase columns, specifically, PrRP analogs: Chromolith RP-18e (Merck, Germany), a silica-based monolithic column (col. size 50 x 3 mm ID) and LEAP2(1-14) analogs: XBridge Premier BEH C18 (Waters, USA), particle size 2.5 µm, VanGuard Fit (col. size 50 x 2.1 mm ID). A gradient elution utilizing 0.1% HCOOH in H_2O and acetonitrile, respectively, was applied. MS signal was measured in multiple reaction monitoring (MRM) mode.

Presented lipidized peptides have been studied extensively in related projects for biological aspects focused on food intake regulation (see elsewhere). Here, the plasma stability of the above mentioned PrRP and LEAP2 analogs were determined by LC-MS. In this context it is important to mention that the sample preparation method preceding LC-MS measurement of the lipopeptide stability in plasma must be developed for each lipopeptide individually. Usually, protein precipitation with various aqueous organic solvents provides an acceptable lipopeptide recovery. We verified that in some cases, specifically utilizing monolitic column Chromolith RP-18e, a direct "dilute and shoot" approach can be applied [1-2].

As can be seen in Figures 2 and 3 *in-vitro* stability of all the studied lipopeptides in plasma has been significantly enhanced with respect to the corresponding non-lipidized analogs. Lipidization proved to be an efficient means of plasma stability protraction. Besides, it is evident that a chemical structure of the linker used for lipidization has a significant influence on the lipopeptide stability. Lipidized peptides with TTDS linker provided relatively low plasma stability being only slightly better than for PrRP3.
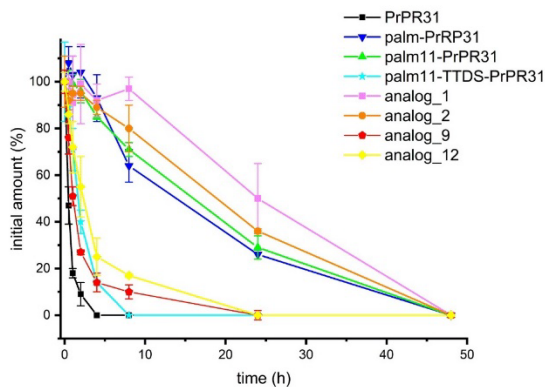
Fig. 2. Stability of PrRPanalogs in rat plasma.   *Fig. 3. Stability of LEAP2 analogs in rat plasma.*
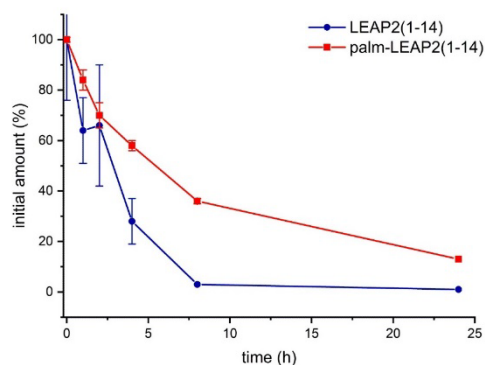
Acknowledgments

References

1. Zemenová, J, Sýkora, D., Freislebenová ,A., Maletínská, L. *Bioanalysis* **9**, 1319-1328 (2017), http://dx.doi.org/ 10.4155/bio-2017-0125
2. Zemenova, J. Sykora, D., Adamkova, H., Maletinska, L., Elbert, T., Marek, A., Blechova, M. *J. Sep. Sci.* **40**, 1032-1039 (2017), http://dx.doi.org/10.1002/jssc.201601141

Synthesis and Characterization of a Supramolecular DNA-Inspired Nanowire

Marta De Zotti[1,2] and Emanuela Gatto[3]

[1]Department of Chemical Sciences, University of Padova, Padova, I-35131, Italy; [2]Centro Interdipartimentale di Ricerca "Centro Studi di Economia e Tecnica dell'energia Giorgio Levi Cases", Padova, I-35131, Italy; [3]Department of Chemical Science and Technologies, University of Rome Tor Vergata, Rome, 00133, Italy

Introduction

In Nature, electron transfer (ET) is performed by means of biomolecules. Proteins and DNA are known to effectively mediate ET, but they offer little stability outside their physiological environment. Natural peptides based on sterically hindered, non-coded α-amino acids are biopolymers that possess - even when short - well-defined helical structures, remarkably stable under extreme environmental conditions. We recently reported a bioinspired approach based on nucleobase pairing, which allows helical peptides to self-organize into molecular wires [1]. We used a helical undecapeptide analog of the natural peptide trichogin GA IV, in which four glycines were replaced by four lysines to reduce flexibility, and the *N*- and *C*-termini were functionalized with thymine and adenine, respectively. Through thymine-adenine hydrogen bonds, we assembled the biodevice onto a gold electrode, capping it with Porphyrin(Zn)-Thymine. Under illumination, the peptide-based supramolecular system could generate current [1] and was found to be very stable over time, also in contact with a solution.

We also describe the effect on ET-through-peptide of a pH-controlled, reversible 3_{10}- to α-helix conversion, with a focus on the effect of the pH-induced conformational change on photocurrent efficiency [2]. The biomolecular devices were characterized by electrochemical and spectroscopic techniques, and were able to generate current under illumination, with an efficiency that is the highest recorded so far with biomolecular systems.

Here, we report the synthesis of the peptide Thymine-[$K^{2,5,6,9}$]tric-Adenine (T-tric-A, Figure 1) and the characterization of its self-assembly in several environments. The primary structure of the peptide is: Thymine-CH$_2$-CO-Aib-Lys-Leu-Aib-Lys-Lys-Leu-Aib-Lys-Ile-Leu-NH-(CH$_2$)$_2$-NH-CO-CH$_2$-Adenine.

Results and Discussion

Trichogin is a naturally-occurring peptaibol, with three Aib residues in its sequence, which make it adopt a well-defined helical conformation [3]. On the other hand, Aib is also a sterically-hindered and poorly-reactive amino acid, therefore the synthesis of Aib-containing peptides needs special adjustments, such as double-coupling reactions both for its insertion and - especially - that of the following residue, since the steric hindrance is more felt when Aib is performing the nucleophilic attack. Nonetheless, Aib at position 8 - and Leu at position 7, as well - are successfully coupled by a single coupling reaction mediated by Oxyma pure and DIC (diisopropylcarbodiimide). This has been found effective for Aib residues at an early stage of the synthesis. The remaining Aib-involving steps have been performed by means of double-coupling reactions, with quantitative yields. Thymine-COOH has been coupled to Aib at position 1 by three subsequent coupling reactions. We tried different active agents, observing a better performance in terms of yield and purity with Oxyma/DIC than with HATU.
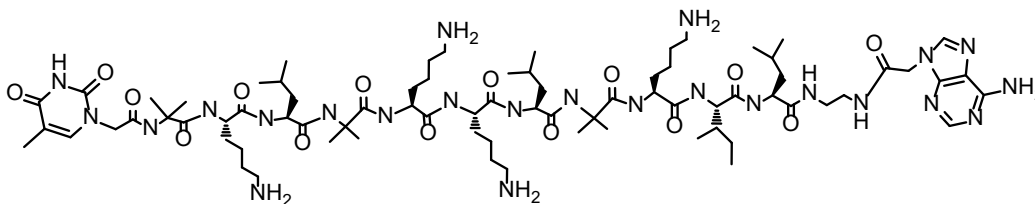
Fig. 1. Chemical structure of peptide T-tric-A.

After cleavage from the resin under mild acidic conditions (1,1,1,3,3,3-hexafluoroisopropanol 30% in CH$_2$Cl$_2$), Adenine-COOH was successfully linked to the C-terminal primary amine of the peptide, by reaction in solution, using 1-Hydroxy-7-azabenzotriazole (HOAt) and N-Ethyl-N'-(3-dimethylaminopropyl)carbodiimide (EDC) as active agents. After Boc removal by treatment with a 3M HCl solution in methanol, the peptide was purified by medium pressure liquid chromatography (Biotage Isolera Prime).

We studied the self-assembly of T-Tr(Lys)-A as a function of peptide concentration by circular dichroism. A R value ($\theta_{222}/\theta_{204}$) above 1 is diagnostic of the presence of aggregation. Our CD analysis (Figure 2) registered aggregation (R>1) at concentrations above 0.2 mM. TEM analysis performed on the same solutions analyzed by CD confirmed that at R>1 molecular wires are formed. Our Diffusion-ordered spectroscopy (DOSY) experiment also highlighted the presence of large, self-assembled structures in solution at a high peptide concentration (Figure 3).
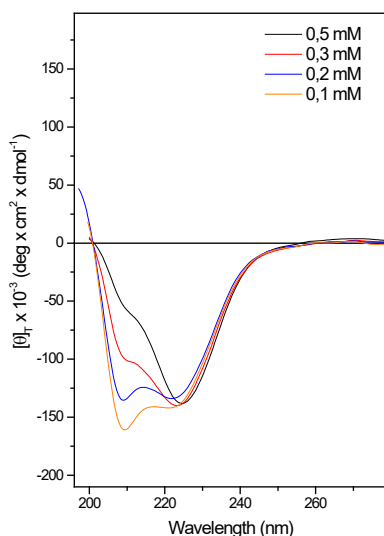
Fig. 2. CD spectra of T-tric-A as a function of increasing peptide concentration in 10:1 v/v acetonitrile/basic water (NaOH 0.1M) solution.

The presence of four Lys residues makes the peptide pH-sensitive [2,4].
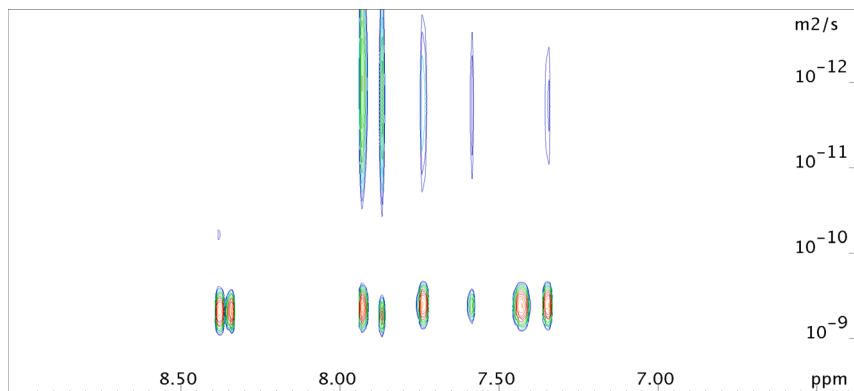
Fig. 3. DOSY map obtained for peptide T-tric-A (2mM in CD$_3$CN/D$_2$O 9:1; 400 MHz, 278K).

We previously reported that Lys-containing trichogin analogs were able to switch their conformation reversibly between fully-developed α-helix and 3$_{10}$-helix in response to pH variation. We thus studied by CD and TEM the self-assembled peptide-based structures at different pH values.
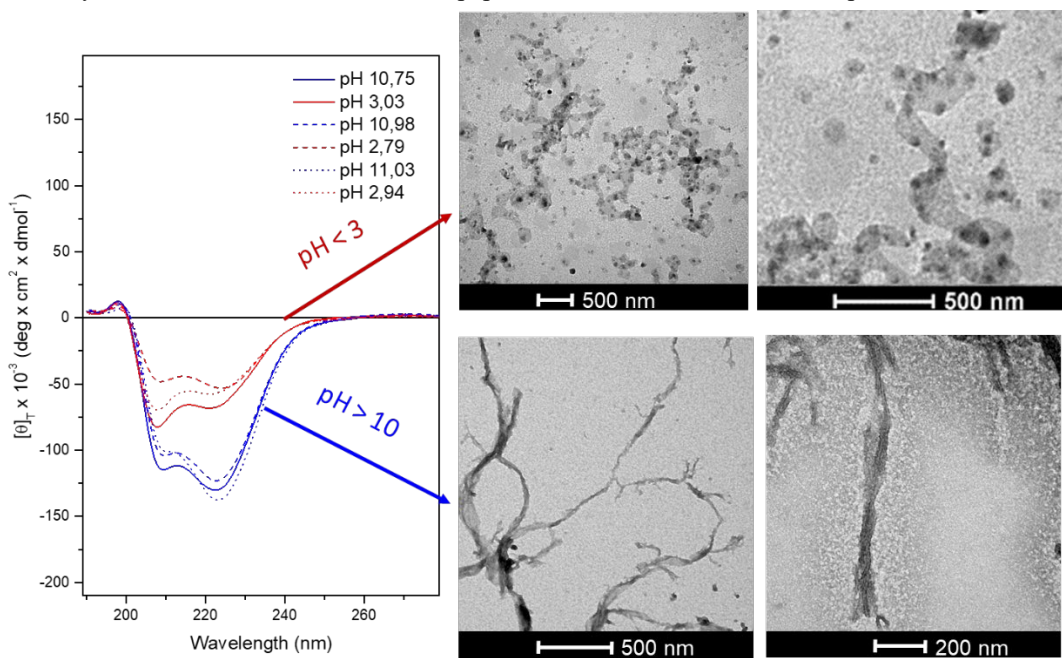
Fig. 4. CD spectra obtained for peptide T-tric-A at different pH values, obtained by switching the pH into the same cuvette [0.3 mM in ACN/NaOH 0.1M 10:1 (starting point)]. TEM images: T-tric-A 0.3 mM in: (i) ACN/(NaOH 0.1mM) 10:1 solution pH 11 (below); (ii) + 2 μl HCl 3M (pH 3) (above).

Figure 4 shows the results from our combined CD and TEM analysis, performed at different pH values, obtained by adding NaOH/HCl alternatively into the CD cuvette and performing both analysis on the same peptide solution. The reversible, conformational transition already detected on the single peptide seems to take place also in the supramolecular assembly, making it a kind of molecular spring. Despite the low peptide concentration - suitable for CD analysis but not for good TEM images - we could unambiguously detect and confirm the presence of the twisted fibers at both pH values tested.

In conclusion, we performed the synthesis of the peptide T-tric-A. The characterization of its self-assembly in several environments highlighted the peptide propensity to form molecular wires, maintaining the ability to reversibly switch its 3D-structure between two helical conformations of different length in response to pH variations.

Acknowledgments

References

1. Gatto, E., et. al. *Angew. Chem. Int. Ed*. **58**, 7308 (2019), https://doi.org/10.1002/anie.201901683
2. Kubitzky, S., et al. *Chem. Eur. J.* **27**, 2810 (2021), https://doi.org/10.1002/chem.202004527
3. Peggion, C., et al. *J. Pept. Sci.* **9**, 679-689 (2003), https://doi.org/10.1002/psc.500
4. De Zotti M., et al., *Org. Biomol. Chem*. **10**, 1285-1299 (2012). https://doi.org/10.1039/C1OB06178J

Novel Antimicrobial Peptide Fluoroquinolone Conjugates

John R. F. B. Connolly, Deirdre Fitzgerald-Hughes, and Marc Devocelle

RCSI University of medicine and health sciences, Department of chemistry, 123 St Stephen's green, Dublin 2

Introduction

Antimicrobial peptides (AMPs) have become of extreme interest over recent decades due to their natural origins, fluidity of amino acid sequences and low promotion of bacterial resistance pathways [1,2]. Unfortunately, these properties, particularly the low levels of bacterial resistance, are not wide spread in small molecule classes of antimicrobial agents, such as fluoroquinolones (FQs) [3]. Research into whether AMPs could enhance small molecule antibiotic agents has recently started to be investigated through either conjugation of small molecule agents or combination studies seeking synergistic properties [4-9]. However, these studies are limited in number and scope as many only provide a single conjugate of FQs to an AMP/amino acid candidate or produce combined dose regimes, with no covalent modifications. In addition, these studies generally have small sample sizes and results, such as MIC values, are varied. Building on this work, a novel fluoroquinolone-AMP conjugate consisting of several repeating units of ciprofloxacin has been produced. The rationale of this approach is to use the cationic charge and hydrophobic properties of ciprofloxacin, two essential traits of the AMPs' amphiphilic topology, while also keeping some of its original antibacterial activity. The candidates will be tested against gram-positive and gram-negative bacteria to assess their activity, as well as further studies to reveal mechanistic action of the peptide. They will aim in particular to evaluate if activity within the ciprofloxacin remains, once part of a larger AMP structure, or whether any advantages on conjugating FQs to AMPS, such as higher salt concentration tolerance or lower proteolytic susceptibility previously published about [4], are also present in these fluoroquinolone-AMP candidates.

Results and Discussion

To test this hypothesis a simple peptide sequence was designed to minimally retain two units contributing to the amphiphilic topologies and net cationic charge AMPs generally possess. As can be seen in Figure 1 the Cip residue is bound through the carboxyl group to the lysine ε-amino group. Arginine was chosen as a cationic unit while Cip was chosen as a cationic and hydrophobic unit, both contributing to the overall net charge. Ciprofloxacin was bound through the carboxyl group as this method of conjugations is well documented in the literature for FQs [4,6,9,10] so would help expedite the formation of initial candidates. A decamer with sequence H-[Lys(Cip)Arg]$_5$-NH$_2$ (**1**) was successfully synthesised. However, a significant byproduct was also detected. Coupling of the Cip unit to the free amine of a resin-bound peptide was difficult due to the length of the peptide chain causing steric bulk for amino acids close to the *C*-terminus and the inactivity of the carboxyl group owed to conjugation within the bicyclic ring. This difficulty required multiple coupling procedures with a particularly active coupling reagent, in this case HATU. Unfortunately, this uronium reagent can also react with the free amine of the lysine if reaction of the carboxyl group is not kinetically favourable. This leads to a guanylation to a lysine's ε-amino group which can been seen in Figure 1 producing **2** [11]. This impurity could not be separated out via HPLC completely, therefore for initial susceptibility testing a combination of **1** and **2** was evaluated against *E. coli* ATCC 25922 and *S. aureus* ATCC 25923. Minimum Inhibitory Concentration (MIC) for these strains were higher than the highest concentration tested (256 μg/mL). This suggested that the amphiphilic topology of an AMP was not being met and the net charge of these peptides were too high. Interestingly, the parent peptide consisting of H(ArgTrp)$_5$NH$_2$ (**3**) also had a relatively high MIC against the same strains of *S. aureus* and *E. coli* with concentrations of 16μg/mL and 32-64μg/mL respectively. A new candidate was then hypothesised to increase hydrophobicity and include more varied residues, as in the sequence H-Lys(Cip)IleArgLys(Cip)ValArgLys(Cip)IleArg-NH$_2$ (**4**). Complete sequence assembly was performed to yield the resin-bound Fmoc-Lys(Mtt)IleArg(Pbf)Lys(Mtt)ValArg(Pbf)Lys(Mtt)Ile-Arg(Pbf)-Resin (**5**). Coupling of the Cip residue via HATU through the free ε-amino group was attempted by manual solid phase synthesis. Again, due to the aforementioned challenges with coupling
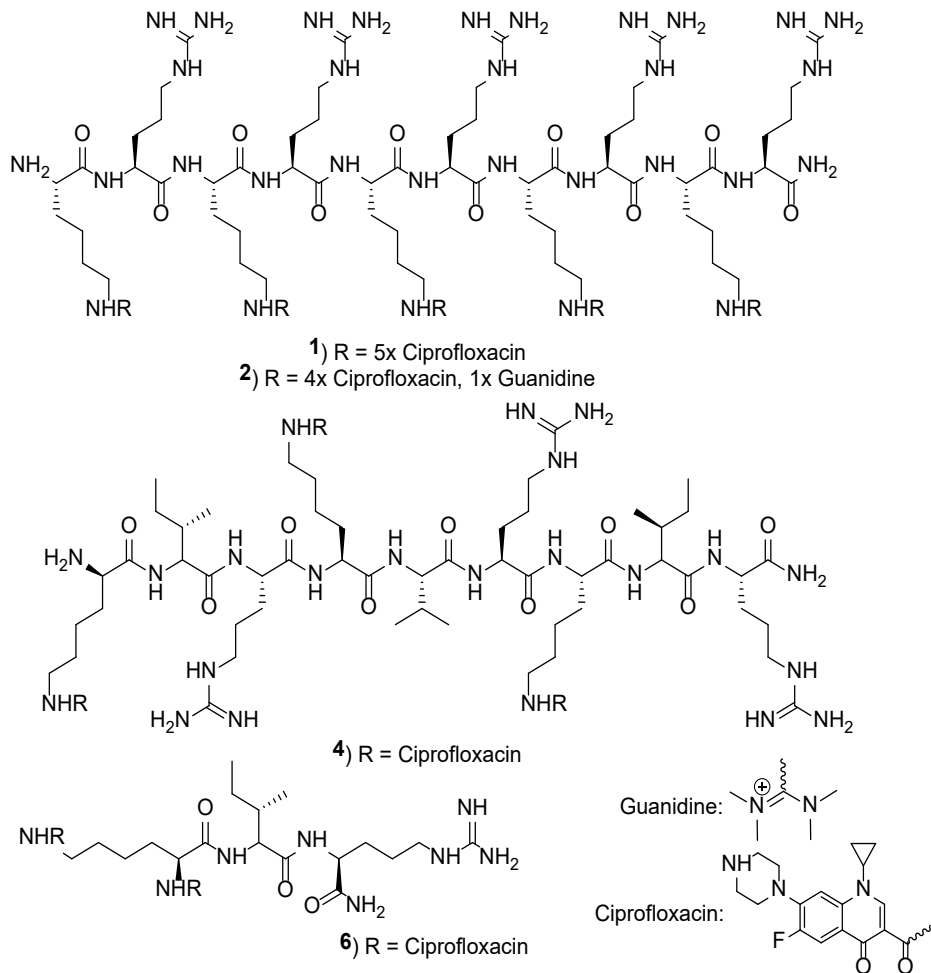
Fig. 1. Chemical structure of AMP-FQ candidates Top) 1/2, middle) 4 and bottom) 5 with corresponding side chains present during synthesis.

as well as the increased steric hindrance of the branched residues, isoleucine and valine, only single and double Cip units were present, with no fully conjugated three Cip unit peptide detected in Figure 2. Several different methods were trialled to address this issue. Firstly, preactivation of the carboxyl group via an N-hydroxysuccinimide (NHS) ester was pursued. Although several attempts were made, no product was detected for the NHS ester of either BOC or FMOC protected Ciprofloxacin. Conventional coupling reagents were then pursued including HATU and PyBrop. In addition to coupling reagents, Ciprofloxacin was also converted into the acyl chloride *in situ* and then reacted with the free ε-amino group. After multiple couplings via each method, no amidation of the latter group was observed for all three sites. A new synthetic pathway was then devised to produce the 9-mer sequence stepwise, with the first three amino acids being coupled forming a tripeptide with lysine at the *N* terminus. The Cip unit would then be conjugated to the terminal lysine R group and upon successful coupling the peptide backbone would be extended until the next lysine were the Cip coupling would be repeated. This would produce the nonamer in three tripeptide steps and ensure the peptide chain causes minimal steric hindrance as the free ε-amino would always be on the *N* terminus.

As a proof of concept, the tripeptide H-Lys(Mtt)IleArg(Pbf)-Resin bound (**6**) was synthesised and coupled to Cip. Preliminary results seem encouraging with conjugates containing a single Cip unit and double Cip unit (due to an unwanted loss of the *N*-terminal Fmoc group, caused by the automated synthesis) on the ε and α-amino groups. However, the by-product containing one Cip unit and one guanidine unit was also identified when using HATU.

Fig. 2: MALDI-TOF positive ion spectra containing derivatives of top) **3** *and bottom)* **4** *and* **5**.

Acknowledgments

References

1. Scott, R. W.; Tew, G. N. *Curr Top Med Chem* **2017**, *17* (5), 576–589, https://doi.org/10.2174/1568026616666160713130452
2. Das, P. et al. *Nature Biomedical Engineering* **2021**, 1–11, https://doi.org/10.1038/s41551-021-00689-x
3. Tyson, G. H.; Li, C.; Hsu, C.-H.; Bodeis-Jones, S.; McDermott, P. F. *Frontiers in Microbiology* **2019**, *10*, https://doi.org/10.3389/fmicb.2019.02826
4. Rodriguez, C. A. et al. *Front. Chem.* **2014**, *2*, https://doi.org/10.3389/fchem.2014.00071
5. Kampshoff, F. et al. *Antibiotics* **2019**, *8* (2), 60, https://doi.org/10.3390/antibiotics8020060
6. Ptaszyńska, N. et al. *International Journal of Molecular Sciences* **2020**, *21* (13), 4696, https://doi.org/10.3390/ijms21134696
7. Ptaszyńska, N. et al. *ACS Chem. Biol.* **2019**, acschembio.9b00538, https://doi.org/10.1021/acschembio.9b00538
8. Li, W. et al. *Chem. Soc. Rev.* **2021**, *50* (8), 4932–4973, https://doi.org/10.1039/D0CS01026J
9. Khairunnisa, A. G. et al. *Current Drug Delivery* **2015**, *12* (1), 108–114
10. Ahmed, M.; Kelley, S. O. *ACS Chem. Biol.* **2017**, *12* (10), 2563–2569, https://doi.org/10.1021/acschembio.7b00540
11. Vrettos, E. I. et al. *RSC Adv.* **2017**, *7* (80), 50519–50526, https://doi.org/10.1039/C7RA06655D

Design and Synthesis of Gonadotropin Releasing Hormone (GnRH) Peptide Analogues Conjugated with Anthraquinone for Selective Immunosuppression

Georgia Biniari[1], Agathi Nteli[1], Carmen Simal[1], Christos Markatos[2], Vlasios Karageorgos[2], Alexios Vlamis-Gardikas[1], George Liapakis[2], and Theodore Tselios[1]

[1]Department of Chemistry, University of Patras, 26504 Rion, Greece
[2]Department of Pharmacology, School of Medicine, University of Crete, 71003 Heraklion, Greece

Introduction

Gonadotropin Releasing Hormone (GnRH or LHRH) is a decapeptide responsible for the control and secretion of the gonadotropin hormones (LH and FSH) and therefore the regulation of the reproductive axis [1]. Altered GnRH peptide analogues have been used for the treatment of fertility problems and hormone-dependent cancer [1,2]. Drug delivery systems based on GnRH (GnRH conjugates) constitute a more targeted approach for the treatment of hormone-dependent cancer, compared to the effective but with serious side effects conventional chemotherapy protocols. The advantage of the targeted approach stems from the fact that tumor cells express GnRHR receptors in elevated levels compared to healthy cells [3,4]. The development of a novel and targeted cancer treatment with reduced side effects remains a challenge for the pharmaceutical industry. In this study, a modified anthraquinone molecule was conjugated with GnRH peptide analogues via a disulfide bond [4-7]. The overall aim is the selective binding of the peptide analogue to the GnRH receptors expressed in hormone-dependent cancer cells. Release of the cytotoxic compound in situ is expected via reduction of the disulfide bond by the thioredoxin system.

Experimental

Synthetic Procedures
Leucoquinizarin was used as the starting material for the synthesis of anthraquinone analogue and was modified for the insertion of a thiol group. The GnRH peptide analogues were synthesized step by step by conventional SPPS, following the Fmoc/tBu methodology using Ethyl Indole AM resin, in order to obtain the ethylamide *C*-terminal. The peptide analogues A and B were rationally designed and synthesized to simulate the structure of Leuprolide (agonist of GnRH). The conjugation between anthraquinone analogue and mutated peptide analogues was achieved via a disulfide bond (Figure 1).

Results

Analytical RP-HPLC and ESI-MS of synthesized conjugates
The purification and the identification of the analogues were achieved by Reverse Phase-High Performance Liquid Chromatography (RP-HPLC) and Electrospray Ionization Mass Spectrometry (ESI-MS) respectively (Figure 2).
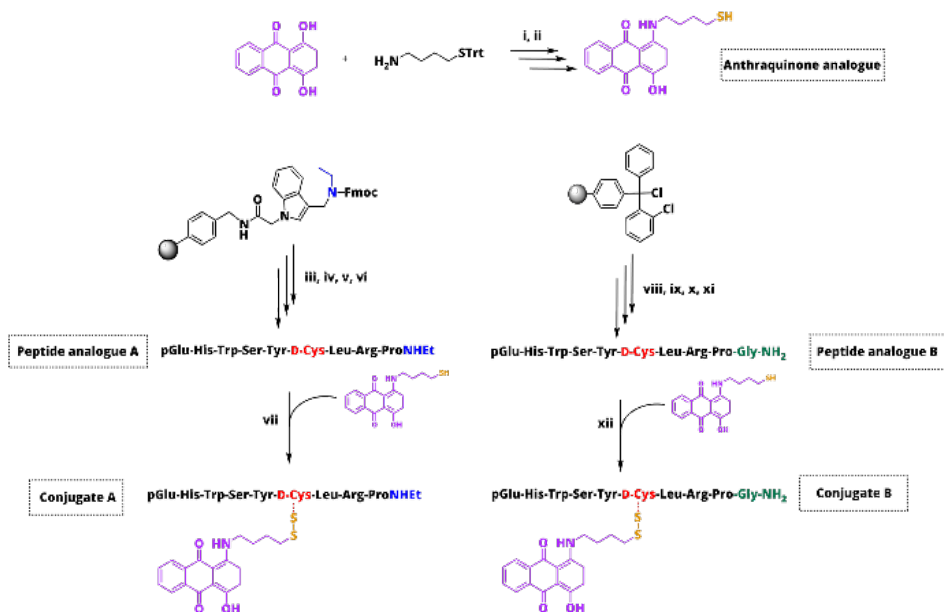
Fig. 1. Synthetic route of the final conjugates A and B. i) Modification of leucoquinizarin (a: EtOH, reflux; b: O₂); ii) Removal of Trt-protecting group (TFA/DCM/TES, 94:3:3); iii) Attachment of the first amino acid on the resin (Fmoc-Pro-OH, HOBt, DIC); iv) Synthesis of the desired peptide sequence, (a: 25% piperidine/DMF; b: Fmoc-AA-OH, HOBt, DIC); v) Peptide cleavage from resin (TFA/DCM, 1:1); vi) Removal of protecting groups (TFA/DCM/Anisole/H₂O, 90:7:2:1); vii) Formation of disulfide bond in DMSO/DIPEA; vii) Esterification of Fmoc-Rink Amide linker on the resin (DIPEA); viii) Synthesis of the desired peptide sequence, (a: 25% piperidine/DMF; b: Fmoc-AA-OH, HOBt, DIC); ix) Peptide cleavage from resin (DCM/TFE, 7:3); x) Removal of protecting groups (TFA/DCM/Anisole/H₂O, 95:2:2:1); xi) Formation of disulfide bond in DMSO/DIPEA.
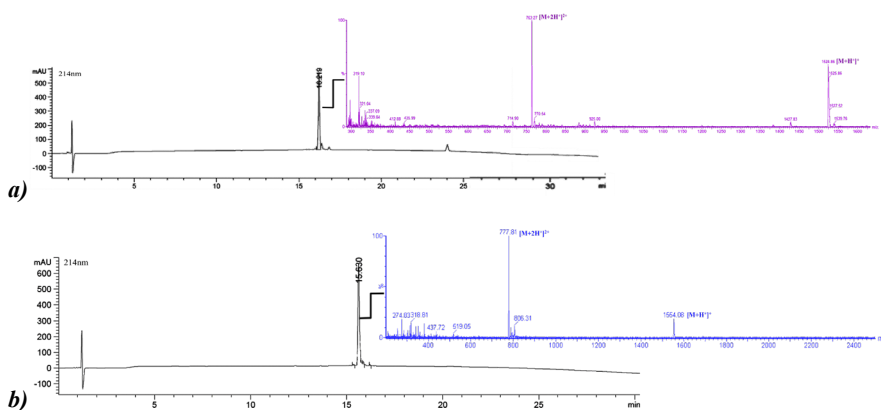
Fig. 2. Analytical RP-HPLC and ESI-MS of the synthesized a) final conjugate A; t_R: 16.22 min; Purity: 94%; MW=1524.78 and b) final conjugate B; t_R: 15.63 min; Purity: 97%; MW=1552.64. Column: Agilent ZORBAX C18; Conditions: 10%(AcN) - 100% (AcN) in 30 min.

	Leuprolide [DLeu⁶,ProNHEt⁹]GnRH	Final Conjugate A	Final Conjugate B
$LogIC_{50}$	-9.20	-9.16	-8.70
IC_{50} (nM)	0.64	0.69	2.00
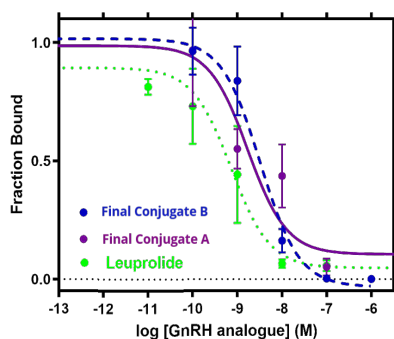
Fig. 3. Competition binding isotherms of synthesized conjugate A and B compared to Leuprolide.

Binding affinity assay

The binding affinity of the synthesized conjugates for the human GnRH receptor was determined using competition experiments in HEK 293 cells, while the [^{125}I-D-Tyr^6,His^5]GnRH and Leuprolide were used as radioligand and control respectively (Figure 3).

Conclusions

The synthesis of all analogues was achieved successfully without serious synthetic problems. The binding affinity showed that synthesized conjugates A and B interacted with GnRH receptor in a dose-dependent manner and they showed better binding score compared to Leuprolide. Moreover, the synthesized molecules are very promising as drug leads and could be used for further in vitro and in vivo evaluation against hormone-dependent cancer.

Acknowledgements

References

1. Schally, A.V., et al. *Biochem. Biophys. Res.Commun*. **43**(2), 393-399 (1971), https://doi.org/10.1016/0006-291X(71)90766-2
2. Laimou, D., et al. *Amino Acids* **39**(5), 1147-1160 (2010), https://doi.org/10.1007/s00726-010-0549-8
3. Emons, G., et al. *Gynecol. Oncol*. **133**(3), 427-432 (2014), https://doi.org/10.1016/j.ygyno.2014.03.576
4. Tzoupis, H., et al. *Cur. Med Chem*. **27**(36), 6136-6158 (2020), https://doi.org/10.2174/0929867326666190712165444
5. Sayyad, N., et al. *Eur. J. Med. Chem*. **166**, 256-266 (2019), https://doi.org/10.1016/j.ejmech.2019.01.041
6. Landys, K., et al. *Invest. New Drugs* **3**(2), 133-137 (1985), https://doi.org/10.1007/BF00174160
7. Tapeinou, A., et al. *Eur. J. Med. Chem*. **143**, 621-663 (2018), https://doi.org/10.1016/j.ejmech.2017.11.064

Analysis of Mannan (Polymannose)-Peptide Conjugate by Competitive ELISA

Areti Gkika[1], Maria-Eleni Androutsou[2], Pigi Katsougkraki[1], Alexios J. Aletras[1], and Theodore Tselios[1]

[1]Department of Chemistry, University of Patras, 26504 Rion Patras, Greece; [2]Vianex S.A., 18th km Athens- Lamia National Road, Nea Erythrea, 14671 Athens, Greece

Abstract

Multiple sclerosis (MS) is an autoimmune disease whereby the myelin of the central nervous system (CNS) is destroyed, leading to paralysis and serious health problems [1]. The main proteins of the membrane sheath of myelin are: i) myelin basic protein (MBP); ii) myelin oligodendrocyte glycoprotein (MOG), iii) myelin-associated glycoprotein (MAG) and iv) proteolipid protein (PLP) [2,3]. Immunodominant epitopes of myelin proteins are involved in pathogenesis of MS. Thus, the 35-55 sequence of MOG protein is an autoantigen of MS and induces *in vivo* Experimental Autoimmune Encephalomyelitis (EAE-animal model of MS) [3]. Moreover, the conjugate of this epitope with mannan (polysaccharide) was found to inhibit the EAE symptoms and could be a new and promising approach for MS treatment [4,5]. In the present study, a competitive ELISA was developed using the MOG_{36-55} peptide for the coating of polystyrene microtiter plates, polyclonal antibodies produced in rabbits after immunization with this peptide, and the mannan-MOG conjugates as competitors. The first approach was to test the stability of mannan-MOG conjugates during storage conditions and their potency after modifications at the peptide sequence that may occur spontaneously. The developed methodology is possible to be used in further analysis of mannan – peptide conjugate in combination with *in vivo* experiments

Methods

Synthesis and coupling of the immunodominant epitopes to mannan

The studied peptides were synthesized by Fmoc/tBu methodology using 2-chlorotrityl chloride resin (CLTR-Cl). The synthesized peptides were purified and identified by semi preparative HPLC and mass spectrometry (ESI-MS) respectively with a purity yield more than 98%. Mannan (poly-mannose from Saccharomyces Cerevisiae), was oxidized to poly-aldehyde using sodium periodate ($NaIO_4$) and purified by size exclusion chromatography (Sephadex G-25 Medium column). The purified oxidized form of mannan was mixed with the peptides and incubated at room temperature for 48 hours. The conjugation of aldehydes, after the oxidation of mannan, with the amines of the Lys residues {$[KG]_5$ linker} of the peptides was achieved via base Schiff formation, while the completion of the conjugation reaction was confirmed by sodium dodecyl sulphate-polyacrylamide gel electrophoresis (SDS-PAGE) [5].

Evaluation of the stability of mannan-peptide conjugates with ELISA

A competitive ELISA was developed using $[KG]_5MOG_{35-55}$ peptide with the sequence H-Lys-Gly-Lys-Gly-Lys-Gly-Lys-Gly-Lys-Gly-Met[35]-Glu[36]-Val[37]-Gly[38]-Trp[39]-Tyr[40]-Arg[41]-Pro[42]-Pro[43]-Phe[44]-Ser[45]-Arg[46]-Val[47]-Val[48]-His[49]-Leu[50]-Tyr[51]-Arg[52]-Asn[53]-Gly[54]-Lys[55]-OH. Affinity purified polyclonal antibodies against peptide MOG_{36-55} (sequence 36-55 of $[KG]_5MOG_{35-55}$) were produced in rabbits via immunization process by Davids Biotechnologies GMBH (Germany), while the epitope recognized by the antibodies is located into sequence 38-49.

The developed ELISA includes the following procedure:
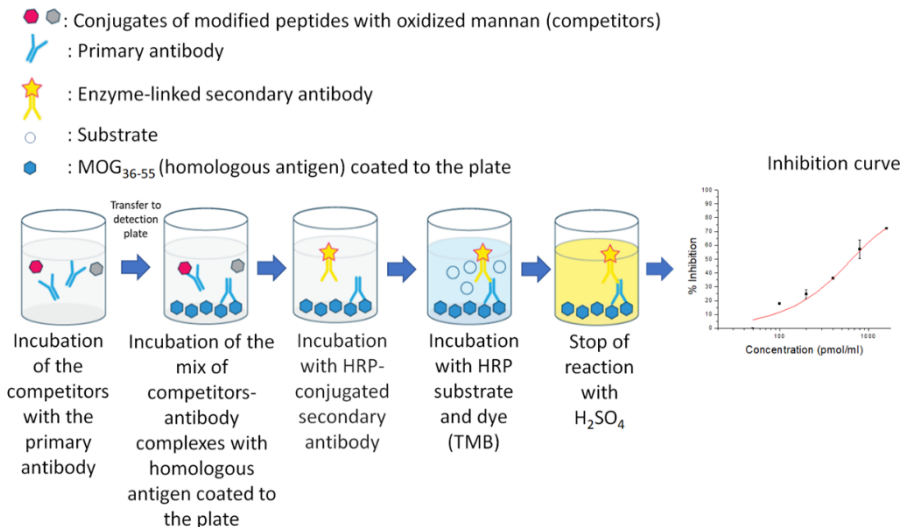
Several modifications of peptide sequence may occur during the peptide synthesis and storage. For the purpose of this study, we have also synthesized and analyzed the oxidized Met in MOG_{35-55} epitope conjugated to mannan. Thus, the following conjugates were studied:

i) Man^{ox} -$[KG]_5MOG_{35-55}$

ii) Man^{ox} - $[KG]_5MOG_{35-55}(Met(O)^{35})$

iii) Man^{ox} - $[KG]_5MOG_{35-55}$, stored at -20°C for at least 36 months

The ability of anti-MOG_{36-55} antibody to react with oxidized mannan (cross-reactivity) was further examined, to investigate the detection of any false-positive result. The results demonstrated that the antibody does not recognize the oxidized mannan.

The Coefficient of Variation (CV) was calculated to be 14.56% and 4.45% for Inter and Intra assay, respectively, so the competitive ELISA is repeatable and accurate and can be used to evaluate the stability of the conjugate.

Results

The study of the conjugates by competitive ELISA, showed that possible alterations of MOG_{35-55} epitope (chemical and/or conformational changes) affect the recognition from the specific anti-MOG_{36-55} antibody (Figure 1).

- The conjugate of mannan with wild type peptide led to a range of inhibitions 0-80% for the studied concentrations (■, red line).
- The Met oxidation is a common mutation that is easily achieved during the deprotection step of peptides. This mutation leads in enhanced reaction for all the examined concentrations of the conjugate Man_{ox}-$[KG]_5MOG_{35-55}(Met(O)^{35})$ with anti-MOG_{36-55} antibody and subsequently to a reduced range of inhibition 35-70% (▶, purple line).
- The examined conjugate when stored at -20°C, led to a lower binding affinity between the anti-MOG_{36-55} antibody and the conjugate (at lower concentrations) and subsequently to a reduced range of inhibition 25-55% (□, green line).

Except for the chemical modifications, the reduced range of inhibition of studied peptides conjugated with mannan in comparison with the wild type may occurs due to conformational changes of conjugates that reduce the recognition of the peptide by the antibody.
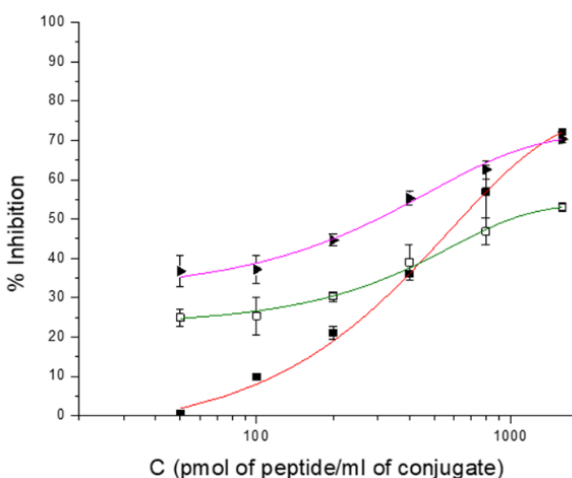
Fig. 1. Inhibition curves of conjugates of oxidized mannan with the modified peptide analogues of MOG_{35-55} using polyclonal antibodies against MOG_{36-55} and increased concentration (50-1600pmol peptide/ml) of: Man^{ox} -$[KG]_5MOG_{35-55}$ (■, red line); $Manox$ - $[KG]_5MOG_{35-55}$, stored at -20ºC (□, green line); $Manox$ - $[KG]_5MOG_{35-55}(Met(O)^{35})$ (►, purple line). Each data point represents the mean value of a triplicate measurement ± SD.

The study of the conjugates by competitive ELISA, showed that possible alterations of MOG_{35-55} epitope (chemical and/or conformational changes) affect the recognition from the specific anti-MOG_{36-55} antibody (Figure 1).

Conclusions

The mannan-$[KG]_5MOG_{35-55}$ conjugate is of great interest in the fight against MS and is a promising candidate for clinical studies [4,6]. The developed methodology is sensitive and reliable and could be used to control mutations of peptide sequence during storage.

Acknowledgments

References

1. Mantzourani, E.D., et al. *Curr. Med. Chem*. **12**, 1521-1535 (2005), https://doi.org/10.2174/0929867054039053
2. Androutsou, M.E., et al. *Med. Chem*. **14**, 120-128 (2018), https://doi.org/10.2174/1573406413666170906123204
3. Amor, S., et al. *J. Immunol*. **153**, 4349-4356 (1994)
4. Tseveleki, V., et al. L. *Exp Neurol*. **267**, 254-267 (2015), https://doi.org/10.1016/j.expneurol.2014.10.019
5. Tapeinou, A., et al. *Anal Biochem*. **485**, 43-45 (2015), https://doi.org/10.1016/j.ab.2015.06.010
6. Dagkonaki, A., et al. *Front. Immunol*. **11**, 1-18 (2020), https://doi.org/10.3389/fimmu.2020.575451

Peptaibol Production and Characterization from *Trichoderma Asperellum* and their Action as Biofungicide

Pamela Alfaro-Vargas[1], Alisson Bastos-Salas[1,2], Rodrigo Muñoz-Arrieta[1], Reinaldo Pereira-Reyes[3], Mauricio Redondo-Solano[2], Julián Fernández[4], Aníbal Mora-Villalobos[1], and José Pablo López-Gómez[1,5]

[1]*National Center for Biotechnological Innovations, San José, 1174-1200, Costa Rica;* [2]*Faculty of Microbiology, University of Costa Rica, San José, 11501, Costa Rica;* [3]*National Nanotechnology Laboratory, San José, 1174-1200, Costa Rica;* [4]*Instituto Clodomiro Picado, University of Costa Rica, San José, 11501, Costa Rica;* [5]*Microbiome Biotechnology Department, Leibniz Institute for Agricultural Engineering and Bioeconomy, Potsdam,14469, Germany*

Introduction

Peptaibols (P_{aib}) are a large family of bioactive peptides composed of 7 to 20 amino acid residues (linear or cyclic) [1,2]. P_{aib} are characterized by the presence of a high proportion of 2-aminoisobutyric acid (Aib), an acetyl or acyl group in the *N*-terminal residue and a *C*-terminal amino alcohol [3,4]. These peptides are assembled by a multienzyme complex called non-ribosomal peptide synthetases (NRPSs), which allows the incorporation of non-proteinogenic amino acids such as Aib [1,5,6]. Their amphipathic nature allows the formation of permanent transmembrane pores that causes the exchange of cytoplasmic material and eventual cell death [2,7].

The bioactivity of P_{aib} against parasites, viruses, bacteria, and pathogenic fungi has previously been reported [1,2]. In addition, its bioactivity has been proved in therapies against cancer, Alzheimer, and some human and animal diseases thanks to their antifungal, antitrypanosomal and anthelmintic activity [2,3,5,7,8].

Trichoderma is one of the most isolated and studied ascomycetes due to its agro-industrial importance as a biocontrol organism and producer of secondary metabolites with biological activity like P_{aib} [9,10]. Some *Trichoderma* strains are currently being used, and even commercialized, as biocontrollers because of their antimicrobial properties [11,12]. However, the whole microorganism is commercialized, not the active compound (P_{aib}). Optimizing the production and isolation of P_{aib} is critical when only the pure active component is required, such as in biomedical applications e.g., the treatment of cancer or Alzheimer [5,8,13]. Likewise, purified P_{aib} could be beneficial in agricultural applications such as biocontrol in post-harvest products, where it is better to apply a treatment free of microorganisms to avoid contamination of the final product.

The present work aimed to produce P_{aib} for their extraction and characterization as a potential biofungicide. The work included the optimization of fungal growth conditions for P_{aib} production. Afterward, mass-spectrometry techniques were applied for the identification and sequencing of P_{aib}. In addition, the biological effect of the biofungicide was evaluated against four phytopathogenic fungi *in vitro* and *in vivo* in tomatoes infected with *Alternaria alternata*. Furthermore, electron microscope images were used to study the effect of P_{aib} on the structure and morphology of the treated fungi.

Results and Discussion

Optimization of *T. asperellum* fermentation for P_{aib} production was carried out to determine the best carbon source, additive amino acid, elicitor and their optimal concentrations. P_{aib} production was optimized in flask by adding sucrose, 2-aminoisobutyric acid, and *Fusarium oxysporum* cell debris. Figure 1 shows the surface response graph obtained with the central composite model where the maximum point of P_{aib} production is located at 2.634 g/L Aib and 0.866 g/L *F. oxysporum* with 30 g/L sucrose.

P_{aib} produced were purified, sequenced and identified by HPLC coupled to mass spectrometry. The mass spectra showed the presence of ions characteristic of trichotoxins with values between 1676 m/z and 1768 m/z. The fragments detected corresponded to ions with m/z 1676, 1691, 1704, 1705, 1718, 1726, 1742 and 1768. Six P_{aib} were identified as trichotoxins of 18 amino acid residues. The general sequence obtained corresponded to Ac-Aib-Gly-Aib-Lxx-Aib-Gln-Aib-Aib-Aib/Ala-Ala-
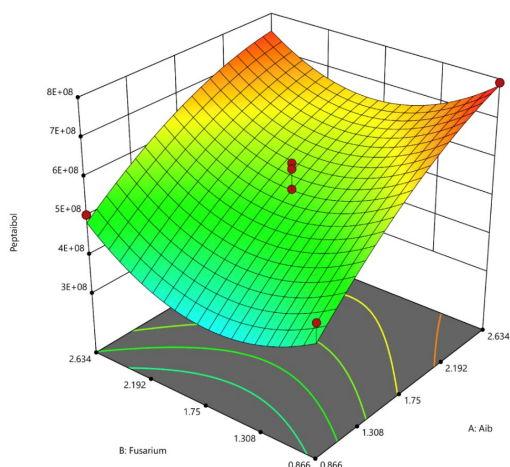
Fig. 1. Surface response graph of the central composite model generated for the optimization of P_{aib} produced in the fermentation of T. asperellum.

Aib/Ala-Aib-Pro-Lxx-Aib-Aib/Vxx-Gln/Glu-Valol, differences are observed in the sequences in the positions 9, 11 and 16 (Table1).

Table 1. Differences between the sequences of the six trichotoxins of the P_{aib} produced by T. asperellum. Vxx:valine/isovaline.

Trichotoxin	m/z	9	11	16
T5D2[1]	1676	Ala	Ala	Aib
1690	1691	Ala	Ala	Vxx
1703A[3]	1704	Aib	Ala	Vxx
A-40[2]	1705	Aib	Aib	Aib
1717A[3]	1718	Aib	Aib	Vxx
A-50 G[1]	1726	Aib	Ala	Vxx

Source: [1][14], [2][15], [3][16]

The biological activity of the P_{aib} extract was evaluated in *vitro* against four phytopathogenic fungi. Antifungal activity assays proved the efficiency of the P_{aib} extract to inhibit the growth of *Colletotrichum gloeosporioides*, *Botrytis cinerea*, *A. alternata* and *F. oxysporum* with a growth inhibition of 92.2, 74.3, 58.4 and 36.2%, respectively (Figure 2). Additionally, the extract completely inhibited the germination of *A. alternata* spores on tomatoes (Figure 3). The tomatoes treated with the extract showed no growth of the fungus, even after 15 days which suggests that the P_{aib} extract is not only effective in the short term but that it can show a continuous inhibitory effect even after two weeks. The incidence of the disease in tomatoes treated with the P_{aib} extract was 0% (same as with clotrimazole), while the untreated fruit (extract without P_{aib}) showed a 92.5% incidence of infection.

SEM results showed how P_{aib} generates damage in the morphology of hyphae and spores of the treated fungi. The images showed noticeable differences between the structures of the fungi treated with P_{aib} and the control (Figure 4). While the control showed hyphae with smooth surfaces and normal conidia, all the images of the treated fungi showed dehydrated hyphae with granules and an evident damage to the fungus wall. These results indicate that the P_{aib} extract could be used as a growth inhibitor against phytopathogenic fungi of agricultural relevance.

Results from this study suggest that environmental soil fungus from Costa Rica may represent an interesting source of known and new P_{aib} and antimicrobial compounds of biotechnological interest. Future studies may incorporate the determination of effective application levels in the field, the validation of proposed treatment against other species and strains and best use strategy on the product.
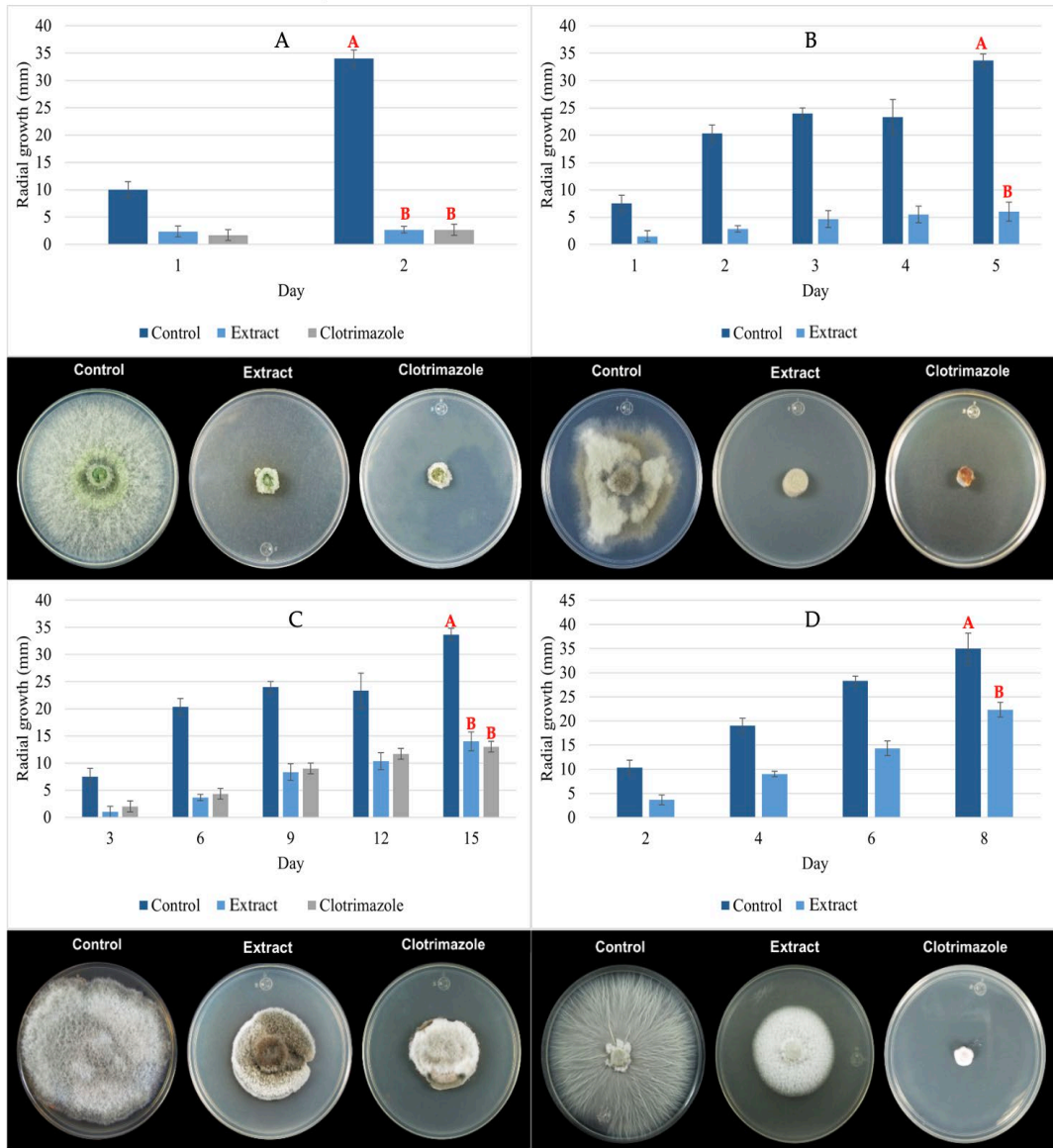
Fig. 2. Inhibition effect of P$_{aib}$ against mycelial growth of (A) C. gloeosporioides, (B) B. cinerea, (C) A. alternata and (D) F. oxysporum on PDA media after treatment with 800 µg mL^{-1} of P$_{aib}$ extract. Different letters represent significant differences between treatments.
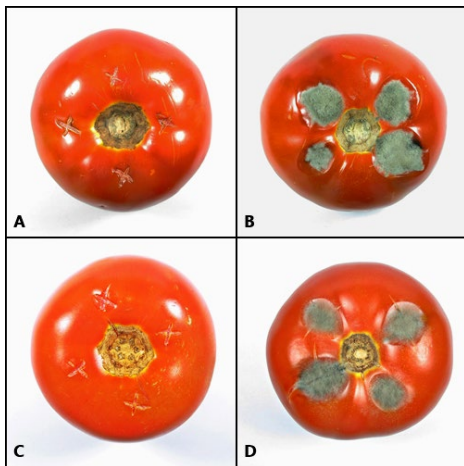
Fig. 3. Effect of P_{aib} on growth of A. alternata in tomatoes 8 days after spore inoculation and application of treatment. (A) extract with P_{aib}, (B) control, (C) clotrimazole, and (D) sterile distilled water.
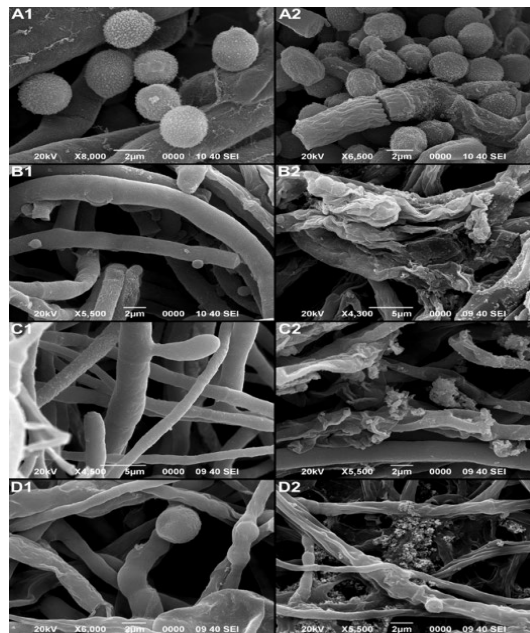
Fig. 4. SEM images showing the effects of P_{aib} over the morphology of untreated fungus (1) and fungi treated with P_{aib} (2). (A)C. gloeosporioides, (B) B. cinerea, (C) A. alternata and(D) F. oxysporum.

Acknowledgments

References

1. You, J., et al. *Proc. Natl. Acad* **114**, E8957-E8966 (2017), https://doi.org/10.1073/pnas.1707565114
2. Das, S.,et al. *Arch. Biochem. Biophys* **658**,16-30 (2018), https://doi.org/10.1016/j.abb.2018.09.016
3. Marik, T., et al. *Chem. Biodivers* **14**, (2017), https://doi.org/10.1002/cbdv.201700033
4. Zeilinger, S., et al. *Trichoderma Research* 39-55 (2020), https://doi.org/10.1016/B978-012 819453-9.00002-7
5. Degenkolb, T., et al. *Chem. Biodiver.* **5**, 671-680 (2008), https://doi.org/10.1002/cbdv.200890064
6. Guha, S., et al. *Chem. Rev.* **119**, 6040-6085 (2019), https://doi.org/10.1021/acs.chemrev.8b00520
7. Daniel, J., et al. *Antibiot.* **60**, 184-190 (2009), https://doi.org/10.1038/ja.2007.20
9. Marik, T., et al. *Front. Microbiol.* **10,** (2019), https://doi.org/10.3389/fmicb.2019.01434
10. Yang, P., et al. *Biocontrol Sci. Technol.* **00**, 1-16 (2017), https://doi.org/10.1080/09583157.2017.1318824
11. Vinale, F., et al. *Soil Biol. Biochem.* **40**,1-10 (2007), https://doi.org/10.1016/j.soilbio.2007.07.002
12. Mukherjee, P., et al. *Rev. Phytopathol.* **51**,105-129 (2013), https://doi.org/10.1146/annurev-phyto-082712 102353
13. Shi, M., et al. *Mol. Cancer* **9**, 1-15 (2010), https://doi.org/10.1186/1476-4598-9-26
14. Brito, J., et al. *Korean Phys. Soc.* **3**, 1-10 (2014), https://doi.org/10.1186/2193-1801-3-600
15. Bruckner, H., et al. *Biochim. Biophys.* **827**, 51-62 (1985), https://doi.org/10.1016/0167-4838(85)90100-1
16. Chutrakul, C., et al. *Chem. Biodivers.* **5**, 1694-1706 (2008), https://doi.org/10.1002/cbdv.200890158

Novel AChE Inhibitory Peptides with Application in Aquaculture: A Bioinformatic Approach Through QSAR

Tanya Román[1,2], Constanza Cárdenas[2], Claudio Álvarez [3,4], Paula Santana[5], and Fanny Guzmán[2]

[1]*Programa de Doctorado en Biotecnología Pontificia Universidad Católica de Valparaíso y Universidad Técnica Federico Santa María, Chile;* [2]*Núcleo de Biotecnología Curauma, Pontificia Universidad Católica de Valparaíso, Chile;* [3]*Laboratorio de Fisiología y Genética Marina (FIGEMA), Centro de Estudios Avanzados en Zonas Áridas (CEAZA), Chile;* [4]*Facultad de Ciencias del Mar, Universidad Católica del Norte, Chile;* [5]*Instituto de Ciencias Químicas Aplicadas, Facultad de ingeniería, Universidad Autónoma de Chile*

Introduction
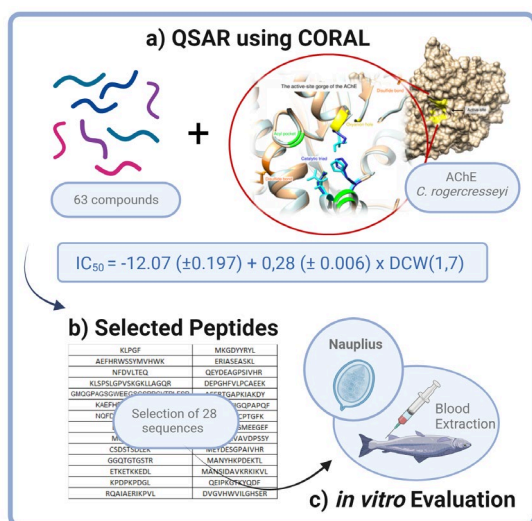
Fig. 1. a) QSAR design using CORAL. b) Selection of peptides with a promising IC$_{50}$. c) Antiparasitic activity and hemolytic activity.

In Chile, the salmon aquaculture industry is highly vulnerable to infections by ectoparasites, such as *Caligus rogercresseyi* [1], that greatly affect the fish's immune system making salmon susceptible to many diseases, thus causing large economic losses. Control of the sea louse relies on chemical treatments with organophosphates as Azamethiphos, able to inhibit the acethylcholinesterase (AChE) enzyme in the parasite; however, in 2014 reduced sensitivity was detected in Chile [2]. For this reason, in the search for new strategies for parasites elimination the use of new molecules like peptides able to inhibit the AChE in this parasite is proposed [3].

Up to now, studies of peptides in fish have focused on their bactericidal or antiviral properties, with little evidence of their participation in the control of parasites [4], so the use of antiparasitic peptides (APPs) is proposed to control or eliminate this kind of pest.

For this reason, bioinformatics tools were used under the application of Quantitative Structure-Activity Relationship (QSAR) [5] procedures in order to identify the main properties and structural characteristics responsible for antiparasitic activity, performing a simulation with active peptides described in the literature, followed by evaluation and construction of models with good statistical quality for validation.

The results allowed us to obtain 21 sequences with a promising IC$_{50}$. These sequences were synthesized by solid phase peptide synthesis using the Fmoc strategy and they were evaluated with the larval stage, nauplius of *C. rogercresseyi*. Four of those peptides showed antiparasitic activity with no hemolytic activity at the concentrations tested.

Results and Discussion

Initially a homology model was built for the *C. rogercresseyi* AChE 3D structure with ITasser server [6], and compared with the *Homo sapiens* structure (PDB ID 4EY4). High similarity was obtained, with conservation of the amino acids in the active site of the catalytic triad: SER203, GLU334, HIS447 are in blue color, and SER171, GLU299, HIS413 are in cyan color in Fig 2, referring to *H. sapiens* and *C. rogercresseyi* respectively. As can also be seen, the acyl pocket (in green), oxyanion hole (in yellow) and disulfide bonds (in orange) are superimposed. This similarity allows us to use the information of compounds directed against the human enzyme, taking advantage of the information obtained in databases and literature (Figure 2).
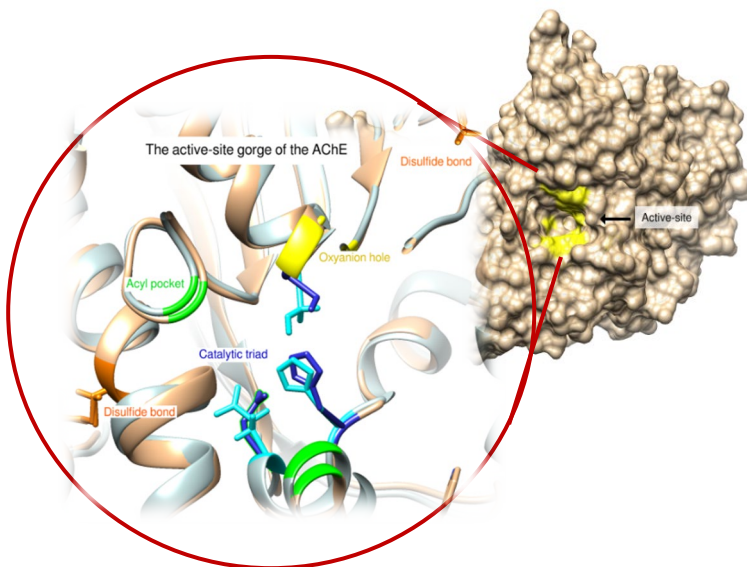
Fig. 2. Surface of the predicted 3D structure of C. rogercresseyi and the active-site gorge of the AChE.

The construction of the QSAR model was carried out with the CORAL software. The compounds for the construction of the model were obtained from databases and literature with specific quantitative information about their activity. Compounds SMILES (Simplified Molecular Input Line Entry Specification) were used for their characterization. We used a total of 63 compounds and evaluated a set of 956 peptides obtained from *Salmo salar* mucus. The obtained model (Equation 1) resulted in the selection of 21 peptides with potential inhibitory activity of the enzyme AChE.

$$\text{Equation 1: } IC50 = -12.07 \ (\pm 0.197) + 0.28(\pm 0.006) * DCW\,(1,7)$$

The selected peptide sequences were synthesized by the Fmoc/tBu standard solid phase strategy using a "tea-bag" protocol [7]. All peptides were characterized by electrospray-mass spectrometry (ESI–MS) in an LCMS-2020 ESI–MS equipment (Shimadzu Corp., Kyoto, Japan) and by high-performance liquid chromatography (HPLC) in a JASCO system (JASCO Corp., Tokyo, Japan).

The antiparasitic activity of the synthesized peptides were evaluated through screening of lethality. Lethality was determined considering death when they remain immobile lying at the bottom of the well. These larval stages were recorded using an optical microscope (Olympus model BX41) fitted with a 10 X objective. Through this assay, it was possible to obtain four peptide sequences (AS4525, AS4528, AS4531 and AS4532) with a lethality effect greater than 90% against the nauplius stage of *C. rogercresseyi* after 60 hours of exposure at a peptide concentration of 100 µM (Figure 3).

a)
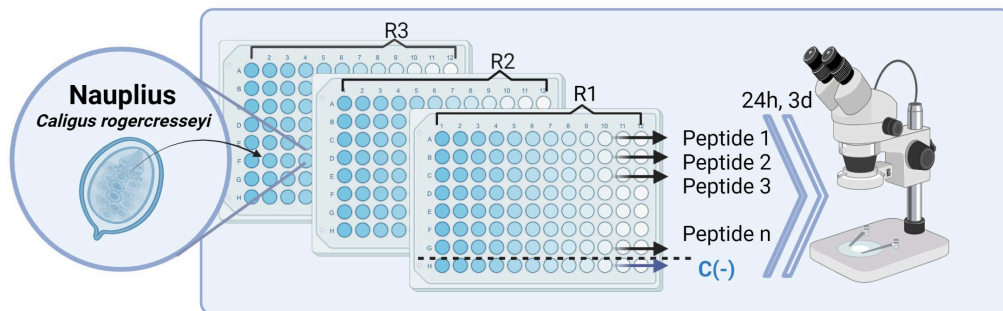
b)
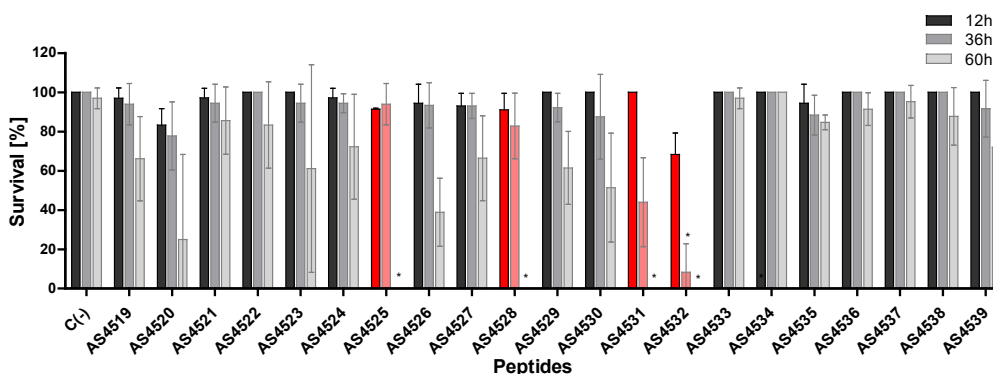
Fig. 3. a) Methodological design to assess lethality of Caligus rogercresseyi using 12 replicates, in triplicate for each peptide and with a photoperiod of 11:13 (light: dark) during 3 days b) Effect of peptides on lethality of the nauplius stage of C. rogercresseyi.
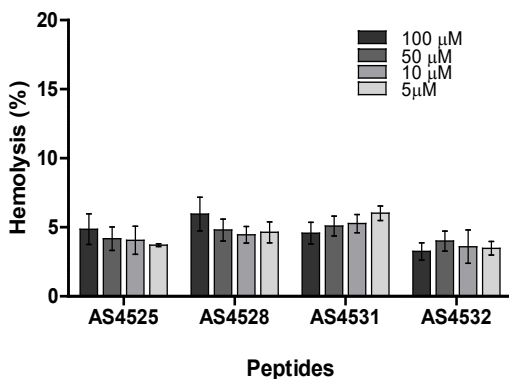
Fig. 4. Evaluation of cytotoxicity of selected peptides using different peptide concentrations.

On the other hand, the measurement of the hemolytic activity of the four selected peptides showed an effect of less than 6% at a concentration of 100 µM, showing no toxicity (Figure 4). These results are promising, placing peptides as alternatives in the treatment of the parasite for the replacement of organophosphates compounds by less toxic and environmentally friendlier compounds.

It is further necessary to verify if the target of action is the AChE enzyme and determine its mechanism of action. These aspects will be addressed in future works.

Acknowledgments

References

1. Carvajal, J., González, L., George-Nascimento, M. *Aquaculture* **166**, 241-246 (1998), https://doi.org/10.1016/S0044-8486(98)00301-9
2. Agusti-Ridaura, C., Dondrup, M., Horsberg, T.E., Leong, J.S., Koop, B.F., Bravo, S., Mendoza, J., and Kaur K. *Parasites Vectors* m11, 570 (2018), https://doi.org/10.1186/s13071-018-3151-7
3. Helgesen, K.O., Bravo, S., Sevatdal, S., Mendoza, J. and Horsberg T.E. *J Fish Dis*. **37**, 877-890 (2014), https://doi.org/10.1111/jfd.12223
4. Masso-Silva, J.A. and Diamond, G. *Pharmaceuticals* **7**, 265-310 (2014), https://doi.org/10.3390/ph7030265
5. Patel, H.M., Noolvi, M.N., Sharma, P., Jaiswal, V., Bansal, S., Lohan, S., Kumar, S.S., Abot, V., Dhimna, S. and Bhardwaj V. *Med Chem Res* **23**, 4991-5007 (2014), https://doi.org/10.1007/s00044-014-1072-3
6. Yang, J., Yan, R., Roy, A., Xu, D., Poisson, J., Zhang, Y. *Nat Methods* **12**(1), 7-8 (2015), https://doi.org/10.1038/nmeth.3213
7. Guzmán, F., Gauna, A., Luna, O., Román, T., Álvarez, C., Albericio, F., et al. *Amino Acids* **52**(8),1201-1205 (2020), https://doi.org/10.1007/s00726-020-02883-8

Study on the Possibility of Cross-Interactions of Selected Growth Factors with Specific and Non-Specific Antibodies

Katarzyna Czerczak-Kwiatkowska, Justyna Fraczyk, and Beata Kolesińska

Institute of Organic Chemistry, Department of Chemistry, Łódź University of Technology,
Żeromskiego 116, 90- 924 Łódź, Poland

Introduction

Proteins are the basic building blocks of living organisms. They also play a key role in a variety of biological processes, such as catalyzing chemical reactions, transporting various compounds, immunological reactions, and signaling between cells [1]. All biological processes are regulated by protein complexes, the activity of which is controlled by protein-protein interactions (PPI) [2,3]. A specific type of PPI is the interaction between antibodies and protein antigens. Essentially, each individual antibody is able to bind specifically to one unique epitope due to a unique antigen-binding site located at the end of the variable region on the antibody. However, an epitope (linear or conformational) may be present in more than one protein antigen. Thus, one antibody can potentially recognize two or more proteins if the proteins are highly homologous and contain the same epitope. This results in the possibility of cross-interaction with other proteins [4-6]. It is commonly believed that the molecular mimicry of epitopes is the cause of the development of many autoimmune and neoplastic diseases [7-11].

Growth factors are specialized proteins (polypeptides) involved in intercellular communication. They activate the body's repair mechanisms. Among the growth factors, over 30 compounds can be distinguished. The most commonly used ones in widely understood medicine are Epidermal Growth Factor (EGF), Vascular Endothelial Growth Factor (VEGF), Platelet-Derived Growth Factor (PDGF), Fibroblast Growth Factor (FGF), and Transforming Growth Factor (TGF). EGF is a common mitogenic factor that stimulates the proliferation and differentiation of various cell types, especially fibroblasts and epithelial cells, and accelerates wound healing. EGF activates the EGF receptor (EGFR/ErbB), which in turn initiates intracellular signaling. EGF supports the differentiation, maturation, and survival of different neurons as well and has a neuromodulatory effect on different types of neurons in the CNS [12,13]. Transforming growth factor alpha (TGF-α) belongs to the epidermal growth factor family. TGF stimulates fibroblasts to produce collagen and stimulates DNA synthesis, proliferation, and differentiation of various types of cells. The expression of TGF-α is highly regulated in response to exogenous cellular signals, including cytokines and other growth factors. This growth factor has been found to be essential for the proper development of many tissues and organs. TGF-α also plays a role in many neoplastic diseases [14]. VEGF stimulates the processes of angiogenesis, i.e. the formation of blood vessels, and activates microcirculation. VEGF is considered a major regulator of angiogenesis in disease states such as cancer, diabetes, and macular degeneration [15,16]. By acting on the appropriate receptors or their isoforms, growth factors trigger cascades of various processes in the body [17-19] which are either harmful or constitute targets in the design of new drugs [20-23]. On the other hand, crosstalk between growth factors and other proteins is widely known, resulting in the formation of new networks of protein-protein interactions and ultimately obtaining different biological responses [24-28].

As a result of our research on the selection of protein fragments involved in the regeneration process of damaged tissues, we have shown [29] that for selection it is possible to use polyclonal antibodies specific to a protein, because finally the set of fragments forming the outer sphere of the protein is obtained. This is due to the fact that the amino acid sequence is important in the recognition of an antigen by antibodies, but a very important factor determining the interaction is the appropriate display of protein fragments, which allows the formation of an antigen-antibody complex. Additionally, polyclonal antibodies are known to recognize many antigens of the one antigen.

The aim of this study was to test the ability to interact with overlapping decapeptide libraries covering entire growth factors such as epidermal growth factor, transforming growth factor alpha, and vascular endothelial growth factor A with specific polyclonal antibodies and non-specific antibodies. Conducting these studies should provide answers to questions about possible cross-interactions between anti-growth factor antibodies and native growth factors. Finding growth factor fragments

incorrectly recognized by anti-growth factor antibodies should, on the one hand, broaden the knowledge of their possible application, as well as provide an answer to the possibility of non-specific interaction of growth factor fragments with various receptors. Experimental studies based on dot-blot tests of libraries of overlapping decapeptides constituting maps of proteins from the growth factor family with antibodies were extended to modeling the interactions of growth factor fragments with selected receptors. It was assumed that both "correct pairs" (ligand-receptor) and "incorrect pairs" (non-specific ligand-receptor) would be used in further research.

Results and Discussion

In the first stage of the research, the syntheses of libraries of fragments of the selected growth factors immobilized on the cellulose surface were carried out. The libraries of fragments of TGF-α, EGF, and VEGF A were obtained. The first stage of the synthetic work involved the incorporation of the isocyanurate derivative on the surface of the cellulose matrix [30,31] (Figure 1). As our research has shown, the isocyanurate derivatives can be used in the SPOT peptide synthesis (modified cellulose as a solid phase) according to the Fmoc/tBu strategy. By using piperidine, it was possible to remove the Fmoc group, which makes it suitable to continue peptide synthesis according to the classical solid phase synthesis procedure. Synthetic protocols [32] were adapted to the synthesis of libraries of decapeptide fragments derived from TGF-α, EGF, and VEGF A. Libraries of decapeptides being overlapping fragments of selected growth factors (reading frame shifted by 1 amino acid residue) was synthesized. Synthesized libraries consisted of 41 fragments for TGF-α, 44 fragments for EGF, and 233 fragments for VEGF A. These libraries were used in subsequent stages to study the ability of interaction with polyclonal antibodies (both specific and non-specific). To visualize peptide-antibody complexes secondary antibodies labeled with horseradish peroxidase (HRP) were used. In order to test the ability of synthesized libraries to interact with specific or non-specific antibodies against growth factors, polyclonal anti-EGF, anti- TGF-α, and anti-VEGF A were used. All performed reactions either with specific or non-specific antibodies showed that there are recognizable decapeptides in each setup (Figure 2).
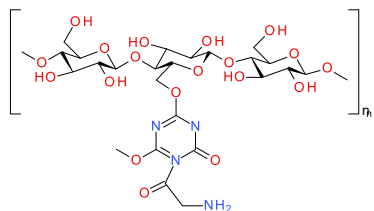
Fig. 1. Isocyanurate derivative immobilized on cellulose prior to peptide synthesis.

EGF and TGF-α belong to growth factors that interact with the same receptor (EGFR), which of course results in the activation of the same processes in the cell [33,34]. Despite the fact that EGF and TGF-α bind to the same receptor, reactions with antibodies specific to them allowed for the selection of structurally diverse fragments. For both EGF and TGF-α 4 fragments were selected. As a result of interactions of the library of EGF-derived decapeptides with anti-TGF-α antibodies 4 fragments were selected, and for TGF-α-derived decapeptides with anti-EGF antibodies it was 1 fragment was found (Figure 3). These fragments partially overlap. In contrast, the fragment 29-38 EGF recognized by anti-TGF-α antibodies is not identified by anti-EGF antibodies, although it partially overlaps with the adjacent active fragments. It can be found that overlapping fragments contain residues conserved for EGF-family proteins. Apart from these residues, there are also others that are similar or the same for both sequences.
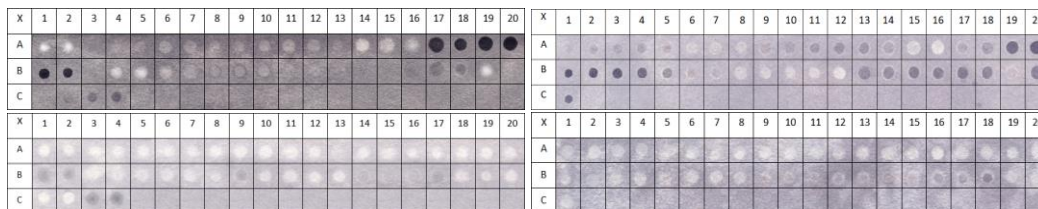
Fig. 2. Exemplary scans of cellulose matrices with peptide libraries of EGF (left) and TGF-α (right) after reactions with polyclonal antibodies: specific (top) and non-specific (bottom).

Analyzing this fact, it can be concluded that the spatial structure of EGF and TGF-α molecules allows for the exposition of similar fragments, which is visible in the above list of fragments selected in reactions with specific antibodies. Binding to the receptor as well as immunization in the process of obtaining antibodies is conditioned by the spatial structure and the appropriate amino acid sequence. It has been found that, despite the presence of a few constant amino acid residues in both sequences, the differences that exist may be of crucial importance in antibody formation. Hence the fact that despite binding to the same receptor, the results of the reaction with EGF and TGF-α antibodies are not identical. For VEGF A interaction with specific polyclonal antibodies resulted in six recognizable fragments. VEGF A belongs to another family of growth factors, but reaction with non-specific antibodies showed, that its fragments may be misrecognized by anti-EGF and anti-TGF-α antibodies. The conducted studies with non-specific anti-EGF and anti-TGF-α antibodies clearly showed that as a result of an incorrect recognition, a significantly greater number of VEGF fragments were selected, than with specific anti-VEGF antibodies. It is worth emphasizing that all selected fragments using specific anti-VEGF antibodies were also found in the dot-blot test with non-specific antibodies. It is also interesting that the VEGF fragments recognized by anti-EGF and anti-TGF-α antibodies were highly compatible. Even for structurally different fragments of the VEGF165 isoform (no reaction with specific anti-VEGF antibodies, one fragment was selected in the test with anti-EGF and anti-TGF-α antibodies. What is surprising, is the almost complete structural homology of the fragments found (you only move one amino acid). Some similarities can be found by analyzing the sequences of the identified fragments. The EGF fragment 33-47 and the TGF-α fragment 29-47 recognized by the anti-EGF antibodies are largely identical. This sequence also includes the aminoacids constant for proteins from the EGF family. Similar sequence is also found in VEGF A 166-175 fragment.
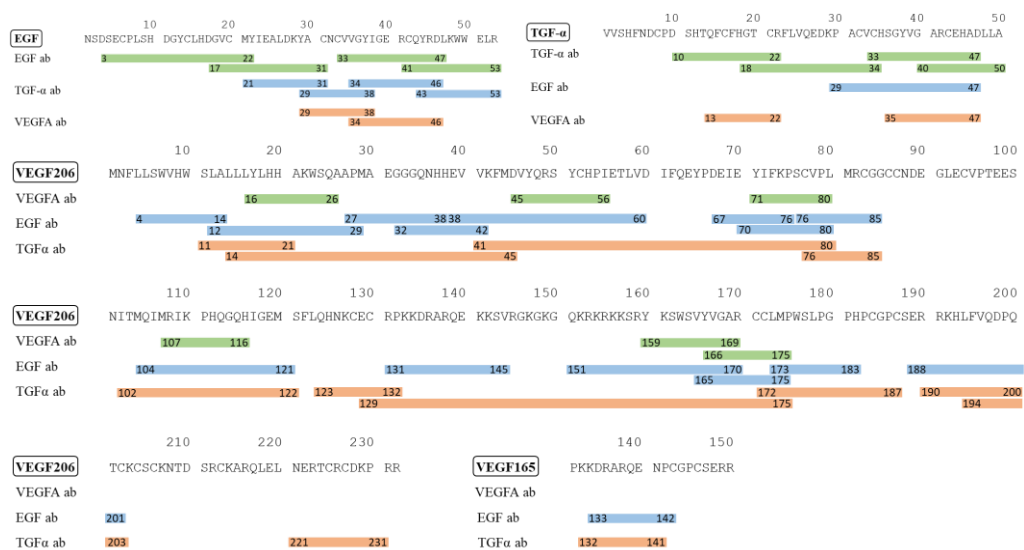
Fig. 3. Graphic scheme of interactions between protein fragments and specific/non-specific polyclonal antibodies.

The results of studies on the cross-interaction of anti-EGF and anti-TGF-α antibodies with VEGF indicate a very high probability of incorrect recognition of growth factors by non-specific antibodies, produced against structurally and functionally different growth factors. Dividing proteins into short peptides show that even between those from different families structural similarities/homology may be found. This fact may indicate that these structures can possibly activate improper proteins during PPI's. Also, studies on mistaken interactions open a new way to design new, unexpected peptides able to interact with selected proteins/receptors.

Acknowledgments

References

1. Lu, H., et al. *Signal Transduct. Target Ther*. **5**, 213 (2020), https://doi:10.1038/s41392-020-00315-3
2. Stelzl, U., et al. *Cell* **122**, 957-968 (2005), https://doi:10.1016/j.cell.2005.08.029
3. Rual, J.F., et al. *Nature* **437**, 1173-1178 (2005), https://doi.org/10.1038/nature04209
4. Augustyniak D., et al. *Curr Med. Chem*. **24**, 4002-4037 (2017), https://doi:10.2174/0929867324666170508110222
5. Jain, D., et al. *Biochem. J*. **476**, 433-447 (2019), https://doi:10.1042/BCJ20180670
6. Leach, M.W., et al. *Toxicol. Pathol*. **38**, 1138-1166 (2010), https://doi:10.1177/0192623310382559
7. Wildner, G., et al. *Front. Immunol*. **11**, 580636 (2020), https://doi:10.3389/fimmu.2020.580636
8. Rees, A.R., *MAbs* **12**, 1729683 (2020), https://doi:10.1080/19420862.2020.1729683
9. Peng, H.-P., et al. *PNAS* **111**, E2656-E2665 (2014), https://doi.org/10.1073/pnas.1401131111
10. Chiaro, J., et al. *Cancer Immunol. Res*. **9**, 981-93 (2021), https://doi.org/10.1158/2326-6066.CIR-20-0814
11. Eisen, H.N. *Annu. Rev. Immunol*. **19**, 1-21 (2001), https://doi.org/10.1146/annurev.immunol.19.1.1
12. Schneider, M.R., et al. *J. Cell. Physiol*. **218**, 460-466 (2009), https://doi:10.1002/jcp.21635
13. Wong, R.W.C., et al. *Cytokine Growth Factor Rev*. **15**, 147-156 (2004), https://doi:10.1016/j.cytogfr.2004.01.004
14. Booth, B.W., et al. *Growth Factors* **25**, 227-235 (2007), https://doi:10.1080/08977190701750698
15. Nieves, B.J. *BioFactors* **35**, 332-337 (2009), https://doi.org/10.1002/biof.46
16. Corvol P. *Bull. Acad. Natl. Med*. **192**, 289-300 (2008), PMID: 18819684
17. Peach, C.J., et al. *Int. J. Mol. Sci*. **19**, 1264 (2018), https://doi:10.3390/ijms19041264
18. Chen, J., et al. *Physiol. Rev*. **96**, 1025-1069 (2016), https://doi:10.1152/physrev.00030.2015
19. Singh, B., et al. *Semin. Cell Dev. Biol*. **28**, 12-21 (2014), https://doi:10.1016/j.semcdb.2014.03.003
20. Mitchell, R.A., et al. *Exp. Cell Res*. **371**, 1-19 (2018), https://doi:10.1016/j.yexcr.2018.08.009
21. Shaik, F., et al. *Biomolecules* **10**, 1673 (2020), https://doi:10.3390/biom10121673
22. Martin-Fernandez, M.L., et al. *Cells* **8**, 316 (2019), https://doi:10.3390/cells8040316
23. Ferrara, N. *Trans Vis. Sci. Tech*. **5**, 10 (2016), https://doi:10.1167/tvst.5.2.10
24. Latko, M., et al. *Cells* **8**, 455 (2019), https://doi:10.3390/cells8050455
25. Luo, K. *Cold Spring Harb Perspect. Biol*. **9**, a022137 (2017), https://doi:10.1101/cshperspect.a022137
26. Tsuda, T. *Int. J. Mol. Sci*. **19**, 2787 (2018), https://doi:10.3390/ijms19092787
27. Munger, J.S., et al. *Cold Spring Harb Perspect. Biol*. **3**, a005017 (2011), https://doi:10.1101/cshperspect.a005017
28. Bjorkelund, H., et al. *PLoS ONE* **6**, e16536 (2011), https://doi.org/10.1371/journal.pone.0016536
29. Kolasa, M., et al. *Int. J. Mol. Sci*. **22**, 13584 (2021), https://doi.org/10.3390/ijms222413584
30. Kaminski, Z.J., et al. *Chem. Biodiv*. **14**, e1700444 (2017), https://doi:10.1002/cbdv.201700444
31. Bak, A., et al. *Comb. Chem. High Throughput Screen*. **17**, 141-156 (2014), https://doi:10.2174/13862073113169990054
32. Fraczyk, J., et al. *J. Pep. Sci*. **24**, e3063 (2018), https://doi:10.1002/psc.3063
33. Winkler, M.E., et al. *Biochemistry* **28**, 6373-6378 (1989), https://doi:10.1021/bi00441a033
34. Ebner, R., et al. *Cell R*egul. **2**, 599-612 (1991), https://doi:10.1091/mbc.2.8.599

Design, Synthesis and Biological Evaluation of Fluorinated Cathepsin D Inhibitors

Francesco Terzani[1], Karine Guitot[1], Julia Kaffy[1], Johanne Leroy-Dudal[2], Evelyne Chelain[1], and Julien Pytkowicz[1]

[1]CY Cergy Paris Université, CNRS, BioCIS, 95000, Cergy Pontoise, France, Université Paris-Saclay, CNRS, BioCIS, 92290, Châtenay-Malabry, France; [2]CY Cergy Paris Université, ERRMECe, EA1391, Equipe MECuP, 95000, Cergy Pontoise, France

Introduction

Aspartic peptidases, like Cathepsin D, are involved in many pathologies affecting human population like hypertension, Alzheimer Disease (AD) and Acquired Immune Deficiency Syndrome (AIDS). Moreover, this enzyme, is considered as a potential target for the treatment of breast cancer. In this context the development of efficient inhibitors and inhibitor screening methods is a major need for the scientific community [1]. Pepstatin A is a penta-peptide, containing two residues of the γ-amino acid Statin, considered as the gold standard among the natural inhibitors of Cathepsin D. Nevertheless, due to its poor selectivity and its poor metabolic stability, no applications have been found for the treatment of the diseases mentioned above with this molecule. The synthesis and the evaluation of peptide-like ligands of Cathepsin D containing fluorine atoms constitutes an innovative strategy that could lead to the development of new molecules as ^{19}F NMR probes and/or new potential inhibitors towards Cathepsin D [2]. The introduction of fluorinated amino acids in the peptide scaffold, in fact, could: *(i)* transform the ligand into an efficient ^{19}F NMR probe opening the way to NMR's based functional assays [3]; *(ii)* help the cellular membrane uptake; *(iii)* improve the bioavailability [4].

Results and Discussion

Structures of the synthesized pepstatin A analogues are summarized in Figure 1. We initially chose to increase locally the hydrophobicity replacing the *N*-terminal isovaleryl moiety of pepstatin A with a trifluoroacetyl group in order to quickly access to the fluorinated analogue **1**. All the syntheses were carried out on solid support *via* classical Fmoc-based solid phase synthesis (SPPS). Chlorotrityl resin was used instead of Wang resin because of the free hydroxyl group of Wang resin and the risk of side reactions due to the presence of the free hydroxyl of the statin residues. A series of classical Fmoc-aa coupling/deprotection reactions yielded the pentapeptide Val-Val-Sta-Ala-Sta, then a trifluoroacety-lation was carried out directly on the resin using ethyl trifluoroacetate and the analogue **1** was obtained in an overall yield of 31% after cleavage and purification.

The synthetic pathway for the analogues **2** and **3** incorporating (*R*) and (*S*) enantiomers of *N*- protected trifluoromethyl alanine (Z-TfmAla) in *N*-terminal position is reported in Scheme 1. These modifications should increase the affinity of these inhibitors for Cathepsin D and improve their metabolic stability by the presence of a fluorinated and quaternarized amino acid. For synthetic convenience, *N*-Cbz protected trifluoromethylated amino acid were used and the protecting group was then preserved in the final inhibitor since *N*-Cbz inhibitors of CatD have already been found in the literature. After coupling of the first amino acid, Fmoc-statin, on the chlorotrityl resin in the presence of DIPEA, deprotection with a 20% solution of piperidine in DMF allows to carry out the coupling reaction of the second amino acid in the presence of HBTU and DIPEA. These steps are repeated with each amino acid to be coupled until the tetrapeptide Val-Sta-Ala-Sta is obtained. Finally, the fluorinated analogues **2** and **3** were obtained by coupling the previously synthesized (*R*) or the (*S*) Cbz-TfmAla on the tetrapeptide respectively in 16% and 28% yield.

The synthesis of analogue **4**, with a (*S*)-TFM (TFM = trifluoromethionine) instead of Valine, was therefore considered; we indeed hypothesized that the incorporation of a fluoroalkyl side chain at the P1 position would increase the potency of the inhibitor. During the synthesis, the unexpected epimerization of the TFM allowed us to obtain analogue **5** incorporating a (*R*)-TFM. We initially considered the synthesis of analogue **4** by coupling the isoval-TFM building block to the Val-Sta-Ala-Sta tetrapeptide. However, during the coupling reaction, the undesired isomerization of the TFM led to a mixture (50/50) of diastereomers **4** and **5**. The two diastereomers could be separated, characterized
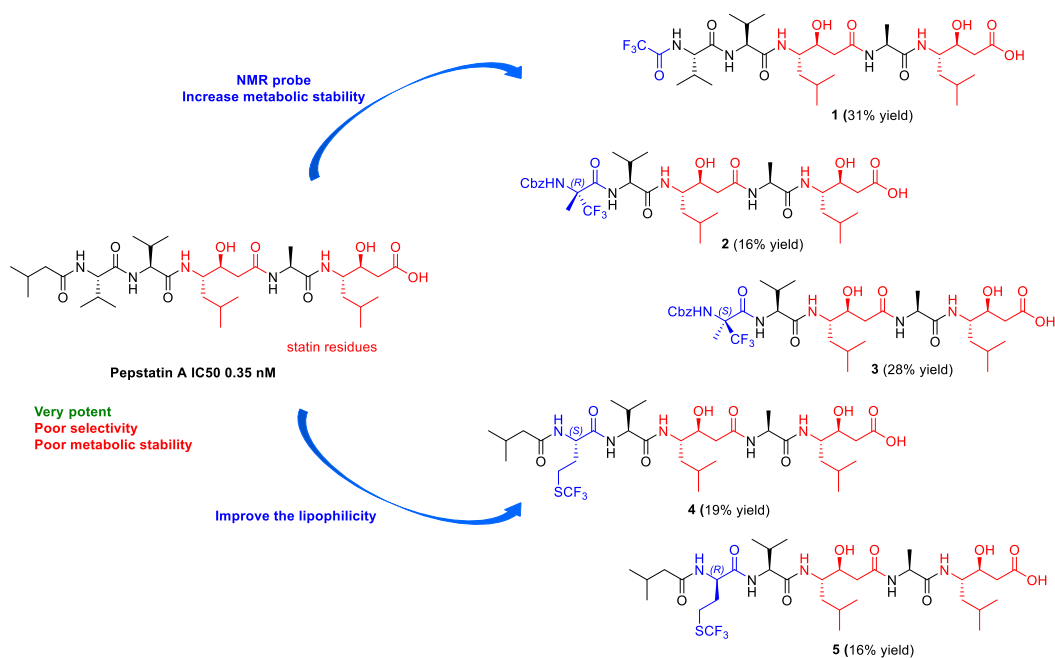
Fig. 1. Structure of the fluorinated analogues of Pepstatin A.
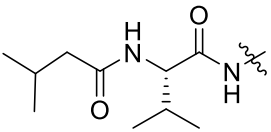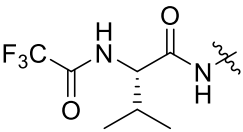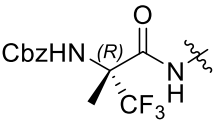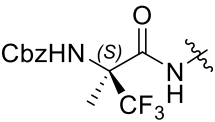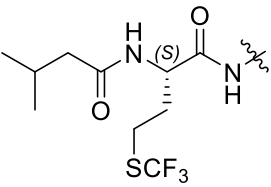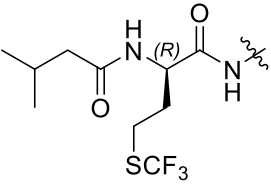
and tested. In order to avoid this epimerization and to be able to identify each diastereomer, we decided to couple the (*S*) Fmoc-protected TFM on the Val-Sta-Ala-Sta tetrapeptide, and then to carry out an acylation of the *N*-terminus by isovaleric chloride. The compound **4** has been cleaved from the resin, purified by semi-prep HPLC, and obtained in 19% overall yield.

Once the fluorinated analogues of Pepstatin A were synthesized, fluorescence tests were carried out in order to evaluate the inhibitory activity of these new analogues. All the tests were initially performed on Pepsin (cheaper and easier to handle) before being carried out on cathepsin D (Table 1). Surprisingly, as shown in Table 1, analogue **5** incorporating an (*R*)-isovaleryl trifluoromethionine in the *N*-terminal position instead of (*S*)-isovaleryl valine, showed a very interesting and better inhibitory activity than that of pepstatin A
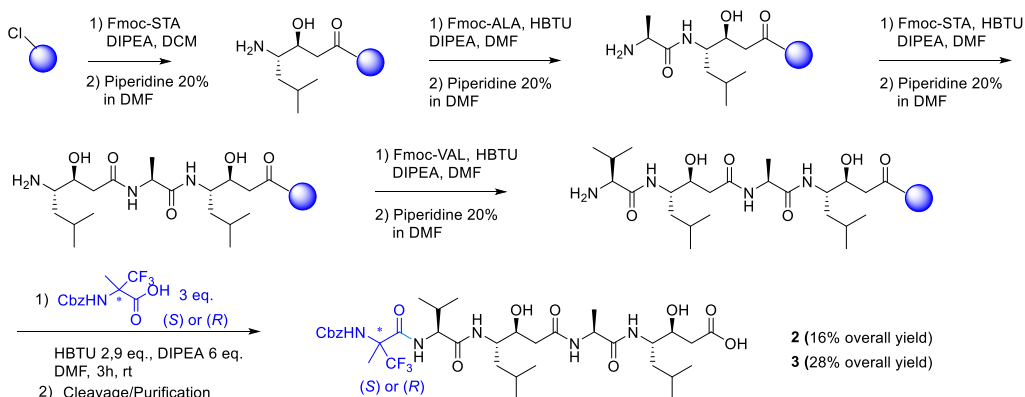
*Scheme 1. Synthesis of the fluorinated analogues **2** and **3** of Pepstatin A.*

*Table 1. Inhibitory activities of **1**-**5** against Pepsin and Cathepsin D.*

Compound	Structure of the N-terminus fragment	IC$_{50}$ (nM) against Pepsin	IC$_{50}$ (nM) against Cath D
Pepstatin A		50	5
1		>4000	>2000
2		375	65
3		48	28
4		775	58
5		31	0.4

References

1. Dash, C., et al. *Crit. Rev. Biochem. Mol. Biol.* **38**, 89-119 (2003), http://dx.doi.org/10.1080/713609213
2. Salwiczek, M., et al. *Chem. Soc. Rev.* **41**, 2135-2171 (2012), https://doi.org/10.1039/C1CS15241F
3. Huhmann, S., et al. *Beilstein J. Org. Chem.* **13**, 2869 (2017), https://doi.org/10.3762/bjoc.13.279
4. Chen, H., et al. *Chem. Soc. Rev.* **42**, 7971-7982 (2013), https://doi.org/10.1039/C3CS60129C
5. Devillers, E., et al. *Amino Acids* **48**, 1457-1468 (2016), https://doi.org/10.1007/s00726-016-2200-9

New Generation of Polyethylene Glycol (PEG)-Based Peptidomimetics of Antimicrobial Peptides (AMPs)

Conor Shine[1], Jamie MacLennan[1], Deirdre Fitzgerald-Hughes[2], and Marc Devocelle[1]

[1]*The Royal College of Surgeons in Ireland, Department of Chemistry, 123 St. Stephens Green, Dublin, Ireland;*
[2]*The Royal College of Surgeons in Ireland, Department of Microbiology, Beaumont Hospital, Dublin, Ireland*

Introduction

Peptidomimetic conversion of Antimicrobial Peptides (AMPs) is one of the main medicinal chemistry approaches currently investigated to improve their therapeutic potential as antibiotic candidates. AMP analogues generated by this approach range from type-1 (*e.g.*, inverso or beta-amino acid peptides and peptoids) to type-3 (*e.g.*, brilacidin) peptidomimetics. Polymer-based mimetics, encompassing functionalised poly(norbornene), poly(acrylic) and nylon-3 backbones, have also been developed [1]. Considering the number of clinically approved polyamide-based biopharmaceuticals including Polyethylene Glycol (PEG) in their structures, we investigated the use of functionalised PEGs as peptidomimetics of AMPs (Figure 1) [2]. These 'pegtides' were produced by co- and post-polymerisation functionalisation of two substituted ethylene oxide monomers, as analogues of cationic and hydrophobic residues in AMPs. This approach has also been independently applied to AMP mimetics produced from three substituted oxirane monomers, allowing the addition of hydrophilic repeating units [3].
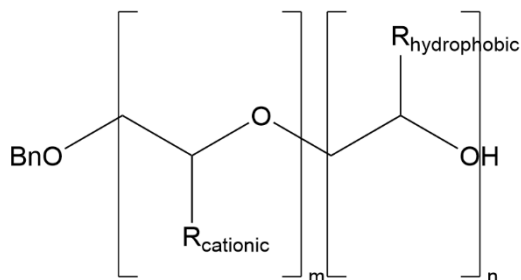
Fig. 1. Structure of the pegtide where $R_{cationic}$ is typically an arginine-like side-chain while $R_{hydrophobic}$ can be, for example, a tryptophan-like or valine-like side-chain.

Preliminary susceptibility and antibiofilm assays performed with the first generation of antimicrobial pegtides, as random copolymers with cationic (guanidyl side-chain) and hydrophobic (n-alkyl/branched/aromatic side-chain) repeating units, showed that the activities of these candidates remained lower than the one of a prototypical AMP ((Arg-Trp)$_5$ decapeptide), in particular against Gram-negative bacteria. However, the parent peptides of these mimetics were themselves analogues of AMPs, where amino acids commonly found in these amphipathic peptides are replaced by analogous residues (*e.g.*, (2-naphtyl)alanine, in place of tryptophan). To improve the activity of these PEG-based mimetics against both Gram-negative and Gram-positive bacteria, we have developed novel oxirane monomers allowing the preparation of PEG-based copolymers, functionalized with side-chains matching those of amino acids frequently selected in optimised AMP sequences. Their use in the production of novel antimicrobial pegtides is presented here.

Results and Discussion

The monomers were synthesized in a chiral fashion by employing the Sharpless asymmetric dihydroxylation (Figure 2).
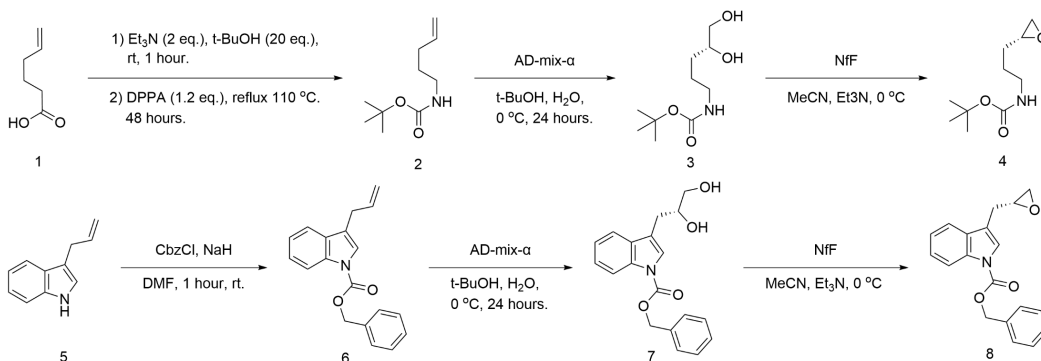
Fig. 2. Reaction schemes for the synthesis of chiral oxirane monomers 4 and 8 bearing protected amino acid side-chain functionalities.

Nonafluorobutanesulfonyl fluoride (NfF) was used to convert the chiral diols to their respective chiral epoxides as standard epoxidation methods could not be employed to compound 6 as the indole ring was extremely susceptible to oxidation. Compound 4 is Boc-deprotected post-polymerization and guanylated to afford the cationic arginine-like residue while compound 8 is complementary Cbz-deprotected by hydrogenation post-polymerization to afford the tryptophan-like residue (Figure 3).
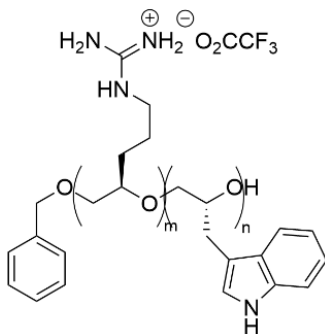
Fig. 3. Structure of the pegtide after post-polymerisation deprotection and guanylation.

Benzyl alcohol is used as an initiator to polymerize compounds 4 and 8 by anionic ring-opening polymerization. The NMR spectra of compounds 4, 8 and the copolymer are shown in figures 4, 5 and 6 respectively.
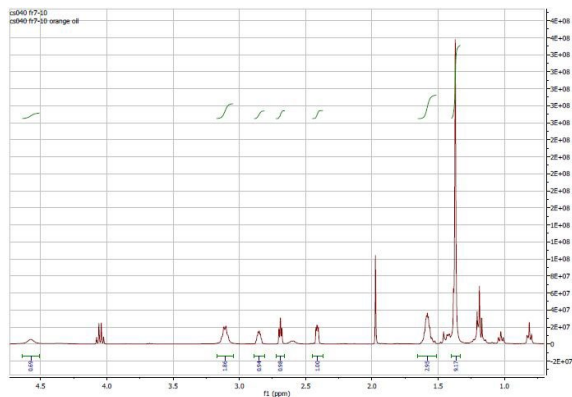
Fig. 4. NMR spectrum of compound 4.
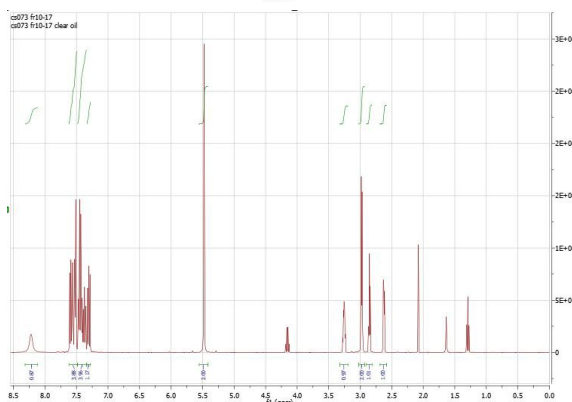
Fig. 5. NMR spectrum of compound 8.
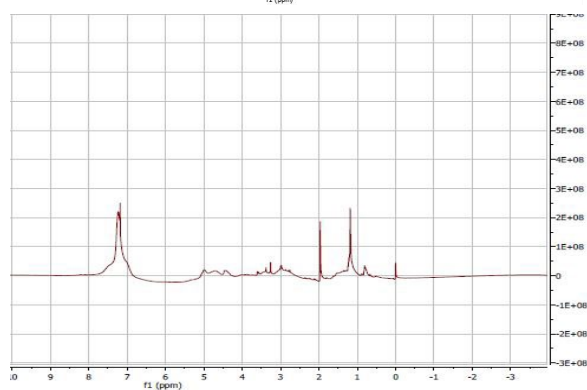
Fig. 6. NMR spectrum of deprotected and guanylated pegtide.

Acknowledgments

References

1. Scott, R.W., Tew, G.N. *Curr Top Med Chem*. **17**, 576-589 (2017), https://doi.org/10.2174/1568026616666160713130452
2. Devocelle, M., et al. *Proceedings of the 35th European Peptide Symposium* 175-176 (2018), http://dx.doi.org/10.17952/35EPS.2018.175
3. Kim, M., et al. *ACS Nano* **15**, 9143-9153 (2021), https://doi.org/10.1021/acsnano.1c02644

Development of Innovative Bio-Tools for a cTnI-Detection Assay

Evgenia Fotou, Vasiliki Moulasioti, Vassilios Moussis, and Vassilios Tsikaris

Section of Organic Chemistry & Biochemistry, Department of Chemistry,
University of Ioannina, Ioannina, Greece

Introduction

Cardiac troponin I (cTnI) constitutes a biomarker for acute myocardial infarction diagnosis [1]. cTnI tests are ELISA-based and require at least two specific antibodies, particularly expensive. Chickens are excellent experimental animals for antibodies' production. Chicken antibodies (IgY) can be isolated from eggs since they pass from serum to egg yolk [2]. Also, chicken produces higher titer antibodies than other animal species with lower cost. Subsequently, the number of experimental animals significantly decreases, while chickens do not forbear painful blood sampling [3]. This study aimed to develop innovative and low-cost specific bio-tools and techniques to detect the cTnI. For this purpose, a series of haptens (consequently possible antigenic epitopes) were selected based on the homology, antigenicity, and hydrophilicity [4-7]. Also, based on our previous studies we exploited two sequential oligopeptide carriers developed in our lab (SOC & CPSOC) [8] to anchor the desired haptens, expecting to enhance in this way the animal immunoresponse but also be usable as adsorbents on ELISA plates during immunoassays. The haptens and peptide carriers were synthesized in SPPS and then linked via thioether bonds to form possible immunogenic conjugates. Experimental animals (laying hens) were immunized with the conjugates. The peptide conjugates were injected into three chickens, following two different approaches that differed in immunogen concentration and the intervals between immunizations. The first approach: 4 injections of immunoconjugate (1 mg/ml)/animal/10 days. The second approach: 3 injections of a mix of immunoconjugates (four immunogenic complexes with a decreasing concentration from 0,3 to 0,1 mg/ml) in one animal in intervals three and five weeks respectively. The antibodies were isolated from their eggs and then purified. The antibodies were tested for their specificity against the peptide conjugates and the cTnI by ELISA assays. Furthermore, an ELISA was utilized to detect cTnI by using commercial anti-cTnI antibodies IgG as capture antibodies and the produced IgY antibodies as detection antibodies.

Results and Discussion

The epitope mapping of cTnI in combination with previous studies, conducted in our lab, resulted in the selection of four peptide sequences which are cTnI[19-31], cTnI[66-77], cTnI[110-122], cTnI[118-131]. The synthesized conjugates are listed in Table 1. Indicatively the ESI-MS spectra and RP-HPLC chromatograms of the two later conjugates are depicted in Figure 1 and they attest the successful synthesis of the conjugates.
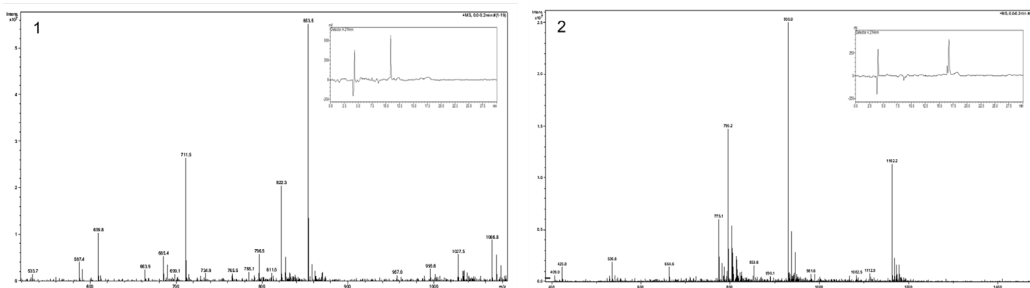
Fig. 1. ESI-MS spectra and RP-HPL chromatograms of peptide conjugates: 1. CPSOC(3,9-Acm;6,12-cTnI[66-77]) Expected MW: 4263,96 and Found MW: 4262,10 ± 0,61. 2. CPSOC(3,9-Acm;6,12-cTnI[110-122]) Expected MW: 4646,48 and Found MW: 4644,86 ± 0,25.

Table 1. Peptide conjugates and column that were used for IgY antibodies production & purification, and their abbreviations.

Peptide conjugate / column	Abbreviation
CH_3CO-[(K-Aib-C(3,9-CH_2CONH_2; 6,12-CH_2CO-E^{66}RRGEKGRALST^{77}-NH_2)]$_4$-NH_2	CPSOC(3,9-Acm; 6,12-cTnI$^{66-77}$)
CH_3CO-[K-Aib-C(3,9-CH_2CONH_2; 6,12-CH_2CO-R^{110}YDIEAKVTKNIT^{122}-NH_2)]$_4$-NH_2	CPSOC(3,9-Acm; 6,12-cTnI$^{110-122}$)
CH_3CO-[K(R^{19}RRSSNYRAYATE^{31})-Aib-G]$_4$-NH_2	SOC-cTnI$^{19-31}$
CH_3CO-[K(T^{118}KNITEIADLTQKI^{131})-Aib-G]$_4$-NH_2	SOC-cTnI$^{118-131}$
Sepharose-C_3H_6O-S-CH_2CO-Ahx-R^{19}RRSSNYRAYATE^{31}-NH_2	Seph@Ahx-cTnI$^{19-31}$

The IgY antibodies' specificity for the immunoconjugates and the entire protein cTnI was tested by a series of ELISA assays, in which the conjugates or the whole protein (cTnI) were coated to the plates and then the produced antibodies were added. The anti-IgY*HRP was used for signal induction and the samples were measured at 450 nm in an ELISA reader. Antibodies from the same hens before immunizations were used as negative control. Also, ELISA sandwich-type assays were designed and performed to detect the cTnI. For this purpose, anti-cTnI (IgG) commercial antibodies were used as capture antibodies, while the antibodies produced against the mixture of the four immunogenic conjugates were used as detection antibodies.

IgY antibodies' specificity for the conjugates 1. SOC-cTnI$^{19-31}$ and 2. SOC-cTnI$^{118-131}$, which were produced according to the 1st approach are illustrated in Figure 2A. Figure 2 B shows the corresponding results for the antibodies produced against the four conjugates 1. SOC-cTnI$^{19-31}$, 2. CPSOC(3,9-Acm; 6,12-cTnI$^{66-77}$), 3. CPSOC(3,9-Acm; 6,12-cTnI$^{110-122}$), 4. SOC-cTnI$^{118-131}$, namely with the 2nd approach.

The anti-SOC-cTnI$^{19-31}$ IgY antibodies were passed through the synthesized column Seph@Ahx-cTnI$^{19-31}$ and the fractions were used to test the specificity of the purified IgY antibodies for the immunoconjugate SOC-cTnI$^{19-31}$. The results are shown in Figure 2C. The IgY antibodies purified by dialysis were used for comparison.

The results of the ELISA that performed to check the specificity of the isolated IgY antibodies against the whole protein cTnI are depicted in Figure 3A. Also, the purified IgY antibodies with affinity chromatography were tested for their specificity for the cTnI as shown in Figure 3B. The IgY antibodies purified by dialysis and a positive control (anti-cTnI, IgY) were used for comparison.

Figure 3C summarizes the results of the sandwich ELISA that used to detect the cTnI. The specific ELISA was performed by using two different anti-cTnI IgGs as capture antibodies and the produced IgY as detection antibodies. IgY non-specific antibodies were used as negative control. According to the Figure 3C, it is inferred that the antibodies produced against the mixture of the four epitopes function in all cases as cTnI detection antibodies.

In conclusion, the produced anti-cTnI chicken antibodies recognized the immunogenic conjugates and human cTnI, while the produced bio-tools are appropriate for using them in cTnI detection assays. The results of the present work showed that the immunized experimental animals produced high titer and specific antibodies against the immunogenic conjugates, which can detect the cTnI. Also, the produced antibodies purified by dialysis can be utilized without further purification to detect the cTnI. Furthermore, our data indicated that the oligopeptide carriers (SOC & CPSOC) [8] are useful in antibodies' production and ELISA assays by exposing immunogenic peptides, confirming our previous studies. Also, our study suggests that the isolated IgY antibodies from the hens' eggs are suitable and relatively inexpensive tools for developing diagnostic tests. The high efficiency of IgY production significantly reduces the number of experimental animals and the used ones do not get harmed.
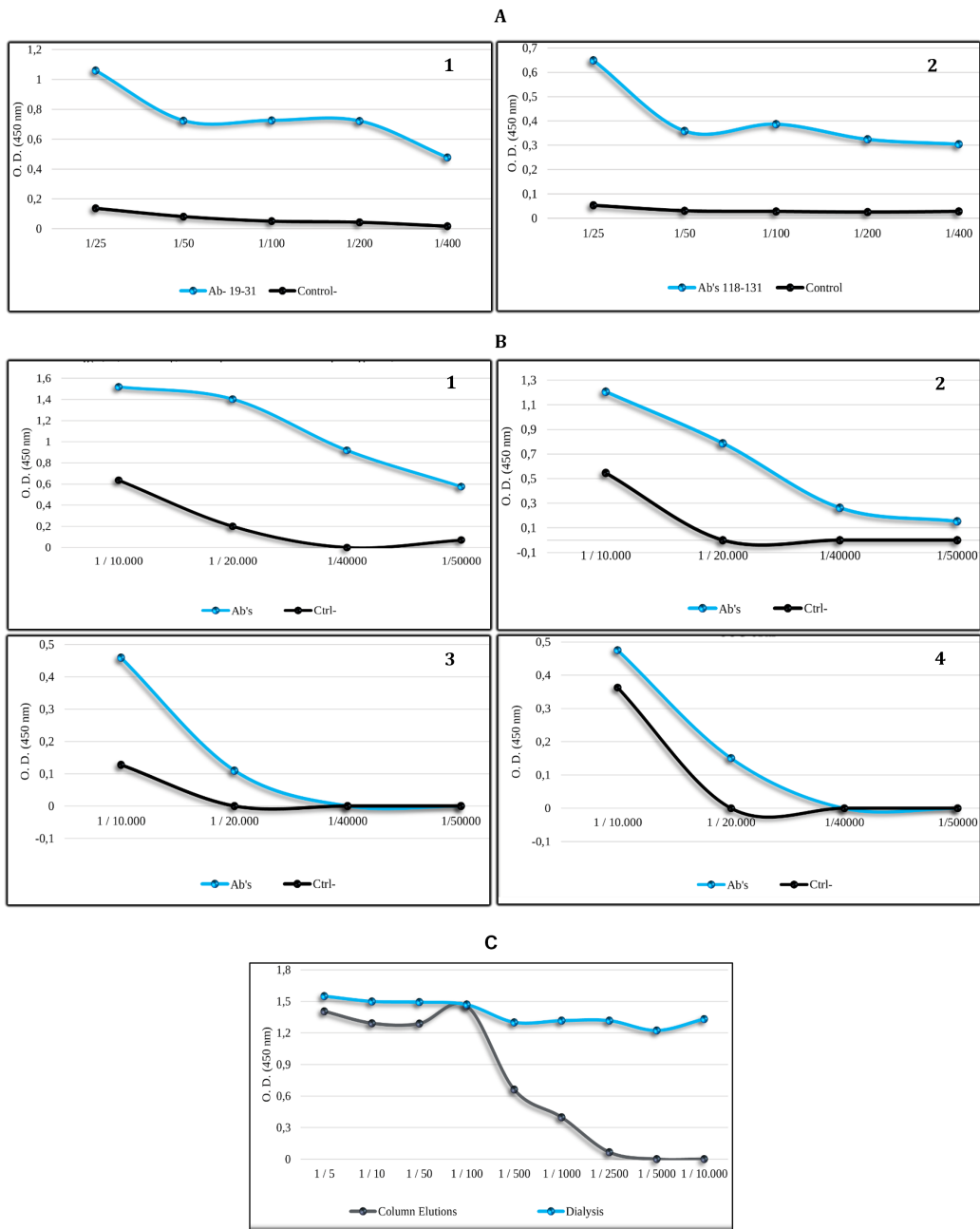
Fig. 2. Specificity of the produced IgY against (A) one epitope/animal (1st approach): 1) SOC-cTnI$^{19-31}$ & 2) SOC-cTnI$^{118-131}$ and (B) mixture of four epitopes/animal (2nd approach): 1) SOC-cTnI$^{19-31}$, 2) CPSOC(3,9-Acm; 6,12-cTnI$^{66-77}$), 3) CPSOC(3,9-Acm; 6,12-cTnI$^{110-122}$), 4) SOC-cTnI$^{118-131}$. (C) Specificity of IgY antibodies, purified with affinity chromatography, for the conjugate SOC-cTnI$^{19-31}$.
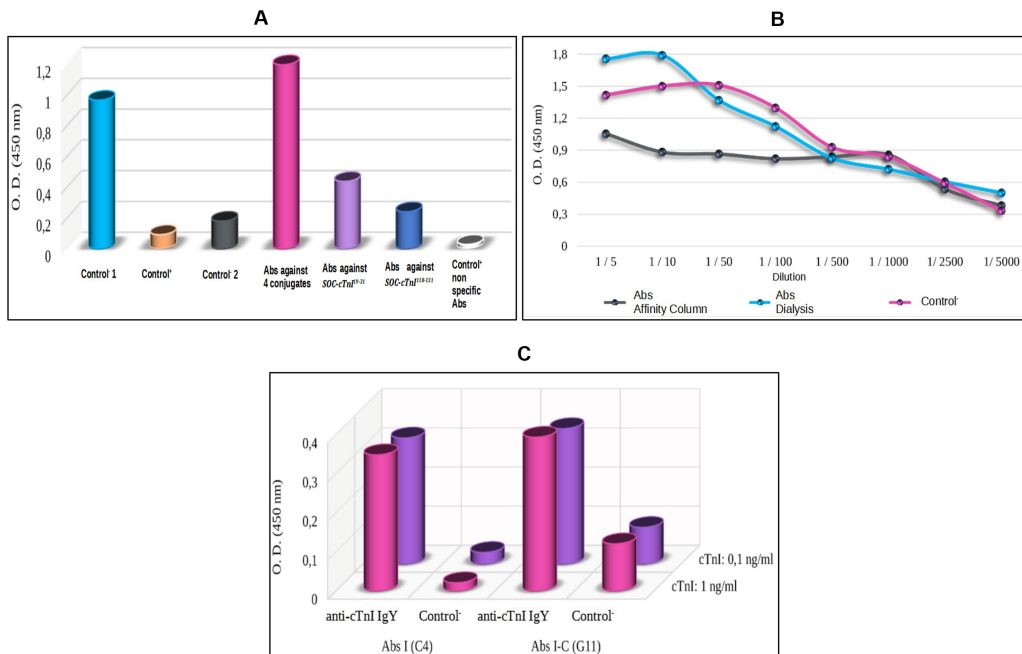
Fig. 3. (A) Results of the ELISA performed for the cTnI detection by the produced IgY. A positive (cyan) & three negative (orange, grey, white) controls were used. (B) Results of the ELISA used to test the specificity of IgY antibodies, purified with affinity chromatography, for the total cTnI. IgY antibodies purified with dialysis were used for comparison and a positive control (pink, anti-cTnI IgY) was used too. (C) Results of the sandwich ELISA used to detect cTnI. Anti-cTnI IgGs were used as capture antibodies and the produced IgY as detection antibodies. IgY non-specific antibodies were used as negative control.

References

1. Thygesen, K., et al. *J. Am. Coll. Cardiol*. **72**, 2231 LP - 2264 (2018), https://doi.org/10.1016/j.jacc.2018.08.1038
2. Schade, R., et al. *Altern Lab Anim*. 1-26 (2005), http://doi.org/10.1177/026119290503300208
3. Zhang, X., et al. *Biol. Rev*. **92**, 2144-2156 (2017), https://doi.org/10.1111/brv.12325
4. http://www.blast.ncbi.nlm.nih.gov/Blast.cgi
5. http://www.ncbi.nlm.nih.gov/BLAST/fasta.shtml
6. https://www.ncbi.nlm.nih.gov/tools/cobalt/re_cobalt.cgi
7. https://www.ebi.ac.uk/Tools/msa/clustalo/
8. Papadopoulos, C., et al. *J Pep Sci*. **27**(11) e3359 (2021), https://doi.org/10.1002/psc.3359

Design and Synthesis of Selective Ion Channel Blocker Peptide Toxin Analogs

Zsolt Bozsó[1], Ferenc Bogár[1], János Szolomájer[1], Zoltán Kele[1], Ágota Csóti[2], Tibor G. Szántó[2], György Panyi[2], and Gábor K. Tóth[1]

[1]Department of Medical Chemistry, Albert Szent-Györgyi Medical School, University of Szeged, Szeged, H- 6720, Hungary; [2]Department of Biophysics and Cell Biology, Faculty of Medicine, University of Debrecen, Debrecen, H-4032, Hungary

Introduction

Voltage-gated ion channels are pore-forming transmembrane proteins, which are important mediators of electrical signals and maintain ion homeostasis in cells [1]. Due to their prime role in signal transduction and cellular regulations, malfunctions of the ion channels can lead to the development of several diseases involving the cardiac, neuronal, immune, and endocrine systems [2,3,4]. Venomous peptides of natural origin (from snakes, scorpions, spiders, frogs, and cone snails) act upon ion channels. Besides their therapeutic importance, these toxins can be used to elucidate the mechanism of action of the channels [2]. However, their application is restricted by the limited selectivity between the numerous ion channels. We tried to investigate the possibility to design and synthesize more selective potassium channel blockers.

Results and Discussion

We have selected three peptides for our studies:
- Iberiotoxin (IbTx) has subnanomolar activity and it is fairly selective for the KCa1.1 channel,
- Agitoxin (AgTx2) has a similarly high affinity for both Kv1.1 and Kv1.3 channels,
- Kaliotoxin (KTX1) blocks Kv1.1 and Kv1.3 channels with nanomolar and KCa1.1 channels with micromolar affinity.

The disulfide bridge pattern of the 3 toxins is identical: abcabc. Our derivatives were synthesized by microwave-assisted solid phase peptide synthesis using N^{α}-Fmoc protected amino acids. Oxidation of the peptides were carried out on air at pH=7.5 (0.1 M NH$_4$OAc). We have examined the effect of the peptides on ion channels Kv1.1, Kv1.3, and KCa1.1 using patch clamp method. None of our analogs acted on the Kv1.1 channel.

First, a chimera of the three toxins was designed (ZFPK in Table 1). Some amino acids of the IbTx were exchanged with the corresponding residues of AgTx2 and KTX1. Namely, V9G, and L20A mutations were done, and the VDR block (between positions 23 and 25) and the C-terminal YQ were replaced with MRF and TPK, respectively.

The mutations resulted in the loss of activity toward the KCa1.1 channel, at the same time the ZFPK peptide blocked the Kv1.3 channel (Figure 1 and 2) So, although only a few amino acids were incorporated into the sequence of IbTx, the new analog rather acted as AgTx2. This result is in agreement with the literature [6 and references therein]: It is reported that Val at position 9 in IbTx is too bulky for the interaction with the turret of the S5-S6 loop of Kv1.3 and Shaker channels. Moreover, when Gly10 (note that position 10 in AgTx2 is corresponding to position 9 in IbTx) of AgTx2 was mutated to Val the affinity of the peptide was greatly decreased toward the Shaker channel. It was shown that Phe[25] and Pro[37] is an important determinant of the binding of AgTx2 to the Shaker channel. All of these 3 residues important for the binding of AgTx2 to Kv1.3 and Shaker were incorporated into these IbTx-based ZFPK chimeras.

In the next analog (ZFYQ) the Val at position 10 and the C-terminal of the IbTx were restored (Table 1). These changes were enough to gain back the activity toward the KCa1.1 channel, but the response of the Kv1.3 channel for ZFYQ was markedly less than that of ZFPK (Figure 1 and 2). It was noticed that the Arg between the 3rd and 4th Cys is shifted by one position in our chimeras (ZFYQ and ZFPK) compared to AgTx2 and KTX1. To check if this affects the interaction with Kv1.3 channel Phe[21] was omitted from the sequence (Table 1, desF[21]-ZFYQ). As it is seen in Figure 1 and 2, this slight modification altered the behavior of the peptide: the effect on Kv1.3 and KCa1.1 channels were

Table 1. Sequence alignment of the parent and the synthesized peptides. Z=pyroglutamic acid, the altered residues of IbTx analogs are marked with boldface characters.

Code	Sequence
IbTx	ZFTDVDCSVSKECWSVCKDLFGVDRGKCMGKKCRCYQ
AgTx2	GVEINVKCSGSPQCLKPCKDAGMRFGKCMNRKCHCTPK
KTX1	GVPINVSCTGSPQCIKPCKDAGMRFGKCMNRKCHCTPK
ZFPK	ZFTDVDCSGSKECWSVCKD**AFG****MRF**GKCMGKKCRC**TPK**
ZFYQ	ZFTDVDCSVSKECWSVCKD**AFG****MRF**GKCMGKKCRCYQ
desF21-ZFYQ	ZFTDVDCSVSKECWSVCKD**A****GMRF**GKCMGKKCRCYQ
ZFYQ-RRR	ZFTDVDCSVSKECWSVCKD**AFG****RRR**GKCMGKKCRCYQ
ZFYQ-MRR	ZFTDVDCSVSKECWSVCKD**AFG****MRR**GKCMGKKCRCYQ
ZFYQ-RWR	ZFTDVDCSVSKECWSVCKD**AFG****RWR**GKCMGKKCRCYQ
ZFYQ-DWR	ZFTDVDCSVSKECWSVCKD**AFG****DWR**GKCMGKKCRCYQ
IbTx-R25Cit	ZFTDVDCSVSKECWSVCKDLFGVD**X**GKCMGKKCRCYQ **X**=citrulline
IbTx-G30Dab	ZFTDVDCSVSKECWSVCKDLFGVDRGKCM**X**KKCRCYQ **X**=2,4-diaminobutyric acid
IbTx-R34E	ZFTDVDCSVSKECWSVCKDLFGVDRGKCMGKKC**E**CYQ

restored and diminished, respectively. (Note that in this study only 100 nM concentration of the peptides were used.)

Homology model on the binding of the IbTx to its ion channel and *in silico* residue scanning experiments on positions 23-25 revealed that the exchange of these residues to RRR, MRR, DWR, or RWR might result in a stronger interaction with the ion channels. Thus, the corresponding analogs were synthesized and tested. The result shows that only ZFYQ-RWR-b and ZFYQ-RRR affected the blockade of the Kv1.3 ion channel. None of the new analogs act on the KCa1.1 channel. (a and b indexes in the names designate peptides with the same sequences having different disulfide bridge patterns.)

It seems that the analogs with an Arg residue at position 23 (desF^{21}-ZFYQ, ZFYQ-RWR-b, ZFYQ-RRR) can close – at least partially - Kv1.3 channel and an aromatic residue at position 24 is beneficial (desF^{21}-ZFYQ and ZFYQ-RWR). Indeed, this position corresponds to position 25 in AgTx2, which contains a Phe here.

The homology model elucidated that Arg^{25} of IbTx forms a salt bridge with Asp^{357} of the KCa1.1 channel. To test this hypothesis this residue was changed to citrulline, which has a similar size to Arg, and can form H-bond, but cannot form a salt bridge. R25Cit mutant has no affinity to the KCa1.1 channel (Figure 2.). This is in agreement with our previous measurements: Only peptides with Arg at position 25 (ZFYQ-RWR-a, ZFYQ-RRR, ZFYQ-MRR) blocked KCa1.1 – at least to some extent.

Gly^{30} has a key role in the insensitivity of the IbTx toward Kv1.3. Other toxins (charybdotoxin, AgTx2, KTX1) contain an Asn in this position, which forms an H-bond with Asp^{381} of the channel. It was shown earlier that IbTx G30N has an affinity to Kv1.3 [7]. We wanted to see what will be the effect of the incorporation of 2,4-diaminobutyric acid into position 30. This residue would be able to form not only an H-bond but a salt bridge with Asp^{381}. This mutation did not increase the affinity to Kv1.3, but it did to the KCa1.1 channel.

Vm24 (α-KTx 23.1) is a 36-residue Kv1.3-blocker peptide from the venom of the scorpion *Vaejovis mexicanus smithi*. Vm24 blocks the Kv1.3 channel with high affinity (Kd = 2.9 pM) and displays excellent selectivity against several ion channels. However, at high peptide concentrations (over 10 nM) it also blocks other ion channels including Kv1.1, Kv1.2, and KCa3.1. A natural analog of Vm24 called sVmKTx differ from the parent peptide only in a single residue: namely Vm24 contains lysine at position 32 and sVmKTx has glutamate here. Although the affinity of sVmKTx decreased to 770 pM concerning the Kv1.3 channel, it does not block any other ion channel even at 100 nM (and in some cases at 2.5 µM) concentrations. Molecular dynamics simulations showed that K32E mutation led to the decreased structural fluctuation of the N-terminal segment of the mutant peptide. This difference was preserved after their binding to Kv1.3 [5].

If we compare the sequence of Vm24 (AAAISCVGSPECPPKCRAQGCKNGKCMNRKCKCYYC) and IbTx (Table 1), it is visible that Lys^{32} in Vm24 corresponds to Arg^{34} in IbTx. As a consequence of that IbTx-R34E was prepared and examined. The mutated peptide was able to act on the Kv1.3 channel with a small affinity, but with higher selectivity, since it lost its activity on the KCa1.1 channel.

Conclusion

The selectivity of IbTx can be altered by the mutation of a couple of residues. Incorporation of Gly at position 9, the exchange of the C-terminal residues of IbTx to that of AgTx2, and the presence of Arg and an aromatic residue at positions 23 and 24, respectively, resulted in an increase in affinity and sometimes in selectivity toward the Kv1.3 ion channel. Arg^{25} is an important determinant of the binding to KCa1.1. Replacement of Gly^{30} with 2,4-diaminobutyric acid did not increase the affinity toward Kv1.3, so a salt bridge between this residue and Asp^{381} of Kv1.3 was not formed, probably. R34E mutation might have some beneficial effects by increasing the selectivity of the chimera.

In the future, we will check the additivity of the findings listed above by synthesizing such analogs of $desF^{21}$-ZFYQ and ZFYQ-RWR which have a Gly at position 9. Further increase in affinity and selectivity can be expected by incorporating again the *C*-terminal residues of AgTx2 and the effect of R34E replacement should be studied more.
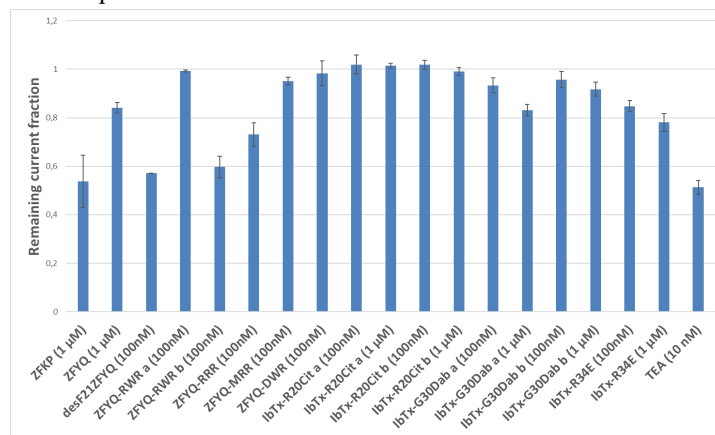
Fig. 1. The electrophysiological effect of analogs on Kv1.3 channel.
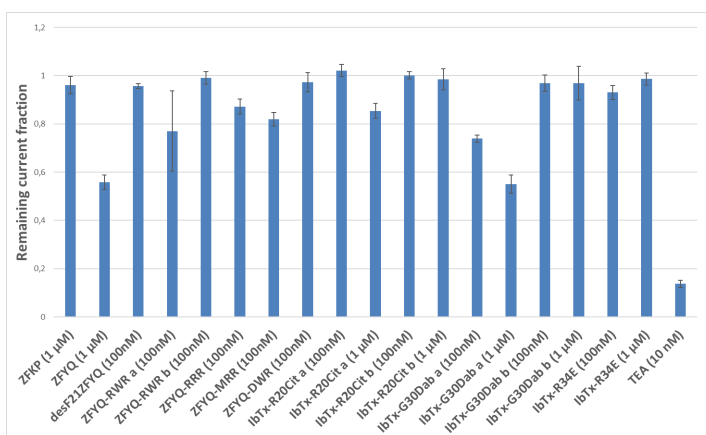
Fig. 2. The electrophysiological effect of analogs on KCa1.1 channel.

Acknowledgments

References

1. Catterall, W.A., et al. *Toxicon* **49**, 124-141 (2007), https://doi.org/10.1016/j.toxicon.2006.09.022
2. Bajaj, S. and Han, J. *Frontiers in Pharmacology* **10**, Article 58 (2019), https://doi.org/10.3389/fphar.2019.00058
3. Oliveira, I.S., et al. *Venom Anim Toxins incl Trop Dis* **25**, e148118 (2019), https://doi.org/10.1590/1678-9199-JVATITD-1481-18
4. Varga, Z. et al. *Biologia Futura* **72**, 75-83 (2021), https://doi.org/10.1007/s42977-021-00071-7
5. Csóti, Á., et al. *Biochemical Pharmacology* **199**, 115023 (2022), https://doi.org/10.1016/j.bcp.2022.115023
6. Gao, Y.-D. and Garcia, M.L. *Proteins: Struct, Func. and Gen.* **52**, 146-154 (2003), https://doi.org/10.1002/prot.10341
7. Schroeder, N., et al. *FEBS Letters* **527**, 298-302 (2002), https://doi.org/10.1016/S0014-5793(02)03256-8

Cationic Hylin Bioactive Peptides from *Boana pulchella* (Anura: Hylidae): Activity, Structure, and Interaction with Lipid Membranes

Silvana Aguilar[1], Andrés E. Brunetti[2,3], Aisel Valle Garay[4], Liem Canet Santos[4], Luis O. Perez[5], Daniel Moreira[6], Lorena Cancelarich[1], Eder Alves Barbosa[5,6], Néstor G. Basso[7], Sonia María de Freitas[4], Julián Faivovich[8], Guilherme Brand[4], Gabriela M. Cabrera[9], José R.S.A. Leite[6,10], and Mariela M. Marani[1]

[1]IPEEC-CONICET, Consejo Nacional de Investigaciones Científicas y Técnicas, 9120 Puerto Madryn, Argentina; [2]Faculdade de Ciências Farmacêuticas de Ribeirão Preto, Departamento de Ciências Biomoleculares, Universidade de São Paulo, 14040-903 Ribeirão Preto, Brasil; [3]Laboratorio de Genética Evolutiva, Instituto de Biología Subtropical (CONICET-UNaM), Facultad de Ciencias Exactas Químicas y Naturales, Universidad Nacional de Misiones, N3300LQH, Posadas, Argentina; [4]Instituto de Biologia, Departamento de Biologia Celular, Laboratório de Biofísica Molecular, Universidade de Brasília (UnB), Brasília, DF, 70910-900, Brasil; [5]IPCSH-CONICET, 9120, Puerto Madryn, Argentina; [6]Núcleo de Pesquisa em Morfologia e Imunologia Aplicada, NuPMIA, Faculdade de Medicina, Universidade de Brasilia, UnB, Brasilia, 70910-900, Brasil; [7]IDEAus-CONICET, 9120, Puerto Madryn, Argentina; [8]División Herpetología, Museo Argentino de Ciencias Naturales 'Bernardino Rivadavia' (CONICET), Buenos Aires, Argentina; [9]Facultad de Ciencias Exactas y Naturales, Departamento de Química Orgánica, Universidad de Buenos Aires, Ciudad Universitaria, C1428EHA Buenos Aires, Argentina; [10]Laboratorio de Espectrometria de Massa, EMBRAPA Recursos Genéticos e Biotecnología, Brasil; Laboratorio de Sintese e Análise de Biomoléculas, Instituto de Química, Universidade de Brasília, Brasil

Introduction

Amphibians are an important source of antimicrobial peptides (AMPs), which are an essential component of their innate immune system contributing to the neutralization or elimination of microorganisms [1,2]. Each species produces its own set of AMPs.

The primary mechanism of action of AMPs typically involve nonspecific electrostatic interactions with bacterial membranes, and proceed through the aggregation of AMPs in the bacterial membrane, affecting its integrity and leading to cell death.

The *Boana* genus is one of the most species-rich clades of the hylid family with a widespread distribution in South America [3]. It has been poorly studied in terms of their AMP profile. To our knowledge, no research have explored the potential mechanism of action of AMPs from *Boana* spp., with the exception of some analogues[4,5].

Based on our results, the possible mechanism of action of these novel molecules and the importance of environmental polarity were discussed.
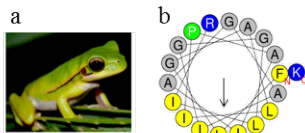
Fig. 1. a) Male adult specimen of Boana pulchella (photo by Andrés Brunetti). b) Helical wheel projection of the AMP hylin-Pul3 identified in the skin secretion of B. pulchella.

Results and Discussion

Our study identified novel peptide sequences from the skin of the tree frog *Boana pulchella* (Figure 1a) using molecular and mass spectrometry analyses. Five unique and novel full-length prepro-peptide cDNAs were identified after cloning, size evaluation, selection of the amplified insert fragments, and sequencing. Precursors showed the typical tripartite structure of AMPs. The analysis of the primary sequences of the peptides identified from the lyophilized crude skin extract of *B. pulchella* by RP-HPLC followed by LC-ESI-MS/MS revealed the presence of several peptides including acidic and amidated C-terminus fragments of the mature peptides identified from mRNAs. This post-transcriptional modification occurs commonly in AMPs and is necessary for membrane binding [6].

Mature peptide sequence alignment with previously described AMPs showed a similarity of 68-84% of four of these peptides with hylin–Prs1 identified from *Boana prasine* [7] and 52-74% with hylin b1, and hylin b2 isolated from *Boana lundii* [8].

Hylin primary sequences are cationic (+1 or +3), with 18 and 20 residues and only Pro7 and Gly11 conserved in all family members. Despite this variability, all hylins exhibit a characteristic amphipathic arrangement with most of the hydrophobic residues (58-68%), such as Leu, Ile, Val, Phe, or Ala, located at the same face (Figure 1b), and the basic amino acids located at the *C*-terminus.

Circular dichroism (CD) was used to evaluate the secondary structure that Fmoc/tert-butyl-synthetized peptides adopt in the presence of neutral and anionic membrane environments. Soluble peptides exhibited a negative band centered at 195–197 nm matching the π-π* transition, typical of unordered conformations. For mature hylin peptides, a high dichroic signal at 195 nm, 208 nm, and 220–230 nm can be observed, compatible with the formation of an α-helical secondary structure upon binding to DMPG:DMPC (1:2) LUVs (Figure 2a) and, to a lesser extent, to pure DMPC. The evaluated fragments hylin-Pul1(12–19) and hylin-Pul2(12–19) did not show significant variations in spectral features when LUVs were added.

Dynamic light scattering (DLS) was used to evaluate the effects of peptides on the size of vesicles mimicking the plasma membrane of eukaryotic and prokaryotic cells. On DMPC membranes, none of the peptides nor any of the fragments were able to increase the size of the vesicles. However, larger particles resulted from the aggregation or fusion of the vesicles in the presence of hylin peptides (Figure 2b).
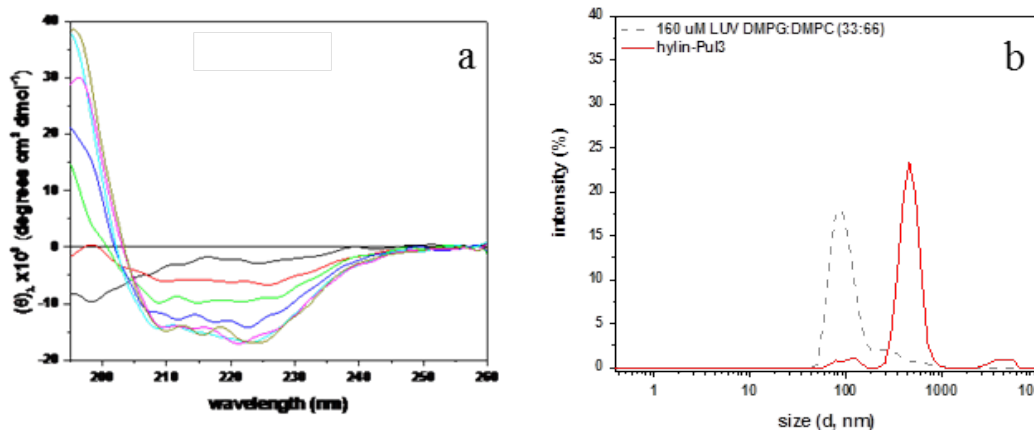
Fig. 2. a) Far-UV CD spectra of the most active peptide, hylin-Pul3,in 10 mM Tris-HCL with 0.15 M of NaCl at pH 7.4 buffer with LUVs DMPG:DMPC (1:2) are shown as follows: soluble peptides 40 μM (black lines) and six peptide:lipid molar ratios 1:1 (red), 1:2 (green), 1:4 (blue), 1:8 (cyan), 1:16 (magenta), and 1:32 (dark yellow).b) Dynamic light scattering of hylin-Pul3 interacting with LUV DMPG:DMPC (33:66) membranes. Size distributions by scattered intensity of particles after peptide addition to LUVs is shown.

Hemolytic activity and antimicrobial activity against *Escherichia coli* and *Staphylococcus aureus* were used to characterize the activity of peptides and fragments. Results of antimicrobial assays of purified synthetic hylin-Pul1, hylin-Pul2, hylin-Pul3, hylin-Pul4, prasin b-Pul, and some of their fragments are summarized in Table 1. Hylin-Pul3 exhibited the most potent antimicrobial activity against the Gram-positive bacteria *S. aureus*, with a MIC concentration of 14 μM. Hemolysis assay of hylin-Pul3 showed less than 2% hemolytic activity on human red blood cells (RBCs) when assessed at concentrations corresponding to *S. aureus* MIC, indicating a selective effect towards bacteria cells.

Table 1. Antimicrobial activity determination of peptides from the skin of B. pulchella.

Name	Sequence	MIC			
		E. coli		S. aureus	
		µg/ml	µM	µg/ml	µM
hylin-Pul1	FLGALIPAITGLIGGLINR-NH$_2$	200	102	200	102
ylin-Pul1(1-11)	FLGALIPAITG	≥ 800	N/D	≥ 800	N/D
hylin-Pul1(12-19)	LIGGLINR-NH$_2$	≥ 800	N/D	≥ 800	N/D
hylin-Pul2	FLGALIPAAIGLISGLIKK-NH$_2$	200	102	400	205
hylin-Pul2(12-19)	LISGLIKK-NH$_2$	≥ 800	N/D	≥ 800	N/D
hylin-Pul3	FLGALIPAIAGAIGGLIRK-NH$_2$	200	108	25	14
hylin-Pul3(1-11)	FLGALIPAIAG	≥ 800	N/D	≥ 800	N/D
hylin-Pul3(12-19)	AIGGLIRK-NH$_2$	≥ 800	N/D	≥ 800	N/D
hylin-Pul4	FFGALIPAVAGAIGGFFRK-NH2	100	52	50	26
prasin b-Pul	GALEIFKKYRLPKCF-NH$_2$	200	110	400	221

N/D: not determined

The adoption of a cationic amphipathic α-helix conformation allows an efficient interaction with bacterial outer membranes, as observed for several AMPs. Here, the adoption of such structure by the novel hylin peptides is greatly influenced by their environment. This was evidenced by disordered conformations of all mature hylin-Pul peptides in aqueous solution and a shift to helical conformations in the presence of LUVs mimicking prokaryotic and eukaryotic membranes. Noteworthy, higher fractional helicity values (fH) were observed when peptides interacted with vesicles containing anionic head groups (DMPG:DMPC).

Taken together, far-CD and dynamic light scattering data indicate that, although peptides in helical conformation co-absorb and are selectively bound regardless of membrane composition, the subsequent hydrophobic interaction can alter membrane structure to different degrees depending on membrane composition [9].

In conclusion, we present the identification, synthesis, and biological activities of novel hylin peptides isolated from the skin secretion of *Boana pulchella*. Their antimicrobial activity, as well as their interaction with lipid vesicles, indicates a nonspecific mode of interaction with bacterial membranes. Thus, the hylin peptides from *Boana pulchella* show the typical mechanism of action of α-helix amphibian peptides in bacterial membranes. Our findings highlight the role of membrane composition in inducing a stable conformation and activity of these AMPs against bacteria.

Acknowledgments

References

1. Patocka, J., et al. *Curr Med Chem* **26**(32), 5924-5946 (2019), https://doi.org/10.2174/0929867325666180713125314
2. Kumar, P., et al. *Biomolecules* **8**(1), 4 (2018), https://doi.org/10.3390/biom8010004
3. Faivovich, J., et al. *South Am J of Herpetol* **13**, 1-32 (2018), https://doi.org/10.2994/SAJH-D-17-00115.1
4. Vignoli, Muniz, G.S., et al. *Biochem Biophys Rep* **24**,100827 (2020), https://doi.org/10.1016/j.bbrep.2020.100827
5. Park, H.J., et al. *Eur J Pharm Sci* **175**, 106205 (2022), https://doi.org/0.1016/j.ejps.2022.106205
6. Shahmiri, M. and Mechler, A. *The EuroBiotech Journal* **4**(1), 25-31 (2020), https://doi.org/10.2478/ebtj-2020-0004
7. Brunetti, A.E., et al. *ISME J* **16**(3), 788-800 (2022), https://doi.org/10.1038/s41396-021-01121-7
8. Castro, M.S., et al. *Protein Pept Lett* **12**(1), 89-93 (2005), https://doi.org/10.2174/0929866053405977
9. Gong, H., et al. *ACS Appl Mater Interfaces* **12**(40), 44420-44432 (2020), https://doi.org/10.1021/acsami.0c09931

Discovery of Stapled Peptides as Efficient BCL-xL Inhibitors

Peiyu Zhang [1,2] and Andrew J Wilson [1,2*]

[1]*School of Chemistry, University of Leeds, Woodhouse Lane, Leeds, LS2 9JT, UK;* [2]*Astbury Centre for Structural Molecular Biology, University of Leeds, Woodhouse Lane, Leeds, LS2 9JT, UK*

Introduction

Protein-protein interactions (PPIs) play essential roles in regulating cellular processes, thus represent an important class of targets for drug discovery. The B cell CLL/lymphoma-2 (BCL-2) family of proteins control the intrinsic apoptotic pathway and can be divided into two major classes: proapoptotic members and prosurvival members [1]. In cancer cells, the overexpression of pro-survival proteins can block proapoptotic signaling by sequestering the BH3-only proteins (proapoptotic). Selective inhibition of BCL-xL, a prosurvival member, is of interest due to its functional roles in solid tumors and drug resistance [2]. Using peptides as inhibitors of PPIs is a promising approach because of their larger size and ability to directly mimic native binding domains. Although small molecules have been reported to inhibit BCL-xL, selective inhibition of BCL-xL using stapled peptides remains underexplored. Recently, our group developed a stapling method using dibromomaleimide (DBM) for crosslinking two cysteines/homocysteines [3]. In this study, we performed a DBM staple scan on a peptide sequence based on a potent BH3 domain in combination with virtual alanine scanning, to identify efficient and selective peptide-based BCL-xL inhibitors. One stapled peptide showed improved inhibitory potency (IC_{50}) in a fluorescence anisotropy (FA) competition assay compared to the wild-type and the linear precursor.

Results and Discussion

We designed a number of peptides by inserting a pair of cysteines into a 23-mer BH3 sequence at *i*, *i*+4 positions. After Fmoc-based solid-phase peptide synthesis, the peptides were cleaved and purified by a prep-HPLC. The linear peptides were treated with TCEP and each maleimide-staple was installed using dibromomaleimide (Figure 1).
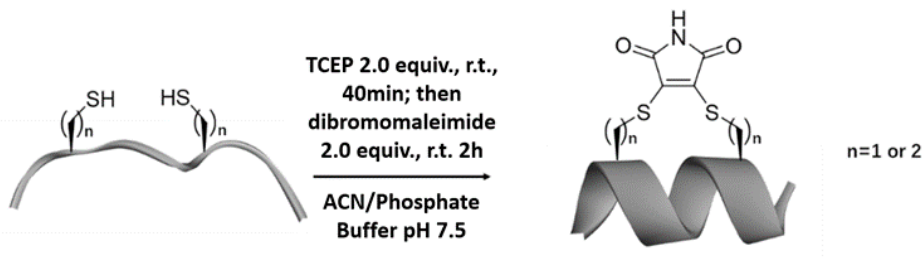
Fig. 1. A representative scheme of synthesis of stapled peptide using dibromomaleimide.
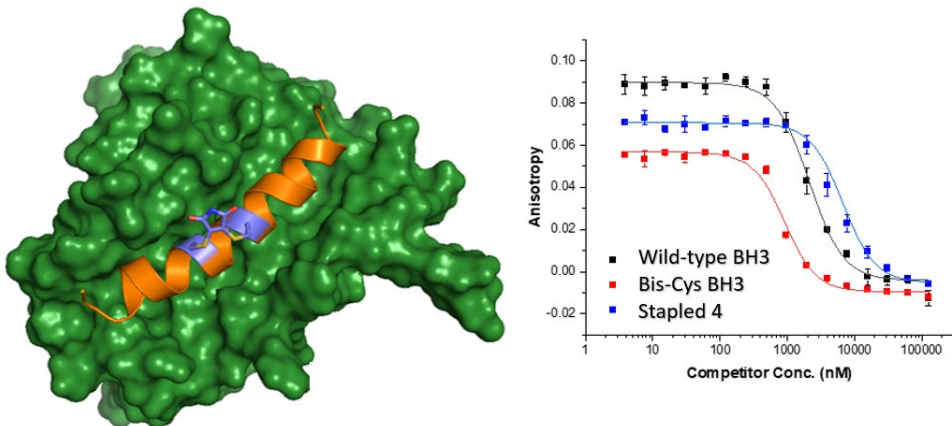
Fig. 2. A representative diagram of a stapled peptide binds to BCL-x$_L$ and FA results of the peptides.

To establish a fluorescence anisotropy assay for screening, we prepared a tracer peptide, FAM-Ahx-BH3, by adding an aminohexanoic (Ahx) linker and a carboxyfluorescein (FAM) group at the *N*-terminus of the 23-mer BH3 sequence. In our direct titration experiment, the tracer bound to the BCL-x$_L$ with an affinity of $K_d = 38$ ($\pm$ 6) nM. Thereafter, the designed peptides were tested in competition assays. Surprisingly, one peptide, *Staple 4*, showed slightly improved potency in comparison to the Wild-Type BH3, whereas the linear peptide, Bis-Cys BH3, showed decreased potency (Figure 2).

Thus we have broadened the scope of the maleimide constraint in the construction of PPI inhibitors in this work and identified promising starting points for identification PPI inhibitors as potential therapeutics for treatment of BCL-x$_L$-overexpressed cancers.

Acknowledgments

References

1. Singh, R., Letai, A., Sarosiek, K. *Nat. Rev. Mol. Cell Biol.* **20**, 175-193 (2019), https://doi.org/10.1038/s41580-018-0089-8
2. Trisciuoglio, D., Tupone, M.G., Desideri, M., Di Martile, M., Gabellini, C., Buglioni, S., Pallocca, M., Alessandrini, G., D'Aguanno, S., and Del Bufalo, D. *Cell Death & Disease* **8**, 3216 (2017), https://doi.org/10.1038/s41419-017-0055-y
3. Grison, C.M., Burslem, G.M., Miles, J.A., Pilsl, L.K.A., Yeo, D.J., Imani, Z., Warriner, S.L., Webb, M.E., and Wilson, A.J. *Chem. Sci.* **8**, 5166-5171 (2017), https://doi.org/10.1039/C7SC01342F

Discovery of Internal Ligand Inhibitors Targeting SHANK1 PDZ Domain Guided by Dynamic Ligation Screening Strategy

Yue Li[1], Stuart L. Warriner[1,2], and Andrew J. Wilson[1,2]

[1]*School of Chemistry, University of Leeds, Woodhouse Lane, Leeds, LS29JT, UK;* [2]*Astbury Centre for Structural Molecular Biology, University of Leeds, Woodhouse Lane, Leeds, LS29JT, UK*

Introduction

Protein-protein interactions have received extensive recent attention as targets for drug discovery given their key role in controlling many biological processes. In terms of the model PPI studied here, we choose the SHANK1 PDZ domain as the target protein. An accumulating body of research shows that mutation in SHANK genes often will interfere with the structure and function of their corresponding product proteins, leading to various neurological disorders and psychiatric diseases [1]. As one of the best-known and largest PPI modules, the PDZ domain is responsible for supporting the intracellular communication network at the postsynaptic site (Figure 1).
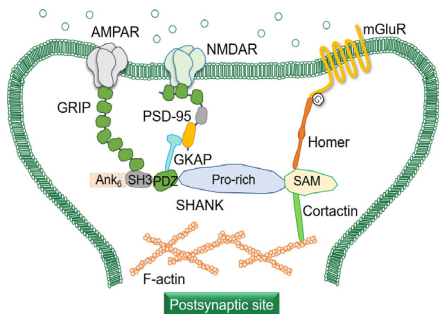
Fig. 1. Scheme illustration role of SHANK and its interacting proteins in the postsynaptic site.

Typically, SHANK PDZ binds to *C*-terminal PBMs in a β-strand conformation, such as the reported examples – *β*PIX/SHANK1 PDZ PPI (Figure 2A) [2] and GKAP/SHANK1 PDZ PPI (Figure 2B) [3]. Hegedüs et al used a dynamic ligation screening workflow (Figure 3) to identify peptide fragment hybrids bearing N-terminal modifications with strong affinity for SHANK1 PDZ (Figure 2C) [4], however no promising *C*-terminal fragments were identified. Internal ligands that bind PDZ domains have been identified as alternative motifs in modulating SHANK proteins in recent years (Figure 2D) [5] and may represent promising starting points for identification of *C*-terminal peptide-fragment hybrids.

(A) βPIX ($_{642}$DETNL$_{646}$)/SHANK1 PDZ PPI [K_d = 41 (±1) μM]

(B) GKAP ($_{661}$EAQTRL$_{666}$)/SHANK1 PDZ PPI [Kd = 2 (±0.3) μM]

(C) 4-A047/SHANK1 PDZ PPI [Kd=1.45 (±0.05) μM]

(D) ARAP3$_{1414-1428}$/SHANK1 PDZ PPI[Kd = 3 (±0.3)]
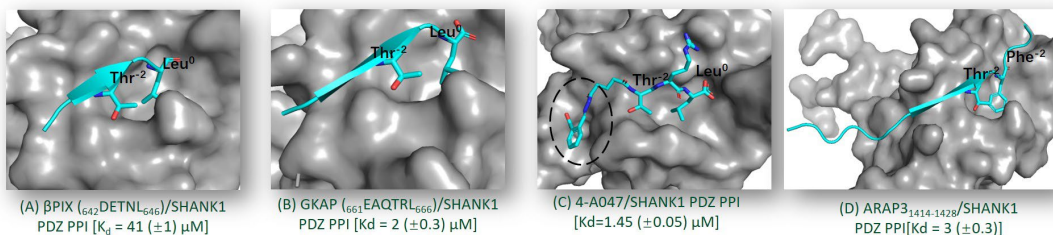
Fig. 2. Ribbon diagrams of typical PPIs of SHANK1 PDZ domain with C-terminal ligands (A-C) and with internal ligand (D).

Results and Discussion

Inspired by prior research on SHANK1 PDZ ligands, we seek to design novel internal ligand inhibitors with the SHANK1 PDZ domain as target. The main strategy is based on the dynamic ligation screening method [4] combined with fluorescent anisotropy assays.

First of all, an artificial sequence PSSMI generated through position-specific scoring experiments in a recently published paper [5] was chosen as precursor after determining the binding affinity (0.81 ± 0.08 μM) of its fluorescently labelled analogue FAM-Ahx-PSSMI and its
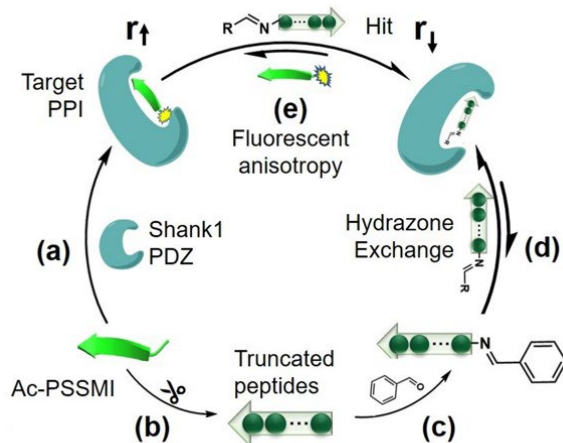
Fig. 3. Schematic illustrating the dynamic ligation screening approach for identification of peptide fragment hydrazones that inhibit strand mediated PPIs.

competition inhibitory activity (3.9 ± 0.1 μM) against FAM-Ahx-PSSMI, where the SHANK1 PDZ domain (656-762) was the target protein.

To further improve the inhibitory activity of designed peptides and explore the function of hybrid short linear motifs (SLiMs) in modulating the PPI of SHANK1 PDZ with internal ligands, we truncated the acetylated peptide Ac_PSSMI from the *N*-terminus, *C*-terminus and both sides.

Based on our truncation studies, we chose phenylhydrazone analogues of PSSMI with *N*-terminal acetamides as templates for subsequent screening. Hydrazone exchange reactions were involved in the dynamic ligation screening experiments (Figure 3). By employing a library containing 165 aldehyde fragments, as a result, a series of potential hydrazones were obtained, and inhibitory activities against FAM_Ahx_PSSMI were established. Resynthesis, purification of promising fragment peptide hydrazones and full dose response analysis confirmed this approach could identify potent *C*-terminal peptide-fragment hybrids with single digit μM IC_{50} values. These results pave the way to further develop short linear internal ligands for SHANK1 PDZ domain.

Acknowledgments

References

1. Monteiro P., et al. *Nature Reviews Neuroscience* **18**, 147-157 (2017), https://doi.org/10.1038/nrn.2016.183
2. Liu, J., et al. *PloS one* **11**, e0149580 (2016), https://doi.org/10.1371/journal.pone.0149580
3. Celis, S., et al. *Chemical Science* **12**, 4753-4762 (2021), https://doi.org/10.1039/d1sc00023c
4. Hegedüs, Z., et al. *Chemical Science* **12**, 2286-2293 (2015), https://doi.org/10.1039/d0sc05694d
5. Ali, M., et al. *Current research in structural biology* **3**, 41-50 (2021), https://doi.org/10.1016/j.crstbi.2021.01.001

Novel Polymyxins with Reduced Toxicity and Modulated Spectrum of Activity

J. García-Gros[1], R. Segovia[1], J. Solé[1], M. Gros[1], A. M. Marqués[2], Y. Cajal[3,4], and F. Rabanal[1*]

[1]*Department of Inorganic and Organic Chemistry, Faculty of Chemistry;* [2]*Laboratory of Microbiology, Faculty of Pharmacy and Food Sciences;* [3]*Department of Pharmacy, Pharmaceutical Technology and Physical Chemistry, Faculty of Pharmacy and Food Sciences, University of Barcelona;* [4]*Institute of Nanoscience and Nanotechnology (IN2UB), 08028 Barcelona, Spain*

Introduction

Antibacterial resistance to almost all available antibiotics is increasing worldwide, and Gram-negative multidrug-resistant bacteria are particularly worrisome. Moreover, the extensive use of antibiotics in the context of the COVID-19 pandemic has accelerated the threat of running out of them. Here, we report a series of polymyxin E (colistin) synthetic analogues with a disulfide bond-containing scaffold and modifications in the hydrophobic domains (Figure 1). By means of biophysical techniques, we explore the interaction of these compounds with models that mimic the bacterial inner and outer membranes, resulting in a selective effect on anionic membranes.

Results and Discussion

Design and synthesis

In previous work, we demonstrated that the introduction of a disulfide bond within the macrocycle peptide structure reduces the toxicity compared to that displayed by natural polymyxins [1,2]. In the present work, we have modulated the hydrophobicity of these molecules by changing the length of the fatty acyl chain and the amino acid at position 6. All analogues have been synthesized by Fmoc/tBu solid-phase peptide synthesis (SPPS).
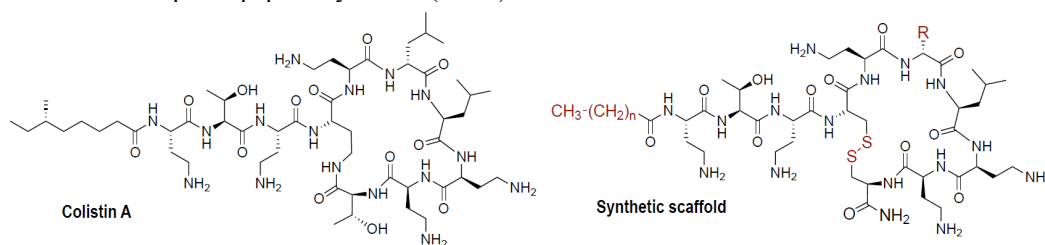
Fig. 1. Structure of natural colistin A (left) and general structure of the synthetic analogues (right).

In vitro activity and hemolysis assays

The activity against bacteria has been assessed in terms of the minimum inhibitory concentration. Two Gram-negative bacteria (*Escherichia coli* and *Pseudomonas aeruginosa*) and one Gram-positive (*Staphylococcus aureus*) have been evaluated. Hemolytic activity was assessed using fresh rabbit erythrocytes and determined by measuring the absorbance at 540 nm of released hemoglobin in the supernatant after peptide exposure. As it can be shown in Table 1, a minimum length of seven carbons in the fatty acyl chain is needed for activity. Analogues with longer acyl chains induce higher degree of hemolysis (Figure 2). On the other hand, the sPE-10 analogue showed selectivity towards *P. aeruginosa* and very low hemolytic activity.
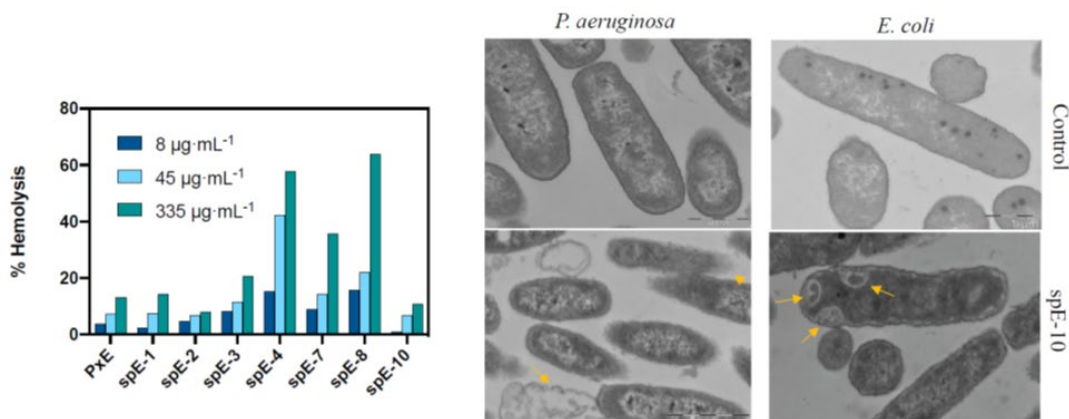
Fig. 2. Hemolysis induced by synthetic analogues(left). TEM images for control samples and bacteria treated with analogue spE-10 at its MIC value (right). Yellow arrows indicate rupture of the cell membrane and cytoplasmic clear zones.

Transmission electron microscopy

The effect of analogue spE-10 on *E. coli* and *P. aeruginosa* has been studied by transmission electron microscopy (TEM). As shown in Figure 2, the treatment of *P. aeruginosa* with spE-10 causes significant rupture of the cell membranes and cytoplasmic clear zones. In the case of *E. coli*, this analogue similarly induces the formation of intracellular membranous structures and cytoplasmic clear zones.

Table 1. Sequences and antimicrobial activities of the peptide analogues determined as the minimal inhibitory concentration (MIC) calculated for different bacteria strains.

	Sequence	*MIC (µg.mL⁻¹)*		
		EC¹	*PA*	*SA*
spE-1	hexanoyl-Dab-Thr-Dab-<u>Cys</u>-Dab-*Leu*-Leu-Dab-Dab-<u>*Cys*</u>	>32	>32	>32
spE-2	octanoyl-Dab-Thr-Dab-<u>Cys</u>-Dab-*Leu*-Leu-Dab-Dab-<u>*Cys*</u>	16	4	>32
spE-3	decanoyl-Dab-Thr-Dab-<u>Cys</u>-Dab-*Leu*-Leu-Dab-Dab-<u>*Cys*</u>	8	2	8
spE-4	dodecanoyl-Dab-Thr-Dab-<u>Cys</u>-Dab-*Leu*-Leu-Dab-Dab-<u>*Cys*</u>	8	1	8
spE-7	decanoyl-Dab-Thr-Dab-<u>Cys</u>-Dab-*Nle*-Nle-Dab-Dab-<u>*Cys*</u>	2	2	8
spE-8	dodecanoyl-Dab-Thr-Dab-<u>Cys</u>-Dab-*Nle*-Nle-Dab-Dab-<u>*Cys*</u>	4	4	4
spE-10	heptanoyl-Dab-Thr-Dab-<u>Cys</u>-Dab-*Aoc*-Nle-Dab-Dab-<u>*Cys*</u>	8	1	>32
Polymyxin B	R1-Dab-Thr-Dab-<u>Dab</u>-Dab-*Phe*-Leu-Dab-Dab-<u>Thr</u>	1	0.5	>32
Colistin	R1-Dab-Thr-Dab-<u>Dab</u>-Dab-*Leu*-Leu-Dab-Dab-<u>Thr</u>	1	0.5	>32

D-amino acids are denoted in italics, and underlined residues denote bond formation. R1: natural mixture of branched C7-C9 fatty acyl moieties

Biophysical studies

The binding affinity of colistin and the synthetic analogues with model lipid membranes has been studied by using monolayers at the air-water interface. Different lipid compositions including LPS, POPE:POPG (6:4), POPG and POPC have been tested. According to the results obtained, the synthetic analogues as well as colistin show a high binding affinity for LPS, which mimics the outer membrane of Gram-negative bacteria. In contrast, the change in surface pressure for zwitterionic POPC membrane is low, indicating a low affinity of the analogues and colistin to bind the eukaryotic membrane model.

Colistin is able to induce the aggregation of vesicles forming clusters, what facilitates the selective exchange of phospholipids. The change in light scattering of the synthetic analogues has been evaluated with liposomes of POPE:POPG and, like colistin, the lipopeptides show an increase of the scattered light, indicating vesicle aggregation (Figure 3). In order to study if the analogues induce mixing, a FRET experiment using vesicles containing 0.6% NBD-PE (donor vesicles) and vesicles containing 0.6% Rh-PE (acceptor vesicles) was conducted. All synthetic analogues induced the lipid mixing between anionic vesicles of POPE:POPG (6:4), similarly to colistin.

Table 2. Increase in surface pressure ($\Delta\pi/mN\cdot m^{-1}$) upon penetration of the antimicrobial lipopeptides into monolayers.

Composition*	Increase in surface pressure ($\Delta\pi/mN\cdot m^{-1}$)							
	spE-1	spE-2	spE-3	spE-4	spE-7	spE-8	spE-10	PxE
LPS	10.6	9.5	10.0	11.4	14.2	12.5	14.8	11.1
POPE:POPG	4.1	6.4	7.9	9.1	6.8	9.8	8.2	7.9
POPG	2.8	4.3	5.7	5.8	8.2	7.4	0.8	5.3
POPC	0.3	0.6	1.3	2.1	1.4	1.3	1.8	0.8

Monolayers mimic the outer membrane of Gram- (LPS), the cytoplasmic membrane of Gram- (POPE/POPG 6:4), or of Gram+ (POPG), or the eukaryotic membrane (POPC)
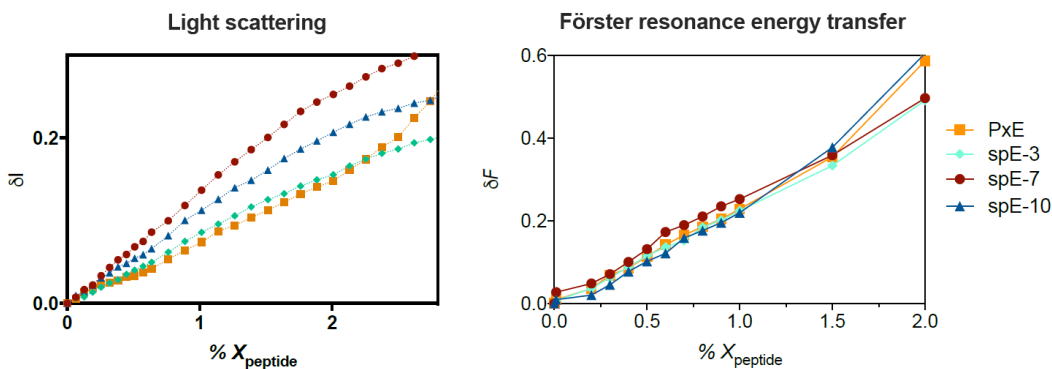
Fig. 3. Change in light scattering (left). On the right, increase in FRET intensity as a function of the mole fraction of lipopeptide added to a (1:1) mixture of vesicles containing 0.6% NBD-PE or Rh-PE.

Finally, we studied the ability of our compounds to induce the leakage of aqueous contents, indicating leaky membrane fusion. In this sense, the increase of fluorescence of ANTS co-encapsulated with the fluorescence quencher DPX was measured. In Figure 4, leakage at three relevant concentrations is shown. As it can be observed, upon peptide addition in membranes of POPE:POPG (6:4), leakage is low in all cases, and at MIC concentrations it remains below 5%, thus indicating a low permeabilization effect in the Gram-negative model.
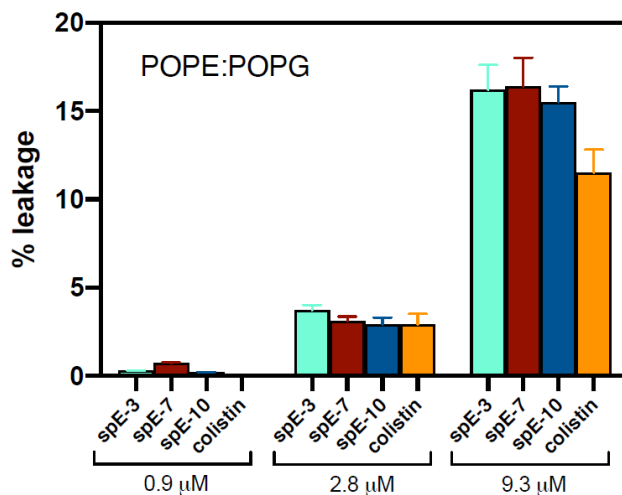
Fig. 4. Leakage from vesicles of POPE/POPG (6:4) at three peptide concentrations. Lipopeptides were added to liposomes co-encapsulating ANTS (12.5 mM) and DPX (45 mM), and leakage was determined as the increase in ANTS fluorescence intensity at 530 nm (excitation 350 nm, lipid concentration 107 μM).

Acknowledgments

Abbreviations

EC: *Escherichia coli*; PS: *Pseudomonas aeruginosa*; SA: *Staphylococcus aureus*; LPS: Lipopolysaccharide from Salmonella enterica serotype Minnesota Re 595 (Re mutant); POPE: 1-palmitoyl-2-oleoylsn-glycero-3-phosphoethanolamine; POPG: 1-Palmitoyl-2-oleoyl-sn-glycero-3-phospho-(1'-rac-glycerol); POPC: 1-palmitoyl-2-oleoyl-glycero-3-phosphocholine; ANTS: 8-aminonaphthalene-1,3,6-trisulfonic acid; DPX: p-Xylene-bis(N-pyridiniumbromide).

References

1. Rabanal, F., Grau-Campistany, A., Vila-Farrés, X., Gonzalez-Linares, J., Borràs, M., Vila, J., Manresa, A., Cajal, Y. *Sci. Rep.* **5**, 10558 (2015), https://doi.org/10.1038/srep10558
2. Rabanal, F., Cajal, Y. *Nat. Prod. Rep.* **34**, 886-908 (2017), https://doi.org/10.1039/C7NP00023E
3. Segovia, R., Solé, J., Marqués, A.M., Cajal, Y., Rabanal, F. *Pharmaceutics* **13**, 2180 (2021), https://doi.org/10.3390/pharmaceutics13122180

Search for Peptidomimetic Inhibitors of the VEGF-A₁₆₅ / NRP-1 Complex with Modification of the *C*-Terminal Arginine

Dagmara Tymecka[1], Patrycja Redkiewicz[2], Piotr F.J. Lipiński[2], and Aleksandra Misicka[1]

[1]Faculty of Chemistry, University of Warsaw, Warsaw, 02-093, Poland; [2]Department of Neuropeptides, Mossakowski Medical Research Institute Polish Academy of Sciences, Warsaw, 02-106, Poland

Introduction

Neuropilin-1 (NRP-1) is a cell surface receptor involved in a wide variety of signaling pathways, including physiological and pathological processes of angiogenesis. Its overexpression is associated with tumor aggressiveness and metastasis, which is observed, inter alia, in breast, colon cancer or brain tumors [1]. One of the most important ligands of NRP-1 and the main mediators of angiogenesis is vascular endothelial growth factor A₁₆₅ (VEGF-A₁₆₅), which acts as a pro-angiogenic factor by interacting with the b1 domain of NRP-1. Compounds that block this interaction are potential inhibitors of the VEGF-A₁₆₅/NRP-1 complex that may find application in the diagnosis and therapy of cancer. One of significant achievements in this field was the identification of the heptapeptide Ala-Thr-Trp-Leu-Pro-Pro-Arg (A7R), which selectively inhibits the binding of VEGF-A₁₆₅ to NRP-1 and reduces angiogenesis and breast cancer growth *in vivo* [2,3]. Based on the structure of the A7R *C*-terminal tetrapeptide, we designed stronger inhibitors, in particular: Lys(Har)-Dap-Pro-Arg (**1**) and Lys(Har)-Dab-Pro-Arg (**2**). However, detailed stability studies of these compounds in human plasma (*in vitro*) have shown that the first cleavage site is a detachment of the *C*-terminal arginine by carboxypeptidases, resulting in a loss of activity since arginine is a key element in the interaction between these inhibitors and NRP-1 [3,4].

Results and Discussion

The aim of the present study was to obtain more stable (and active) analogs of these branched peptidomimetics (**1** and **2**). For this purpose, we decided to replace *C*-terminal arginine with its mimetics. In our previous work [4], based on molecular dynamics, we put forward an interaction model for compounds **1** and **2**. According to this model: (i) the branched peptidomimetics adopt more than one binding pose at the NRP-1 binding cleft, with two poses (Figure 1, BP1 and BP2) being dominant
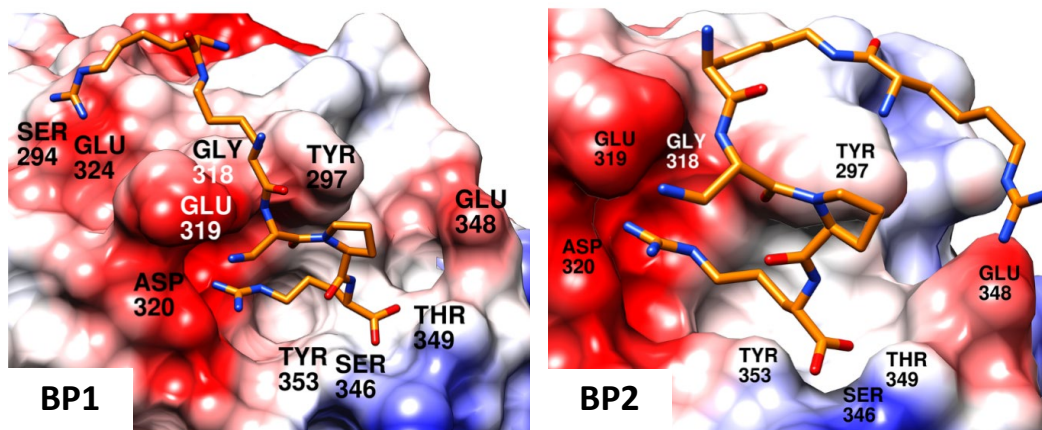
Fig. 1. Two dominant binding poses (PB1 and PB2) found in molecular dynamics simulations for Lys(Har)-Dap-Pro-Arg as complexes with b1 domain of NRP-1. The NRP-1 receptor is depicted as an electrostatic color-coded surface (red: negative charges, white: neutral, blue: positive). Colors of ligands are orange, red and blue for carbon, oxygen and nitrogen, respectively.

and in mutual equilibrium; (ii) the peptidomimetics insert their *C*-terminal Arg residue in the shallow cleft at the protein surface and form several interactions, including H-bonds to Asp320, Ser346, Thr349 (Figure 1); (iii) the middle and *N*-terminal parts of the peptidomimetic retain some residual mobility and switch between positioning BP1 and BP2, forming several interactions in each, including H-bonds to Gly318, Glu319, Glu324, Ser294, Tyr297, Glu348.

With our desire to replace the *C*-terminal Arg, we took the described above model as a starting point for designing new compounds. We analyzed several possible modifications to the *C*-terminus and confronted them with our previous model through molecular docking. Our speculation was that it should be possible to shorten the arginine side chain to Agb (2-amino-4-guanidino-butyric acid) or even Agp (2-amino-3-guanidino-propionic acid). Given that Lys(Har)[1] and Dap/Dab[2] side-chains are long and flexible, it was envisaged that some shortening in Xaa[4] should be tolerated. The first and second residue should still be able to reach their interaction partners (Figure 1). And shorter Xaa[4] should be still able to interact with Asp320 and Ser346/Thr349 (Figure 2A and 2B). We contemplated also extending the Xaa[4] residue to Har (homoarginine). According to crystal structure 5IJR [5], Har can be accommodated in the cleft although with some displacement of the binding mode compared to if Arg is present in the cleft. We supposed however that interactions of Lys(Har)[1] and Dap/Dab[2] would allow retaining significant affinity. Furthermore, it was interesting to see if the *C*-terminal residue with an aromatic ring could gain some affinity due to forming aromatic interactions with Tyr297 (Figure 2D). Finally, a kind of an acid-test to the importance of guanidine-Asp320 interactions was provided by a Cit[4]-analogue, which is able to form one H-bond without charge-assistance (Figure 2C). This analogue was quite decently scored by docking.

To evaluate the accuracy of the design assumptions the inhibitory activity of the obtained compounds on VEGF-A$_{165}$ binding to the NRP-1 was estimated *in vitro* by modified competitive Enzyme-Linked Immunosorbent Assay (ELISA), following the previously described protocol [6]. Obtained results revealed that extension of Arg[4] side chain (**1** and **2**) by introducing one methylene
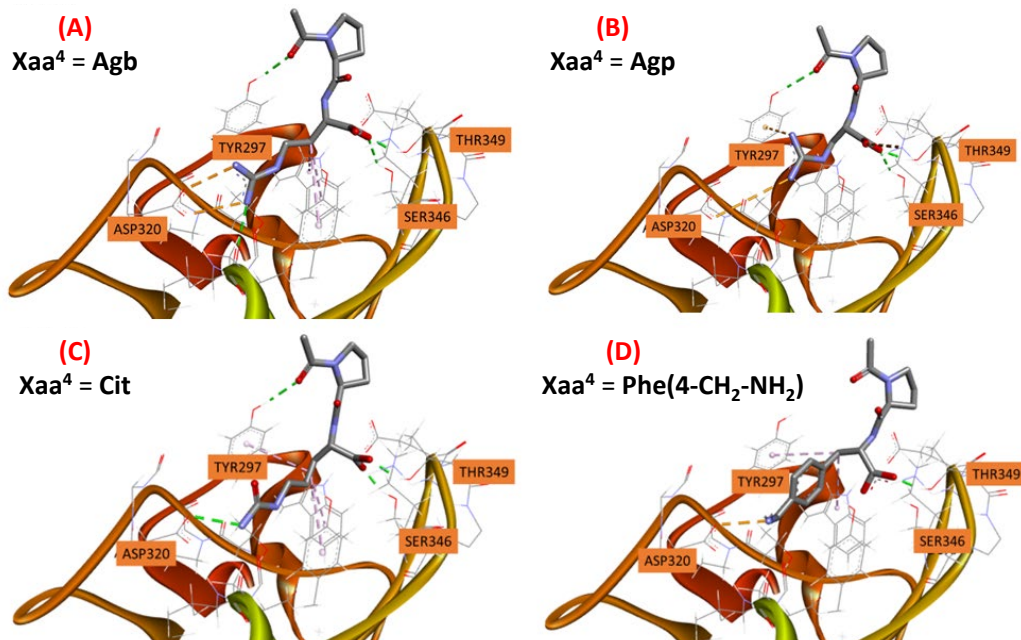
Fig. 2. Predicted binding poses for the C-terminal part of the analogues with (A): Agb^4, (B): Agp^4, (C): Cit^4 and (D): Phe(4-CH$_2$NH$_2$)^4. Protein atoms shown as lines. Ligand atoms shown as sticks (only Pro^3-Xaa^4 part). Only selected residues of the NRP-1 binding cleft shown. Hydrogen display in the ligands suppressed. Dotted lines represent interactions (green – H-bond, orange – electrostatic, pink – hydrophobic).

Table 1. Inhibitory effect of obtained peptidomimetics on VEGF-A$_{165}$ binding to NRP-1.

No	Structure	IC$_{50}$ [µM] ± SD
A7R	Ala-Thr-Trp-Leu-Pro-Pro-Arg	11.3 ± 3.2
1	Lys(Har)-Dap-Pro-Arg	8.4 ± 1.6
2	Lys(Har)-Dab-Pro-Arg	4.7 ± 0.6
3	Lys(Har)-Dap-Pro-Har	29.2 ± 1.8
4	Lys(Har)-Dab-Pro-Har	14.3 ± 2.3
5	Lys(Har)-Dap-Pro-Agb	87.5 ± 10.3
6	Lys(Har)-Dab-Pro-Agb	105.7 ± 17.4
7	Lys(Har)-Dap-Pro-Agp	147.6 ± 45.9
8	Lys(Har)-Dab-Pro-Agp	164.7 ± 21.1
9	Lys(Har)-Dap-Pro-Cit	169.7 ± 55.6
10	Lys(Har)-Dab-Pro-Cit	193.3 ± 20.6
11	Lys(Har)-Dap-Pro-Phe(4-CH$_2$-NH$_2$)	22.8 ± 5.9
12	Lys(Har)-Dab-Pro-Phe(4-CH$_2$-NH$_2$)	19.8 ± 1.8

group to obtain Har[4] (**3** and **4**, respectively), gives only a slight decrease in inhibitory activity as compared to the parent compounds. However, contrary to our speculation, shortening the Arg[4] side chain (**1** and **2**) to Agb (- 1 x CH$_2$, **5** and **6**) or further to Agp (- 2 x CH$_2$, **7** and **8**) leads to a significant reduction in the inhibition of VEGF-A$_{165}$ binding to NRP-1. Similarly, replacement of the guanidine group (Arg[4], in **1** and **2**) by the urea group (Cit[4], **9** and **10**), therefore limiting the interactions (with Asp320), in the shallow binding cleft, to only one H-bond without charge-assistance (salt bridge) significantly reduces the inhibitory activity. Interestingly, the replacement of the alkyl side chain of Arg[4] by the aromatic ring of Phe(4-CH$_2$-NH$_2$) with a simultaneous change of the guanidine to an amino group (**1** and **2** *vs.* **11** and **12**, respectively), resulted in a slight decrease in activity, comparable to that for Har.

Conclusions

In conclusions, our experimental results showed that:
- position of the guanidinium group (which strongly depends on the length of the methylene chain) in relation to Asp320 has a crucial effect on the inhibitory activity that changes as follows:

  Arg (3x CH$_2$) ≈ Har (4x CH$_2$) > Agb (2x CH$_2$) > Agp (1x CH$_2$);
- limited number of the interaction between the side chain of *C*-terminal residue and Asp320 strongly reduces inhibitory activity

  Arg (guanidine group) >> Cit (urea group)
- replacement of ionic interaction with aromatic interaction (inside the binding cleft) allows to maintain inhibitory activity at a similar level

  Arg (guanidine group) ≈ Phe(4-CH$_2$-NH$_2$) (aromatic ring).

Unfortunately, the synthesized analogues are all weaker inhibitors of the VEGF-A$_{165}$/NRP-1 complex than expected, based on the modelling in the design stage. One of the possible reasons for

this disagreement might be that the design was based on static dockings without accounting for flexibility of the protein binding cleft and the possibility of dual/multiple binding modes. However, further studies using the molecular dynamics are warranted to understand and rationalize the obtained experimental data and to guide future designs.

Acknowledgments

References

1. Douyère, M., et al. *Frontiers in Oncology* **11**, 665634 (2021), https://doi.org/10.3389/fonc.2021.66563
2. Starzec, A., et al. *Life Sciences* **79**, 2370-2381 (2006), https://doi.org/10.1016/j.lfs.2006.08.005
3. Starzec, A., et al. *Peptides* **28**, 2397-2402 (2007), https://doi.org/10.1016/j.peptides.2007.09.013
4. Tymecka, D., et al. *European Journal of Medicinal Chemistry* **158**, 453-462 (2018), https://doi.org/10.1016/j.ejmech.2018.08.083
5. Mota, F., et al. *The FEBS Journal* **285**, 1290-1304 (2018), https://doi.org/10.1111/febs.14405
6. Puszko, A.K., et al. *Medicinal Chemistry Communications* **10**, 332-340 (2019), https://doi.org/10.1039/c8md00537k

Effect of Doubling Peptide Length on the Microscopic, Macroscopic and Biological Properties of Hydrogels

Julie Heremans[1], Lucie Chevillard[2], Morgane Mannes[1], Jessica Mangialetto[3], Jacinta F. White[4], Arthur Lamouroux[1], James Gardiner[4], Bruno Van Mele[3], Niko Van den Brande[3], Richard Hoogenboom[5], Annemieke Madder[6], Vicky Caveliers[7], Bruno Mégarbane[2], Sophie Hernot[7], Steven Ballet[1], and Charlotte Martin[1]

[1]Research Group of Organic Chemistry, Vrije Universiteit Brussel, Brussels, B-1050, Belgium; [2]INSERM, UMR-S 1144, Université de Paris, Paris, F-75006, France;[3] Physical Chemistry and Polymer Science, Vrije Universiteit Brussel, Brussels, B-1050, Belgium; [4]CSIRO Manufacturing, Bayview Avenue, Clayton, VIC 3169, Australia; [5]Supramolecular Chemistry Group, Department of Organic and Macromolecular Chemistry, Ghent University, Ghent, 9000, Belgium; [6]Organic and Biomimetic Chemistry Research Group, Ghent University, Ghent, 9000, Belgium; [7]In Vivo Cellular and Molecular Imaging, Vrije Universiteit Brussel, Brussels, 1090, Belgium

Introduction

Subcutaneous administration is often the preferred drug administration route, especially for biologicals characterized by a limited oral bioavailability. In view of chronic diseases and the associated frequent drug administrations, subcutaneous sustained drug delivery formulations were developed, of which hydrogels represent one promising subclass [1-4]. Hydrogels, classified as functional biomaterials, can be defined as a three-dimensional fiber network composed of hydrophilic polymers, which retain large amounts of water. More specifically, amphipathic peptides as low-molecular-weight building blocks render peptide-based hydrogels biocompatible, biodegradable and easy to manufacture and functionalize. Additionally, as their nanofiber network is formed through self-assembly based on non-covalent interactions (e.g. β-sheets) (Figure 1), they can be easily injected [5-7].
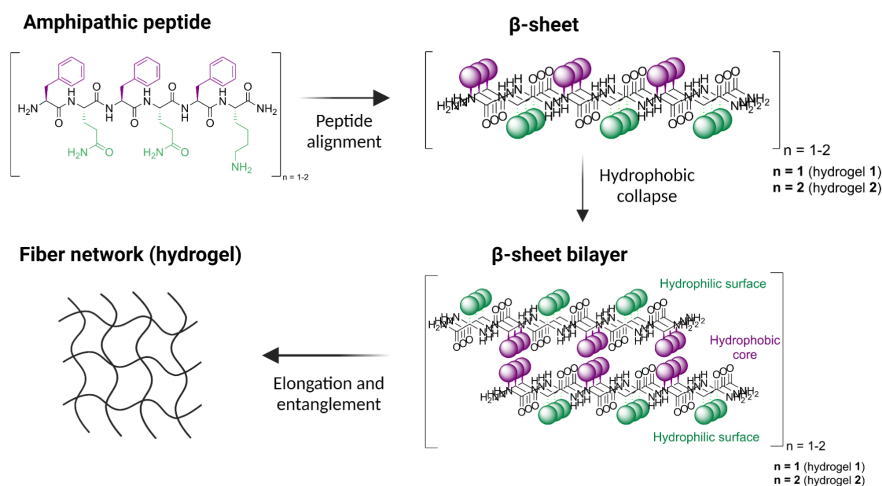
Fig. 1. Illustration of the self-assembly process of amphipathic peptide-based hydrogelators. The chemical structure of the hydrogelator is composed of alternating hydrophobic amino acids (in purple) and hydrophilic amino acids (in green).

In prior work, several hexapeptide sequences (e.g. H-FEFQFK-NH$_2$, H-FQFQFK-NH$_2$) have already demonstrated their efficacy in the delivery of therapeutically relevant molecules [8,9]. In this study, further extension of the drug release time period was aimed for by doubling the hydrogelator length, from a hexamer H-FQFQFK-NH$_2$ (hydrogel **1**) up to a dodecamer H-FQFQFKFQFQFK-NH$_2$ (hydrogel **2**), which was hypothesized to increase the amount of intermolecular interactions between the peptide chains. The effect of this doubled peptide length on the hydrogel's fiber and network morphology (microscopic), mechanical properties (macroscopic) and *in vivo* gel stability and drug release behaviour (biological properties) was evaluated.

Results and Discussion

In order to determine the influence of doubling the peptide length on the hydrogel properties, several experiments were performed using various techniques, including cryogenic and negative staining transmission electron microscopy (TEM), dynamic rheometry, *in vivo* SPECT/CT imaging and the *in vivo* hot-plate test (an antinociceptive model).

Hydrogel characterization

First of all, analyses of the two hydrogels by Fourier Transform Infrared (FT-IR) spectroscopy confirmed the presence of β-sheets as secondary structures within the entangled nanofiber networks, since a clear amide I band was visible within the 1610–1640 cm^{-1} spectral region. Subsequently, characterization of the fiber/network morphology was performed by cryogenic and negative staining TEM, which revealed that both hydrogel **1** and **2** (Figure 1) were able to form a highly intertwined nanofiber network, but there was a clear impact of the hydrogelator length on fiber morphology. While hydrogel **1** forms very long fibrils with some linear aggregation into tape like structures, hydrogel **2** forms shorter, more flexible fibrils with also some circular features in the network.

Lastly, an assessment of the hydrogel's mechanical or viscoelastic properties was possible *via* dynamic rheometry, applying a 5-step procedure after injection of the samples in between the rheometer plates. The first 2 hour time sweep (25ºC, 0.5% strain, 0.15 Hz frequency) indicated that the obtained storage moduli (G') are around 5 times higher than the corresponding loss moduli (G''), resulting in a dominant elastic or gel-like behaviour for both hydrogel systems. Remarkably, the G' of hydrogel **2** (2% w/v) (60 ± 10 Pa) is substantially lower than the G' of hydrogel **1** (2% w/v) (660 ± 160 Pa), suggesting that doubling the hydrogelator length adversely affects the gel strength (a lower rigidity was observed). Considering the cryo-TEM results, this might be explained by the shorter dodecamer fibrils and therefore lower cross-linking density of its fiber network. In step 4, an *in situ* destruction of the gels was performed (strain from 0.01% to 500%), which resulted in a phase angle (δ) increase to 90°, implying a successful viscous deformation. More importantly, a full recovery of the moduli was achieved for both gels (step 5) after destruction, with a faster recovery for hydrogel **2**, confirming the injectability of the two systems (i.e. thixotropic behaviour). Overall, as it seems challenging to relate the mechanical properties of the gels *before in vivo* injection to their observed drug release behaviour *after* injection (*vide infra*), a first experiment was performed where the mechanical properties were measured of the hydrogel **2** residue dissected from the mouse at 6h post *in vivo* injection. The resulting storage modulus (ca. 6500 Pa) was significantly higher than the pre- injection modulus (ca. 60 Pa), suggesting an influence of subcutaneous medium on the hydrogel **2** assembly and stiffness.

In vivo (SPECT/CT) imaging

After a thorough *in vitro* validation of the two hydrogels, their *in vivo* stability was investigated using non-invasive nuclear SPECT/CT imaging, which was possible by radiolabeling a fraction of the hydrogel network with radioactive isotope [111]Indium (using DOTA as chelator). Following injection of the ^{111}In-labelled formulations, the hydrogel volume at the injection site could be estimated by measuring the remaining radioactivity at the injection site over time. These results showed that hydrogel **2** was significantly more stable compared to hydrogel **1**, which seems to be supportive of different drug release mechanisms for the two gels (mainly diffusion-based and erosion-based, respectively).

The higher *in vivo* stability of hydrogel **2** also resulted in a more prolonged release profile of two different peptide drugs (i.e. cargoes), as observed in an *in vivo* drug release study where the ^{111}In-labelled drug was followed at the injection site via SPECT/CT imaging (Figure 2).
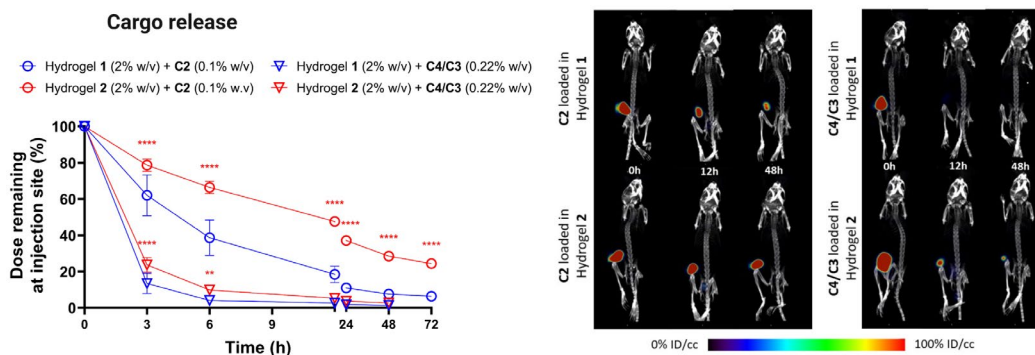
Fig. 2. In vivo release profile (left) of cargoes **C2** (0.1% w/v) and **C4/C3** (1:1.2) (0.22% w/v) from hydrogels **1** and **2** (2% w/v gels in PBS). The radioactive signal at the injection site was quantified at different time-points post-injection, representing the remaining dose over time, presented as mean ± SD (n = 4): (**) $P < 0.01$, (****) $P < 0.0001$, hydrogel **2** vs. hydrogel **1**. Corresponding SPECT/CT images (right) were scaled to the same level (0-100 %ID/cc).

Note that the release timeframe not only depends on the hydrogel system, but also on the cargo encapsulated. For example, the longer peptide cargo **C2** (0.1% w/v) was released from hydrogel **1** within approximately 24h, while a shorter peptide cargo, mixture **C4/C3** (1:1.2) (0.22% w/v), was released already within 6h (Figure 2). This suggests that the cargoes' physicochemical properties can influence the resulting release kinetics and are therefore important to consider.

In vivo efficacy

To evaluate the final *in vivo* efficacy of the two gels as drug delivery platform, an acute thermal nociceptive model, the hot-plate test, was performed. In specific, the mouse is restrained on a heated plate of 52 °C, at several time-points after injection of a co-formulation of the analgesic tetrapeptide **C3** (H-Dmt-DArg-Phe-Phe-NH$_2$, 74 μmol/kg) with hydrogel **1**, hydrogel **2** or a 0.9% NaCl solution. The results indicated that both sustained release formulations exerted prolonged analgesic effects compared to the immediate release formulation (**C3** in 0.9% NaCl solution). More importantly, hydrogel **2** caused a significant painkilling effect up to 48h post-injection, while this was up to 24h for hydrogel **1**. This longer therapeutic effect was aimed for, as it will provide a more consistent pain control and better quality of life for patients diagnosed with chronic pain.

Acknowledgements

References

1. Ruiz, M.E., Montoto, S.S. *ADME Processes in Pharmaceutical Sciences*, Springer, 97-133 (2018), http://dx.doi.org/10.1007/978-3-319-99593-9_6
2. Chen, W., et al. *Advanced Drug Delivery Reviews* **127**, 20-34 (2018), http://dx.doi.org/10.1016/j.addr.2018.01.016
3. Gulati, N., Gupta, H. *Recent Patents on Drug Delivery & Formulation* **5**(2), 133-145 (2011), http://dx.doi.org/10.2174/187221111795471391
4. Shi, Y., Li, L. *Expert Opinion on Drug Delivery* **2**(6), 1039-1058 (2005), http://dx.doi.org/10.1517/17425247.2.6.1039
5. Thambi, T., et al. *Journal of Controlled Release* **267**, 57-66 (2017), http://dx.doi.org/10.1016/j.jconrel.2017.08.006

6. Fichman, G., Gazit, E. *Acta biomaterialia* **10**(4), 1671-1682 (2014),
   https://doi.org/10.1016/j.actbio.2013.08.013
7. Martin, C., Ballet, S. *The Royal Society of Chemistry* 112-140 (2021),
   https://doi.org/10.1039/9781839163975-00112
8. Martin, C., et al. *Materials Today Chemistry* **3**, 49-59 (2017),
   http://dx.doi.org/10.1016/j.mtchem.2017.01.003
9. Martin, C., et al. *Journal of Medicinal Chemistry* **61** (21), 9784-9789 (2018),
   http://dx.doi.org/10.1021/acs.jmedchem.8b01282

Divalent Metal Ions Boost Effect of Nucleic Acids Delivered by Cell-Penetrating Peptides

Maria Maloverjan[1], Abhijit Biswas[1], Kärt Padari[2], Aare Abroi[1], Ana Rebane[3], and Margus Pooga[1]

[1]*Institute of Technology, University of Tartu, 1 Nooruse Street, Tartu, 50411, Estonia;* [2]*Institute of Molecular and Cell Biology, University of Tartu, 23b Riia Street, Tartu, 51010, Estonia;* [3]*Institute of Biomedicine and Translational Medicine, University of Tartu, 14b Ravila Street, Tartu, 50411, Estonia*

Introduction

Nucleic acids can be used as therapeutic agents for various medical purposes, starting from treatment of genetic diseases and finishing with vaccination [1,2]. Therapeutic nucleic acids include short non-coding single- or double-stranded nucleic acids, e.g. antisense oligonucleotides (ASOs) [3] and small interfering RNAs (siRNAs) [4], as well as longer coding nucleic acids, e.g. plasmid DNA (pDNA) [5] and messenger RNA (mRNA) [6,7]. The key issue with successful use of nucleic acids in live systems is their insufficient stability and efficiency. Being large and negatively charged molecules, nucleic acids cannot effectively penetrate cell membrane, thus providing insufficient effect in the case of intracellular targets [8]. Furthermore, unmodified nucleic acids are rapidly degraded by extra- and intracellular nucleases [9,10].

For cellular delivery of nucleic acids, numerous delivery systems have been developed, including liposomes [11], polyplexes [12], dendrimers [13], and peptides [14]. Among them, lipid formulations are currently most widely used in clinics, including those developed for delivery of mRNA-based vaccines that helped to fight the COVID-19 pandemic overworld [1,2]. However, it has been shown that cell-penetrating peptides (CPPs), up to 30 amino acid residues long peptides with ability to cross biological membranes, can be considered a promising alternative to lipids, often showing comparable efficiency, at the same time displaying lower cytotoxicity [15].

However, the efficiency of peptide-mediated delivery is still generally lower than that of the commercial lipid-based transfection systems. One of the most significant hindrances that can reduce productive delivery is inefficient endosomal escape of the CPP-nucleic acid complexes, which leads to eventual degradation of cargo molecules [16,17]. There are different ways to increase endosomal escape of peptide particles, e.g. adding endosomolytic moieties or strengthening proton sponge effect. In the current research, we were looking for novel safe and effective approaches for enhancing transfection efficiency of complexes formed from CPP and nucleic acids, without increasing concentration of the peptide.

Calcium has been known for a long time as a compound that is able to condense nucleic acids, facilitating transfection of viral DNA [18] and has also been recently used to condense siRNA to nanoparticles, providing more efficient transfection [19]. Recently, calcium has been used to facilitate transfection of CPP-nucleic acid nanoparticles. In the current study, we added Ca2+ as well as a range of other metal ions with different valencies to non-covalently formed complexes of CPP and nucleic acids and tested the efficiency of transfection in cell culture conditions. We used PepFect14 (PF14), a stearylated amphipathic CPP (stearyl-AGYLLGKLLOOLAAAALOOLL, where O = ornithine) that has been developed in 2011 by Ezzat *et al.* [20] and has been shown to efficiently deliver different types of cargo molecules [15,20,21].

We have found that adding calcium and magnesium chloride to the complexes during their preparation can greatly enhance efficiency of CPP-mediated transfection of splice-correcting ASO into cultured cells. Similar effects were also achieved in the case of pDNA, siRNA and mRNA, and in different cell lines. We also observed significant changes in intracellular distribution and trafficking of complexes prepared with the addition of calcium chloride [22], with ion-supplemented particles showing more extensive nuclear localization and, most likely, more efficient endosomal escape. Interestingly, also some salts of mono- and trivalent metals provided an increase in the expression of the reporter protein similar to that of CaCl2 and MgCl2. Importantly, particles containing CaCl2 and MgCl2 did not have any cytotoxic effect on cell lines that we used. Altogether, our results indicate that efficiency of CPP-mediated transfection can be greatly enhanced by the addition of calcium, magnesium and some other cations.

Results and Discussion

First, we tested the effect of adding $CaCl_2$ and $MgCl_2$ to the complexes of CPP and nucleic acid in the luciferase-based reporter system. For this, a reporter cell line with aberrant splicing, HeLa pLuc 705, was used. This cell line contains firefly luciferase gene that is interrupted by the second intron of beta-globin. The intron contains a mutation in the position 705 of the respective gene that prevents normal splicing, so that a part of the intron is retained, causing beta-thalassemia in humans or lack of functional luciferase in the reporter cell line. When splice-correcting oligonucleotide (SCO-705) is added, an aberrant splicing-inducing site is blocked, splicing occurs normally and functional luciferase is produced. Thus, luminescence intensity can be used to estimate productive transfection of the SCO. For formation of nanoparticles, CPP and SCO (final concentration 100 nM) were mixed at a molar ratio 5 in Milli-Q water, and after 15 min incubation, $CaCl_2$ or $MgCl_2$ solution was added to preformed complexes. After 15 min, solutions were diluted with pre-warmed growth medium 10-fold to reach the final volume, applied to the HeLa pLuc 705 cells and incubated for 24 h.

Fig. 1. Effect of $CaCl_2$ and $MgCl_2$ on rescue of luminescence in HeLa pLuc 705 cells by the SCO-PF14 complexes.

Titration of $CaCl_2$ and $MgCl_2$ resulted in a concentration-dependent increase of biological effect of the SCO-PF14 complexes, reaching 130-fold increase, compared to untreated cells (Figure 1). Addition of other divalent metal ions that are biologically relevant – Zn^{2+}, Mn^{2+}, Fe^{2+} and Cu^{2+} – did not result in any positive change in splicing correction.

Fig. 2. Viability of HeLa pLuc 705 cells in the presence of $CaCl_2$, $MgCl_2$, $ZnCl_2$ and $MnCl_2$ at various concentrations.

While $CaCl_2$ and $MgCl_2$ were not toxic for HeLa pLuc 705 cells, some other divalent ions were highly cytotoxic already at sub millimolar concentrations, as measured with WST-1 assay (Figure 2).

Endosomal entrapment is the major bottleneck that reduces productive delivery of CPP complexes, so that only a small proportion of cargo reaches cytosol and can be biologically active. To investigate whether endosomal trapping is a significant hindrance to the activity of ion-complemented PF14-SCO complexes, we used an endosome-destabilizing compound chloroquine (Figure 3). HeLa pLuc 705 cells were incubated with nanoparticles in the growth medium containing 100 µM chloroquine for 4 h. After that, the solutions were exchanged to fresh growth medium and luciferase activity was measured the next day. In line with what was expected, chloroquine enhanced the efficiency of PF14-SCO complexes (over 9-fold increase of luminescence). However, the positive effect of chloroquine decreased at higher calcium ion concentrations, indicating that calcium-complemented complexes are less dependent on additional endosome destabilizing, being more successful at endosomal escape.

Next, we wanted to know if the same effect could be achieved with other types of nucleic acids. For that, we prepared complexes

Fig. 3. Change in the effect of SCO-705 transfected into HeLa pLuc 705 cells with PF14 particles formed with or without addition of $CaCl_2$, upon addition of an endosome-destabilizing compound chloroquine (B).

of PF14 and pDNA (Figure 4A), siRNA targeting luciferase expressed by U87-MG Luc2 cells (Figure 4C), and mRNA encoding luciferase (Figure 4B). As a result, we observed very similar positive effects of calcium and magnesium chloride in the case of all nucleic acid types tested. In most cases, adding $CaCl_2$ resulted in a more significant increase in effect than $MgCl_2$, in line with what was observed for SCO. Interestingly, adding $CaCl_2$ alone, i.e. without the peptide, is sufficient to facilitate transfection of siRNA, which has been shown also by other research groups. The most prominent effect on the activity of cargo was observed in the case of mRNA, reaching several hundred fold difference in luminescence between complexes with and without $CaCl_2$.

In addition, we broadened our selection of metal salts, including also mono- and trivalent metals, such as sodium, potassium and aluminum, and combining them with various anions. We observed a positive effect on splicing switching by PF14-SCO complexes in the case of many salts tested (Figure 5). Interestingly, aluminum salts generally started being efficient already at low concentrations, while efficiency of sodium and potassium salts usually increased with raising concentration. Some salts, like $AlCl_3$ and $BiCl_3$, showed cytotoxicity and, as a result, reduced efficiency.

Fig. 4. Effect of adding $CaCl_2$ and $MgCl_2$ to the complexes of PF14 and (A) luciferase-encoding plasmid pGL3 in HeLa cells; (B) luciferase-encoding mRNA in HaCaT cells; and (C) luciferase-targeting siRNA in U87-MG Luc2 cells.

Fig. 5. Effect of adding various salts to the complexes of PF14 and SCO-705 in HeLa pLuc 705 cells.

Altogether, our data shows a significant impact of various salts that dissociate in water on the efficiency of CPP-mediated transfection of nucleic acids of different sizes and chemistries. The resulting biological effect of a cargo molecule can be increased over 10-fold by simply adding a salt solution to CPP-nucleic acid complexes during preparation. The resulting complexes are non-cytotoxic and are efficient in different cell lines. Still, the exact mechanism of this effect remains not fully understood, although some of our results indicate that divalent metal ions might act by facilitating endosomal escape of nanocomplexes. Describing CPP-nucleic acid complexes prepared with addition of a full panel of biocompatible salts and investigating mechanism of such transfection in more detail is of high interest and a subject of further research.

Acknowledgments

References

1. Polack, F.P., et al. *New England Journal of Medicine* **383**, 2603-2615 (2020), https://doi.org/10.1056/NEJMoa2034577
2. Baden, L.R., et al. *New England Journal of Medicine* **384**, 403-416 (2021), https://doi.org/10.1056/NEJMoa2035389
3. Temsamani, J., Guinot, P. *Biotechnol Appl Biochem* **26 (Pt 2)**, 65-71 (1997),
4. Song, E.W., et al. *Nature Medicine* **9**, 347-351 (2003), https://doi.org/10.1038/nm828
5. Romero, N.B., et al. *Human Gene Therapy* **15**, 1065-1076 (2004), https://doi.org/10.1089/hum.2004.15.1065
6. Reichmuth, A.M., et al. *Ther Deliv* **7**, 319-334 (2016), https://doi.org/10.4155/tde-2016-0006
7. van den Brand, D., et al. *European Journal of Pharmaceutics and Biopharmaceutics* **141**, 180-190 (2019), https://doi.org/10.1016/j.ejpb.2019.05.014
8. Dagle, J.M., et al. *Antisense Research and Development* **1**, 11-20 (1991), https://doi.org/10.1089/ard.1991.1.11
9. Sajid, M.I., et al. *Pharmaceuticals* **13**, (2020), https://doi.org/ARTN 294 10.3390/ph13100294
10. Houseley, J., Tollervey, D. *Cell* **136**, 763-776 (2009), https://doi.org/10.1016/i.cell.2009.01.019
11. Felgner, P.L., et al. *Proc Natl Acad Sci USA* **84**, 7413-7417 (1987), https://doi.org/10.1073/pnas.84.21.7413
12. Kichler, A. *J Gene Med* **6 Suppl 1**, S3-10 (2004)
13. Chung, H.H., et al. *Biopolymers* **76**, 83-96 (2004), https://doi.org/10.1002/bip.10597
14. Betts, C.A., Wood, M.J. *Curr Pharm Des* **19**, 2948-2962 (2013)
15. Urgard, E., et al. *Nucleic Acid Ther* **27**, 295-302 (2017), https://doi.org/10.1089/nat.2017.0670
16. Wan, Y., et al. *Current Medicinal Chemistry* **22**, 3326-3346 (2015), https://doi.org/10.2174/0929867322666150825162941
17. Abes, S., et al. *J Control Release* **110**, 595-604 (2006), https://doi.org/10.1016/j.jconrel.2005.10.026.
18. Graham, F.L. *Current Contents/Clinical Medicine*, 16-16 (1988)
19. Goldshtein, M., et al. *International Journal of Pharmaceutics* **515**, 46-56 (2016), https://doi.org/10.1016/j.ijpharm.2016.10.009
20. Ezzat, K., et al. *Nucleic Acids Res* **39**, 5284-5298 (2011), https://doi.org/10.1093/nar/gkr072
21. Veiman, K.L., et al. *Mol Pharm* **10**, 199-210 (2013), https://doi.org/10.1021/mp3003557
22. Maloverjan, M., et al. *Cells* **11**, (2022), https://doi.org/ARTN 756 10.3390/cells11040756

IgY Antibody Production Against Phospholipases A2 from *Vipera berus* and *Vipera ammodytes* Snake Species

Vasiliki Moulasioti[1], Evgenia Fotou[1], Vassilios Moussis[1], Dionysios Sgouras[2], and Vassilios Tsikaris[1]

[1]*Section of Organic Chemistry and Biochemistry, Department of Chemistry, University of Ioannina, Ioannina, 45110, Greece;* [2]*Laboratory of Medical Microbiology, Hellenic Pasteur Institute, Athens, 11521, Greece*

Introduction

Snakebite envenomation is a neglected disease that has a remarkable impact on Public Health worldwide [1]. In Europe, medically important cases of snakebite are mainly caused by three snake species of the *Vipera* genus (*V. berus, V. aspis*, and *V. ammodytes*). Snake venom is a complex mixture of proteins, peptides, enzymes, etc., and it is known that its toxicity is not a result of all its components [2]. PLA2s, which are found in the venom of most snakes, are among the most lethal toxins and may represent a promising target to produce a broad-spectrum antivenom [3]. Moreover, currently used snake antivenoms are produced in horses immunized with whole venoms, but the derived antibodies can induce early or late adverse reactions [4]. On the contrary, chickens constitute an alternative to conventional antivenom production due to their economic, productive, and ethical advantages. In this study, two appropriate peptide epitopes from the *C*-terminal segment of PLA2s of *Vipera berus* and *Vipera ammodytes* snake species were synthesized and conjugated to the CPSOC(3,9Acm) peptide carrier. Hens were used for vaccination with the immunogenic, and the specific IgY antibodies were isolated from the egg yolk to investigate the potency of recognizing both immunogenic conjugates and viper venom.

Methods

Peptide synthesis and Thioether bond formation
The peptide synthesis for both peptides (abbrv: pep1, pep2) was performed by the stepwise solid-phase peptide synthesis on a Rink-Amide (AM) resin using the Fmoc/tBu methodology. Thioether conjugates {abbrv: pep1-CPSOC(3,9Acm), pep2-CPSOC(3,9 Acm)} were formed between the CPSOC(3,9Acm) carrier and the antigenic epitopes. Iodoacetyl-peptides were dissolved in a H_2O/AcN (1:1), carrier CPSOC(3,9Acm) was added to the solution in solid form and small portions. The reaction was performed under inert conditions. At the end of the reaction, the solution was acidified until pH reached 2–3. The peptide and conjugates purity was checked by analytical RP-HPLC, and the correct molecular masses were confirmed by LTQ-ORBITRAP HR-ESI-MS.

Immunization protocol and IgY isolation from egg yolk
Two hens were used for the immunizations. The first one (HenA) was immunized with the pep1-CPSOC(3,9Acm) conjugate and the second one (HenB) with the mixture of both conjugates. For the first immunization, conjugates (0.6mg/ml) were dissolved in 0.5 ml H_2O and mixed with an equal volume of Freund's complete adjuvant, whereas the other three doses consisted of conjugates (0.2 mg/ml) emulsified with Freund's incomplete adjuvant. All doses were administered intramuscularly, in four different places and the eggs were obtained after each immunization. Standard protocol of Polyethylene glycol (PEG) 6000 was used to isolate the IgY antibodies from the egg yolk [5].

Immunochemical assay
To determine the IgY binding activity, ELISA wells were coated with the antigen (5μg/well of conjugates or 1 μg/well of snake venom) at 37°C for 1.5h and blocked with 3% skim milk in PBS for 1h at 37°C. The preimmunization- or fourth-immunization-induced IgY was added to the wells in various dilutions and incubated for 1.5h at 37°C. After removing unbound IgY, the HRP-conjugated anti-chicken IgY was added, and the wells were incubated for another 1h at 37°C. For color development, 3,3′,5,5′tetramethylbenzidine (TMB) substrate solution was added, and the reaction was stopped by adding 0,2N HCl. Absorbance was measured at 450nm.

Results and Discussion
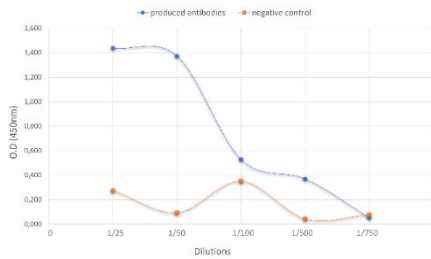
Fig. 1. Schematic representation of the produced antibodies ability to recognize the viper venom.
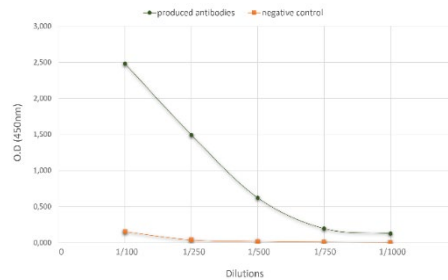
Fig. 2. Schematic representation of the specificity of the produced antibodies against the mixture of the conjugates.
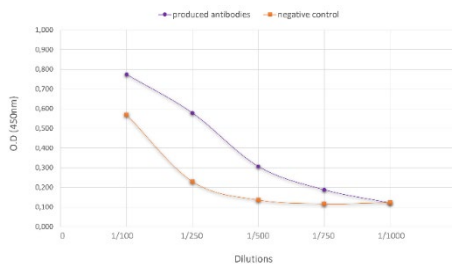
Fig. 3. Schematic representation of the specificity of the produced antibodies against the pep1-CPSOC(3,9Acm) conjugate.

Table 1. Results of the antibody binding activity to pep1-CPSOC(3,9Acm) conjugate (HenA).

Dilutions	Produced antibodies (O.D)	Negative control (O.D)
1/25	1,438	0,274
1/50	1,373	0,092
1/100	0,528	0,350
1/500	0,369	0,042
1/750	0,053	0,076

Table 2. Results of the antibody binding activity to the mixture of immunogenic conjugates (HenB).

Dilutions	Produced antibodies (O.D)	Negative control (O.D)
1/100	2,480	0,152
1/250	1,492	0,039
1/500	0,622	0,018
1/750	0,196	0,009
1/1000	0,128	0,006

Table 3. Results of the antibody binding activity to the viper venom (antibodies from HenB).

Dilutions	Produced antibodies (O.D)	Negative control (O.D)
1/100	0,774	0,469
1/250	0,578	0,229
1/500	0,307	0,136
1/750	0,188	0,116
1/1000	0,121	0,123

The results of this study show that the antibodies produced by the immunization of hens can successfully recognize the immunogenic conjugates. More specifically, the hen immunized with the mixture of conjugates shows a higher antibody titer compared to the one immunized with only pep1-CPSOC(3,9Acm) conjugate. Interestingly, preliminary experiments show strong evidence that the produced antibodies can recognize the *Ammodytes meridionalis* venom, but further research is needed to optimize the assay conditions. Further experiments are in progress to optimize the ELISA assay and examine the ability of antibodies to recognize other viper venoms intending to perform *in vivo* experiments.

References

1. Scheske, L., et al. *Int. J. Heal. Policy Manag*. **4**(7), 447-457, (2015), https://doi.org/10.15171/ijhpm.2015.75
2. Latinović, Z., et al. *J. Proteomics* **146**, 34-47, (2016), https://doi.org/10.1016/j.jprot.2016.06.020
3. Xiao, H., et al. *Biomed Res. Int*. (2017), https://doi.org/10.1155/2017/6592820
4. León, G., et al. *Toxicon* **76**, 63-76, (2013), https://doi.org/10.1016/j.toxicon.2013.09.010
5. Polson, A., et al. *Immunol. Commun* **9**(5), 475-493, (1980), https://doi.org/10.3109/08820138009066010

Raman Spectroscopy with Nanoparticles for Investigation of Protein Tyrosine Oxidation

Jaroslav Šebestík

Institute of Organic Chemistry and Biochemistry, Czech Academy of Sciences, Prague, 166 10, Czech Republic

Introduction

Reactive oxygen and nitrogen species play important physiological and pathological roles [1,2]. They are signaling molecules and are used by the immune system as a defense against pathogens [3,4]. If they appear in high concentrations and cannot be quenched by antioxidants, oxidative stress occurs [5,6]. Oxidative stress is implicated, for example, in Diabetes mellitus type 2, or in many neurodegenerative diseases [2,5,6].
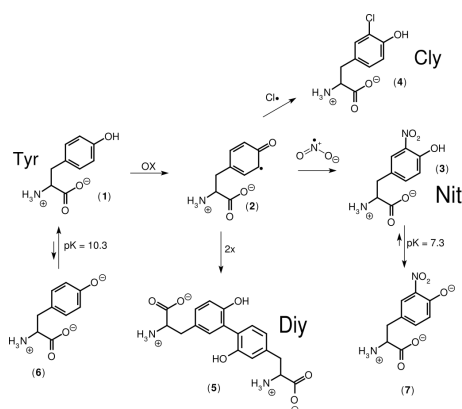
Fig. 1. Oxidized tyrosines [3,4].

For example, nitration, halogenation, and crosslinking of tyrosines are important post-translational modifications (Figure 1) and can influence protein structure [4]. The nitration is an early-stage marker of oxidative stress and neurodegeneration [7]. To understand the effect of oxidation on biophysical functions, we selectively synthesized a series of oxidized peptides and proteins. We have described the synthesis of selectively nitrated synuclein segments using Fmoc-Nit(Bn)-OH [8]. In addition to that other oxidized tyrosines can be inserted into peptides and proteins [8-10]. We have shown that double nitration significantly affected the vibrational circular dichroism spectra of synuclein segments, whereas chlorination did not cause any significant structural changes [9,10]. We used various nanoparticles to visualize protein tyrosine oxidation by surface-enhanced Raman spectroscopy (SERS), and identified markers for nitrated proteins [7,10]. We also used the SERS for studies of a neuroregenerative drug [11].

Results and Discussion

We have photochemically prepared nanosilver as a SERS substrate [7]. By adjusting the irradiation light, we could tune both plasmonic bands of pink-silver. The band yielded from the green light scattering was visible by naked-eye and was important for enhanced Raman scattering.

Protein tyrosine nitrations were monitored using surface enhanced Raman spectroscopy (SERS) with green or red laser excitation [7,10]. Two modes of measurement were used: native and induced ones. In both modes, the analyzed protein sample was mixed with silver colloid. In the induced mode, the hydrochloric acid was added to lower pH and initiate aggregation of the colloid. The induced mode is more universal for measurement of tyrosine nitration i.e., it works with many types of silver colloids such as chemical brown silver [10] and photochemical pink silver [7].

For induced mode, the characteristic pattern observed in Raman spectrum is a change of tyrosine fingerprint vibrations in region between 810 and 890 cm^{-1} [7,10]. This change is caused by strong domination of δ_{NO2} enhanced by silver surface at ca 825 cm^{-1}. The induce mode can serve for nitration detection down to 500 nM [10].

For native mode with pink-silver [7], the most dominant became the asymmetric vibration of nitro group at (1523-1527 cm^{-1}, $\nu_{NO2,as}$). This vibration in native mode can serve for nitration detection down to 114 nM [7]. Symmetric nitro band (1338-1343 cm^{-1}, $\nu_{NO2,symm}$) was visible marker of YYACAYY peptide nitration [7]; however, when the bigger synuclein models were used, the region was dominated by other vibrations of amino acids and could not serve for reliable detection of nitration [10].
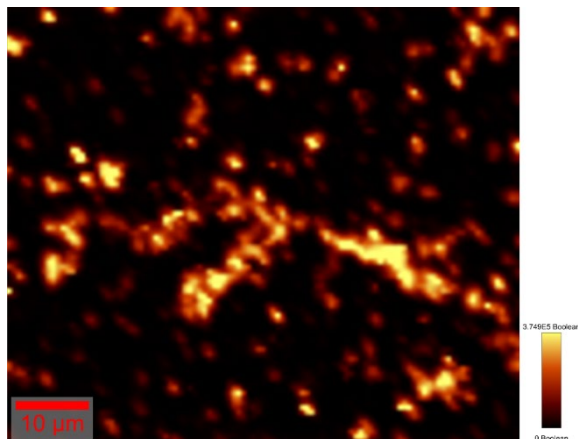
We have also investigated the possibility to measure the SERS using Raman microscope. For that purpose, we have covalently anchored the silver or gold nanoparticles on glass surface using known-techniques [12-14]. The measurement in solid state brought some difficulties such as sample burning at higher powers of laser. We have achieved optical and Raman co-localization of aggregated microparticles on the surfaces. These microparticles can interact for instance with nitrobenzene – a model of nitrated species (Figure 2).

Fig. 2. Raman intensity of nitrobenzene sample with pink-silver anchored on glass surface.
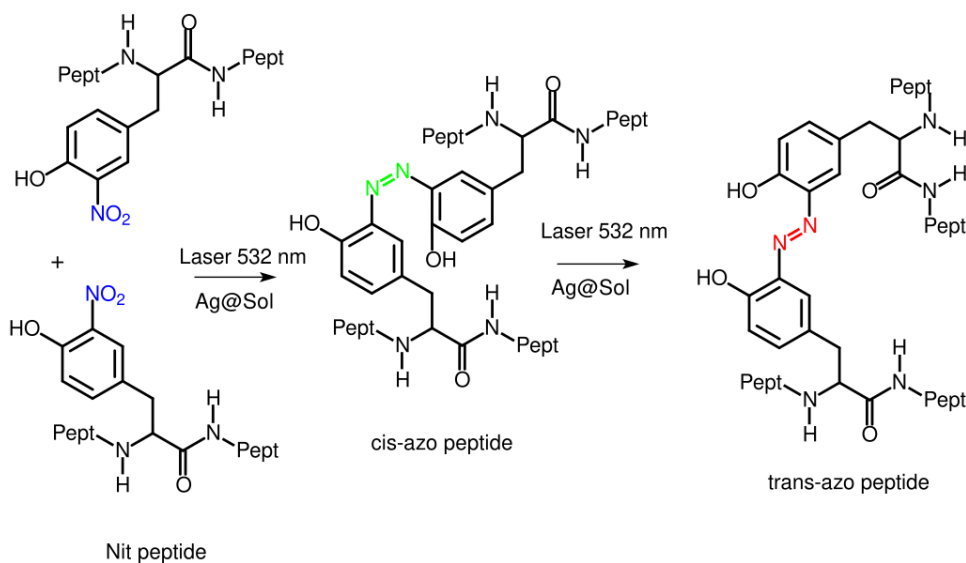
Fig. 3. Photochemical formation of azo-peptides [10].

In physics, it is well known – Heisenberg's uncertainty principle – saying that you cannot study the system without influencing it. The same is also valid for SERS studies: when the peptide is anchored on silver surface and irradiated with light it may undergo various chemical transformations.

On brown silver with [Nit1]enkephalin, we have observed a conversion of nitro group to azo bond, which was accompanied with the crosslinking of two peptide chains together [10] (Figure 3). According to the observed Raman signals, the cis-azo bond was formed at the beginning, and later it was followed by isomerization to trans-azo peptide.

The pink-silver provided access to Cys(tBu) deprotection through the anchoring to the silver surface (Figure 4). The reaction was confirmed by an observation of S-Ag vibration and Cys vibrations

in Raman spectra [7]. This strategy is advantageous for syntheses of peptides bearing Cys residue. Protection group prevents unwanted dimerization of peptides via disulfide bridge formation. When the peptide reached the proximity of silver surface, tBu is removed and peptide stays anchored to the surface for measurement.
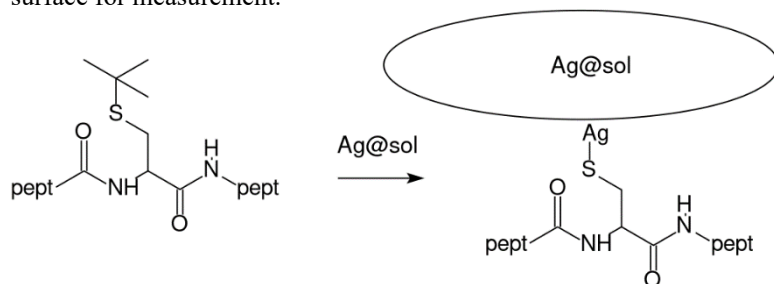
Fig. 4. Removal of tBu group by direct anchoring on silver surface [7].

Acknowledgments

References

1. Madkour, L.H. *J. Global Pharma Technol.* **2**, 1-23 (2019), http://doi.org/10.1038/s41573-021-00233-1
2. Ježek, J., et al. *Prog. Drug Res.* **72**, 99-134 (2017), https://doi.org/10.1007/978-3-319-63953-6_6
3. Radi, R. *Proc. Natl. Acad. Sci. USA* **101**, 4003-4008 (2004), http://doi.org/10.1073/pnas.0307446101
4. Radi, R. *Acc. Chem. Res.* **46**, 550-559 (2013), https://doi.org/10.1021/ar300234c
5. Sies, H. *Antioxidants* **9**, art. no. 852 (2020), http://dx.doi.org/10.3390/antiox9090852
6. Forman, H.J. and Zhang, H. *Nat. Rev. Drug Discovery* **20**, 689-709 (2021), http://doi.org/10.1038/s41573-021-00233-1
7. Sokolová, M., et al. *Amino Acids* **54**, 1261-1274 (2022), https://doi.org/10.1007/s00726-022-03178-w
8. Niederhafner, P., et al. *Amino Acids* **48**, 1087-1098 (2016), https://doi.org/10.1007/s00726-015-2163-2
9. Niederhafner, P., et al. in Futaki, S. and Matsuzaki, K. (Eds), *Peptide Science 2018*, pp 59-60, Osaka, 2019
10. Niederhafner, P., et al. *Amino Acids* **53**, 517-532 (2021), https://doi.org/10.1007/s00726-020-02911-7
11. Hamissa, M.F., et al. *J. Mol. Struct.* **1250**, art. no. 131828 (2022) https://doi.org/10.1016/j.molstruc.2021.131828
12. Klimpovuz, C.R. and Oliveira, M.M. *Chem. Papers* **75**, 2639-2646, (2021) https://doi.org/10.1007/s11696-020-01499-2
13. Pasternack, R.M., et al. *Langmuir* **24**, 12963-12971 (2008) https://doi.org/10.1021/la8024827
14. Haddada, M.B., et al. *Gold Bull* **46**, 335-341 (2013) https://doi.org/10.1007/s13404-013-0120-y

Magnetic Affinity Nanoparticles for Bevacizumab Adsorption

Gabriela R. Barredo-Vacchelli[1,2], Silvana L. Giudicessi[1,2], Fernando Albericio[3,4], Osvaldo Cascone[1,2], and Silvia A. Camperi[1,2]

[1]Universidad de Buenos Aires, Facultad de Farmacia y Bioquímica, Cátedra de Biotecnología, CABA, 1113, Argentina; [2]Instituto NANOBIOTEC UBA-CONICET, CABA, 1113, Argentina; [3]School of Chemistry & Physics, University of KwaZulu-Natal, Durban, 4001, South Africa; [4]CIBER-BBN, Networking Centre on Bioengineering, Biomaterials and Nanomedicine, and Department of Organic Chemistry, University of Barcelona, Barcelona, 08028, Spain

Introduction

The vascular endothelial growth factor (VEGF) stimulates tumor angiogenesis by targeting its receptor (VEGFR) [1]. The IgG monoclonal antibody bevacizumab, produced in CHO cells, is used for cancer treatment due to its capability of targeting the endothelial growth factor A (VEGF-A) and inhibiting angiogenesis [2]. Bevacizumab purification step may account for as much as 70% of the total manufacturing cost because of the high purity necessary for its parenteral administration. Nowadays, its purification is achieved by protein A affinity chromatography (AC). However, protein A is a very expensive ligand and harsh elution conditions are required to recover bevacizumab from the AC column, which can damage the mAb as well as the protein A ligand [3].

Recently, we have reported a short peptide contained in VEGF that binds to bevacizumab with high affinity and selectivity and demonstrated that this peptide bound to agarose can be used to purify bevacizumab at a lower cost and no harsh elution conditions [4]. However, conventional chromatography requires a previous clarification step to avoid column clogging.

Unlike conventional chromatography, magnetic nanoparticle (MNP) purification allows the extraction of the target directly from the cell culture without needing clarification steps [5]. In this work, bevacizumab purification with MNP with a peptide ligand immobilized is assessed.

Results and Discussion

Ac-PHQGQHIGVSK-NH$_2$ was synthesized by solid phase peptide synthesis (SPPS) with Fmoc/tBu chemistry using Rink amide-MBHA and analyzed by matrix-assisted laser desorption/ionization (MALDI)-time of flight (TOF) mass spectrometry (MS) and RP-HPLC (Figures 1-2). Lys was incorporated at the *C*-termini to facilitate its subsequent immobilization through its ξ-amino group on *N*-hydroxysuccinimidyl ester (NHS)-activated magnetic beads according to Pierce instructions (https://static.thermoscientific.com/images/D20904~.pdf).
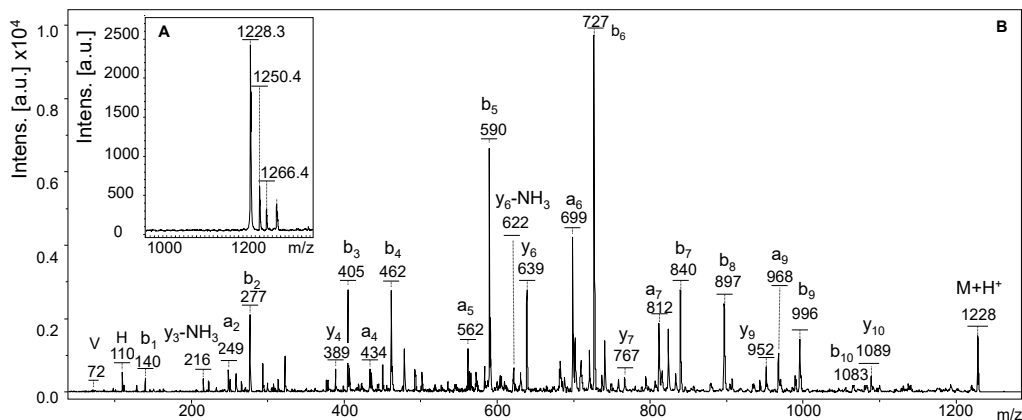
Fig. 1. PHQGQHIGVSK-NH$_2$ MS and MS/MS analysis (A) MALDI TOF MS: Signals at m/z 1228.3; 1250.4 and 1266.4 correspond to the M+H$^+$; M+Na$^+$ and M+K$^+$ respectively. (B) MS/MS: ions form the series, "b","a" and "y" are indicated.
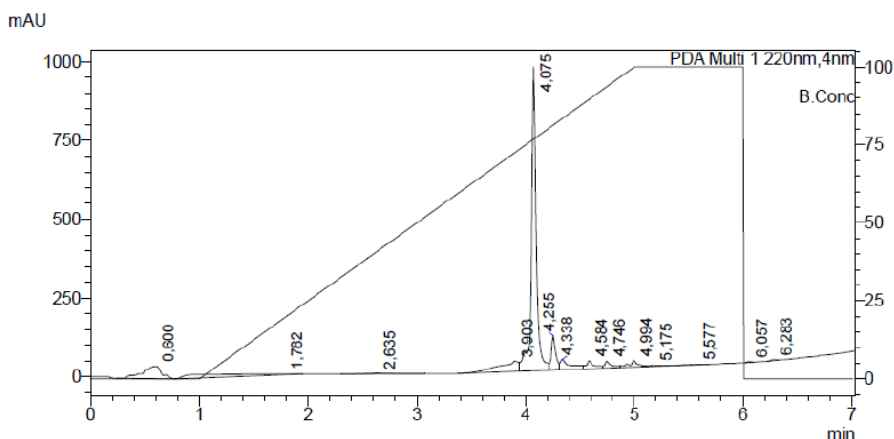
Fig. 2. Ac-PHQGQHIGVSK-NH₂ RP-HPLC analysis. RP column (C18 3.5μm, 4.6x50mm). Solvent A: 0.045% TFA in H₂O, Solvent B: 0.036% TFA in acetonitrile.

The amount of peptide immobilized, measured indirectly by quantifying the *N*-hydroxysuccinimide released as a result of peptide immobilization, was 1.1 nmol/mg of MNP. This value was higher than that reported for IgG immobilization in the data sheet (0.17 nmol of IgG/ mg of MNP; https://static.thermoscientific.com/images/D20904~.pdf).

MNP with the peptide immobilized were added to microtubes with a suspension of CHO cell culture containing bevacizumab in adsorption buffer (20 mM phosphate, 1M $(NH_4)_2SO_4$, pH 7.0). The MNP were separated after a short period of incubation by using a magnetic rack. After washing the beads with the adsorption buffer, elution buffer (20 mM phosphate buffer, pH 7.0) was added, and MNP were separated from the eluted bevacizumab for their reuse (Figure 3).
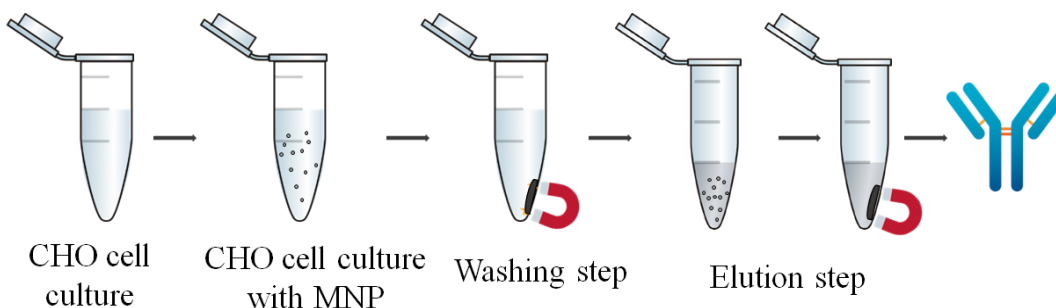
Fig. 3. Bevacizumab purification using Ac-PHQGQHIGVSK-MNP. Adsorption buffer: 20 mM phosphate buffer, 1 M (NH4)₂SO₄, pH 7.0. Elution buffer: 20 mM phosphate buffer, pH 7.0.
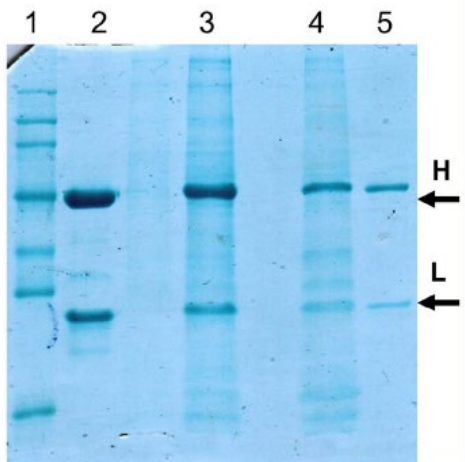
Fig. 4. SDS-PAGE under reduction conditions.
1) Molecular weight marker. 2) Pure bevacizumab.
3) Bevacizumab-producing CHO cell culture.
4) Washing fraction. 5) Elution fraction. H: Bevacizumab heavy chain. L: Bevacizumab light chain.

An excess of bevacizumab crude sample was added to determine the MNP maximum adsorption capacity by measuring the elution fraction protein content by Bradford reagent [6]. The capacity was 16 μg of bevacizumab/mg of MNP, corresponding to 32 mg of bevacizumab/ml of MNP (considering MNP density of 2.0 g/cm^3). Samples were evaluated by SDS-PAGE under reduction conditions. As it is observed in the elution fraction (line 5), MNP adsorbed bevacizumab selectively (Figure 4). As an excess of sample had been added, bevacizumab was also observed in the elution fraction together with the contaminants (lane 4).

Ac-PHQGQHIGVSK-MNP could purify the bevacizumab, although with some loss of it due to the small amount of MNP used for this test.

Peptide-MNP can be useful for bevacizumab purification from culture media without prior clarification and for easy sampling for quality control during the production process.

Acknowledgments

References

1. Ferrara, N., et al. *Nature Medicine* **9**, 669-676 (2003), https://doi.org/10.1038/nm0603-669
2. Roviello, G., et al. *European Journal of Cancer* **75**, 245-258 (2017), https://doi.org/10.1016/j.ejca.2017.01.026
3. Ramos-de-la-Peña, A.M., et al. *Journal of Separation Science* **42**, 1816-1827 (2019), https://doi.org/10.1002/jssc.201800963
4. Barredo, G.R., et al. *Protein Expression and Purification* **165**, 105500 (2020), https://doi.org/10.1016/j.pep.2019.105500
5. Holschuh, K. and Schwammle, A.K. *Journal of Magnetism and Magnetic Materials* **293**, 345-348 (2005), https://doi.org/10.1016/j.jmmm.2005.02.050
6. https://static.thermoscientific.com/images/D20904~.pdf

Total Bound Nitrogen Analysis for the Quantification of Immobilized Peptides on Dynabeads

Peter Boelens[1], Sylvia Schöne[2], Stephan Weiss[2], and Franziska Lederer[1]

[1]Helmholtz-Zentrum Dresden-Rossendorf, Helmholtz Institute Freiberg for Resource Technology, D-09599 Freiberg, Germany; [2]Helmholtz-Zentrum Dresden-Rossendorf, Institute of Resource Ecology, D-01328 Dresden, Germany

Introduction

According to the most recent listing reported by the European Commission, rare-earth elements (REEs) are the critical raw materials with the highest supply risk, whereas their recycling rates remain very low in the European Union [1]. End-of-life fluorescent lamps are a promising secondary source of REEs, but their recycling requires innovative separation processes [2,3]. By using phage surface display, Lederer and co-workers identified selectively surface-binding peptides that specifically bind to fluorescent lamp phosphors [4]. In a following study, Schrader et al. immobilized these peptides on coated well plates to investigate their binding to various REE phosphors [5]. The immobilization was facilitated by an activation with benzotriazole-1-yl-oxytripyrrolidinophosphonium-hexafluoro-phosphate (PyBOP) in the aprotic solvent *N*-Methyl-2-pyrrolidone (NMP) in the presence of the sterically hindered base diisopropylethylamine (DiPEA), a coupling reaction commonly used for chemical peptide synthesis. Recently, we investigated the immobilization method presented by Schrader et al. for the functionalization of Dynabeads [6]. Dynabeads are highly spherical and monodisperse composite magnetic beads, consisting of superparamagnetic iron oxide nanoparticles dispersed in a polystyrene matrix. They are commercially available with various surface coatings. The functionalization of amine coated Dynabeads with phosphor binding peptides, immobilized with the coupling reaction described above, did not change the Dynabeads' zeta potential and had no significant effect on the interaction with REE phosphors [6]. On the other hand, we found that the immobilization onto carboxylic acid coated Dynabeads changed the Dynabeads' zeta potential and isoelectric point. We also observed that this immobilization had a detrimental effect on the interaction of the beads with the targeted phosphor particles and suggested that this may be an indication of polymerization of the peptides on the Dynabeads' surfaces. In this work, we present a quantitative analysis of the total bound nitrogen (TN_b) for the quantification of the immobilized peptides on the Dynabeads.

Materials and Methods

A peptide with the amino acid sequence RCQYPLCS (FL464) was obtained from DGpeptides, Co., Ltd., whereas PyBOP, DiPEA and NMP were purchased from Carl Roth GmbH + Co. KG. The functionalization of M-270 amine and carboxylic acid coated Dynabeads (ThermoFisher Scientific Inc.) with diameters of 2.8 µm was conducted as described by Boelens et al. [6]. Briefly, 1.8 mg amine and carboxylic acid coated Dynabeads were each mixed with 1.0 mg of the peptide, 10 molar equivalents of PyBOP and 20 molar equivalents of DiPEA, as compared to the peptide concentration, in NMP with a total volume of 1 mL. Additionally, we prepared control samples in which the Dynabeads were mixed with the reagents without the presence of the peptide. All samples were prepared in triplicate. The samples were incubated in an overhead shaker for 120 minutes. Subsequently we washed the samples twice with NMP and four times with deionized water by collecting the Dynabeads with a permanent magnet and refreshing the supernatant. Next, we lyophilized the samples overnight to completely remove all traces of NMP and finally, we dissolved the Dynabeads in 5 mL of a 2 M HCl solution prior to TN_b analysis with a multi N/C 2100S (Analytik Jena GmbH).

The multi N/C 2100S was originally developed for analysis of environmental samples, such as soils and (waste)waters. The working principle of this setup for determination of the samples' TN_b content is based on a sample injection into a combustion tube, where the sample is digested at high temperature and a platinum catalyst facilitates the total conversion of nitrogen to NO-gas, which is detected by a chemoluminescence detector.

Results and Discussion

The mechanisms of the peptide immobilization onto the amine and carboxylic acid coated Dynabeads are depicted in Figure 1A and Figure 1B, respectively, as intended by Boelens et al. [6]. As PyBOP activates carboxylic acid groups for a coupling reaction with nucleophilic amines, based on the structure of the peptide FL464, we assumed that the peptides' *C*-terminus would bind to the surface of amine coated Dynabeads, whereas both the *N*-terminus and the guanidino group in the arginine sidechain could bind to the surface of carboxylic acid coated Dynabeads. Figure 1C shows the TN_b concentration in the samples of the amine coated Dynabeads, incubated without peptide (NH2 DB control) and with peptide (FL464@NH2 DB), and in the samples of the carboxylic acid coated Dynabeads, incubated without peptide (COOH DB control) and with peptide (FL464@COOH DB). The incubation with the peptide did not significantly change the TN_b concentration of the samples with amine coated Dynabeads ($p = 0.25$), indicating that the peptide immobilization on these beads may not have been successful, which is in line with findings of the beads' zeta potential and interaction with REE phosphors [6]. On the other hand, the immobilization of FL464 onto carboxylic acid coated Dynabeads significantly increased the TN_b concentration from 4.10 ± 0.06 mg.L^{-1} to 5.94 ± 0.30 mg.L^{-1} (p = 0.0033).
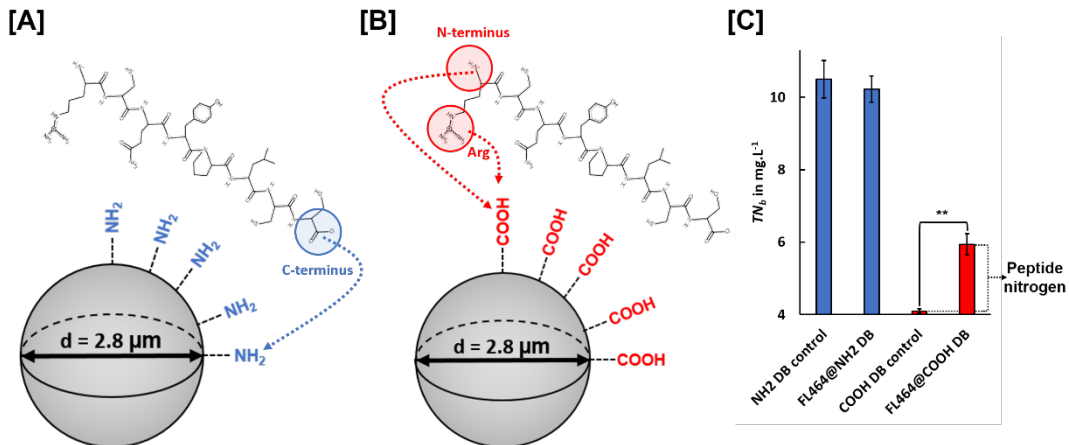
Fig. 1. Intended coupling reaction mechanism of the peptide FL464 to the surface of [A] amine coated and [B] carboxylic acid coated Dynabeads. The structures of the peptide were drawn with the online tool available under: http://www2.tulane.edu/~biochem/WW/PepDraw/.[C] TN_b concentration of the various samples, as determined with a multi N/C 2100S (Analytik Jena GmbH). The error bars depict one standard deviation.

From the obtained difference of the TN_b concentrations between the samples without and with peptides and the known size, shape, and amount of the Dynabeads, the surface density of the immobilized peptide, σ_{pept}, can be calculated according to the equation:

$$\sigma_{pept} = \frac{\Delta TN_b . N_A}{\Pi . M_N . n_N . d^2 . c_{particle}}$$

where ΔTN_b corresponds to the difference in the TN_b concentration in the samples with and without peptide, N_A stands for the Avogadro constant and M_N, n_N, d and $c_{particle}$ respectively represent the molar mass of nitrogen, the number of nitrogen atoms per peptide molecule, the bead diameter and the particle concentration of the beads.

Hence, we estimate a σ_{pept} on the carboxylic acid coated Dynabeads of 11.2 peptide equivalents per nm^2. This very high value may indicate, besides an immobilization, a polymerization of the peptide, which could confirm our previously suggested explanation.

Conclusions

In this work, we used a multi N/C 2100S (Analytik Jena GmbH) to investigate the chemical immobilization of the REE phosphor binding peptide FL464 onto M-270 amine and carboxylic acid coated Dynabeads by TN_b analysis. We found that the incubation with the peptide not significantly change the TN_b concentration of the samples with amine coated Dynabeads ($p = 0.25$), whereas it very significantly increased the TN_b concentration of carboxylic acid coated Dynabeads ($p = 0.0033$), from which we could estimate $\sigma_{pept} = 11.2$ peptide equivalents.nm^2. These results are well in line with our previous findings [6]. More generally, the high reproducibility, the quantification limit in the $< \mu g.L^{-1}$ range and the sample volume in the mL range, could make the presented method an interesting tool for various peptide-related analyses.

References

1. European Commission, Study on the EU's list of Critical Raw Materials - Final Report (2020).
2. Patil, A.B., Paetzel, V., Struis, R.P.W.J., Ludwig, C. *Separations* **9** (2022), https://doi.org/10.3390/separations9030056
3. Binnemans, K., Jones, P. *Journal of Rare Earths* **32**, 195-200 (2014), https://doi.org/10.1016/S1002-0721(14)60051-X
4. Lederer, F., Curtis, S., Bachmann, S., Dunbar, S., MacGillivray, R. *Biotechnol. Bioeng.* **114**, (2016), https://doi.org/10.1002/bit.26240
5. Schrader, M., Bobeth, C., Lederer, F. *ACS Omega XXXX*, (2021), https://doi.org/10.1021/acsomega.1c04343
6. Boelens, P., Bobeth, C., Hinman, N., Weiss, S., Zhou, S., Vogel, M., Drobot, B., Azzam, S.S.A., Pollmann, K., Lederer, F. *J. Magn. Magn. Mater.* 169956 (2022), https://doi.org/10.1016/j.jmmm.2022.169956

Peptides Conjugated-Magnetite Nanoparticles for Heavy-Metal Detoxification

Ximena Carolina Pulido[1], Ginna Niyireth Navarro Durán[1,2], Anderson Guarnizo[1], Maryeimy Varón-López[2], and Fanny Guzmán[3]

[1]Grupo de Química Aplicada a Procesos Ecológicos, Departamento de Química, Facultad de Ciencias, Universidad del Tolima, Ibagué, Colombia; [2]Grupo de Genética y Biotecnología Vegetal y Microbiana, Departamento de Biología, Facultad de Ciencias, Universidad del Tolima, Ibagué, Colombia; [3]Núcleo de Biotecnología Curauma, Pontificia Universidad Católica de Valparaíso, Valparaíso, Chile

Introduction

Environmental pollution has increased proportionally with economic growth, generating a loss in the quality of air, water and soil because industrialization and mining directly or indirectly discharge large amounts of toxic metals, such as cadmium and lead, threatening the environment. Therefore, it is recognized as one of the most important problems of the 21st century [1]. Heavy metals are considered strong environmental contaminants, their toxicity being a problem of growing importance from ecological, evolutionary, nutritional, and environmental perspectives [2]. This is because, once emitted, they are neither chemically nor biologically degradable, affecting the quality of the different ecosystems with repercussions on the entire food web and generating problems for human health [3]. Nanotechnology has gained attention in recent decades due to the unique physical properties of nanoscale materials. In the case of magnetite nanoparticles, due to their large surface area, it is possible to modify their surface with specific molecules, such as peptides, to increase the heavy metal affinity [4]. As mentioned before, metals, especially non-essential ones, have toxic effects on living beings. As a consequence of exposure to these metals, cells have developed a series of detoxification mechanisms, such as bioprecipitation, bioadsorption and bioaccumulation, among others. In the latter case, the cells, when in contact with metals such as Cd and Pb, synthesize molecules with the ability to chelate them; among these molecules are metallothioneins, phytochelatins and glutathione [4]. Nanotechnology has gained attention in recent decades due to the unique physical properties of nanoscale materials, such as magnetite, known for its magnetic properties and its large surface area, which allows its surface to be modified with functional groups that can form specific molecules like heavy metals [5]. Functionalized magnetite nanoparticles (MNPs) to remove heavy metals in water are becoming very important for the recovery of aquatic ecosystems, since they are excellent sorbents of these metallic contaminants, and their superparamagnetic properties prevent their agglomeration and allow them to be quickly removed along with the contaminants from the solutions by magnetism [6]. Solutions are currently being sought hand in hand with nanotechnology to reduce the concentrations of heavy metals in different aquatic ecosystems. According to that, this research aims to test the capacity of peptide nanoconjugates for the removal of cadmium and lead in aqueous solutions.

Results and Discussion

Two peptide nanoconjugates were synthesized. First, the synthesis of magnetite nanoparticles (Fe_3O_4 MNPs) was carried out by co-precipitation of Fe(II) and Fe(III) in ammonia solution. Then these nanoparticles were directly functionalized with glutathione (MNPs@GSH). On the other hand, modified MNPs on their surface with (3-aminopropyl) triethoxysilane (APTES) were used to be then functionalized with previously protected and activated phytochelatin 2 (MNPs@APTES-PC2).

As a first step, the adsorption of cadmium and lead on MNPs@APTES-PC2 at pH 6 and different initial concentrations of Cd(II) and Pb(II) (1, 10, 30, 50 and 100 ppm) was evaluated. The concentrations of both metals were measured by atomic absorption spectroscopy (Table 1). The nanoconjugate MNPs@APTES-PC2 had a lead removal of 95% at 1 ppm from aqueous solution, followed by 57.9% removal at 10 ppm. As seen, as the Pb concentration increased, the percent removal decreased.

Table 1. Percentages of Cd and Pb removal by MNPs@APTES-PC2.

Metal	Initial Concentration (ppm)	% Removal
Cd	1	0.1
	10	2
	30	18.2
	50	13.3
	100	7.2
Pb	1	95
	10	57.9
	30	24.8
	50	17.5
	100	12.1

The highest percent of Cd removal was 18.2% at 30 ppm, followed by 13.2% at 50 ppm. Also in this case, its removal decreased with increasing concentrations, implying that this nanoconjugate has a sufficient number of adsorption sites to adsorb metal ions. However, at higher concentrations, the adsorption sites of the nanoadsorbents would become saturated due to the increasing ratio between the number of metal ions and the number of adsorption sites [7].

Table 2. Adsorption isotherm parameters for the removal of Cd(II) and Pb(II) from aqueous solution with MNPs@APTES-PC2.

Isotherm	Parameters	Metal	
		Cd(II)	Pb(II)
Langmuir	K	-0.015	0.128
	b	-39387	30.864
	R^2	0.278	0.957
Freundlich	Kd	0.004	6.988
	$1/n$	2.130	0.332
	R^2	0.939	0.979

To determine the capacity and the adsorption process of the MNPs@APTES-PC2 nanoconjugate, Langmuir and Freundlich isothermal models for Cd(II) and Pb(II) were performed. From the linearized fit it was observed that for the adsorption of both metals the model that better fitted the experimental data was the Freundlich model, being the correlation coefficient R^2 0.939 for Cd(II) and 0.979 for Pb(II) (Table 2). It should be noted that the Freundlich isotherm indicates a heterogeneous nature of the surface, which lacks a plateau, indicating a multilayer adsorption, with different adsorption energies and with non-identical adsorption sites that are not always available [8].

For the nanoconjugate MNPs@GSH, the adsorption experiments with both metals were carried out at pH 6 and at different concentrations (10, 30, 50 and 100 ppm) (Table 3). In the removal assays, it was found that the highest percent removal was for Cd with 27.84% at 50 ppm. The percent removal of Pb with this nanoconjugate was much lower, being 8.20% at a concentration of 10 ppm, again percentage removal of Pb(II) decreased with concentration, exhibiting the same pattern of removal obtained with MNPs@APTES-PC2.

Table 3. Percentages of Cd and Pb removal by MNPs@GSH.

Metal	Initial Concentration (ppm)	% Removal
Cd	10	0.5
	30	0.4
	50	27.8
	100	16.3
Pb	10	8.2
	30	3.47
	50	4.08
	100	1.43

Taking into account the above results, the highest percent removal was for Cd. This agrees with data reported by Jacquart et al. [8], where the complexes with Cd(II) had greater affinity than with Pb(II), and are driven by the enthalpy change that occurs with the thiol groups of GSH and this metal [8]. In GSH-Cd(II) and GSH-Pb(II) complexes, only one thiol group could bind to the metal ion compared to PC2, which can bind up to two ions [9]. In the case of MNPs@GSH, it is not possible to determine which is the adsorption site, since with the functionalization carried out in this study, the GSH was able to bind to the magnetite either by the $-NH_2$ group or by the -SH group, as reported by Maleki et al. al., (2020). In the case of the adsorption of MNPs@GSH with the Cd(II) ion, it can be seen that the adsorption capacity of this nanoconjugate increases at the concentration of 50 ppm and this can be attributed to the increase in the driving force for the mass transfer between the aqueous and the solid phase when increasing the concentration of Cd(II) [9,10].

Table 4. Adsorption isotherm parameters for the removal of Cd(II) and Pb(II) from aqueous solution by MNPs@GSH.

Isotherm	Parameters	Metal removed	
		Cd(II)	Pb(II)
Langmuir	K	-0.012	0.157
	b	-0.865	40
	R^2	0.435	0.917
Freundlich	Kd	0.000	1.100
	$1/n$	2.892	0.299
	R^2	0.674	0.569

In the case of Cd(II) neither the Langmuir nor the Freundlich isothermal models (Table 4) fitted the data with this nanoconjugate, while in the case of Pb(II) removal from aqueous solution, the model that better fitted the experimental data was the Langmuir isotherm, where the correlation coefficient R^2 was greater than 0.90; the parameters resulting from these modeling are shown in Table 2. It should be noted that the Langmuir model indicates that all active adsorption centers are equivalent and that the ability of a molecule to bind to the surface is independent of whether or not there are positions next busy. Furthermore, adsorption is restricted to a monolayer and there are no lateral interactions between the adsorbate molecules [11].

Acknowledgments

References

1. Sharma, B., Dangi, A.K., & Shukla, P. *Journal of Environmental Management* **210**, 10-22 (2018), https://doi.org/10.1016/j.jenvman.2017.12.075
2. García-lestón, J., Pásaro, E., & Laffon, B. *Environment International Journal* **36**, 623-636 (2010), https://doi.org/10.1016/j.envint.2010.04.011
3. Morillo, J., Usero, J., & Rojas, R. *Environ Monit Assess* **139**, 329-337 (2008), https://doi.org/10.1007/s10661-007-9839-3
4. Sruthi, P., Majeed, A., & Jos, S. *Wetlands Ecology and Management* **25**, 129-148 (2016), https://doi.org/10.1007/s11273-016-9513-z
5. Jeevanandam, J., Barhoum, A., Chan, Y. S., Dufresne, A., & Danquah, M. K. *Journal of Nanotechnology* **9**, 1050-1074 (2018), https://doi.org/10.3762/bjnano.9.98
6. Singh, K.K., Senapati, K.K., & Sarma, K.C. *Journal of Environmental Chemical Engineering* **5**(3), 2214-2221 (2017), https://doi.org/10.1016/j.jece.2017.04.022
7. Ouyang, D., Zhuo, Y., Hu, L., Zeng, Q., Hu, Y., & He, Z. *Minerals* **9**(5), 1-16 (2019), https://doi.org/10.3390/min9050291
8. Jacquart, A., Brayner, R., El Hage Chahine, J. M., & Ha-Duong, N. T. *Chemico-Biological Interactions*, *267*, 2 (2017), https://doi.org/10.1016/j.cbi.2016.09.002
9. Ayawei, N., Ebelegi, A.N., & Wankasi, D. *Journal of Chemistry* 1-11 (2017), https://doi.org/10.1155/2017/3039817; Sharma, M., Chaudhary, K., Kumari, M., Yadav, P., Sachdev, K., Janu, V. C., & Gupta, R. *Materials Today Chemistry* **18**, 100379 (2020), https://doi.org/10.1016/j.mtchem.2020.100379
10. Maleki, B., Esmaeilnezhad, E., Choi, H. J., Koushki, E., Rahnamaye Aliabad, H. A., & Esmaeili, M. *Current Applied Physics*, *20*(6), 822–827 (2020), https://doi.org/10.1016/j.cap.2020.03.020
11. Patiha, Heraldy, E., Hidayat, Y., & Firdaus, M. *Materials Science & Engineering* **107**, 1-10 (2016), https://doi.org/10.1088/1757-899X/107/1/012067

Synthesis and Structural Optimization of Macrocyclic BACE1 Inhibitors with a Hydrophobic Cross-Linked Structure

Kazuya Kobayashi, Takuya Otani, Yasunao Hattori, and Kenichi Akaji

Kyoto Pharmaceutical University, Yamashina-ku, Kyoto 607-8412, Japan

Introduction

Alzheimer's disease (AD) is a brain disorder, and its pathological features are senile dementia, neurofibrillary tangles, and neuronal cell death. β-Site amyloid precursor protein cleaving enzyme 1 (β-secretase, hereafter referred to as BACE1) is a promising drug target for treating AD because it catalyzes the first step in the production of amyloid β peptide (Aβ), whose aggregation is one of the causal factors of senile dementia. To date, various BACE1 inhibitors have been reported; however, no therapeutic agents for AD have been developed.

Previously, we reported a superior BACE1 cleavage sequence (H-Ile-Ser-Glu-Ile-Thi-Thi*Nva-Ala-Glu-Phe-Arg-His-NH₂, where * denotes the cleavage site, Thi:2-thienylalanine, Nva: norvaline) that was cleaved ten times faster than wild type and Swedish mutant substrates [1]. We also reported novel BACE1 inhibitors designed by combining this sequence with hydroxyethylamine (HEA)-type transition-state mimetics [2]. X-ray crystallography of the complex formed between BACE1 inhibitor **1** and recombinant BACE1 (rBACE1) revealed a hydrophobic space between the P1 and P3 side chains (PDB ID:4TRW). In this study, based on compound **2**, which showed higher activity than inhibitor **1**, we synthesized and evaluated macrocyclic derivatives bearing a cross-linked structure between P1-P3 side chains of various lengths (Figure 1). Moreover, we introduced methyl substituents at the P3 β- position on the cross-linked structure and a 4-carboxymethylphenyl group into the P1' site.

Results and Discussion

We designed 12- to 15-membered ring macrocyclic inhibitors **9**-**16** bearing an alkane or alkane-type cross-linked structure (Scheme 1). HEA fragments **3** and **4** containing the terminal alkene were
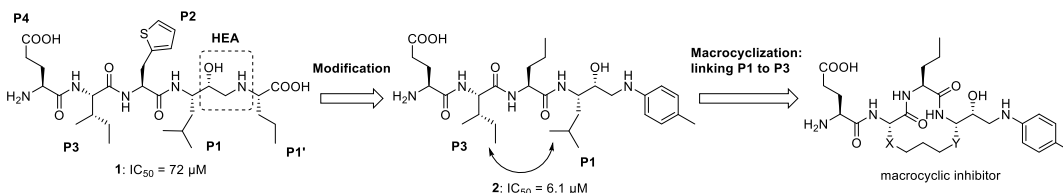
*Fig. 1. Structures of linear inhibitors **1** and **2**, and macrocyclic inhibitors.*
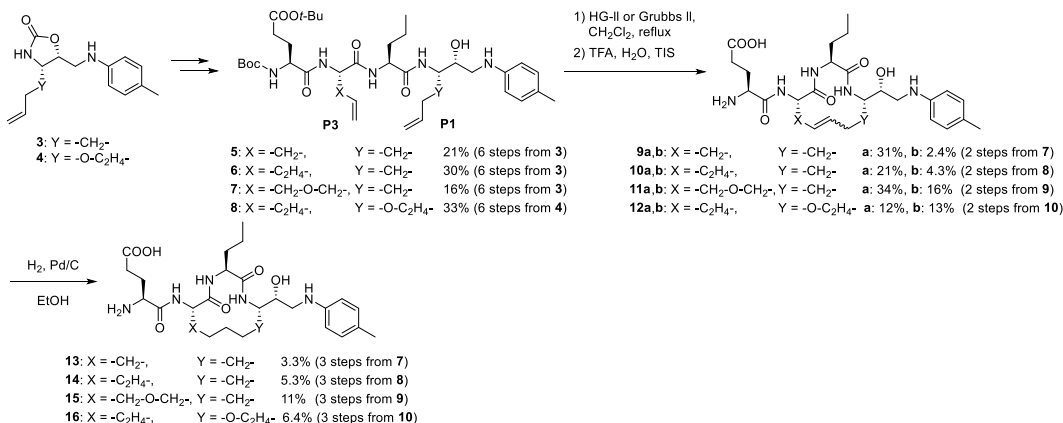
*Scheme 1. Synthesis of 12- to 15-membered macrocyclic inhibitors **9**-**16**.*

Table 1. Inhibitory activities of macrocyclic derivatives.

Compd.	Ring size	IC$_{50}$ (µM)	Compd.	Ring size	IC$_{50}$ (µM)
2	(control)	6.1			
13	12	1400	**15**	14	>1500[b]
9a[a]		>1500[b]	**11a**[a]		>1500[b]
9b[a]		1050	**11b**[a]		>1500[b]
14	13	780	**16**	15	N.D.[c]
10a[a]		380	**12a**[a]		N.D.[c]
10b[a]		1410	**12b**[a]		N.D.[c]

[a]*The alkene geometry could not be determined;* [b]*20~40% inhibition at 1500 µM;* [c]*N.D. = not detected*

prepared from commercially available Boc-Glu(OBzl)-OH or Boc-Asp-OBzl. Sequential condensation of Fmoc-Nva-OH, a P3 fragment and Boc-Glu(O*t*-Bu)-OH and Fmoc deprotection gave cyclization precursors **5**-**8**. Cyclization of the terminal alkenes were conducted by ring-closing metathesis (RCM) reaction. After deprotection, alkene-type macrocyclic derivatives **9**-**12** were obtained. Depending on the order of elution using RP-HPLC, the compounds labelled "a" or "b", which indicated (*E*)- or (*Z*)-alkene, but the alkene geometry could not be determined. They were converted to alkane-type macrocyclic derivatives **13**-**16** by catalytic reduction.

The inhibitory activities of macrocyclic derivatives against rBACE1 are summarized in Table 1. The activities of 12-, 14-, and 15-membered ring derivatives were markedly reduced compared to those of parent compound **2**. However, the 13-membered ring derivative, especially alkene isomer **10b**, showed weak but clear activity. These results suggest that the introduction of a simple cross-linked structure between the P1 and P3 side chains resulted in decreased activity, but that the 13-membered ring was the most suitable ring size for activity.

Docking models of **19a** and **19b** were constructed using Molecular Operating Environment (MOE) software (Figure 2). Linear inhibitor **1** complexed with rBACE1 (PDB ID:4TRW) was
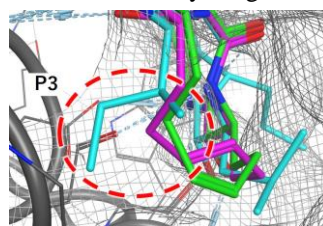
*Fig. 2. Docking models for **10a** and **10b** with rBACE1. The (Z)- and (E)-alkene derivatives and the template compound **1** are shown in green, purple and cyan, respectively. The gray mesh represents the vdW surface of rBACE1.*
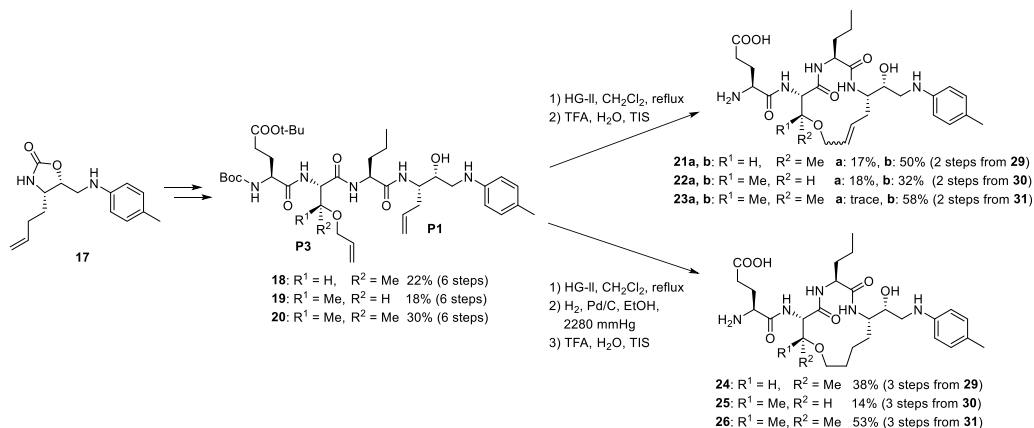
*Scheme 2. Synthesis of β-branched macrocyclic inhibitors **21-26**.*

Table 2. Inhibitory activities of β-branched macrocyclic derivatives.

Compd.	R^1, R^2	IC$_{50}$ (μM)	Compd.	R^1, R^2	IC$_{50}$ (μM)
2	(control)	6.1	**22a**[a]	R^1 = Me, R^2 = H	1000
10a[a]	(macrocycle)	380	**22b**[a]	[(*S*)-methyl]	11.7
21a[a]	R^1 = H, R^2 = Me	1420	**25**		135
21b[a]	[(*R*)-methyl]	117	**23b**	R^1, R^2 = Me	3.9
24		1000	**26**	[dimethyl]	6.1

[a]*The alkene geometry could not be determined*

used as a template for docking. Focusing on the P3 position, the isoleucine side chain of compound **1** occupied the hydrophobic space in the S3 pocket, while the side chain of the macrocyclic derivatives occupied it insufficiently. Based on these results, we assume that the loss of hydrophobic interactions in the S3 pocket resulted in decreased activity.

To increase inhibitory activity, new inhibitors **21**-**26** bearing a branched structure at the P3 β-position were designed and synthesized (Scheme 2). The ring size of these compounds was fixed at 13-membered, and they contained one or two methyl groups at the P3 β-position. The alkene geometries of **21** and **22** could not be determined, whereas those of **23b** could be assigned. Another alkene isomer, **23a**, was obtained in small amounts but was not evaluated.

The inhibitory activities of β-branched macrocyclic derivatives are listed in Table 2. The introduction of the (*R*)-methyl group causes a change in activity. One of the alkene isomers, **21a**, and reductant **24** showed lower activity than the non-branched macrocyclic derivative **10a**; however, another alkene, **21b**, showed about three-fold higher activity than **10a**. This trend was also observed in the (*S*)-methyl derivatives, and the improvement rate was higher than that of the (*R*)-methyl derivatives. The activity of compound **22b** was 10-fold higher than that of compound **21b**. For the dimethyl derivatives **23b** and **26**, further improvements in activity were observed. In particular, (*Z*)-alkene **23b** showed approximately 100-fold higher activity than **10a** and approximately 1.5-fold higher activity than the parent compound **2**. These results reveal that the introduction of methyl groups on the P3 β-position improved inhibitory activity, as expected, and that the (*S*)-methyl group contributed more to activity than the (*R*)-methyl group.

Docking simulation of (*Z*)-alkene **23b** with rBACE1 was performed using MOE software (Figure 3). Focusing on the P3 β-position, the direction of the dimethyl group of **23b** was approximately the same as that of the isoleucine side chain of compound **1**. These two methyl groups are located near the vdW surface of rBACE1, and the pro-(*S*)-methyl group is closer to the vdW surface than the pro-(*R*)-methyl group. These results suggest
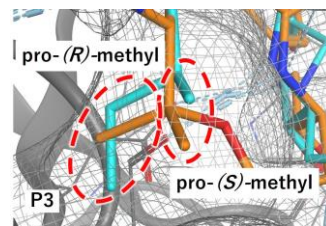
*Fig. 3. Docking model for **23b** with rBACE1. The dimethyl (Z)-alkene derivatives **23b** and the template compound **1** are shown in orange and cyan, respectively. The gray mesh represents the vdW surface of rBACE1.*
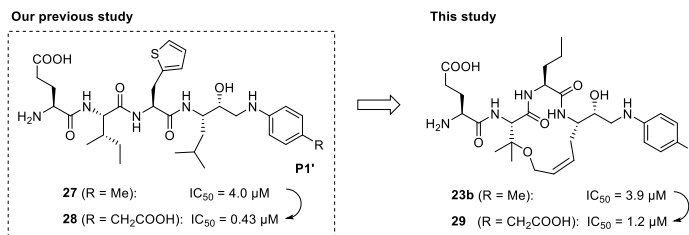
*Fig. 4. Structures and inhibitory activities of P1'-4-carboxymethylphenyl type derivatives **28** and **29**.*

that a stronger hydrophobic interaction with rBACE1 at the S3 pocket was formed by the dimethyl group of **23b** compared to the non-branched derivative **10a**, and that the additional hydrophobic interaction contributed to the enhanced activity of **23b**, which was consistent with the result that (*S*)-methyl derivatives showed higher activity than the corresponding (*R*)-methyl derivatives.

In our previous study, we reported that the introduction of a 4-carboxymethylphenyl group instead of a *p*-tolyl group increased inhibitory activity 10-fold [3]. Based on these results, the dimethyl branched macrocyclic derivative **29** containing a 4-carboxymethylphenyl group at the P1' site was synthesized (Figure 4). The activity of compound **29** was increased approximately 3.2 times from that of compound **23b**. The improvement in the activity of macrocyclic derivatives was lower than that of linear inhibitors in a previous study, but the introduction of a 4-carboxymethylphenyl group at the P1' position led to further improvement in activity.

Acknowledgments

References

1. Kakizawa, T., et al. *Bioorg. Med. Chem.* **19**, 2785-2789 (2011), https://doi.org/10.1016/j.bmc.2011.03.056
2. Hattori, Y., et al. *Bioorg. Med. Chem.* **23**, 5626-5640 (2015), https://doi.org/10.1016/j.bmc.2015.07.023
3. Kobayashi, K., et al. *Bioorg. Med. Chem.* **50**, 116459 (2021), https://doi.org/10.1016/j.bmc.2021.116459

Downsizing Nanobodies: Towards CDR Loop Mimetics Modulating Intracellular Protein-Protein Interactions

Kevin Van holsbeeck[1,2], Baptiste Fischer[3], Simon Gonzalez[1], Charlène Gadais[1], Wim Versées[3], José C. Martins[2], Charlotte Martin[1], Alexandre Wohlkönig[3], Jan Steyaert[3], and Steven Ballet[1]

[1]*Research Group of Organic Chemistry, Vrije Universiteit Brussel, 1050 Brussels, Belgium; [2]NMR and Structure Analysis Unit, Ghent University, 9000 Ghent, Belgium; [3]Structure Biology Brussels, VIB-VUB Center for Structural Biology, Vrije Universiteit Brussel, 1050 Brussels, Belgium*

Introduction

Monoclonal antibodies (ca. 150 kDa) display remarkable specificity and high affinity binding capabilities. However, their therapeutic application is associated with some limitations, including limited *in cellulo* access and high therapeutic costs. These drawbacks entailed the development of miniaturized functional antibody fragments (ca. 15-50 kDa) such as antigen-binding fragments (Fab), single-chain variable fragments (scFv) and recombinant variable single domains such as Nanobodies (Nb) [1]. In addition, smaller synthetic peptides based on (parts of) the antigen-binding site of antibodies or Nanobodies have been investigated as antibody mimetics, although so far with limited success [2].

In this context, we explored the feasibility of developing Nanobody-based peptide mimetics of limited molecular weight (1-2 kDa). Using a structure-based design strategy, several peptidomimetics were developed from the interacting complementarity-determining regions (CDR) of a Nanobody. This Nanobody modulates the nucleotide exchange activity on RAS proteins by interaction with the intracellular RAS:SOS1 complex. The significance of this protein-protein complex is related to the RAS protein. RAS proteins cycle between inactive GDP-bound states and active GTP-bound states, thereby controlling downstream cellular signaling pathways which impact cell proliferation, growth, differentiation, and survival [3]. The cycling between the active and inactive RAS protein states is regulated by guanine exchange factors (GEFs) and GTPase-activating proteins (GAPs). This tight control is deregulated in case of activating mutations in RAS proteins, which may lead to the development of multiple human cancer types and developmental disorders [4]. Direct inhibition of RAS proteins has been perceived as a challenging task [5]. Therefore, modulation of RAS proteins through the regulatory GEF SOS1 represents an attractive alternative therapeutic target.

Results and Discussion

Upon discovery of a Nanobody which modulates the nucleotide exchange activity on RAS proteins by interaction with the intracellular RAS:SOS1 complex, we explored the feasibility to develop Nanobody mimetics based on its crucial complementarity-determining regions (CDR). This was guided through a biochemical nucleotide exchange assay, which follows the nucleotide exchange rate of RAS:GDP towards RAS:GTP catalyzed by SOS1. A co-crystal structure of the Nanobody bound to the RAS:SOS1 protein complex identified the CDR3 loop as an important contributor to the interaction by penetration within a hydrophobic pocket on SOS1 through a β-turn. A linear peptide representing the CDR3 amino acid sequence-maintained ca. 15% of the maximum activation rate of the Nanobody, although with a significantly weakened potency of 500 μM.

Subsequently, multiple peptide analogues were synthesized wherein amino acids residues were substituted. These substitutions indicated the importance of residues located at the β-turn portion of the CDR3 loop for the interaction with SOS1. Introduction of cationic residues at the Ile position resulted in efficacy improvements, especially in case of a D-Arg, which doubled the efficacy of the native peptide. A co-crystal structure of this peptide bound to the RAS:SOS1 complex showed a positioning of the peptide within the same binding pocket as the Nanobody CDR3 loop, although without stabilization of the β-turn structure.

Therefore, the peptide was cyclized by a lactam bridge at the terminal positions to potentially stabilize the formation of the β-turn conformation. Remarkably, this led to an improvement of the potency by a factor 7 compared to the native peptide. In this case, a co-crystal structure of this peptide

bound to the RAS:SOS1 complex shows a strong overlap of the top residues of the peptide with the Nanobody CDR3 loop, thereby validating the anticipated structural stabilization by introduction of the lactam tether. This co-crystal indicated a positioning of the D-Arg side chain towards a negative surface patch of SOS1.

To improve the contact of the D-Arg with SOS1, it was substituted by the extended analogues D- homoarginine and D-Phe(4'-guanidino). This led to either an improvement in the efficacy or potency of the peptides. For the peptide containing the D-Phe(4'-guanidino) residue, a co-crystal structure showed a reorientation of two Glu residues of SOS1 allowing efficient contacts with the amino acid side chain.

To further reduce the conformational flexibility of the peptide, the lactam bridge was substituted by a 1,4-disubstitued 1,2,3-triazole bridge. In addition, the Ala residue was deleted to provide an improved stabilization of the β-turn conformation. This resulted in a peptide showcasing 55% of the maximal activation by the parent Nanobody. Although similar binding positions and contacts were observed as the peptide with the lactam bridge in a co-crystal structure, this peptide allows the formation of more productive hydrogen bonds in the β-turn conformation, comparable to the parent Nanobody CDR3 loop.

By application of a structure-based design strategy, and guided by a biochemical GEF assay, we developed CDR3 loop mimetics able to mimic 55% of efficacy of the parent Nanobody, upon substitution with some (un)natural amino acids and introduction of cyclization tethers. In addition, selected peptidomimetics were found to structurally mimic the native Nanobody CDR3 loop, presenting similar binding poses upon interaction with the RAS:SOS1 complex (as demonstrated by X-ray analysis). With this study, we provided the first solid proof-of-principle that small peptidomimetics can be developed which mimic both structurally and functionally protein-protein interaction modulatory Nanobodies.

Acknowledgments

References

1. Bruce, V.J., Ta, A.N., McNaughton, B.R. *ChemBioChem* **17** (20), 1892-1899 (2016), https://doi.org/10.1002/cbic.201600303
2. Van holsbeeck, K., Martins, J.C., Ballet S. *Bioorg. Chem.* **119** (105563), 1-14 (2022), https://doi.org/10.1016/j.bioorg.2021.105563
3. Simanshu, D.K., Nissley, D.V., McCormick, F. *Cell* **170** (1), 17-33 (2017), https://doi.org/10.1016/j.cell.2017.06.009
4. Pylayeva-Gupta, Y., Grabocka, E., Bar-Sagi, D. *Nat. Rev. Cancer* **11**, 761-774 (2011), https://doi.org/10.1038/nrc3106
5. Spencer-Smith, R., O'Bryan, J.P. *Semin. Cancer Biol.* **54**, 138-148 (2019), https://doi.org/10.1016/j.semcancer.2017.12.005

Various Strategies to Control the Conformation of Peptoids

Claude Taillefumier, Sophie Faure, Maha Rzeigui, Maxime Pypec, Olivier Roy

Université Clermont Auvergne, Clermont Auvergne INP, CNRS, ICCF, F-63000 Clermont−Ferrand, France

Introduction

N-substituted glycines oligomers or peptoids have drawn considerable interest as peptide biomimetics [1]. They possess many desirable attributes such as *in vivo* stability, ease of synthesis, and side chain diversity. Peptoids are also a special class of foldamers, as both *cis*- and *trans*-amide bond conformations are accessible. In this respect, peptoids show similarities to proline-rich sequences. For example, they can adopt type I (PPI) and type II (PPII) helical conformations. This involves regulating amide isomerism in the peptoid backbone. Considerable efforts have been made to control the conformation of peptoids through steric and electronic interactions involving peptoid amides and nearby side chains. Among the best *cis*-amide inducing side chains are the *N*α-chiral aromatic phenylethyl, naphthylethyl and triazolium groups, or the alkyl-ammonium, fluorinated and *tert*-butyl side chains (Figure 1A). Fewer side chains are capable of promoting *trans* peptoid amides. Among these, are the *N*-aryl, *N*-hydroxy, *N*-alkoxy, *N*-acylhydrazide, *N*-imino and *N*-alkylamino groups (Fig. 1B). All these findings are recapitulated in a recent review by Kalita *et al.* [2]. Here we report on our results with the following two sterically demanding aliphatic side chains, *tert*-butyl (*t*Bu) and (*S*)-1-*tert*-butyl(ethyl) (s1tbe), which our group has introduced to the peptoid "tool box" to induce *cis*-amides. In particular, the modulation of peptoid helicity by sequence specific positioning of chiral (*N*s1tbe) and achiral monomers (*Nt*Bu) will be discussed [3,4]. We will also consider the conformation of homologous *β*-peptoid oligomers bearing *Nt*Bu side chains.

Results and Discussion

We first showed in 2013 that the bulky *tert*-butyl side chain is able to freeze peptoid amide-bonds in the *cis* conformation [5]. We then demonstrated that achiral *Nt*Bu-glycine homo-oligomers can preferentially adopt helical folding as a result of weak intramolecular non-covalent interactions, of which some are specific to the *tert*-butyl group (*t*Bu···*t*Bu London interactions) [6]. These results led us to look for another highly congested aliphatic side chain, but this time with a chiral center to control helix handedness. This is how the (*S*)-1-*tert*-butyl(ethyl) side chain (s1tbe) was introduced to the peptoid 'toolbox' [7]. Two families of peptoids (A and B) are presented here. The A family comprises the homo-oligomers Ac-(*N*s1tbe)ₙ-O*t*Bu ranging from monomer to nonamer (Table 1). The B family corresponds to mixed peptoid oligomers comprising *N-tert*-butylglycine (*Nt*Bu) and α-chiral (*S*)-*N*-(1-*tert*-butyl(ethyl)glycine residues (*N*s1tbe) (Table 2). The principle of the submonomer solution-phase synthesis which we adopted to prepare the peptoid molecules is shown in Figure 2. For each oligomer, we determined by integration of the NMR spectra (CDCl₃, CD₃CN and CD₃OD) the overall proportion of *cis* and *trans* rotamers, expressed as the $K_{cis/trans}$ ratio in Tables 1 and 2.
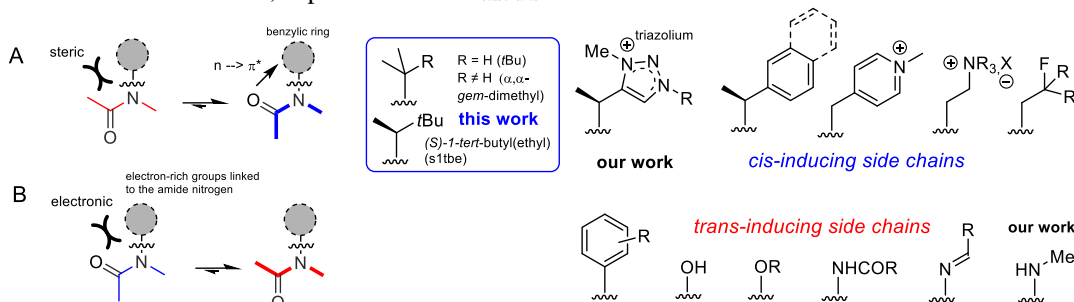
Fig. 1. Key interactions that regulate peptoid amide bond isomerism and summary of the most structuring side chains.

*Table 1. Sequences of peptoids **1-9** (Family A) and overall backbone $K_{cis/trans}$ values as determined by ^{1}H NMR spectra integration in CDCl$_3$, CD$_3$CN and CD$_3$OD.*

peptoid	sequence	CDCl$_3$	CD$_3$CN	CD$_3$OD
		$K_{cis/trans}$	$K_{cis/trans}$	$K_{cis/trans}$
1	Ac-*N*s1tbe-O*t*Bu	0.64	0.67	0.77
2	Ac-(*N*s1tbe)$_2$-O*t*Bu	0.98	1.60	1.68
3	Ac-(*N*s1tbe)$_3$-O*t*Bu	1.95	2.61	3.00
4	Ac-(*N*s1tbe)$_4$-O*t*Bu	>19	10.89	>19
5	Ac-(*N*s1tbe)$_5$-O*t*Bu	18.92	7.96	>19
6	Ac-(*N*s1tbe)$_6$-O*t*Bu	>19	10.39	>19
7	Ac-(*N*sch)$_6$-O*t*Bu	2.71	1.39	
8	Ac-(*N*s1tbe)$_8$-O*t*Bu	>19	8.08	>19
9	Ac-(*N*s1tbe)$_9$-O*t*Bu	>19	12.13	>19

Family A. Table 1 shows a dramatic increase in $K_{cis/trans}$ between trimer **3** and tetramer **4** from 1.95 to >19 in CDCl$_3$, for example, which means that overall the *trans* rotamer population has decreased from 66% to < 4%. The conversion of the trimer to a tetramer thus induces a dramatic increase in conformational order and suggests cooperative folding with chain elongation. The comparison of the $K_{cis/trans}$ values of hexamers **6** ($^{CDCl_3}K_{cis/trans}$ > 19) and **7** ($^{CDCl_3}K_{cis/trans}$ = 2.71) clearly

Fig. 2. Submonomer solution-phase synthesis of α-peptoids oligomers

shows the remarkable *cis*-promoting effect of the s1tbe side chain with respect to the cyclohexylethyl side chain (sch, Figure 2), which has long been considered as a reference. We were able to obtain suitable crystals of compound **5** for X-ray diffraction analysis. In the crystal, peptoid **5** adopts the structure of a nascent right-handed helix with torsion angles consistent with the PPI helix. The solution conformation of this family of peptoids was then investigated by circular dichoism (CD) which confirmed the helical conformation observed in the crystalline state. The CD spectra of peptoids **5**, **6**, **8** and **9** have a similar shape with two negative maxima at about 188 and 225 nm and an intense positive

*Fig.3. CD spectra of peptoids **1-9** at 500 mM. in CH$_3$CN*

maximum at about 209 nm characteristic of the PPI helix (Figure 3). The length-dependent increase in per-amide molar ellipticity (MRE) suggests that helix folding of *N*s1tbe oligomers is probably a cooperative process The comparison of the intensities of the curves of the two hexamers **6** (*N*s1tbe) and **7** (*N*sch), clearly shows that peptoid **7** displays a greater extent of backbone flexibility. This again demonstrates the superiority of the stbe side chain over other aliphatic side chains. We then set out to improve the conformational stability of the *N*s1tbe oligomers and designed a second series of oligomers (Family B) whose sequences incorporate one or more *Nt*Bu units allowing the relevant amides to be fully cis.

Peptoid	Sequence	CDCl₃	CD₃CN
		$K_{cis/trans}$	$K_{cis/trans}$
10	Ac-*N*s1tbe-*N*s1tbe-*N*s1tbe-*N*s1tbe-*N*s1tbe-***Nt*Bu**-O*t*Bu	> 49	> 49
11	Ac-*N*s1tbe-*N*s1tbe-*N*s1tbe-*N*s1tbe-***Nt*Bu**-*N*s1tbe-O*t*Bu	> 15.2	> 11.7
12	Ac-*N*s1tbe-*N*s1tbe-*N*s1tbe-***Nt*Bu**-*N*s1tbe-*N*s1tbe-O*t*Bu	> 14.6	> 10.2
13	Ac-*N*s1tbe-*N*s1tbe-***Nt*Bu**-*N*s1tbe-*N*s1tbe-*N*s1tbe-O*t*Bu	> 18.8	> 10.5
14	Ac-*N*s1tbe-***Nt*Bu**-*N*s1tbe-*N*s1tbe-*N*s1tbe-*N*s1tbe-O*t*Bu	> 14.5	> 11.8
15	Ac-***Nt*Bu**-*N*s1tbe-*N*s1tbe-*N*s1tbe-*N*s1tbe-*N*s1tbe-O*t*Bu	> 20.3	> 13.4
16	Ac-***Nt*Bu**-*N*s1tbe-*N*s1tbe-*N*s1tbe-*N*s1tbe-***Nt*Bu**-O*t*Bu	> 23.3	> 23.3
17	Ac-***Nt*Bu**-***Nt*Bu**-*N*s1tbe-*N*s1tbe-***Nt*Bu**-***Nt*Bu**-O*t*Bu	> 29.1	> 27.8
18	Ac-***Nt*Bu**-***Nt*Bu**-*N*s1tbe-*N*s1tbe-*N*s1tbe-***Nt*Bu**-***Nt*Bu**-O*t*Bu	> 49	> 42.0
19	Ac-***Nt*Bu**-***Nt*Bu**-*N*s1tbe-*N*s1tbe-*N*s1tbe-*N*s1tbe-***Nt*Bu**-***Nt*Bu**-O*t*Bu	> 25.5	> 25.5
20	Ac-***Nt*Bu**-***Nt*Bu**-***Nt*Bu**-*N*s1tbe-*N*s1tbe-*N*s1tbe-***Nt*Bu**-***Nt*Bu**-***Nt*Bu**-O*t*Bu	> 49.0	> 49.0

Family B. The first finding from the comparison of the $K_{cis/trans}$ values (Table 2) of peptoid hexamers **10-15** is that the positioning of a single *cis*-promoting *Nt*Bu residue at the carboxy terminus proves exceptionally efficient to suppress the *trans*-amide rotamers. This is consistent with the known fact that the *C*-terminus of the PPI peptoid helix is structurally more flexible than the *N*-terminus [8]. The second major finding is that peptoid oligomers containing a central chiral segment of 2 to 4 consecutive *N*s1tbe residues, surrounded by *Nt*Bu residues (**16-20**) display the higher overall $K_{cis/trans}$ (% cis = 96-100). In contrast, the incorporation of *Nt*Bu monomers every two *N*s1tbe residues (not shown) does not ensure the complete suppression of peptoid amide *cis-trans* isomerism.

The strongest CD intensity (208 nm) of hexamer **10** within the group of peptoids **10-15** (Figure 4A) is consistent with an all *cis*-amide backbone ($K_{cis/trans}$ > 49 in CDCl₃ and CD₃CN). Comparison of the CD curves of hexamers **10-15** shows that the ellipticity decreases with increasing the distance of the *Nt*Bu residue from the carboxy terminus. Also of note is that a single *Nt*Bu residue, strategically placed at the *C*-terminus, provides a much more stable helical conformation than a homo-oligomeric sequence of the same length (compound **10** *vs* hexamer Ac-(*N*s1tbe)₆-O*t*Bu).
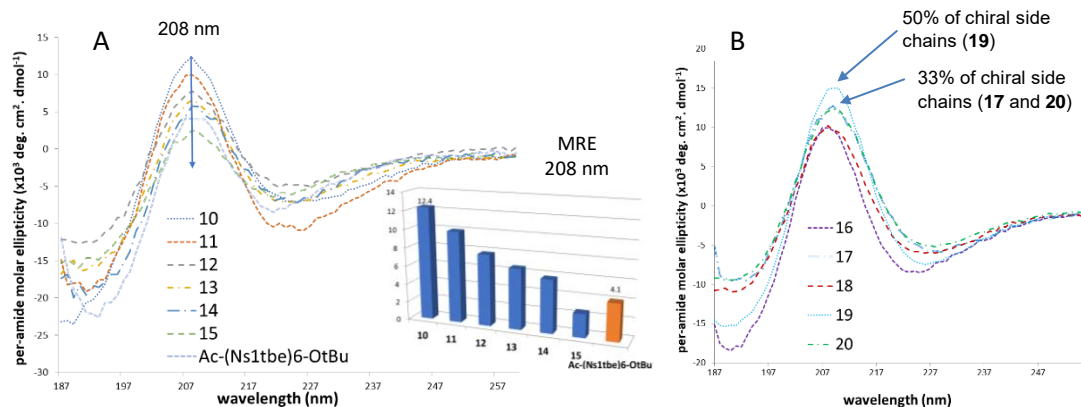
*Fig. 4. CD spectra of peptoids **10-20** and reference compound Ac-(Ns1tbe)₆ in MeOH.*

Regarding the DC curves of peptoids **16-20** (Figure 4B), the most striking observations are the following: the MRE of peptoid **17** is remarkable, considering its short length (hexamer) and low proportion of chiral side chains (33%). The MRE intensity of peptoid **17** at 208 nm is at the same level as that of hexamer **10**, which contains 83% of chiral side-chains. In addition, the CD spectrum of **17** in methanol has comparable shape and intensity to that of the nonamer **20**, also composed of only 33% of chiral residues. The design principle underlying the preparation of compounds **16-20** is thus particularly attractive for attaining stable helical folding with a low content of chiral side chains. The results suggest a sergeants-and-soldiers behaviour, with the central chiral segment imposing its handedness on both ends of the oligomers. This is clearly seen in the crystallographic structure of octamer **19**, the longest linear α-peptoid ever analysed in the crystal state. The structure of **19** is a right-handed PPI-like helix of great regularity despite a chiral content of only 50%.

In continuation of this work, we focused on β-*Nt*Bu oligomers and showed that they can adopt a helical structure with about three residues per turn as already described in the literature [9]. We also proposed a new regular ribbon-like structure [10].

Fig. 5. X-ray structure of octamer 19.

Acknowledgments

References

1. Horne, W.S. *Expert Opin Drug Discov*. **6**, 1247-1262 (2011), https://doi.org/10.1517/17460441.2011.632002
2. Kalita, D., et al. *Chem. Asian J.* e202200149 (2022), https://doi.org/10.1002/asia.202200149
3. Shin, H., et al. *Chem. Commun.* **50**, 4465-4468 (2014), https://doi.org/10.1039/C3CC49373C
4. Rzeigui, M., et al. *J. Org. Chem.* **85**, 2190-2201 (2020), https://doi.org/10.1021/acs.joc.9b02916
5. Roy, O., et al. *Org. Lett.* **15**, 2246-2249 (2013), https://doi.org/10.1021/ol400820y
6. Angelici, G., et al. *Chem. Commun.* **52**, 4573-4576 (2016), https://doi.org/10.1039/C6CC00375C
7. Roy, O., *J. Am. Chem. Soc.* **139**, 13533-13540 (2017), https://doi.org/10.1021/jacs.7b07475
8. Wu, C.W. *J. Am. Chem. Soc.* **123**, 6778-6784 (2001), https://doi.org/10.1021/ja003154n
9. Laursen, J.S. *Nat Commun* **6**, 7013 (2015), https://doi.org/10.1038/ncomms8013
10. Angelici, G., et al. *Org. Biomol. Chem.* 2022, Accepted Manuscript, https://doi.org/inc.bib.cnrs.fr/10.1039/D2OB01351G

Influence of the Daunomycin Position on Bioactivity in Angiopep-2 - Drug Conjugates

Lilla Pethő[1], Rita Oláh-Szabó[1], and Gábor Mező[1,2]

[1]ELKH-ELTE Research Group of Peptide Chemistry, Budapest, 1117 Hungary; [2]Eötvös Loránd University, Faculty of Science, Institute of Chemistry, Budapest, 1117 Hungary

Introduction

Transporting therapeutics through the blood-brain barrier (BBB) is a major challenge in the treatment of brain tumors. The BBB is a semipermeable system and therefore the majority of the active substances are poorly transported through this barrier resulting in decreased therapeutic effects [1]. Angiopep-2 (TFFYGGSRGKRNNFKTEEY) is a peptide containing 19 amino acids that was shown to be a ligand of the low-density lipoprotein receptor-related protein-1 (LRP1). This peptide can cross the blood-brain barrier *via* receptor-mediated transcytosis and simultaneously target glioblastoma, thereby dual targeting may be achieved [2]. Angiopep-2 contains three amino groups (two lysine side chains in positions 10 and 15 and the *N*-terminal), and all these groups were functionalized in previous studies to produce drug-peptide conjugates [3,4]. Using all possible conjugation sites is convenient from the synthetic point of view but is not always necessary for achieving the best effect. In this case the role and importance of each position have not yet been investigated. Hence, in this work, the number and position of the drug molecules in Angiopep-2 based conjugates were in the focus.

Results and Discussion

Conjugates containing one, two, and three daunomycin molecules *via* oxime linkage were prepared. The peptides for conjugation were prepared by SPPS using Fmoc/*t*Bu strategy starting from one batch of Rink-Amide MBHA resin. Before the coupling of the second lysine derivative, the resin was split, and orthogonal protecting schemes were further applied to create the proper conjugation sites (Scheme 1). Before the cleavage of the peptides from the resin, one or more protecting groups were removed selectively, and the resulting free amino groups were modified by Boc-protected aminooxyacetyl (Aoa) moiety. After the peptide cleavage the derivatives containing different number of Aoa were purified by RP-HPLC and used for conjugation with daunomycin (Dau) under slightly acidic condition (0.2 M NH$_4$OAc at pH 5 for overnight). In this way three conjugates with one Dau in different positions, three conjugates with 2 Dau and one with 3 Dau in all possible conjugation sites were produced.

The cytostatic effect of the conjugates was investigated on U87GM human glioblastoma cell line. The cells were incubated with the conjugates in serum free medium for 24 h and after washing the cells were further incubated in fresh serum containing medium for additional 48 h The results indicated significant differences in the antitumor activity of the conjugates, which was not related to the number but rather the position of the drug(s) on the homing peptide (Figure 1). The free Angiopep-2 did not show any effect on tumor cells up to 100 µM concentration. Among the conjugates with only one Dau compound **3** in which Dau was attached to the *N*-terminus showed the highest antitumor effect on glioblastoma cells (*IC$_{50}$*: 10.9 ± 2.8 µM). When the Dau was conjugated to the Lys side chain in position 15 (compound **2**) the effect decreased significantly (*IC$_{50}$*: 30.2 ± 6.4 µM) and conjugate **4** also was not significantly better (*IC$_{50}$*: 24.0 ± 5.9 µM). The conjugates with two drug molecules similar tendency was observed. Compound **7** with Dau at the *N*-terminus and on the Lys side chain in position 10 showed the highest activity (*IC$_{50}$*: 7.8 ± 6.3 µM). When the Lys side chains were used as conjugation sites, the formed compound (**6**) had a moderate activity on U87 cells (*IC$_{50}$*: 21.6 ± 5.4 µM). Surprisingly, conjugate **5** with Dau at the *N*-terminus and Lys side chain in position 15 showed the lowest potency on cells (*IC$_{50}$*: 32.3 ± 8.1 µM). Compound **8** with three Dau had moderate activity as well (*IC$_{50}$*: 23.6 ± 6.3 µM). The data indicated that the side chain of Lys in position 15 is an inadequate

conjugation site for drug delivery. In contrast, the substitution of the *N*-terminal amino group with a drug molecule might be the most efficient choice for drug targeting with Angiopep-2.
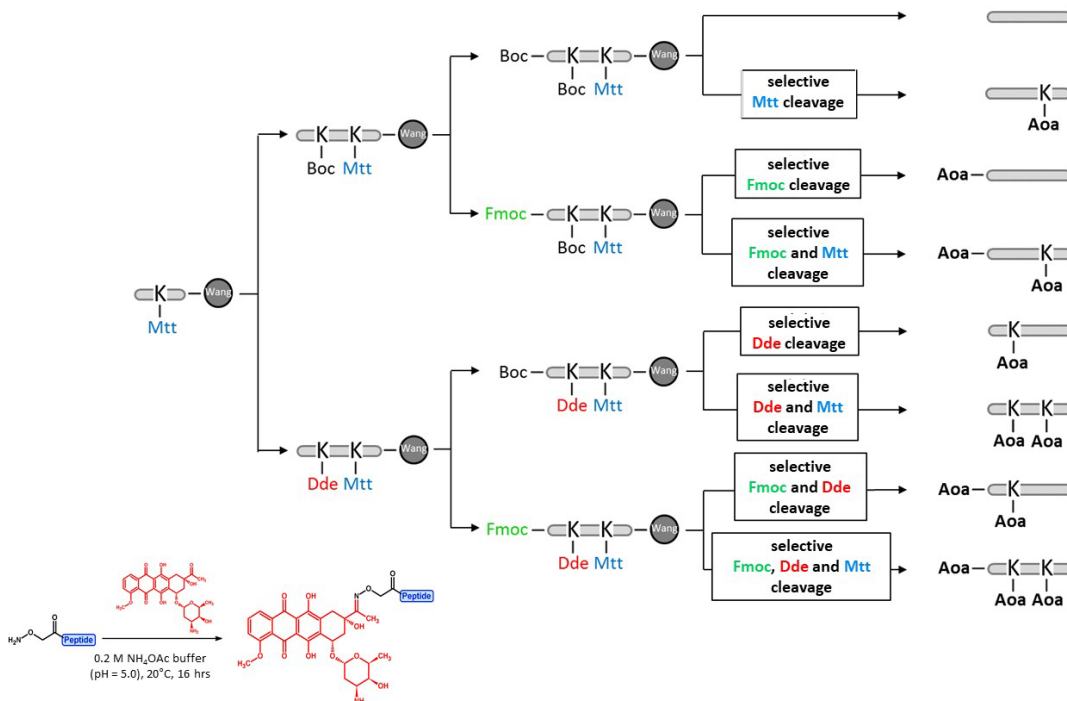
Scheme 1. Synthetic protocol of different Angiopep-2 – daunomycin conjugates using orthogonal side chain protecting groups.
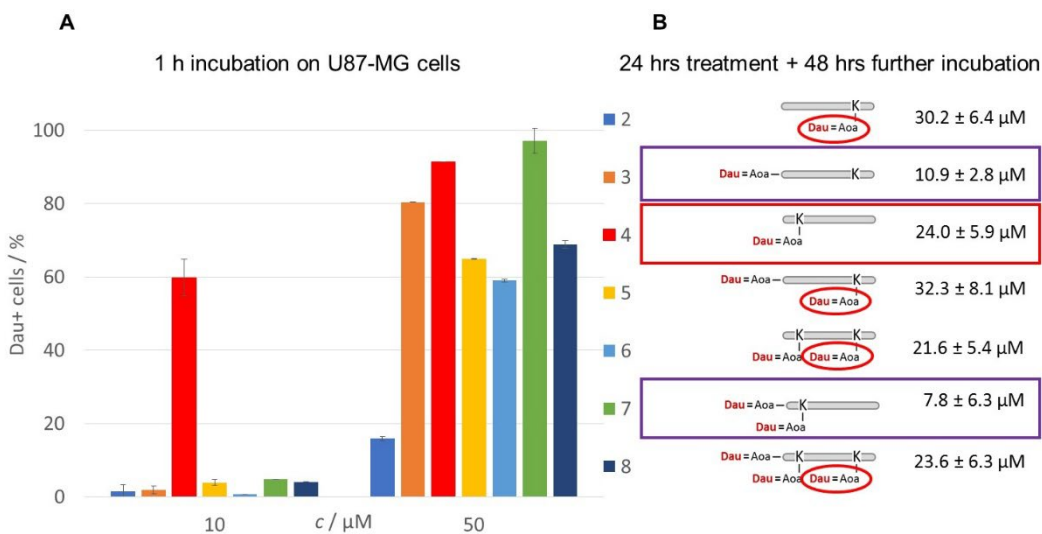
Fig. 1. Cellular uptake (A) and cytostatic effect (B) of Angiopep-2 − daunomycin conjugates.

The antitumor activity of any peptide-drug conjugate is influenced by many factors. One of the main effects is the cellular uptake of the conjugates. Therefore, we compared the cellular uptake of the different conjugates on U87GM glioblastoma cells, which were incubated with the conjugates for 1 h, by flow cytometry. The cellular uptake of the conjugates was concentration dependent. The correlation between the uptake and the cytostatic effect could be established in most cases. Conjugates **3** and **7** entered the cells very efficiently at 50 µM concentration (80% and 97% of cells were Dau+, respectively) while conjugate **2** showed very low uptake (15%) (Figure 1). Interestingly, conjugate **4** that showed moderate cytostatic effect was taken up the most effectively. 90% of the cells were Dau positive at 50 µM concentration, while this value was 60% at a concentration of 10 µM. In contrast, all other compounds showed lower cellular uptake (< 10%) at this concentration. In case of the conjugate with three Dau (**8**) only 70% of the cells were Dau+ at 50 µM concentration.

Since we discovered contradictions between the cellular uptake and cytostatic effect of some conjugates, we studied the degradation of the conjugates in lysosomal homogenates (isolated from rat liver). It is worth mentioning that oxime linkage is quite stable at neutral pH, therefore, there is no early release of drug from the conjugate in the blood circulation in contrast with conjugates containing an ester linkage. The disadvantage of the oxime linkage is that it does not decompose in cells either to release the free drug. However, the smallest metabolites that contain daunomycin linked to one amino acid through Aoa established linker can bind to DNA resulting in antitumor activity [5]. This is the reason that this type of conjugates can be used in higher amount *in vivo* providing higher antitumor effect in comparison with free Dau at the maximum tolerated dose.

The lysosomal degradation was followed by HPLC-MS. The results indicated that in case of compound **3**, the Dau=Aoa-Thr-OH fragment appeared within 1 h, at 6 h it was the main drug containing metabolite and at 72 h, this Dau containing fragment could only be detected (Figure 2). This time dependent pattern was also observed in case of conjugate **2**, where Dau was attached to the side chain of Lys in position 15, and the formed smallest metabolite was H-Lys(Dau=Aoa)-OH. Since this metabolite binds very efficiently to DNA [5], a strong cytostatic effect could be expected in case of compound **2**. As we observed the opposite, we can conclude that the low activity of this compound is related to the low cellular uptake. In contrast, this metabolite was not efficiently released from compound **4**. It was not detectable at 1 h and only a low amount could be observed after 6 h. Even after 72 h the main metabolites were H-Gly-Lys(Dau=Aoa)-Arg-OH and H-Gly-Lys(Dau=Aoa)-OH. Though the efficient cellular uptake, this observation might explain the lower anticancer activity of the conjugate.

Code	Structure	Smallest metabolite Dau=Aoa-Thr-OH (3) or H-Lys(Dau=Aoa)-OH (2,4)		
		1 hr	6 hrs	72 hrs
2	H-TFFYGGSRGKRNNFKTEEY-OH Dau=Aoa	appeared	main product	only detectable
3	Dau=Aoa-TFFYGGSRGKRNNFKTEEY-OH	appeared	main product	only detectable
4	H-TFFYGGSRGKRNNFKTEEY-OH Dau=Aoa	not detectable	appeared	not the main product detected smallest metabolites H-GK(Dau=Aoa)R-OH and H-GK(Dau=Aoa)-OH

Fig. 2. Lysosomal degradation of Angiopep-2 – Dau conjugates with one drug molecule.

To increase the release of the active metabolite in this position, Cathepsin B (lysosomal enzyme) labile peptide spacers were incorporated between the side chain of Lys in position 10 and Dau. For this purpose, GFLG, VA and VAGG were selected. The application of GFLG spacer in conjugate **9** showed an efficient cellular uptake and a moderate improvement in cytostatic effect (IC_{50}: 16.9 ± 5.6 µM) compared to compound **4** (Figure 3). Unfortunately, the release of Dau=Aoa-Gly-OH was also slow and the detected main metabolite at 6 h time point was Dau=Aoa-Gly-Phe-OH. The investigation of VA spacer (conjugate **11**) showed that the antitumor activity was completely lost. This effect could be explained both by the decrease of cellular uptake and lysosomal degradation. Only negligible Dau=Aoa-Val-OH could be detected even after 72 h. The incorporation of two Gly between VA and the Lys side chain (compound **10**) resulted in higher cytostatic effect but there was no significant improvement in comparison with compound **4**. Although the Dau=Aoa-Val-Ala-OH fragment appeared after 1 h and Dau=Aoa-Val-OH was also detected in high amount after 6 h, but the cellular uptake of this conjugate was much lower than that of the conjugates **4** and **9**. According to these results we can conclude that the substitution of Lys side chain in position 10 with an appropriate enzyme labile spacer (GFLG) has a positive effect on the cellular uptake, but the drug release is still hindered. Therefore, we plan to use other properly designed enzyme labile spacers to increase the release of the active metabolite.
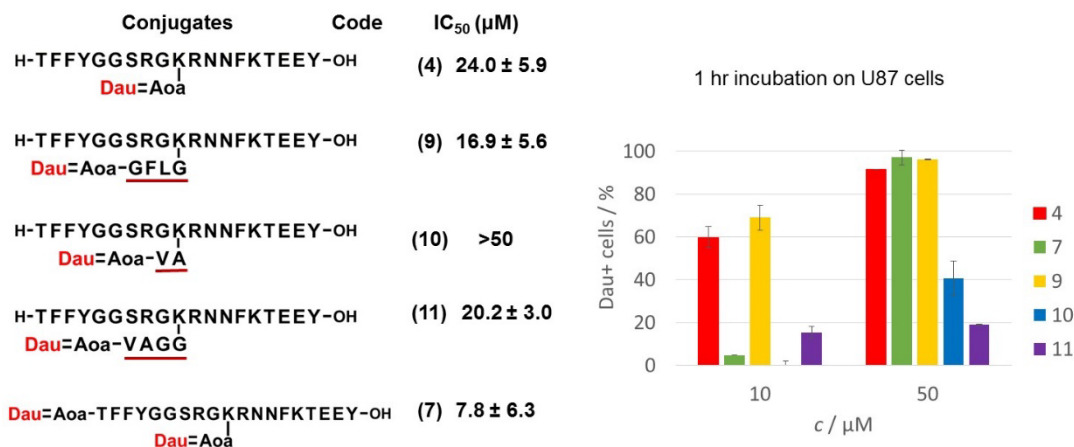
Fig. 3. Cytostatic effect and cellular uptake of Angiopep-2 – daunomycin conjugates with spacers between the homing peptide and the drug molecule.

As summary, we can draw the conclusion that the position of the drug molecule in an Angiopep-2 conjugate has higher influence on the antitumor activity than the number of the conjugated drugs.

Acknowledgments

References

1. Oller-Salvia, B., et al. *Chem. Soc. Rev.* **45**, 4690-4707 (2016), https://doi.org/10.1039/C6CS00076B
2. Demeule, M., et al. *J. Pharmacol. Exp. Ther.* **324**, 1064-1072 (2008), https://doi.org/10.1124/jpet.107.131318
3. Régina, A., et al. *Br. J. Pharmacol.* **155**, 185-197 (2008), https://doi.org/10.1038/bjp.2008.260
4. Ché, C., et al. *J. Med. Chem.* **53**, 2814-2824 (2010), https://doi.org/10.1021/jm9016637
5. Orbán, E., et al. *Amino Acids* **41**, 469-483 (2011), https://doi.org/10.1007/s00726-010-0766-1

Development of Pancreatic Tumor Specific Daunomycin – Peptide Conjugates Using Homing Peptides Selected by Phage Display Technique

Levente Endre Dókus[1], Eszter Lajkó[3], Zsófia A. Szász[3], Diána Vári-Mező [3], Angéla Takács[3], László Kőhidai[3], and Gábor Mező[1,2]

[1]*ELKH-ELTE Research Group of Peptide Chemistry, Budapest, Hungary;* [2]*Eötvös Loránd Universit, Faculty of Science, Institute of Chemistry, Budapest, Hungary;* [3]*Department of Genetics, Cell- and Immunobiology, Semmelweis University, Budapest, Hungary*

Introduction

Pancreatic Ductal Adenocarcinoma (PDAC) is one of the most dangerous cancerous diseases leading to high mortality [1]. This tumor type is only 3-4% of all newly diagnosed cancer cases but the mortality of this disease is more than 80% [2]. Furthermore, the average 5-years survival rate is not more than 10% [3], because approximately 80% of the patients are diagnosed with metastatic or inoperable status. Therefore, new approaches for efficient treatment are necessary. Here we report the development of peptide - drug conjugates which contain daunomycin as anticancer drug attached to different homing peptides *via* oxime bound – a linkage that might be suitable for targeted tumor therapy. In the literature, several peptides can be found that were identified by phage-display technique and recognized PDAC cells with high affinity. However, the efficacy of drug targeting has not been compared. Four of them (**(I)** SYENFSA [4], **(II)** IVRGRVF [4], **(III)** PFWSGAV [5], **(IV)** TMAPSIK [6]) were selected for this study. Based on our previous results four-members conjugate families were designed. Linear and branched structures were synthesized using various enzyme labile spacers for enhanced drug release.

Results and Discussion

For targeting of PDAC cells, sixteen different daunomycin - peptide conjugates were designed and synthesized using the above mentioned four homing moieties (Table 1).

The synthesis of conjugates was carried out by solid phase peptide synthesis, using Fmoc/^{t}Bu technique. To the *N*-terminal α-amino group isopropylidene-protected aminooxyacetyl-group was attached as a linker between the homing part and the payload. The aminooxyacetyl peptide derivatives were cleaved from the resin and the crude products were purified by RP-HPLC. For identification of products ESI-MS was used in all cases. After the cleavage of the isopropylidene-protecting group with 0.2M NH_4OAc buffer solution (pH 5.0), daunomycin was coupled to the aminooxyacetyl moiety forming oxime bond (Figure 1). In the case of eight conjugates cathepsin B enzyme labile spacer was built into the sequences between the homing peptide and the aminooxy moiety that may enhance the intracellular (lysosomal) degradation and the release of the active drug-containing metabolites. In cases of apolar homing peptide sequences (**1**, **2**, **3**) LRRY segment was built in as spacer but the more polar **4** sequence encouraged the application of GFLG spacer [7].

The *in vitro* cytotoxic effect of conjugates was investigated on PANC-1 pancreatic cancer cells by an impedimetric technique, xCELLigence System. The effect of them was characterized also on further three cell lines as control (colon cancer (Colo-205); melanoma (A2058) and non-small cell lung cancer (EBC-1)) for characterization their selectivity using Alamar blue test.
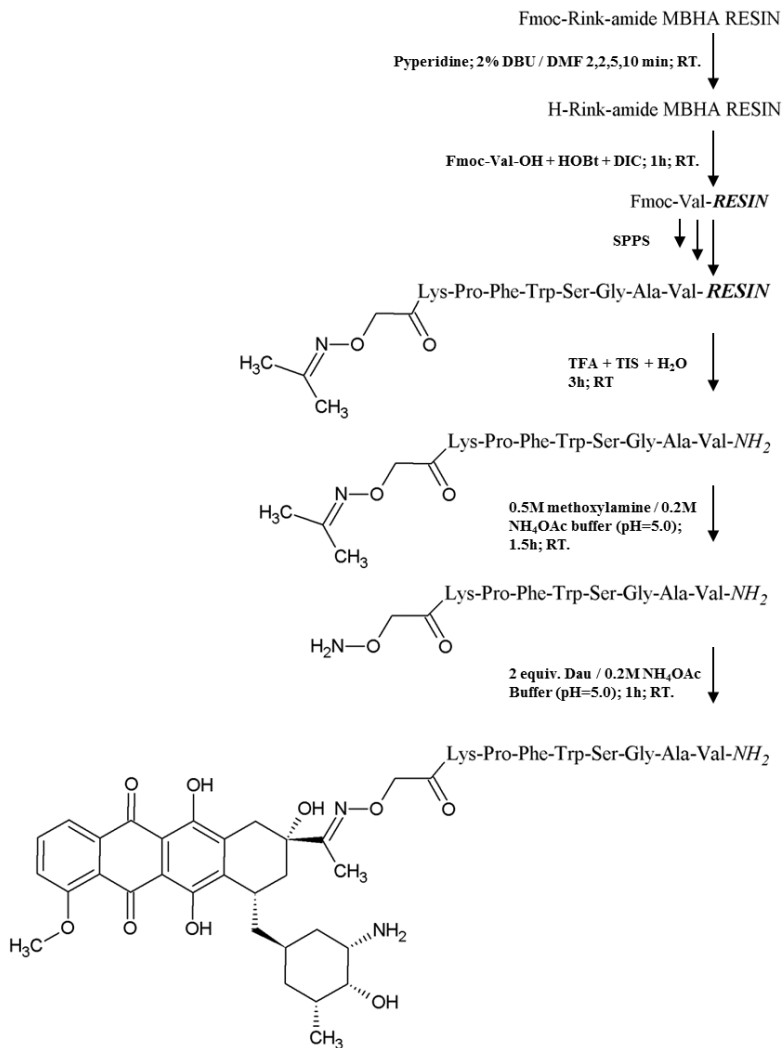
Fig. 1. Outline of synthesis of conjugates.

To investigate further structure-activity relationships Ala-scanning of conjugate **10** was carried out to study the possible positions for further development of more efficient compounds.

Ala-scanning showed that the alanine substitution resulted in the loss of efficiency in all cases except conjugate **22** which presented moderated antitumor effect (Table 2).

The results showed that two conjugates out of four which were designed with homing moieties **I** and **II** did not give significant antitumor effect on PANC-1 cells (conjugates 1-8). However, these 8 conjugates have very poor antitumor effect (50-70 viability %) on one or more of the other control cell lines out of conjugate **6**.

Table 1. Effect of the conjugates on PANC-1 and other cell-lines as control.

CODE	CONJUGATES	Viability % in 10^{-5} M concentration, after 72 h incubation			
		PANC-1[a]	Colo-205[b]	A2058[b]	EBC-1[b]
1	Dau=Aoa-SYENFSA-NH₂	NOT SOLUBLE	66.0±1.9	58.3±1.0	40.1±0.6
2	Dau=Aoa-KSYENFSA-NH₂	117.1±3.5	62.6±3.2	68.9±1.9	83.1±4.6
3	Dau=Aoa-LRRYKSYENFSA-NH₂	107.4±4.4	82.1±2.4	65.6±3.0	75.8±2.0
4	Dau=Aoa-LRRYK(Dau=Aoa)SYENFSA-NH₂	128.0±13.5	56.3±7.6	55.8±2.4	62.8±5.9
5	Dau=Aoa-IVRGRVF-NH₂	89.7±12.0	69.6±1.1	58.0±3.1	50.0±0.5
6	Dau=Aoa-KIVRGRVF-NH₂	105.3±6.4	92.8±2.3	69.4±2.7	78.4±1.8
7	Dau=Aoa-LRRYKIVRGRVF-NH₂	125.0±7.4	63.7 ± 6.7	83.5±6.1	74.4±2.0
8	Dau=Aoa-LRRYK(Dau=Aoa)IVRGRVF-NH₂	122.6±9.0	63.4±6.7	56.0±2.5	70.7±3.7
9	Dau=Aoa-PFWSGAV-NH₂	23.2 ± 3.3	23.8 ± 0.7	38.6 ± 2.6	26.0 ± 0.6
10	Dau=Aoa-KPFWSGAV-NH₂	12.0 ± 2.5	19.6 ± 0.1	41.4 ± 5.0	24.8 ± 0.4
11	Dau=Aoa-LRRYKPFWSGAV-NH₂	85.7 ± 17.2	28.9 ± 0.3	54.7 ± 1.7	35.1 ± 2.7
12	Dau=Aoa-LRRYK(Dau=Aoa)PFWSGAV-NH₂	10.5 ± 0.5	19.4 ± 0.2	26.8 ± 1.7	30.2 ± 0.3
13	Dau=Aoa-TNleAPSIK-NH₂	31.5 ± 3.5	23.0 ± 0.5	44.0 ± 8.2	32.8 ± 0.8
14	Dau=Aoa-KTNleAPSIK-NH₂	120.3 ± 3.6	40.1 ± 2.2	82.7 ± 5.5	64.4 ± 3.3
15	Dau=Aoa-LRRYKTNleAPSIK-NH₂	37.5 ± 2.4	22.7 ± 0.3	43.5 ± 4.7	31.8 ± 1.1
16	Dau=Aoa-LRRYK(Dau=Aoa)TNleAPSIK-NH₂	49.8±1.5	79.3±7.3	26.9±5.8	48.8±2.6

[a]x-Celligence System;[b]Alamar blue assay

Table 2. Effect of the conjugates of Ala-scan on PANC-1 and further cell-lines as control.

CODE	CONJUGATES	Viability % in 10^{-5} M concentration, after 72 h incubation			
		PANC-1[a]	Colo-205[b]	A2058[b]	EBC-1[b]
17	Dau=Aoa-KPFWSGAA-NH₂	99.5±4.6	66.0±1.9	58.3±1.0	40.1±0.6
18	Dau=Aoa-KPFWSAAV-NH₂	101.7±12.1	63.2±1.4	53.1±1.9	33.9±0.5
19	Dau=Aoa-KPFWAGAV-NH₂	120.5±18.9	70.7±2.5	71.2±7.7	70.6±3.7
20	Dau=Aoa-KPFASGAV-NH₂	127.3±21.2	79.2±5.4	73.8±10.2	70.5±1.2
21	Dau=Aoa-KPAWSGAV-NH₂	133.0±7.4	73.3±6.4	73.5±3.7	63.0±2.9
22	Dau=Aoa-KAFWSGAV-NH₂	48.6±1.0	47.5±1.1	32.9±0.9	27.3±0.2
23	Dau=Aoa-APFWSGAV-NH₂	121.9±19.2	63.8±4.8	73.0±2.9	68.5±1.7

[a]x-Celligence System;[b]Alamar blue assay

In contrast, among the conjugates derived from the homing peptide family **III** or **IV** there were active compounds. Conjugates **10** and **12** showed significant antitumor effect on PANC-1 cells. Treatments with these conjugates at 10^{-5} M concentration resulted in lower than 15% viability of cells. Further four derivatives (conjugates **9**, **13**, **15** and **16** have moderate effect on PANC-1 cells. They generated lower than 50% viability.

Conjugates **10** and **12** have low, but significant selectivity to PANC-1 cells, while conjugates **9, 13, 15** and **16** showed approximately similar cytotoxic effect on all cell lines.

The presence of different enzyme labile spacer does not significantly enhance the effectivity of conjugates belong to the groups **III** and **IV**.

Ala-scanning of conjugate **10** showed that the alanine substitution resulted in the loss of efficiency in all cases except conjugate **22** which has moderated antitumor effect.

Acknowledgments

References

1. Jemal, A., et al. *CA Cancer J. Clin.* **57**, 43-66 (2007), https://doi.org/10.3322/canjclin.57.1.43
2. Siegel, R.L., et al. *CA Cancer J. Clin.* **70**, 7-30 (2018), https://doi.org/10.3322/caac.21590
3. Hidalgo, M. *N. Engl. J. Med.* **362**, 1605-1617 (2010), https://doi.org/ 10.1056/NEJMra0901557
4. Nishimoto, T., et al. *Gene Therapy* **16**, 669-680 (2009), https://doi.org/10.1038/gt.2009.1
5. Nishimoto, T., et al. *PLOS ONE.* **7**(9), e45550 (2012), https://doi.org/10.1371/journal.pone.0045550
6. Kelly, K.A., et al. *PLoS Medicine* **5**(4), e85 (2008), https://doi.org/10.1371/journal.pmed.0050085
7. Peterson, J.J., et al. *Bioconj. Chem.* **9,** 618-626 (1998), https://doi.org/10.1021/bc980059j

Enhancing Cell Entry of Peptide Conjugates with Bicycle Formation Through TBMB Rigid Scaffold

Attila Csaba Bató[1*], Ildikó Szabó[2], and Zoltán Bánóczi[1]

[1]*Institute of Chemistry, Eötvös Loránd University, Budapest, Hungary;*
[2]*MTA-ELTE Research Group of Peptide Chemistry, Budapest, Hungary*
e-mail:bs.csabi@gmail.com

Introduction

Delivering therapeutic agents into cells has always been a major challenge. Usually, the conjugates decompose before entering the cells. Bicyclic peptides are promising agents and have some advantages. These peptides are usually not so long typically 9-20 amino acids and thanks to this small size these peptides have the potential to penetrate the cell membrane. Furthermore, the two rings may protect the construct from the enzymatic degradation, so bicyclic peptides remain intact. A sequence containing 3 cysteine residues can be cyclized via its thiol-groups in selective reaction with a small-molecule scaffold. This reaction may form three stable thio-ether bonds between the peptide and the scaffold, constraining the peptide into a bicyclic structure [1,2]. Another approach is the modification of the *N*-terminal amino-group with Dabcyl-group ((4–((4–(dimethylamino)phenyl)azo)benzoyl)) that can also enhance the cellular uptake of the peptides [3].

Results and Discussion

Our aim is to study the effect of bicycle formation on the internalization of different oligoarginines. For this oligoarginines with or without Dabcyl-group were synthesized and reacted with 1,3,5-tris(bromomethyl)benzene. Their labelling for cellular uptake studies was with 5(6)-carboxyfluorescein on the *C*-terminal Lys residue. The oligoarginines were synthesized by standard Fmoc/^{t}Bu strategy. The Dabcyl-group was coupled to the α-amino group of the peptides on the resin. The reaction between the peptides and 1,3,5-tris(bromomethyl)benzene as well as the fluorescent labelling took place in solution. The constructs were purified by RP-HPLC and characterized by analytical RP-HPLC and mass spectrometry (Table 1). The sequences were designed in a way that each loop contains equal number arginine residues.

   In vitro cellular uptake was measured by flow cytometry experiments on cancerous cells. EBC-1 human cancer cells were treated with the solution of the conjugates for 90 min at RT. The fluorescence intensity of treated cells was measured by flow cytometry (Figure 1). The cyclization increased the cellular uptake of the Dabcyl containing octaarginine derivative in comparison with octaarginine. The cytotoxicity was also measured by flow cytometry (Figure 2). The live cells were always 70% or more indicating that these constructs have no cytotoxic effect.

Table 1 Chemical characteristics of conjugates.

Peptide sequence	Code	Rt (min)	$M_{calculated}$	$M_{measured}$
Dabcyl-CR$_2$CR$_2$CK-CF TBMB	D-CR4	14.8	1802.0	1801.8
Dabcyl-CR$_3$CR$_3$CK-CF TBMB	D-CR6	13.8	2114.4	2114.0
Dabcyl-CR$_4$CR$_4$CK-CF TBMB	D-CR8	13.5	2426.8	2426.2
Acyl-CR$_2$CR$_2$CK-CF TBMB	Ac-CR4	12.5	1592.8	1592.7
Acyl-CR$_3$CR$_3$CK-CF TBMB	Ac-CR6	11.4	1905.2	1904.9
Acyl-CR$_4$CR$_4$CK-CF TBMB	Ac-CR8	10.1	2217.6	2217.1
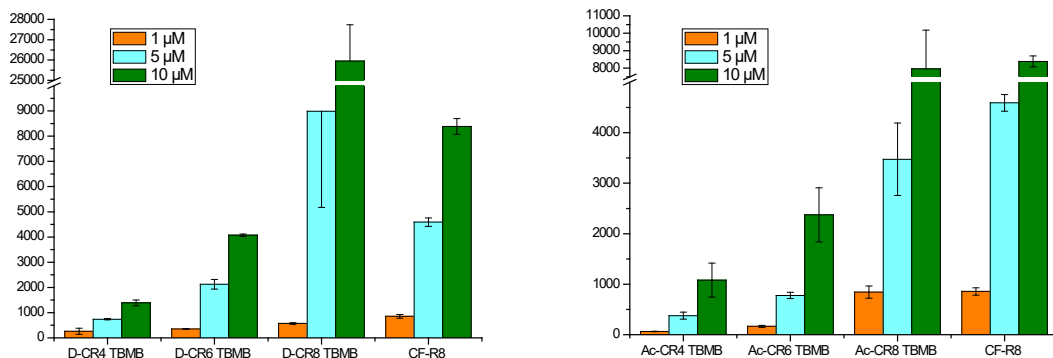
Fig. 1. The effect of bicycle formation on the internalization of oligoarginines with (left) and without Dabcyl-group (right) on EBC-1 cells at RT.
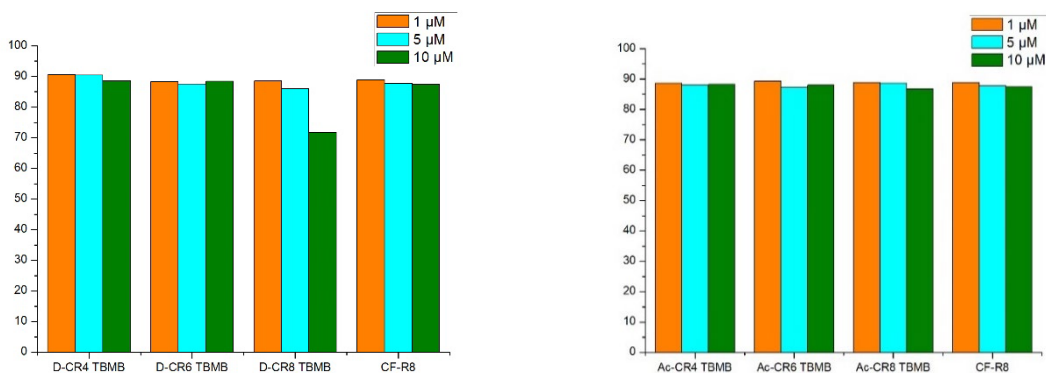
Fig. 2. Cytotoxicity measured by flow cytometry of oligoarginines with (left) and without Dabcyl-group (right).

These results indicate that the cyclization may enhance the internalization of oligoarginine. The bicyclic octaarginines; with or without Dabcyl-group had better or similar uptake than the linear one, respectively. These modifications enhance the internalization while they do not result in cytotoxic effect.

Acknowledgments

References

1. Gemma, E.M., et al. *J. Med. Chem*. **63**(8), 4107-4116 (2020), https://doi.org/10.1021/acs.jmedchem.9b02129
2. Natia, T., et al. *Eur. J. Med. Chem*. **94**, 459-470 (2015), https://doi.org/10.1016/j.ejmech.2015.01.014
3. Szabó, I., et al. *Amino Acids* **53**(7), 1033-1049 (2021), https://doi.org/10.1007/s00726-021-03003-w

Studies on Interactions of Human Serum Albumin with Hot Spots and Peptidic Inhibitors of Insulin and Amylin Aggregation

J. Wasko[1], M. Wolszczak[2], Z.J. Kaminski[1], and B. Kolesinska[1]

[1]Institute of Organic Chemistry, Faculty of Chemistry, Lodz University of Technology, Lodz, 90-924, Poland;
[2]Institute of Applied Radiation Chemistry, Faculty of Chemistry, Lodz University of Technology, Lodz, 93- 590, Poland

Introduction

Human serum albumin (HSA), being a molecule of an increasing number of applications, shows great potential for becoming a safe, multifunctional delivery vehicle for important medications (e.g. phenylbutazone, ketoprofen, liraglutide, warfarin) [1]. HSA has two main binding sites, localizing in IIA (Sudlow site I) and IIIA subdomains (Sudlow site II), with a highly ordered secondary structure, composed mainly of α-helix and stretched chains (Figure 1). The conformational changes of HSA are regulated by pH alteration of the external environment, influencing its transport properties [2]. Nowadays, amyloidosis caused by undesirable polypeptide/protein aggregation is a huge challenge for
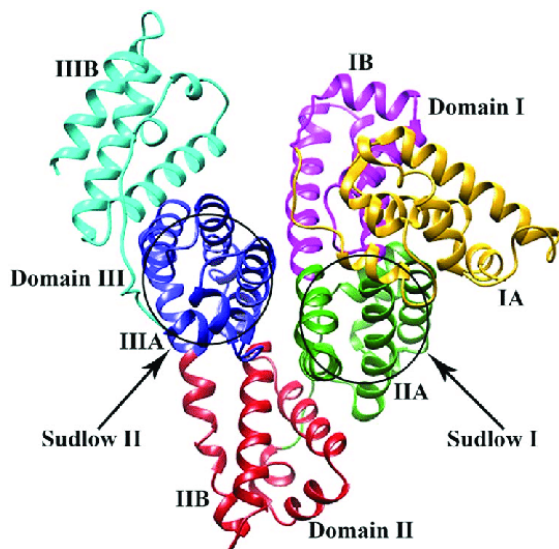
Fig. 1. HSA structure with indicated potential binding sites of external ligands.

scientists. Amyloidosis includes neurodegenerative diseases (Alzheimer's disease, Parkinson's disease), diabetes, cardiac amyloidosis, and others. Scientific work is being intensively carried out on the search for new methods of treating amyloidosis [3,4,5]. It is supposed that HSA could be applied as a drug delivery system (DDS) for inhibitors of pathological protein/polypeptide aggregation, with the aim to alleviate the symptoms and detrimental effects of neurodegenerative and metabolic disorders. On the one side, these inhibitors should be precisely delivered to the target site but on the other side, their immune activity should be minimal. The aim of the study was to check whether HSA can be used as a drug carrier for *N*-methylated analogous amyloidogenic cores (so-called hot spots) [6] of insulin and amylin, which significantly inhibit the aggregation of hormones regulating carbohydrate metabolism and are directly involved in the development of diabetes. The implementation of the research goal required the synthesis of amyloidogenic cores of insulin and amylin hormones and peptidic inhibitors of undesirable aggregation. For synthesis of peptides, 4-(4,6-dimethoxy-1,3,5-triazin-2-yl)-4-methyl-morpholinium p-toluenosulphonate (DMT/NMM/TosO⁻) [7] was used as coupling reagent. Moreover, all peptides were labeled with 4-(1-pyrenyl)butyric acid (PBA), fluorescent dye permitting to monitor their docking to HSA. For selected fragments, it was planned to carry out research using a microscope, microscale thermophoresis (MST), and circular dichroism techniques (CD). Additionally, it was planned to check the effects of glucose and cholesterol concentrations on the inhibitor release from the HSA.

Results and Discussion

All analyzed peptides were synthesized on the chloro-2'-chlorotrityl resin according to Fmoc/tBu methodology. The application of DMT/NMM/TosO⁻ as a coupling agent allowed us to obtain final products with the required efficiency and purity, even in the case of hot-spots fragments showing a

strong tendency to aggregation, as described in the literature [8]. In the next step, all fragments were labeled by using 4-(1-pyrenyl)butyric acid as a fluorescent probe. The optimized reaction conditions let us synthesize peptide-probe conjugates with preserved spectroscopic properties of pyrenyl moiety (Figure 2). Observing the changes in the absorbance and fluorescence spectra of the conjugates, it was possible to assume that they would be able to interact with HSA.
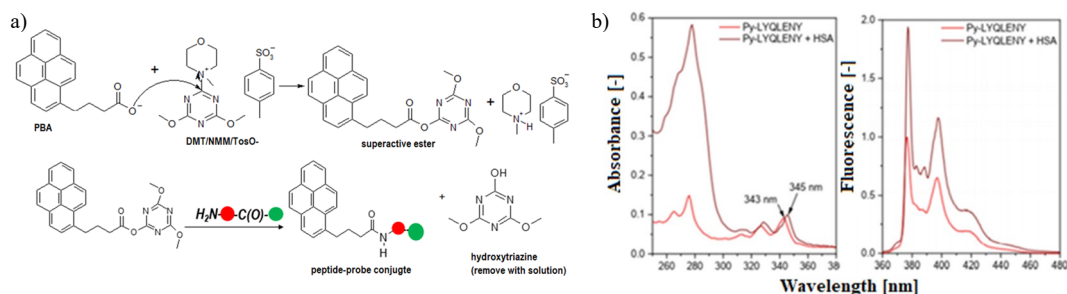
Fig. 2. a) Synthesis of fluorescent labelled conjugates, red spot - peptide chain, green spot - solid phase; b) absorption and fluorescence spectra recorded for labelled amyloidogenic core of insulin in the presence and without addition of HSA.

It has been found that the fluorescent-labeled conjugates derived from insulin and amylin hot spots have shown a tendency to aggregate in the absence of HSA. The addition of HSA resulted in an increase in absorbance, the intensity of the emission of the fluorescence probe, and the visualization of the entire oscillatory structure of the fluorescence spectrum (Figure 2b). These observations indicated changes in the microenvironment within the probe, probably caused by the docking of the conjugate within the HSA region. Only for a labelled amyloidogenic fragment of amylin (Py-FGAIL) on the recorded spectra, was not observed above changes that could point to the lack of persistent interactions of this fragment with HSA or on different places of its docking within plasma protein (Table 1).

Due to the possible influence of pyrenyl moiety on interactions peptides with HSA we also performed studies for unlabelled hot spots fragments of insulin and amylin. Congo red (CR) and thioflavin T (ThT) were used as dyes to study the amyloid structures. The inhibitory effect HSA on the aggregation process for unlabelled amyloidogenic cores of metabolic hormones was observed (Table 2). However, the exception was again amylin fragment (FGAIL) for which on the recorded both absorption spectra for CR as well as fluorescent spectra for ThT we noticed changes characteristic for amyloids formation even in the presence of HSA (the bathochromic shift and CR absorbance decrease as well as the irregular changes fluorescence intensity of ThT). The obtained results were also confirmed in circular dichroism and microscopic studies. The lack of increase in α-helix content on recorded CD spectra for FGAIL fragment after incubation with plasma protein indicated the preservation of the structure typical for amyloid fibers (mainly β-sheet conformation). Moreover, on the microscopic photo, the highest content of amyloid-like fibers in the presence of HSA was observed for amylin fragment. In the case of two tested insulin fragments, noticeable inhibition of their aggregations in the presence of HSA was observed, indicating promising potential of plasma protein in metabolic disorders treatment. If the HSA could limit amyloid formation, it could also act as an effective DDS for *N*-methylated peptidic inhibitors of insulin and amylin aggregation. To test the influence of glucose and cholesterol on the behaviour of the HSA-inhibitor complex, three different glucose solutions and one cholesterol solution were prepared. These were designed to mimic the natural ratios of HSA to the above-mentioned biomolecules in the case of hypoglycemia (1) (<7 mg/ml), normal (2) (7-9.9 mg/ml), and hyperglycemia (3) glucose (10-12.6 mg/ml) as well as a normal (<20 mg/ml) cholesterol level (4). Since the concentration of HSA in human blood ranges from 34 to 50 mg/ml, 40 mg/ml was chosen as the reference value. In the case of diabetes treatment concentration of glucose could have a crucial influence on the possible release of *N*-methylated peptidic inhibitor from HSA, which finally decides about the desired activity of a drug. On the other hand, lipids concentration in the diabetic's bloodstream could also modify HSA structure, as a result

of the protein lipidation process [9]. For examination of the release process of the *N*-methylated fragments of insulin (L'YQLENY, LYQ'LENY, L'YQ'LENY), 2 ml of a given HSA-inhibitor solution were mixed with 2 ml of each glucose/cholesterol solution respectively. All samples were incubated at 37°C for 7 days. The recorded CD spectra for analyzed samples were presented in Figure 3.

Table 1. Spectroscopic changes observed for analyzed conjugates in the presence of HSA.

Analyzed fragment	Fluorescent conjugates	Absorption spectrum	Fluorescence spectrum	
		Bathochromic shift	Increase the fluorescence intensity	Oscillatory structure visualization
Insulin hot-spots	Py-LYQLENY	+	+	+
	Py-VEALY	+	+	+
Amylin hot-spot	Py-FGAIL	-	-	-
N-methylated fragments of insulin	Py-L'YQLENY	+	+	+
	Py-LYQ'LENY	+	+	+
	Py-L'YQ'LENY	+	+	+
	Py-VE'ALYL	+	+	+
	Py-VEAL'YL	+	+	+
	Py-VE'AL'YL	+	+	+

'Y, 'L, 'A – N-methylated amino acids

Table 2. Spectroscopic studies for unlabelled amyloidogenic cores in the presence of HSA.

Studied hot-spot	Decrease in CR absorption	Irregular changes on ThT fluorescence spectra	Increase in α-helix structure on CD spectra	Presence of amyloid fibres on microscopic photos
LYQLENY	-	+/-	+/-	+/-
VEALYL	-	+/-	+/-	+/-
FGAIL	+	+	-	+/-

The spectrum obtained for HSA buffer solution confirms the dominant contribution of α-helix structure in protein conformation, two characteristic minima were observed around 209 and 222 nm as well as a maximum at 195 nm. Based on the rest curves shown in Figure 3a it could be assumed that glycosylation and lipidation of HSA lead to a loss of heart-shape structure of HSA and a reduction in α-helix content. The most similar changes were also recorded for HSA-L'YQLENY sample incubated with glucose solution as well as with cholesterol solution, respectively. It was found that for this *N*-methylated fragment in analyzed conditions its release from HSA structure was the most effective. In the case of two other inhibitors, namely LYQ'LENY and L'YQ'LENY, their interactions with HSA seemed to be stronger, the recorded bands showed totally different spectral shapes in comparison to the first inhibitor. The results obtained from CD measurements were additionally compared with microscale thermophoresis studies

Table 3. The K_d values of inhibitor-HSA complex.

The studied sample	K_d
L'YQLENY + HSA	19.2 nM
LYQ'LENY + HSA	15.6 nM
L'YQ'LENY + HSA	8.07 nM

performed in buffer solution for *N*-methylated inhibitor-HAS complexes. The MST technique allowed us to calculate dissociation constant (K_d) for possible interactions between inhibitors and HSA. It has been found that L'YQLENY-HSA complex showed the highest K_d value which indicated the most effective ligand release from the serum protein structure (Table 3). For the rest inhibitor-HSA complexes, estimated K_d values were lower but still on the same order of magnitude. It could be assumed that also for these inhibitors possible interactions with HSA showed reversible character. This is a very important factor that should be monitored in all paths of developing innovative drug delivery systems allowing for more effective and controlled transport of drugs to the affected sites.
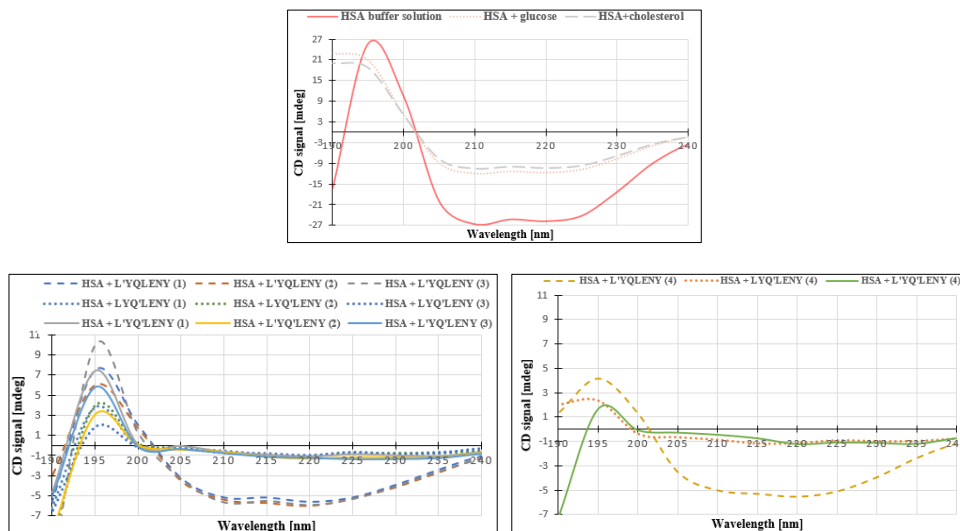
Fig. 3. The CD spectra recorded for: a) HSA in different environments; b) HSA-inhibitor complex: (1) hypoglycemia, (2) normal concentration of glucose, (3) hyperglycemia; c) HSA-inhibitor complex in presence of cholesterol.

Conclusions

The results presented in this paper have shown that all peptide-pyrenyl conjugates with their unlabelled analogues could interact with HSA. The inhibition of the aggregation process for peptides forming amyloid structures suggests that HSA may be an internal stabilizing factor of insulin and its fragments, and therefore could offer a natural, internal inhibitor of the process of their aggregation. Thus, HSA shows the potential to be used as an effective inhibitor for undesirable aggregation of amyloidogenic cores of peptides in the bloodstream, especially from the point of view of diabetes treatment. Moreover, the performed studies provide the first evidence that HSA could be also applied as a drug delivery system for *N*-methylated analogues of hot spots of insulin, to inhibit/limit the aggregation of this hormone within the tissue. The studies on the preparation of HSA complexes with peptide inhibitors of insulin aggregation and the use of HSA as a transporter are ongoing.

References

1. Joseph, K.S., et al. *J. Chromatogr.* A **1216**, 3492-3500 (2009), https://doi.org/10.1016/j.chroma.2008.09.080
2. Fasano, M., et al. *IUBMB Life* **57**(12), 787-796 (2005), https://doi.org/10.1080/15216540500404093
3. Gancar, M., et al. *Sci. Rep.* **10**, 1-10 (2020), https://doi.org/10.1038/s41598-020-66033-6
4. Sirangelo, I., et al. *Int. J. Mol. Sci.* **21**, 2-16 (2020), https://doi.org/10.3390/ijms21134636
5. Malisauskas, R., et al. *Plos One* **10**(3), 1-14 (2015), https://doi.org/10.1371/journal.pone.0121231
6. Swiontek, M., et al. *Molecules* **24**, 3706, 1-20 (2019), https://doi.org/10.3390/molecules24203706
7. Kolesinska, B., et al. *Eur. J. Org. Chem.* 401-408 (2015), https://doi.org/10.1002/ejoc.201402862
8. Swiontek, M., et al. *Molecules* **24**, 1600, 1-20 (2019), https://doi.org/10.3390/molecules24081600
9. Jiang H., et al. *Chem Rev.* **118**(3), 1-2 (2018), https://doi.org/10.1021/acs.chemrev.6b00750

Investigation of the Effect of Aromatic Molecules on the Cell Penetration of Arginine-Rich CPPs

Dóra Barbara Soltész[1], Ildikó Szabó[2], and Zoltán Bánóczi[1]

[1]Department of Organic Chemistry, Eötvös L. University, Budapest, 1117, Hungary;
[2]MTA-ELTE Research Group of Peptide Chemistry, Hungarian Academy of Sciences,
Pázmány P.S. 1/A, Budapest, 1117, Hungary

Introduction

Arginine-rich cell-penetrating peptides (CPPs) are able to transport different cargos into cells, and they are promising subjects of chemical modifications to enhance their cellular uptake efficiency [1]. It was shown by our research group that coupling 4-((4-(dimethylamino)phenyl)azo)benzoyl group (Dabcyl) to tetra- or hexaarginine increases the cell penetration compared to the acetylated peptides [2]. As the Dabcyl group has two aromatic rings, our research group is focused on finding other aromatic molecules with the same penetration enhancing effect as Dabcyl. We investigate the effect of Dabcyl and other aromatic molecules, furthermore aromatic non-natural amino acids on the cellular uptake efficiency of oligoarginine and penetratin derivatives.

Results and Discussion

Our aim is to study the effect of aromatic residues on the intracellular delivery efficiency of arginine-rich CPPs. Therefore, we planned the synthesis of oligoarginines with different number of arginines in their sequence and also penetratin derivatives. The peptides were synthesized with SPPS using Fmoc/^{t}Bu strategy on Rink Amide MBHA resin, and we modified the peptides with various aromatic groups: Dabcyl, 4-(aminomethyl)benzoic acid (AMBA) (Figure 1) and (*E*)-3-(4-hydroxyphenyl)-2-phenylacrylic acid (cis-stilbene derivative), 3-(2-naphthyl)-L-alanine and L-1,2,3,4-tetrahydroisoquinoline-3-carboxylic acid. The fluorescent dye 5(6)-carboxyfluorescein was coupled either to the side chain of an inserted *C*- terminal Lys in solution, or to the *N*-terminal α-amino group of the peptide on solid phase. The fluorescence intensity of EBC-1 cells treated with the conjugates for 90 minutes at room temperature was measured by flow cytometry.

Fig. 1. The structure of Dabcyl acid and AMBA.

In case of the prepared oligoarginine derivatives (from four arginines to eight arginines in their sequence) the Dabcyl group was an effective penetration enhancer, the AMBA modification caused no change in the cellular uptake, and usually the Dabcyl-AMBA tandem group was better than Dabcyl alone (Figure 2). The position of the Dabcyl and 5(6)-carboxyfluorescein was important only in case of one conjugate, the hexaarginine derivative Dabcyl-Arg$_6$-Lys(Cf), where the Cf-Arg$_6$-Lys(Dabcyl) seemed to be a poorer CPP than octaarginine. The results from the concentration-dependent uptake of selected oligoarginine derivatives clearly showed that Dabcyl-AMBA-Arg$_8$-Lys(Cf) is a prominent CPP even at 1.25 µM concentration. Also, Dabcyl-Arg$_6$-Lys(Cf) and Dabcyl-AMBA-Arg$_5$-Lys(Cf) have as similar uptake efficiencies as octaarginine. Regarding the uptake mechanisms, the Dabcyl-AMBA-Arg$_8$-Lys(Cf) peptide enters cells by macropinocytosis, while the Dabcyl-Arg$_6$-Lys(Cf) and Dabcyl-AMBA-Arg$_5$-Lys(Cf) peptides are uptaken mostly by lipid-raft/caveolae-dependent endocytosis, but pinocytosis is also a route for them.

The peptides modified with (*E*)-3-(4-hydroxyphenyl)-2-phenylacrylic acid (St), St.-Arg$_4$-Lys(Cf) and St.-Arg$_2$-Trp-Arg$_2$-Lys(Cf) showed poor cellular uptake, we think it might be the cause of the *E*- conformation (results not shown).

Based on the results of Letoha et al. [3] who showed that dodeca-penetratin can be equally effective as penetratin, we synthesized penetratin and dodeca-penetratin derivatives, and changed the two tryphtophans and the phenylalanine in the sequence either to 3-(2-naphthyl)-L-alanine (Nal) or to 1,2,3,4-tetrahydroisoquinoline-3-carboxylic acid (TIC) (Table 1 and Figure 3). Later Cf-Pen12 was further modified with Dabcyl and/or Nal (Table 1). The result (Figure 4) showed that the Nal modification has a significant enhancing effect on the cellular uptake, and in this case the shortened peptide can be used on EBC-1 cells. The cell penetration efficiencies of the TIC modified peptides are

greatly reduced compared to that of the the unmodified peptides. Probably the TIC caused structural disturbance is the casue of this negative effect. From the results of the uptake of the Dabcyl and/or Nal modified peptides we can conclude that Dabcyl can also enhance the internalisation of penetratin, but it is better to use it alone than in combination with Nal modifications.
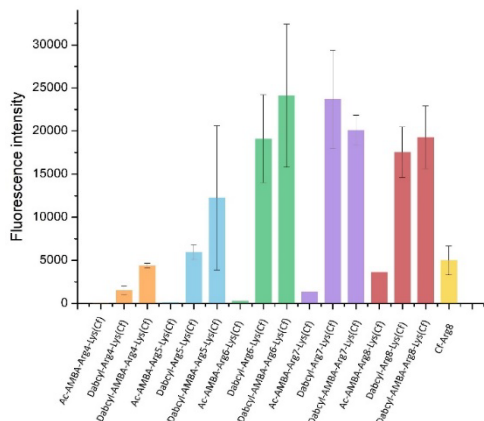
Fig. 2. Internalisation of conjugates into EBC-1 cells at 5 µM concentration at RT.

Table 1. Sequence of synthesized penetratin derivatives.

Abbreviation	Sequence
Cf-Pen	Cf-RQIKIWFQNRRKWKK-NH$_2$
Cf-Pen(Tic)	Cf-RQIKI*TICTIC* QNRRK*TIC* KK-NH$_2$
Cf-Pen(Nal)	Cf-RQIKI*NalNal* QNRRK*Nal* KK-NH$_2$
Cf-Pen12	Cf-RQIKIWFRKWKK-NH$_2$
Cf-Pen12(Tic)	Cf-RQIKI*TICTIC* RK*TIC* KK-NH$_2$
Cf-Pen12(Nal)	Cf-RQIKI*NalNal* RK*Nal* KK-NH$_2$
Ac-Pen12(Cf)	Ac-RQIKIWFRKWKK(Cf)-NH$_2$
Ac-Pen12(Nal)(Cf)	Ac-RQIKI*NalNal* RK*Nal* KK(Cf)-NH$_2$
Dabcyl-Pen12(Cf)	Dabcyl-RQIKIWFRKWKK(Cf)-NH$_2$
Dabcyl-Pen12(Nal)(Cf)	Dabcyl-RQIKI*NalNal* RK*Nal* KK(Cf)-NH$_2$

Fig. 3. The structure of TIC and Nal.

TIC= 1,2,3,4-tetrahydroisoquinoline-3-carboxylic acid

Nal= 3-(2-naphthyl)-L-alanine

Fig. 4. Internalisation of penetratin derivatives and internal standard Cf-Arg$_8$ into EBC-1 cells at 5 µM concentration at RT.

Acknowledgments

References

1. Szabó, I., et al. *Pharmaceutics* **14**, 907-945 (2022), https://doi.org/10.3390/pharmaceutics14050907
2. Szabó, I., et al. *Amino Acids* **53**, 1033-1049 (2021), https://doi.org/10.1007/s00726-021-03003-w
3. Letoha, T., et al. *Journal of Peptide Science* **11**, 805-811 (2005), https://doi.org/10.1002/psc.678

Activatable Antibody Mimetics for the Selective Delivery of Therapeutics

Roberta Lucchi, Sandra Prat, Maria Celia Lucana, Cristina Díaz-Perlas, and Benjamí Oller-Salvia

Institiut Químic de Sarrià - Universitat Ramon Llull, Barcelona, 08017, Spain

Introduction

Antibodies have become an essential tool not only in basic investigation but particularly in diagnosis and therapy. Nowadays, they are established as therapeutics for several indications, including cancer. Antibody therapeutics are directed against targets overexpressed in diseased cells. However, these targets are rarely expressed only in the diseased tissue and many adverse effects arise from their interaction with the intended target in the healthy tissue [1]. These on-target off-site effects significantly reduce the therapeutic window of many antibody therapeutics. To overcome this issue, conditionally-activated antibodies have been developed. Such antibodies are able to engage their target only upon activation mediated by a specific stimulus [2]. Stimuli-responsive antibodies show an increased therapeutic window compared to their non-activatable counterpart and allow targeting of receptors previously considered undruggable. A wide variety of cues can be harnessed to activate antibodies, including internal stimuli, such as enzymes, pH and ion concentration, as well as external ones, such as light. In the context of cancer therapy, the use of protease- or pH-responsive antibodies seems promising, since they rely on the peculiar characteristics of most tumor microenvironments. Among the many inactivation strategies that have been developed, those that rely on steric hindrance are of particular interest. Despite usually showing smaller differences in binding between active and inactive conformation compared to Probodies, which rely on *N*-terminal epitope mimetic extension, methods relying on steric hindrance can be more easily transferred across different antibody specificities and formats.
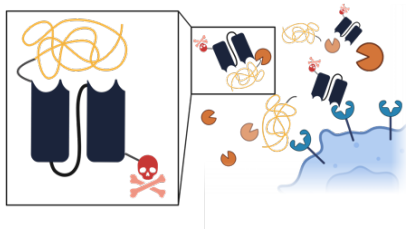
Fig. 1. Schematic representation of the objective of this work.

In our group we are developing new methods to reversibly mask antibodies with high transferability across antibody formats and specificities. Masking moieties used to provide sufficient hindrance with current approaches need to be very large, like in the case of XTENylated antibodies, where *N*-terminal elongations of 600-900 residues are required [3]. This increases considerably the size of the therapeutic, further limiting its diffusion into the tumor tissue. Here we report a new method that enables masking of a single chain variable fragment (scFv) using a protease-cleavable sterically hindering masking moiety of reduced size (Figure 1).

Results and Discussion

scFvs are antibody fragments whose tertiary structure is stabilized by two disulphide bridges. Therefore, their expression in soluble form in bacteria can prove quite challenging, due to the reducing environment in the bacterial cytoplasm. Our scFv was expressed in *E. coli* BL21(DE3) cells in an insoluble form, purified from the inclusion bodies by affinity chromatography, and finally refolded into its active structure by dialysis. The refolded scFv showed the expected mass both on SDS-PAGE analysis and MALDI mass spectrometry. After refolding, the scFv was able to bind specifically to HeLa cells transfected with its antigen, with an apparent K_d in the subnanomolar range (Figure 2).

Once we confirmed that the refolded scFv was active, we mutated residues that were either in more conserved loops around the CDRs or in the CDR themselves into cysteines. These cysteine residues were used as anchor points to site-specifically conjugate peptides and polymers of different sizes via thia-Michael addition. We are currently implementing other strategies we have previously developed based on bioorthogonal chemistry [4,5].

In most of the strategies relying on steric hindrance, such as XTENylation, the masking moiety is expressed with the antibody as an *N*-terminal-extension. Despite the fact that the *N*-terminus is relatively close to the CDRs in the tertiary structure, it is also usually more flexible. This could explain why such big masks are needed to achieve sufficient inactivation. We reasoned that conjugating the masking moiety to more strategically located residues would enable reducing the size of the mask. Successful conjugation was confirmed by Western Blot and LC-MS. The scFv-mask conjugates were assayed in cell binding experiments. We observed apparent K_ds up to 40-fold lower compared to the WT antibody, depending on the site modified and the conjugated mask. Such masks may be removed by tumor-specific proteases.

In parallel, we developed a strategy to generate scFv-drug conjguates by conjugating toxic payloads to this scFv. In particular, we aimed to conjugate the drug at the *C*-terminus of the scFv after introducing a bioorthogonal chemical handle via enzymatic ligation mediated by Sortase A. The transpeptidase was produced in *E. coli* BL21(DE3) cells and purified by affinity chromatography. The ligation reaction was optimized and product formation was observed both with SDS-PAGE (Figure 3) and LC-MS. Conjugates were produced by reacting the bicyclo[6.1.0]non-4-yne (BCN) handle installed on the scFv with tetrazine-functionalized payloads, including toxic molecules and protease-resistant peptides that enable transport across biological barriers [6].

We have shown that our antibody mimetic has high selectivity for target cells. We expect this will translate into reduced on-target off-site effects and, thus, higher selectivity compared to common ADCs in the *in vivo* experiments we will conduct.
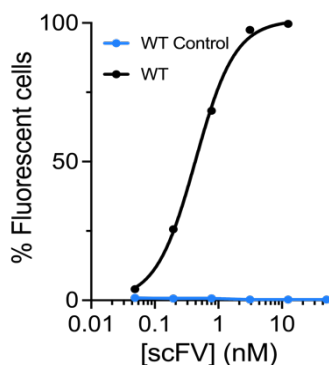
Fig. 2. Binding of refolded scFv on HeLa cells transfected with its target receptor.
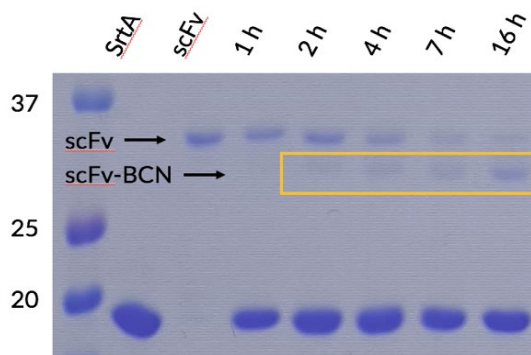
Fig. 3. SDS-PAGE analysis of Sortase A reaction over time.

Acknowledgments

References

1. Hansel, et al. *Nat. Rev. Drug Discov.* **9**(4), 325-338 (2010), https://doi.org/10.1038/nrd3003
2. Lucchi, et al. *ACS Cent. Sci.* **7**(5), 724-738 (2021), https://doi.org/10.1021/acscentsci.0c01448
3. Cattaruzza, et al. [abstract] In: *Proceedings of the Annual Meeting of the American Association for Cancer Research 2020*; *Cancer Res* **80**(16 Suppl) Abstract nr 3376 (2020), https://doi.org/10.1158/1538-7445.AM2020-3376
4. Oller-Salvia, et al. *ACIE.* **57**(11), 2831-2834 (2018), https://doi.org/10.1002/anie.201712370
5. Oller-Salvia *J. Vis. Exp.* **139**, e58066 (2018), https://doi.org/10.3791/58066
6. Lucana, et al. *Pharmaceutics* **13**(12), 2065 (2021), https://doi.org/10.3390/pharmaceutics13122065

Stability of Cryo-Concentrated Complexes

Heleri H. Härk, Ly Porosk, Piret Arukuusk, and Kaido Kurrikoff

Drug Delivery Group, Institute of Technology, University of Tartu, Tartu, 50411, Estonia

Introduction

Nucleic acid-based molecules (NA) have a great potential as therapeutics. However, their clinical use is limited due to their lack of natural mechanisms enabling them to pass biological barriers like cell membranes, blood-brain barrier, endothelium *etc*. This is mainly because of the high molecular weight and negative charge of NA. What is more, these NA-s are generally rapidly degraded by extracellular and intracellular enzymes [1]. Therefore, there is a great need for efficient and non-toxic delivery vectors which are able to cross these barriers and carry macromolecule-based therapeutics with them to the intracellular targets.

Cell-penetrating peptides (CPP) are relatively short (ranging from approximately 5 to 30 residues) amino acid sequences which are able to permeate cell membranes and deliver covalently or non-covalently bound cargo, such as NA (Figure 1) [2]. Although covalent bonding strategy allows number of cargo molecules per CPP to be controlled resulting in a defined structure, non-covalent formulations have their advantages, especially in case of NA, due to simpler preparation and versatility. In case of plasmids (pDNA), which are circular NA molecules, the non-covalent attachment is more preferred as it does not involve complicated modifications of the plasmid. However, as non-covalent bonding strategy is mainly based on electrostatic interactions, the formulated nanoparticles may have heterogeneous size-distribution and low stability [3,4]. Therefore, they are rapidly cleared from the general blood circulation and achieve high tissue accumulation levels only in

Fig. 1. Spontaneous non-covalent formulation of nanoparticles based on electrostatic interactions between positively charged CPP and negatively charged cargo.

case of certain organs when assessed in mammalian organism. Since physical parameters such as size and size distribution influence biodistribution and toxicity of nanoparticles [5], it is important to prepare stable, homogeneous and well-defined nanoparticles for *in vivo* application.

Results and Discussion

Recently, a new formulation approach for CPPs called cryo-concentration was introduced by our research group [6]. Cryo-concentration is based on nanoparticle formulation in diluted solution following their reconstitution in a concentrated, *in vivo* compatible solution after freeze-drying. In more detail, the process involves formulation of CPP-cargo complexes in a 10x diluted concentration compared to the final injection concentration. After reconstitution in water, the obtained cryo-concentrated complexes (CCC) are ready for use in *in vivo* application (Figure 2).

Cryo-concentration enables preparing stable and homogeneous nanoparticles between CPP NF55 and pDNA which do not aggregate after reconstitution, have excellent stability against enzymatic degradation and show significantly higher bioactivity *in vivo* [6]. Additionally, these ready-made
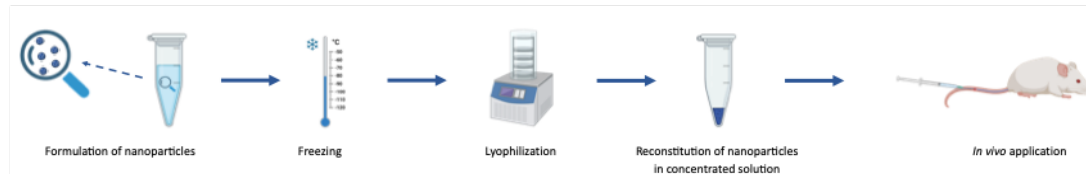

Fig. 2. Process of preparing cryo-concentrating complexes (CCC) from formulation to in vivo application.

CCC-s are convenient to use as they can be used immediately after taking up into solution without further mixing, further incubation processes, nor do they require any additional reagents aside from Milli-Q® grade water.

However, the shelf-life of these nanoparticles is currently unknown. Therefore, the stability of these nanoparticles was tested by storing them at 3 different conditions for 31 weeks: -20 ℃, +4 ℃ and room temperature (RT). Freshly prepared CCC was used as a control throughout the experiments. It was observed that while CCC stored at room temperature began to show decrease of transfection efficacy after 4 weeks, efficacy of CCC stored at -20 ℃ and +4 ℃ remained at the same level with freshly prepared CCC throughout the whole tested time period (Figure 3). Therefore, the CCC approach allows the preservation and use of CPP-NA complexes over extended time period compared to previously used freshly prepared CPP-NA complexes.

As a conclusion, cryo-concentration is a simple and versatile tool to achieve stable and homogeneous nanoparticles with higher bioactivity *in vivo*. They can be conveniently used as there is no need for additional procedures after reconstitution of the nanoparticles. What is more, as the efficacy of CCC stored at +4 ℃ or below remained at the same level with freshly prepared complexes throughout the 31 week-period, the shelf-life of CCC is at least 6 months.
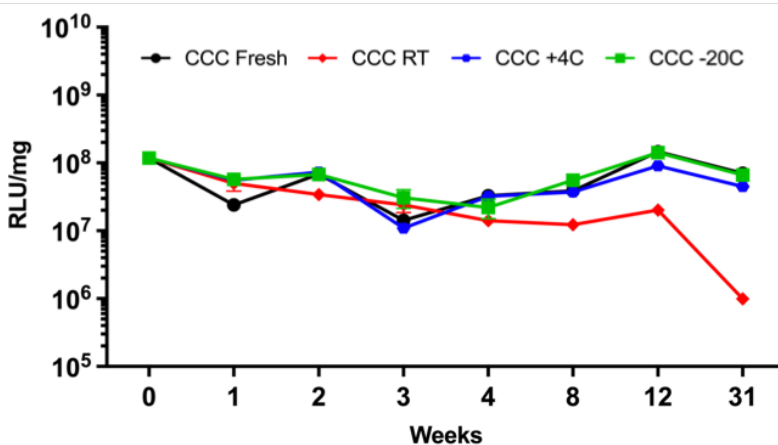
Fig. 3. Stability of cryo-concentrated complexes (CCC) stored at different conditions. Experimental conditions: CHO K1 cells, 10K cells per well, 96 wp, full media, pFluc dose 0.1 g per well. Complexes were formulated between NF55 and pDNA at charge-ratio 3. Luminescence was measured 24 h post-transfection and normalized to protein content.

Acknowledgments

References

1. Margus, H., et al. *Molecular Pharmaceutics* **13**, 172-179 (2016), http://doi.org/10.1021/acs.molpharmaceut.5b00598
2. Langel, Ü. *CPP, Cell-Penetrating Peptides*, Springer Nature Pte Ltd., Singapore, 2019, p.1, http://doi.org/10.1007/978-981-13-8747-0
3. Andaloussi, S.E.L., et al. *Nucleic Acids Research* **39**, 3972-3987 (2011), http://doi.org/10.1093/nar/gkq1299
4. Veiman, K.-L., et al. *Journal of Controlled Release* **209**, 238-247 (2015), http://doi.org/10.1016/j.jconrel.2015.04.038
5. Blanco, E., et al. *Nature Biotechnology* **33**, 941-951 (2015), http://doi.org/10.1038/nbt.3330
6. Freimann, K., et al. *Molecular Therapy - Nucleic Acids* **10**, 28-35 (2018), http://doi.org/10.1016/j.omtn.2017.10.011

Modular Approach to Enhance the Bioactivity of Peptides

Shulamit Fluss Ben-Uliel[1], Faten Habrat Zoabi[1], Moriya Slavin[2], Hadas Sibony-Benyamini[1], Nir Kalisman[2], and Nir Qvit[1]

[1]The Azrieli Faculty of Medicine in the Galilee, Bar-Ilan University, Safed 1311502, Israel; [2]Institute of Life Sciences, The Hebrew University of Jerusalem, Jerusalem 9190401, Israel

Introduction

Bioactive peptides (BPs) are peptides with hormonal or pharmacological properties. The source of BPs can be from natural peptides of endogenic origin, or it can be synthesized in the lab based on rational design or screening. Herein we demonstrate how a BP of interest can be modified to a highly effective research tool as well as therapeutic lead with minimal modifications that can be done in many labs or ordered for a reasonable price [1,2]. Phosphatase and tensin homolog induced kinase 1 (Pink1) is serine/threonine kinase. Pink1 is related to mitochondrial dynamics, and it was demonstrated to regulate mitochondrial homeostasis [3]. We developed a linear peptide that targets Pink1. Based on this peptide we engineered peptide-based targeted peptidomimetics (modified peptides), biomolecular probes, with various properties.

Results and Discussion

As a proof of concept, a linear peptide (aka cargo) was developed to target Pink1 by rational design method (Figure 1). A library of peptides was synthesized to address three goals: to give the peptide 'drug-like' properties, to add an element that will allow a crosslinking experiment to determine the identity of the docking domain in the target protein, lastly to conjugate florescence dye to the peptide that will be used in molecular imaging in H9c2 cells and evaluate the interaction between the peptide and protein of interest. For better solubility and cell penetrating trait a TAT sequence was added to all synthesized peptides (Figure 2).
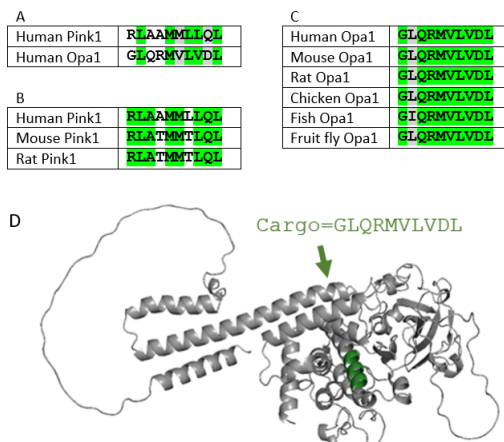
Fig. 1. Rational design of a peptide that target Pink1. Sequence alignment identifies a short sequence of homology between Opa1 and Pink1 (A), which is conserved in evolution (B,C). The Opa1 sequence (light green) is exposed in the C-lobe region of Pink1 (Alphafold predicted model of human Pink1: Q9BXM7) (D). PyMol (Schrodinger LLC) was used to generate the figure.

Peptide Name	Sequence
CVP-198	CH₃-CO-GLQRMVLVDL-K-GG-YGRKKRRQRRR-NH₂
CVP-199	CO-(CH₂)₂-CO-NH / GLQRMVLVDL-K-GG-YGRKKRRQRRR-NH₂
CVP-200	CO-(CH₂)₃-CO-NH / GLQRMVLVDL-K-GG-YGRKKRRQRRR-NH₂
CVP-201	CO-(CH₂)₃-CO₂H / GLQRMVLVDL-K-GG-YGRKKRRQRRR-NH₂
CVP-202	CO-(CH₂)₂-CO₂H / GLQRMVLVDL-K-GG-YGRKKRRQRRR-NH₂
CVP-205	CH₃-CO-C-GLQRMVLVDL-K-GG-YGRKKRRQRRR-NH₂
CVP-206	BDP / CH₃-CO-C-GLQRMVLVDL-K-GG-YGRKKRRQRRR-NH₂

Fig. 2. Schematic structure of the developed library. The cargo in green, addition to the cargo for enabling cyclization/crosslinking/dye conjugation in red, TAT and a linker in blue, cyclazation/precyclyzation/dye in black . BDP= Borondipyrromethene.

Table 1. Summary of the corresponding in vitro K_D values of the peptides binding to Pink1.

Peptide Name	K_D (µM)	Notes
CVP-198	130.47 ± 0.01	Linear peptide
CVP-199	58.31 ± 0.02	Cyclic peptide
CVP-200	138.72 ± 0.30	Cyclic peptide
CVP-201	125.89 ± 0.02	Precyclic peptide
CVP-202	143.09 ± 0.04	Precyclic peptide

Five peptides, CVP-198 - CVP-202, were tested by field effect biosensing to determine their binding to Pink1. CVP-199 a cyclic peptide showed the best K_D values. Cyclization may allow better binding of a peptide to the target protein (Table 1).

CVP-198 and CVP-199 were tested in a comparative experiment to find whether the cyclization gives protection against proteolytic conditions. By HPLC analysis it was showed that CVP-199 the cyclic peptide was more resistant to proteolytic conditions in the presence of trypsin compared to CVP-198 the linear peptide (Figure 3).

CVP-198 was tested in a crosslinking experiment with two kinds of crosslinking agents bis(sulfosuccinimidyl)suberate (BS3) and 4-(4,6-dimethoxy-1,3,5-triazin-2-yl)-4-methyl-morpholinium chloride (DMTMM). The target protein was Pink1. The analyses were done by LC/MS. Eight sequences of a crosslink between the Pink1 sequence and the lysine next to the cargo in peptide CVP-198 using a BS3 crosslinker were found. Using DMTMM crosslinker, two peptide pairs reporting a crosslink between the protein and the peptide were identified. An overlap was made between the computerized model of the protein folding and docking of the peptide and the results of the crosslinking found in the LC/MS analysis (Figure 4). This finding confirms the suitability of the peptide for its docking site according to the rational design and gives structural information about the protein at the binding site. CVP-205 was prepared to allow conjugation to the fluorescent dye, boron-dipyrromethene (BDP). H9c2 rat cardio myoblast cell line was treated with CVP-206 (CVP-205 with fluorescent dye, boron-dipyrromethene (BDP)) in two conditions - without stress and with oxidative stress by hydrogen peroxide (H_2O_2) that induced cellular apoptosis. The cells were analyzed by confocal microscope. H_2O_2 treatment enhanced the localization of Pink1 to the mitochondria surface and the colocalization of Pink1 with the peptide, CVP-206, whereas this enhancement was significantly reduced in control cells (Figure 5). It can be concluded that the peptide reaches the target protein Pink1 in the cells.

This project presents a general approach using an identified peptide and developing various research tools as well as therapeutic leads, which can be customized to other laboratories easily [4].
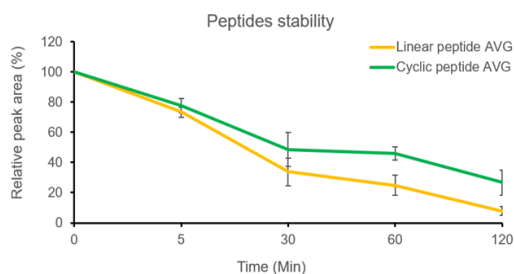
Fig. 3. Stability studies of the linear peptide, CVP-198, and the bioactive backbone cyclic peptide, CVP-199. The stability of the peptides was measured independently under tryptic degradation at 37 ℃ (by trypsin degradation of the peptide) and was determined by HPLC analysis (n=3). The starting time point (0 min, 100%) represents the peptide at the beginning of each experiment. Liner peptide (CVP-198) at 37 ℃ with trypsin (yellow), and cyclic peptide (CVP-199) at 37 ℃ with trypsin (green), were analyzed after 0 min, 5 min, 30 min, 60 min, and 120 min. Separation was performed by HPLC at 214 nm. Peptide amounts were calculated relative to the quantities determined at time point zero.

Crosslinker agent	Pink1 AA number	LC/MS resulting peptides
BS3	137	S**K**PGPDPLDTRR-2
BS3	186	GCSAAVYEATMPTLPQNLEVT**K**STGLLPGR-22
BS3	266	GP**K**QLAPHPNIIR-3
BS3	319	TLFLVM**K**NYPCTLR-7
BS3	547	LTE**K**CCVETK-4
BS3	555	CCVET**K**MK-6
DMTMM	155	LJ**E**YLIGQSIGK-3
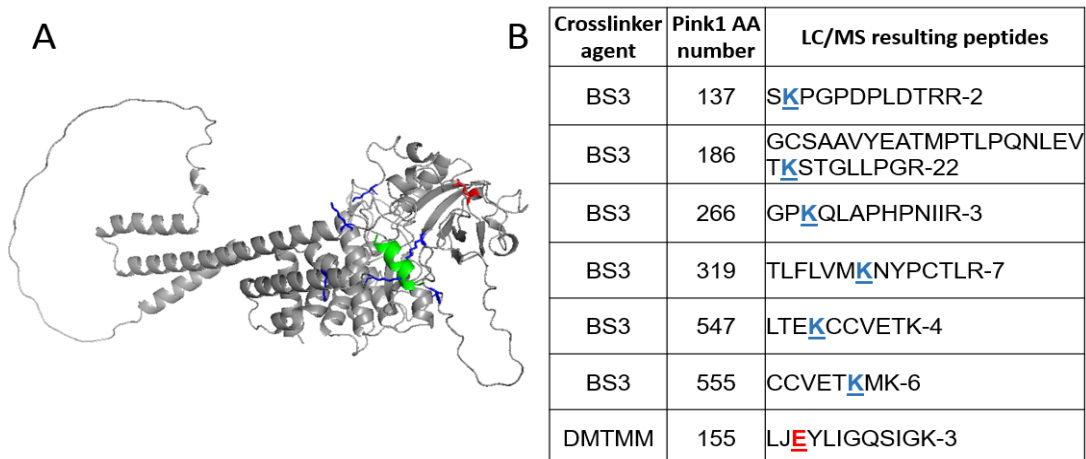
*Fig. 4. Map of the cross-link identified between the peptide CVP-198 and the Pink1 protein (AlphaFold predicted model: Q9BXM7). (**A**) Residues involved in cross-linking contacts are highlighted in blue and red stick structure on the Pink1 protein. CVP-198 peptide (shown in green cartoon structure) and hPink1 protein (shown in grey cartoon structure) (**B**) CVP-198 and Pink1 cross-linking contacts table: The positions involved Pink1 lysine residues, highlighted in the blue, and involved Pink1 glutamic acid residue, highlighted in the red. PyMoL (Schrodinger LLC) was used to generate the figure.*
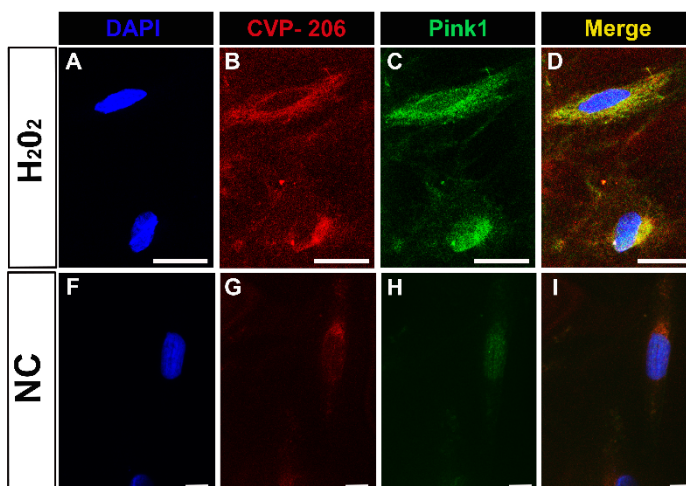
Fig. 5. Colocalization of Pink1 and CVP-206 peptide in H9c2 cells. (A-D) Immunostaining for CVP-206 (1 μM, Red) and Pink1 (Green) after H_2O_2 treatment (1.6 mM for 0.5 hour). (F-I) Immunostaining for Pink1 (Green) and CVP-206 (1 μM, Red) in H9c2 cells with no treatment, Negative control (NC). Nuclei is in blue (DAPI), scale bar indicates 20 μm for CVP-206 staining after H_2O_2, and 10 μm for Negative control (NC) (n=3). Confocal microscopy images were taken at 63x magnification for NC and H_2O_2 treated cells.

Acknowledgments

References

1. Adhikari, S., Leissa, J.A., & Karlsson, A.J. *AIChE Journal* **66**(3), e16776 (2020), https://doi.org/10.1002/aic.16776
2. Akbarian, M., Khani, A., Eghbalpour, S., & Uversky, V.N. *International Journal of Molecular Sciences* **23**(3), 1445 (2022), https://doi.org/10.3390/ijms23031445
3. Wang, N., Zhu, P., Huang, R., Wang, C., Sun, L., Lan, B., & Gao, Y. *Life Sciences* **259**, 118247 (2020), https://doi.org/10.1016/j.lfs.2020.118247
4. Ben-Uliel, S.F., Zoabi, F.H., Slavin, M., Sibony-Benyamini, H., Kalisman, N., & Qvit, N. *International Journal of Molecular Sciences* **23**(11), 6076 (2022), https://doi.org/10.3390/ijms23116076

Peptides Bearing Multiple Post-Translational Modifications as Antigenic Targets for Biomarkers towards Personalized Rheumatology

Cristina García-Moreno[1], María J. Gómara[1], Raimon Sanmartí[2], and Isabel Haro[1]

[1]Unit of Synthesis and Biomedical Applications of Peptides, IQAC-CSIC, Barcelona, 08034, Spain;
[2]Unit of Arthritis, Hospital Clínic of Barcelona, Barcelona, 08036, Spain

Introduction

Rheumatoid arthritis (RA) is an autoimmune rheumatic disease characterized by the presence of autoantibodies resulting from an immune response triggered by proteins that have undergone post-translational modifications (PTMs) [1]. Citrullination (deimination of arginine), is the best-studied PTM in rheumatology, and for a long time, anti-citrullinated protein/peptide antibodies (ACPAs) have been used for RA diagnosis and considered the most relevant serological markers. More recently, other PTMs have been described in the context of RA including homocitrullination (carbamylation) and acetylation, which take place in lysine (Figure 1). Different autoantibodies against these novel modifications (antibodies against modified proteins/peptides, AMPAs) have been linked with interstitial lung disease (ILD), an extra-articular manifestation of RA that entails a high mortality [2,3].

Results and Discussion
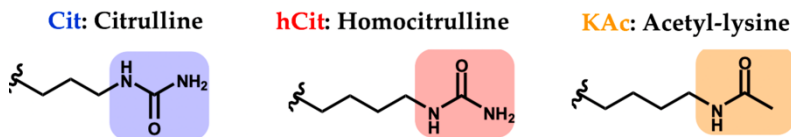
Fig. 1. Chemical structures of relevant PTMs in RA. Citrulline results of the conversion from arginine while homocitrulline and acetyl-lysine come from the conversion of lysine residues.

Previous studies in our group defined a chimeric citrullinated peptide containing α-fibrin and filaggrin domains (CFFCP1, Figure 2) that yielded better results in terms of sensitivity/specificity balance and identified RA patients with poor radiographic outcomes as an antigen compared to the gold standard commercial test [4]. Based on the primary structure of this peptide, a panel of several peptide antigens that resulted from the substitution of lysine for homocitrulline and/or acetyl-lysine were designed (Figure 2), synthesized by solid-phase and tested in a RA population (n=37 RA-ILD vs n=141 RA non-ILD) to study their role as biomarkers linked to the presence of ILD.

The analysis of fine specificities with these novel chimeric peptide antigens demonstrated that IgG was the predominant isotype in the main RA population. IgG and IgA isotypes were more frequent when the antigen was doubly modified (citrullinated/homocitrullinated) compared to anti-ACPA specificities. In addition, all anti-AMPA fine specificities were more frequent in the RA-ILD group. Regarding the IgA isotype, the peptide containing two or three PTMs was able to detect a percentage close to 20% of RA-ILD sera that were negative when analyzed with the peptide bearing a single PTM. Particularly, the mean titers of autoantibodies against the peptide antigen bearing three PTMs, citrullinated/homocitrullinated/acetylated chimeric peptide (CFFCHAP) were statistically significant for IgA and IgM isotypes, but also for IgG ($p < 0.05$) (Figure 3), a finding not observed with the ones against doubly PTM-modified antigens.

Chimeric peptide	α-fibrin(617-631)-S^{306},S^{319} cyclo [Cys^{306,319}] filaggrin(304-324)
CFFCP1	HSTKRGHAKSRPV**Cit**G-HQCHQEST**Cit**GRSRGRCGRSGS
CFFCHP1	HSTKRGHA**hCit**SRPV**Cit**G-HQCHQEST**Cit**GRSRGRCGRSGS
CFFCHP2	HST**hCit**RGHAKSRPV**Cit**G-HQCHQEST**Cit**GRSRGRCGRSGS
CFFCHP3	HST**hCit**RGHA**hCit**SRPV**Cit**G-HQCHQEST**Cit**GRSRGRCGRSGS
CFFCHAP	HST**KAc**RGHA**hCit**SRPV**Cit**G-HQCHQEST**Cit**GRSRGRCGRSGS

Fig. 2. Primary structure of synthetic cyclic fibrin-filaggrin chimeric peptides bearing citrulline, homocitrulline and acetyl-lysine at specific positions of the α-fibrin (617-631) and cyclic filaggrin (304-324) domains.

When analyzing patients according to the presence of erosive disease assessed by radiographs of hands and feet (Larsen score), a higher prevalence of autoantibodies was found in patients with more severe joint damage (Larsen $\geq$ 18) in comparison to those with mild joint destruction (Larsen < 18). The differences were statistically significant in almost all specificities, and especially for IgA and IgM isotypes. Interestingly, only the frequency of antibodies of the IgG isotype against the triple PTM peptide (anti-CFFCHAP-IgG-positive) was higher in patients with severe joint damage, with statistical significance.
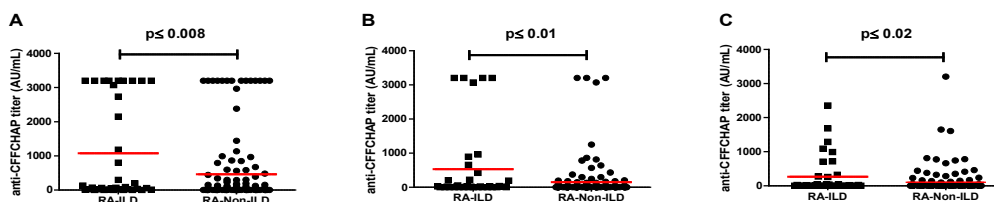
Fig. 3. Comparison of anti-CFFCHAP titers (AU/mL) for RA-ILD vs RA-non-ILD patients. A) IgG; B) IgA and C) IgM isotypes. Horizontal lines depict mean titers. Statistical significances were established as two-tailed p-values < 0.05 after analyzing the continuous variables using the Mann–Whitney U test.

For the first time, we described a novel peptide-based antigen bearing citrulline, homocitrulline and acetyl-lysine into the same peptide sequence to consistently detect severe phenotypes in CFFCHAP positive RA patients. We demonstrated an association between the presence and levels of AMPA titers and severe manifestations of RA such as joint destruction and ILD [5].

Acknowledgments

References

1. Scherer, H.U., et al. *J. Autoimmun*. **110**, 102400 (2020), http://dx.doi.org/10.1016/j.jaut.2019.102400
2. Hyldgaard, C., et al. *Ann. Rheum. Dis.* **76**, 1700-1706 (2017), http://dx.doi.org/10.1136/annrheumdis-2017-211138
3. Castellanos-Moreira, R., et al. *Ann. Rheum. Dis.* **79**, 587-594 (2020), http://dx.doi.org/10.1136/annrheumdis-2019-216709
4. Sanmarti, R., et al. *Arthritis Res. Ther.* **11**, R135 (2009), http://dx.doi.org/10.1186/ar2802
5. García-Moreno, C., et al. *Int. J. Mol. Sci.* **22**, 13290 (2021), https://doi.org/10.3390/ijms222413290

Peptide Inhibitors Based on the *C*-Terminal Tail of Connexin43

Debora Iaculli[1], Arthur Lamouroux[1], Jade Montgomery[2], Mathieu Vinken[3], Brenda R. Kwak[2], and Steven Ballet[1]

[1]Research Group of Organic Chemistry, Vrije Universiteit Brussel, Brussels, 1050, Belgium; [2]Department of Pathology and Immunology, University of Geneva, Geneva, 1211, Switzerland; [3] Department of in Vitro Toxicology and Dermato-Cosmetology, Vrije Universiteit Brussel, Brussels, 1090, Belgium

Introduction

Connexin43 (Cx43), the most abundantly expressed member of the connexin protein family in ventricular cardiomyocytes, oligomerizes into hemichannels (HCs), forming thereafter intercellular channels known as gap junctions (GJ) channels [1]. While GJs are involved in 'healthy' physiological intercellular communication, HCs activities are linked to various pathological states, and therefore hemichannel inhibition might offer a potential therapeutical tool in the treatment of heart diseases. In particular, a segment of amino acids 10 residues long at the *C*-terminal domain (CT) of Cx43 is known to be involved in both intramolecular interactions within Cx43, as well as intermolecular interactions with other proteins, resulting in effects on Cx43 HC trafficking, insertion in GJs and regulation of GJ channel and HC activity [1,2]. Mimetic peptides based on this fragment (*e.g.*, αCT1 [3], which mimics the last 9 amino acids of the CT linked to a cell-penetrating motif) have revealed to be promising therapeutic agents preserving left ventricular cardiac function after ischemia/reperfusion injury [4]. Therefore, in order to pharmacologically improve existing lead sequences, a set of conformationally and proteolytically stabilized peptide inhibitors was designed and tested for their inhibitory capacity by *in vitro* assays. The results constitute a starting point for the development of a set of peptido-mimetics targeted against Cx43 hemichannels with improved bioactivity.

Results and Discussion

A peptide mimicking the last 10 amino acids of the Cx43 CT, **CT10** (Figure 1), has been shown to interact with the L2 region (aa 119-144) of the cytoplasmic loop of the protein. This "loop-tail interaction" is critical in regulating Cx43 HC activity. [3,6,7] In the current work, a set of peptides based on the **CT10** sequence (Figure 2) was rationally designed to investigate the role of individual amino acids in the binding process, to examine the importance of the *N*- and *C*- termini of the peptide sequence and to provide proteolytically more stable analogues to be used as pharmacological tools. As such, a structure-activity relationship (SAR) study based on an Ala-scan was performed to first assess the importance of the positively and negatively charged residues in the sequence. Secondly, the proline residues were replaced in an attempt to elucidate the importance of these amino acids in the bioactivity of the peptide.

Additionally, four cyclic peptides were designed as *N*-terminal acetylated and *C*- terminal carboxamides. In one analogue, a proline residue was replaced by a (4*S*)-4-azidoproline residue, while the *C*- terminal Ile was replaced by a propargylglycine residue, in order to constrain the peptide sequence through the formation of a triazole ring via a copper-catalyzed azide-alkyne cycloaddition (CuAAC) reaction. The length of the covalent tether was also changed, to provide macrocyclized analogues bridged by (*i*, *i+5*) to (*i*, *i+3*) linkages. Finally, the tethering Pro residue was also replaced by propargylglycine (Pra) and azidolysine (Azk) residues, respectively, and the triazole ring was moved closer to the *N*-terminal side of the peptide (Figure 2).
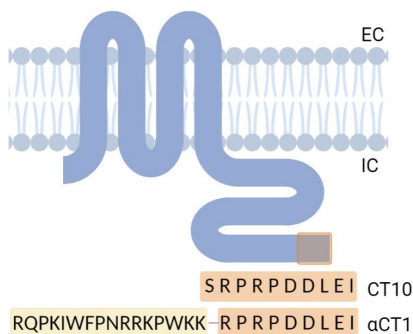

Fig. 1. Topology of a Cx43 monomer. The extra- and intracellular domains are abbreviated EC and IC, respectively. The reference sequences of CT10 and αCT1 are shown, with the mimicked region of the C-tail highlighted in orange.

Next, the peptides were tested *in vitro* for their inhibitory capacity. In the applied assay, ATP release was used as an indicator of hemichannel activity. In the presence of an adequate trigger (in this case, low extracellular Ca^{2+} levels) the channels open and release ATP, while in the presence of an inhibitor the release of ATP is decreased. A non-specific small molecule inhibitor of Cx43, carbenoxolone (Cbx) was used as a control, as well as the aforementioned **αCT1** and **CT10** peptides. None of the substitutions on the linear sequence led to a significant decrease in inhibitory activity compared to the native **CT10** sequence, while all cyclic analogues show an inhibitory capacity comparable to that of **αCT1**, but without bearing a cell-penetrating motif.

In order to evaluate the effect of the macrocyclization on the proteolytic resistance of the peptides, *in vitro* plasma stability experiments were performed. For **αCT1**, presumed plasma protein binding was observed which prevented the half-life to be experimentally determined. For **CT10**, a half-life of 75.86 (± 4.01) minutes was determined in concordance with literature [8,9], while the stapled analogues displayed high stability (half-life > 24 hours). Additionally, circular dichroism (CD) spectroscopy experiments were performed on the linear **CT10** compound and the cyclic analogues to determine whether they adopt some form of secondary structure. However, most peptides were largely unstructured (*i.e.* random coil) even in the presence of the stabilizing agent trifluoroethanol (TFE).

In conclusion, a set of novel peptidomimetic inhibitors of Cx43 HC were identified. Several analogues show a similar bioactivity *in vitro* as the most established inhibitor of Cx43 hemichannels **αCT1**, with the advantage of a shorter, chemically and proteolytically stabilized sequence. These promising results constitute a starting point for the development of potent and stable Cx43 HC inhibitors.
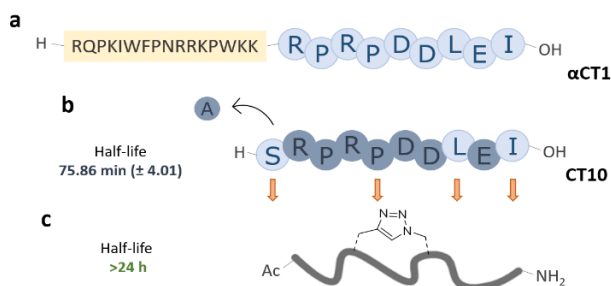
Fig. 2. a) Sequence of the **αCT1** peptide. b) Sequence of the **CT10** peptide. The residues that were replaced by Ala are indicated in grey. The residues that were replaced by (4S)-4-azidoproline, propargylglycine and/or azidolysine are indicated by arrows. c) Generic structure of the macrocyclic peptides presented in this work.

Acknowledgments

References

1. Leybaert, L., et al. *Pharmacol Rev* **69**, 396-478 (2017), https://doi.org/10.1124/pr.115.012062
2. a) Laird, D.W. and Lampe, P.D. *Nat. Rev. Drug. Discov.* **17**, 905-921 (2018), https://doi.org/10.1038/nrd.2018.138. b) Palatinus, J.A. et al. *Biochim. Biophys. Acta* **1818**, 1831-1843 (2012), https://doi.org/10.1016/j.bbamem.2011.08.006. c) Sorgen, P.L. et al. *Int. J. Mol. Sci.* **19**, 1428 (2018), https://doi.org/10.3390/ijms19051428
3. Ponsaert, R., et al. *FASEB J.* **24**, 4378-4395 (2010), https://doi.org/10.1096/fj.09-153007
4. Hunter, A.W., et al. *Molecular Biol. Cell.* **16**, 5686-5698 (2005), https://doi.org/10.1091/mbc.e05-08-0737
5. Jiang, J., et al. *J Am Heart Assoc.* **8**, e012385 (2019), https://doi.org/10.1161/JAHA.119.012385
6. Hirst-Jensen, B.J., et al. *J. Biol. Chem.* **282**, 5801-5813 (2007), https://doi.org/10.1074/jbc.M605233200
7. D'hondt, C., et al. *Biochem. Biophys. Res. Commun.* **432,** 707-712 (2013), https://doi.org/10.1016/j.bbrc.2013.01.066
8. Marsh, S. R., et al. *J. Cardiovasc. Dev. Dis.* **8**, 52 (2021), https://doi.org/10.3390/jcdd8050052
9. Boöttger, R., et al. *PLoS One* **12**, e0178943 (2017), https://doi.org/10.1371/journal.pone.0178943

In vitro Studies on Angiotensin-I Converting Enzyme (ACE I) Inhibitory Activity of Short Synthetic Peptides on Smooth Muscle Preparations (Rat Ileum)

B. Yakimova[1,2], P. Mateeva[2], P. Todorova[2], R. Zamfirova[2], P. Kardaleva[1], and I. Stoineva[1]

[1]Institute of Organic Chemistry with Centre of Phytochemistry, Bulgarian Academy of Sciences, Sofia 1113, Bulgaria; [2]Institute of Neurobiology, Bulgarian Academy of Sciences, Sofia, 1113, Bulgaria

Introduction

It is well known that in the renin-angiotensin system (RAS) ACE I has a significant role, where it acts as a dipeptidyl-carboxypeptidase and cleave the *C*-terminal dipeptide His^9-Leu^{10} from Angiotensin I (AT I) 1 to produce the vasoconstrictor peptide Angiotensin II (AT II) [1]. In order to avoid this negative effect on the living organisms with high blood pressure, it is necessary to search for new inhibitors of ACE I. To shed light on the effect of chemical structure of different inhibitors it is necessary to investigate ACE I isolated from different sources, as well as purified enzyme and segments of rat ileum.

Nowadays, an increasing number of ACE inhibitory peptides have been isolated and identified from the hydrolysates of various natural sources. Most of them are screened based on their *in vitro* ACE inhibitory activities, however the *in vivo* antihypertensive effects of most of them have not been confirmed.

The purpose of the present study was to investigate *in vitro* effects of low molecular weight synthetic peptides obtained by SPPS as novel inhibitors of Angiotensin-I converting enzyme, for better understanding of the relationship structure/activity and the intermolecular-interaction mechanism.

Results and Discussion

The synthesis of each of the target peptides: H-Val-Ala-Trp-OH, H-Val-Ala-Pro-OH, H-Leu-Ala-Pro-OH, H-Leu-Lys-Pro-OH, H-Ile-Ala-Lys-OH, was realized by Fmoc strategy of SPPS. The TBTU/DIPEA method was used for coupling of each amino acid. For the synthesis of the peptides with free *C*-terminal group 2 chlortrityl chloride resin (ClTR) and Wang resin were used by us successfully. In the Figure 1 is shown the reaction scheme of the synthesis of H-Leu-Ala-Pro-OH.
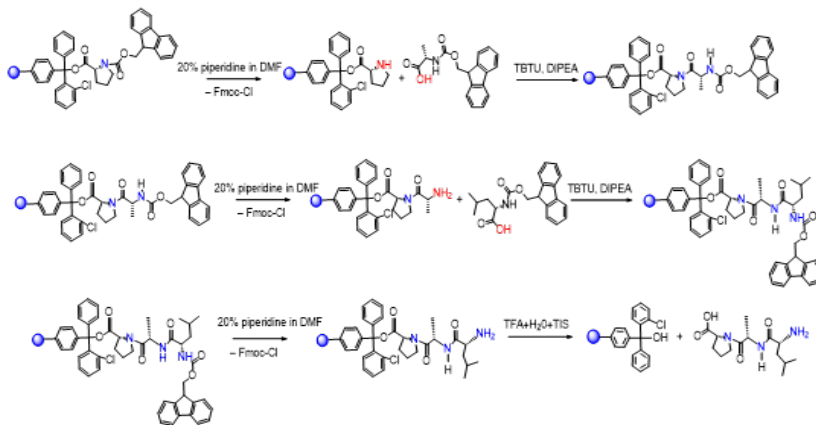

Fig. 1. Scheme of synthesis of H-Leu-Ala-Pro-OH. Reagents and conditions: H-Pro-2-ClTrt resin, Fmoc-Ala, Fmoc-Leu, HOBT, TBTU, DIPEA, TFA / triisopropylsilane / H₂O (95: 2.5: 2.5), room temperature, 1.5 h reaction time.

Table 1. Calculated EC_{50} values for rat ileum contractions after different concentrations of AT-I. EC_{50}ratio is the ratio of EC_{50} in the presence of inhibitor divided by EC_{50} of agonist (AT I) alone.

Concentration	Control –AT I EC_{50}	EC_{50} ratio			
		0.01 µM	0.1 µM	1 µM	10 µM
LAP	11.0^{-8}		3.562	4.55	
VAP	1.5^{-8}			1.777	5.947
LKP	5.5^{-8}		3.075	3.506	
IAK	3.04^{-8}		2.914	7.573	
VAW	1.98^{-8}		3.494	3.995	
LIS	4.09^{-8}	8.11	18.14		
Average±SD	$6.2^{-8} \pm 4.3$				

Spontaneously hypertensive rats (SHR) are a well- known animal model to study the pathophysiology of hypertension and have been widely used in scientific research [2,3]. The most widely used method described in the literature for determination the inhibitory activity of different compounds on ACE activity in isolated organs is the introduction of two or three different concentrations AT I in the incubation medium in presence or absence of inhibitor. For the purpose of our research, we performed preliminary experiments with rat ileum, replacing the single administration of AT I with cumulative (ATI 10^{-9}M – 10^{-6}M). We have found that this kind of preparation is sufficient sensitive to AT I and can be used for the purpose of our study. The cumulative input allows us to be more detailed monitoring the inhibitory effect of the peptides at all concentrations used AT I.
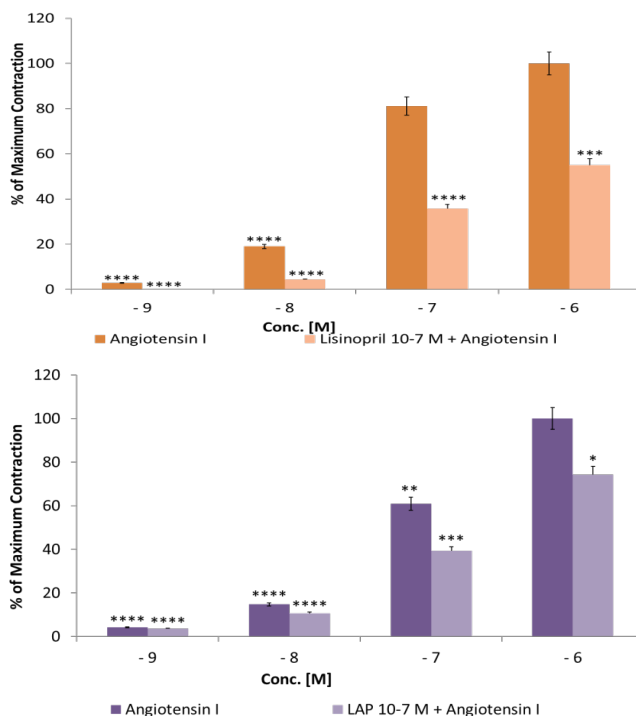

Fig. 2. Effects of Lisinopril and LAP on the angiotensin-induced contractions of rat ileum segments.

The effect of different ACE inhibitors on the contractile response of rat ileum after AT I cumulative application (reported by EC_{50}) is most significantly expressed by the ratio of EC_{50} calculated of the control curve (without inhibitor) and EC_{50} determined of the curve in the present of investigated peptide (so-called EC_{50} ratio) (Table 1).

All investigated tripeptides Val-Ala-Pro (VAP), Val-Ala-Trp (VAW), Leu-Lys-Pro (LKP), Leu-Ala-Pro (LAP), Ile-Ala-Lys (IAK) tested at 2 concentrations decreased dose-dependently AT I-induced contractions of the segments (Figure 2). This suggests that most likely these compounds specifically inhibit ACE activity.

The contractions induced by cumulatively applied AT1 ($10^{-9}M$ – $10^{-6}M$) were considered as control values and compared to those obtained after a 2 min incubation of the muscle segments with the peptides tested ($10^{-7}M$, $10^{-6}M$). Lisinopril in the same concentrations was also used like a test compound.

Studies have shown that the C-terminal aminoacid of an inhibitory peptide highly influences its binding to ACE I. It is established that potential ACE inhibitors are comprised of hydrophobic (aromatic or branched side chains) amino acid residues at the C-terminus where the utmost preferred aminoacid is proline [4].

Our results confirm that hydrophobic C-terminal proline in position 3 is very important for the inhibitory effect of the new synthetic compounds. Furthermore, the replacement in the second posittition of positively charged amino acid lysine (LKP) with hydrophobic alanine significantly increases the inhibitory activity of the new compound (LAP). The combination Ala^2-Pro^3 leads to an enhanced inhibitory effect. The combination Ala^2-Pro^3 enhances the inhibitory effect. Differences between the peptides inhibitory potency were observed when comparing their effect on biological object - smooth muscle preparations (rat ileum) due to AT-I induced contractions. Differences between the peptides inhibitory potency were observed comparing their effects on AT I induced smooth muscle contractions (rat ileum). It is important to note that, in addition to direct inhibition of ACE, other physico-chemical characteristics (e.g., transport through the cell membrane) are responsible for differences in the inhibitory activity of different peptides-the short peptide sequences are easily absorbed into the blood circulation and retain their activity. An understanding of the correlation between the peptide sequence and its bioactivity as an inhibitor is crucial in generating the potentially active peptide ACE inhibitors.

Acknowledgments

References

1. Wu, J., Liao, W., Udenigwe, C.C. *Trends Food Science & Technology* **69**, 214-219 (2017), https://doi.org/10.1016/j.tifs.2017.07.011
2. Majumder, K., Panahi, S., Kaufman, S., & Wu, J. P. *Journal of Functional Foods* **5**, 187-194 (2013), https://doi.org/10.1016/j.jff.2012.10.004
3. Grootaert, Ch., Matthijs, B., Voorspoels, S., Possemiers, S., Smagghe, G., Camp, *J. Food &Function* **8**, 3847-3855 (2017), https://doi.org/10.1039/C7FO00839B
4. Norris, R., FitzGerald, R.J. *Bioactive food peptides in health and disease* (Hernandez-Ledesma.B. editor.), 45-72 (2013), https://doi.org/10.5772/51710

Unravelling the Role of Membrane Active Peptide CorTS 1

Aditi Arora[1], Sujithra Shankar[1], Sushmita G Shah[2], and Archana Chugh[1]*

[1]Kusuma School of Biological Sciences, Indian Institute of Technology Delhi, New Delhi, 110016 India;
[2]Senior Consultant Ophthalmologist, Eye Life Hospital, Mumbai, 400052 India

Introduction

Quality of human life is significantly affected by impaired vision. According to a recent WHO estimate, at least 2.2 billion people around the world suffer from vision impairment or blindness, out of which in almost 1.2 billion people the occurrence of the condition could have been prevented or treated [1]. Human eye is a unique organ with its intricate anatomical structure involving complex arrangement of tissue layers. Several physiological and anatomical barriers such as ocular static and dynamic barriers, nasolachryimal drainage, tear turnover, reflex blinking prevent permeation of any exogenous material into ocular tissues. Consequently, it becomes difficult to achieve desirable therapeutic drug concentration in different eye segments [2]. Hence, various strategies are being developed for efficient drug delivery to deeper ocular tissues.

Cell penetrating peptides (CPPs)-based therapeutics is one such promising approach that employs bioactive peptides with cell permeating potential and the capacity to enhance the curative effects of drugs. Cell penetrating peptides have been mainly employed for intracellular delivery of cargoes such as nanosized nucleic acids, small molecule drugs and drug carrying nanoparticles. Recently studies have demonstrated successful application of CPPs for efficient drug delivery to ocular tissues as well [3-6]. Investigations into the immunomodulatory effects of CPPs in ocular diseases have also been reported [7-10]. Hence, further research in different aspects of CPP functions can facilitate the development of optimized therapy against various infectious and non-infectious ocular diseases.

Our group has developed a novel corneal targeting CPP- CorTS 1 (Corneal Targeting Sequence 1) for efficient drug delivery to anterior eye segment [11]. CorTS 1 has been designed by substituting Arginine residue in lieu of X in conserved LRR motifs- LXXLXLXXNXL. Based on the sequence composition it was hypothesized that the arginine residues will confer the peptide with cell permeating potential and presence of leucine residues will aid interaction of peptide with collagen rich extracellular matrix of stromal layer of cornea. Thus, aiding in development of a corneal targeting cell penetrating peptide. The peptide shows a dose dependent uptake via both energy dependent and energy independent mechanism in Human Corneal Epithelial cell line (HCE) without any effect on cell viability. Interestingly, potent antimicrobial action against MRSA and *Fusarium dimerum* has also been shown by the peptide [11]. Encouraged by this finding we are further investigating the role of CorTS 1 in immune-modulation by evaluating its effect on proinflammatory cytokines. Moreover, interaction of peptide with plasma membrane of HCE cells has been also assessed using scanning electron microscopy (SEM) to gain better understanding of internalization pathway.

Results and Discussion

In our previous study we have reported that for its internalization in HCE cells, CorTS 1 employs both ATP dependent (such as via endocytosis) and independent pathways. Herein, to gain further insight into the mechanism of uptake we have performed co-localization study with lysotracker DND-99 dye and FITC labelled CorTS 1. As shown in Figure 1, both yellow (from superimposition of green labelled peptide and red lysotracker stain) and green colored vesicular structures are observed in CorTS 1 treated cells suggesting that the peptide is utilizing both endosome dependent and independent pathways for its translocation in HCE cells. Thus, corroborating the results obtained in our prior study.

Furthermore, we have investigated the nature of interaction between the peptide and cell membrane of HCE cells using SEM. Interestingly, no significant changes in the topology of cell membrane were observed on treatment with CorTS 1 (Figure 2). Therefore, further experiments are required for better understanding of nature of direct penetration pathways that CorTS 1 utilises for its entry in HCE cells.
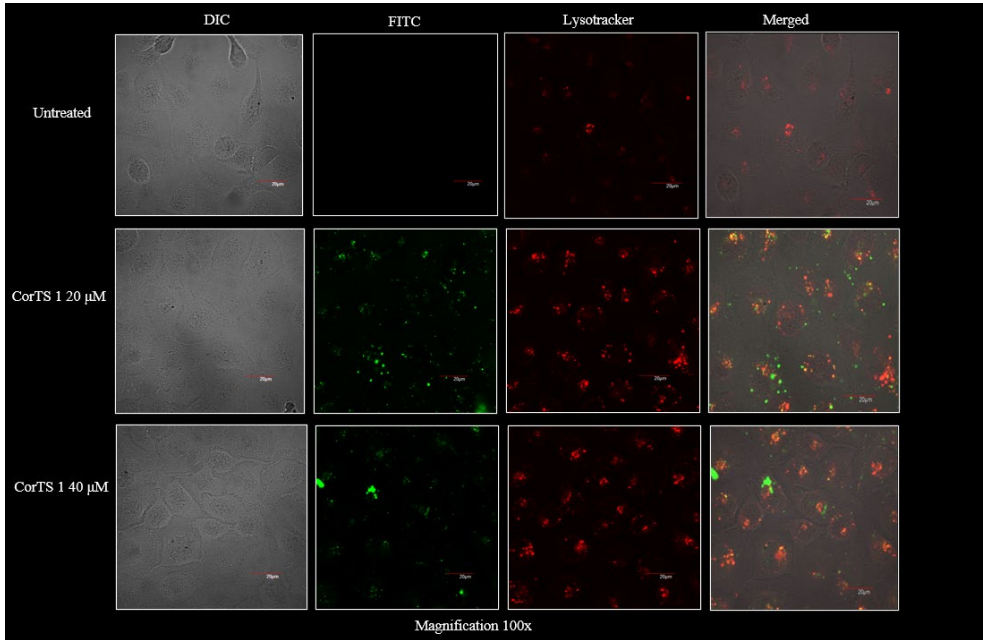
Fig. 1. Subcellular localization of CorTS 1 peptide in HCE cells as examined by staining the cells with lysotracker red DND-99.
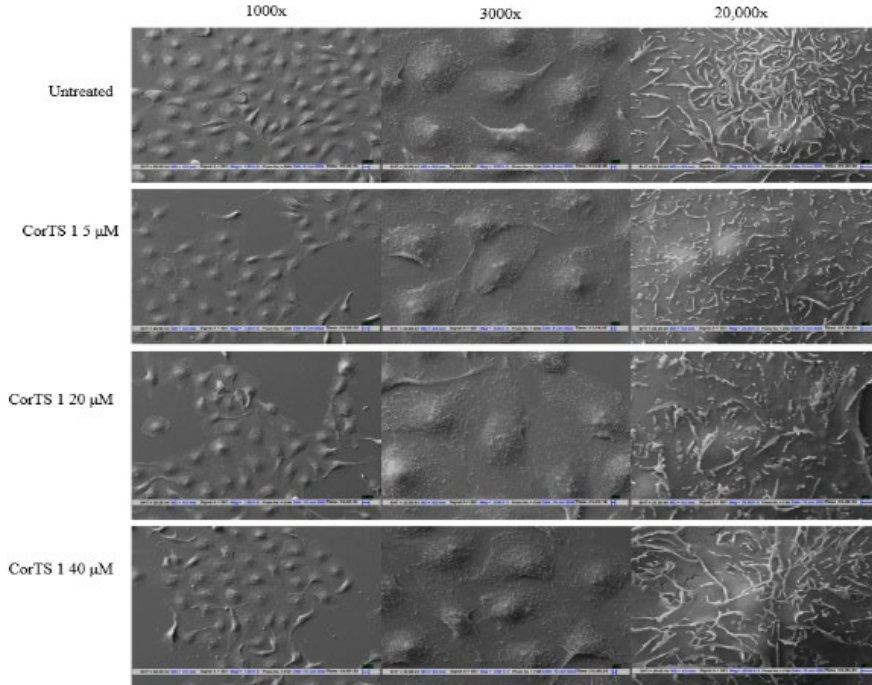

Fig. 2. SEM analysis of HCE cells after CorTS 1 treatment for 15 minutes at 37℃ and 5% CO$_2$.

CorTS 1 has also demonstrated strong antimicrobial action against deadly microbes including MRSA and *Fusarium dimerum* with MIC values of 10.53μM and 21.05 μM, respectively [11]. Based on these findings we were encouraged to investigate if the peptide also possesses immunomodulation potential. For this purpose, the effect of peptide treatment on the release of TNF-α by LPS stimulated THP1 cells was evaluated using ELISA. Preliminary studies have shown an approximately 2.3 times reduction in the TNF-α levels on application of CorTS 1 at a concentration of 20 μM.
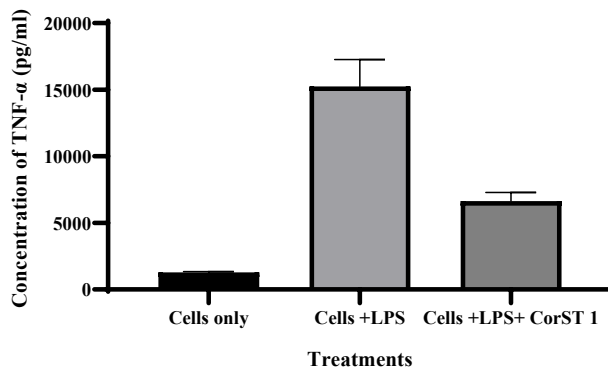

Fig. 3. Evaluation of TNF-α levels in LPS stimulated THP1 cells on CorTS 1 treatment.

Additionally, further investigation into the role of CorTS 1 in immunoregulation and management of microbial keratitis are currently underway.

Acknowledgements

References

1. "Blindness and vision impairment," 2021, [Online]. Available: https://www.who.int/news-room/fact-sheets/detail/blindness-and-visual-impairment
2. Gaudana, R., Ananthula, H.K., Parenky, A., and Mitra, A.K. *AAPS J.* **12**(3), 48-360 (2010), https://doi.org/10.1208/s12248-010-9183-3
3. Johnson, L.N., Cashman, S.M., and Kumar-Singh, R. *Mol. Ther.* **16**(1), 107-114 (2008), https://doi.org/10.1038/sj.mt.6300324
4. Jain, A., Shah, S.G., and Chugh, A. *Pharm. Res.* **32**(6), 1920-1930 (2015), https://doi.org/10.1007/s11095-014-1586-x
5. Chu, Y., et al. *Int. J. Nanomedicine* **12**, 353 (2017), https://doi.org/10.2147/IJN.S126865
6. Wang, Y., et al. *Nat. Commun.* **10**(1), 804 (2019), https://doi.org/10.1038/s41467-019-08690-4
7. Ildefonso, C.J., et al. *Invest. Ophthalmol.* Vis. Sci. **57**(2), 372-386 (2016), https://doi.org/10.1167/iovs.15-17703
8. Ahmed, C.M., Massengill, M.T., Brown, E.E., Ildefonso, C.J., Johnson, H.M., and Lewin, A.S. *Exp. Eye Res.* **177**, 12-22 (2018), https://doi.org/10.1016/j.exer.2018.07.020
9. Marques, R.E., et al. *J. Neuroinflammation* **14**(1), 1-14 (2017), http://dx.doi.org/10.1186/s12974-019-1686-y
10. Ahmed, C.M., Ildefonso, C.J., Johnson, H.M., and Lewin, A.S. *PLoS One* **15**(2), e0227524 (2020), https://doi.org/10.1371/journal.pone.0227524
11. Shankar, S., Shah, S.G., Yadav, S., and Chugh, A. *Eur. J. Pharm. Biopharm.* **166**, 216-226 (2021), https://doi.org/10.1016/j.ejpb.2021.06.014

Selection of Fragments of Collagen II Useful in Regenerative Medicine

Piotr Rosiak, Angelika Becht, Aleksandra Czerchawy, Katarzyna Czerczak-Kwiatkowska, Joanna Wasko, Justyna Fraczyk, and Beata Kolesinska

Institute of Organic Chemistry, Department of Chemistry, Łódź University of Technology,
Żeromskiego 116, 90-924 Łódź, Poland

Introduction

At present, much emphasis is placed on the research of collagen-based scaffolds. Collagen, due to its properties and functions, and its widespread presence in the composition of almost every tissue, is one of the main research objects in modern regenerative medicine. From the point of view of the development of materials mimicking the natural matrix, the most important are collagens I, II, and III, able to form macrostructures in the form of fibers that are able to imitate ECM. It has been shown that collagen can also be used to obtain multidimensional porous structures [1]. Literature data show that scaffolds based on native collagen has the ability to initiate and support the tissue regeneration process. In the form of a hydrogel, the collagen materials even initiate the chondrogenesis process [2]. However, materials made of native, unmodified collagens are characterized by unsatisfactory mechanical properties and low structural stability [1]. For this reason, work was undertaken to modify scaffolds made of native collagen or to obtain composite materials in which the non-collagen fraction responsible for improving the strength properties will not eliminate the desired biocompatibility and bioresorbability. Strategies for cross-linking the native collagen backbone allow for enhancement of its mechanical and structural properties. Additionally, this process allows for extending the biodegradation time [3]. The cross-linking of collagen fibers adversely affects the activity of cells embedded in the modified material [4]. However, the negative influence of modified collagen on the cellular response *in vivo* has led to attempts to use mixtures of natural or synthetic polymers with collagen. Composites of collagen and synthetic polymers have found wide applications in tissue engineering [5,6]. Natural polymers are widely used in tissue engineering due to their similarity to native ECM [7]. Moreover, there are many literature reports that indicate that it is possible to use short peptides as scaffolds and their positive influence on the life processes of cells. The self-organizing peptides RADA16-I and RADA16-II form materials that favor the proliferation and differentiation of neuronal stem cells [8]. Another example of a self-organizing peptide that positively affects the proliferation processes and the ability to take up vital functions by cells is the RAD peptide [9]. KLD-12 peptide is used for the regeneration of cartilage tissue, e.g. for repairing intervertebral discs [10]. In order to obtain a material providing a comprehensive ECM substitute, work has been undertaken to combine raw materials with fiber morphology and fragments responsible for the interaction of the natural extracellular matrix with the surrounding environment. The primary method was to directly link a functional cell-interacting fragment to the *C*-terminus of the self-assembled peptide. Typically, a linker of two glycine residues is inserted between the self-assembled peptide and the functional fragment to improve the display of the active fragment. Research on this type of conjugate resulted in obtaining material consisting of the RADA16-I peptide and two RGD peptides, which showed the ability to stimulate proliferation in tests performed with fibroblasts. The use of the PRG motif derived from the laminin sequence made it possible to obtain derivatives significantly improving the activity of periodontal ligament fibroblasts [11].

The aim of our research was to select fragments of human collagen II useful for tissue regeneration. It was assumed that the key is to select the exposed fragments of collagen II, which should guarantee their biological activity. This assumption is due to the fact that the protein-protein / protein-peptide interaction takes place only at the junction of the outer domains of proteins. Assuming this assumption, the use of polyclonal antibodies that recognize structurally diverse and exposed fragments of a given protein should allow for the reconstruction of the external structure of collagen II. Despite the fact that the selected fragments form immune complexes with antibodies (i.e. they are immunologically active), due to their "length" they are too weak antigens to trigger the activation of the immune system, and in addition, they are fragments of human proteins, which further reduces the possibility of triggering activation the immune system in humans.
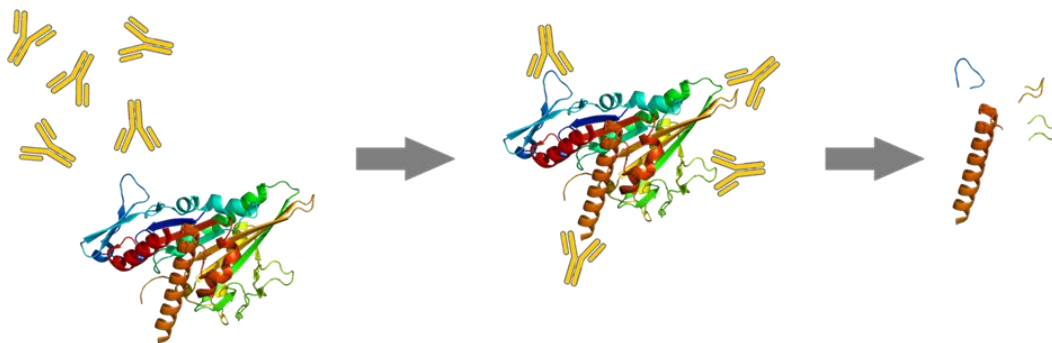
Fig. 1. Schematic diagram of the search for biologically active fragments of collagen II.

Results and Discussion

Results As part of the research, attempts were made to select biologically active fragments of collagen II, expecting that they would have the function of a native protein. The implementation of the aim of the work required dividing the research part into several stages: 1) synthesis of a collagen II fragment library comprising whole proteins, 2) selecting biologically active fragments, 3) checking the biological activity of selected fragments.

The automatic SPOT method with the use of cellulose modified with 1,3,5-triazine derivative [12] was used to synthesize the library of collagen II fragments immobilized on cellulose. The 1,3,5-triazine derivative acts as a linker separating the peptide from the cellulose matrix and ensuring its appropriate exposure to interaction with antibodies [13].
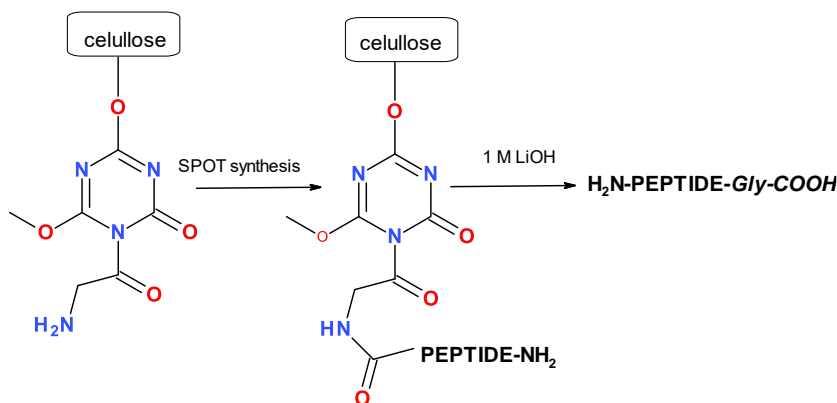
Fig. 2. Cellulose matrix with an immobilized 1,3,5-triazine derivative and a glycine residue (H₂N-Gly-iso-methoxy-1,3,5-triazine linker), to which subsequent amino acids of the synthesized peptides are attached.

4-(4,6-Dimethoxy-1,3,5-triazin-2-yl)-4-methyl-morpholinium p-toluenosulphonate (DMT/NMM/TosO⁻) was used as a coupling reagent in the synthesis of peptides by the SPOT method [14]. Collagen II contains 1487 amino acid residues, so the library of cellulose-immobilized non-overlapping collagen II fragments comprised 148 decapeptides and one heptapeptide. Transformation to a 256-point greyscale of the dot-blot-stained cellulose matrix allowed for the quantification of the binding capacity of the antibodies to collagen II fragments. This approach made it possible to select the fragments that make up the outer sphere of the protein.

From the 149-component library of collagen II fragments, 26 fragments were selected for further study. Out of 26 selected decapeptides, 4 formed complexes with polyclonal antibodies and were classified as very strong (++), 19 as strong (+), for the three decapeptides marked as +/- the results were not

identical and it was difficult to assign them to the group + or inactive fragments, therefore it has been assumed that they will be included in the pool of tested fragments. The next stage of research was to find the right fragments recognized by polyclonal antibodies, which should be included within 26 fragments selected in the first screening. These studies were necessary because at the first screening stage, collagen division was based on an arbitrary division of the protein into non-overlapping decapeptide fragments. It was assumed that epitope mapping of the selected 26 fragments would be performed, shifting the reading frame by five amino acid residues towards both the *N*- and *C*-terminus. The synthesis of cellulose-immobilized peptides followed the synthetic protocol described above. Finally, for the selected 26 fragments of collagen II, a 296-component library of immobilized decapeptides was obtained.

Table 1. Collagen II fragments able to interact with polyclonal anti-collagen II antibodies. Results of the dot blot test with polyclonal antibodies with a library of non-overlapping collagen fragments (1st screening) and a library resulting from epitope mapping of selected fragments (2nd screening).

Entry	1st screening		2nd screening	
	Fragment	Strength of interaction	Fragment	Strength of interaction
1	11-20	++	10-23	++
2	31-40	+/-	25-41	+
3	41-50	+	42-55	++
4	241-250	+	236-248	+
5	271-280	+	273-287	++
6	281-290	+	283-295	+
7	321-330	+	316-331	++
8	431-440	+	426-441	+
9	511-520	+	511-520	+
10	541-550	+/-	536-552	+
11	551-560	+/-	554-565	+
12	621-630	+	620-635	+
13	701-710	+	696-711	++
14	711-720	+	714-725	++
15	931-940	+	927-945	+
16	971-980	+	971-987	+
17	981-990	+	984-995	+
18	1131-1140	+	1130-1144	++
19	1181-1190	+	1181-1194	++
20	1331-1340	++	1327-1338	++
21	1341-1350	+	1344-1355	+
22	1371-1380	++	1367-1384	++
23	1391-1400	+	1385-1396	+
24	1431-1440	+	1427-1440	+
25	1441-1450	+	1443-1454	+
26	1451-1460	++	1449-1461	++

The possibility of cleavage of the peptide from the modified cellulose matrix in the presence of a diluted LiOH solution allowed for the cleavage of the collagen II fragments selected in the first screening and the use of an equimolar mixture of 26 selected collagen II fragments: 11-20G, 31-40G, 41-50G, 241-250G, 271-280G, 281-290G, 321-330G, 431-440G, 511-520G, 541-550G, 551-560G, 621-630G, 701-710G, 711-720G, 931-940G, 971-980G, 981- 990G, 1131-1140G, 1181-1190G, 1331-1340G, 1341-1350G, 1371-1380G, 1391-1400G, 1431-1440G, 1441-1450G, 1451-1460G in biological studies (in each cleaved peptide at the C-terminus present there is a Gly residue derived from the isocyanurate linker). An assessment of biological activity was performed on human Hs 680 fibroblasts. One of the tests was the PrestoBlue viability and proliferation test, which allows determining the viability of cells and their ability to proliferate. Another test used was ToxiLight™ Bioassay allowing the measurement of cytotoxicity. Damage to *in vitro* cultured cells and loss of cell membrane integrity results in leakage of many compounds into the surrounding medium. The ToxiLight test is based on the quantitative measurement of adenylate kinase (AK) released from damaged cells, which allows for an accurate and sensitive determination of cytotoxicity and cytolysis.
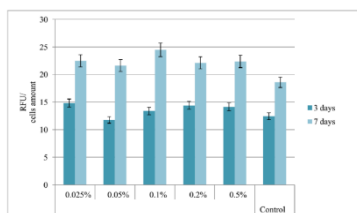

Fig. 3. Viability (proliferation) of Hs 680 cells cultured with the addition of an equimolar mixture of increasing concentration of collagen II fragments as a percentage of the total cell count in the culture. PrestoBlue assay. RFU- Relative Fluorescence Units.
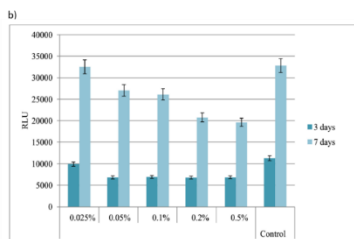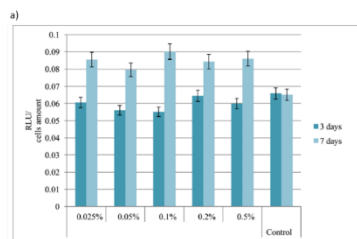

Fig. 4. Cytotoxicity of Hs 680 cell with the addition of an equimolar mixture of collagen II fragments, a) ToxiLight assay, b) ToxiLight 100 Lysis Control assay. RLU - Relative Light Units.

The amount of ATP is determined as a result of the conversion of luciferin in the presence of luciferase. As a result, the intensity of the emitted light is linearly dependent on the concentration of AK.

Preliminary results of the research indicate that selected fragments of collagen II can be used to obtain materials useful in regenerative medicine.

Acknowledgments

References

1. Dong, C., et al. *Polymers* **8**, 42 (2016), https://doi.org/10.3390/polym8020042
2. Zuber, M., et al. *Int. J. Biol. Macromol.* **80**, 366-374 (2015), https://doi.org/10.1016/j.ijbiomac.2015.07.001
3. Yamada, S.K., et al. *Biomed Res. Int.* **2014**, 302932 (2014), https://doi.org/10.1155/2014/302932
4. Pawelec, K.M., et al. J. *Mater. Chem. B* **4**, 6484-6496 (2016), https://doi.org/10.1039/c6tb00807k
5. Zhang, Q., et al. *Int. J. Biol. Macromol.* **76**, 94-101 (2015), https://doi.org/10.1016/j.ijbiomac.2015.01.063
6. Jia, L., et al. *Mater. Sci. Eng. C* **33**, 4640-4650 (2013), https://doi.org/10.1016/j.msec.2013.07.021
7. Yan, F., et al. *Neural Regen. Res.* **10**, 1421-1426 (2015), https://doi.org/10.4103/1673-5374.163466
8. Wang, S., et al. *Tissue Eng. Part A* **14**, 227-236 (2008), https://doi.org/10.1089/tea.2007.0143
9. Yuan, Y., et al. *Transplant. Proc.* **40**, 2571-2574 (2008), https://doi.org/10.1016/j.transproceed.2008.08.017
10. Miller, R.E., et al. *Clin. Orthop. Relat. Res.* **469**, 2716-2724 (2011), https://doi.org/10.1007/s11999-011-1891-1
11. Kumada, Y., et al. *PLoS One* **5**, 1-7 (2010), https://doi.org/10.1371/journal.pone.0010305
12. Kaminski, Z.J., et al. *Chem. Biodiv.* **14**, e1700444 (2017), https://doi.org/10.1002/cbdv.201700444
13. Fraczyk, J., et al. *J. Pept. Sci.* **24**, 1-12 (2018), https://doi.org/10.1002/psc.3063
14. Kolesinska, B., et al. *Eur. J. Org. Chem.* 401-408 (2015), https://doi.org/10.1002/ejoc.201402862

Bifunctional Opioid/Melanocortin Peptidomimetics for Use in Neuropathic Pain

Aleksandra Misicka-Kęsik[1,2], Ewa Witkowska[1,2], Magda Popławska[1], Katarzyna Witoszka[1], Beata Wileńska[1,2], Jolanta Dyniewicz[1], Krzysztof Różycki[1], Kacper Błaziak[1,2], Joanna Starnowska-Sokół[1,3], Anna Piotrowska[1,3], and Barbara Przewłocka[1,3]

[1]*NEURO-OPIOMEL sp. z o. o., Krasińskiego 22, 05-820 Piastów, Poland;* [2]*Faculty of Chemistry, University of Warsaw, Pasteura 1, 02-093 Warsaw, Poland;* [3]*Department of Pain Pharmacology, Maj Institute of Pharmacology, Polish Academy of Science, Smętna 12, 31-343 Kraków, Poland*

Introduction

Neuropathic pain results from a damage of the nervous system. and belongs to the category of chronic pain. The use of conventional opioid agonists for the treatment of chronic pain with neuropathic component is limited due to their weaker analgesic effects and the potential occurrence of undesirable side effects such as constipation, respiratory depression, tolerance and dependence. After the first post-injury period, when the endogenous antinociceptive (opioid) system is activated, other endogenous systems come into play as counteractants of the elicited opioid activity. These systems generate pronociceptive compounds that exert their effect through non-opioid receptors and weaken the effect of analgesics [1].

One of the most promising strategies in the search for new analgesics for this type of pain is to design compounds that activate the opioid system and simultaneously block the pronociceptive systems. A number of such endogenous pain-enhancing systems have been described [2], among them the melanocortin system (MC), particularly the melanocortin 4 (MC4) receptor, is of great interest [3,4].

Based on the above strategy, we have designed and evaluated for biological activity several bifunctional peptidomimetics [5-7] which consist of an opioid agonist (fragment of enkephalin [8]) and a melanocortin-4 (MC4) receptor antagonist (fragment of SHU9119 [9]), joined by linkers of varying length and rigidity. Three of them containing flexible linkers, namely one or two 6- aminohexanoic acid (Ahx) residues, were found to be very effective at low doses in reducing allodynia and hyperalgesia (von Frey and Cold Plate, respectively) that characterize neuropathic pain, while showing little activity in acute pain. An important element of preclinical studies of bifunctional peptidomimetics was the demonstration that the compounds we synthesized were much more potent than the mixture of parent compounds. Moreover, looking for an effect in neuropathic pain, we compared different forms (acetate and trifluoroacetate) and routes of administration of selected peptidomimetics in a neuropathic pain model.

The structure and possible application(s) of our compounds are subject to intellectual property rights protection, including but not limited to patent protection (US11041010) and pending patent protection (PL422093, PCT/IB2018/054925).

We have now started developing a larger-scale synthesis of our compounds and a series of analytical, physicochemical, biological, and biochemical tests necessary to begin preclinical studies on these compounds. In this publication we present several aspects of our research.

Results and Discussion

The three most efficient peptidomimetics mentioned above NOM1 (Tyr[1]-D-Ala[2]-Gly[3]-Phe[4]-**Ahx**[5]-Nle[6]-c[Asp[7]-His[8]-D-Nal(2')[9]-Arg[10]-Trp[11]-Lys[12]]-NH_2), NOM2 (Tyr[1]-D-Ala[2]-Gly[3]-Phe[4]-**Ahx**[5]-**Ahx**[6]-Nle[7]-c[Asp[8]-His[9]-D-Nal(2')[10]-Arg[11]-Trp[12]-Lys[13]]-NH_2) and NOM3 (Dmt[1]-D-Ala[2]-Gly[3]-Phe[4]-**Ahx**[5]-Nle[6]-c[Asp[7]-His[8]-D-Nal(2')[9]-Arg[10]-Trp[11]-Lys[12]]-NH_2) were synthetized on a Rink amide AM resin (IRIS, 0,35 mmol/g) using the standard Fmoc strategy and carbodiimide (DIC) as a coupling reagent. The final crude peptides were purified by RP-HPLC and characterized by ESI MS method. The exchange of trifluoroacetates with acetates was performed using AG 1-X2 (acetate), 200-400 mesh ion exchange resin (BioRad). Before the upscaling of the synthesis, it was checked which step was the

most advantageous to carry out the cyclization (the formation of the lactam bond). For that purpose, three syntheses of the NOM3 were performed. In the first synthesis, cyclization was performed after attachment of Asp[7] residue, in the second - after attachment of Nle[6] residue and in the third - after the peptide chain has been assembled. After removing the peptides from the resin, the crude products were analysed by HPLC and the chromatograms were compared. The best result was achieved in the case of heptapeptide cyclization (the second synthesis)- 58% of NOM3 (HPLC). In the other two syntheses - the first and the third (cyclization of hexapeptide and dodecapeptide), 21% of NOM3 (HPLC) and a mixture of products were obtained, respectively.

Preclinical studies were performed in a model of neuropathic pain after chronic constriction injury to the sciatic nerve (CCI) in mice. The pain sensitivity characteristic of neuropathic pain was measured 7-14 days after nerve injury using two tests: von Frey filaments (tactile stimulus) and cold plate (thermal stimulus). Importantly, the behavioural tests have shown that the new bifunctional structure causes a stronger analgesic effect than the mixture of its components, i.e. the opioid and the MC4 antagonist. Figure 1A shows a comparison of the effect provided by the mixture of parent compounds, NOM1 and NOM2, in the cold plate test. As can be seen, the analgesic effect of NOM1 and NOM2 is significantly stronger. Moreover, the effect delivered by these peptidomimetics lasts much longer than the effect provided by the parent compounds and their mixture, what is clearly visible in Figure 1B when the the areas under the curve (AUC) are compared.

Administration of these two forms (acetate and trifluoroacetate) of peptidomimetics in a mouse model of neuropathic pain showed similar potency after intraperitoneal administration. Figure 2 shows the analgesic effects provided by two forms of NOM3. The analgesic effects provided by the two forms, as observed at different time points, are not significantly different, which indicates the possibility of using the form recommended in preclinical studies.
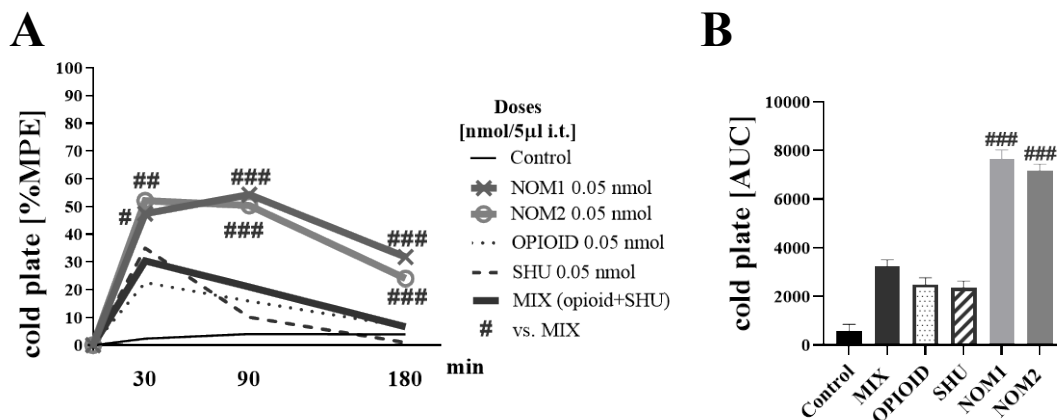

Fig. 1. Comparison of effects of hybrid structure NOM1 and NOM2 (0.05 nmol) with mixture of parent compounds (MIX = 0.05 nmol opioid + 0.05 nmol SHU9119) on: (A) hypersensitivity to thermal stimuli (cold plate), and (B) the effect by the area under the curve (AUC), as measured 30, 90, and 180 min after administration in CCI-exposed mice.
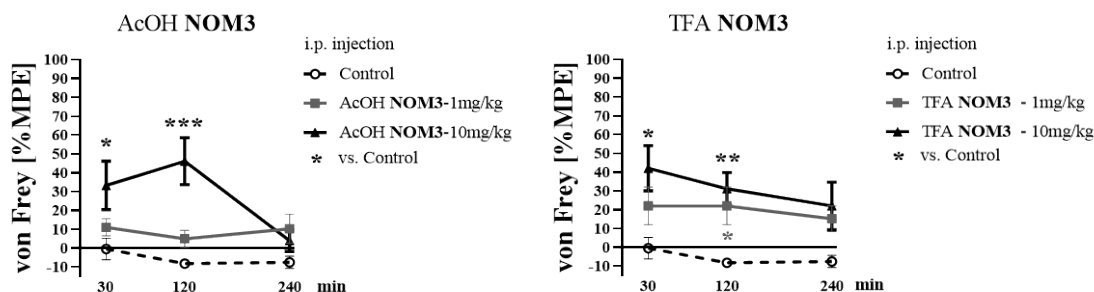
Fig. 2. Analgesic effect of NOM3 in two forms (acetate and trifluoroacetate) after intraperitoneal injection in mouse neuropathic pain model (chronic constriction injury to the sciatic nerve – CCI).

A comparison of the effects of peptidomimetics following intraspinal (by lumbar puncture), intravenous and intraperitoneal administration in a mouse model of neuropathic pain was also performed. The results of these studies are shown in Figure 3.
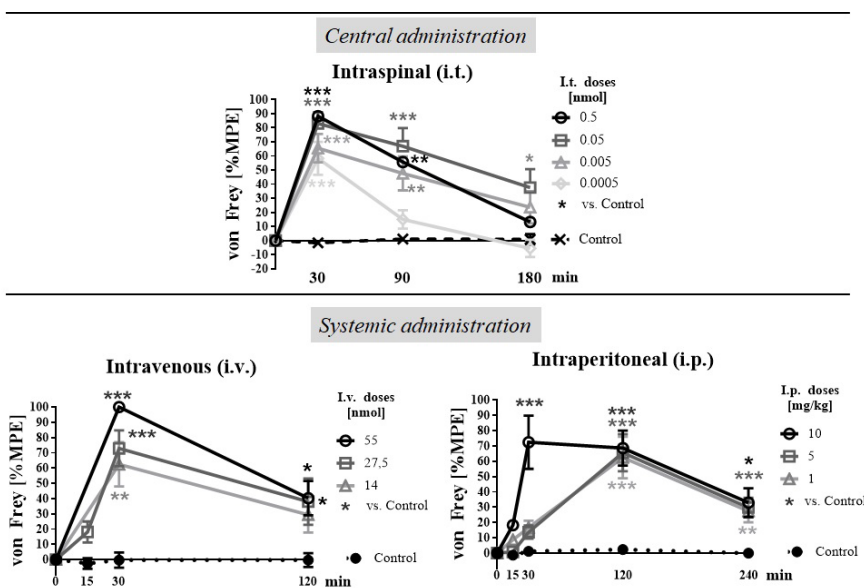

Fig. 3. Analgesic effect of NOM1 in different administration routes (Intraspinal – i.t., intravenous – i.v., and intraperitoneal – i.p.) in mouse neuropathic pain model.

Peptides intended for preclinical research must not contain trifluoroacetate ions, due to their harmful properties. Therefore, the replacement of these counterions with other ones is necessary. The HPLC-MS/MS method was developed to determine the concentration of TFA in synthetic samples. The multiple reaction monitoring (MRM) method in negative ion mode was used to follow the precursor-fragment ion transitions presented on the figure below (Figure 4). The calibration curve was prepared based on five different standard sample solutions. The representative peak area of the main MS2 transition was tracked in the test sample and compared with calibration linear equation resulting in TFA concentration in the test sample. The LC-MS/MS system consisted of LC-2050C 3D Liquid

Chromatograph and triple quadrupole mass spectrometer LCMS-8045 (Shimadzu), equipped with an ESI source and the polar type of column (30 mm × 2.1 mm) at 40 ℃ were used in the study. The water-based and organic mobile phases were used for mixture separation: (A) ammonium acetate/acetic acid water solution and (B) a mixture of AcCN:MeOH:HCOOH. The 3.5-minute-long gradient program at a flow rate of 0.8 ml/min was used. The electrospray (ESI) parameters were optimized to collect the most ion transitions *via* multiple reaction monitoring (MRM) method in negative ion mode.
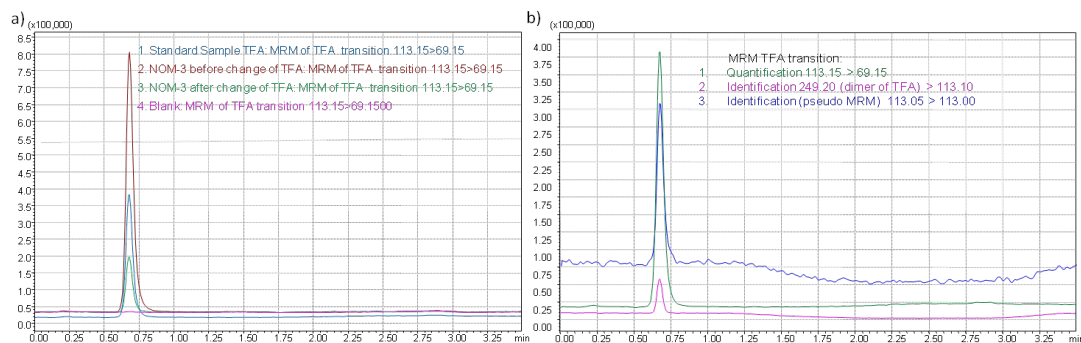

Fig. 4. Overlay TFA MRM transitions recorded for: a) 1. standard sample, 2. compound NOM3 before exchange of TFA to AcOH, 3. NOM3 after exchange of TFA to AcOH, 4. blank. b) MRM TFA transitions 1. Quantification 113.15/69.15, 2. Identification 249.20 (dimer of TFA)/113.10 3. Identification (pseudo MRM) 113.05/113.00.

Our studies showed that tested bifunctional peptidomimetics exhibit significantly greater analgesic activity compared to the action of the mixture of their components (opioid agonist and MC4 receptor antagonist). The best efficiency of peptidomometics was observed after spinal administration, but a similar effect was also obtained after intravenous administration, which is the basis for the selection of a drug formulation for use in the treatment of neuropathic pain. Moreover, the tested compounds show antinociceptive activity in both forms (acetate and trifluoroacetate) in rodents, which indicates the possibility of using the form recommended in preclinical studies.

The results of our research on bifunctional peptidomimetics offer hope for the development of new potential drugs for the treatment of neuropathic pain.

Acknowledgments

References

1. Vanderah, T.W. *Med Clin North Am* **91**, 1-12 (2007), https://doi.org/10.1016/j.mcna.2006.10.006
2. Nickel, F.T., et al. *Eur. Neuropsychopharmacol* **22**, 81-81 (2012), https://doi.org/10.1016/j.euroneuro.2011.05.005
3. Starowicz, K., et al. *Pain* **117**, 401-411 (2005), http://dx.doi.org/10.1016/j.pain.2005.07.003
4. Starowicz, K., et al. *Pharmacol. Rep.* **61**, 1086-1095 (2009), https://doi.org/10.1016/S1734-1140(09)70171-9
5. Starnowska-Sokół, J., et al. *Neuropharmacology* **178**, 108232 (2020), https://doi.org/10.1016/j.neuropharm.2020.108232
6. Piotrowska, A., et al. *Pain* 2021, **162**, 432-445 (2022), http://dx.doi.org/10.1097/j.pain.0000000000002045
7. Witkowska, E., et al. *Int J Mol Sci* **23,** 674 (2022), http://dx.doi.org/10.3390/ijms23020674
8. McGregor, W.H., et al. *Life Sci.* **23**, 1371-1376 (1978), https://pubs.acs.org/doi/abs/10.1021/jm00018a005
9. Hruby, V.J., et al. *J. Med. Chem.* **38**, 3454-3461 (1995), https://doi.org/10.1021/jm00018a005

Inhibition of the Angiotensin II Type 2 Receptor AT2R is a Novel Therapeutic Strategy for Glioblastoma

Richard Perryman[1#], Alexander Renziehausen[1#], Hamidreza Shaye[2,3#], Androniki D. Kostagianni[4], Antonis D. Tsiailanis[4], Tom Thorne[5], Maria V. Chatziathanasiadou[1,4], Gregory B. Sivolapenko[6], Mohamed Ahmed El Mubarak[6], Gye Won Han[3], Barbara Zarzycka[3,7], Vsevolod Katritch[3,8], Guillaume Lebon[9], Cristiana Lo Nigro[10], Laura Lattanzio[10], Sophie Morse[11], James Choi[11], Kevin O'Neill[1,12], Zoe Kanaki[13], Apostolos Klinakis[13], Tim Crook[1], Vadim Cherezov[2,3*], Andreas G. Tzakos[4,14*], and Nelofer Syed[1*]

[1]*John Fulcher Neuro-Oncology Laboratory, Department Brain Sciences, Imperial College, London, UK;* [2]*Department of Chemistry, University of Southern California, Los Angeles, CA 90089, USA;* [3]*Bridge Institute, University of Southern California, Los Angeles, CA 90089, USA;* [4]*Department of Chemistry, University of Ioannina, Ioannina, Greece;* [5]*Department of Computer Science, University of Surrey, Surrey, UK;* [6]*Laboratory of Pharmacokinetics, Department of Pharmacy, University of Patras, Patras, Greece;* [7]*Division of Medicinal Chemistry, Amsterdam Institute for Molecules, Medicines and Systems (AIMMS), Vrije Universiteit Amsterdam, De Boelelaan 1108, 1081 HZ Amsterdam, The Netherland;* [8]*Department of Quantitative and Computational Biology, University of Southern California, Los Angeles, CA 90089, USA;* [9]*Insitut de Génomique Fonctionnelle, University of Montpelier, CNRS, INSERM, Montpellier, France;* [10]*Department of Oncology, Ospedale San Croce e Carle, Cuneo, Italy;* [11]*Department of Bioengineering, Imperial College London, London, UK;* [12]*Department of Neurosurgery, Charing Cross Hospital, London, UK;* [13]*Centre for Basic Research, Biomedical Research Foundation of the Academy of Athens, Greece;* [14]*University Research Center of Ioannina (URCI), Institute of Materials Science and Computing, Ioannina, Greece*

Introduction

The prognosis for patients with glioblastoma (GBM) remains poor, therefore novel therapeutic approaches to address this unmet clinical need are urgently required. We illustrate that angiotensin II (AngII), a peptide involved in salt and water balance, is produced endogenously by GBM cells and promotes proliferation of these cells, via the type 2 receptor of AngII (AT_2R). We repurposed EMA401, a peripherally restricted AT2R selective antagonist, originally developed for the treatment of neuropathic pain. We show that EMA401 efficiently inhibits proliferation of GBM spheroids that express AT2R, and prevents both invasiveness and angiogenesis. We enhance the central nervous system (CNS) penetration of EMA401, through the generation of a novel compound, A3E. The novel compound demonstrated superior efficacy both *in vitro* and *in vivo* with minimal toxicity. This study demonstrates that inhibition of AT_2R is a new and promising candidate target for systemic therapy of GBM [1].
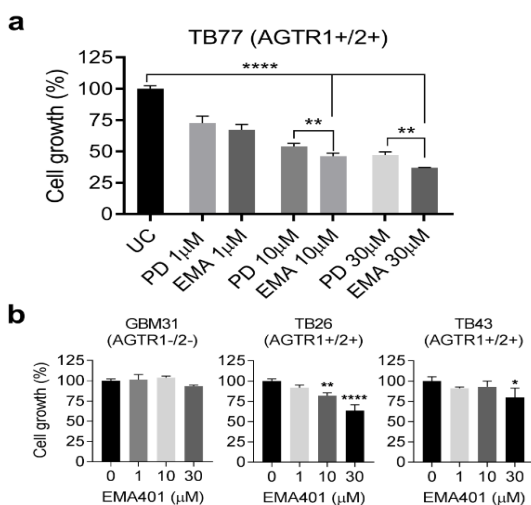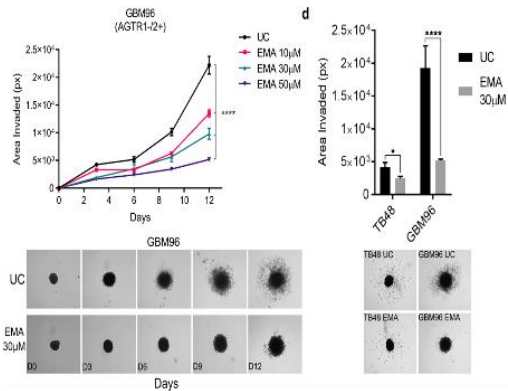
Fig. 1. EMA401 significantly inhibits the growth of GBM cells via AT2R.

Results and Discussion

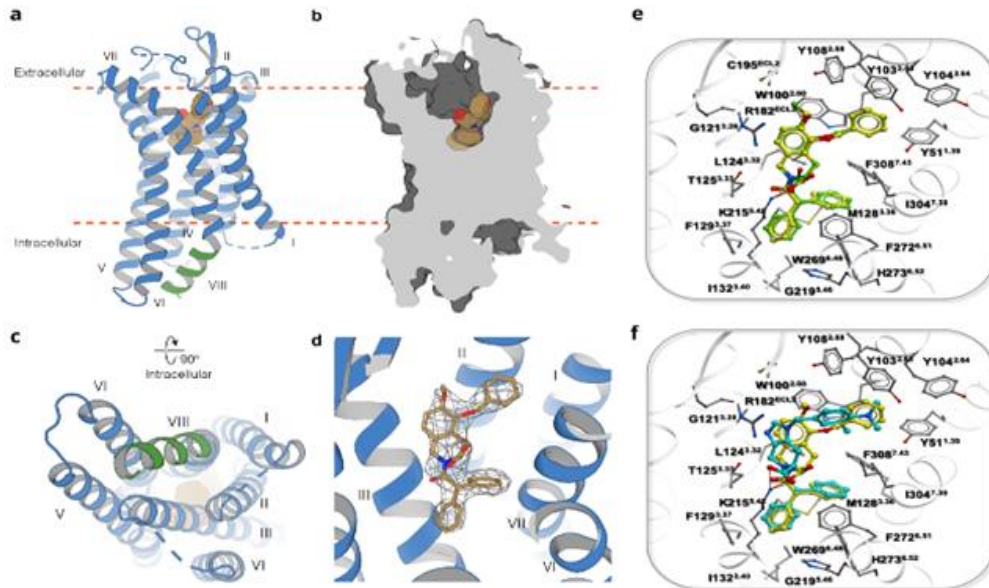Here we show that AT_2R signalling [2], has an significant role in promotion of

Fig. 2. Evaluating spheroid growth, spheroid invasion and the ability of GBM cells to induce angiogenesis when treated with angiotensin receptor antagonists.

GBM tumor growth and invasiveness. This study follows our previous work in which we reported that AT_2R inhibition with EMA401 inhibits proliferation, invasiveness, and angiogenesis in metastatic melanoma [3]. The AngII receptors differ functionally between cancer types. Furthermore, the effects of each receptor also depend on the microenvironmental stressors present in the vicinity of cancer cells. Here we show that under conditions of starvation stress (the norm in most tumor microenvironments), AT_2R adopts a promoting function, therefore selective antagonism has anti-tumor effects.

Herein, we reported that in low serum conditions, AngII minimally increased the growth of GBM lines and primary cultures which expressed AT1R but not AT2R. Selective antagonism of AT2R by PD123319 blocked the enhanced growth conferred by exogenous AngII, but no effects were observed with treatment with losartan, which is a selective AT1R antagonist. Our results indicate that under growth factor limiting conditions, AngII confers a growth advantage to GBM which is transduced via AT2R. PD123319 inhibited the proliferation of AT2R expressing cells in the absence of exogenous AngII, and effects were significant in two of these cell lines (8MG: P<0.05 and TB77: P<0.0001). These results demonstrate that under low serum conditions, autocrine production of AngII promotes cell growth of GBM cells via AT2R signaling.

EMA401 demonstrated significantly more potent growth inhibition than PD123319 (P=0.0011). Similar activity was observed in additional primary GBM cultures expressing AGTR2 (TB26, TB43). Notably, the AGTR2 negative GBM31 cell line was insensitive to EMA401. EMA401 significantly reduced the invasiveness of GBM96 cells in a dose-dependent manner. TB48 spheroids exhibited

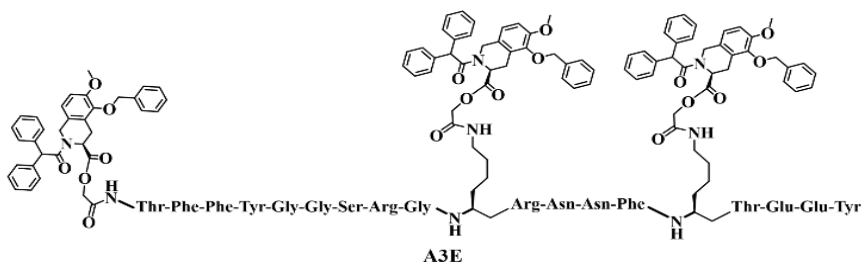*Fig. 3. AT2R-EMA401 structure and details of AT2R-ligand interactions.*

190

Fig. 4. Structure of A3E (Angiopep-2-EMA401).

lower invasive properties than GBM96, but invasiveness was nonetheless significantly reduced by 30 μM EMA401 (Figures 1,2).

Next, we determined the crystal structure of EMA401 bound to AT2R. The AT2R structure is comprised of an heptahelical transmembrane bundle (7TM helices I-VII), three extracellular loops (ECLs 1-3), three intracellular loops (ICLs 1-3), and an intracellular amphipathic helix VIII. The crystal structure of AT_2R bound to EMA401 was determined and revealed the receptor to be in an active-like conformation with helix-VIII blocking G protein or β-arrestin recruitment. Based on our X-ray structure of EMA401 bound to AT2R (Figure 3), it is evident that its carboxylic acid group is essential for forming interactions with key AT2R residues.

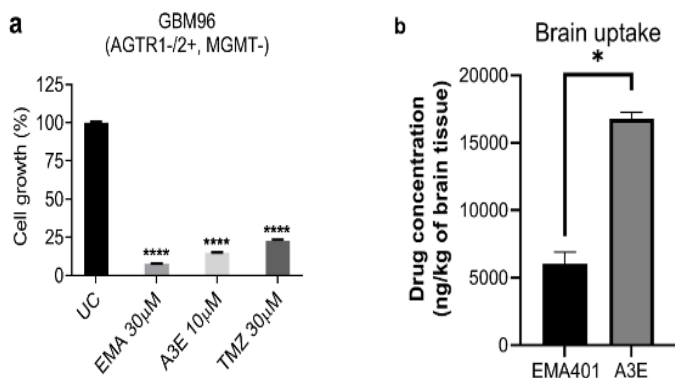Despite the inhibitory effect of EMA401 in GBM promotion, a potential obstacle to its clinical use of

Fig. 5. a) The effects of EMA401 and A3E on proliferation in primary GBM cultures b) Brain biodistribution of EMA401 after intravenous injection of EMA401, and A3E.

is the reported inability of the molecule to efficiently penetrate the intact BBB [4]. To enhance the likelihood of using EMA401 as a potential GBM therapeutic, either a structural derivatization or proper formulation has to be performed. On the basis of our X-ray structure of EMA401 bound to AT2R, it is evident that its carboxylic acid group is essential for forming interactions with key AT2R residues. We therefore use this group as a reactive handle to conjugate three EMA401 units, via cleavable ester bonds to Angiopep-2, to generate A3E. (Figure 4) Angiopep-2 is a molecule that potentiates the CNS delivery of drugs typically unable to pass the BBB [5-7].

The *in vitro* anti-proliferative effect of A3E was at least as potent as EMA401 in all primary GBM cell lines that has been tested. In addition, through biodistribution studies we demonstrated that A3E notably increased CNS penetration of EMA401 with respect to the native EMA401 (Figure 5).

Together, these observations prompted us to test A3E in an orthotopic model of GBM. A3E demonstrated a clear inhibitory effect on tumor growth, whereas native EMA401 did not affect tumor size, due to its inability to penetrate the BBB. Moreover, weight (a marker of systemic impact of tumor growth) was preserved in mice treated with A3E but not in controls or EMA401 treated mice (Figures 6 and 7).

Overall, this study validates AT2R as a viable therapeutic target in GBM and affirm A3E as a leading candidate for further clinical development. Given the high frequency of AT2R expression, our results support further investigation of the RAS and its therapeutic modulation in GBM.
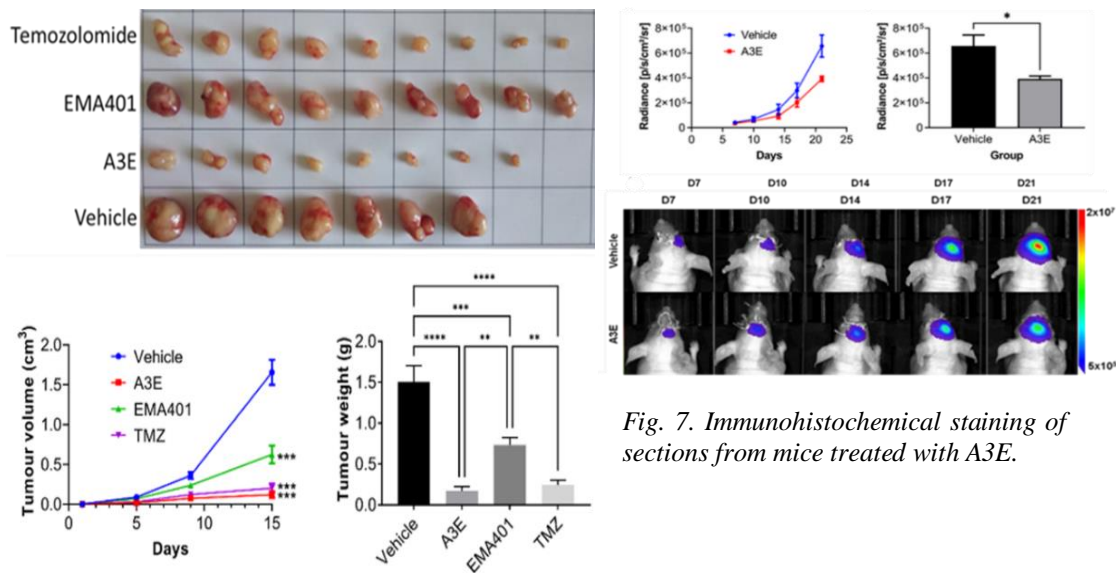
Fig. 6. Average volume and weight of subcutaneous U87-GFP/luc tumors in NSG mice after 21 days of treatment with EMA401, A3E, TMZ (30 mg/kg, n = 9) or vehicle.

Fig. 7. Immunohistochemical staining of sections from mice treated with A3E.

Acknowledgments

References

1. Perryman, R., et al. *Proceedings of the National Academy of Sciences* **119**(32), e2116289119 (2022), https://doi.org/10.1073/pnas.2116289119
2. Valenzuela, R., et al. *Cell Death & Disease* **7**(10), e2427-e2427 (2016), https://doi.org/10.1038/cddis.2016.327
3. Renziehausen, A., et al. *Oncogene* **38**(13), 2320-2336 (2019), https://doi.org/10.1038/s41388-018-0563-y
4. Anand, U., et al. *Eur J Pain* **17**(7), 1012-1026 (2013), https://doi.org/10.1002/j.1532-2149.2012.00269.x
5. Wang, L., et al. *J Drug Target* **23**(9), 832-846 (2015), https://doi.org/10.3109/1061186X.2015.1025077
6. Figueiredo, P. et al. *Int J Pharm* **511**(2), 794-803 (2016), https://doi.org/10.1016/j.ijpharm.2016.07.066
7. Gao, H., et al. *Mol Pharm* **11**(8), 2755-2763 (2014), https://doi.org/10.1021/mp500113p

Selection of the Fragments of the BMP-2 Protein.
Components of Materials for Bone Tissue Regeneration

D. Zielinski[1], A. Becht[1], J. Fraczyk[1], M. Kaminska[2], B. Kolesinska[1], and J. Wasko[1]

[1]*Institute of Organic Chemistry, Faculty of Chemistry, Lodz University of Technology, Lodz, 90-924, Poland*
[2]*Division of Biophysics, Institute of Materials Science and Engineering, Lodz University of Technology, Stefanowskiego 1/15, 90-924 Lodz, Poland*

Introduction

Bone morphogenetic protein 2 (BMP-2 Figure 1) belongs to the transforming growth factor β (TGF-β) superfamily that plays essential roles in many processes, including cardiogenesis, neurogenesis, and osteogenesis. BMP-2 by associating with type I receptor BMPR1A and type II receptor BMPR2 initiates the canonical signalling cascade reactions leading to bone and cartilage tissue regeneration. It has been identified and characterized by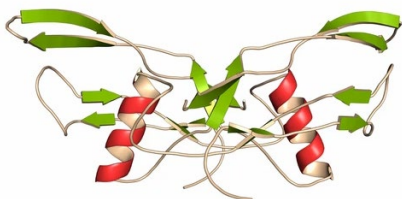 over twenty BMPs in mammals, but the multifaceted action of BMP-2 in tissue regeneration attracts the most attention of scientists [1,2]. This biomolecule consists of 396 amino acids, from which 19 create signaling sequence and its secondary structure is highly ordered, constituted mainly from β-sheet and α-helix chains [3]. BMP-2 is an FDA-approved osteoinductive growth factor applied as a bone graft substitute. Nowadays physicians use INFUSE® Bone Graft, which contains BMP-2 adsorbed to a collagen sponge, during spinal cord injuries treatment [4]. However, after surgery, some undesirable effects such as infections, severe swelling, heterotopic ossification or urogenital problems have been detected in patients [5]. This led to the hypothesis that these adverse events might be eliminated by reducing the delivered growth factor amount to a suitable yet clinically relevant dose. Therefore, the development of a delivery system that provides a sustained release of the protein at sufficient concentrations is a challenge of high priority. On the other hand, it has been searching for new modifications of BMP-2 with lower immunoactivity. One of the approaches postulates finding shorter BMP-2 fragments with high osteoinductive character and selectively interacting with bone morphogenetic protein receptors on mesenchymal stem cells but with less effect on the human immune system [6,7].

Fig. 1. BMP2 structure [3].

This paper will present studies leading to the implementation of the last hypothesis in medical practice. In this aim it has been performed: 1) synthesis of the library of immobilized BMP-2 fragments on cellulose according to SPOT methodology using a triazine coupling reagent and a linker based on 1,3,5-triazine derivatives; 2) selection of BMP-2 fragments reproducing the external sphere of the protein, capable of interacting with specific anti-BMP-2 polyclonal antibodies, in the dot-blot test; 3) synthesis of selected peptides on the 2-chlorotrityl chloride resin, according to Fmoc/tBu methodology, applying triazine coupling reagent (DMT/NMM/TosO⁻); 4) checking the influence and cytotoxicity of the synthesized peptides on cells line; 5) checking the usefulness of BMP-2 fragments useful in regenerative medicine on cell viability.

Results and Discussion

Our studies started from the initial preparation of cellulose matrix, namely its functionalization using 1,3,5-triazine derivative (DCMT) (Figure 2a) [8]. In the next step immobilized on cellulose matrix DCMT was transformed into a triazine-based coupling reagent using *N*-methylmorpholine (NMM) and next treated with Fmoc-glycine to obtain a stable linker for peptide synthesis. At elevated temperature, O → N rearrangement was performed to the stable form of the isocyanurate derivative [9]. Finally, the functionalized cellulose matrix could have been successfully used for SPOT peptide synthesis according to the Fmoc/tBu protection strategy. We synthesized 39 element library of
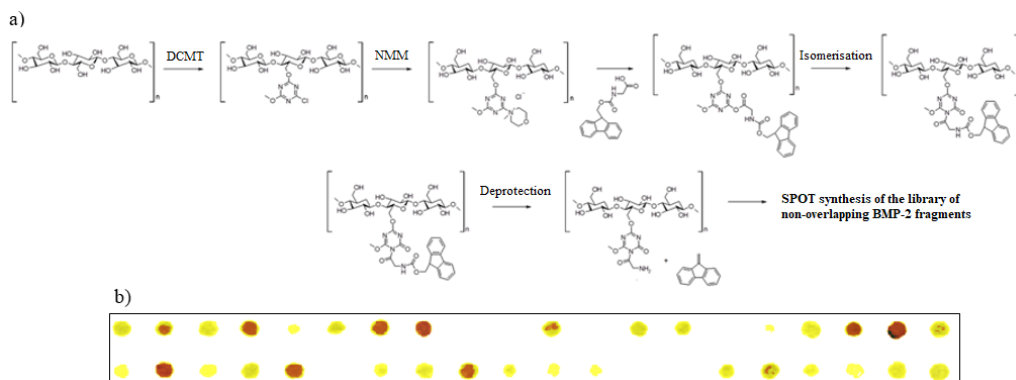
Fig. 2. a) Cellulose functionalization and immobilization BMP-2 fragments library according to SPOT methodology using a linker based on 1,3,5-triazine derivatives (DCMT) and a triazine coupling reagent; b) selection of BMP-2 fragments reproducing the external sphere of the protein in the dot-blot test.

decapeptides and one hexapeptide of BMP-2 which in the next step were treated with polyclonal *anti-*BMP-2 antibodies.

The strength of possible interactions peptide-antibody was determined according to the standard procedure, by measuring the coloration of the spot after treatment with antihuman secondary antibodies labeled with horseradish peroxidase. In the next stage of the research, modelling of the selected nine fragments strongly interacting with polyclonal antibodies was performed. Molecular modeling and optimization of the structure of the BMP-2 protein required the use of an optimized model of the structure of the whole protein (Figure 3). For this purpose, the structure available in the AlphaFold database was used. The model AlphaFold Model AF-P12643-F1 was used. The model of matching the protein structure is very high (pLDDT> 90) or it is characterized by high certainty (90> pLDDT> 70). The use of an optimized protein structure enabled imaging in the Swiss-Pdb Viewer 4.1.0 program [10,11].
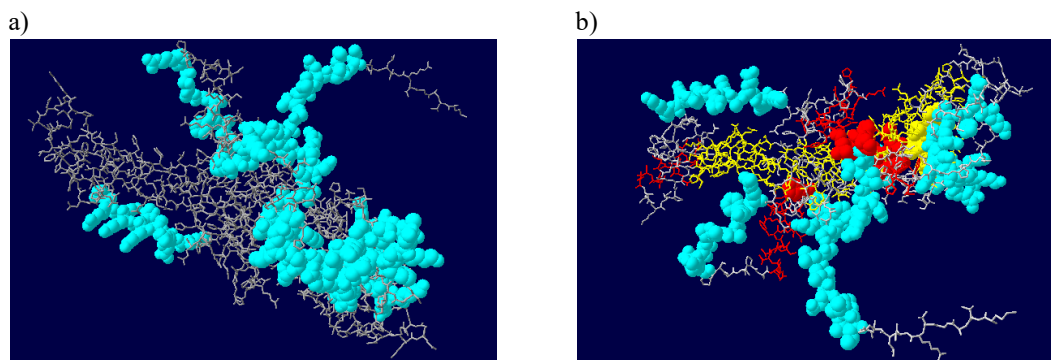
Fig. 3. a) Location of nine strongly interacting fragments with polyclonal antibodies on the structure of BMP-2; b) location of nine fragments strongly interacting with polyclonal antibodies on the structure of BMP-2, taking into account the secondary structure, fragments with β-sheet conformation are marked in yellow, fragments with helical conformation are marked in red.

Based on the structure imaging in the Swiss-Pdb Viewer program, the following secondary structure models were distinguished in the BMP-2: fragments of the alpha helix structure: 47(Asp)-61(Phe), 77(Pro)-87(Ser), 97(His)-103(Ala), 210(Thr)-218(Ala), 254(Glu)-258(Ser), 306(Ser)-308(Phe), 341

194

(Asn)-352(Val) and the fragment with the β-sheet structure: 107(Asn)-112(Phe), 128(Thr)-132(Phe), 144(Phe)-154(Arg), 167(Phe)-177(Ile), 188(Val)-198(Asn), 203(Arg)-209(Val), 225(Gly)-231(Ala), 263(Leu)-269(His), 297(Lys)-304(Phe), 313(Trp)-315(Val), 318(Pro)-326(His), 360(Cys)-367(Ser), 369(Ile)-375(Asp), 389(Val)-396(Arg).

In the fragments selected in the dot-blot test, helical fragments are compacted: 51-61, 77-80, 101-103, 211-218, 341-352 and β-sheet fragments: 107-110, 128-132, 167-176, 188-198, 225-231, 263-269, 297-300, 360-677, 369-370, 389-396.

The applied model of the protein structure confirmed the assumptions that the external sphere of the protein is largely responsible for interactions with polyclonal antibodies. A large area of the protein structure is characterized by a high value of the fitness parameter (pLDDT > 70).

Based on the obtained results we selected 9 decapeptides from the external sphere of BMP-2 which were able to have strong interactions with polyclonal antibodies (Figure 2b). Subsequently, these peptides ([11]LLLPQVLLGG[20], [31]RKFAAASSGR[40], [61]FGLKQRPTPS[70], [71]RDAVVPPYML[80], [171]INIYEIIKPA[180], [181]TANSKFPVTR[190], [211]PAVMRWTAQG[220], [241]KRHVRISRSL[250], [281]KRQAKHKQRK[290]) were synthesized on 2-chlorotrityl chloride resin under SPPS conditions using a triazine coupling agent (DMT/NMM/TosO⁻) [12]. The final monoisotopic masses and purity of products were assessed using high-performance liquid chromatography coupled with electrospray mass spectrometry. It has been found that the purity of the crude products was in the range of 80-98%. The purified BMP-2 fragments were tested for their cytotoxicity against human osteoblasts-femoral (HO-f) and human osteosarcoma (Saos-2) cell lines (Figure 4).
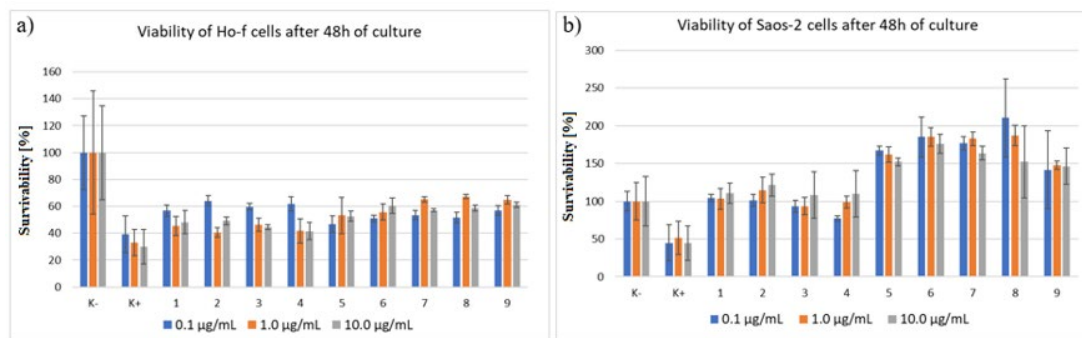

Fig. 4. The survivability diagrams of Ho-f (a) and Saos-2 (b) cells in the presence of BMP-2 fragments.

Cells cultured in a medium without the addition of any substances or harmful agents were used as the Control⁻ (K⁻), while cells treated with DMSO on the second day of incubation were used as the Control⁺ (K⁺). A colorimetric MTT assay was used to estimate the cytotoxicity of peptides. It has been found that the survivability of Ho-f cells in presence of each analyzed peptide was higher in comparison to a positive control (K⁺) (Figure 4a). This was the first important clue that reflects the possible potential of BMP-2 fragments in regenerative medicine. Moreover, the concentration of the peptides had a crucial influence on cell proliferation – its increase not in all cases favoured cell growth. The very interesting results were obtained for the more resistant cell line Saos-2 (Figure 4b). Namely, also in this case, it was observed a remarkable increase in cell survivability, even more than it was noticed for cells cultured in a medium without the addition of any substances (K⁻). Furthermore, for peptides 5-9 cells proliferation was the most effective, which meant that different decapeptides might have differential osteogenic activity.

Based on the results shown in this paper it can be concluded that the triazine coupling reagent was effective both for immobilization BMP-2 fragments on cellulose as well as in SPPS synthesis. Moreover, the selected fragments of the external sphere of BMP-2 can be successfully used as scaffolds in regenerative medicine. On the other hand, the osteogenic activity of the selected peptides might be regulated by their concentration within the damaged tissue. The synthesis of covalent polysaccharide-peptide conjugates as well as biological research are still continuing.

Acknowledgments

References

1. Halloran, D., et al. *J. Dev. Biol*. **8**, 1-3 (2020), https://doi:10.3390/jdb8030019
2. Mandal, C.C., et al. *J. Biol. Chem*. **291**, 1148-1161 (2016), https://doi:10.1074/jbc.M115.668939
3. https://www.uniprot.org/uniprotkb/P12643/entry#structure [access date: 21.09.2022]
4. Mumcuoglu, D., et al. *J. Transl. Sci*. **3**, 1-11 (2017), https://doi:10.15761/JTS.1000195
5. James, A.W., et al. *Tissue Eng. Part* B **22**, 284-297 (2016), https://doi:10.1089/ten.teb.2015.0357
6. Kim, H.K., et al. *Exp. Mol. Med*. **49**, e328 (2017), https://doi:10.1038/emm.2017.40
7. Pountos, I., et al. *BMC Medicine* **14**, 103 (2016) https://doi:10.1186/s12916-016-0646-y
8. Fraczyk, J., et al. *J. Pep. Sci*. **24**, 1-20, (2018), https://doi.10.1002/psc.3063
9. Kaminski, Z.J., et al. *Pol. J. Chem*. **70**, 1316-1323 (1996)
10. Jumper, J., et al. *Nature* **596**, 583-589 (2021), https://doi.org/10.1038/s41586-021-03819-2
11. Varadi, M., et al. *Nucleic Acids Res.* **50**, D439-D444 (2022), https://doi.org/10.1093/nar/gkab1061
12. Kolesinska, B., et al. *Eur. J. Org. Chem*. 401-408 (2015), https://doi.org/10.1002/ejoc.201402862

Amadori and Heyns Rearrangement Products as Possible Galectin-3 Ligands

Andreja Jakas[1], Ramya Ayyalasomayajula[2], and Mare Cudic[2]

[1]Rudjer Bošković Institute, Division of Organic Chemistry and Biochemistry, Bijenička c. 54, 10000 Zagreb, Croatia; [2]Florida Atlantic University, Department of Chemistry and Biochemistry, 777 Glades Rd., Boca Raton, FL 33431, USA

Introduction

The Amadori and Heyns rearrangements are two well-known reactions in carbohydrate chemistry occurring at the first stage of Maillard reaction. The Amadori rearrangement is a reaction between reducing sugars as *a*-hydroxy aldehydes and suitable amines leading to *a*-amino ketones. The introduction of an amino group at position C-1 of aldoses with concomitant isomerization leads to 1-amino-1-deoxyketoses (Figure 1A). The Heyns rearrangement employs ketoses as *a*-hydroxy ketones as starting materials and proceeds *via* a glycosylamine to the corresponding 2-amino-2-deoxyaldoses (Figure 1B). After the cascade of reactions, the final step of Maillard reaction called also the non-enzymatic browning produces advanced glycation end products (AGE). Maillard reaction occurs during the food processing as well as in the human body as a process of aging and especially during disease such as diabetes when the AGE products accumulate causing many problems.

Receptor for advanced glycation end products (RAGE) and its ligands have been considered as important pathogenic triggers for the progression of number of diseases. Preventive and therapeutic strategies focusing on RAGE is of great importance. Galectin-3 has been increasingly recognized as an important modulator of several biological functions, and galectin-3 participates in the pathogenesis of diabetic complications via its receptor function for advanced glycation end-products (AGEs) and advanced lipoxidation end-products (ALEs). We want to investigate the possibility of galectin-3 to react with early stage products of Maillard reaction before AGE formation.

Results and Discussion

In this study, the early products of the Maillard reactions 1-amino-1-deoxyketoses (Amadori compounds) (Figure 1A, **1-5**) [1] and 2-amino-2-deoxyaldoses (Heyns compounds) (Figure 1B, **6-8**) [2] were prepared from the endogenous opioid pentapeptide leucine-enkephalin (YGGFL, **4**), leucine-enkephalin methyl ester (**3**), structurally related tripeptide (YGG, **2**, **6**), amino acid (Y, **1**), and biologically important tetrapeptide LSKL (**5**, **7**, **8**). The strong evidence indicates that galectin-3 participates in the pathogenesis of diabetic complications *via* its receptor function for advanced glycation end-products (AGEs). Thus, the interactions of the early-stage Maillard reaction model compounds (**1-8**) with galectin-3 were investigated by using AlphaScreen competitive binding assay (Figure 2). The affinity level of galectin-3 for Amadori and Heyns compounds depends on sugar moiety, as well on peptide, or amino acid in model compounds.

AlphaScreen utilizes bead-based chemistry to study biological interactions in a high throughput manner in a multi-well format. Binding of molecules captured on the beads leads to a broad energy transfer from one bead to the other, ultimately producing an amplified luminescent/fluorescent signal. We used a histidine (nickel chelate) detection kit from PerkinElmer in this study. His-tagged galectin-3 was bound to nickel chelate acceptor beads (capacity = 600 nM), whereas streptavidin-coated donor beads (capacity = 30 nM) were used to attach to biotin asialofetuin (ASF) [3]. The multivalent glycoprotein ASF, which possesses nine *N*-acetyllactosamine (LacNAc) binding sites, was chosen as the galectin-3 binding partner since the binding constant of galectins for the first LacNAc epitope was reported to be in the nanomolar range with a gradient of decreasing binding constants of the remaining epitopes.

The best results were obtained for Amadori compound **4** and Heyns compound **6** (Figure 3) which suggest the importance of amino acids with aromatic side chains, Tyr and/or Phe, for binding to galectin-3. Interestingly, Amadori compound **3**, bearing the protected *C*-terminal carboxyl group,
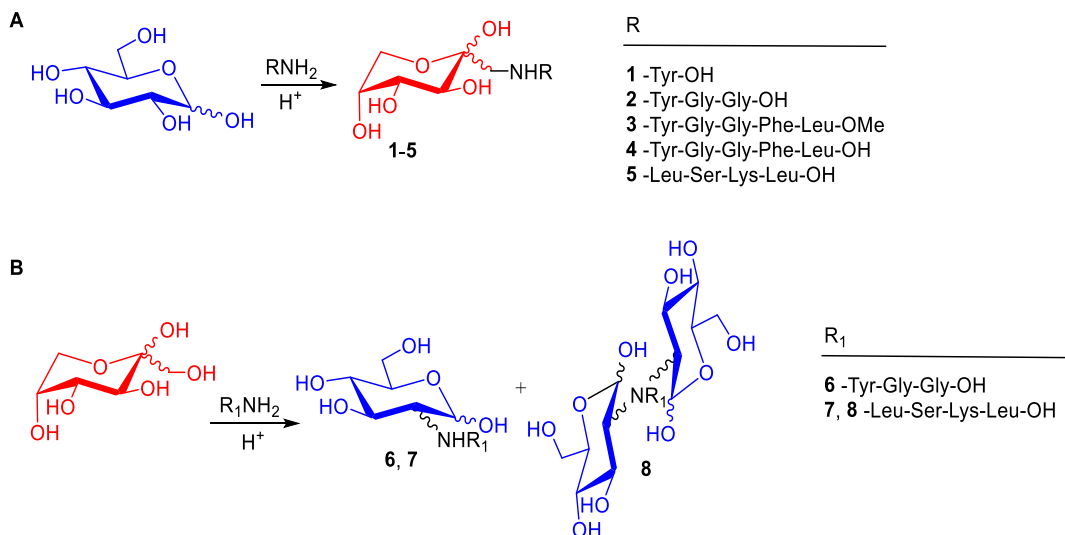
Fig. 1. A) Amadori rearrangement reaction and Amadori products of Y (**1**), YGG (**2**), YGGFL-OMe (**3**), YGGFL (**4**) and LSKL (**5**); B) Heyns rearrangement reaction and Heyns products of YGG (**6**), and LSKL (**7**, **8**).
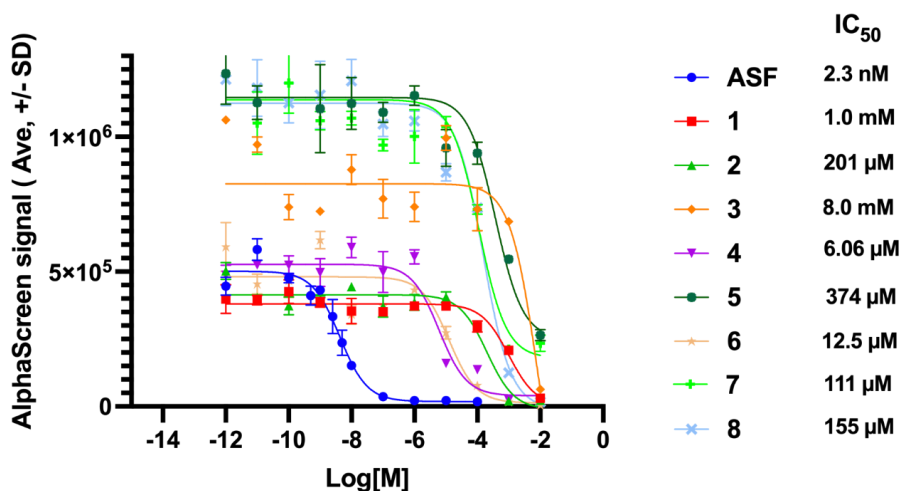
Fig. 2. Inhibition of binding of biotinylated asialofetuin (ASF) (5 nM) to galectin-3 (200 nM) by **1**-**8** (final concentrations of 0–10 mM). The final concentration of the beads was 25 μg/mL. The assay buffer consisted of 25 mM Hepes (pH 7.4) containing 100 mM NaCl and 0.05% Tween 20. Curves, AlphaScreen signal counts (counts per second) vs log [inhibitor, M], were plotted as means of five replicate measurements.

exhibited significant drop in affinity compared to **4**. This underscores the critical role carboxylate plays in improving binding affinity of **4**. Heyns compound **6**, that carries the same peptide sequence as Amadori compound **2**, but differs in sugar moiety, showed higher affinity for galectin-3. Neither Amadori or Hyens compounds of tetrapetide LSKL (**5**, **7**, **8**) showed notable affinity for galectin-3, possibly due to lack of aromatic residues.
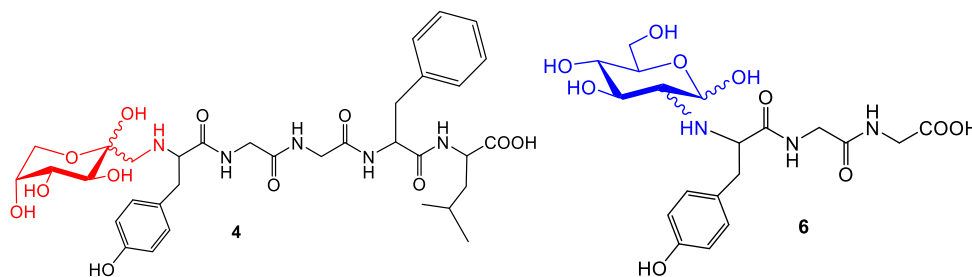
*Fig. 3. The most potent Amadori **4** and Heyns compound **6** for galectin-3 complexation.*

Acknowledgments

References

1. Jakas, A., and Horvat, Š. B*iopolymers* **69**, 421-431 (2003), https://doi.org/10.1002/bip.10338
2. Jakas, A. Katić, A., Bionda, N., and Horvat, Š. *Carbohydr. Res.* **343**, 2475-2480 (2008), https://doi.org/10.1016/j.carres.2008.07.003
3. Yegorova, S., Chavaroche, A.E., Rodriguez, M.C., Minond, D., Cudic, M. *Anal Biochem.* **439**, 123-131 (2013), https://doi.org/10.1002/cbic.201600285

NMR Structural Elucidation of Mannan (Polymannose) Conjugate with the Myelin Oligodendrocyte Glycoprotein 35-55 Epitope (MOG$_{35\text{-}55}$)

Areti Gkika[1], Nikoletta Zoupanou[2], Maria-Eleni Androutsou[3], Thomas Mavromoustakos[2], and Theodore Tselios[1]

[1]*Department of Chemistry, University of Patras, 26504 Rion Patras, Greece; [2]Department of Chemistry, National and Kapodistrian University of Athens, 10679 Athens, Greece; [3]Vianex S.A., 18th km Athens-Lamia National Road, Nea Erythrea, 14671 Athens, Greece*

Abstract

Multiple sclerosis (MS) is a slowly progressive, chronic inflammatory, autoimmune disease of the Central Nervous System (CNS), characterized by destruction of the myelin sheath leading to paralysis and serious health problems [1-4]. The myelin oligodendrocyte glycoprotein MOG is a main myelin protein and is implicated in the progress of MS [1, 5]. The epitope 35-55 from MOG protein is an autoantigen associated with the pathogenesis of MS and the induction of Experimental Autoimmune Encephalomyelitis (EAE; animal model of MS) in mice [5]. Moreover, the conjugate of 35-55 epitope with mannan polysaccharide was found to inhibit the EAE symptoms and could be a promising candidate for MS treatment [6, 7].

Mannose, mannan polysaccharide (Figure 1), oxidized mannan and the conjugates of immunodominant MOG$_{35\text{-}55}$ epitope with mannan in oxidized form were studied by high field nuclear magnetic resonance (NMR) spectroscopy to explore the structural characteristics of mannan and its conjugate with MOG$_{35\text{-}55}$ epitope. This study under progress aims: (a) to detect spatial interactions between MOG$_{35\text{-}55}$ epitope and mannan that possibly determine the active conformation of the complex; (b) stability of the product under storage conditions at room and cold temperatures; (c) degree of oxidized mannan achieved in the synthesis.

Methods

Samples for NMR analysis

The samples used for NMR analysis were mannose, mannan, oxidized mannan and conjugates of oxidized mannan with the immunodominant epitope MOG$_{35\text{-}55}$. Oxidized mannan was synthesized after oxidation of mannan to poly-aldehyde using sodium periodate (NaIO$_4$) and purified by size exclusion chromatography (Sephadex G-25 Medium column) and the conjugates of oxidized mannan with the peptide [KG]$_5$MOG$_{35\text{-}55}$ were synthesized by mixing of the peptide with the oxidized mannan and incubation at room temperature for 48h. The conjugation was achieved by formation of Schiff base between the aldehydes of the oxidized polysaccharide and the free amines of the peptide. The liquid samples of oxidized mannan and conjugates were lyophilized. Two additional conjugates that were stored +5°C and at -20°C for at least 3 years, were also lyophilized. Afterwards all samples mannose (15.25mg), mannan (17.78mg), oxidized mannan (24.72mg) and conjugates (23.91mg, 25.08mg and 25.0mg for fresh, at -20°C and 5°C respectively) were dissolved in 750μL of D$_2$O and 0.67mM NaTMSP (internal reference).

NMR analysis

The experiments were performed, using Agilent Technologies VNMRS 800MHz spectrometer (Bruker Biospin - TCI probe - Four channel AVANCE NEO console). The structural elucidation of samples of mannose, mannan, oxidized mannan and conjugates of oxidized mannan with [KG]$_5$MOG$_{35\text{-}55}$, was achieved by analysis of 1D (^{1}H, ^{13}C) and 2D homonuclear and heteronuclear experiments (2D COSY, 2D ROESY, 2D TOCSY, 2D HSQC and 2D HMBC) (Figure 2).
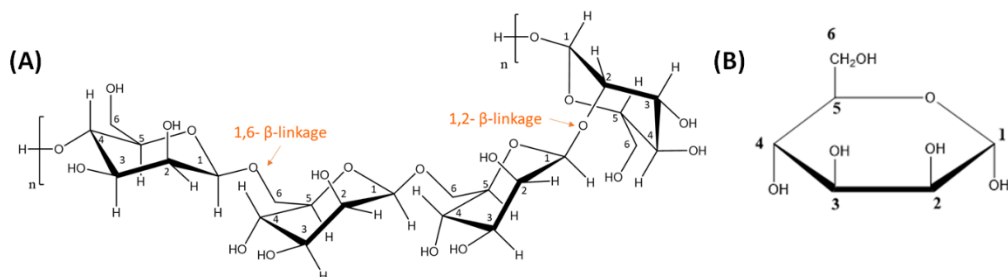
Results

Fig. 1. Structure of mannan from Saccharomyces Cerevisiae (poly-mannose) (**A**); structure of D-mannose (**B**).

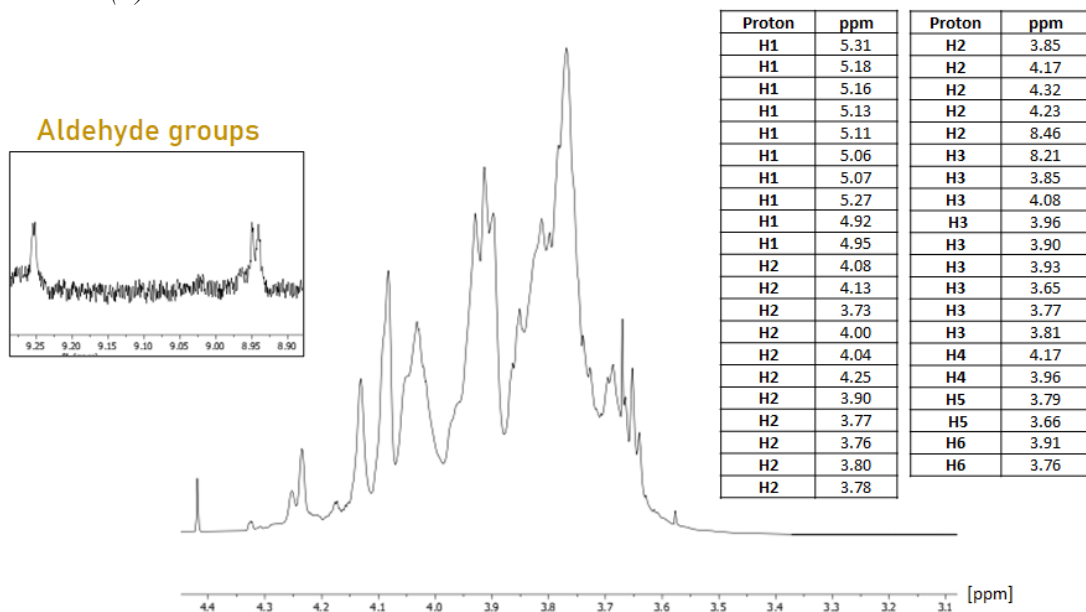| Proton	ppm	Proton	ppm
H1	5.31	H2	3.85
H1	5.18	H2	4.17
H1	5.16	H2	4.32
H1	5.13	H2	4.23
H1	5.11	H2	8.46
H1	5.06	H3	8.21
H1	5.07	H3	3.85
H1	5.27	H3	4.08
H1	4.92	H3	3.96
H1	4.95	H3	3.90
H2	4.08	H3	3.93
H2	4.13	H3	3.65
H2	3.73	H3	3.77
H2	4.00	H3	3.81
H2	4.04	H4	4.17
H2	4.25	H4	3.96
H2	3.90	H5	3.79
H2	3.77	H5	3.66
H2	3.76	H6	3.91
H2	3.80	H6	3.76
H2	3.78		

Fig. 2. Representative part of the 800MHz ^{1}H NMR spectrum of oxidized mannan. Peaks at 8.98ppm and 9.25ppm correspond to aldehyde groups which are formed after the oxidation of mannan with $NaIO_4$. The complexity and overlapping of the ^{1}H NMR peaks constituting the spectrum explains the subtle different environment of the protons. The table includes the chemical shifts (ppm) of the protons of oxidized mannan.

Conclusions

i.   The oxidation of mannan leads to the emergence of two peaks at the ^{1}H NMR which correspond to the formed dialdehyde. These two peaks are not observed after the conjugation reaction of oxidized mannan with the peptide.

ii. The peaks correspond to the Schiff bases which are formed between the amines of the peptide and the aldehydes and are observed at the range 6.0-8.0ppm. In this range are also observed peaks that correspond to the peptide.

iii. The conjugate, based on the NMR spectrum, for the three samples (fresh prepared; at least 3 years stored at +5ºC; at least 3 years stored at -20ºC) is stable under storage conditions.

iv. The degree of oxidation in the oxidized mannan was found after comparison of the aldehyde peak and one anomeric to be 9.7%.

Acknowledgments

References

1. Androutsou, M.E., et al. *Med. Chem*. **14**, 120-128 (2018), https://doi.org/10.2174/1573406413666170906123204
2. Dagkonaki, A., et al. *Front. Immunol*. **11**, 1-18 (2020), https://doi.org/10.3389/fimmu.2020.575451
3. Mantzourani, E.D., et al. *Curr. Med. Chem*. **12**, 1521-1535 (2005), https://doi.org/10.2174/0929867054039053
4. Tapeinou, A., et al. *Eur. J. Med. Chem*. **143**, 621-631 (2018), https://doi.org/10.1016/j.ejmech.2017.11.063
5. Amor, S., et al. *J. Immunol*. **153**, 4349-4356 (1994)
6. Tseveleki, V., et al. L. *Exp Neurol*. **267**, 254-267 (2015), https://doi.org/10.1016/j.expneurol.2014.10.019
7. Tapeinou, A., et al. *Anal Biochem*. **485**, 43-45 (2015), https://doi.org/10.1016/j.ab.2015.06.010

Design, Synthesis, and Characterization of Aza-BODIPY-Peptide Conjugates Derived from LfcinB: Approximation to Photodynamic Therapy

A. Verónica Rodríguez-Mayor[1], Maricela Morales[1], Zuly J. Rivera[2], Javier E. García[2], Norberto Farfan[3], and Rosa Santillan[1]

[1]Departamento de Química- CINVESTAV. 07360, CDMX, México; [2]Facultad de Química, Departamento de Química Orgánica, UNAM. 04510, CDMX, México; [3]Facultad de Ciencias, Universidad Nacional de Colombia, 111321, Bogotá D.C. Colombia

Introduction

In 2020, the World Health Organization had reported 19 million cases of cancer. Among the available treatments for cancer, the most frequently used are surgery, radiotherapy and chemotherapy while immunotherapy and photodynamic therapy have also become available recently [1,2]. In spite of constant efforts to provide treatments that improve the survival and quality of life of people around the world; the high cost, low availability, and adverse side effects require the development of therapeutic alternatives more specific, selective and with less adverse effects [3].

Phototheranostics is a promising strategy for precise tumor treatment. It consists of optical diagnosis, photodynamic therapy, and photothermal therapy. Aza-boron-dipyrromethenes (aza-BODIPYs) are excellent photosensitizer candidates due to their properties such as absorption/emission close to the near-infrared region, potential to generate highly reactive oxygen species and photothermal conversion efficiency. Conjugation of aza-BODIPY photosensitizers with amphiphilic molecules can provide selectivity in target tumor sites, enhanced permeability and retention effect, improving diagnosis and therapeutic efficacy [4].

Peptides have been considered promising candidates for the design and development of anticancer therapeutic agents, in addition to presenting high selectivity for cancer cells and fewer adverse effects. Some promising peptides that have been studied are those derived from Bovine Lactoferricin (LfcinB). LfcinB is an Antimicrobial peptide (AMP) that has shown activity against Gram positive and Gram-negative bacteria, fungi, parasites, viruses, and tumor cells [5-7]. Further studies have shown that the minimum motif with activity is the hexapeptide RRWQWR [8,9] and that peptide derivatives [7,10] containing this sequence show significant activity against bacterial and cancer cell lines.

On the other hand, aza-BODIPY derivatives have shown cytotoxic activity against several cancer lines [11-13] and may be promising therapeutic molecules. The design of molecules with optical properties, such as Boron aza-dipyrromethes (aza BODIPY), is an area of interest currently. These compounds belong to the BODIPY (Boron dipyrromethene) family and are characterized by having a nitrogen atom in the *meso* position of the structure (Figure 1). These compounds are chromophores with characteristics which include: high photostability, structural versatility and the possibility of modifying the periphery of the core allowing to enhance the chemical and optical properties [14].

The possibility to achieve structural diversity and generate molecules with optical and therapeutic properties from a small number of units is attractive. BODIPY-peptide conjugates having low toxicity and high specificity towards target cells, with potential application in phototherapy and imaging [15-17] have been reported, however, to our knowledge, no reports on the conjugation of aza-BODIPYs with peptides have been described.

This work describes the design and synthesis of modified peptides derived from Bovine Lactoferricin (LfcinB) and their conjugation with aza-BODIPY type donor-acceptor-donor molecules with thiophene and methoxy groups. Conjugation of the Aza-BODIPY fragment at the *N*-terminal end of the peptide chain using click chemistry is expected to provide new molecules with favorable optical properties and antitumoral activity that will be evaluated as therapeutic agents in photodynamic therapy.

Results and Discussion

Aza-BODIPY molecules with Donor-Acceptor-Donor architecture were designed to give emission bands shifted towards the NIR by incorporation of electron-donor groups such as amino phenyl, p-methoxyphenyl, and thiophene in the periphery. For conjugation with peptides, we envisioned to functionalize the aza-BODIPYs with maleimide or alkyne groups to obtain monomeric conjugates (with a unit of peptide) or dimeric conjugates (with two units of peptide) (Figure 1).
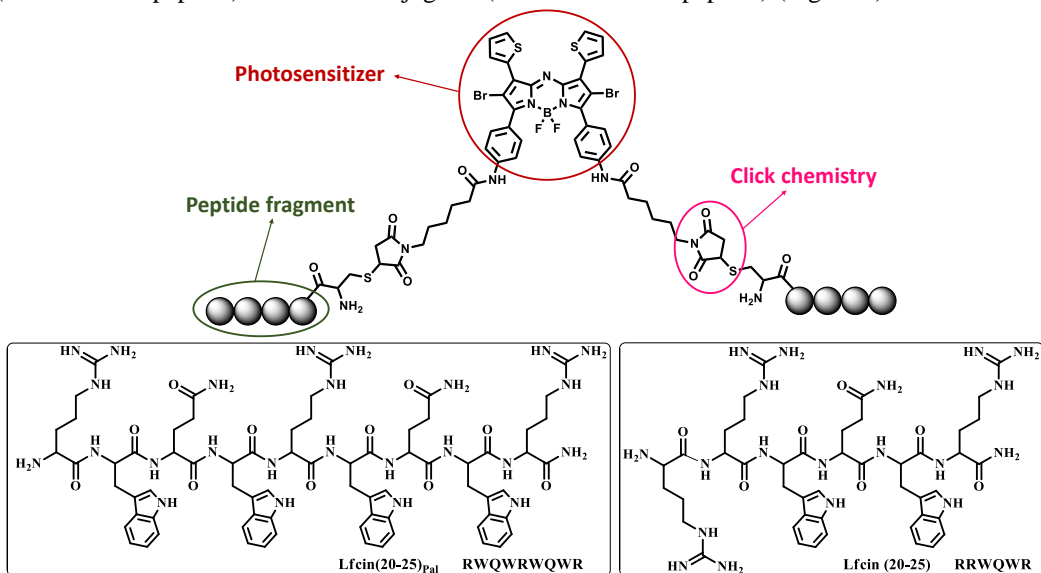

Fig. 1. Structural design of aza-BODIPY-peptide conjugates derived from LfcinB. Peptides Lfcin(20-25) and Lfcin(20-25)$_{pal}$ are represented by circles.

Peptides derived from LfcinB containing cysteine and Lys(N$_3$) residues in the *N*-terminal end, were also designed to be conjugated to aza-BODIPY by click chemistry [18,19]. The peptides were obtained by manual SPPS (Solid Phase Peptide Synthesis) using the Fmoc/tBu strategy and characterized by HPLC and mass spectrometry MALDI-TOF (Table 1).

Table 1. Characterization of peptides HPLC and MALDI-TOF data.fig.

Peptide	Chromatography [a]		Mass Spectrometry	
	$t_{(R)}$ (min)	Area (%)	[M+H]$^+$	m/z
RRWQWR	5.3	99	986,536	985,279
K(N$_3$)-RRWQWR*	5.4	83	1139,631	1139,781
C-RRWQWR*	4.9	97	1088,545	1088,224
RWQWRWQWR	6.9	97	1485,753	1484,589
K(N$_3$)-RWQWRWQWR*	6.8	65	1693,848	1640,678
C-RWQWRWQWR*	6.5	96	1588,762	1589,101

* Crude peptide [a]Peptides were analyzed using a Linear gradient from 5% to 50% of B solvent (ACN-TFA 0.05%) in A solvent (H$_2$O-TFA 0.05%) on Chromolith$^@$ Performance RP-18e column for 8 min

The synthesis of the aza-BODIPY derivatives was carried out by the O'Shea method [20] starting by condensation of *p*-amino-acetophenone or *p*-methoxy-acetophenone to give the α, β-unsaturated ketone, followed obtention of the corresponding nitroketone by Michael addition which upon

cyclization provides the aza-dipyrromethene intermediate. Finally, coordination using boron trifluoride provides the desired aza-BODIPYs which can be conjugated to the peptide molecule using click chemistry.
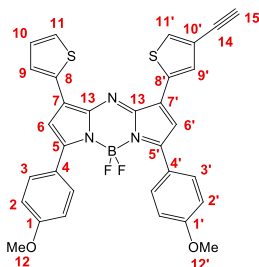

Fig. 2. Aza-BODIPY functionalized with alkyne group.

^{1}H NMR (500 MHz, CDCl$_3$) δ 8.06 and 8.01 (1H each, *J* = 8.9 Hz, H-3 and H3'), 7.91 (d, *J* = 3.8 Hz, 1H, H-11), 7.72 (d, *J* = 3.9 Hz, 1H, H-11'), 7.55 (d, *J* = 5.0 Hz, 1H, H-9), 7.31 (d, *J* = 3.9 Hz, 1H, H-9'), 7.19 (dd, *J* = 5.0, 3.8 Hz, 1H, H-10), 6.99 (1H each, *J* = 8.9, H-2 and H-2'), 6.93 and 6.87 (1H each, H-6 and H-6'), 3.88 (3H each, H-12 and H-12'), 3.54 (s, 1H, H-15).

^{1}H NMR (500 MHz, CDCl$_3$) δ 8.14 (s, 2H, H-12), 7.96 (d, *J* = 8.6 Hz, 4H, H-3), 7.86 (d, *J* = 3.6 Hz, 2H, H-11), 7.58 (d, *J* = 8.6 Hz, 4H, H-2), 7.51 (d, *J* = 5.0 Hz, 2H, H-9), 7.14 (dd, *J* =5.0, 3.6 Hz, 2H, H-10), 6.88 (s, 2H, H-6), 6.63 (s, 4H, H-20), 3.47 (t, *J* = 7.0 Hz, 4H, H-18), 2.60-1.09 (m, 12H).
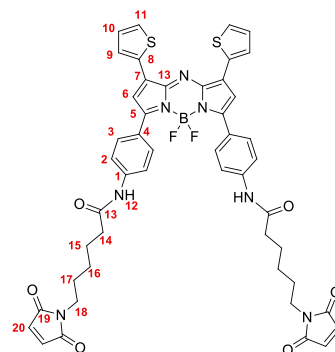

Fig. 3. Aza-BODIPY functionalized with maleimide group.

Two Aza-BODIPY compounds containing alkyne and maleimide groups with donor-acceptor architecture were synthesized and characterized by NMR and MS-ESI. Peptides were synthesized and characterized by HPLC and mass spectrometry MALDI-TOF, obtaining a high chromatographic purity of 95% except for the peptides with Lys(N3) residues which had 83% and 65% chromatographic purity, respectively. The compounds obtained will be halogenated and subsequently will be linked to peptide sequences with anticancer properties to evaluate their cytotoxic activity in photodynamic therapy.

Acknowledgments

References

1. Siegel, R.L., et al. *Cancer J. Clin.* **70,** 7-30 (2020), https://doi.org/10.3322/caac.21590
2. Agostinis, P., et. al. *Cancer J. Clin.* **61**, 250-281 (2011), https://doi.org/10.3322/caac.20114
3. Ferreiro, J.R., et al. *Gac Med Bilbao* **100**, 69-74 (2003),
4. Chen, D.Z. et al. *ACS Appl. Mater. Interfaces* **12**, 26914-26925 (2020), https://doi.org/10.1021/acsami.0c05021
5. Sinha, M., et al. *Int J Pept.* **2013,** 1-46 (2013), https://doi.org/10.1155/2013/390230
6. León-Calvijo, M.A., et al. *Biomed Res. Int.* **2015**, 1-8 (2015), https://doi.org/10.1155/2015/453826
7. Barragán-Cárdenas, A., et al. *RSC Adv.* **10**, 17593-17601 (2020), https://doi.org/10.1039/d0ra02688c
8. Richardson, A., et al. *Biochem. Biophys. Res. Commun.* **388**, 736-741 (2009), https://doi.org/10.1016/j.bbrc.2009.08.083
9. Hilchie, A.L., et al. *Exp. Mol. Pathol.* **95**, 192-198 (2013), https://doi.org/10.1016/j.yexmp.2013.07.006
10. Vargas Casanova, Y., et al. *Molecules,* **22**, 1641-1652 (2017), https://doi.org/10.3390/molecules22101641
11. Treekoon, J., et al. *Org. Biomol. Chem.* **19**, 5867-5875 (2021), https://doi.org/10.1039/d1ob00400j
12. Tian, J., et al. *Chem. Sci.* **6**, 5969-5977 (2015), https://doi.org/10.1039/c5sc01721a

13. Yu, Z.J., et al. *J. Med. Chem.* **63**, 9950-9964 (2020), https://doi.org/10.1021/acs.jmedchem.0c00882
14. Kubheka, G., et al. *Molecules.* **25**, 3689 (2020), https://doi.org/10.3390/molecules25163689
15. Zhao, N., et al. *Bioconjug. Chem.* **28**, 1566-1579 (2017), https://doi.org/10.1021/acs.bioconjchem.7b00211
16. Kaufman, N.E.M., et al. *J. Med. Chem.* **62**, 3323-3335 (2019), https://doi.org/10.1021/acs.jmedchem.8b01746
17. Williams, T.M., et al. *Photochem. Photobiol.* **96**, 581-595 (2020), https://doi.org/10.1111/php.13234
18. Rostovtsev, V.V., et al. *Angew. Chemie - Int. Ed.* **41**, 2596-2599 (2002), https://doi.org/10.1002/1521-3773(20020715)41:14<2596::AID-ANIE2596>3.0.CO;2-4
19. Nair, D.P., et al. *Chem. Mater.* **26**, 724-744 (2014), https://doi.org/10.1021/cm402180t
20. Killoran, J., et al. *Chem. Commun.* **317,** 1862-1863 (2002), https://doi.org/10.1039/b204317c

Overcoming the Challenges in Machine Learning-Guided Antimicrobial Peptide Design

Fabien Plisson

CINVESTAV Unidad Irapuato, Department of Biotechnology and Biochemistry. Km 9.6 Libramiento Norte Carretera Irapuato-León, C.P. 36824 Irapuato, Guanajuato, Mexico

Introduction

Antimicrobial peptides (AMPs) are rich and structurally polypeptide sequences of 12-50 residues that can kill pathogens by either disrupting their membranes or interacting with their intracellular targets [1,2]. Their direct antibacterial activities and the lack of bacterial resistance have stimulated their therapeutic avenues against antibiotic-resistant infections [3]. Major limitations preventing AMPs from translating into clinics are their low metabolic stability, poor oral bioavailability and high toxicity. Reducing hurdles to clinical trials without compromising the therapeutic promises of peptide candidates becomes an essential step in peptide-based drug design. Artificial intelligence (AI) algorithms intertwine predictive and generative models to design optimal AMP sequences rationally [4,5]. Here, we present some of the current challenges to develop robust and fair models for the discovery and design of safe AMPs.
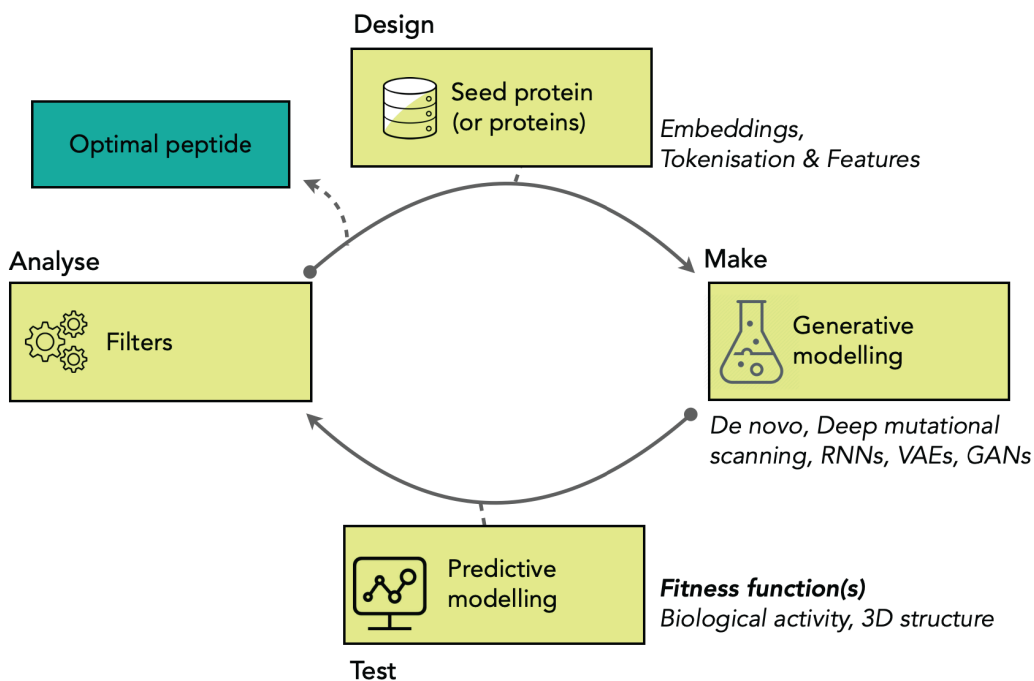

Fig. 1. Streamlining the DMTA cycle for computational peptide design - Machine learning (ML) and deep learning (DL) models are cost-effective and time-saving strategies used to predict biological activities from primary sequences or generate novel sequences.

Results and Discussion

Use the right descriptors. Traditional machine learning (ML) algorithms require features/variables (*e.g.*, amino acid composition, *k*-mers, global physicochemical properties) to illustrate the diversity of peptide sequences and their biological functions. The right "encoding" strategy is key to maximize the performance of ML models [6]. Dimensionality reduction techniques allow the rapid visualization of one or more peptide space(s). In Figure 2, we mapped 56 physicochemical descriptors used to predict the hemolytic activity of antimicrobial peptides and reduced to a bidimensional t-distributed Stochastic Neighbouring Embedding (t-SNE) manifold [7]. On the left side of the figure, we displayed the training set Hemo-PI-1 (N=1,104) and on the right, the testing set Antimicrobial Peptide Database (APD, N=3,081). Our features informed the model to distinguish between hemolytic (purple) and non-hemolytic sequences (orange). Nearly 70% of APD were predicted as hemolytic peptides.
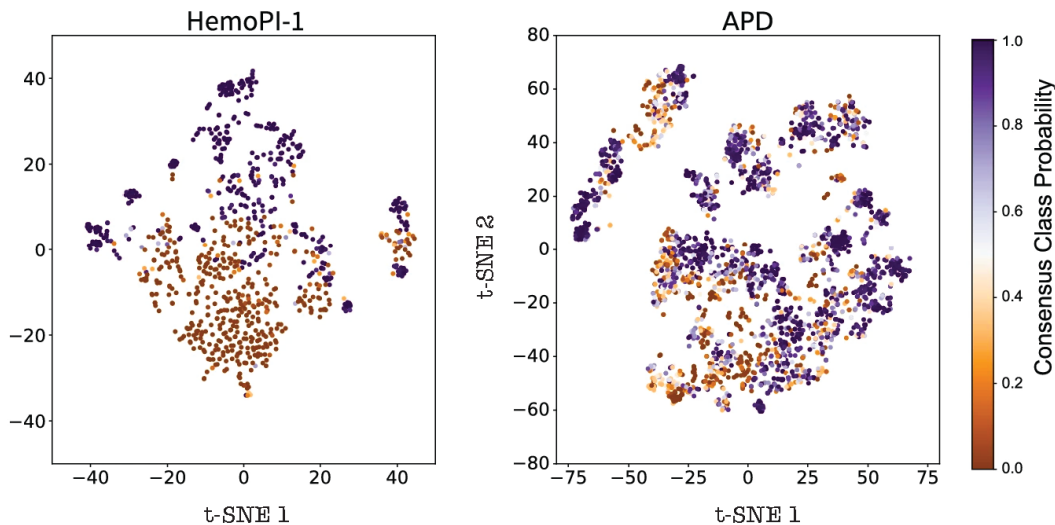

Fig. 2. T-SNE projections showing the distributions of HemoPI-1 training model (left) and APD testing dataset (right) with their respective consensus class probabilities, extracted from [7].

Mitigate imbalance and algorithmic bias. AI-powered peptide models are predominantly built from primary sequences. Sequence homology and structural information are often undermined. Taxonomic bias in AMP predictive models was recently brought to our attention [8] whereas the AMP structural folds remain mostly unknown – only 2.5% have been characterized experimentally (*i.e.*, X-ray or nuclear magnetic resonance) [9]. It is therefore crucial to identify the most reliable, fast, and efficient peptide structure prediction method to estimate the peptide structural landscape. Here, we explored the structural landscape of 5,840 sequences from GRAMPA [10], the Giant Repository of AntiMicrobial Peptide Archive using the Peptide Secondary Structure Prediction method PEP2D [11] for its ability to measure the 3 secondary states (H:Helix, E:Strand or Sheet and C:Coil) over a medium-large dataset of sequences. In Figure 3, we mapped the structural landscape of GRAMPA and its subsets using the 3 secondary states in terms of percentage in a ternary plot. Each face (or axis) of the ternary plot indicates the content of a peptide sequence in a single secondary state. The global AMP structure is represented with a dot at the intersection of the three axes. In Figure 3 (left), we summarized GRAMPA structural landscape where the dataset appeared as predominantly made of alpha-helical structures – highest density between 40 and 80% in helical content. On the right side of the figure, we mapped two GRAMPA subsets with reported antimicrobial activity against Gram-negative bacteria *Escherichia coli*. The top ternary plot shows that the majority of 4,540 sequences are likely to adopt an alpha-helical structure and occupies the same structural landscape than the entire GRAMPA dataset. The bottom ternary plot illustrates the

structural landscape of 3,367 sequences used by Dean and co-workers to train their model against *E. coli*.[12]. In their study, the authors voluntarily excluded cysteine- and proline-rich sequences from the original dataset, which led to a training set entirely made of alpha-helical and coiled structures.
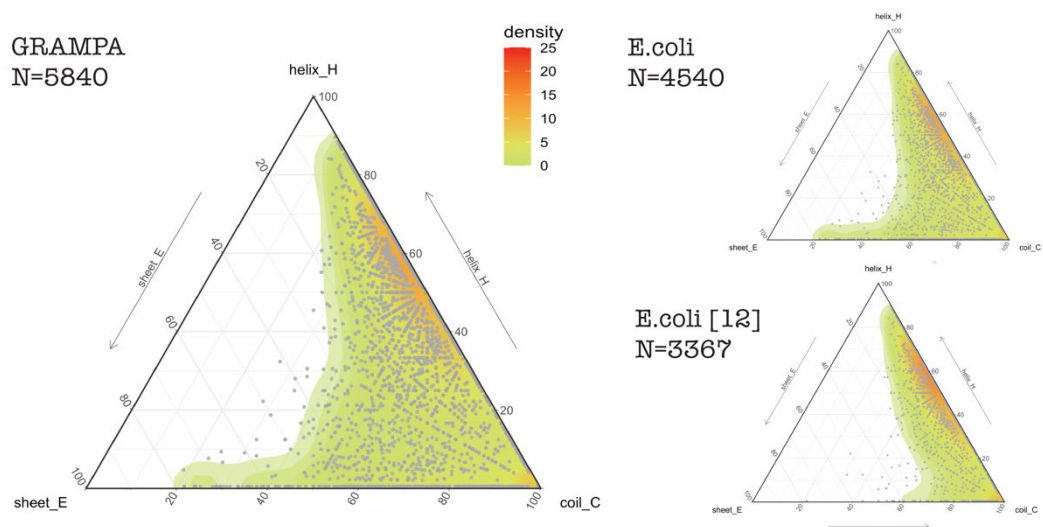

Fig. 3. *Ternary plots showing the structural landscapes of three AMP datasets, i.e., GRAMPA, GRAMPA E.coli subset, E.coli subset[12]. Each landscape is mapped according to the calculated contents (%)) in the three possible secondary structures, namely, helices (H), strands or sheets (E), or coils (C) for each peptide sequence.*
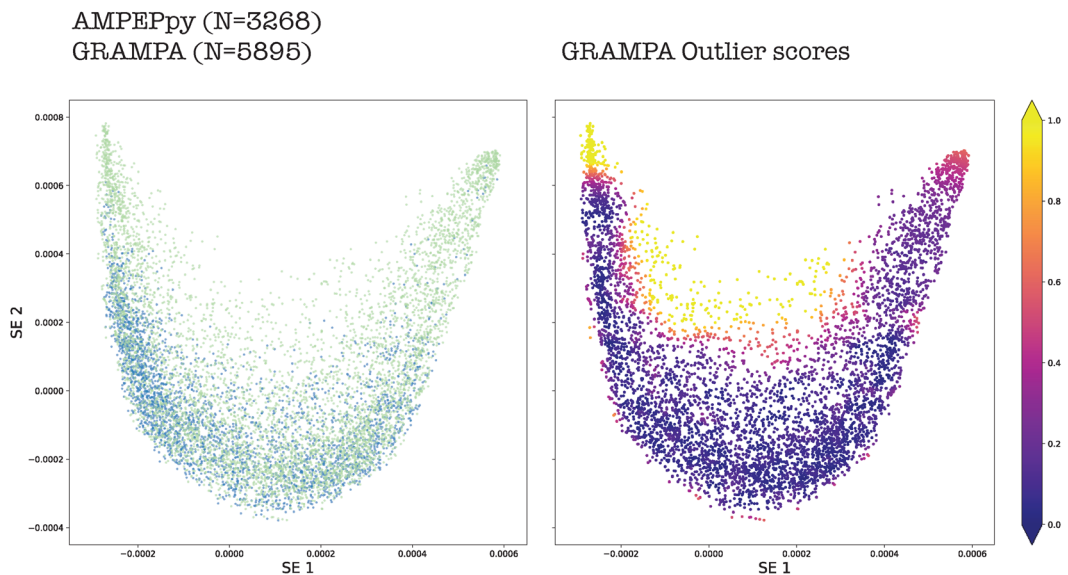

Fig. 4. *Bidimensional spectral embeddings (SE) of two datasets; the positive training set AMPEPpy (N=3,268, blue) and the testing set GRAMPA (N=5,895, green). On the right side, Local Outlier Factor method best detected GRAMPA outliers shown in yellow (outlier score gradient).*

Consider limits of model predictability. Limitations in peptide predictive and generative modeling lie in the diversity of peptide sequences and biological information. Detecting the boundaries of the applicability domain (sequence space where predictions are considered reliable) is key to build robust AI models. It implies identifying the peptide sequences "within-distribution" (inliers) and "out-of-distribution" (outliers). We co-ranked several dimensionality reduction techniques including principal component analysis, t-SNE and spectral embedding. In Figure 4 (left), we described two datasets – positive training set AMPEPpy (N=3,268, blue) [13] and GRAMPA (N=5,895, green) after reducing 83.9 millions of pairwise Smith-Watermann distances into bidimensional spectral embeddings (SE). We implemented multivariate outlier detection methods with Python module PyOD [14] to the reduced peptide sequence space, and we associated an outlier score (gradient) to each sequence. In Figure 4 (right), we displayed the results after applying the Local Outlier Factor method that best detected GRAMPA outliers shown in yellow.

Acknowledgments

References

1. Hancock, R. & Sahl, H.G. *Nature Biotech.* **24**, 1551-1557 (2006), https://doi.org/10.1038/nbt1267
2. Nguyen, L.T., Haney, E.F., & Vogel, H.J. *Trends in Biotechnology* **29** (9), 464-472 (2011), https://doi.org/10.1016/j.tibtech.2011.05.001
3. Haney, E.F., Straus, S.K., & Hancock, R. *Frontiers in chemistry* **7**, 43 (2019), https://doi.org/10.3389/fchem.2019.00043
4. Fjell, C., Hiss, J., Hancock, R., & Schneider, G. *Nature Reviews Drug Discovery* **11**, 37-51 (2012), https://doi.org/10.1038/nrd3591
5. Melo, M.C.R., Maasch, J.R.M.A., & de la Fuente-Nunez, C. *Communications Biology* **4**, 1050 (2021), https://doi.org/10.1038/s42003-021-02586-0
6. Erjavac, I., Kalafatovic, D., & Mauša, G. *Artificial Intelligence in Life Sciences* **2**, 100034 (2022), https://doi.org/10.1016/j.ailsci.2022.100034
7. Plisson, F., Ramírez-Sánchez, O., & Martínez-Hernández, C. *Scientific Reports* **10**, 16581 (2020), https://doi.org/10.1038/s41598-020-73644-6
8. Rázai, Z., Kiss, J., & Nagy, N.A. *Scientific Reports* **11**, 17924 (2021), https://doi.org/10.1038/s41598-021-97415-z
9. Van Oort, C.M., Ferrell, J.B., Remington, J.M., Wshah, S., & Li, J. *Journal of Chemical Information and Modelling* **61**(5), 2198-2207 (2021), https://doi.org/10.1021/acs.jcim.0c01441
10. Witten, J. & Witten, Z. *bioRxiv* 692681 (2019), https://doi.org/10.1101/692681
11. Singh, H., Singh, S., & Raghava G.P.S. *bioRxiv* 558791 (2019), https://doi.org/10.1101/558791
12. Dean, S.N., Alvarez, J.A.E., Zabetakis, D., Walper, S.A., & Malanoski, A.P. *Frontiers in Microbiology* **12**, 725727 (2021), https://doi.org/10.3389/fmicb.2021.725727
13. Lawrence, T.J., Carper, D.L., Spangler, M.K., Carrell, A.A., Rush, T.A., Minter, S., Weston, D.J., & Labbé, J.L. *Bioinformatics (Oxford, England)* **37**(14), 2058-2060 (2021), https://doi.org/10.1093/bioinformatics/btaa917
14. Zhao, Y., Nasrullah, Z., & Li, Z. *Journal of Machine Learning Research* **20**(96), 1-7 (2019), https://jmlr.org/papers/v20/19-011.html

Synthesis, Conformation, and Electrochemical Studies of Dap Homo-Peptides and their Ferrocenyl-Conjugates

Barbara Biondi[1], Annalisa Bisello[2], Roberta Cardena[2], Renato Schiesari[2], Marco Crisma[1], Marzio Rancan[3], Saverio Santi[2], and Fernando Formaggio[1,2]

[1]CNR-Institute of Biomolecular Chemistry, Padova, 35131 Padova, Italy; [2]Department of Chemical Sciences, University of Padova, Padova, 35131, Italy; [3]CNR-Institute of Condensed Matter Chemistry and Technologies for Energy (ICMATE), Padova, 35131 Padova, Italy

Introduction

Electron transfer processes in proteins depend primarily on the distance between the centres involved but are heavily mediated by the nature of the amino acid side chains, by backbone conformations and H-bonds [1-3]. In particular, the macrodipole moment generated by ordered structures (*e.g.*, helices) appears to play a relevant role. In this contribution we report synthesis and analyses of new ferrocenyl-peptide systems (Figure 1), characterized by helical homo-peptide spacers (Dap), with pendant ferrocenyl (Fc) moieties [4].
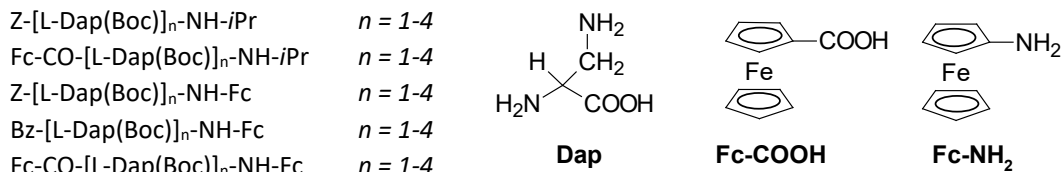
Z-[L-Dap(Boc)]$_n$-NH-*i*Pr   *n = 1-4*
Fc-CO-[L-Dap(Boc)]$_n$-NH-*i*Pr   *n = 1-4*
Z-[L-Dap(Boc)]$_n$-NH-Fc   *n = 1-4*
Bz-[L-Dap(Boc)]$_n$-NH-Fc   *n = 1-4*
Fc-CO-[L-Dap(Boc)]$_n$-NH-Fc   *n = 1-4*

Dap   **Fc-COOH**   **Fc-NH$_2$**

Fig. 1. Chemical structures of the Fc-peptide conjugates synthesized and studied in this work.

Results and Discussion

Synthesis and conformation

All syntheses were performed in solution as previously reported [5,6]. SPPS is feasible [7], but we chose the stepwise solution synthesis as it allowed us to study peptides of intermediate length as well. Our peptides adopt β-turn/3$_{10}$-helical conformations both in solution and in the crystal state. In particular, we solved the X-ray crystal structures for Fc-CO-[L-Dap(Boc)]$_2$-NH-Fc [8] and for Bz-[L-Dap(Boc)]$_2$-NH-Fc (Figure 2, left) [4]. Both dipeptides maintain the same conformation in chloroform solution, as assessed by 2D NMR techniques [4,8]. In particular, they form a β-turn, stabilized by an intramolecular H-bond. In addition, two *intraresidue* H-bonds are observed: they connect the side-chain CO of each Dap residue to its α-NH. The FT-IR analysis as well [4,8] points to the formation of helical structures in the same solvent of the NMR measurements.

Cyclic Voltammetry

In a 3$_{10}$- or α-helix, the carbonyl groups generate a macrodipole, with the positive pole oriented towards the *N*-terminus, that strongly affects the oxidation potential of the metal group. By elongating the peptide chain, oxidation in the Fc-CO-[L-Dap(Boc)]$_n$-NH-*i*Pr series becomes more difficult, whereas in the Z-[L-Dap(Boc)]$_n$-NH-Fc becomes easier (Figure 2, right) [4]. This effect is due to the peptide macrodipole, thus confirming the helical conformation.
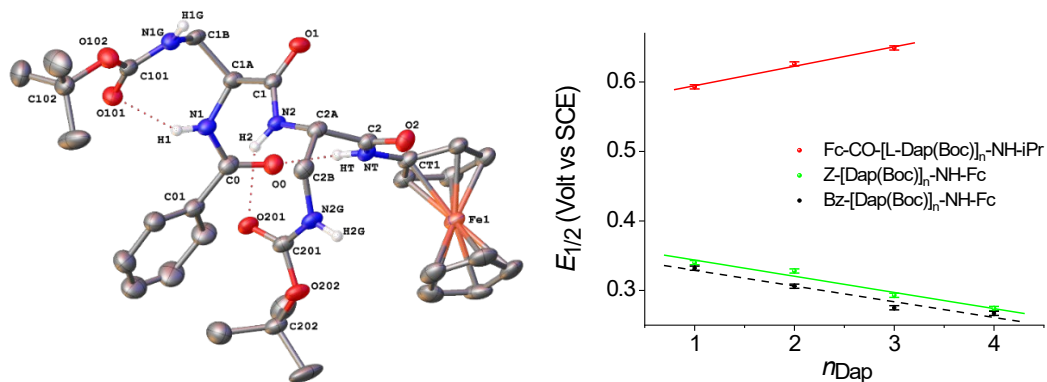
Fig. 2. **Left**: *X-Ray diffraction structure of Bz-[L-Dap(Boc)]₂-NH-Fc, with atom numbering (from ref. 4, with permission). H-atoms of the ferrocene unit, aliphatic carbon atoms and benzyl ring are omitted for clarity. H-bonds are indicated by dotted red lines.* **Right**: *variation in oxidation potentials of Z-[L-Dap (Boc)]ₙ-NH-Fc (n = 1-4), Bz-[L-Dap(Boc)]ₙ-NH-Fc (n = 1-4), and Fc-CO-[L-Dap (Boc)]ₙ-NH-iPr (n = 1-3). Each potential is obtained as the mean value of manifold measures (error bars ± 3 mV) (from ref. 4, with permission).*

Conclusions

Conformational studies in solution (¹H NMR, IR, and CD) and in the crystal state (X-ray diffraction) revealed the tendency of side-chain protected, Dap homo-peptides to adopt β-turn or helical conformations. Our cyclic voltammetry and spectroscopic (UV-Vis variations upon oxidation, not shown) analyses, [4,8] performed to map the peptide-mediated charge transfer, highlighted the influence of the molecular skeleton on the redox and optical properties of the molecules.

Acknowledgments

References

1. Donoli, A., Marcuzzo, V., Moretto, A., Crisma, M., Toniolo, C., Cardena, R., Bisello, A., Santi, S. *Biopolymers* **100**, 14-24 (2013), https://doi.org/10.1002/bip.22197
2. Donoli, A., Marcuzzo, V., Moretto, A., Toniolo, C., Cardena, R., Bisello, A., Santi S. *Org. Lett.* **13**, 1282-1285 (2011), https://doi.org/10.1021/ol102864s
3. Antonello, S., Formaggio, F., Moretto, A., Toniolo, C., Maran, F. *J. Am. Chem. Soc.* **125**, 2874-2875 (2003), https://doi.org/10.1021/ja029787e
4. Biondi, B., Bisello, A., Cardena, R., Schiesari, R., Facci, M., Cerveson, L., Rancan, M., Formaggio, F., Santi, S. *Eur. J. Inorg. Chem.* e202100966 (2022), https://doi.org/10.1002/ejic.202100966
5. Santi, S., Bisello, A., Cardena, R., Tomelleri, S., Schiesari, R., Biondi, B., Crisma, M., Formaggio, F. *ChemPlusChem* **86**, 723-730 (2021), https://doi.org/10.1002/cplu.202100072
6. Biondi, B., Cardena, R., Bisello, A., Schiesari, R., Cerveson, L., Facci, M., Rancan, M., Formaggio, F., Santi, S. *ChemElectroChem* **8**, 2693-2700 (2021), https://doi.org/10.1002/celc.202100597
7. Slootweg, J.C., Prochnow, P., Bobersky, S., Bandow, J.E., Metzler-Nolte, N. *Eur. J. Inorg. Chem.* 360-367 (2017), https://doi.org/10.1002/ejic.201600799
8. Santi, S., Biondi, B., Bisello, A., Cardena, R., Schiesari, R., Tomelleri, S., Crisma, M., Formaggio, F. *Molecules* (2022), accepted for publication.

Synthesis and Analysis of Structure-Activity Relationship of Antimicrobial Peptide Conjugates Incorporating a Plant Defence Elicitor

Gerard Riesco-Llach[1], Pau Caravaca-Fuentes[1,2], Àngel Oliveras[1], Sergio Gil-Caballero[3], Esther Badosa[2], Anna Bonaterra[2], Emilio Montesinos[2], Marta Planas[1], and Lidia Feliu[1]

[1]*LIPPSO, Department of Chemistry, University of Girona, Girona, 17003, Spain;*
[2]*Laboratory of Plant Pathology, Institute of Food and Agricultural Technology-CIDSAV-XaRTA,*
University of Girona, Girona, 17003, Spain; [3]*Serveis Tècnics de Recerca (NMR),*
University of Girona, Parc Científic i Tecnològic, Girona, 17003, Spain

Introduction

According to United Nations, it is expected that at the end of this century the world population will rise to more than 10 thousand million. In this context, agriculture will face major challenges in terms of food production. One of the main threats are plant diseases caused by bacteria and fungi which have a huge impact on crop production involving important economic loses. It is worth noting that there are not many effective methods to tackle some of these diseases, and the antibiotics available are not authorized in Europe. Within this field, antimicrobial peptides have attracted much attention as new agents to control phytopathogens: apart from being more environmentally friendly than traditional pesticides they are less prone to causing the appearance of resistant strains [1].

Different strategies have been described to enhance the biological profile of antimicrobial peptides such as the incorporation of a fatty acid chain to increase the interaction with bacterial membranes or even the combination of two peptides with different biological activity to obtain a new bifunctional sequence [2,3,4].

In our group we have recently reported the synthesis of peptide conjugates incorporating an antimicrobial sequence, derived from the lead peptide **BP100** (KKLFKKILKYL-NH$_2$), and a plant defense elicitor. These conjugates were screened for their antimicrobial activity against bacterial pathogens, their hemolytic activity, and their effect on plant defense gene expression [5].

Based on the promising biological activity profile exhibited by this collection of peptide conjugates, the aim of this work was to perform a structure-activity relationship analysis. For this purpose, we selected 6 peptide conjugates including highly and poorly active sequences and with a range of hemolysis to relate their biological activity with physicochemical parameters that govern their mechanism of action.

Results and Discussion

Peptide conjugates were designed by combining an antimicrobial peptide (**BP16**, **BP100**, or **BP475**) at the *N*- or *C*- terminus of a reported plant defence elicitor peptide (**flg15**, **BP13** or **Pep13**). Their synthesis was performed on solid phase following a 9-fluorenylmethoxycarbonyl (Fmoc)/*tert*-butyl (*t*Bu) strategy using a ChemMatrix resin as solid support. For the preparation of peptide amides, a Fmoc-Rink amide linker was employed, whereas a PAC linker was used for those containing a carboxylic acid at the *C*-terminus. Peptide elongation was carried out through sequential steps of Fmoc removal with piperidine/DMF and coupling of the protected amino acids with *N*,*N*- diisopropylcarbodiimide (DIC) and ethyl 2-cyano-2-(hydroxyimino)acetate (Oxyma). For the sequences incorporating a fatty acid at the side-chain of a lysine (**BP475**), this residue was incorporated as Fmoc-Lys(ivDde)-OH. The 1-(4,4-dimethyl-2,6-dioxocyclohex-1-ylidine)-3-methylbutyl (ivDde) group was chosen because it is stable to the treatments with piperidine and can be removed with hydrazine, allowing the selective derivatization of this residue. Finally, an acidolytic cleavage afforded the expected peptide conjugates which after purification were obtained in excellent HPLC purities and were characterized by ESI-HRMS (Table 1).

Table 1. Sequences of the peptide conjugates, HPLC retention times (t_R) and purities, and mass spectrometry results.

Peptide conjugate	Sequence[a]	t_R (min)	Purity (%)	ESI-HRMS
flg15-BP475	Ac-RINSAKDDAAGLQIA-KKLfKKILKK(COC$_3$H$_7$)L-NH$_2$	6.79	97	1511.4329
BP475-flg15	Ac-KKLfKKILKK(COC$_3$H$_7$)L-RINSAKDDAAGLQIA-OH	6.03	>99	1511.9271
Pep13-BP100	VWNQPVRGFKVYE-KKLFKKILKYL-NH$_2$	6.14	>99	1512.4007
BP100-Pep13	KKLFKKILKYL-VWNQPVRGFKVYE-OH	5.53	>99	1512.8950
BP13-BP16	FKLFKKILKVL-KKLFKKILKKL-NH$_2$	7.85	>99	1372.4666
BP16-BP13	KKLFKKILKKL-FKLFKKILKVL-NH$_2$	7.68	>99	1372.4627

[a]COC$_3$H$_7$, butanoyl. *Lowercase letters correspond to* D-*amino acids*

Peptide conjugates were tested *in vitro* against six plant pathogenic bacteria: *Xanthomonas axonopodis* pv. vesicatoria (*Xav*), *Xanthomonas fragariae* (*Xf*), *Xanthomonas arboricola* pv. pruni (*Xap*), *Erwinia amylovora* (*Ea*), *Pseudomonas syringae* pv. syringae (*Pss*) and *Pseudomonas syringae* pv. actinidiae (*Psa*). For all of them, the minimum inhibitory concentration (MIC) was determined (Figure 1A). Peptides incorporating **flg15** or **Pep13** were more active against these phytopathogens than those containing **BP13**. In particular, **flg15-BP475**, **BP475-flg15**, **Pep13-BP100** and **BP100-Pep13** exhibited MIC values <6.2 µM against at least five of the bacteria tested. Moreover, the hemolytic activity of the peptides was assessed by determining hemoglobin release from erythrocytes at 150 µM peptide concentration (Figure 1B). In this case, peptide conjugates derived from **BP13** were the most hemolytic, with hemolysis >85%. In contrast, **BP475-flg15** was not hemolytic and the other conjugates showed hemolysis between 25 and 45%.

These biological results can be related to physicochemical parameters of the peptide conjugates such as the charge, the hydrophobicity, or the secondary structure that they adopt. In this context, we elucidated the structure of six peptide conjugates by NMR in presence of 30% CF$_3$CD$_2$OD (TFE-d$_3$). The secondary structure was predicted by the Chemical Shift Index based on the ^{1}H-, ^{13}C- and ^{15}N-chemical shifts and was confirmed by NOESY and TOCSY correlations [6].

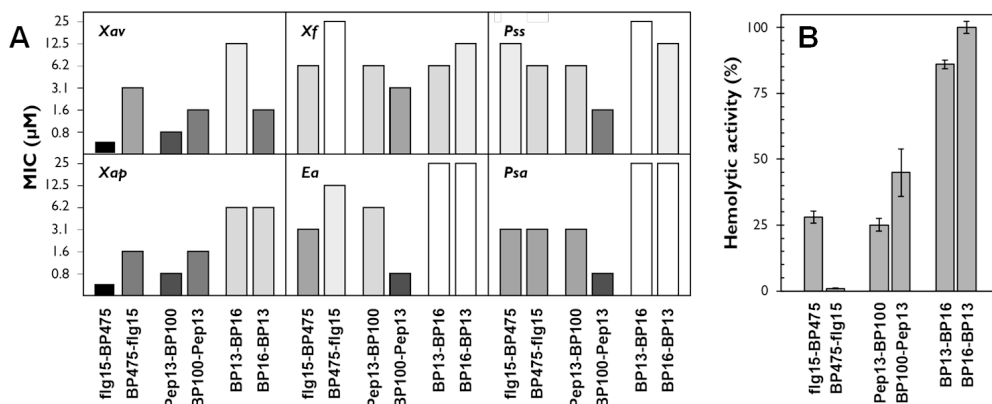*Fig. 1. A) Antibacterial activity (MIC) of selected peptide conjugates against Xanthomonas axonopodis pv. vesicatoria (Xav), Xanthomonas fragariae (Xf), Xanthomonas arboricola pv. pruni (Xap), Erwinia amylovora (Ea), Pseudomonas syringae pv. syringae (Pss) and Pseudomonas syringae pv. actinidiae (Psa). For each sequence the lowest value of the MIC range is represented. B) Hemolysis of the peptide conjugates at 150 µM, expressed as a percentage compared to melittin.*
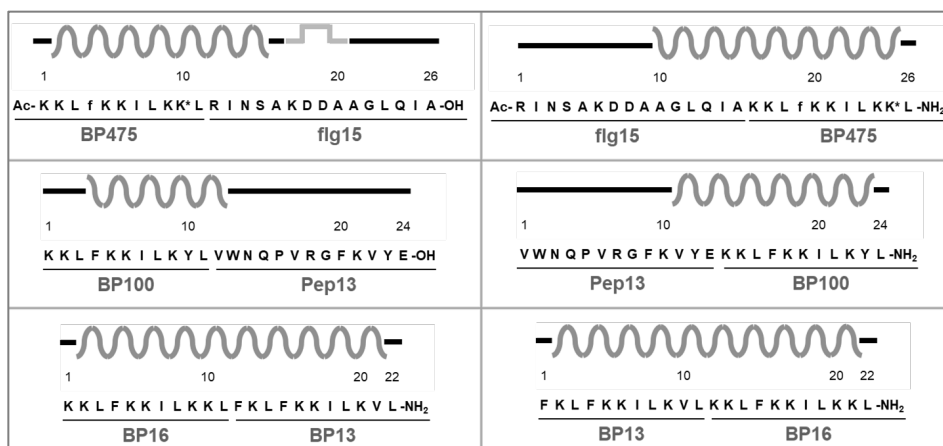
*Fig. 2. Schematic representation of the secondary structure of peptide conjugates predicted by NMR. Dark grey curves mark the α-helical region; grey lines β-turns; and black lines assign residues in a random coil. Lipopeptide **BP475** incorporates a butanoyl group at the side-chain of the lysine with an asterisk, and a D-Phe which is written in lowercase letter.*

As shown in Figure 2, in **flg15-BP475, flg15-BP475, Pep13-BP100** and **BP100-Pep13**, the most active peptide, the antimicrobial fragment (**BP475** or **BP100**) folded into an α helix, whereas the elicitor moiety (**flg15** or **Pep13**) remained unstructured as a random coil. In addition, these peptides have a low hydrophobic moment (0.12-0.33) and a positive charge of +5 or +6. In contrast, **BP13-BP16** and **BP16-BP13**, which showed the worst biological activity profile were completely structured as an α helix and have significantly higher hydrophobicity (>0.80) and charge (+10).

Furthermore, peptide conjugate **flg15-BP475** was characterized by NMR in presence of anionic SDS-d_{25} and zwitterionic DPC-d_{38} micelles to mimic biological membranes. Results showed a similar Hα chemical shift to that observed in presence of 30% CF_3CD_2OD, thus displaying a similar folding. These results point out that TFE constitutes a suitable solvent to analyze these peptide conjugates. Moreover, NMR results were in agreement with those obtained from circular dichroism (Figure 3A), suggesting that in all conditions tested, except for in water, **flg15-BP475** partially folds into an α-helix.

In order to analyze the interactions of the folded peptide **flg15-BP475** with the environment, we used Mn^{2+} as a hydrophilic paramagnetic probe, which results in the selective quenching of the solvent-
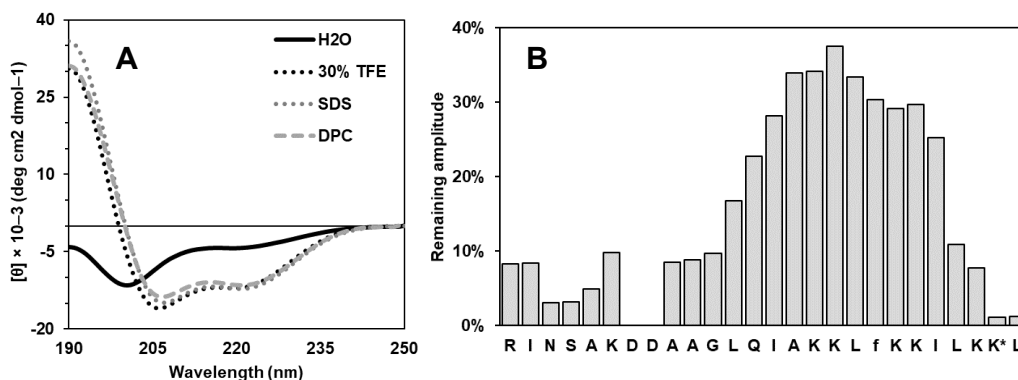

*Fig. 3. A) Circular dichroism of **flg15-BP475** B) Relative change of intensities of Hα-NH TOCSY cross peaks acquired in DPC micelles after the addition of $MnCl_2$.*

exposed residues [7]. The relative change in the intensity of the signals was quantified by determining the remaining amplitude in the Hα/NH TOCSY cross-peaks before and after the addition of MnCl$_2$ (Figure 3B). Residues Ala[10] to Lys[24], that fold into an α-helix, are less exposed to the solvent and, thus, strongly interact with the micelles, showing a remaining amplitude of the cross peaks >10% after the addition of Mn^{2+}.

Overall, this study suggests the importance of a moderate amphipathic character and a positive charge around +5 for an optimal biological profile. In future works, we expect to relate all these physicochemical parameters with the mechanism of action of these peptide conjugates.

Acknowledgments

References

1. Kumar, P., Kizhakkedathu, J.N., Straus, S.K. *Biomolecules* **8**, 1-24 (2018), http://dx.doi.org/10.3390/biom8010004
2. Badosa, E., Planas, M., Feliu, L., Montesinos, L., Bonaterra, A., Montesinos, E. *Microorganisms* **10**, 1784 (2022), http://dx.doi.org/10.3390/microorganisms10091784
3. Oliveras, À., Baró, A., Montesinos, L., Badosa, E., Montesinos, E., Feliu, L., Planas, M. *PLoS ONE* **13**, e0201571 (2018), http://dx.doi.org/10.1371/journal.pone.0201571
4. Oliveras, À., Moll, L., Riesco-Llach, G., Tolosa-Canudas, A., Gil-Caballero, S., Badosa, E., Bonaterra, A., Montesinos, E., Planas, M., Feliu, L. *Int. J. Mol. Sci.* **22**, 6631 (2021), http://dx.doi.org/10.3390/ijms22126631
5. Oliveras, À., Camó, C., Caravaca-Fuentes, P., Moll, L., Riesco-Llach, G., Gil-Caballero, S., Badosa, E., Bonaterra, A., Montesinos, E., Feliu, L., Planas, M. *Appl. Environ. Microbiol.* **88**, e0057422 (2022), http://dx.doi.org/10.1128/aem.00574-22
6. Hafsa, N.E., Arndt, D., Wishart, D.S. *Nucleic Acids Res.* **43**, 370-377 (2015), http://dx.doi.org/10.1093/nar/gkv494
7. Pandit, G., Ilyas, H., Ghosh, S., Bidkar, A.P., Mohid, S.A., Bhunia, A., Satpati, P., Chatterjee, S. *J. Med. Chem.* **61**, 7614-7629 (2018), http://dx.doi.org/10.1021/acs.jmedchem.8b00353

Binding of Captopril and Bioactive Tripeptides Val-Pro-Pro and Ile-Pro-Pro to Angiotensin I-Converting Enzyme (ACE I): Insights from DFT

B. Yakimova[1,2], S. Angelova[3], and I. Stoineva[1]

[1]*Institute of Organic Chemistry with Centre of Phytochemistry, Bulgarian Academy of Sciences, 1113 Sofia, Bulgaria;* [2]*Institute of Neurobiology, Bulgarian Academy of Sciences, Sofia, 1113, Bulgaria;* [3]*Institute of Optical Materials and Technologies "Acad. J. Malinowski", Bulgarian Academy of Sciences, 1113 Sofia Bulgaria*

Introduction

Hypertension, or high blood pressure, is one of the most important risk factors for cardiovascular disease and death. It is a common condition that will catch up with most people who live into older age. Angiotensin-I-converting enzyme *(*ACE) inhibitors (Captopril, Enalapril, Lisinopril, Benazepril, Fosinopril, etc.) are a major class of antihypertensive drugs - they are commonly prescribed to treat high blood pressure and related conditions. ACE belongs to the group of zinc peptidases with HEXXH sequence segment or zincins, subdivision gluzincins (with motif His-Glu-Xaa-Xaa-His, Xaa stands for any amino acid) [1,2]. In the HEXXH motif the two His residues, together with the *C*-terminus Glu, ligate the essential zinc atom, and the Glu in the HEXXH motif has a catalytic function [3]. Possible alternative therapies for treatment of (pre)hypertension are nutraceuticals and functional foods that claim some physiological benefits. For example, food-derived proteins release variety of bioactive peptides which are similar in structure to peptide sequences acting in the organism and therefore can modulate their physiological functions. It emerges that milk-derived peptides Val-Pro-Pro (VPP) and Ile-Pro-Pro (IPP) exert mild inhibitory activity against ACE [4,5]. These peptides have been shown to decrease blood pressure in hypertensive subjects [6] and are expected to play a vital role in the prevention of hypertension and hypertension-related disorders [7,8]. The aim of our *in silico* (DFT) study is to model the binding of milk-derived bioactive tripeptides Val-Pro-Pro and Ile-Pro-Pro and of the pharmaceutical drug Captopril (Figure 1) to the Zn^{2+}-HEXXH metal-binding motif of ACE I.
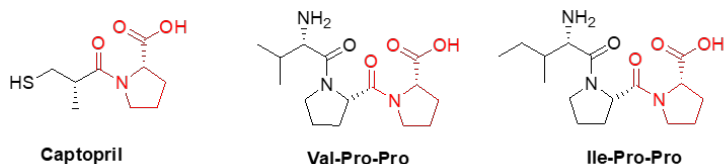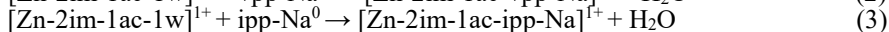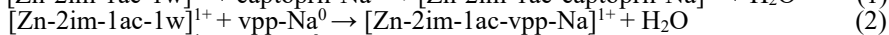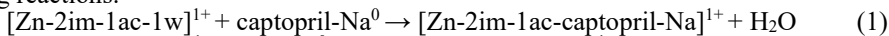

Fig. 1. Molecular structure of Captopril, Val-Pro-Pro and Ile-Pro-Pro.

Results and Discussion

In answering the question which inhibitor (drug or tripeptide) binds more readily to the HEXXH motif, we determined how strong the modeled tetra/penta-coordinated HEXXH motif interacts with the monosodium salts of the inhibitors by examining the change in the Gibbs energy (ΔG) in the following reactions:

$$[\text{Zn-2im-1ac-1w}]^{1+} + \text{captopril-Na}^0 \rightarrow [\text{Zn-2im-1ac-captopril-Na}]^{1+} + H_2O \qquad (1)$$
$$[\text{Zn-2im-1ac-1w}]^{1+} + \text{vpp-Na}^0 \rightarrow [\text{Zn-2im-1ac-vpp-Na}]^{1+} + H_2O \qquad (2)$$
$$[\text{Zn-2im-1ac-1w}]^{1+} + \text{ipp-Na}^0 \rightarrow [\text{Zn-2im-1ac-ipp-Na}]^{1+} + H_2O \qquad (3)$$

To simplify the system, we use models for the amino acid residues that interact with metal cation(s) in the studied centers in a direct manner. The following models were considered (in accordance to the pK_a values of the amino acid side chains [9,10]) for the purpose of the current study: the side chains of usually deprotonated Asp/Glu were modeled as acetates (CH_3COO^-), whereas those of the neutral His were represented by methylimidazole ($C_4N_2H_6$).

B3LYP/6-31+G(3d,p) level of theory was chosen for all molecular electronic structure calculations in the gas phase, $\varepsilon=1$, and in protein environment, $\varepsilon=4$. This functional/basis set combination has been recently shown to be reliable in studying the function of the zinc cation in two centers of rhodopsin [11]. Monosodium salts of Captopril, Val-Pro-Pro and Ile-Pro-Pro inhibitors were optimized and these structures were used to build up models of HEXXH motif bound to

inhibitor molecules after a displacement of a water molecule (Figure 2). The arrangement of the amino acid models was preserved in the binding site/inhibitor constructs.

The binding of Captopril with deprotonated sulfhydryl group (such a structure was used in the simulation of the docking interactions of captopril to ACE I [12]) is predicted to be highly favorable, characterized with negative $\Delta G^1/\Delta G^4$ values (-86.3 kcal mol^{-1} and -31.0 kcal mol^{-1}, respectively).

+ captopril-Na^{1-}
- H$_2$O

ΔG^1 = -86.3 kcal mol^{-1}
ΔG^4 = -31.0 kcal mol^{-1}

[Zn-2im-1ac-captopril-Na]^0

[Zn-2im-1ac-1w]$^{1+}$

+ vpp-Na^0
- H$_2$O

ΔG^1 = -13.9 kcal mol^{-1}
ΔG^4 = -1.7 kcal mol^{-1}

[Zn-2im-1ac-vpp-Na]$^{1+}$

+ ipp-Na^0
- H$_2$O

ΔG^1 = -13.6 kcal mol^{-1}
ΔG^4 = -1.3 kcal mol^{-1}
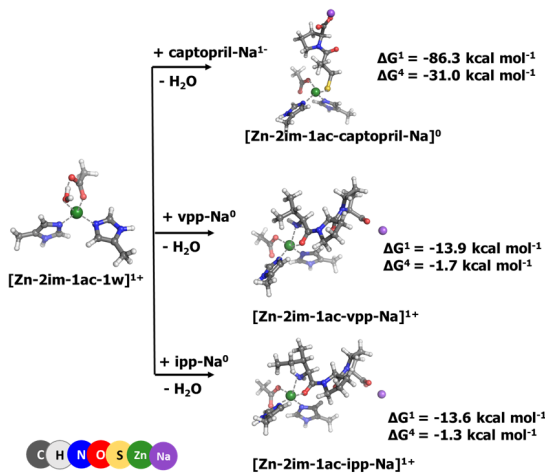
C H N O S Zn Na

[Zn-2im-1ac-ipp-Na]$^{1+}$

Fig. 2. Optimized geometries of the binding site model, [Zn-2im-1ac-1w]$^{1+}$, and binding site/inhibitor constructs. Gibbs energies of complex formation calculated for B3LYP/6-31+G(3d,p) optimized octahedral [Zn-2im-1ac-captopril-Na]$^{1+}$, [Zn-2im-1ac-vpp-Na]$^{1+}$ and [Zn-2im-1ac-ipp-Na]$^{1+}$ structures.

Val-Pro-Pro and Ile-Pro-Pro tripeptides coordinate to the metal cation via the valine's/isoleucine functional groups. Valine and isoleucine (along with leucine), are known as "branched chain amino acids" - they contain nonlinear aliphatic side chains (isopropyl and *sec*-butyl, respectively).

Valine NH$_2$ group plays a significant role in the binding site/inhibitor complex formation and influences the Val-Pro-Pro affinity towards Zn^{2+} binding site [13]. Similar effect can be supposed for the isoleucine NH$_2$ group. For Val-Pro-Pro the interactions with Zn^{2+}-HEXXH binding motif are predicted to be favorable in both the gas phase and protein environment, characterized with negative ΔG^1=-13.9 kcal mol^{-1} and ΔG^4=-1.7 kcal mol^{-1}.

For Ile-Pro-Pro the interactions with Zn^{2+}-HEXXH binding motif are predicted to be favorable in both the gas phase and protein environment, characterized with negative ΔG^1=-13.6 kcal mol^{-1} and ΔG^4=-1.3 kcal mol^{-1}.

The results obtained are in line with the tendency of Zn^{2+} to form complexes readily with S-donor ligands (Captopril). The interactions of Val-Pro-Pro and Ile-Pro-Pro with Zn^{2+}-HEXXH binding motif are expected to be favorable in both the gas phase and protein environment, but the ΔG values are indicative for a much lower activity of the tripeptide (compared to the drug molecule). Val-Pro-Pro and Ile-Pro-Pro do not differ significantly in their affinity for the Zn^{2+}-HEXXH binding motif.

Acknowledgments

References

1. Rawlings, N.D., Barrett, A.J. *Chapter 77 - Introduction: Metallopeptidases and Their Clans*; Rawlings, N. et al. Eds.; Academic Press, 2013; pp 325-370, https://doi.org/10.1016/B978-0-12-382219-2.00077-6
2. Spyroulias, G.A., et al. *Curr. Top. Med. Chem.* **4**(4) (2004), https://doi.org/10.2174/1568026043451294
3. Williams, T.A., Corvol, P., Soubrier, F. *J. Biol. Chem.* **269** (47), 29430-29434 (1994),
4. Yamamoto, N., Takano, T. *Food / Nahrung* **43(**3), 159-164 (1999), https://doi.org/10.1002/(SICI)1521-3803(19990601)43:3<159::AID-FOOD159>3.0.CO;2-R
5. Nonaka, A., et al. *Hypertens. Res.* **37**(8), 703-707 (2014), https://doi.org/10.1038/hr.2014.72
6. Hata, Y., et al. *Am. J. Clin. Nutr.* **64**(5), 767-771 (1996), https://doi.org/10.1093/ajcn/64.5.767
7. Mohanty, D.P., et al. *Saudi J. Biol. Sci.* **23**(5), 577-583 (2016), https://doi.org/10.1016/j.sjbs.2015.06.005
8. Chanson-Rolle, A., Aubin, F., Braesco, V., Hamasaki, T., Kitakaze, M. *PLoS One* **10**(11), e0142235 (2015)
9. Voet, D., Voet, J.G. *Biochemistry*, 4th Edition; John Wiley & Sons, Inc., 2010
10. Daniel, A.G., Farrell, N.P. *Metallomics* **6**, 2230-2241 (2014)
11. Kircheva, N., et al. *Inorg. Chem.* (2020), https://doi.org/10.1021/acs.inorgchem.0c02664
12. Dalkas, G.A., et al. *J. Pept. Sci.* **16**(2), 91-97 (2010), https://doi.org/10.1002/psc.1201
13. Kircheva, N., et al. *Biophys. Chem.* **276**, 106626 (2021), https://doi.org/10.1016/j.bpc.2021.106626

Biomimetic Macrocyclic Inhibitors of Human Cathepsin D

Radka Houštecká[1], Lucie Marešová[-1], Martin Hadzima[1], Jindřich Fanfrlík[1], Jiří Brynda[1], Lenka Pallová[1], Iva Hánová[1], Martin Lepšík[1], Martin Horn[1], Martin Smrčina[2], Pavel Majer[1], and Michael Mareš[1]

[1]*Institute of Organic Chemistry and Biochemistry of the Czech Academy of Sciences, Prague, Czech Republic;*
[2]*Icagen Inc., Tucson Research Center, Oro Valley, USA*

Introduction

Human cathepsin D (CatD), a pepsin-family aspartic protease, plays an important role in tumor progression and metastasis. Here, we report the development of biomimetic inhibitors of CatD as novel tools for regulation of this therapeutic target. We designed a macrocyclic scaffold to mimic the spatial conformation of the minimal pseudo-dipeptide binding motif of pepstatin A, a microbial oligo-peptide inhibitor, in the CatD active

site. A library of more than 30 macrocyclic peptidomimetic inhibitors was employed for scaffold optimization, mapping of subsite interactions, and profiling of inhibitor selectivity. Furthermore, we solved high-resolution crystal structures of three macrocyclic inhibitors with low nanomolar or subnanomolar potency in complex with CatD and determined their binding mode using quantum chemical calculations. The study provides a new structural template and functional profile that can be exploited for design of potential chemotherapeutics that specifically inhibit CatD and related aspartic proteases.
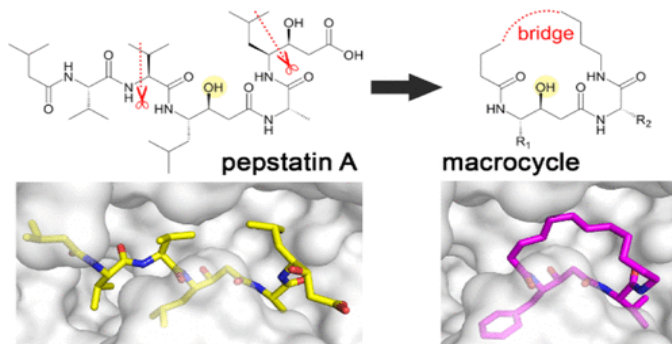
Results and Discussion

- We designed and synthesized a set of macrocyclic peptidomimetic inhibitors that were used for analysis of the macrocyclic scaffold and specificity of S1 and S2′ subsites of HCD (Figure 1).
- The high resolution crystal structures of three macrocyclic inhibitors in complex with HCD were determined. Their binding mode was investigated using quantum chemical calculations (Figure 2).
- The work identified a novel inhibitor scaffold and interaction hot spots that can be exploited for the rational design of specific inhibitors of HCD and related aspartic peptidases as potential chemotherapeutics (Figure 3).

The high affinity of naturally occurring pepstatin A for human CatD makes it an attractive template for biomimetic inhibitor design [1]. Here, we used the crystal structure of the CatD−pepstatin A complex and previously obtained SAR data as guides for rational design of small peptidomimetic inhibitors [2,3]. We aimed to avoid the inherent difficulties connected with use of linear peptides as therapeutics. Linear peptides suffer from poor oral absorption, short duration of action, proteolytic instability, and rapid biliary clearance. In contrast, cyclic peptidomimetics in general have better pharmacokinetic properties and are being increasingly employed in drug development [4-7].

First, we evaluated linear fragments of pepstatin A to assess size requirements for the inhibitory motif. Second, we analyzed pepstatin A bound in the active site of human CatD. The inhibitor adopts a U-shaped conformation with several side chains in positions that can be effectively connected by an aliphatic bridge to impose conformational constraint by cyclization. Based on these data, we designed a functional macrocyclic scaffold with minimized size. High-resolution crystal structures of CatD−macrocycle complexes revealed that this scaffold stabilizes the active site conformation seen in pepstatin A and forms a comparable number of atomic contacts and hydrogen bonds as the larger structure of the parent ligand. Quantum chemical calculations of the interaction energies of

macrocycles demonstrated the critical role of the statin residue, which is correctly positioned in the scaffold to interact with the enzyme catalytic center. The results of the structural analysis are in line with findings that proteases recognize peptide ligands with extended β-strand conformation and that this extended-like conformation can be induced in short peptides by macrocyclization to improve their affinity [8,9].
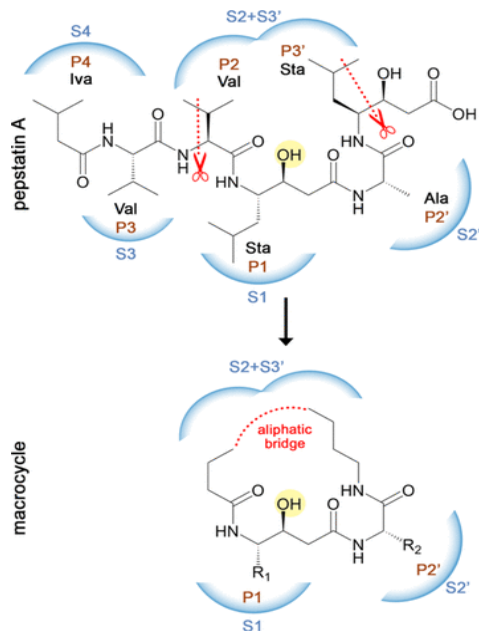
Fig. 1. Schematic representation of the rational design of the macrocyclic inhibitor scaffold. The scaffold mimics the spatial conformation of pepstatin A, a natural linear oligopeptide inhibitor, in the active site of human CatD (PDB: 1LYB). Binding subsites (S) are marked and colored in blue; corresponding inhibitor positions (P) are in brown. The central hydroxyl group of the statine residue that interacts with the catalytic aspartates of CatD is highlighted in yellow. Lines with scissors indicate the region used for macrocycle scaffold design. Pepstatin A structure: Iva-Val-Val-Sta-Ala-Sta, where Iva is isovaleryl and Sta is statine.

We prepared a library of more than 30 macrocyclic compounds (Table 1) with variable bridge size and various side chains in the P1 and P2′ positions. SAR analysis revealed that the minimized scaffold effectively potentiates inhibition, and we identified human CatD inhibitors with low nanomolar and subnanomolar potency. The inhibitor selectivity can be altered by residue substitutions in macrocycles to preferentially target human CatD or its close homologues from the A1 family of aspartic proteases. Notably, the developed compounds display favorable drug-like properties comparable to those reported for other medicinally relevant macrocycles [4-7]. They meet Lipinski's "rule of five" criteria and other physicochemical parameters for drug design that pepstatin A generally does not. Furthermore, the macrocycles are proteolytically stable and noncytotoxic, and parameters such as solubility and cell permeability can be controlled by structural substitutions. In conclusion, we present new biomimetic macrocyclics as a powerful template for further optimization and future development of potential chemotherapeutics against pathologies associated with human CatD and CatD-like proteases.
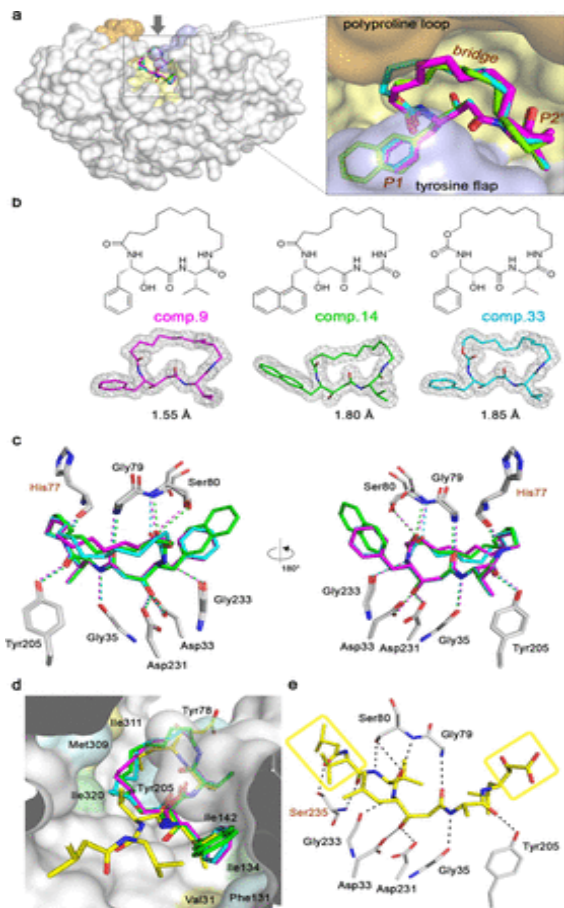
Fig. 2. Crystal structures of human CatD in complex with three macrocyclic inhibitors (*9*, *14*, and *33*, PDB codes 6QCB, 6QBG, and 6QBH). (*a*) Top view of the CatD active site with the superimposed macrocyclic inhibitors. The enzyme is shown as semitransparent surface and the inhibitors as sticks (*9*, magenta; *14*, green; *33*, cyan). The active site residues are colored as follows: Tyr flap residues are pale blue, polyproline loop residues are pale orange, and the rest of the residues are light yellow. (b) Chemical structures and electron density maps of macrocyclic inhibitors. The $2F_o$ - F_c maps are contoured at 1.2σ. (c) Hydrogen bond networks (dashed lines) formed between CatD and macrocyclic inhibitors are shown in two views rotated by 180°. Inhibitors are colored as in (b); interacting enzyme residues are gray. Heteroatoms have standard color coding. (d) Superposition of macrocyclic inhibitors colored as in (b) and pepstatin A (yellow) in the CatD active site. The enzyme is in semitransparent surface representation, and residues that form hydrophobic interactions with inhibitors are highlighted. The residues interacting with the macrocycles are pale cyan, with pepstatin A are yellow, and with both inhibitors are pale green. (e) Hydrogen bond network (dashed lines) formed between CatD and pepstatin A. Pepstatin A is colored yellow; interacting enzyme residues are gray. Yellow boxes indicate segments of pepstatin A that are absent in the macrocycle scaffold. Residues labeled in brown form pepstatin A-specific hydrogen bonds; macrocycle-specific hydrogen bonding is labeled in (c).
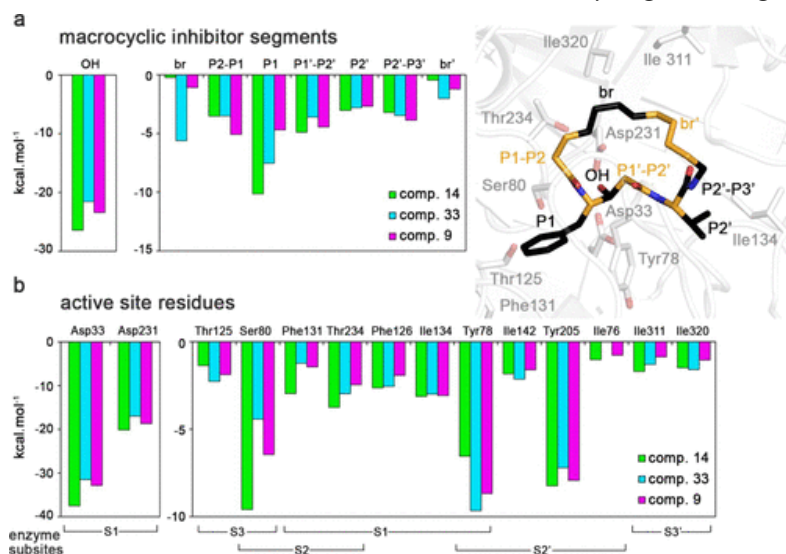

Fig. 3. Quantum chemical calculations of interaction "free" energies of three crystallographically characterized macrocyclic inhibitors in the CatD active site. The 3D view shows fragmentation of an inhibitor into segments (alternating black and orange) and the active site residues of CatD (gray) used for the calculations (PDB code 6QCB). (a) Contributions of individual inhibitor segments. (b) Contributions of the active site residues obtained from a "virtual glycine" scan.

Table 1. Substitution Analysis of Macrocyclic Inhibitors of Human CatD. Compounds with variation at the R_1 substituent (a) and the R_2 substituent (b) are ordered according to their potency.

a

Compound	R_1	IC_{50} (nM)
14	(2-naphthylmethyl)	0.6 ± 0.1
15	(3,4-difluorobenzyl)	3.1 ± 0.6
16	(3,4-dichlorobenzyl)	4.2 ± 0.7
17	(4-fluorobenzyl)	4.7 ± 0.7
9	(benzyl)	5.8 ± 0.7
18	(cyclohexylmethyl)	9.0 ± 0.7
19	(benzylthiomethyl)	20 ± 4
7	(isobutyl)	22 ± 5
20	(4-hydroxybenzyl)	39 ± 9
21	(4-benzyloxybenzyl)	55 ± 5
22	(indol-3-ylmethyl)	190 ± 20
23	(mercaptomethyl)	340 ± 38
24	(thiazolylmethyl)	600 ± 145

b

Compound	R_2	IC_{50} (nM)
25	(pyridin-3-ylmethyl)	1.1 ± 0.2
26	(sec-butylmethyl)	3.8 ± 0.7
9	(isobutyl)	5.8 ± 0.7
27	(cyclohexylmethyl)	8.2 ± 0.7
28	(benzyl)	15 ± 3
29	(acetamidopentyl)	16 ± 1
30	(phenethyl)	27 ± 3
8	(isopropyl)	68 ± 16
31	(2-hydroxypropyl)	500 ± 55
32	(benzyloxymethyl)	560 ± 130

Acknowledgments

References

1. Knight, C.G. *Biochem. J.* **155**, 117-125 (1976), http://dx.doi.org/10.1042/bj1550117
2. Majer, P. *Protein Sci.* **6**, 1458-1466 (1997), http://dx.doi.org/10.1002/pro.5560060710
3. Baldwin, E.T. *Proc. Natl. Acad. Sci. U.S.A.* **90**, 6796-6800 (1993), http://dx.doi.org/10.1073/pnas.90.14.6796
4. Cummings, M.D. *J. Med. Chem.* **62**, 6843-6853 (2019), http://dx.doi.org/10.1021/acs.jmedchem.8b01985
5. Giordanetto, F. *J. Med. Chem.* **57**, 278-295 (2014), http://dx.doi.org/10.1021/jm400887j
6. Marsault, E. *J. Med. Chem.* **54**, 1961-2004 (2011), http://dx.doi.org/10.1021/jm1012374
7. Mallinson, J. *Future Med. Chem.* **4**, 1409-1438 (2012), http://dx.doi.org/10.4155/fmc.12.93
8. Tyndall, J. *Curr. Med. Chem.* **8**, 893-907 (2001), http://dx.doi.org/10.2174/0929867013372715
9. Madala, P.K. *Chem. Rev.* **110**, PR1-PR31 (2010), http://dx.doi.org/10.1021/cr900368a

Bifunctional Opioid-Neuropeptide FF Ligands as Analgesics with Reduced Side Effects

Jolien De Neve[1], Simon Gonzalez[1], Claire Herby[2], Séverine Schneider[2], Valérie Utard[3], Rosine Fellmann-Clauss[3], Khadija Elhabazi[3], Charlotte Martin[1], Frédéric Bihel[2], Frédéric Simonin[3], and Steven Ballet[1]

[1]*Research Group of Organic Chemistry, Department of Bioengineering Sciences and Chemistry, Vrije Universiteit Brussel, Pleinlaan 2, 1050 Brussels, Belgium;* [2]*Laboratoire d'Innovation Thérapeutique, Faculté de Pharmacie, UMR 7200, CNRS Université de Strasbourg, Illkirch, France;* [3]*Biotechnologie et Signalisation Cellulaire, UMR 7242 CNRS, Université de Strasbourg, Illkirch, France*

Introduction

The development of safer analgesics remains one of the main challenges in contemporary medicine. The "gold standard" opioids, used to treat moderate to severe pain, are unavoidably linked to adverse side effects, such as tolerance, respiratory depression, constipation, and physical dependence [1]. All of these side effects have an inevitable impact on the quality of life. To overcome this burden, the development of dual ligands, also called hybrids or bifunctional ligands, has increased over the past decade, more specifically by co-targeting opioid and non-opioid receptors involved in nociception [2,3]. Herein, the aim was to synthesize opioid-neuropeptide FF hybrids with selective G protein signaling over β-arrestin recruitment at the μ-opioid receptor (MOR). G protein signaling is responsible for pain relief, while the β-arrestin recruitment is linked to receptor internalization and, hence, desensitization, and flanked by opioid-induced side effects [3,4,5]. As non-opioid receptors, the neuropeptide FF 1 and 2 receptors (NPFF1/2R) are known to be involved in opioid-induced analgesic tolerance, among other side effects [3]. Interestingly, antagonism of the NPFF1/NPFF2 receptors prevents the increase of analgesic tolerance and opioid-induced hyperalgesia [3,7,8]. After screening a first set of OPFF hybrids [3], a subsequent series based on lead sequence **1** (Figure 1), was developed and underwent biological *in vitro* evaluation. Subsequently, only the best analogues were selected to be tested *in vivo* for an assessment of common opioid side effects.
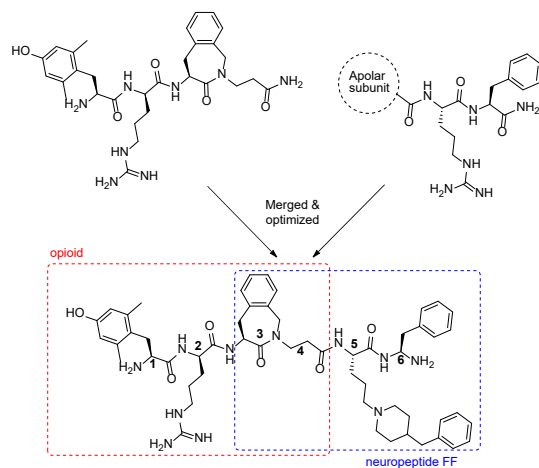

*Fig. 1. Fusion of the opioid peptide **KGOP01** and minimal NPFF pharmacophores led after optimization to the merged lead peptide **1**.*

Results and Discussion [9]

In this study, a new series of opioid-neuropeptide FF (OPFF) hybrids was synthesized, based on the lead peptide **1** (Figure 1). Peptide **1** consists of an opioid pharmacophore: H-Dmt-D-Arg-AbaβAla-, and a NPFF pharmacophore (here Bpa-Phe-NH$_2$). The opioid pharmacophore constituted a previously optimized opioid peptide **KGOP01**, while the standard NPFF pharmacophore consists of RF-NH$_2$ like moieties. This latter one was optimized to provide the Bpa-Phe-NH$_2$ moiety.

All hybrids were synthesized by solid phase peptide synthesis (SPPS) using the classical Fmoc/*t*Bu strategy with the Rink Amide AM resin as solid support. Coupling conditions were HBTU/DIPEA, DIC/Oxyma Pure or DIC/HOBt. The synthesis of Fmoc-Bpa-OH was performed, as previously described [10]. In addition, all constrained dipeptides, incorporated in position 3 & 4, were manually synthesized in our lab, according to known procedures [3,11,12].

Table 1. *In vitro data of the most promising compounds.*

Code	Sequence	MOR		NPFF1	NPFF2
		cAMP EC_{50}/E_{max}	β-arrestin-2 EC_{50}/E_{max}	IC_{50} antagonist IC_{50} binding	IC_{50} antagonist IC_{50} binding
1	H-Dmt-D-Arg-Aba-βAla-Bpa-Phe-NH$_2$	13 ± 3 nM 90 ± 3 %	133 ± 18 nM 43 ± 2 %	≈ 5 μM $K_i = 228 \pm 58$ nM	5 μM $K_i = 7.1 \pm 3.6$ nM
2	H-Dmt-D-Pro-Aba-βAla-Bpa-Phe-NH$_2$	11 ± 1 nM 53 ± 1 %	No recruitment	≈ 5 μM $K_i = 1.1 \pm 0.2$ μM	≈ 5 μM $K_i = 27 \pm 8$ nM
3	H-Dmt-*N*(Me)-D-Ala-1Ana-Gly-Bpa-Phe-NH$_2$	4.9 ± 0.5 nM 76 ± 0.1 %	No recruitment	> 5 μM $K_i = 1.2 \pm 0.01$ μM	≈ 5 μM $K_i = 58 \pm 6$ nM
4	Guanidyl-Dmt-D-Arg-Aba-βAla-Bpa-Phe-NH$_2$	14 ± 2 nM 58 ± 5 %	119 ± 97 nM 15 ± 8 %	< 5 μM $K_i = 85 \pm 0.4$ nM	< 5 μM $K_i = 5.1 \pm 0.9$ nM
5	H-Dmt-*N*(Me)-D-Ala-1Ana-βAla-Bpa-Phe-NH$_2$	4.8 ± 1.8 nM 77 ± 5 %	No recruitment	> 5 μM $K_i = 1.5 \pm 0.2$ μM	> 5 μM $K_i = 38 \pm 3$ nM

Subsequently, the *in vitro* profiles (Table 1) of the OPFF hybrid peptides were determined at the human MOR, by examining the cAMP inhibition and the β-arrestin-2 recruitment. In addition, affinity and activity at the NPFF receptors were tested on the most favorable peptides.

Conclusions

As shown in Table 1, peptides **2-5** presented lowered β-arrestin-2 recruitment, together with a selectivity of NPFF1/NPFF2. Consequently, these peptides were tested *in vivo*. Upon investigation of acute analgesia, all peptides showed a prolonged duration of action, as compared to morphine. Gratifyingly, peptide **5** showed an enhanced analgesic activity, in comparison to the previous lead peptide **1**. In contrast to morphine, preliminary data also indicated that peptide analogues **4** and **5** induce no hyperalgesia. Altogether, the hybrids **4** and **5** were selected as lead compounds to be further evaluated *in vivo* during future endeavors.

Acknowledgments

References

1. De Neve, J., et al. *RSC Med. Chem.* **12(6)**, 828-870 (2021), https://doi.org/10.1039/D1MD00041A
2. Gadais, C., et al. *Molecules* **26(17)**, 5406 (2021), https://doi.org/10.3390/molecules26175406
3. la Rochelle, A.D., et al. *Pain* **159(9)**, 1705-1718 (2018), https://doi.org/10.1097/j.pain.0000000000001262
4. Bohn, L.M., et al. *Science* **286**, 2495-2498 (1999), https://doi.org/10.1126/science.286.5449.2495
5. Raehal, K.M., et al. *J. Pharmacol. Exp. Ther.* **314**, 1195-1201 (2005), https://doi.org/10.1124/jpet.105.087254
6. Raehal, K.M., et al. *Handb. Exp. Pharmacol.* **219**, 427-443 (2014), https://doi.org/10.1007/978-3-642-41199-1_22
7. Elhabazi, K., et al. *Br. J. Pharmacol.* **165**, 424-435 (2012), https://doi.org/10.1111/j.1476-5381.2011.01563.x
8. Simonin, F., et al. *Proc. Natl. Acad. Sci. USA* **103**, 466-471 (2006), https://doi.org/10.1073/pnas.0502090103
9. De Neve, et al. Manuscript in preparation.
10. Schneider, S., et al. *Org. Biomol. Chem.* **13**, 7020-7026 (2015), https://doi.org/10.1039/c5ob00828j
11. Gonzalez, S., et al. *J. Med. Chem.* **63(21)**, 12929-12941 (2020), https://doi.org/10.1021/acs.jmedchem.0c01376
12. Trân, K., et al. *J. Med. Chem.* **64(9)**, 5345-5364 (2021), https://doi.org/10.1021/acs.jmedchem.0c01941

Unveiling Activity Determinants of [10]Panx1

Anne Caufriez[1,2], Arthur Lamouroux[2], Charlotte Martin[2], Andrés Tabernilla[1], Mathieu Vinken[1*], and Steven Ballet[2*]

[1]*Research group of In Vitro Toxicology and Dermato-cosmetology, Department of Pharmaceutical and Pharmacological sciences, Vrije Universiteit Brussel, Brussels,1090, Belgium;* [2]*Research Group of Organic Chemistry, Departments of Chemistry and Bioengineering sciences, Vrije Universiteit Brussel, Brussels,1050, Belgium, * Shared equal seniorship*

Introduction

Pannexin1 channels are heptameric conduits that allow the passage of ions and other molecules such as adenosine triphosphate (ATP) across the cell plasma membrane, thereby playing a role in multiple pathophysiological responses linked to inflammation [1,2]. Although pannexin1 channels are seen as highly interesting drug targets, the search for appropriate blockers is an arduous process [3,4]. As one of the known inhibitors' main problems is specificity, the pannexin1 field turned to peptides [5,6]. To this date, a peptide mimicking a ten amino-acid long sequence of the first extracellular loop of the pannexin1 protein, named [10]Panx1, remains one of the most commonly used pannexin1 channel inhibitor *in vitro*, yet is not fit for *in* vivo purposes because of poor stability [7,8]. The goal of this study was to identify important amino acid side chains of the lead sequence involved in the peptide protein interaction and to pinpoint scissile amide bonds in order to enable a more rational approach for the optimization of the sequence.

Results and Discussion

Important side chains were uncovered through the synthesis and *in vitro* testing of an Ala scan of the [10]Panx1 sequence (Figure 1). All analogs were obtained *via* Fmoc-solid phase peptide synthesis. Subsequently, the peptides were evaluated in an *in vitro* pannexin1 channel assay, in which their capacity to reduce pannexin1-mediated extracellular ATP release was compared with that of the lead sequence, after opening the channels through osmotic shock. Both [10]Panx1 and lanthanum, another well-known inhibitor of pannexin1 channel activity, were included in the assays as controls. *In vitro* testing of the Ala scan showed that replacing glutamine at position three (compound 9) and aspartic acid at position eight (compound 6) of the sequence abolished [10]Panx1's inhibitory potency significantly (Figure 1). Precipitation was observed in the case of the peptide in which glutamine was substituted by alanine. Hence, a more soluble analog was synthesized and compared against the respective control (Figure 1).
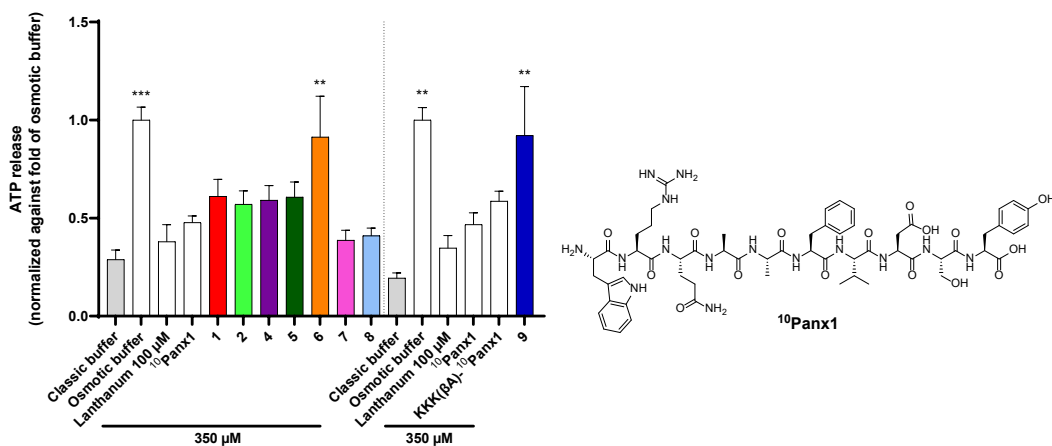

Fig. 1. Structure of the lead sequence [10]Panx1 and evaluation of [10]Panx1 and analogs.

Despite the many advantages of peptides as therapeutics, one of the major drawbacks in the field is proteolytic instability [9]. [10]Panx1, as an unmodified linear peptide, is highly prone to be cleaved by different proteases, as reflected by a half-life of merely a few minutes in human plasma. Well-established techniques such as terminal modification and chiral switches were used to increase proteolytic stability. Both acetylation of the *N*-terminus (compound 12) and *C*-terminal amidation (compound 11) on their own as well as the combination of these two modifications (compound 13) did not alter the inhibitory activity (Figure 2). The latter did however increase the half-life by almost a ten-fold (Figure 2). Chiral switches of the tryptophan created a loss in activity (compound 14), while the opposite holds true for the tyrosine at the *C*-terminus (compound 16). Combining the terminal modifications with the integration of a D-tyrosine (compound 16) increased the plasma half-life up to more than a 20-fold, in comparison to the $t_{1/2}$ of the lead sequence (Figure 2). Additionally, the all D-amino acid containing sequences with (compound 17) and without (compound 10) terminal modifications did not show any loss of activity in the pannexin1 channel assay (Figure 2). In conclusion, we have obtained fully stable [10]Panx1 analogs with a similar inhibitory activity as the lead sequence.
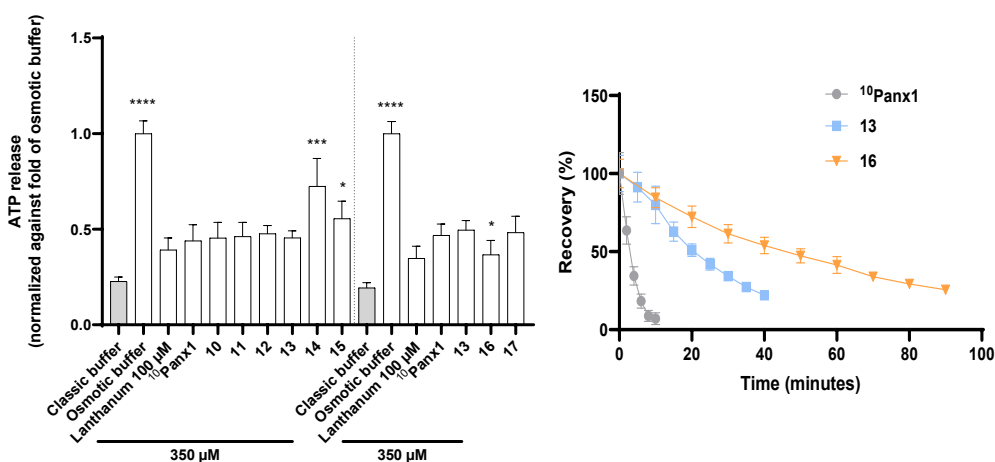
Fig. 2. Inhibitory activity and plasma stability testing of stabilized [10]Panx1 analogs.

Acknowledgments

References

1. Jin, Q., et al. *Cell Research* **30**, 449-451 (2020), https://doi.org/10.1038/s41422-020-0310-0
2. Koval, M., et al. *Purinergic Signalling* **17,** 521-531 (2021)*,* https://doi.org/10.1007/s11302-021-09804-8
3. Dahl, G., et al. *Neuropharmacology* **75**, 583-593 (2013), https://doi.org/10.1016/j.neuropharm.2013.02.019
4. Willebrords, J., et al. *Pharmacology & Therapeutics* **180**, 144-160 (2017), https://doi.org/10.1016/j.pharmthera.2017.07.001
5. Pelegrin, P., and Surprenant, A. *EMBO journal* **25**, 5071-5082 (2006), https://doi.org/10.1038/sj.emboj.7601378
6. Caufriez, A., et al. *Expert Opinion on Drug Discovery* **15**, 1213-1222 (2020), https://doi.org/10.1080/17460441.2020.1773787
7. Pelegrin, P., and Surprenant, A. *J.Biol.Chem.* **282**, 2386-2394 (2007), https://doi.org/10.1074/jbc.M610351200
8. Maes, M., et al. *Archives of Toxicology* **91**, 2245-2261 (2017), https://doi.org/10.1007/s00204-016-1885-6
9. Muttenthaler, M., et al. *Nature Reviews Drug Discovery* **20**, 309-325 (2021), https://doi.org/10.1038/s41573-020-00135-8

Comparison Between Diverse Nitroxide Spin Labels in Synthetically Accessible Peptides

Barbara Biondi[1], Victoria N. Syriamina[2], Antonio Barbon[3], Fernando Formaggio[1,3], Claudio Toniolo[1,3], and Sergei A. Dzuba[2]

[1]CNR-Institute of Biomolecular Chemistry, Padova, 35131 Padova, Italy; [2]RAS-Institute of Chemical Kinetics and Combustion, 630090 Novosibirsk, Russian Federation; [3]Department of Chemical Sciences, University of Padova, 35131 Padova, Italy

Introduction

Site-directed spin labeling (SDSL) in combination with electron paramagnetic resonance (EPR) spectroscopy is a very effective biophysical method to analyze structure and dynamics of proteins under physiological conditions [1,2]. To evaluate the reliability in distance measurements of different spin labels, we designed and synthesized a 20-mer long model peptide and two analogs (Figure 1) with a well-defined Aib-generated, stable α-helical structure. We introduced, at fixed separations (14 residues, about 2.2 nm), two α-amino acid residues of the helicogenic 2,2,6,6-tetramethylpiperidine-1-oxyl-4-amino-4-carboxylic acid (TOAC) or two S-(1-oxyl-2,2,5,5-tetramethyl-2,5-dihydro-1H-pyrrol-3-yl)methyl (MTSL) groups conjugated to cysteines (Cys) in the sequence, respectively (Figure 2). The latter nitroxyl labeling methodology is by far the most widely utilized in protein investigations.

Ac-20-NH$_2$	Ac-Aib-Lys-Aib-Ala-(Aib-Lys-Aib-Ala)$_3$-Aib-Ala-Aib-Lys-NH$_2$	**I**
Ac-[TOAC^{3,17}]-20-NH$_2$	Ac-Aib-Lys-**TOAC**-Ala-(Aib-Lys-Aib-Ala)$_3$-**TOAC**-Ala-Aib-Lys-NH$_2$	**II**
Ac-[Cys(MTSL)^{4,18}]-20-NH$_2$	Ac-Aib-Lys-Aib-Cys(**MSTL**)-(Aib-Lys-Aib-Ala)$_3$-Aib-Cys(**MSTL**)-Aib-Lys-NH$_2$	**III**

Fig. 1. Amino acid sequences of the 20-mer model peptide (I) and its two analogs (II and III).
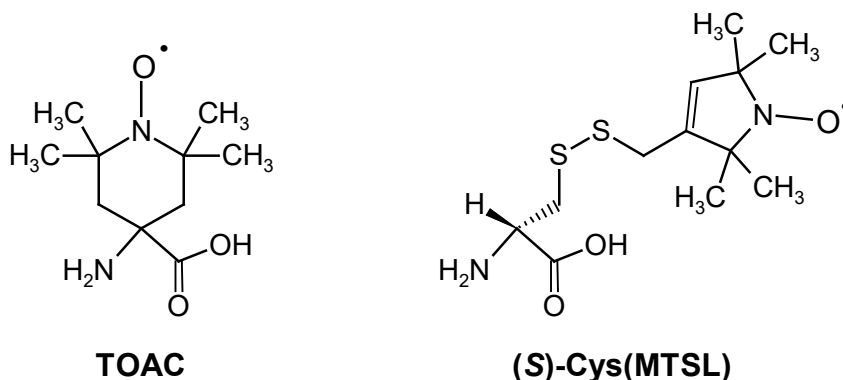

Fig. 2. Chemical structures of the TOAC and (S)-Cys(MTSL) spin labeled residues.

Results and Discussion

Through an in-depth conformational analysis (FT-IR absorption, CD and NMR), we confirmed a stable α-helical structure for all three peptides in different (water, methanol) environments. Our detailed EPR

analysis took advantage from both continuous-wave (CW) and double electron-electron resonance (DEER) experiments. The DEER data indicated a much narrower distance distribution for the TOAC-labeled peptide as compared with that of its MTSL-labeled counterpart (Figure 3). In the latter case, the experimental distance distribution exhibits two maxima which unambiguously point to the existence of two labeled conformers. We conclude that TOAC labels are much more rigid than MTSL labels, therefore providing more precise data on distance distributions in helical peptides.
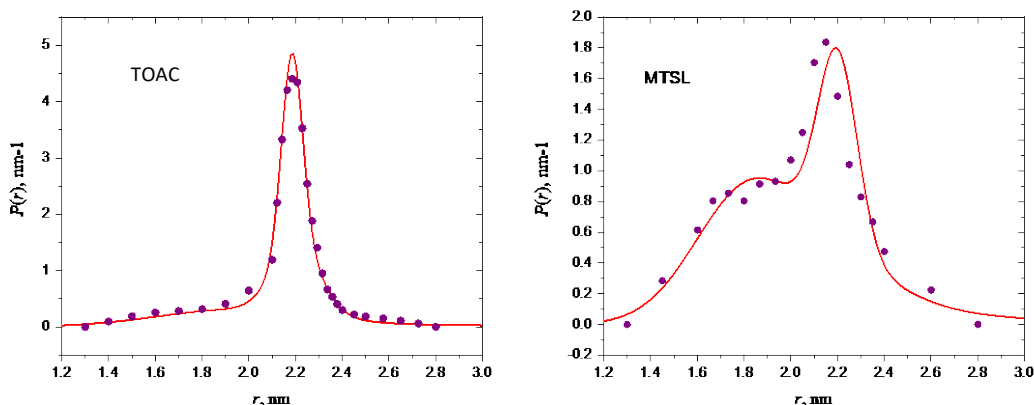
Fig. 3. These representations describe the obtained distance distributions employing the multi-Gaussian approximation (red curve) and the distance discretization (blue points).

Acknowledgments

References

1. Jeschke, G. *Annu. Rev. Phys. Chem.* **63**, 419-446 (2012), https://doi.org/10.1146/annurev-physchem-032511-143716
2. Roser, P., Schmidt, M.J., Drescher, M., Summerer, D. *Org. Biomol. Chem.* **14**, 5468-5476 (2016), https://doi.org/10.1039/C6OB00473C

Design of a Thermostable WW Domain Scaffold

Christina Lindner and Franziska Thomas (PI)

Institute of Organic Chemistry, Heidelberg University, Heidelberg, 69120, Germany

Introduction

The current goal of research in the field of synthetic chemistry is the design and production of peptide- and protein structures that function as biological synthesis machines [1]. At the beginning of the *de novo* design of peptide catalysts, the focus was set on α-helical structural motifs such as the coiled coil [2]. Based on the fact that these are relatively rigid and self-assembling scaffolds, current scientific efforts are on the design of smaller single chain β-sheet motifs such as the WW domain [3-7].

In this project, the WW domain was selected as potential scaffold for the design of miniaturized enzymes due to its properties as a small independently folding protein motif. It is a protein interaction module with 34-40 amino acid residues and has a flexible binding site [8] (Figure 1).
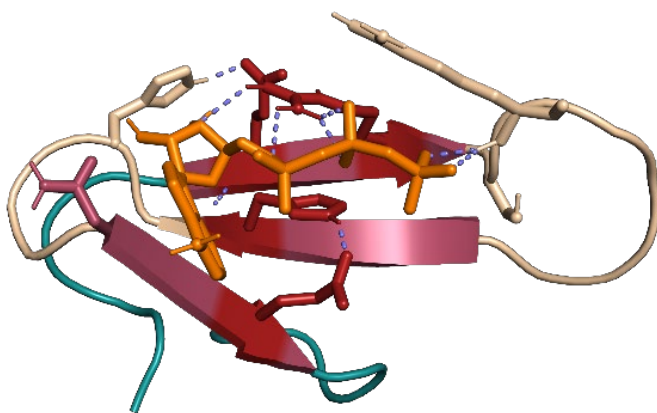
Fig. 1. Visual representation of a designed ATP-binding WW domain [9]. The graph was created in PyMol, the N-&-C-terminus are displayed in green, the β-sheets in raspberry, the loops in wheat color and the ATP in orange. The important binding residues of the WW domain peptide are shown in red, whereas the polar contacts are violet.

Results and Discussion

To establish the WW domain as a scaffold, it is important to deepen the knowledge of the sequence-to-structure-to-function relationships and to investigate the possibilities of binding pocket engineering. Thus, binding- and structure relevant amino acid residues on variable sequence positions were identified based on the generation of a consensus sequence by aligning the sequences of 85 WW domains. This consensus sequence served as a starting point for the design of a temperature-stable WW domain based basic scaffold. 9 CD thermal denaturation examinations of the most promising candidate exhibited a melting temperature of 89 °C and a K_D value in micromolar range in fluorescence-based binding studies (Figure 2).
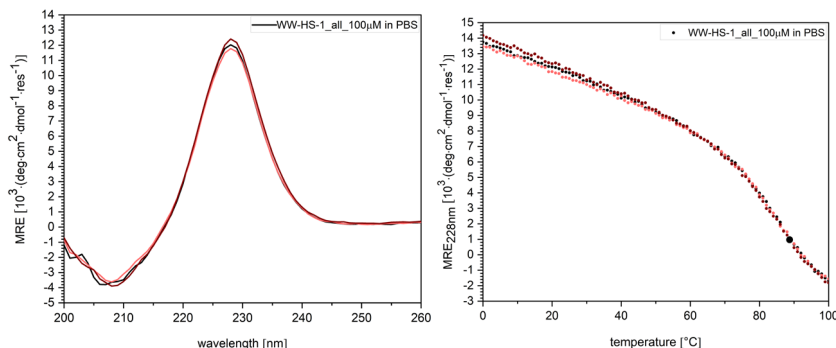

Fig. 2. Left CD spectra of WW-hs1 at 20 °C (n=3). Right CD thermal denaturation curves (n=3). T_M= 89 °C.

Conclusion

According to the findings, the WW domain is robust to mutations in terms of structural stability. In addition, there was a successful identification of structure-relevant and stabilizing amino acid residues in strand and loop regions, which led to the generation of a thermostable WW domain with a melting temperature of 89 °C, compared to 55 °C for the natural reference peptide hPin1$_{WW}$.

Outlook

The future aim is to construct different binding properties onto the basic WW domain template, leading to the design of mini phosphate receptors and phosphatases (Figure 3).
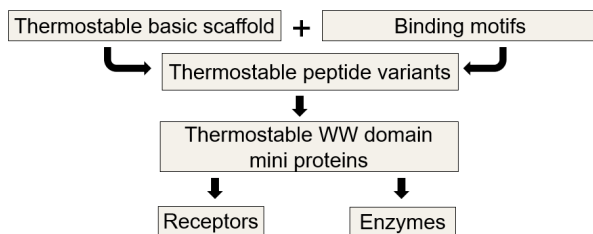
Fig. 3. Overview over the future steps towards mini receptors and enzymes.

Acknowledgements

References

1. Huang, P.-S., et al. *Nature* **537** (7620), 320 (2016), https://doi.org/10.1038/nature19946
2. Lee, D. H., et al. *Nature* 525-528 (1996), https://doi.org/10.1038/382525a0
3. Vishwanath, et al. *Prog. Biophys. Mol. Biol.* **116**, (2-3), 151 (2014), https://doi.org/10.1016/j.pbiomolbio.2014.08.003
4. Camarero, J.A., et al. *Angew. Chem. Int. Ed.* **37**(3), 347 (1998), https://doi.org/10.1002/(SICI)1521-3773(19980216)37:3<347::AID-ANIE347>3.0.CO;2-5
5. Toepert, F., et al. *Angew. Chem. Int. Ed*. **40**(5), 897 (2001), https://doi.org/10.1002/1521-3773(20010302)40:5<897::AID-ANIE897>3.0.CO;2-X
6. Coin, I., et al. *Nat. Protoc.* **2**(12), 3247 (2007), https://doi.org/10.1038/nprot.2007.454
7. Mende, F., et al. *J. Am. Chem. Soc.* **132** (32), 11110 (2010), https://doi.org/10.1021/ja101732a
8. Otte, L., et al. H. *Protein Sci*. **12**, 491 (2003), https://doi.org/10.1110/ps.0233203
9. Neitz, H., et al. *Chem. Science* **31** (2022), https://doi.org/10.1039/D2SC01078J

Two Self-Assembly Pathways of a Peptide Hydrogel Studied by Atomic Force Microscopy

J. Bertouille[1], S. Kasas[2,3], C. Martin[1], U. Hennecke[1], S. Ballet[1], and R.G. Willaert[3,4]

[1]*Research Group of Organic Chemistry, Vrije Universiteit Brussels, Brussel, 1050, Belgium;* [2]*Laboratory of Biological Electron Microscopy, Ecole Polytechnique Fédérale de Lausanne, Lausanne, 1015, Switzerland;* [3]*International Joint Research Group VUB-EPFL BioNanotechnology & NanoMedicine, Vrije Universiteit Brussel, Brussels, 1050, Belgium; Ecole Fédérale Polytechnique de Lausanne, Lausanne, 1015, Switzerland;* [4]*Research Group Structural Biology Brussels, Alliance Research Group VUB-UGent NanoMicrobiology, Vrije Universiteit Brussel, Brussels, 1050, Belgium*

Introduction

Peptide-based hydrogels are being investigated over almost 30 years for, amongst others, drug delivery, tissue engineering and wound healing [1,2]. The hierarchical self-assembly of the peptides is steered by the amino acid composition and external physicochemical parameters. The macroscopic properties of the resulting soft materials will depend on the fibril and network morphology. One class of peptide-hydrogels comprise β-sheet based materials. Here, the formed β-sheets will elongate and form a fibril. These fibrils will align and interact with each other forming the cross-links needed for hydrogel network formation. Unfortunately, the full assembly mechanisms of these networks are not revealed yet. Common techniques to investigate the network morphology, such as atomic force
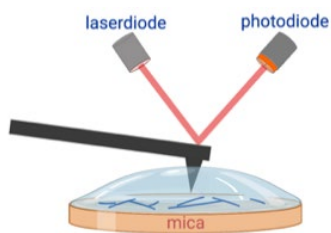

Fig. 1. Illustration of the AFM set-up.

microscopy (AFM) in air and cryogenic electron microscopy (cryo-EM), lack dynamic features. Additionally, the sample preparation might influence the self-assembly process. In this work, peptide self-assembly dynamics were investigated under native conditions by means of high-speed atomic force microscopy (HS-AFM) experiments in liquid [3]. The general AFM set-up is depicted in Figure 1. We optioned for a model peptide, KFE8 (Ac-FKFEFKFE-NH$_2$) [4], which is known to form β-sheet containing hydrogels due to its alternating hydrophobic and hydrophilic amino acids. After the formation of a β-sheet double layer to create a hydrophobic core, it was described that this peptide will form helical ribbons as intermediate structures before evolving into larger fibrils.

Results and Discussion

In the first experiments, the self-assembly was followed *in-situ,* meaning the fibril formation took place at the interface between the mica surface and the water droplet. The scans, recorded with a speed up to 0.3 frames per second, were combined in videos and selected scans are depicted in Figure 2. It was observed that the formation of the fibrils occurred mostly via secondary nucleation. Besides, a bi- directional growth was visualized, the fibril elongated until the growing end reached the surface of another fibril. To form a network structure, the fibrils further branched and aligned. A stabilized 2D network was formed within a few minutes. Remarkably, polymorphism and the existence of different intermediate morphologies was not observed.
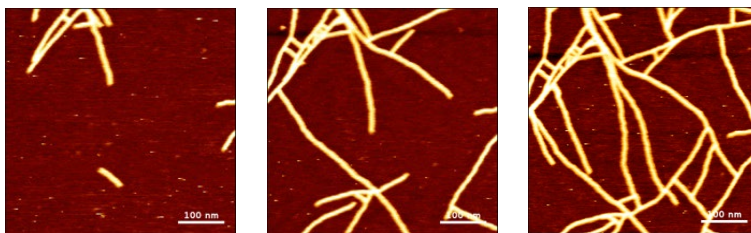
Fig. 2. AFM scans of the in-situ self-assembly at 85 s, 127 s and 235 s.

In a subsequent experiment, the self-assembly occurred in solution without being in contact with the mica surface (*ex-situ)*. Aliquots of this solution were dropped on mica and scanned in liquid. After the fast formation of large spherical aggregates during the first seconds, helical ribbons were observed on the AFM micrographs (Figure 3). Over time, these ribbons elongated prior to condensation towards nanotubes, being the most stable morphology. Both the nanotubes and the intermediate ribbons aligned sideways and formed cross-links. Under the applied conditions, slow kinetics were observed, the transition to a mature network required over 3 months. The material visible in the background of the images, consists of the 2D network formed on the mica surface, indicating the existence of two self-assembly pathways.
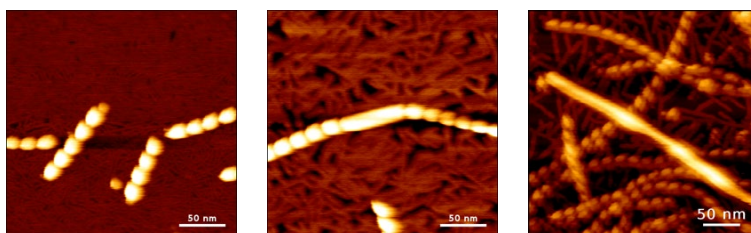

Fig. 3. AFM scans of the ex-situ self-assembly, fltr: the formation of helical ribbons, the structural change from ribbons to nanotubes and the presence of a nanotube.

In conclusion, two distinct self-assembly mechanisms were revealed, being at the surface-liquid interface and in the bulk solution. For the former, a fast-growing network composed of small uniform fibrils is formed, while for the latter, a more extended network resulted after the formation of an intermediate morphology. Both processes could be captured at high resolution and dimensions of these structures could be determined. Moreover, our findings provided novel dynamic insights into the understanding of a β-sheet forming peptide-based material (KFE8). This technique leads the way to further studies on the influence of physicochemical parameters and peptide composition on the assembly kinetics and morphological transitions of self-assembling systems.

Acknowledgments

References

1. Zhang, S., Holmes, T., Lockshin, C., and Rich, A. *Proc. Natl. Acad. Sci. USA* **90**, 3334-3338 (1993), https://doi.org/10.1073/pnas.90.8.3334
2. Fu, K., Wu, H., and Su, Z. *Biotechnol. Adv*. **49**, 107752-107769 (2021), https://doi.org/10.1016/j.biotechadv.2021.107752
3. Bertouille, J., Kasas, S., Martin, C., Hennecke, U., Ballet, S., and Willaert R.G. Manuscript submitted.
4. Marini, D.M., Hwang, W., Lauffenburger, D.A., Zhang, S., and Kamm R.D. *Nano Letters* **2**, 295-299 (2002), https://doi.org/10.1021/nl015697g

Protocol for the Computational Optimization of Modified Peptides as Potential Protease Inhibitors

Rodrigo Ochoa and Pilar Cossio

Biophysics of Tropical Diseases, Max Planck Tandem Group, University of Antioquia,
050010 Medellin, Colombia

Introduction

From the repertoire of targets, enzymes interacting with peptide substrates constitutes one of the most interesting groups to block due to their impact as key drivers in many biological processes. Information about natural substrates as well as potential inhibitors has contributed to understand the specificity of these enzymes, and the mechanisms to recognize certain molecular binders, as in the case of proteases [1]. Many of these proteases have been identified in pathogens, or as crucial molecular components in the modulation of human diseases [2]. For example, structures of proteases have been characterized and used to design novel inhibitors of emerging viruses [3]. This is the case of the 3CL protease or main protease (Mpro) characterized for SARS-CoV-2 that since its report has motivated the publication of various studies aiming to understand its mechanism of action and screening of potential inhibitors [4,5]. Another example is cathepsin S, a protease involved in the human immunological response pathway. The overexpression of this protease is associated with some autoimmune diseases, motivating the characterization of its structure to provide new clues for designing novel binders able to control their deleterious effects [6].

Thanks to the availability of these protease structures, researchers have applied different computational strategies to design novel inhibitors, some of them mimicking the mechanism of action of their natural substrates [7]. This is the case of modified peptides composed of non-natural amino acids (NNAA), which can be associated with improved pharmaceutical properties [8,9]. These NNAAs can be computationally parameterized and included in common simulation and modelling techniques [10]. This provides valuable resources to support the engineering and design of modified peptides through computational strategies, allowing, for example, the design of novel inhibitors against proteases responsible to cleave natural peptides [11].

Something crucial is to employ computational strategies to explore efficiently both the conformational and sequence space of the peptides. In the case of the sampling techniques, there are multiple alternatives from classic to enhanced molecular dynamics simulations [12]. These trajectories can be used to score protein-peptide complexes and allow the modification of their sequences based on accepting random or guided modifications [13,14,15]. Something required is the definition of a molecular target structure bound to a peptide, which can be obtained from either a crystal structure or through docking methodologies. These targets are usually proteins that can be inhibited using peptides as potential drug-like molecules. In this work, we applied the design protocol PARCE [16] using crystal structures of two proteases of relevance, a cathepsin S and SARS-CoV-2 main protease docked with 3-mer modified peptides as starting points. The selected candidates were ranked and proposed as potential inhibitor candidates for further experimental validations.

Results and Discussion

In this work we generated a protocol to design modified peptides composed of non-natural α-L-amino acids and some basic D-amino acids. Using as input a protein-peptide complex, several mutations were attempted with a set of parameterized NNAAs. The mutations are sampled with RosettaCommons (https://www.rosettacommons.org/), and a consensus scoring or metropolis Monte Carlo criterion can be applied to accept or reject the mutations. An application using two known protease systems was included to design novel 3-mer modified peptides.

Parameterization of non-natural amino acids
Based on the information of α-L- and D-NNAAs derived from the SwissSideChain database [17], a total of 83 NNAAs were selected to perform the mutations. All the NNAAs contain chemical modifications only on the side chain, and they can be sampled using molecular dynamics (MD) simulations with the CHARMM27 force field available in SwissSideChain.

Application using proteases structures

We selected two proteases' structures from the PDB that has been co-crystallized with 3-mer modified peptides. One is the SARS-CoV-2 Mpro structure (PDB id 6fv2) [18], and the second is a cathepsin S structure (PDB id 2f1g) [19]. In both cases, the bound peptides are composed of NNAAs that are not part of the parameterized NNAA dataset. Based on that, we modelled a group of 3-mer peptides using combinations from a set of 14 NNAAs available in RDKit (https://rdkit.org/) to run conformer predictions. The conformer library was docked using AutoDock Vina [20], and the bound peptides with the best energies were used as starting points for the design of modifications. In the case of Mpro, the sequence was DGN (D-glutamine), ORN (ornithine) and DME (D-methionine). For cathepsin S, the 3-mer was DAR (D-arginine), ORN (ornithine) and DPR (D-proline). A graphical representation of the structures and the docked poses are shown in Figure 1.

Both complexes were used as references to design variants with higher affinities. For the design, we initially attempted a run using a single scoring function with a Metropolis Monte Carlo criterion to accept the mutations. A total of 400 mutations were attempted, and the score evolution was monitored to identify the accepted candidate sequences. We found a high number of accepted sequences (85)
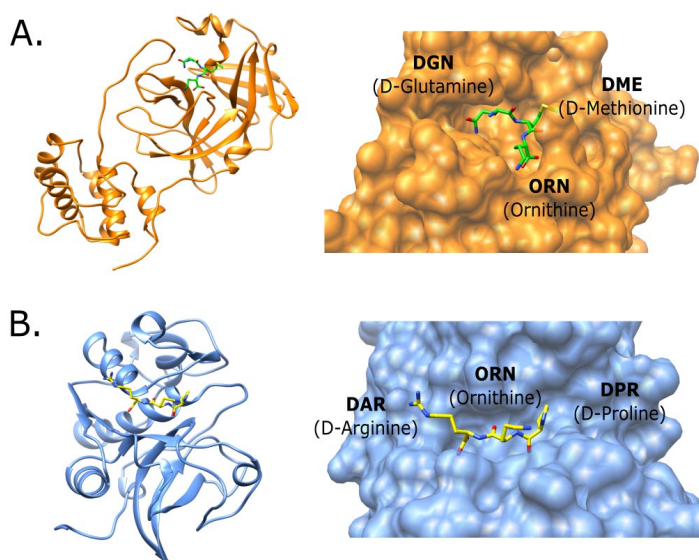
Fig. 1. Structures of the two proteases that were included for the application. (A) Structure of a SARS-CoV-2 Mpro structure (PDB id 6fv2) bound to the starting 3-mer peptide DGN (D-glutamine), ORN (ornithine) and DME (D-methionine. (B) Structure of the cathepsin S structure (PDB id 2f1g) bound to the 3-mer peptide DAR (D-arginine), ORN (ornithine) and DPR (D-proline).

from the 400 iterations (see Figure 2). However, relying in one single scoring function can be risky given the intrinsically errors associated [21]. Because of that, the next step was to run the design with a consensus setup, using two thresholds of three and four scoring functions to accept the mutations from the original six.

After running the design with a threshold of three and 200 mutation attempts, we found more difficulties to converge the scoring functions after the planned number of iterations. This is mostly given by the small size of the peptide sequences, which can change drastically the average scores from one iteration to the next. For example, we obtained for the Mpro system a total of 20 candidates, but with a noticeable lack of convergence. For the cathepsin S, the results were similar with a total of 34 accepted molecules. To avoid these issues, we increased the threshold from three to four scoring functions to accept the mutations. In that scenario, a lower number of sequences were accepted, but we got a better performance of the scoring functions during the iterations. An example with four of the

six scoring functions values for the accepted sequences during the 200 mutation attempts is shown in Figure 3.

We found that from the six scoring functions, only NNscore [22] finished the design run with sequences having more positive scores with respect to the original molecules. This is expected given the stochastic nature of the sequence space search, where the scores can also increase in energy to overcome local barriers. Also, by setting a higher threshold, the number of accepted sequences was lower in both cases, with a total of six peptides for each system. Despite the numbers, there are higher probabilities to obtain candidates with better average scores than the reference.

The NNAAs that are part of the prioritized molecules are: DGN (D-glutamine), DME (D-methionine), ALO (allo-threonine), BB8 (phenylserine), C2N (3-chloro-l-alanine), PF5 (pentafluoro-phenylalanine), HOX (4-amino-L-phenylalanine), MEG ((3s)-3-methyl-l-glutamic acid), DLY (D-lysine), DAL (D-alanine), ALC (3-cyclohexyl-alanine), WFP (3,5-Difluoro-phenylalanine), 2FM (s-(difluoromethyl)-homocysteine), ABA (2-Aminobutyric acid), PHI (4-iodo-phenylalanine) and TYI (3,5-diiodotyrosine).
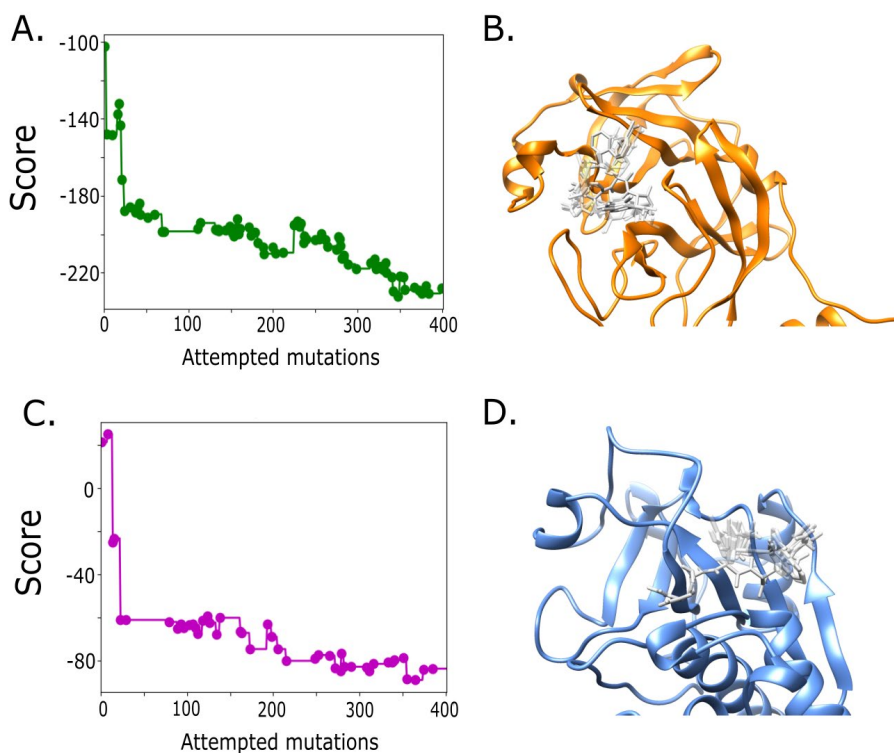
Fig. 2. Evolution of the Rosetta scoring function after 400 mutation attempts using a Metropolis criterion for Mpro (A) and cathepsin S (C). The dots in the curve represent the mutations that were accepted. A structural representation of the accepted modified peptides is shown for Mpro (B) and cathepsin S (D).

Finally, to show the connection between our design protocol and the possibility to implement MD simulations to re-rank the candidates, all the peptides were subjected to 100 ns MD with the modified CHARMM27 force field available at the SwissSideChain database. The trajectories were scored using the same six scoring functions of the design, and an average ranking was calculated to prioritize the candidates. As a perspective, the user has the possibility to re-rank the molecules using more exhaustive sampling methodologies before moving to experimental validations.
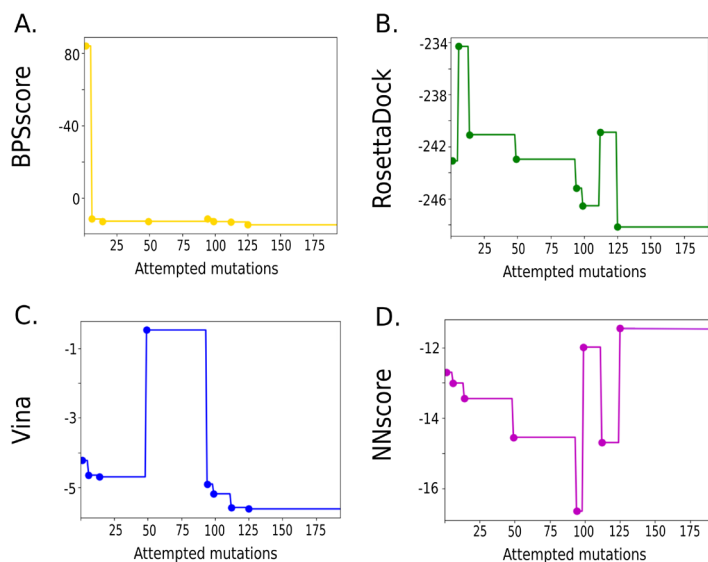
Fig. 3. Evolution of some of the scoring functions using a consensus criterion. We used a total of six scoring functions to calculate the consensus with a threshold of four after attempting 200 mutations. The dots in the curve represent the mutations that were accepted. The shown scoring functions are (A) BPSScore, (B) RosettaDock, (C) Vina and (D) NNscore.

Acknowledgments

References

1. Ochoa, R., et al. *BMC Bioinformatics* **21**, 1-20 (2020), https://doi.org/10.1186/s12859-020-03931-6
2. Drag, M. and Salvesen, G.S. *Nat. Rev. Drug Discovery* **9**, 690-701 (2010), https://doi.org/10.1038/nrd3053
3. Zhou, Y., et al. *Antiviral Res.* **116**, 76-84 (2015), https://doi.org/10.1016/j.antiviral.2015.01.011
4. Zhang, L., Lin, D., Sun, X., et al. *Science* **368**, 409-412 (2020), https://doi.org/10.1126/science.abb3405
5. Macchiagodena, M., et al. *Chem. Phys. Lett.* **750**, 137489 (2020), https://doi.org/10.1016/j.cplett.2020.137489
6. Tato, M., Kumar, S., Liu, Y., et al. *Sci. Rep.* **7**, 1-15 (2017), https://doi.org/10.1038/s41598-017-01894-y
7. Mulligan V.K., et al. *Proc. Nat. Acad. Sci.* **118**, e2012800118 (2021),
   https://doi.org/10.1073/pnas.2012800118
8. Gentilucci, L., et al. *Cur. Pharm. Des.* **16**, 3185-3203 (2010), https://doi.org/10.2174/138161210793292555
9. Vagner, J., et al. *Cur. Opin. Chem. Biol.* **12**, 292-296 (2008), https://doi.org/10.1016/j.cbpa.2008.03.009
10. Lenci, E. and Trabocchi, A. *Chem. Soc. Rev.* **49**, 3262-3277 (2020), https://doi.org/10.1039/D0CS00102C
11. Fear, G., et al. *Pharmacol. Therap.* **113**, 354-368 (2007), https://doi.org/10.1016/j.pharmthera.2006.09.001
12. Miao, Y. and McCammon J.A. *Mol. Simul.* **42**, 1046-1055 (2016),
    https://doi.org/10.1080/08927022.2015.1121541
13. Ochoa, R., et al. *J. Chem. Inf. Mod.* **59**, 3464-3473 (2019), https://doi.org/10.1021/acs.jcim.9b00403
14. Ochoa, R., et al. *Front. Mol. Biosci.* **8**, 636562 (2021), https://doi.org/10.3389/fmolb.2021.636562
15. Ochoa, R., et al. *Frontiers in Immunology* **13**, 862851 (2022), https://doi.org/10.3389/fimmu.2022.862851
16. Ochoa, R., et al. *Comp. Phys. Commun.* **260**, 107716 (2021), https://doi.org/10.1016/j.cpc.2020.107716
17. Gfeller, D., et al. *Nucl. Acids Res.* **41**, D327-D332 (2012), https://doi.org/10.1093/nar/gks991
18. Zhang, L., et al. *J. Med. Chem.* **63**, 4562-4578 (2020), https://doi.org/10.1021/acs.jmedchem.9b01828
19. Tully, D., et al. *Bioorg. Med. Chem. Lett.* **16**, 1975-1980 (2006), https://doi.org/10.1016/j.bmcl.2005.12.095
20. Trott, O. and Olson, A.J. *J. Comput. Chem.* **31**, 455-461 (2010), https://doi.org/10.1002/jcc.21334
21. Michel, J. and Essex, J.W. *J. Comp. Aided Mol. Des.* **24**, 639-658 (2010), https://doi.org/10.1007/s10822-010-9363-3
22. Durrant, J.D. and McCammon, J.A. *J. Chem. Inf. Mod.* **51**, 2897-2903 (2011), https://doi.org/10.1021/ci2003889

From a Bioinformatic Approach to Synthetic Conformational Peptide Epitopes to Disclose Molecular Mechanism of Aberrant Glucosylation in Multiple Sclerosis

Michele Casoria[1,2,3], Paolo Rovero[2,4], Gianni Cardini[1,3], Marina Macchiagodena[1,3], Anna Maria Papini[2,3], Claudia Andreini[3,5], and Marco Pagliai[1,3]

[1]Research Unit of Computational Chemistry, University of Florence, 50019 Sesto Fiorentino, Italy; [2]Interdepartmental Research Unit of Peptide and Protein Chemistry and Biology, University of Florence, 50019 Sesto Fiorentino, Italy; [3]Department of Chemistry "Ugo Schiff", University of Florence, 50019 Sesto Fiorentino, Italy; [4]Department of Neurosciences, Psychology, Drug Research and Child Health Section of Pharmaceutical Sciences and Nutraceutics, University of Florence, 50019 Sesto Fiorentino, Italy; [5]Magnetic Resonance Center - University of Florence, 50019 Sesto Fiorentino, Italy

Introduction

Multiple Sclerosis (MS) is a chronic, inflammatory, demyelinating disease of the central nervous system. MS is accepted to be a group of diseases that have not been yet completely characterized.

Autoantibodies (Abs) circulating in blood can be used as specific biomarkers relevant for an early diagnosis or prognosis of a disease form. To this end, a 'chemical reverse approach' based on the use of patient sera to screen focused libraries of synthetic modified peptides, can lead to the identification of selective antigenic probes able to characterize specific and high affinity Abs. MOG (myelin oligodendrocyte glycoprotein) is a glycoprotein present in the CNS (central nervus system) of mammalians and represents 0.01-0.05% of total myelin proteins. Mog possesses two potential transmembrane domains and one *N*-linked glycosylation site on MOG exposed on the outermost surface of myelin making it an ideal target antigen for Ab-recognition. [Asn31(Glc)]-hMOG(30-50) (Table 1) was the first *N*-glucosylated MOG peptide able to recognize specific IgG Abs in sera of a multiple sclerosis patient population (Figure 1) while the unglucosylated analogue hMOG(30-50) was inactive[1].

Fig. 1. IgG Ab titers to glycopeptides [Asn31(Glc)]- hMOG(30-50) (1) and CSF114(Glc)(2).

Starting from hMOG(30-50), a structure-activity relationship study allowed to design a scrambled sequence characterized by a β-hairpin structure optimally exposing the minimal epitope Asn(Glc). This peptide termed CSF114(Glc) [2] recognized Abs with higher affinity and greater specificity [3].
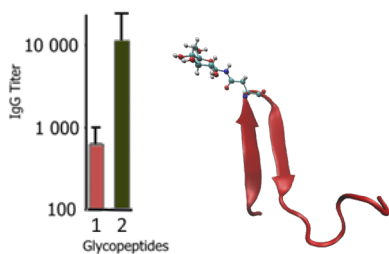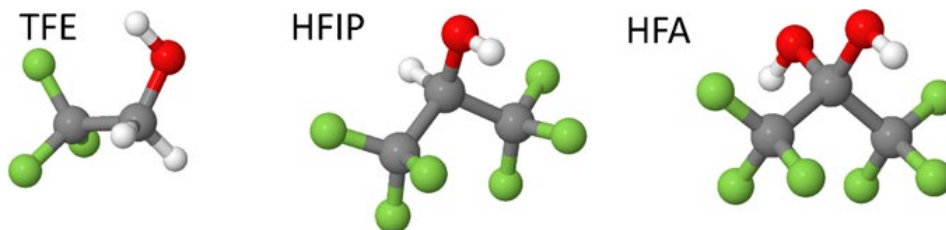

Fig. 2. Molecular structure of TFE, HFIP, and HFA biomimetic solvents.

Table 1. Peptide sequences used in the simulation systems.

Name	Sequence
hMOG(30-50)	KNATGMEVGWYRPPFSRVVHL
[Asn31(Glc)]-hMOG(30-50)	KN(Glc)ATGMEVGWYRPPFSRVVHL
CSF114	TPRVERNGHSVFLAPYGWMVK
CSF114(Glc)	TPRVERN(Glc)GHSVFLAPYGWMVK

Results and Discussion

Molecular dynamics (MD) simulations of two N-glucosylated versus the unglucosylated analog peptides were performed to achieve structural properties of different peptide epitopes, using three different mixtures of biomimetic solvents: trifluoroethanol (TFE), hexafluoro-2-propanol (HFIP) and hexafluoroacetone (HFA) (Figure 2). The effectiveness of structure-inducing cosolvent depends on its percentage in the mixture. Mixed water-alcohol solvents (TIP3P model has been adopted for water) [4] may approximate the dielectric constant of protein interiors. In the case of peptides, the folding in these solutions represents an intrinsic propensity to adopt a specific secondary structure in the corresponding protein region, otherwise unstructured in aqueous solution. This solvent mixture is a stabilizing agent, which increases the intrinsic tendency of the amino acid sequence to fold in defined secondary structures. As general trend, HFIP and HFA are considered stronger structural inducers than TFE, suggesting that the ability of the cosolvent is related to the presence of F atoms, and as consequence additional F atoms would be more effective. The lowest energy form of TFE has a gauche configuration, while the trans conformer is less stable, being its energy > 2.0–2.5 kcal/mol [5]. This is in agreement with the hypothesis that TFE molecules form a 50:50 mixture of trans and gauche conformations around the C–C–O–H frame in solution. HFA is known to form stable hydrates. The monohydrate is a solid melting at 46°C, the trihydrate can be distilled and melts at -11°C. Both these hydrates are formed bubbling gaseous HFA into water. If the molar ratio of the components in solution is 1:1, only the monohydrate is formed. Hydrated fluoroketones can be considered as fluoroalcohols, i.e., geminal diols. HFIP has a high tendency to form micelle-like clusters with a maximum effect at about 30% (v/v).
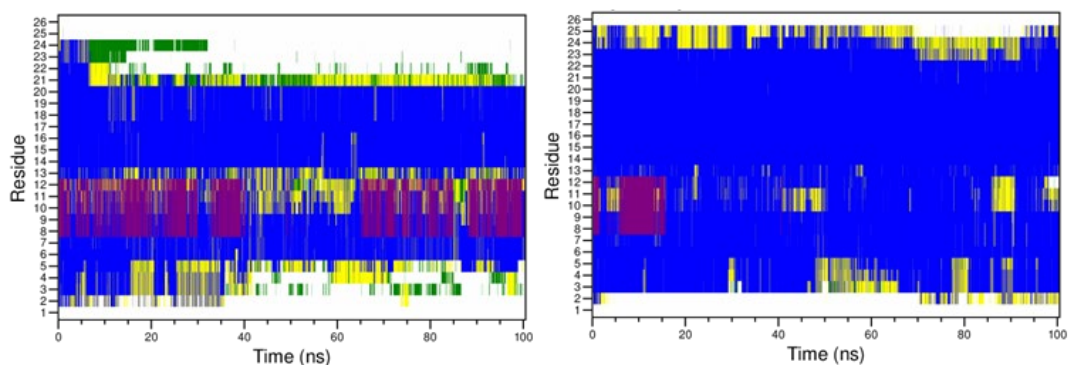

Fig. 3. DSSP analysis of Melittin in HFA with both GAFF (left) and with improved FFs (right).

We report herein, an improved Force Field (FF) for TFE, HFIP, and HFA that use the General Amber Force Field (GAFF) [6], to describe bonded and Lennard-Jones parameters. Atomic charge was reparametrized by using Mulliken population Analysis [7] considering the bulk solvent effects in the Conductor-like Polarizable Continuum Model (C-PCM) [8]. As case study, to verify the accuracy and reliability of the FFs, was chosen Melittin (MLT), a component of the venom of *Apis mellifica*. MLT is a 26-mer peptide that is unstructured in water at low pH but adopts an α-helical conformation when it is bound to the membrane as well as when alcohols are present. MLT consists of two α-helical regions and these portions are connected through Thr11 and Gly12. In Figure 3, we report the (DSSP) define secondary structure of protein analysis showing a more stable structure when the improved FF is used. These FFs have been employed to simulate the structure-based designed type I' β-turn peptide CSF114, hMOG(30-50), CSF114(Glc), and Asn31(Glc)]hMOG(30–50) with the glucosyl moiety added thanks to the tool doGlycans[9].

Previously, NMR-based conformational studies revealed that Asn31(Glc)]hMOG(30–50) and hMOG(30-50) adopted similar conformations in water/HFA (50:50 v/v) solution [10]. The specific autoantibody binding site on hMOG(30-50) was related to the *N*-linked glucose moiety suggesting it as minimal epitope. During simulation of hMOG(30-50) in HFA, the average time development of hydrogen bond distances for i-(i+3) backbone (left) and i-(i+2) CO on Asn side-chain (right), suggest that hMOG(30-50) adopts an Asn-turn (Figure 4). That can explain the lower antibody titer detected in MS sera.

NMR-based conformational studies on CSF114 show the presence of a β-hairpin structure (i.e. a β-turn flanked by two antiparallel β-sheet) in HFA/water 50/50 v:v [11]. DSSP graph (Figure 5) shows the ability of improved FFs reproducing the structure of the designed type I' β-turn peptide CSF114 (Glc).

Future studies will be aimed to correlate aberrant asparagine-glucosylation (N-Glc) and ability to detect autoantibodies in MS patient sera. We will focus on bioinformatics to characterize consensus sequences in myelin proteins in order to identify *de novo* peptides. These *de novo* sequences will be studied by molecular dynamics to verify secondary structures in water and biomimetic solvents. Then the optimized structure will be synthesized and tested for antibody recognition in MS.
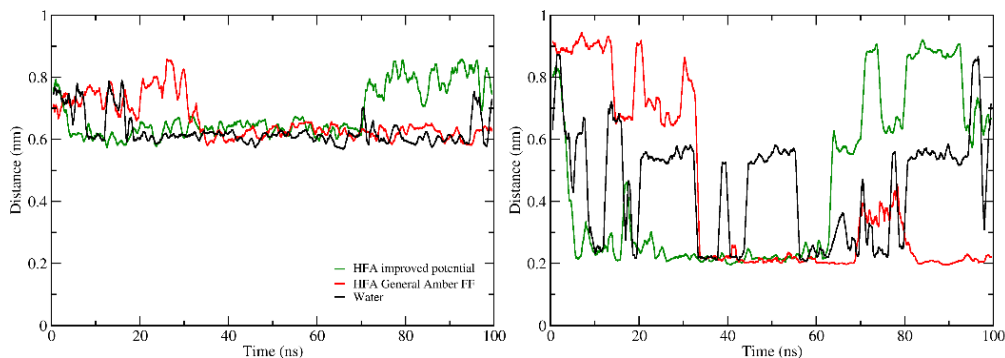

Fig. 4. Average time development of 30Lys-O-33Thr-H hydrogen bond distances (β-turn, left) and 31Asn-CO-33Thr-H (Asn-turn, right) for hMOG(30-50) in HFA and water simulation.
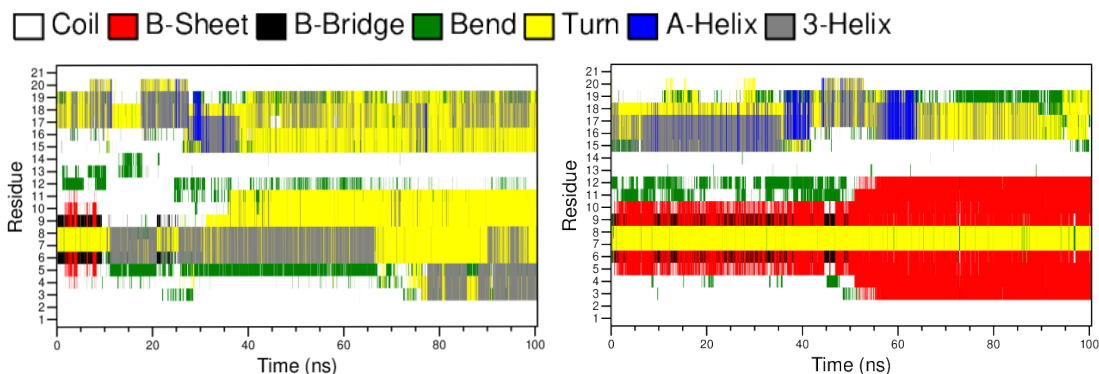
Fig. 5. DSSP graph of CSF114(Glc) in TFE using GAFF (left) and the improved FF (right).

Acknowledgments

References

1. Mazzucco, S., et al. *Bioorg. Med. Chem. Lett.* **9**, 167-172 (1999), https://doi.org/10.1016/S0960-894X(98)00698-2
2. Lolli, F., et al. *PNAS* **102**, 10273-10278 (2005), https://doi.org/10.1073/pnas.0503178102
3. Lolli, F., et al. *J. Neuroimmunol*. **167**, 131-137 (2005), https://doi.org/10.1016/j.jneuroim.2005.05.016
4. Jorgensen, W.L., et al. *J. Chem Phys*. **79**, 926-935 (1983), https://doi.org/10.1063/1.445869
5. Li-Hong, X., et al. *J. Chem Phys* **103**, 9541-9548 (1995), https://doi.org/10.1063/1.469968
6. Procacci, P. *J. Chem. Inf. Model* **57**, 1240-1245 (2017), https://doi.org/10.1021/acs.jcim.7b00145
7. Macchiagodena, M., et al. *Chem. Phys. Lett.* **677**, 120-126 (2017), https://doi.org/10.1016/j.cplett.2017.04.004
8. Barone, V., et al. *J. Chem Phys* **102**, 1995-2001 (1998), https://doi.org/10.1063/1.469968
9. Danne, R., et al. *J Chem Inf Model* **57,** 2401-240 (2017), https://doi.org/10.1021/acs.jcim.7b00237
10. Carotenuto, A., et al. *J. Med. Chem*. **44**, 2378-2381 (2001), https://doi.org/10.1021/jm010811t
11. Carotenuto, A., et al. *J. Med. Chem.* **49**, 17 (2006), https://doi.org/10.1021/jm060117j

O-Aminoanilides in Protein Synthesis: *N*-Acylureas, Aryloxycarbonyl-*o*-Aminoanilides and Benzotriazoles

Iván Sánchez-Campillo[1], Judit Miguel-Gracia[1], Periklis Karamanis[2], and Juan B. Blanco-Canosa[1]

[1]*Institute for Advanced Chemistry of Catalonia (IQAC- CSIC), Barcelona, 08034, Spain;* [2]*School of Chemistry, University College of Dublin (UCD), Dublin, D04 N2E2, Ireland*

Introduction

Peptide α-thioesters (peptide-COSR) play a key role in native chemical ligation (NCL). They react chemoselectively with peptides featuring *N*-terminal cysteine residues, forming a native amide bond [1,2]. The synthesis of peptide-COSR by Fmoc-solid phase peptide synthesis (Fmoc-SPPS) is a non-direct process because piperidine induces thioester aminolysis. Several methods have been described for the synthesis of these important intermediates, but the lack of reproducibility and cumbersome steps did not result in any general protocol. Thus, in 2008 the *N*-acyl-benzimidazolinone (Nbz) method was introduced, which relies on the 3,4-diaminobenzoic acid for the syntheses of peptide-Nbz-CONH$_2$ that are precursors of peptide-COSR (Figure 1) [3]. Herein we recapitulate the family of *o*-aminoanilide linkers used in protein synthesis.
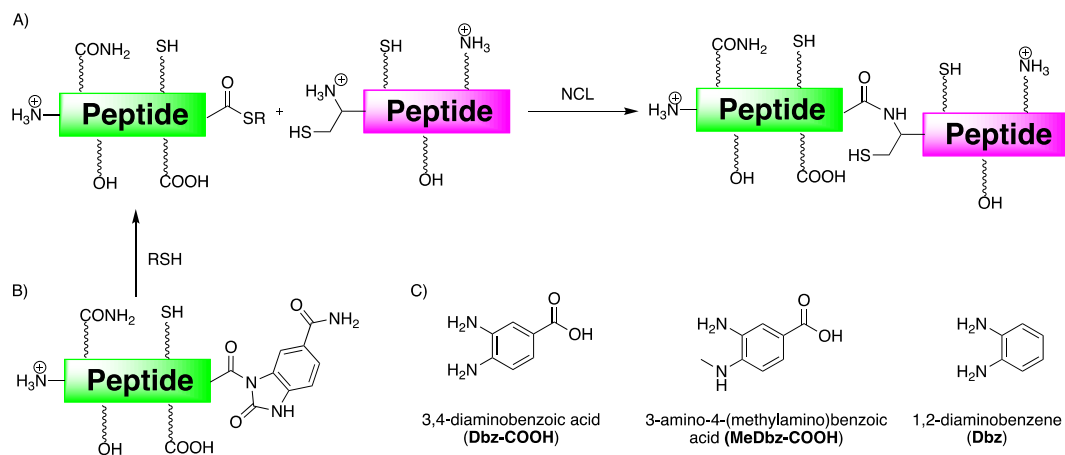
Fig. 1. A) The native chemical ligation (NCL) reaction. B) N-acyl-benzimidazolinone peptide (Peptide-Nbz-CONH$_2$) precursor of peptide-COSR. C) 3,4-diamonobenzoic acid, 3-amino-4-(methylamino)benzoic acid, and 1,2-diaminobenzene scaffolds.

Results and Discussion

Peptide-(*N*-acyl-benzimidazolinone) (peptide-Nbz-CONH$_2$) are prepared from 3,4-diaminobenzoic acid (Dbz-COOH) [3,4]. Starting from an aminomethylated resin functionalized with an acid labile linker (Rink, PAL, Sieber…), incorporation of Dbz-COOH followed by chemoselective monoacylation yields the Fmoc-Xaa$_1$-Dbz-CONH-resin (**1**, Xaa$_1$ = any amino acid, Figure 2). Next, stepwise chain elongation using Fmoc-SPPS leads to the target peptide sequence (peptide-Dbz-CONH-resin, **2**). The resulting *o*-aminoanilide peptide **2** is then acylated using *p*-nitrophenyl chloroformate, which under basic conditions undergoes intramolecular cyclization to give the peptide-Nbz-CONH-resin (**3**). TFA-mediated acidolytic cleavage of **3** releases the unprotected peptide-Nbz-CONH$_2$ (**4**), which under an excess of a thiol compound undergoes an intermolecular

N -to-*S* acyl exchange that forms the peptide-COSR (**5**). Alternatively, the presence of an *N*-terminal Cys-peptide yields the ligated product (**6**) in a one-pot NCL.

In addition, peptide **2** has a second reaction pathway via benzotriazole (Bt) derivatives [5,6]: activation with sodium nitrite at pH 3 and low temperature (~ -15ºC) leads to a peptide-Bt-CONH$_2$ (**7**) that, upon addition of a thiol compound, undertakes thioesterification followed by NCL (Figure 2).

Unfortunately, the chemoselectivity of the *o*-aminoanilide peptide **2** is compromised in Gly-rich sequences, resulting in the acylation of the free *o*-aminoanilide (Figure 2, **8**) [6]. Therefore, we developed the second generation of Dbz linkers to overcome this problem: 3-amino-4-methylamino-benzoic acid (MeDbz-COOH, Figure 3) [8]. The MeDbz-COOH is incorporated in the *C*-terminal position of peptides following a similar synthetic scheme as for Dbz-COOH. However, it behaves more robustly and can bear strong coupling microwave coupling conditions without noticeable
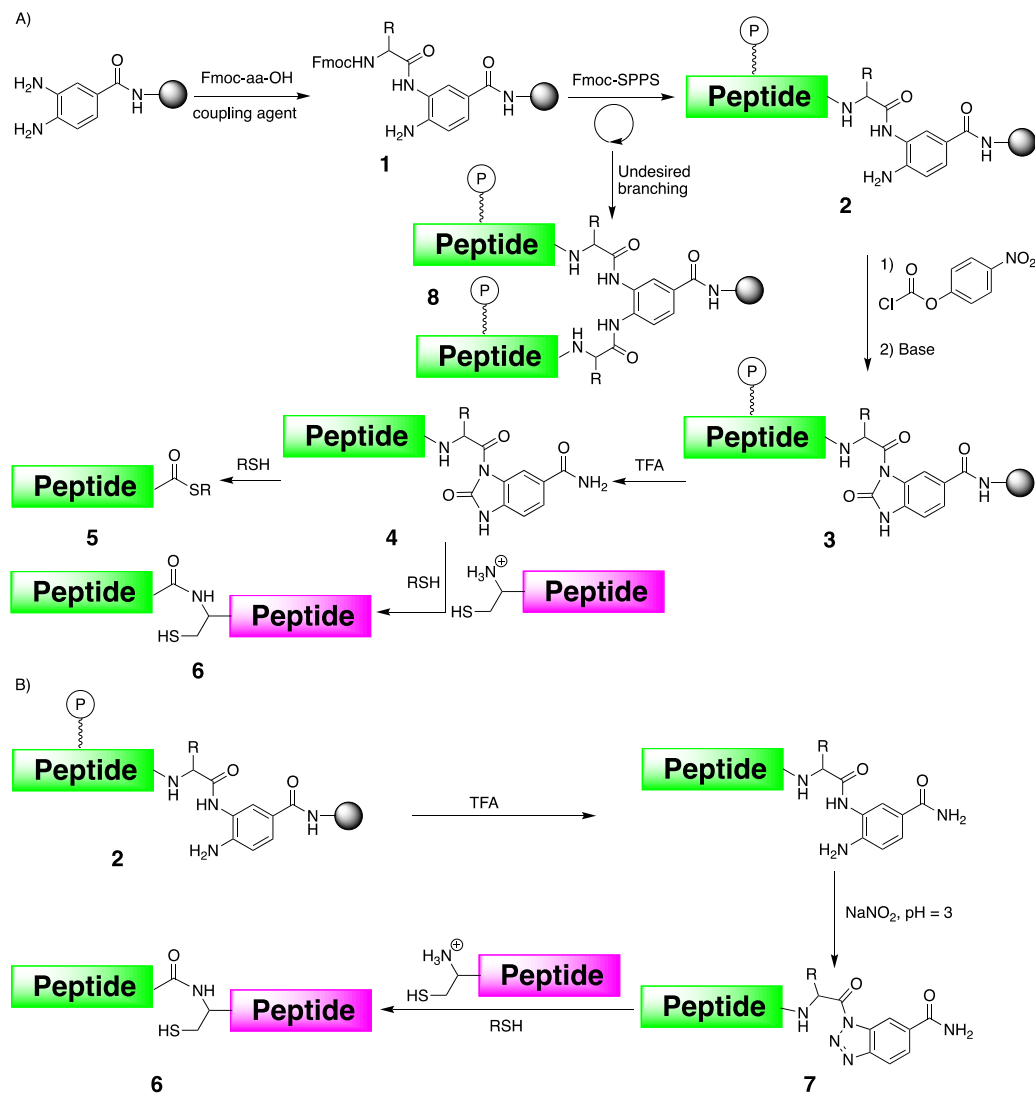
Fig. 2. A) Synthetic scheme for peptide-Nbz-CONH$_2$ and NCL. B) Synthetic route for peptide-Bt-CONH$_2$ and NCL. P = protecting group.

secondary acylations. Similarly to that peptide **2**, peptide-MeDbz-CONH-resin (**9**) can be converted into peptide-MeNbz-CONH-resin and then cleaved to give peptide-MeNbz-CONH$_2$ (**10**). Alternatively, acylation with *p*-cyanophenyl chloroformate followed by TFA-mediated cleavage affords the peptide-(*p*CN-Phoc)MeDbz-CONH$_2$ (**11**) [9]. Both peptides, **10** and **11**, undergo thiolysis in the presence of thiols, and NCL. In addition, the slower reactivity of **11** enables the use of (*p*CN-Phoc)MeDbz-CONH$_2$ peptides in sequential one-pot ligations under kinetic control [9,10].

The interesting properties of Dbz-CONH$_2$ and MeDbz-CONH$_2$ peptides as surrogates of peptide-COSR via peptide-Nbz/MeNbz-CONH$_2$ or peptide-Bt-CONH$_2$ motivated the search for an *o*-aminoanilide surrogate that would combine the advantages of both and keep the robustness of MeDbz-CONH$_2$ peptides. Thus, we found that 1,2-diaminobenzene linked to a PAL-resin can
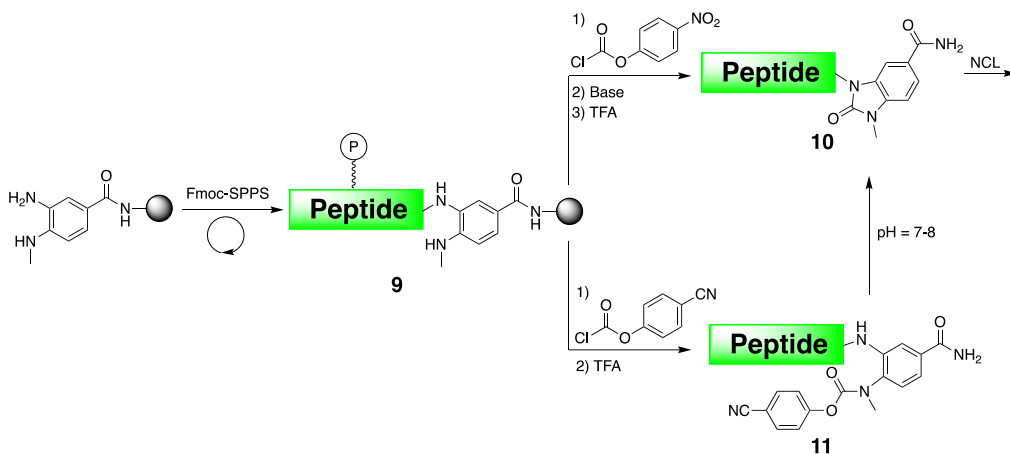
Fig. 3. Synthesis of peptide-MeNbz-CONH$_2$ and peptide-(pCN-Phoc)MeDbz-CONH$_2$ surrogates for peptide-COSR.
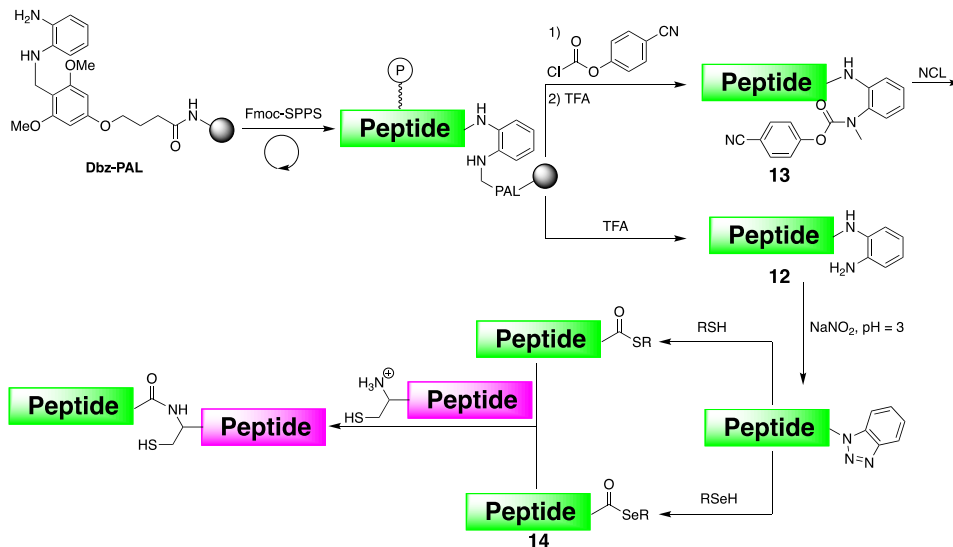
Fig. 4. Synthesis of peptide-Dbz-PAL-resin and pathways for the preparation of peptide-(pCN-Phoc)Dbz, peptide-COSR, and peptide-SeR.

generate a peptide-Dbz (**12**) after TFA cleavage, or a peptide-(*p*CN-Phoc)Dbz (**13**) precursor of peptide-Nbz (Figure 4) [11]. The Dbz-PAL-resin is chemoselective, but it does not impair the acylation in the presence of strong electrophiles such as chloroformates. In addition, we have found that peptide-Bt is labile enough to undergo transselenoesterication in the presence of benzeneselenol. C-terminal peptide-selenoesters (peptide-COSeR, **14**) react outstandingly fast with *N*-terminal cysteine and selenocysteine-peptides. Here, we have developed an efficient strategy for the synthesis of peptide-COSeR that hold a great deal of promise for chemical protein synthesis.

Conclusions

The synthesis of peptide-COSR and peptide-COSeR for NCL can be efficiently accomplished by the different moieties derived from *o*-aminoanilides. Activation via *N*-acylurea or *N*-acylbenzotriazole leads to precursors that undergo transthioesterification or transselenoesterification in the presence of the corresponding thiols or selenols.

Acknowledgments

References

1. Dawson, P.E., et al. *Science* **266**, 776-779 (1994), https://doi.org/10.1126/science.7973629/
2. Hackeng, T.M., et al *Proc. Natl. Acad. Sci. USA* **96**, 10068-10073 (1999), https://doi.org/10.1073/pnas.96.18.10068
3. Blanco-Canosa, J.B. and Dawson, P.E. *Angew. Chem. Int. Ed.* **47**, 6851-6855 (2008), https://onlinelibrary.wiley.com/doi/10.1002/anie.200705471
4. Tiefenbrunn, T.K., et al. *Biopolymers* **94**, 405-413 (2010), https://onlinelibrary.wiley.com/doi/10.1002/bip.21486
5. Wang, J.-X., et al. *Angew. Chem. Int. Ed.* **54**, 2194-2198 (2015), https://onlinelibrary.wiley.com/doi/10.1002/anie.201408078
6. Weidmann, E., et al. *Org. Lett.* **18**, 164-167 (2016), https://doi.org/10.1021/acs.orglett.5b03111
7. Mahto, S.K., et al. *ChemBiochem* **12**, 2488-2494 (2011), https://dx.doi.org/10.1002%2Fcbic.201100472
8. Blanco-Canosa, J.B., et al. *J. Am. Chem. Soc*. **137**, 7197-7209 (2015), https://doi.org/10.1021/jacs.5b03504
9. Palà-Pujadas, J., et al. *Angew. Chem. Int. Ed.* **57**, 16120-16125 (2018), https://doi.org/10.1002/anie.201810712
10. Bang, D., et al. *Angew. Chem. Int. Ed.* **45**, 3985-3988 (2006), https://onlinelibrary.wiley.com/doi/10.1002/anie.200600702
11. Sánchez-Campillo, I., et al. *Chem. Sci.* in press (2022), https://doi.org/10.1039/D2SC04158H

Design of Novel Alkylselenol Catalysts Enabling Peptide Thioester and Protein Chemical Synthesis

Florent Kerdraon[1], Benoît Snella[1], Vincent Diemer[1], Vangelis Agouridas[1,2], and Oleg Melnyk[1]

[1]Univ. Lille, CNRS, Inserm, CHU Lille, Institut Pasteur de Lille, U1019 - UMR 9017 - CIIL - Center for Infection and Immunity of Lille, F-59000 Lille, France; [2]Centrale Lille, F-59000, Lille, France

Introduction

Thioesters are pivotal intermediates in the native chemical ligation-mediated synthesis or semisynthesis of proteins. Their preparation very often occurs through a thiol-thioester exchange step which involves thiol-based catalysts [1,2]. Although the selenol group also presents interesting properties in this regard, selenol-based catalysts have been largely overlooked. In this study, we designed various selenocysteamine-derived alkyl selenols in the form of the corresponding diselenide precursors **1**-**3** (Figure 1a) and assessed their capacity to promote the formation of thioesters from *bis*(2-sulfanylethyl)amido (SEA) peptides **4** (Figure 1b) [3,4]. The more promising candidate was then used to prepare granulysin (9-GN), a 9 kDa human protein involved in immunity.
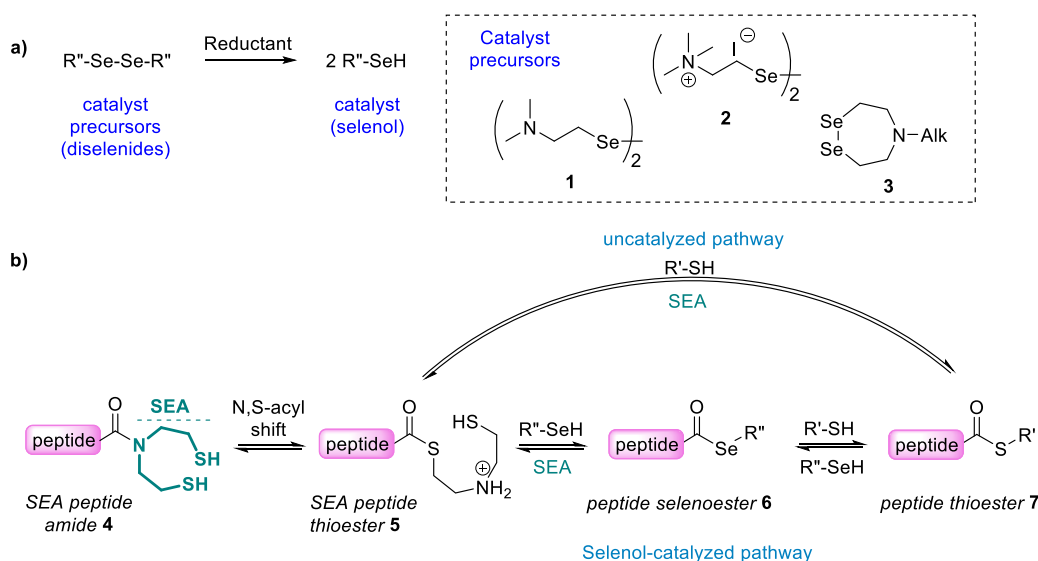

Fig. 1. a) Selenol-based catalysts in the form of their diselenide precursors; b) Principle of the selenol-catalyzed thiol-thioester exchange from SEA-peptides.

Results and Discussion

The exchange reactions were conducted on a 10-mer model peptide in the presence of a selenol-based catalyst introduced at various concentrations and were monitored by HPLC (Figure. 2a,b). The data showed that selenols derived from diselenides **1** and **3** were almost equally efficient for accelerating the formation of MPA-thioester **9** from SEA-peptide **8** when introduced at 25 mM or more (50 mM total selenol concentration) (Figure 2c). Diselenide **2** was found not as potent as **1** or **3**. From a synthetic perspective, catalyst precursors **1** and **2** could be obtained at the gram scale, in fewer chemical steps and in higher yield than compound **3**. Alltogether, these results prompted us to use diselenide **1** as a precatalyst for the total chemical synthesis 9-GN granulysin.
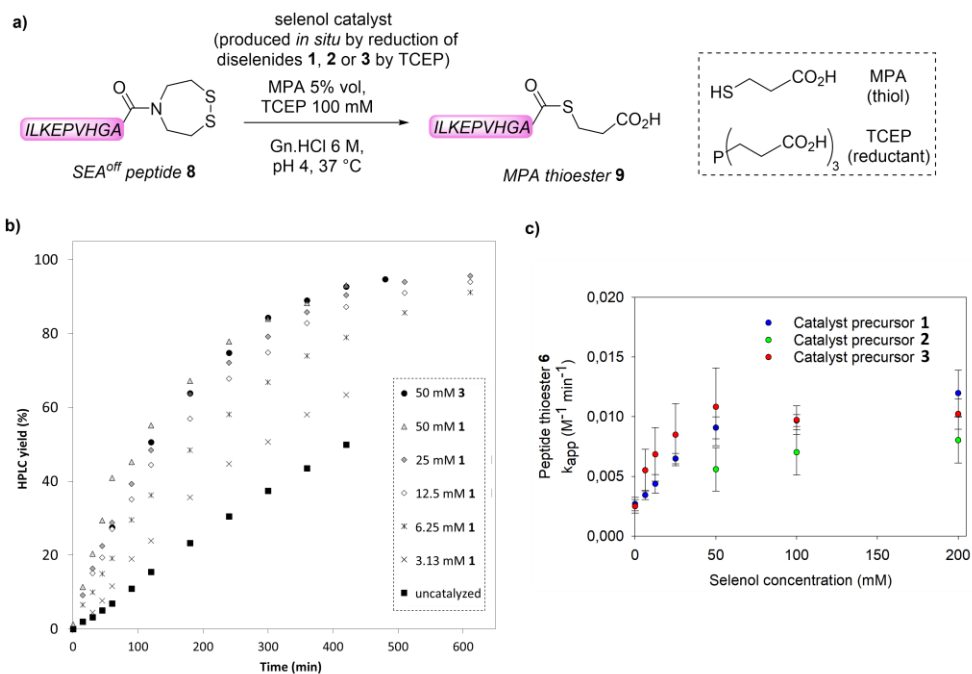
*Fig. 2. a) Model reaction for the SEA/MPA thiol-thioester exchange; b) HPLC monitoring of the reaction (yields calculated on the basis of the UV signal at 215 nm); c) Influence of catalyst's nature and concentration on the rate of the thiol/thioester exchange (apparent second order rate constants of peptide **9** formation determined by nonlinear regression fitting).*

9-GN is a human cytotoxic, chemoattractant and proinflammatory protein secreted by specialized cells from the immune system in response to infections. The design of 9-GN analogues with potential therapeutic interest motivated the development of an efficient and modular synthetic route (Figure 3a). In this approach, diselenide **1** was used as the precatalyst to successfully accelerate the formation of the central segment B in the form of an MPA-thioester from a SEA precursor. The linear polypeptide **9-GN-l** obtained after the concatenation of two additional segments by NCL was folded and the formation of the native pattern of disulfide bonds was determined by trypsic digestion under non-reducing conditions and mass spectrometry. The UPLC-MS analysis of **9-GN** highlights the quality of the protein obtained by the designed synthetic route (Figure 3b).
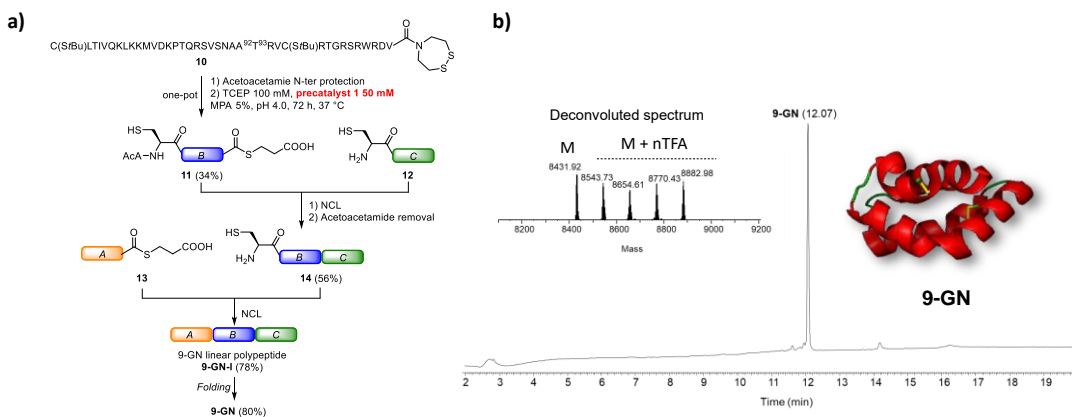
Fig. 3. a) Synthetic approach toward native 9-GN protein; b) UPLC-MS characterization of folded synthetic 9-GN protein.

Conclusion

We evidenced that the *bis*(2-sulfanylethyl)amido (SEA)/thiol exchange process could be efficiently catalyzed by selenocysteamine-derived selenols. These compounds can be easily synthesized at the multigram scale from cheap and commercially available starting materials. As catalysts, they are bench-stable for months in the form of their diselenide precursors and can be used for chemical protein synthesis as illustrated with the production of native 9 kDa granulysin.

References

1. Agouridas, V., et al. *Chem. Rev.* **12**, 7328-7443 (2019), http://dx.doi.org/10.1021/acs.chemrev.8b00712
2. Diemer, V., et al. *Chemistry* **28**, e202104229 (2022), https://doi.org/10.1002/chem.202104229
3. Kerdraon, F., et al. *Molecules* **26**, 1386 (2021), https://doi.org/10.3390/molecules26051386
4. Cargoët, M., et al. *J. Org. Chem.* **83**, 12584-12594 (2018), https://doi.org/10.1021/acs.joc.8b01903

Expanding the Protein Chemical Synthesis Toolbox with
N- Selenoethyl Cysteine

Vincent Diemer[1], Olga Firstova[1], Vangelis Agouridas[1,2], and Oleg Melnyk[1]

[1]Univ. Lille, CNRS, Inserm, CHU Lille, Institut Pasteur de Lille, U1019 - UMR 9017 - CIIL – Center for Infection and Immunity of Lille, F-59000 Lille, France; [2]Centrale Lille, F-59000 Lille, France

Introduction

Assembling peptide segments by native chemical ligation (NCL) is an efficient and powerful strategy for accessing native or modified proteins (Figure 1a) [1-3]. In this field, we recently reported that *N*-selenoethyl cysteine (SetCys) residue behaves as a redox-controlled cysteine (Cys) surrogate, and as such enables to temporally mask the reactivity of key Cys residues involved in peptide assemblies by NCL [4]. The interest of SetCys relies on its capacity to lose spontaneously its selenoethyl appendage after reduction of the cyclic selenosulfide bond (Figure 1b). Although breaking carbon-nitrogen bonds usually requires harsh conditions, we discovered that the SetCys conversion into Cys optimally occurs under mild conditions (pH 6, 37°C) [4]. We show here that the rate of the SetCys conversion into Cys can be controlled by choosing the combination of reductants (phosphine/thiol) used for inducing the ring-opening of the SetCys residue, thereby increasing its scope in protein chemical synthesis.
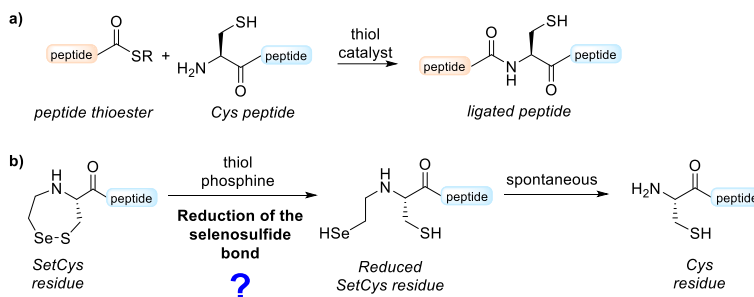

Fig. 1. a) NCL reaction. b) SetCys as a redox controlled Cys surrogate.

Results and Discussion

Peptide **1** was used as a model compound to investigate the impact of thiols and phosphines that are classically employed as additive in NCL reactions on the kinetics and the mechanism of the SetCys conversion into Cys (Figure 2). No reaction was observed in the presence of MPAA (4-mercaptophenylacetic acid), the gold standard catalyst used to accelerate the NCL reaction [4]. In contrast, the addition of water-soluble alkyl or aryl phosphines into the reaction mixture cleanly induced the conversion of SetCys into Cys.

In the presence of TCEP (*tris*(2-carboxyethyl)phosphine), we showed that the rate of the reaction was independent of the phosphine, the thiol additive and the SetCys peptide concentrations [5]. This result points towards a mechanism in which the Se-S bond is directly and quickly reduced by the phosphine (Figure 2b, path a). The ring-opening of SetCys is so fast in these strong reducing conditions that the rate of the whole process is dictated by the subsequent cleavage of the selenoethyl appendage.
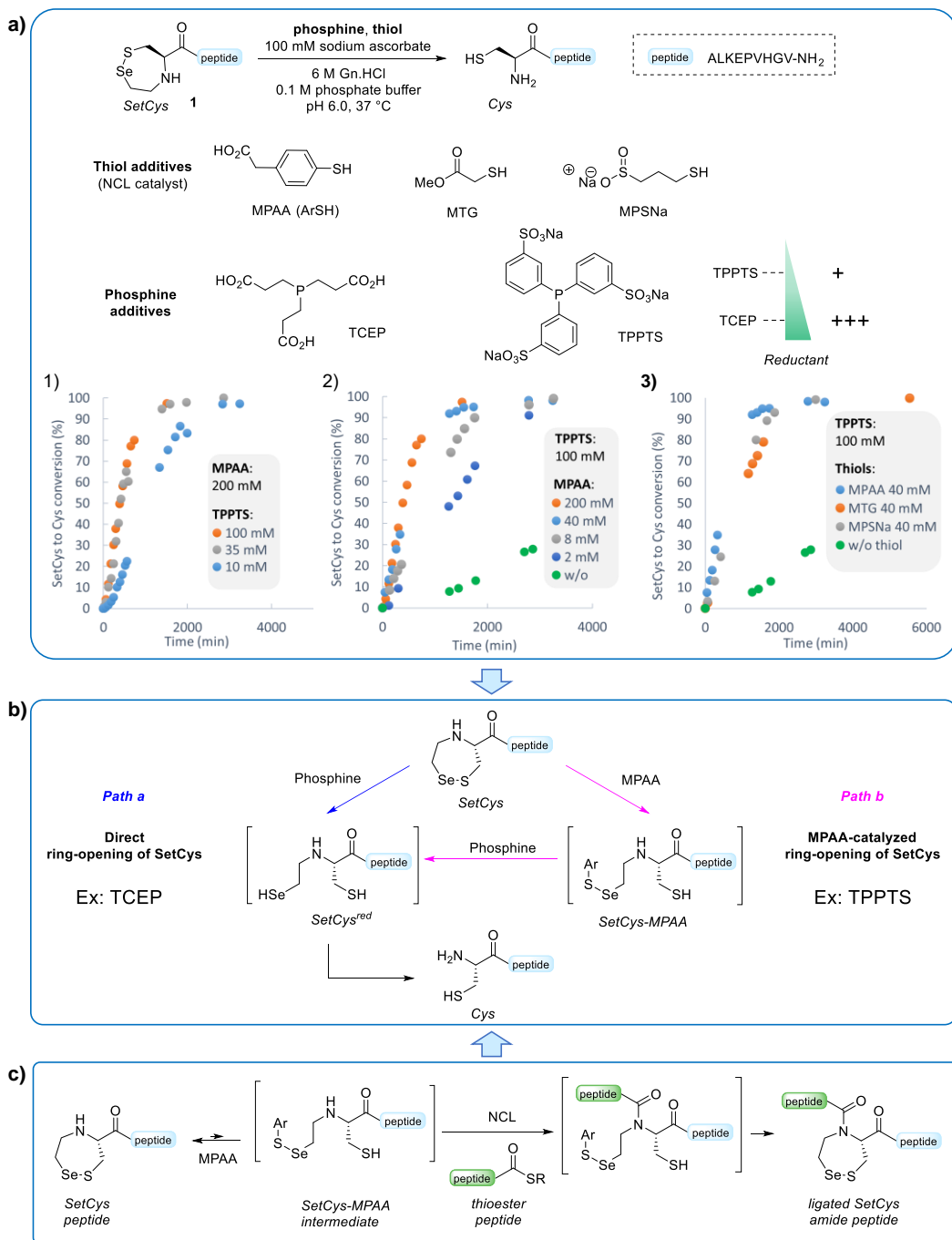
Fig. 2. Study of the SetCys to Cys conversion: effect of the thiol and phosphine additives on the rate of the reaction. a) Model reaction and kinetic data. b) Main mechanisms for the SetCys reduction by phosphines. c) Evidence for SetCys opening by the thiol catalyst.

The situation is clearly different when a less reactive phosphine such as TPPTS (3,3′,3″-phosphanetriyltris(benzenesulfonic acid) trisodium salt) was used as reductant [5]. We found that the

rate of the SetCys to Cys conversion depends in this case on the aryl phosphine concentration (Figure 2a, graph 1), and this up to 35 mM, a concentration above which the reduction process involving TPPTS is no longer rate limiting. Furthermore, we discovered that the SetCys conversion into Cys was efficiently catalysed by MPAA (Figure 2a, graph 2). Very slow in the absence of MPAA (t½ 75.4 h), the reaction is more than 10-fold faster when MPAA is present at 200 mM (t½ 6.5 h). A screening of the reaction conditions showed that the MPAA was the most efficient additive among the tested thiols (Figure 2a, graph 3).

Such an acceleration of the SetCys to Cys conversion in the presence of MPAA led us to postulate a second mechanism for SetCys reduction where the Se-S bond is initially cleaved by the thiol additive in a step which is rate limiting (Figure 2b, path b). The product of SetCys opening by MPAA is postulated to be an alkyl aryl selenosulfide, due to the higher affinity of thiolate nucleophiles for selenium [6-8]. This intermediate is then reduced by TPPTS into a free selenol, a step that triggers the cleavage of the C-N bond and the formation of the target Cys peptide. Although the intermediate alkyl aryl selenosulfide has never been detected by simply incubating SetCys peptides in presence of MPAA, some experiments argue for its formation in situ (Figure 2c). In particular, the formation of SetCys amide peptides by an NCL-like mechanism can occur only if the cyclic structure of the SetCys residue is transiently opened by MPAA during the ligation.

To sum up, the ring-opening of SetCys *via* the reduction of its selenosulfide bond is a fast process in the presence of strong reductant such as TCEP. In these conditions, the rate of SetCys to Cys conversion is dictated by the intramolecular substitution process leading to C-N bond cleavage. In contrast, the SetCys reduction is significantly slower with TPPTS, a milder reductant compared to TCEP, delaying the subsequent conversion of SetCys into Cys. However, we discovered that the lower reducing power of TPPTS can be efficiently balanced by the addition of thiol catalysts. Such a finer tuning of the SetCys reactivity through the combination of phosphine and thiol additives will certainly open the way towards new redox-controlled strategies for concatenating peptide segments by NCL.

Acknowledgments

References

1. Diemer, V., Firstova O., Agouridas V., Melnyk O. *Chemistry* **28**, 16, e202104229 (2022), https://doi.org/10.1002/chem.202104229
2. Agouridas, V., El Mahdi, O., Diemer, V., Cargoet, M., Monbaliu, J.-C.M., Melnyk O. *Chem. Rev.* **12**, 7328-7443 (2019), https://doi.org/10.1021/acs.chemrev.8b00712
3. Agouridas, V., El Mahdi, O., Melnyk, O. *J. Med. Chem.* **63**, 15140-15152 (2020), https://doi.org/10.1021/acs.jmedchem.0c01082
4. Diemer, V., Ollivier, N., Leclercq, B., Drobecq, H., Vicogne, J., Agouridas, V., Melnyk, O. *Nat. Commun.* **11**, 2558 (2020), https://doi.org/10.1038/s41467-020-16359-6
5. Firstova, O., Melnyk, O., Diemer, V. *J. Org. Chem.* **87**, 14, 9426-9430 (2022), https://doi.org/10.1021/acs.joc.2c00934
6. Steinmann, D., Nauser, T., Koppenol, W.H. *J. Org. Chem.* **75**, 6696-6699 (2010), https://doi.org/10.1021/jo1011569
7. Lothrop, A.P., Snider, G.W., Ruggles, E.L., Patel, A.S., Lees, W.J., Hondal, R.J. *Biochemistry* **53**, 654-663 (2014), https://doi.org/10.1021/bi400658g
8. Bachrach, S.M., Demoin, D.W., Luk, M., Miller J.V. *J. Phys. Chem. A* **108**, 4040-4046 (2004), https://doi.org/10.1021/jp037972o

Practical and Straightforward Stereoselective Synthesis of (*S*)-5,5,5,5',5',5'-hexafluoroleucine

Aline Delamare,[1] Guillaume Naulet,[1] Brice Kauffmann,[2] Gilles Guichard,[1] and Guillaume Compain[1]

[1]Univ. Bordeaux, CNRS, Bordeaux INP, CBMN, UMR 5248, IECB, F-33600 Pessac, France;
*[2]Univ. Bordeaux, CNRS, INSERM, IECB, UAR 3033, F-33600 Pessac, France*

Introduction

Fluorinated amino acids in drug design and protein science are currently the focus of intensive research [1,2]. The hydrophobic properties of fluorine combined with its small Van der Waals radius are interesting features for modulating lipophilicity of hydrophobic amino acids while retaining the morphology of the parent version. In addition, polyfluorinated versions of proteinogenic hydrophobic amino acids have proved particularly well suited to study the structure and function of proteins using ^{19}F NMR experiments [3]. In this respect, 5,5,5,5',5',5'-hexafluoroleucine which bears six fluorine atoms and displays a significantly higher hydrophobicity than the corresponding canonical version is a key fluorinated amino acid [4,5]. Only few synthetic pathways of this enantiopure fluorinated amino acid have been reported, and these syntheses involve the use of hexafluoroacetone or hexafluorothioacetone dimer [6-9]. In this study, we report a new route to access (*S*)-5,5,5,5',5',5'hexafluoroleucine using 2-(bromomethyl)-1,1,1,3,3,3-hexafluoropropane. The synthetic pathway is based on the homologation of chiral nickel complex, notably developed and exemplified by the group of Soloshonok [10-12] and more recently by the group of Koksch [13] for the synthesis of other α-amino acids with fluorinated side chains. The protocol enables the incorporation of the hexafluoroisobutyl side chain in one step through an original cascade reaction [14]. The method is highly practical and amenable to large scale synthesis.

Results and Discussion

Optimization of reaction conditions

We started by evaluating the alkylation reaction on chiral nickel complex **1** using NaOH powder in THF at -20 C (Table 1, entry 1). Unfortunately, the desired product **2** was formed with a very low yield (6%, entry 1) and the pentafluoroalkenylated compound **3** was obtained as the predominant product (55% yield). The structure of diastereoisomers (*S,S*)-**2** and (*S,S*)-**3** was confirmed by X-ray analysis (*Fig. 1*). Despite the successful alkylation of **1**, an elimination of fluoride is thus taking place at some point in the process. We tested other alkali metal bases, LiOH, KOH and tBuOK (entries 2-4), but compound **2** was still the minor compound (6-15%). We also tested alkali metal bases in DMF to see if a more polar solvent could favour the formation of the hexafluorinated compound (Table 2, entries 5-8). However, compound **2** was not observed with NaOH, LiOH and tBuOK. In contrast, CsOH tends to favour the formation of compound **2** (23% yield) and lower the yield of compound **3**. These observations indicate the crucial role of the fluoride counter ion by dictating the solubility of the salt. The fluoride released during the reaction (1 equiv.) is trapped by alkali metals (*i.e.* LiF, NaF, KF) to form insoluble fluoride salts precluding further reaction. With CsOH, the resulting fluoride salt is more soluble and the hydrofluorination of **3** is thus more favoured. To see whether the addition of a crown ether could capture the metal and preserve the nucleophilicity of the fluoride, we tested the combination of 15-crown-6 with NaOH (Table 1, entry 9). Surprisingly, this condition favoured the formation of the elimination product **3**, which was obtained in a yield higher than without the crown ether (61% versus 55% respectively). In these conditions, only trace amount of **2** could be detected in the crude NMR compare to 6 % yield obtained without crown ether. As the pentafluoroalkene moiety should be quite electrophilic due to the presence of five electron-withdrawing fluorine atoms, we tested whether the elimination could be reversed by using a source of fluoride as a base. To our delight, compound **2** was successfully isolated with a good 66% yield using a large quantity of TBAF (10 equiv., entry 10).

Table 1. Optimization of reaction conditions.
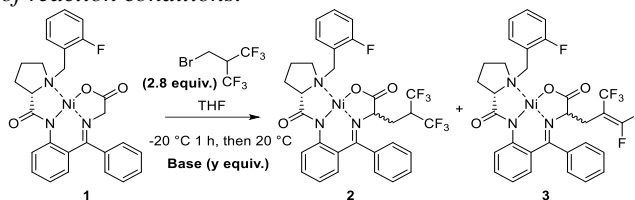
Entry	Base (y)	Solvent	Reaction Time (h)	Yield		
				1	2[a]	3[a]
1	NaOH (4)	THF	4	20 %	6 %	55 %
2	LiOH (4)	THF	4	40 %	15 %	38 %
3	KOH (4)	THF	4	32 %	6 %	44 %
4	tBuOK (4)	THF	4	20 %	13 %	47 %
5[b]	NaOH (4)	DMF	4	nd	-	23 %
6	LiOH (4)	DMF	4	-	-	53 %
7[c]	tBuOK (4)	DMF	5.5	nd	-	52 %
8	CsOH (4)	DMF	4	-	23 %	35 %
9[d]	NaOH (4)	THF	4	25 %	Trace	61 %
10	TBAF (10)	THF	3	-	66%	-

[a] Compounds 2 and 3 were obtained as a mixture of diastereoisomers, the diastereoisomeric ratio ((S,S)-2:(S,R)-2 and (S,S)-3:(S,R)-3) determined by ^{19}F NMR was between 88:12 and 93:7 for all tested conditions. [b] 1/2/3 ratio: 68:1:31, determined by ^{19}F NMR. [c] 1 equiv. of 2-(bromomethyl)-1,1,1,3,3,3-hexafluoropropane was added after 4.5 h of reaction at 20 °C; 1/2/3 ratio: 25:0:75, determined by ^{19}F NMR. [d] 5 equiv. of 15-crown-5 were added

Mechanism insights

The reactivity of the fluorinated electrophile was studied in the presence of TBAF and the reaction was followed by ^{19}F NMR (Figure 2A). After few minutes, the brominated reagent undergoes an elimination of HBr to produce hexafluoroisobutylene (HFIB), and the latter one is relatively stable in the reaction medium beyond 3 h. Indeed, this reaction is favoured due to the presence of two CF_3 groups which extensively contribute to enhancing the acidity of the central C–H bond. Consequently, the alkylating reagent in the reaction is unlikely to be the bromo derivative but rather the alkene instead. Then, we performed *in situ* NMR experiments to monitor the reaction of **1** (Figure 2B).
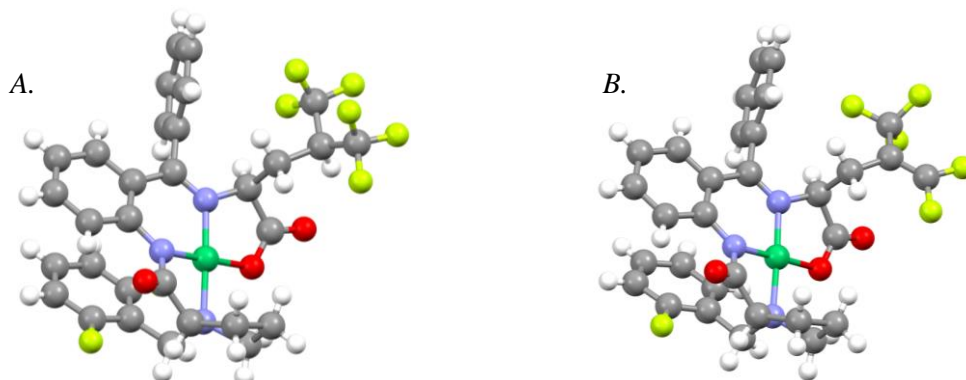
Fig. 1. X-ray structures of compounds (S,S)-2 (A.) and (S,S)-3 (B.).

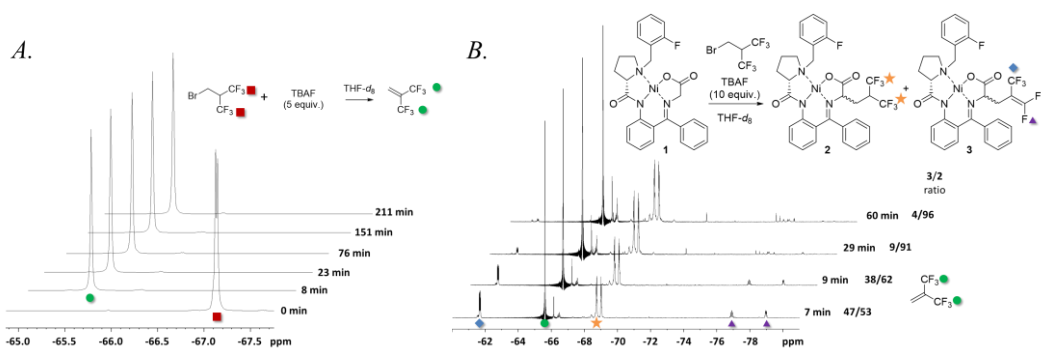*Fig. 2. In situ ¹⁹F NMR experiments.*

The formation of both compounds **2** and **3** was rapidly observed (after only 7 minutes). Then, the proportion of compound **3** started to decrease progressively over time with a concomitant increase in the intensity of the signal corresponding to compound **2**. These observations indicate that compound **3** is formed first and then converted into compound **2**, thus suggesting that TBAF promotes the addition of HF to the alkene.

The mechanism depicted on Figure 2 has been proposed (Figure 3). The brominated reagent rapidly undergoes an elimination of HBr under basic conditions to provide HFIB. In parallel, the deprotonation of the nickel complex leads to the formation of enolate, which then reacts with HFIB through an allylic shift (S_N2' mechanism). This provides the elimination product **3**. Then, the excess of fluoride ions efficiently reacts with **3** (hydrofluorination) to give compound **2**. In contrast, the use of alkali metal bases leads to insoluble fluoride salts and **3** is obtained predominantly.

Multi-gram scale synthesis

This methodology is compatible with a multi-gram scale procedure as shown in Figure 4. The two diastereoisomers (*S*,*S*)-**2** and (*S*,*R*)-**2** were successfully separated by flash chromatography affording pure (*S*,*S*)-**2** with a diastereomeric ratio > 99:1. The hydrolysis of the alkylated complex (*S*,*S*)-**2** afforded hexafluoroleucine (*S*)-**4** with an almost quantitative yield (Figure 4). The N-Fmoc or N-Boc protected derivatives (respectively (*S*)-**5** and (*S*)-**6**) can be obtained using FmocOSu or Boc₂O respectively, directly after hydrolysis of the alkylated nickel complex without intermediate purification. After the hydrolysis of complexes (*S*,*S*)-**2**, the chiral ligand derived from proline can be recovered quantitatively and reused to synthesise the Ni(II) complex (*S*)-**1**. Excellent enantiomeric ratios > 99:1 were found for (*S*)-**4** (Marfey's derivatization method).
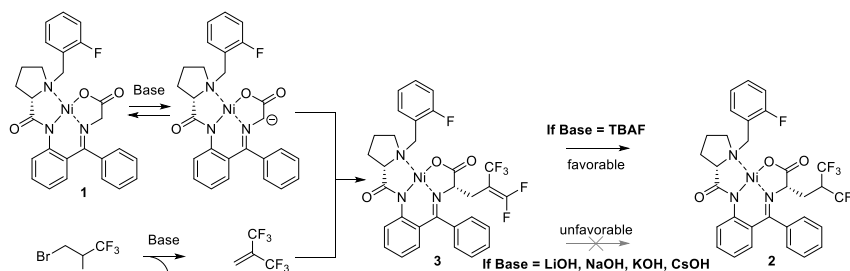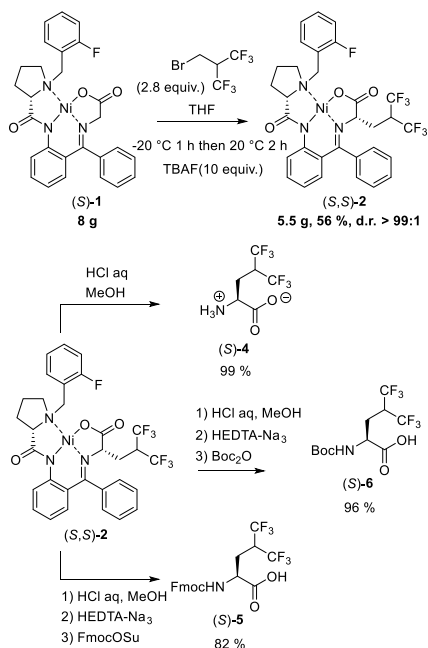

Fig. 3. Proposed mechanism.

Fig. 4. Large-scale synthesis of (S)-5,5,5,5',5',5'-hexafluoroleucine and its N-Boc and N-Fmoc protected derivatives.

Conclusions

In summary, we report a hexafluoroisobutylation cascade reaction mediated by TBAF for the synthesis of enantiopure (S)-5,5,5,5',5',5'-hexafluoroleucine. The reaction is based on the nucleophilic attack on HFIB, rapidly formed under basic conditions from 2-(bromomethyl)-1,1,1,3,3,3-hexafluoropropane. HFIB reacts first with the deprotonated Schiff base complex through a S_N2' mechanism promoting a fluoride β-elimination affording a fluoroalkene group. Unfortunately, when using alkali metal bases, the reaction provides predominantly this undesired alkene. However, we found that the use of TBAF as a base allows the efficient and selective formation of the hexafluoro-isobutylated compounds by promoting the addition of HF to the alkene. *In situ* NMR data support the cascade elimination/allylic shift/hydrofluorination mechanism. This method is highly practical since the brominated reagent is liquid at room temperature, unlike HFIB. Hydrolysis of the nickel complex readily affords the (S)-fluorinated amino acid, as well as N-Boc and N-Fmoc-protected derivatives with high enantiopurity. The finding that the whole procedure is amenable to multi-gram-scale synthesis bodes well for a broader use of this polyfluorinated leucine analogue to engineer peptides and proteins for applications in medicinal chemistry and chemical biology.

Acknowledgments

References

1. Mei, H., et al. *Eur. J. Med. Chem.* **186**, 111826 (2020), https://doi.org/10.1016/j.ejmech.2019.111826
2. Berger, A.A., et al. *Acc. Chem. Res.* **50**, 2093-2103 (2017), https://doi.org/10.1021/acs.accounts.7b00226
3. Miller, M.A., et al. *ChemBioChem* **21**, 3451-3462 (2020), https://doi.org/10.1002/cbic.202000297
4. Huhmann, S., et al. *Beilstein J. Org. Chem.* **13**, 2869-2882 (2017), https://doi.org/10.3762/bjoc.13.279
5. Marsh, E.N.G. *Acc. Chem. Res.* **47**, 2878-2886 (2014), https://doi.org/10.1021/ar500125m
6. Xing, X., et al. *Org. Lett.* **3**, 1285-1286 (2001), https://doi.org/10.1021/ol015567e
7. Anderson, J.T., et al. *Org. Lett.* **4**, 4281-4283 (2002), https://doi.org/10.1021/ol026922j
8. Chiu, H.-P., et al. *J. Am. Chem. Soc.* **128**, 15556-15557 (2006), https://doi.org/10.1021/ja0640445
9. Chiu, H.-P., et al. *Org. Lett.* **9**, 5517-5520 (2007), https://doi.org/10.1021/ol702470j
10. Wang, Y., et al. *Amino Acids* **49**, 1487-1520 (2017), https://doi.org/10.1007/s00726-017-2458-6
11. Aceña, J.L., et al. *J. Fluorine Chem.* **155**, 21-38 (2013), https://doi.org/10.1016/j.jfluchem.2013.06.004
12. Romoff, T.T., et al. *Org. Process Res. Dev.* **21**, 732-739 (2017), https://doi.org/10.1021/acs.oprd.7b00055
13. Hohmann, T., et al. *J. Org. Chem.* **87**, 10592-10604 (2022), https://doi.org/10.1021/acs.joc.2c00522
14. Delamare, A., et al. *Chem. Sci.* **13**, 9507-9514 (2022), https://doi.org/10.1039/D2SC02871A

Adhesion Miniproteins for Tissue Engineering – From Molten Globule to Active Metalloprotein

Florian Häge and Franziska Thomas

Institute for Organic Chemistry, Heidelberg University, Im Neuenheimer Feld 270, 69120 Heidelberg, Germany, Email: Florian.Haege@oci.uni-heidelberg.de

Introduction

Tissue Engineering requires extracellular matrix (ECM)-like scaffold materials to support the formation of tissue from cells. Our goal is to create a biomimetic material that uses immobilized designed miniproteins mimicking the Ca^{2+}-carbohydrate-interaction of Laminin or other LG domain-containing ECM proteins and the cell-surface receptor Dystroglycan [1].

As designed peptides tend to bind their targets with a weaker affinity, we chose a tight-binding natural model – calmodulin [2] – to achieve a micromolar binding affinity similar to the LG domain-calcium interaction [3].
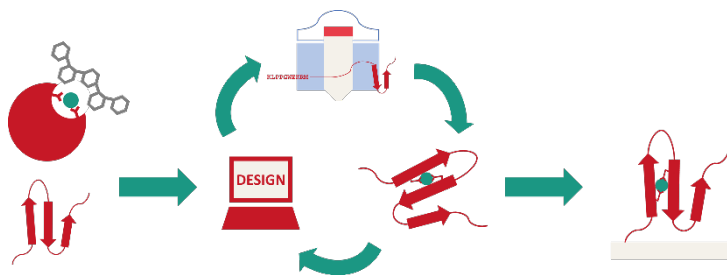
Fig. 1. Design of an ECM-mimetic material.

Design Strategy

The peptides were designed intuitively from a natural model and a small β-peptide scaffold (Figure 1). For this, the active center of the natural model protein – calmodulin – was overlaid with the crystal structure of the scaffold domain (Figure 2). Once a fitting position was found, the Scaffold was mutated to imitate the binding site of the natural model. Rosetta Relax for geometry optimization and evaluation.
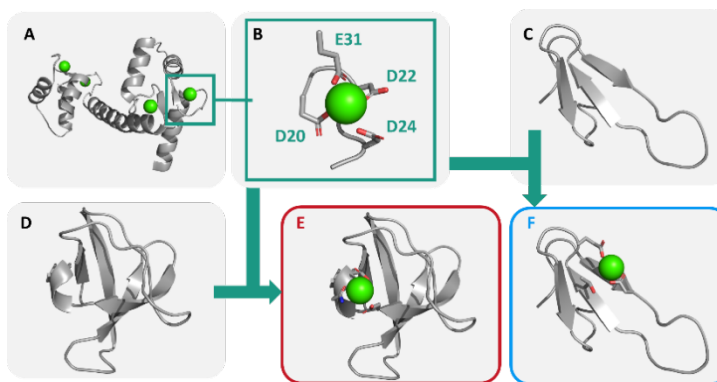

Fig. 2. Concept of the intuitive Design of adhesion miniproteins. (A) Natural model: calmodulin, (B) active center, (C) WW domain, (D) SH3 domain and designed peptides (E) Scan 1 and (F) WWcalm 3.1.

Structural Analysis

CD spectroscopy was used to determine the secondary structure of the newly designed peptides Scan and WWcalm, based on calmodulin and the SH3 and WW domains respectively (Figure 3).
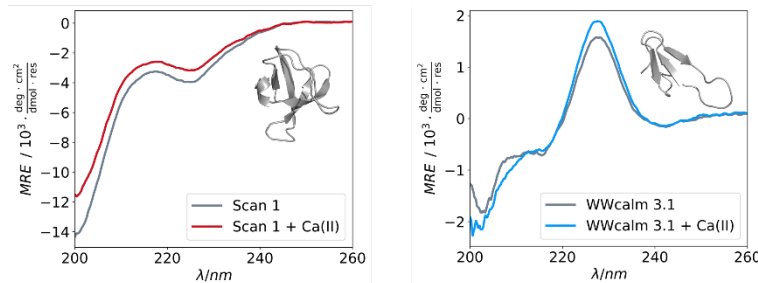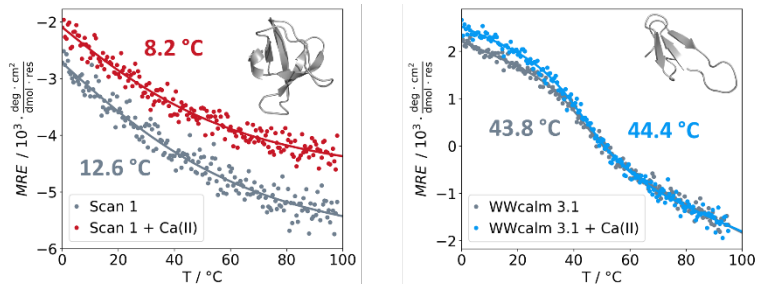

Fig. 2. CD spectra of (left) Scan 1 and (right) WWcalm 3.1 in the absence (grey) and presence of Ca^{2+} (colored) in buffered solution (NEM, pH 7.2).

Fig. 3. Thermal denaturation curves of (left) Scan 1 and (right) WWcalm 3.1 in the absence (grey) and presence of Ca^{2+} (colored) in buffered solution (NEM, pH 7.2).

Stability Improvement

A more stable mutant of WWcalm 3.1 was designed using our WW domain library. The Design of a stable Scan peptide was unsuccessful (Figure 4 and 5).
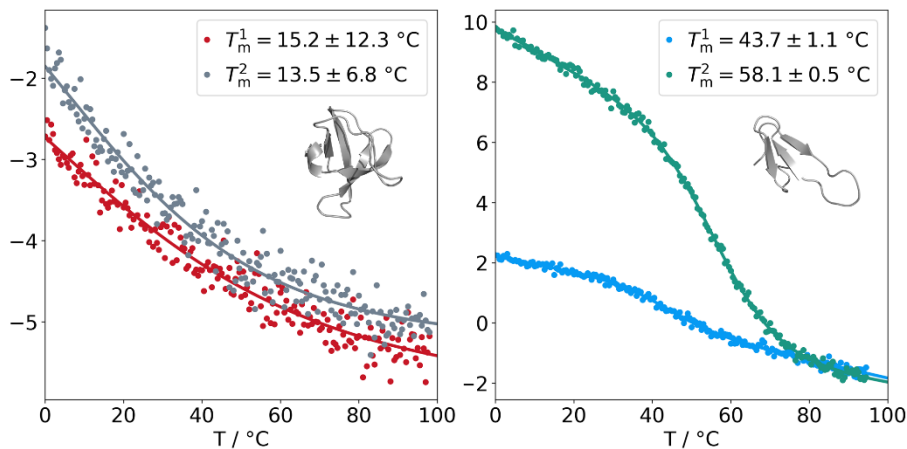
Fig. 4. Left: Thermal denaturation curves of Scan1-2. Right: Thermal denaturation curves of WWcalm 3.1-2.

Table 1. Protein domains or designed Peptides and their dissociation constants for Ca²⁺.

	Calmodulin	*Laminin*	*Neurexin*	*Scan1*	*WWcalm3.1*	*WWcalm3.2*
K_d [μM]	0.53 - 1.18	$5 - 300$	400	108 ± 94	14.5 ± 6.5	80 ± 210
Ca²⁺-binding domain	EF-hand	LG3-5	LG2	EF-hand	EF-hand	EF-hand
Reference	[2]	[3]	[5]	Design	Design	Design

Competitive Binding Assay

The UV-signal of Br₂-BAPTA at 263 nm is calcium-dependent (Figure 6). With its K_d identified, we used the dye to determine our peptides' K_d in a competitive binding experiment (Figure 7) based on a protocol by Linse et al. [4].
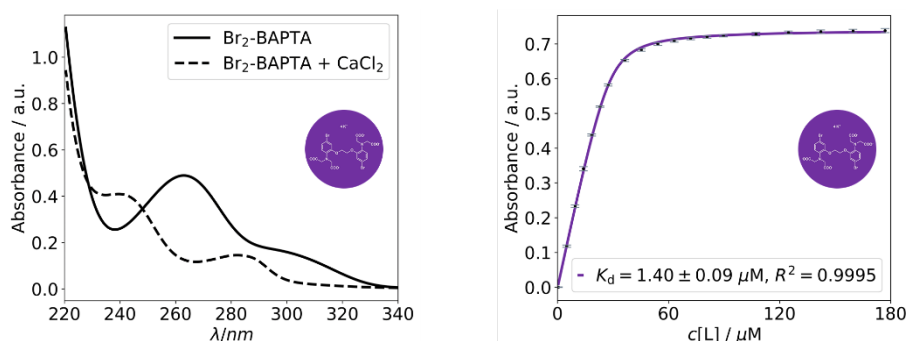
Fig. 5. Left: UV spectrum of Br2-BAPTA in the presence (dashed) and absence (straight) of Ca2+.

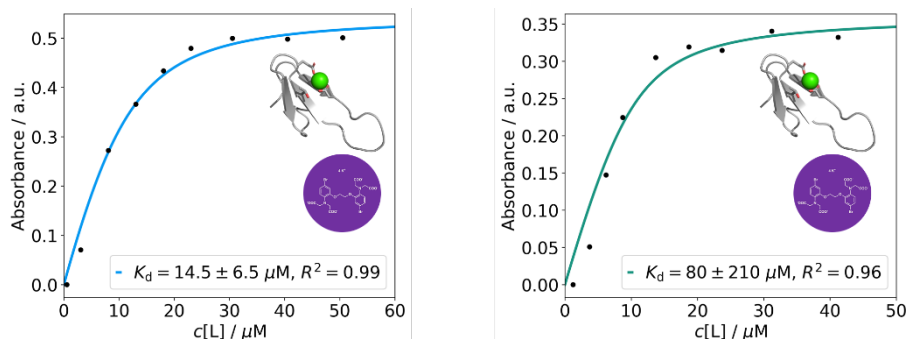*Fig. 6. Competitive Ca²⁺-Binding assays of WWcalm3.1 (left) and WWcalm3.2 (right) versus Br₂-BAPTA.*

Conclusions

We designed three Ca²⁺-binding peptides based on the WW and SH3 domains. Structural analysis showed correct folding and structural changes upon Ca²⁺ addition. Stabilization of the metastable Scan was unsuccessful.

We determined K_d values for Scan 1 (108 µM), WWcalm 3.1 (14.5 µM) and 3.2 (80 µM) in the range of LG domains. The carbohydrate-binding will be investigated next.

Acknowledgments

References

1. Hohenester, E. *Curr Opin Struct Biol* **56**, 56-63 (2019), https://doi.org/10.1016/j.sbi.2018.11.007
2. Zhang, M., et al. *Structure* **20**(5), 911-923 (2012), https://doi.org/10.1016/j.str.2012.03.019
3. Paulsson, M. *JBC* **263**(11), 5425-5430 (1988), https://doi.org/10.1074/jbc.M702963200
4. Linse, S., et al. *JBC* **266**(13), 8050-8054 (1991), https://doi.org/10.1016/S0021
5. Dempsey, C.E., et al. *Front Mol Biosci* **6**(18), 1-19 (2019), https://doi.org/10.3389/fmolb.2019.00018

Fast-SEA: Modifying Proteins in the Nanomolar Concentration Range with an NCL Inspired Ligation

Benjamin Grain[1], Benoît Snella[1], Jérôme Vicogne[1], Birgit Wiltschi[2], Oleg Melnyk[1], and Vangelis Agouridas[1,3]

[1]Univ. Lille, CNRS, Inserm, CHU Lille, Institut Pasteur de Lille, U1019 - UMR 9017 - CIIL - Center for Infection and Immunity of Lille, F-59000 Lille, France; [2]Institute of Bioprocess Science and Engineering, University of Natural Resources and Life Sciences, Vienna; [3]Centrale Lille, F-59000, Lille, France

Introduction

Chemical Protein Synthesis has greatly benefitted from the properties of the thioester functional group, in particular with the development of the Native Chemical Ligation (NCL) reaction (Figure 1a) [1,2]. However, NCL-based modification of proteins suffers from the moderate reactivity of classical alkyl and aryl thioesters, especially in highly dilute media [3]. Seeking for fast reactive thioesters surrogates, we have discovered that oxalyl derivatives of bis(2-sulfanylethyl)amides (^{oxo}SEA) in the form of a latent thioester precursor could act as powerful and chemoselective acylating agents of β-aminothiols upon activation by reductants (Figure 1b) [4].
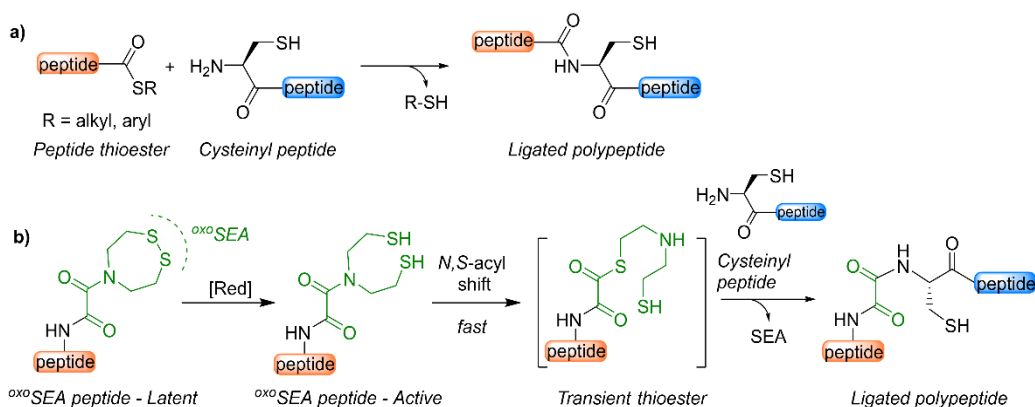

Fig. 1. a) Principle of the Native Chemical Ligation reaction; b) Principle of the ^{oxo}SEA-mediated ligation.

Results and Discussion

The SPPS-compatible lysine derivative **1** featuring an ^{oxo}SEA moiety on its side chain was prepared at the gram scale with 17% overall yield and its structure was validated through X-ray diffraction (Figure 2a,b).

The residue was incorporated into short model peptides of type **2**, which served as reactants to assess the reactivity of the ^{oxo}SEA group in the presence of a cysteinyl peptide **3** (Figure 2c). The study enabled to establish that the formation of ligation product **4a** through the ^{oxo}SEA-mediated ligation reaction of peptides **2a** and **3a** was: *i)* highly efficient even at peptide concentrations in the nanomolar concentration range, *ii)* rapid (~30 M^{-1} s^{-1} as compared to 0.3-4 M^{-1} s^{-1} for classical thioesters [5]), *iii)* triggered on-demand by the addition of a reductant (Figure 2d).
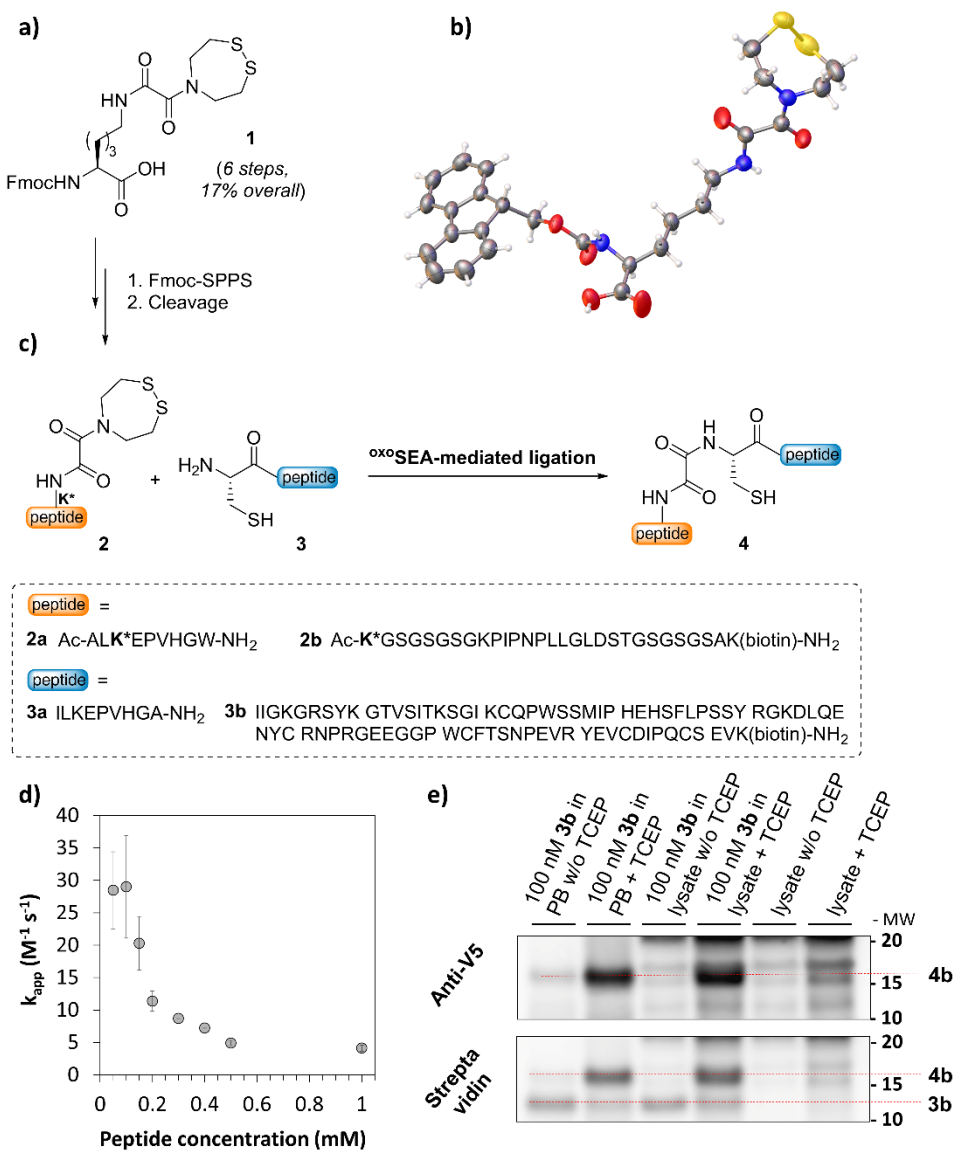
Fig. 2. a) Structure of Fmoc-Lys(*oxo*SEA)-OH synthetic residue **1**; b) Crystal structure of compound **1** with ellipsoids shown at the 50% probability level (ccdb 2164270); c) Sequence of the peptides used for the study of the *oxo*SEA-mediated ligation; d) Apparent second order rate constant of peptide **4a** formation determined by nonlinear regression fitting. The data correspond to the mean ± standard error (95% confidence limit interval) determined from three independent replicates. Conversion to ligated peptide **4a** from peptides **2a** and **3a** was performed using the following experimental conditions: 1 equiv. **2a**, 1.2 equiv. **3a**, 200 mM 4-mercaptophenylacetic acid (MPAA), 100 mM TCEP, pH 5.5, 37 °C in 6 M guanidinium chloride in 100 mM phosphate buffer; e) Western-blot analysis of the formation of **4b** in a crude THP-1 whole cell protein extract (1.6 µg µL-1) supplemented with 100 nM **3b** (i.e. 93 ng µL-1) in the presence of a 15-fold excess of **2b**.

260

To challenge the performance of the ᵒˣᵒSEA-mediated ligation at the protein level, an ᵒˣᵒSEA peptide derived from V5 peptidic tag **3a** and a *C*-terminally biotinylated kringle 1 domain of the hepatocyte growth factor (K1/HGF) equipped with an *N*-terminal cysteine **3b** were prepared (Figure 2c,e). Those were ligated in a crude protein extract of a THP-1 whole cell lysate supplemented with 100 nM of **3b** in the presence of a 15-fold excess of **3a**. Monitoring of the reaction was achieved by SDS-PAGE separation followed by Western Blot analysis and specific detection by anti-V5 monoclonal antibody labelled with horseradish peroxidase (HRP) and streptavidin-HRP. Formation of ligated product **4b** was successfully observed in the presence of TCEP, thereby demonstrating the chemoselectivity and the efficiency of the ᵒˣᵒSEA-mediated process.

Conclusion

The spectacular reactivity of this activatable oxalyl thioester surrogate allows to perform peptide and protein modification through a chemoselective ligation reaction. The latter proceeds extremely fast in aqueous media, under mild conditions and in highly dilute medium which can be as complex as a cell lysate. Introduced within peptide segments in the form of a lysine derivative, oxalyl thioesters offer an interesting extension to NCL as a conjugation method and might be useful for the development of novel crosslinking strategies or the polycondensation of water-soluble (bio)molecules.

Acknowledgments

References

1. Dawson, P.E., et al. *Science* **266**, 776-779 (1994), http://dx.doi.org/10.1126/science.7973629
2. Agouridas, V., et al. *Chem. Rev.* **12**, 7328-7443 (2019), http://dx.doi.org/10.1021/acs.chemrev.8b00712
3. Saito, F., et al. *ACS Chem. Biol.* **10**, 1026-1033 (2015), http://dx.doi.org/10.1021/cb5006728
4. Snella, B., et al. *Angew. Chem. Int. Ed.* **61**, e202204992 (2022), http://dx.doi.org/10.1002/anie.202204992
5. Diemer, V., et al. *Nat. Commun.* **11**, 2558 (2020), http://dx.doi.org/10.1038/s41467-020-16359-6

The Protein Chemical Synthesis Database (pcs-db.fr)

Vangelis Agouridas[1,2], Ouafâa El Mahdi[3], and Oleg Melnyk[1]

[1]Univ. Lille, CNRS, Inserm, CHU Lille, Institut Pasteur de Lille, U1019 - UMR 9017 - CIIL - Center for Infection and Immunity of Lille, F-59000 Lille, France; [2]Centrale Lille, F-59000, Lille, France
[3]Faculté Polydisciplinaire de Taza, University Sidi Mohamed Ben Abdellah, BP 1223 Taza Gare, Morocco

Introduction

Since 1994, chemoselective amide-bond forming reactions, of which the Native Chemical Ligation (NCL [1]), the Serine Threonine Ligation (STL [2]) or the KetoAcid HydroxylAmine ligation (KAHA [3]) are the more popular, have revolutionized chemical protein synthesis (CPS) by enabling the concatenation of unprotected, polyfunctionalized peptide segments in water under mild conditions (Figure 1). Such reactions have provided the means for successful applications in chemical biology, medicinal chemistry [4], materials science and nanotechnology research.
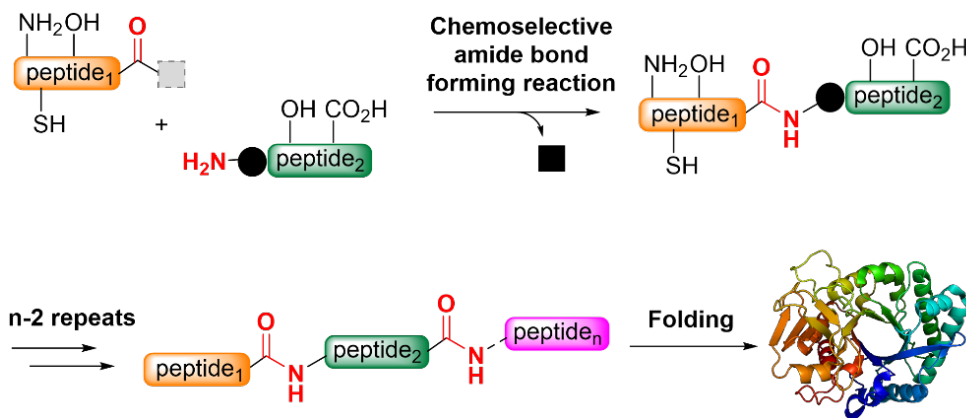

Fig. 1. General principle of amide-bond forming native ligation reactions.

These advances, which are described in a prolific literature, are presented in a freely available database: the Protein Chemical Synthesis database (pcs-db.fr) [5]. The present proceeding article describes the logical and conceptual design of the latter and how it can be exploited as a bridge between the research and teaching communities to promote chemical protein synthesis.

Material and methods

The PCS-db was built around three levels of information, mined from over 700 articles in the literature. In this context, synthetic targets of biological significance were retained whereas methodological studies using model peptides only were not considered. The different levels of information deal with:

-    the identity of synthesized proteins (name, year of publication, length, bibliographical reference),

-    the synthetic design of protein targets (type of ligation chemistry applied, number of ligations, nature of the junction residues, use of amino acid surrogates, thiol auxiliaries and/or the application of post-ligation treatments),

-    the presence of modifications (mutations, post-translational modifications, tags or presence of non canonical amino acids).

The various items were reported in a table file, which was processed with a cloud-based self-service to provide users with an intuitive, clear and comprehensive interface (Figure 2). In total, the PCS-db counts more than 1300 entries with around 15 descriptors each and can be interrogated through four independent search modules, all connected to the main database.
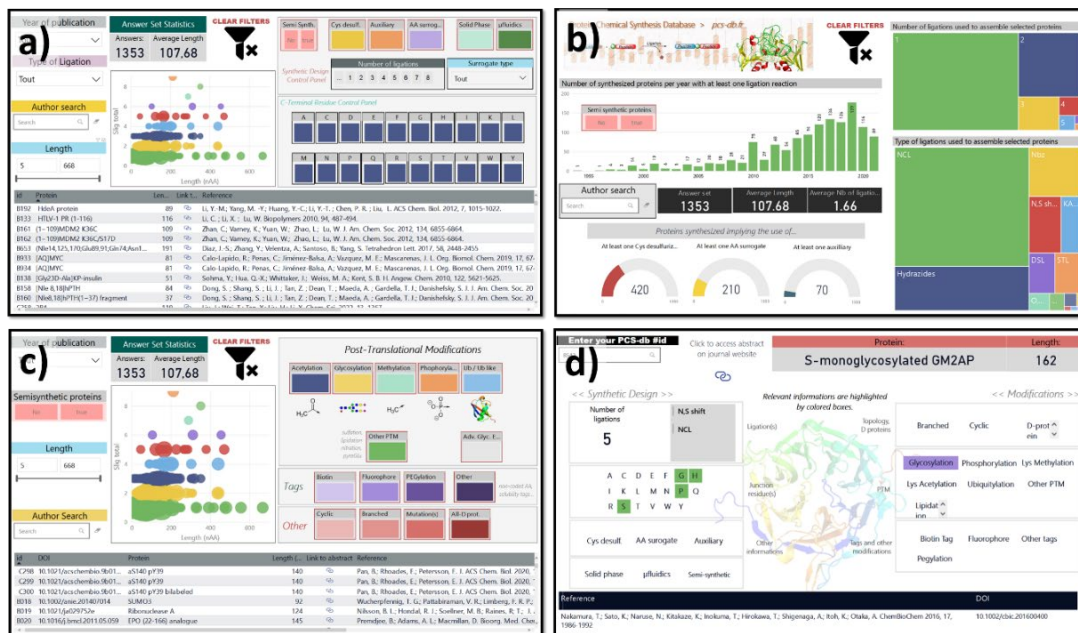

Fig. 2. The various modules of the PCS-db; a) the PCS-db module is the main module and is devoted to synthetic design; b) PCS-GO is a graphical companion providing synoptic views; c) PCS-PTM is a module devoted to modified synthetic proteins; d) PCS-id is a reverse look-up directory that allows to retrieve an entry from a #PCS-id.

The website also contains instructions, introductory bibliography and much more to discover online.

Results and discussion

The PCS-db offers researchers the possibility to achieve targeted bibliographical research ideally complementing well-established resources. By providing straightforwardly accessible information on the synthetic design of protein targets, the database can be perceived as a support decision tool for synthetic design selection. The database also reinforces the Research-Teaching Nexus by providing a structured learning environment.

Apart from practical aspects that allow instructors to find up-to-date articles or refresh their slides, the database can prove a useful support to teaching. Thanks to its comprehensive nature, data can be exploited to put the topic in perspective which is a concern hardly overcome by students when they are first introduced to new concepts or techniques. In the specific case of the PCS-db, we mean for example how the domain has quantitatively evolved over the years in terms of successfully synthesized targets and where a specific methodology stands compared to the other ones for a given period of time.

Also, the use of a database might orient teaching towards an inductive and more student-centered instruction. As databases are most often designed according to an entity-relationship model, deciphering the conceptual and logical design levels of the PCS-DB may help students acquiring a deeper understanding of the topic. For example, by formulating relevant queries in the context of driven homeworks, they should be able, alone or in a group, to identify, to evaluate and to analyze the main factors that govern the reactivity in amide-bond forming ligation reactions. Eventually, the results

of their research can be discussed in the classroom with the instructor and serve as a basis to develop the main concepts of ligation chemistry more in detail. Conversely, teachers can easily browse the PCS-DB and quickly build whole sets of relevant research articles to design a suitable learning environment for case-based studies.

The PCS-DB can also be further exploited for assessments. In this context, the instructor will let the students define their own search criteria, pick up, summarize and present a series of relevant articles to address a specific issue or limitation of amide-bond forming ligation reactions.

Conclusion

In its current state, the PCS database offers an efficient, interactive and free web-based tool on chemoselective amide-bond forming ligation reactions. Researchers, instructors or students can use it regardless of their knowledge of the field. The content of the PCS-DB is regularly updated to include the most recent contributions in the field and new features are to be implemented to offer a more accurate view of the topic.

References

1. Dawson, P.E., et al. *Science* **266**, 776-779 (1994), http://dx.doi.org/10.1126/science.7973629
2. Zhang, Y., et al. *Proc. Natl. Acad. Sci.* **110**, 6657-6662 (2013), http://dx.doi.org/ 10.1073/pnas.1221012110
3. Bode, J.W., et al. *Angew. Chem. Int. Ed.* **45**, 1248-1252 (2006), http://dx.doi.org/10.1002/anie.200503991
4. Agouridas, V., et al. *J. Med. Chem.* **63**, 15140-15152 (2020), http://dx.doi.org/10.1021/acs.jmedchem.0c01082
5. Agouridas, V., et al. *Bioorg. Med. Chem.* **25**, 4938-4945 (2017), http://dx.doi.org/10.1016/j.bmc.2017.05.050

First Application of the Combined *o*-NPS Nα-Protection/Carpino's Acylfluoride Cα-Activation Methods to the SPPS of Very Hindered Peptide Sequences

Alessandro Moretto[1], Quirinus B. Broxterman[2], Claudio Toniolo[1], and Fernando Formaggio[1]

[1]Department of Chemical Sciences, University of Padova, Padova, 35131, Italy;
[2]InnoSyn BV, Geleen, 6167 RD, The Netherlands

Introduction

We developed a novel, improved dyad of α-amino protection/α-carbonyl activation procedures in SPPS. This combination demonstrated to be very appealing, in particular with the sterically hindered, Cα-tetrasubstituted α-amino acids. The *ortho*-nitrophenylsulfenyl (*o*-NPS) α-amino protection (Figure 1), which cannot generate the chirally dangerous and poorly reactive 5(4H)-oxazolone intermediate, was used in conjunction with the Carpino's highly efficient α-aminoacyl fluoride (Figure 1) C-activation approach [1].
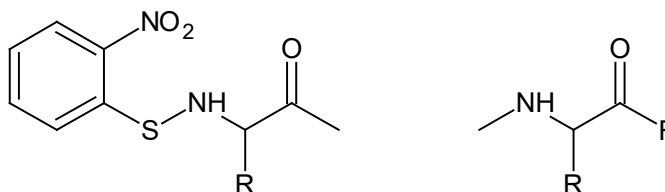

Fig. 1. Chemical structures of the derivatives o-NPS-α-aminoacyl (left) and α-aminoacyl fluoride (right) moieties.

Results and Discussion

In the course of our experiments, we modified gradually the spatial congestion of the -NH$_2$ moiety of the amino substrates along with the properties of the reaction conditions, in particular the coupling efficacy of the carboxyl component.

We first SPPS synthesized the pentapeptide Fmoc-(Aib)$_4$-L-Ala-OH using the Carpino's procedure, specifically with Fmoc-Aib-F and the Fmoc-L-Ala-SASRIN α-amino acid resin. This method is confirmed to be *highly efficient*.

Then, by employing the same SPPS procedure as above, we made an attempt to prepare the *much more hindered* tetrapeptide sequence -[D-(αMe)Val]$_4$-, using five equivalents of Fmoc-D-(αMe)Val. In this case, the synthesis essentially *failed* and the desired final compound was *not* found.

In the third step, our synthetic target was the tripeptide *o*-NPS-L-(αMe)Phg-Aib-D-(αMe)Phg-O*t*But by *solution* methods. We utilized o-NPS-Aib-F and (separately) the two enantiomeric *o*-NPS-(αMe)Phg-F. The α-amino group of the nucleophile was preactivated with BTSA [N,O-*bis*-(trimethylsilyl)-acetamide]. The final product was obtained in excellent (92%) yield after chromatographic purification.

We *initially* applied the o-NPS protection to *SPPS* for the production of the longer hexapeptide -L-Ala-(Aib)$_4$-L-Ala- by use of the *milder* Carpino's activation *HATU/HOAt* [2] method, Fmoc-L-Ala-SASRIN, and o-NPS-Aib-OH. The expected product was generated in a *very limited* percentage.

Our next step was the *first* application of the o-NPS-/-CO-F dyad to *SPPS* [in the synthesis of the pentapeptide sequence -L-Ala-(Aib)$_3$-L-Ala-]. Here, we took advantage of Fmoc-L-Ala-SASRIN and

o-NPS-Aib-F. Satisfactorily, the *largely major* peak in HPLC is that corresponding to the target product.

Finally, we prepared by SPPS *the very much congested* (at its *N*-terminus) tripeptide -[L-(αMe)Phg]₂-L-Ala-OH. To this end, we exploited *o*-NPS-L-(αMe)Phg-F and BTSA (N,O-bis(trimethylsilyl)acetamide). The HPLC and mass spectrometry results are *extremely* promising (88% overall yield).
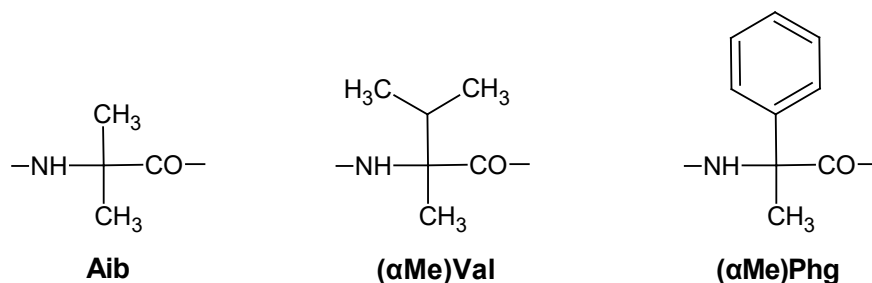

Fig. 2. Chemical structures of the C^α-tetrasubstituted α-amino acids used.

References

1. Carpino, L.A., Sadat-Aalaee, D., Chao, H.G., and DeSelms R.H. *J. Am. Chem. Soc.* **112**, 9651-9652 (1990), http://dx.doi.org/10.1021/ja00182a041
2. Carpino, L.A. *J. Am. Chem. Soc.* **115**, 4397-4398 (1993), http://dx.doi.org/10.1021/ja00063a082

Synthesis of Fluorinated Amino Acids for the Design of Injectable Hydrogels

Aurélie Honfroy[1,2,3], Grégory Chaume[1], Thierry Brigaud[1], Nathalie Lensen[1], Sophie Hernot[2], Steven Ballet[3], and Charlotte Martin[3]

[1]*CNRS, BioCIS, CY Cergy Paris University, Cergy-Pontoise, 95000, France; [2]In Vivo Cellular and Molecular Imaging, Vrije Universiteit Brussels, Brussels, 1050, Belgium; [3]Research Group of Organic Chemistry, Vrije Universiteit Brussels, Brussels, 1050, Belgium*

Introduction

Amphipathic peptides, composed of alternating hydrophobic and hydrophilic amino acids, have been shown to form self-assembled hydrogels. These hydrogels proved adequate drug delivery platforms that can deliver pharmaceutical cargoes in a stable and prolonged manner when injected subcutaneously [1]. Such systems can increase patient compliance by limiting the number of injections required for the efficient treatment of chronic diseases. Currently, however, the drug release window of these peptide hydrogels is limited to a maximum of four days and this window ideally needs to be extendable for optimal use in diverse clinical settings.

As the role of fluorine within medicinal chemistry continues to develop, fluorinated amino acids have shown their utility in promoting and stabilizing well-defined secondary structures, as well as increasing local hydrophobicity and enhancing the biological profile of drug candidates [2]. Thus, the rational introduction of fluorine atoms into peptide hydrogels might provide access to a new class of injectable controlled-delivery systems that can take advantage of the favorable properties of fluorine atoms. Two strategies are investigated for the synthesis of fluorinated peptide hydrogels based on a previously developed hexapeptide consensus sequence. The first relies on the incorporation of fluorinated amino acids along the hydrophobic face of the amphipathic peptide of type 1 (Figure 1a), the second concerns the design of fluorinated β-hairpin peptide hydrogelator of type 2 (Figure 1b). Several Fmoc-protected amino acids were synthesized for introduction into those peptides, including the trifluoromethionine (TFM) and the CF_3-pseudoproline ($CF_3\psi$Pro) (Figure 2).

Results and Discussion

For the design of peptides of type **1**, TFM has been considered for its capacity to increase the hydrophobicity of peptides [3]. The synthesis has been performed by adapting procedures reported in the literature [4]. Starting from L-homocystine, the Fmoc-TFM-OH building block ready-to-use for solid phase peptide synthesis (SPPS) was obtained with an overall yield of 36% over 4 steps (Figure 2a).

Regarding the design of β-hairpins of type **2**, several turn motifs including fluorinated residues were prepared to promote the formation of β-sheet and eventually help the self-assembly process to form hydrogels. To this end, Fmoc-Lys(Alloc)-$CF_3\psi$Pro-OH and Fmoc-Pro-$CF_3\psi$Pro-OH were chosen. Because of the lack of nucleophilicity of the amino group and the steric bulkiness of the vicinal CF_3-group of the $CF_3\psi$Pro residue, the dipeptide building blocks have been synthesized according to our optimized conditions using activated amino acids as acyl chloride (Figure 2b)[5]. A series of the two dipeptides with different configurations were obtained with overall yields between 12-66%.
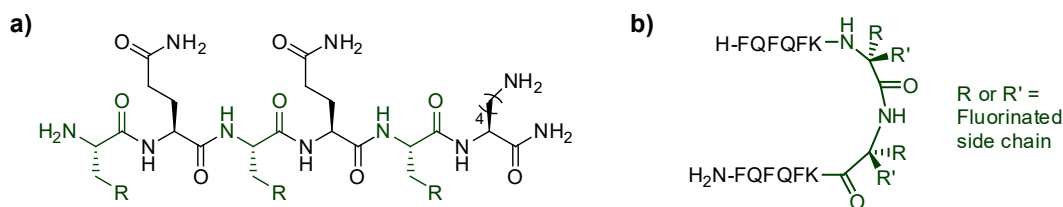

*Fig. 1. a) Type **1**: Hexapeptide sequence; b) Type **2**: β-hairpin sequence.*

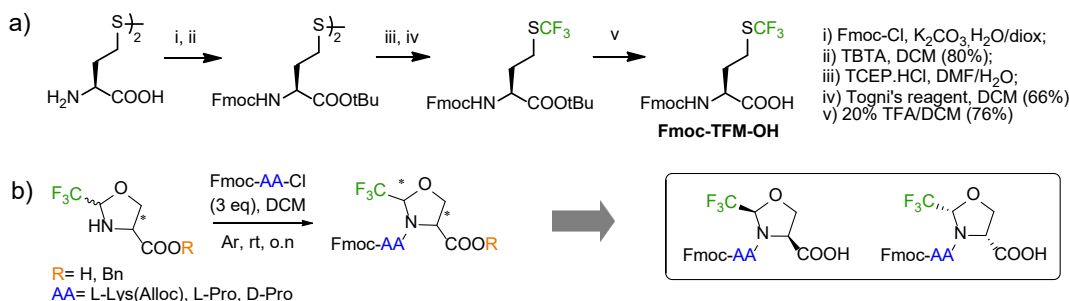*Fig. 2. a) Synthesis of Fmoc-TFM-OH; b) Coupling conditions of the CF₃ψPro residue using acyl chloride and the prepared building blocks.*

Subsequently, a set of linear fluorinated hexapeptides of type **1** has been designed, by substituting the phenylalanine residues from the hydrophobic face with different fluorinated amino acids, including TFM as well as several commercial fluorinated phenylalanine derivatives. After the synthesis, the gelation properties of the resulting fluorinated hydrogelators have been assessed qualitatively using the inverted tube test. The minimum gelation concentration has been determined using PBS buffer as trigger, according to an established protocol [1]. The results suggested that, in general, the substitution of all phenylalanine positions by a fluorinated residue increased the hydrophobicity of the peptide, while decreasing the stiffness of the gels. Also, the single substitution of the phenylalanine at the *C*- terminal position afforded hydrogels with interesting gel properties, as already observed in a previous study [6]. To evaluate the structuration occurring during the self-assembly, FT-IR spectroscopy has been performed and displayed the typical signature of the presence of β-sheet for most of the formed gels.

In parallel, β-hairpin hydrogelators of type **2** have been designed by connecting two strands based on the hexamer consensus sequence, through a β-turn motif based on the well-known D-Pro-Pro motif as β-turn inducer. A set of fluorinated β-hairpin hydrogelators have been successfully synthesized incorporating the CF₃ψPro residue to functionalize the β-turn motif of the hairpin sequence. Interestingly, several sequences showed promising gel properties and, again, FT-IR characterization showed β-sheet structuration. A more extensive characterization will be performed, including circular dichroism (CD) and nuclear magnetic resonance (NMR), to better understand the self-assembly process of these hydrogelators.

In summary, fluorinated building blocks have been successfully synthesized and introduced into peptides using SPPS. In the next step, quantitative assessment of the gel strength will be performed using dynamic rheometry. Subsequently, the release properties of the most promising sequences will be further investigated *in vitro* using different cargoes.

Acknowledgments

References

1. (a) Martin, C., et al. *J. Med Chem.* **61**, 9784-9789 (2018), https://doi.org/10.1021/acs.jmedchem.8b01282 ;
   (b) Martin, C., et al. *Mater. Today Chem.* **3**, 49-59 (2017), http://dx.doi.org/10.1016/j.mtchem.2017.01.003
2. Sloand, J.L., et al. *Pept. Sci.* **113**, e24184 (2021), https://doi.org/10.1002/pep2.24184
3. Gadais, C., et al. *ChemBioChem.* **19**, 1026-1030 (2018), http://dx.doi.org/10.1002/cbic.201800088
4. (a) Almaliti, J., et al. *Eur. J. Med. Chem.* **161**, 416-432 (2019), https://doi.org/10.1016/j.ejmech.2018.10.024;
   (b) McConathy, J., et al. *J. Med. Chem.* **45**, 2240-2249 (2002), https://doi.org/10.1021/jm010241x; Gadais, C., et al. *Eur. J. Org. Chem.* **2**, 246-251 (2017), https://doi.org/10.1002/ejoc.201601318
5. Chaume, G., et al. *J. Org. Chem.* **78**, 10144-10153 (2013), https://doi.org/10.1021/jo401494q
6. Bettens, T., et al. *Mater. Adv.* **2**, 4792-4803 (2021), https://doi.org/10.1039/D1MA00455G

Chemical Synthesis of Palmitoylated Histone Protein

Hironobu Hojo[1], Fumika Nakatani[1], and Isao Suetake[2]

[1]Institute for Protein Research, Osaka University, Suita, Osaka 565-0871, Japan; [2]Department of Nutritional Sciences, Nakamura Gakuen Graduate School University, Fukuoka 814-0198, Japan

Introduction

Histone proteins H2A, H2B, H3 and H4 form a histone core, which is composed of two copies of each of them. The core is wrapped around by DNA to form a nucleosome. The *N*-terminus of each histone protein in nucleosome receives many post-translational modifications, such as acetylation, methylation and phosphorylation. These modifications are dependent on the changes in the living environments, diseases and foods, which results in the epigenetic regulation of genes. Recently, an unusual modification of histone was found [1]: an *O*-palmitoylation of histone H4 of Ser[47]. Due to the hydrophobicity of the palmitoyl (Pal) group, this modification will lead to the local increment of the hydrophobicity on highly basic histone, and then donate novel function(s) by possible change of nucleosome structure and/or its interactor(s). Therefore, the detailed analysis of this modification will lead to the discovery of the novel function of histone modification. Here, we report the total chemical synthesis of Ser(Pal)[47]-histone H4.

Results and Discussion

The structure of Ser(Pal)[47]-H4 is shown in Figure 1. In this synthesis, the thioester method, which uses the direct aminolysis of the amino-protected peptide thioester by the other segment [2], was used. As the middle segment having the Pal group is expected to be highly hydrophobic, we postulated that the thioester method, which uses an organic solvent for coupling, is advantageous to condense segments including hydrophobic ones. The segment coupling was designed to be performed at the *C*-terminus of Gly[28,56], in order to avoid the potential danger of racemization of the *C*-terminal amino acids during the condensation reaction. Three segments, which correspond to H4(1-28) **1**, H4(29-56) **2**, H4(57-102) **3**, were prepared by the solid-phase peptide synthesis (SPPS).
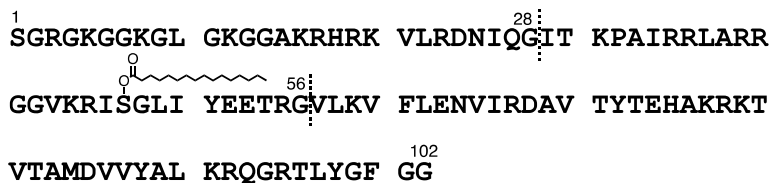


```
 1
SGRGKGGKGL GKGGAKRHRK VLRDNIQGIT KPAIRRLARR

          O
          ‖
          O                 56
GGVKRISGLI YEETRGVLKV FLENVIRDAV TYTEHAKRKT

                       102
VTAMDVVYAL KRQGRTLYGF GG
```

Fig. 1. Structure of Ser(Pal)[47]-histone H4. The broken lines indicate the sites of segment coupling.

To efficiently assemble the entire sequence, three segments were ligated in one-pot using the reactivity difference between the aryl and alkyl thioesters, following the previously developed method [3]. Therefore, segment **1** was prepared as a reactive aryl thioester, whereas segment **2** as an alkyl thioester, which is only activated by the addition of silver ions. The synthesis of these thioesters was realized by the post-synthetic thioesterification method using the *N*-alkylcysteine as the *N*-to-*S* acyl shift device [4]. The side chain amino protection was achieved by the hydrophilic and acid/base stable 4-pyridylmethoxycarbonyl (*i*Noc) group [5]. This group can be easily removed by Zn in acetic acid treatment after the ligation.
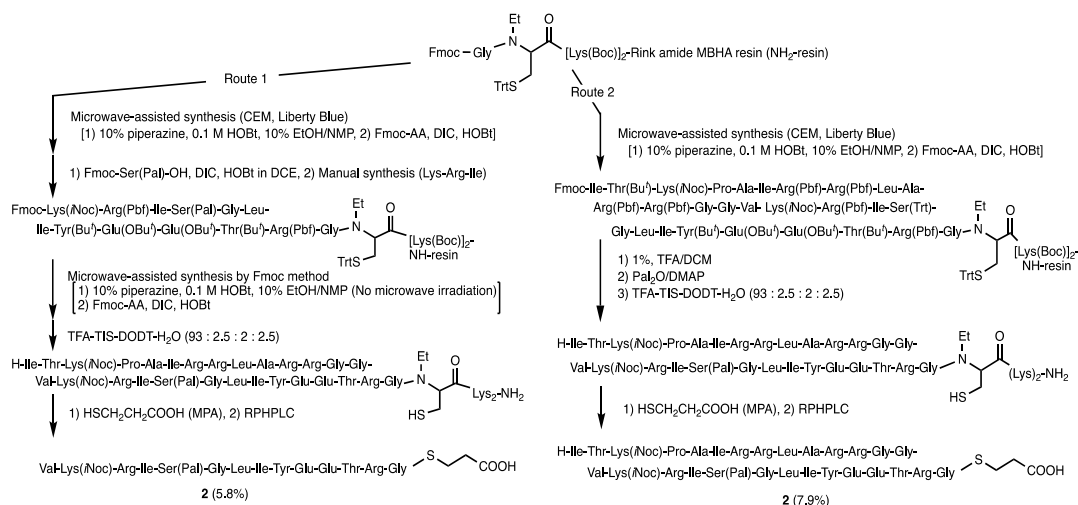
Fig. 2. Two synthetic routes of segment 2. Fmoc-Ser(Pal)-OH and Fmoc-Lys(iNoc)-OH were introduced manually.

For the introduction of the palmitoyl group to the side chain hydroxy group of Ser[47], two synthetic routes were examined: 1) introduction of the preformed Fmoc-Ser(Pal)-OH during SPPS of segment **2**, 2) introduction of Fmoc-Ser(Trt)-OH for Ser[47] during SPPS, followed by on-resin selective removal of Trt group and palmitoylation. In the first method, when standard microwave synthesis (CEM, Liberty Blue) was applied, the purity of the product was low, which might be due to the partial decomposition of the *O*-palmitoyl group during the piperidine treatment. Therefore, the microwave irradiation was switched off during the piperidine treatment and the desired product was successfully obtained after thioesterification reaction in 5.8% isolated yield (Fig. 2, Route 1). In Route 2, the standard microwave synthesis could be applied and segment **2** was obtained in 7.9% yield. Route 2 is better than Route 1 in point of the yield and the applicability of the standard microwave protocol.

Three segments were then condensed by the one-pot thioester method as shown in Figure 3. The peptide aryl thioester **1** and palmitoylated peptide alkyl thioester **2** were dissolved in DMSO containing HOOBt, and DIEA was then added to initiate the reaction. The reaction efficiently proceeded within 12 h to give the intermediate alkyl thioester **4**. Without purification, peptide **3** and silver ions were added to the mixture to perform the second ligation. This reaction also proceeded efficiently to give the polypeptide **5**. The Fmoc group

Fig. 3. Ligation to obtain Ser(Pal)[47]-histone H4.

removal by piperidine followed by the *i*Noc group removal by Zn in acetic acid treatment efficiently proceeded to give the desired product **6** in 20% overall yield [6]. From the SPPS of the segment to the ligation reaction, no major solubility problem was observed.
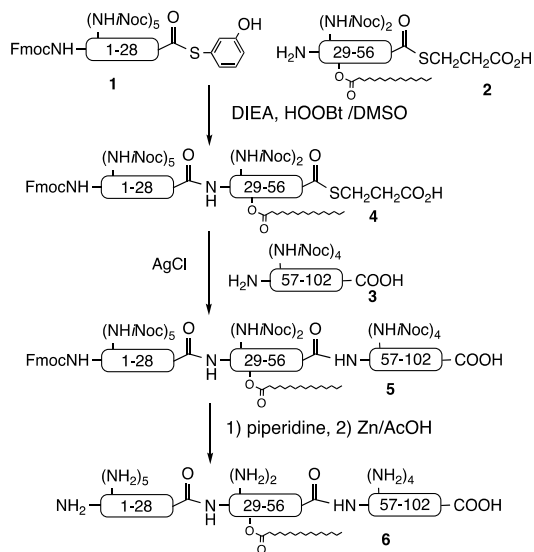
The introduction of the palmitoylated H4 into the nucleus as well as the nucleosome formation using palmitoylated H4 are being undertaken.

References

1. Zou, C., et al. *J. Biol. Chem.* **286**, 28019-28025 (2011), https://doi.org/10.1074/jbc.M111.253385
2. Hojo, H., Aimoto, S. *Bull. Chem. Soc. Jpn.* **64**, 111-117 (1991)
3. Asahina, Y., et al. *Angew. Chem. Int. Ed.* **52**, 9733-9737 (2013), https://doi.org/10.1002/anie.201303073
4. Hojo, H., et al. *Tetrahedron Lett.* **48**, 25-28 (2007), https://doi.org/10.1016/j.tetlet.2006.11.034
5. Veber, D.F., et al. *J. Org. Chem.* **42**, 3286-3288 (1977), https://doi.org/10.1021/jo00440a018
6. Hojo H., Suetake, I., *Arkivoc* part iv, 186-197 (2021), https://doi.org/10.24820/ark.5550190.p011.361

Studies Towards the Chemical Synthesis of Sonic Hedgehog

Iván Sánchez-Campillo[1], Judith Palà-Pujadas[2], and Juan B. Blanco-Canosa[1]

[1]Chemical Biology, Institute for Advanced Chemistry of Catalonia (IQAC-CSIC), Jordi Girona 18-26, 08034 Barcelona, Spain; [2] The Donnelly Centre, University of Toronto, M5S 3E1 Toronto, Canada

Introduction

Sonic Hedgehog (ShhN) is an extracellular protein, responsible for the activation of the Hedgehog (Hh) signaling pathway. Hh is present in all metazoans and it carries out an important role in embryo development, by regulating cell proliferation and differentiation into tissues and organs. In adults, it remains quiescent, while it still regulates cell population and growth (Figure 1) [1].

A quite interesting fact about Hh and ShhN is their role in cancer disease. Aberrant signaling of Hh, especially by overexpression of ShhN, has been related to the development of many types of cancer, i.e. pancreatic, glioblastoma, and basal cell carcinoma, while the inhibition of the Hh activity has been demonstrated to stop cell proliferation. Therefore, Hh proteins are attractive as targets for anti-cancer drug discovery [2].

Out of all the possible targets, ShhN is the most attractive one. It is located in the extracellular matrix, enabling easier drug targeting because it does not need to be delivered inside the cell. Despite that, only 3 inhibitors targeting ShhN have been described [2,3]. ShhN is a challenging target to study due to its hydrophobic nature. Native human ShhN is a 174-mer protein that bears two post-translational modifications (PTM): an N-terminal palmitoylation and a *C*-terminal cholesterol ester. These lipidations impair its recombinant expression and chemical synthesis.

Considering its interest in medicine and the synthetic challenge, this project aims to synthesize native ShhN by chemical means and use the synthetic ShhN for drug discovery.
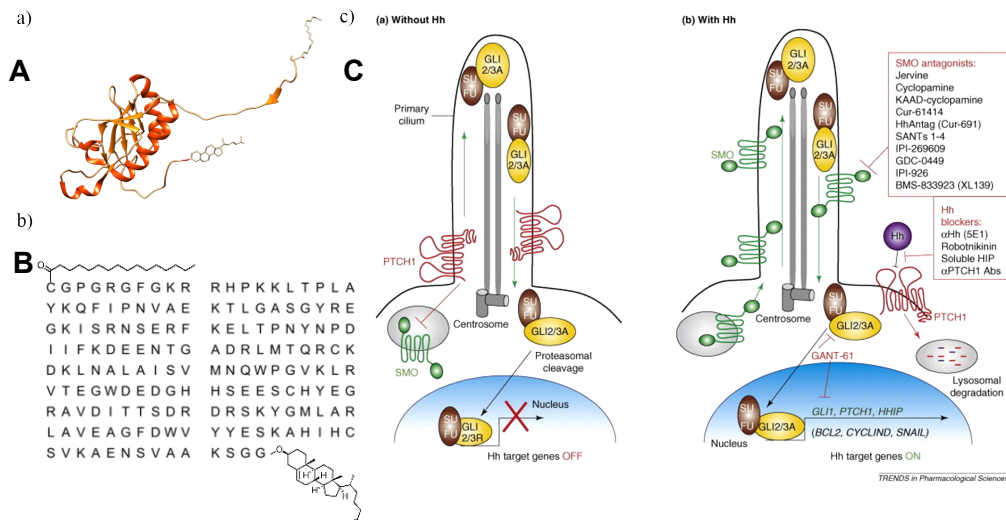

Fig. 1. ShhN and the Hh signaling pathway. a) X-ray structure of ShhN (PDB: 6RVD). b) Primary sequence of ShhN. c) Overview of the Hh pathway and its inhibitors (picture from reference 2).

Methodology

In our group, we rely on the Dbz linkers to synthesize peptide thioesters for native chemical ligation (NCL). First reported by Dawson et. al. [4], these linkers based on *o*-aminoanilides are compatible with Fmoc/*t*Bu SPPS and can be activated by two different pathways, one as *N*-acylbenzimidazolinone (Nbz) and the other as *N*-acylbenzotriazole, both enabling thioesterification and subsequent ligation in the presence of *N*-terminal Cys-containing peptides (Figure 2).

To avoid the branching peptides that can be formed in the *p*-amino position, the methylated MeDbz was developed [5]. This strategy fixed the issue, but it is only reactive through the Nbz (MeNbz) pathway. Most recently, we reported a linker based on 1,2-diaminobenzene which reacts through both pathways, avoids branching, and enables selenoester preparation through the benzotriazole pathway [6].

State of the art

Based on our previous work in which an ShhN analog-bearing biotin at the C-terminus was synthesized [7], the native ShhN is retrosynthetically divided into five fragments (Figure 3). The palmitic acid is introduced in SPPS and the cholesterol is introduced by reaction of Gly-Cholesterol with the fully protected fragment Cys^{160}-Gly^{173}–MeNbz-G. Fragments 2 and 4 bear the MeNbz precursor, the aryloxycarbonyl-*o*-methylaminoanilide (Figure 2, route A), which is cyclized into MeNbz under ligation conditions. These peptides enable kinetically controlled ligations (KCL), as they react slower than those that are prepared as 2-mercaptoethanosulfonic acid thioesters (fragments 1 and 3).
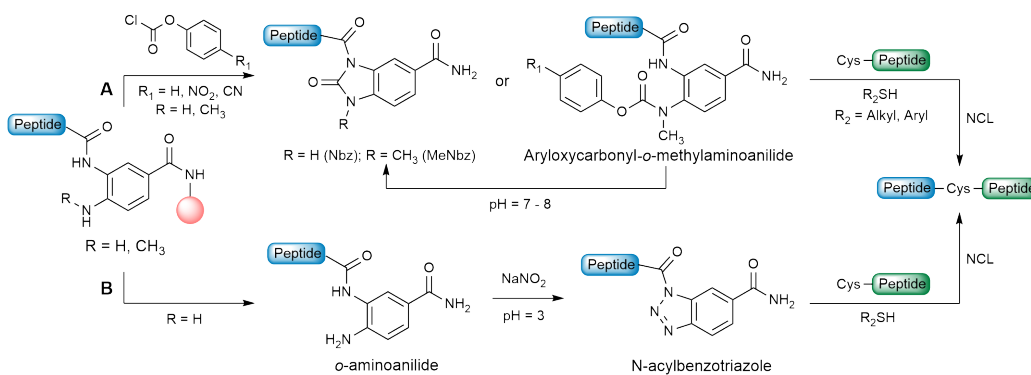
Fig. 2. The Dbz linkers and their application to Native Chemical Ligation (adapted from ref 6). Route A is the Nbz / MeNbz pathway. Route B is the N-acylbenzotriazole pathway.

ShhN only comprises 3 Cys residues, therefore, residues 35 and 122 are mutated into Cys to desulfurize them into native Ala positions after ligation. Moreover, Cys^1 is protected with Acm to prevent its desulfurization, and Cys^{79} is protected with thiazolidine (Thz) to avoid the intramolecular cyclization. The synthetic scheme pointed out in Figure 3 leaves the ligation of fragment 5 for the last step of the synthesis to minimize the purification steps of this hydrophobic fragment during the synthesis. Remarkably, fragment 1 is still soluble, possibly likely due to the content of Arg and Lys residues in its sequence.

So far, the five fragments have been synthesized and purified, and the first two ligations are being scaled up (Figure 4). Ligations of fragments 1 and 2, as well as fragments 3 and 4, proceed at 10 mM total peptide concentration in guanidinium/- phosphate buffer. 4-Mercaptophenol (4-MPOH) is used as a thiol catalyst. The control of the pH and reaction time enables the two KCL to maintain the MeNbz precursors intact.
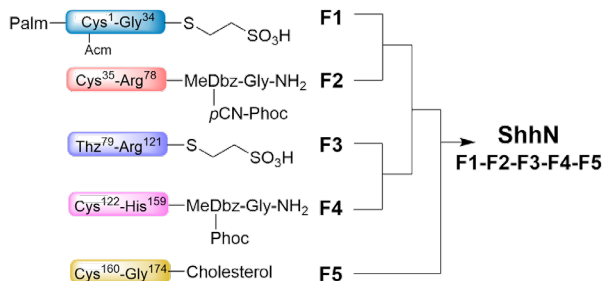

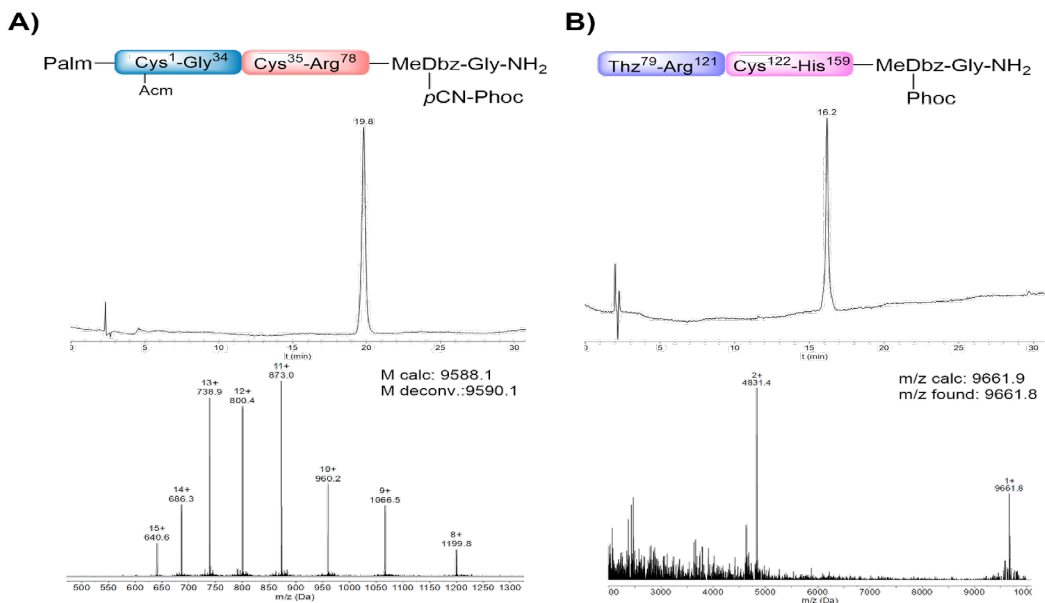*Fig. 3. The proposed synthetic route to ShhN.*

Fig. 4. a) Fragment 1-2. RP-HPLC (C_{18}, 0 to 70% ACN, 30 min) and ESI-MS. b) Fragment 3-4. RP-HPLC (C_3, 0 to 70% ACN, 30 min) and MALDI-TOF.

Acknowledgments

References

1. Lum, L. and Beachy, P.A. *Science* **304**, 1755-1759 (2004), https://doi.org/10.1126/science.1098020
2. Scales, S.J. and de Sauvage, F.J. *Trends Pharmacol. Sci.* **30**, 303-312 (2009), https://doi.org/10.1016/j.tips.2009.03.007
3. Owens, A.E., de Paola, I., et. al. *J. Am. Chem. Soc.* **139**, 12559-12568 (2017), https://doi.org/10.1021/jacs.7b06087
4. a) Blanco-Canosa, J.B. and Dawson. P.E. *Angew. Chem. Int. Ed.* **47**, 6851-6855 (2008), https://doi.org/10.1002/anie.200705471, b) Mahto, S. K., Howard, C.J. et al. *ChemBioChem* **12**, 2488-2494 (2011), https://doi.org/10.1002/cbic.201100472, c) Zhao, Z., Mousa, R. and Metanis, N. *Chem. Eur. J.* **28**, e202200279 (2022), https://doi.org/10.1002/chem.202200279, d) Maity, S., Jbara, M., Mann, G. et al. *Nat. Protoc.* **12**, 2293-2322 (2017), https://doi.org/10.1038/nprot.2017.049
5. a) Blanco-Canosa, J.B., Nardone, B., et. al. *J. Am. Chem. Soc.* **137**, 7197-7209 (2015), https://doi.org/10.1021/jacs.5b03504, b) Sakamoto, K., Tsuda, S., et al. *Chem. Commun.* **53**, 12236-12239 (2017), https://doi.org/10.1039/C7CC07817J, c) Acosta, G.A., Royo, M., et al. *Tetrahedron Letters* **58**, 2788-2791 (2017), https://doi.org/10.1016/j.tetlet.2017.06.008, d) Gless, H.B. and Olsen, C.A. *J. Org. Chem.* **83**, 10525-10534 (2018), https://doi.org/10.1021/acs.joc.8b01237
6. Sánchez-Campillo, I., Miguel-Gracia, J., et. al. *Chem. Sci.* Advance Article (2022), https://doi.org/10.1039/D2SC04158H
7. Palà-Pujadas, J., Albericio, F., and Blanco-Canosa, J.B. *Angew. Chem. Int. Ed.* **57**, 16120-16125 (2018), https://doi.org/10.1002/anie.201810712

Epitope Determination of DNA and RNA Aptamers as Antibody Alternatives by Affinity-Mass Spectrometry Open New Perspectives for Peptide Biomarkers and Molecular Diagnostics

Michael Przybylski[1], Nico Hüttmann[1,2], Loredana Lupu[1], Pascal Wiegand[1], Stephan Rawer[1], Wolfgang Kleinekofort[1], Maxim V. Berezovski[2], Marc Vogel[3], and Beatrix Süß[3]

[1]*Steinbeis Centre for Analytical Biochemistry and Biomedical Mass Spectrometry, Marktstrasse 29, 65428 Ruesselsheim am Main, Germany; and Rhein Main University, Department of Engineering, 65428 Ruesselsheim am Main, Germany;* [2]*University of Ottawa, Department of Chemistry and Biomolecular Sciences, Ottawa, Canada;* [3]*Techn. University Darmstadt, Department of Synthetic Biology, Schnittspahnstr. 10, 64287 Darmstadt, Germany*

Introduction

Aptamers are short single stranded DNA or RNA oligonucleotides that have recently gained attention as new therapeutic structures vis-à-vis classical IG-type antibodies. In contrast to antibodies, aptamers are chemically synthesized and show a number of unique features, e.g. in bioassays and drug development. As "chemical antibodies", aptamers are less immunogenic and do not interfere with cell viabilities, since they specifically bind and release cells, suggesting their potential for the evaluation of biomarkers. Aptamers are typically produced using the SELEX (Systematic Evolution of Ligands by EXponential Enrichment) procedure [1] with high affinities towards a biomolecular target. The production of aptamers solely in vitro, their chemical synthesis, and high affinity to specific targets have created high interest for development of alternatives to antibodies. However, determinations of aptamer epitopes of protein antigens, as key criteria for their functional specificity have rarely been achieved.

We report here the first epitope and affinity determinations illustrated for DNA protein aptamers in comparison to monoclonal and polyclonal antibodies. Epitopes were identified for two DNA aptamers (60 and 64 bases) against C-MET, a cancer diagnostic protein, obtained by SELEX from a random DNA library [2]. Proteolytic affinity-mass spectrometry in combination with SPR biosensor analysis (PROTEX-SPR-MS) was used as the principal tool for epitope determination [3]. Moreover, a molecular comparative study of a DNA aptamer and a monoclonal antibody against tumor necrosis factor-alpha protein (TNFα) revealed identical epitope peptides, associated with high affinities (K_D, 7 and 13 nM). The molecular identification of DNA aptamer epitopes from specific protein targets, reported here for the first time, indicate that they have comparable recognition properties to the structure-based recognition of variable antibody sequences.

Materials and Methods

Proteins and selection of aptamers
Synthetic DNA aptamers of C-Met (CNL0003 and CNL0004) consisting of 60 and 64 bases [4] were obtained by SELEX from a large DNA library. A DNA aptamer of TNFα (VR11) [5] composed of 26 bases was produced using the filter SELEX procedure with recombinant TNFα. All aptamers were prepared with 5'-amino groups (5AmMC12).

Proteolytic digestion
Tryptic digestion was performed with an enzyme-substrate ratio of 1:100. High pressure digestion was performed with a Barocycler 2320EXT instrument (Pressure Biosciences, Boston/USA) [2]. Affinity microcolumns were prepared with NHS/EDC-activated Sepharose microbeads, using 40 μg aptamer.

Epitope identification and affinity determinations
Epitope analyses were carried out by epitope-extraction- MS, using 10 μg of tryptic digestion mixture incubated with the aptamer or antibody immobilized on Sepharose resin. After incubation for 2 hrs, the affinity column was washed with ammonium bicarbonate until no background signal was observed

by MALDI-MS. Epitope fractions were eluted with 100 µl 0.1% TFA. MALDI-MS was performed with a Bruker Autoflex III Smartbeam-MS (Bruker Daltonics, Bremen, Germany). SPR Analysis was performed with an Ametek 2CH7500 instrument using 1 x 1 cm gold chips with self-prepared 40 nm gold layer. Affinity determinations and K_D values were obtained with the TraceDrawer 1.7.1 software. Epitope peptides were synthesized by Fmoc-SPPS (Applied Biosystems ABI-433A synthesizer).

Epitope identification and affinity determination using PROTEX-SPR-MS

Figure 1 shows the analytical platform of the SPR-MALDI-MS combination, comprising an autosampler connected to an SPR chip, connection of autosampler and SPR, and a transfer line from SPR to MALDI-MS. The SPR-MS combination can utilize all major biosensor types and microfluidic systems such as prism-based SPR and SAW-biosensors. An SPR fluidic module compatible with both ESI-MS and MALDI-MS has been optimized for protein digestion mixtures containing the immobilized antibody or aptamer. The SPR sensorgram is determined in a first step, and K_D determinations of the chip- immobilized antibody or aptamer interacting with the epitope peptide(s) is performed at different concentrations over the SPR chip. Following removal of unbound components by washing, the epitope(s) are eluted at slightly acidic aqueous conditions and spotted on the MALDI target plate (Figure 2).

Affinity determinations of the aptamer complexes with the C-Met protein were carried out by SPR analysis on self-assembled monolayer (SAM) gold chips, by immobilization of either the aptamers or the protein on the chip surface using standard SAM technology [2]. Binding constants were determined with dilution series of protein and aptamers, respectively. The K_D determinations of the CLN00003 and CLN00004 aptamers revealed 223 nM and 535 nM, respectively. Epitope extraction by PROTEX-SPR-MS was confirmed by replications with an affinity column.

Epitope extraction of aptamer CLN0004 showed a single linear epitope. In contrast, the aptamer CLN0003 revealed an assembled epitope comprised of two peptides within adjacent sequence domains, C-Met [524-543] and [557-568]. The high affinities of epitope peptides were established by synthesis and SPR determinations (K_{DS}, <1 µM). Structure modelling of the aptamers was consistent with the identified epitopes.
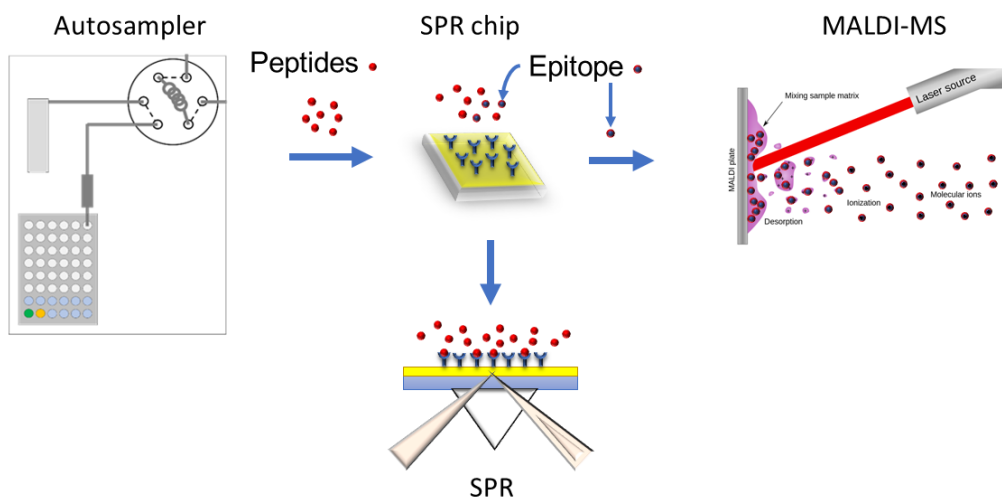
Fig. 1. Analytical platform for the Chip-SPR–MALDI-MS epitope analyzer. An autosampler/valve system connects the biosensor chip with the MALDI-target plate (multi-well plate) for the MALDI-MS analysis. Sample injection is performed on the SPR chip containing the immobilized antibody or aptamer. Peptide mixtures injected over the antibody channel provide the SPR sensorgram of binding epitope(s), and eluted epitope peptide(s) are spotted on the MALDI target plate. K_D determination of the antibody-bound protein and peptide fragments is performed by injecting a dilution series over the SPR chip.

Antibody- and DNA-Aptamer- complexes of Tumor-necrosis-factor-alpha reveal identical molecular epitopes

A comparative study of a DNA aptamer and a monoclonal antibody against tumor necrosis factor-alpha protein (TNFα) was performed by PROTEX-SPR-MS and provided the identification of identical epitope peptides.
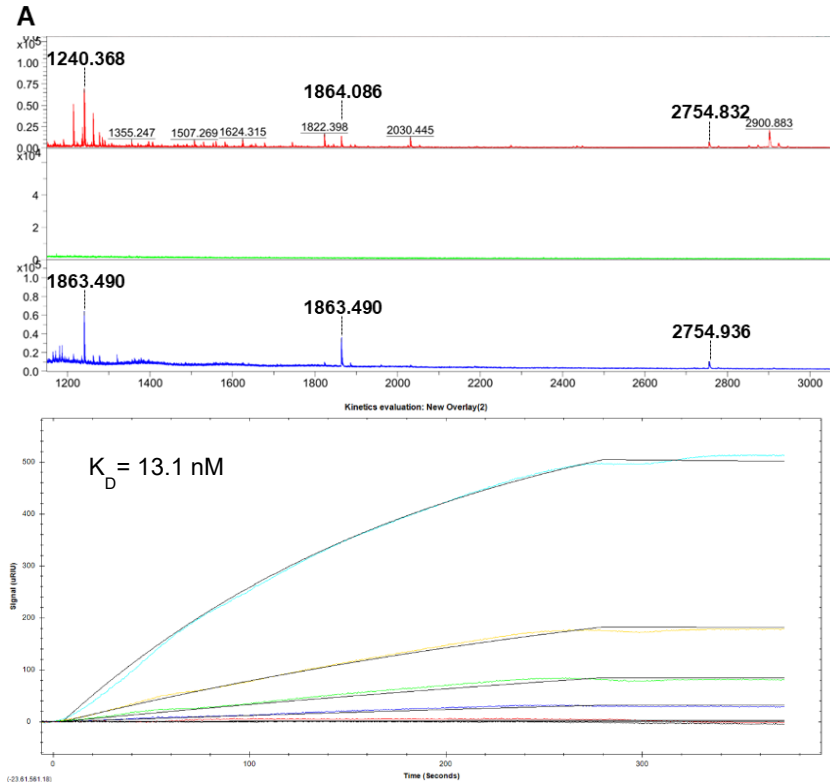
Fig. 2. (A) Epitope identification of TNFα- aptamer by proteolytic epitope extraction and sequential MALDI-MS analysis of supernatant, last wash and epitope elution fractions. B. Anti-TNF alpha antibody interacting with TNF alpha protein- Dilution series (28-950 nM) of intact TNF alpha protein. Identical molecular epitopes (Figure 2A), both associated with high affinities (K_D, 7 and 13 nM) for aptamer and antibody, respectively. (TNFα- [7-31] TPSDKPVAHVVANPQAEGQLQWLNR at $[M+H]^+ = 1864.1$ m/z and [66-82] GQGCPSTHVLLTHTISR by $[M+H]^+ = 2755.6$ m/z).

GQGCPSTHVLLTHTISR
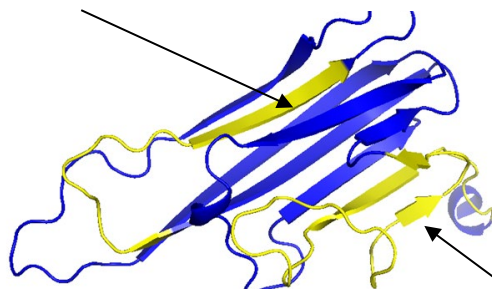
TPSDKPVAHVVANPQAEGQLQWLNR

Fig. 3. Ribbon representation of TNFα protein with associated epitope identified (in yellow) from both aptamer and antibody. Epitopes are visualized on the TNFα monomer.

Summary and Conclusions

The molecular comparison of epitopes of TNFα -antibodies and aptamers identified here for the first time opens new perspectives for specific biomarker elucidation and clinical diagnostics. In contrast to antibodies showing both high immunogenicity and considerable stability problems, DNA aptamers exert high stability, specificities, and affinities. Moreover, aptamers generally have low immunogenicity.

References

1. Boussebayle, A., et al. *Methods* **161**, 10-15 (2019), https://doi.org/10.1016/j.ymeth.2019.04.004
2. Lupu, L., et al. *Int J Mol Sci* **22**(23), 12832 (2021), https://doi.org/10.3390/ijms222312832
3. Lupu, L., et al. *ChemMedChem* **15**, 363 (2020), https://doi.org/10.1002/cmdc.201900489
4. Boltz, A., et. al. *J Biol Chem* **286**(24), 21896-21905 (2011), https://doi.org/10.1074/jbc.M111.238261
5. Orava, E., et. al. *ACS Chem. Biol.* **8**, 1, 170-178 (2013), https://doi.org/10.1021/cb3003557

Bioactive Peptides from Salmon Collagen: An *in silico* Approach

Constanza Cárdenas[1], Tanya Román[1,2], Claudio Alvarez[3,4], Paula Santana[5], and Fanny Guzmán[1]

[1]Nucleo de Biotecnología Curauma. Pontificia Universidad Católica de Valparaíso. Valparaíso, Chile.; [2]Programa de Doctorado en Biotecnología. Pontificia Universidad Católica de Valparaíso y Universidad Federico Santa María. Valparaíso, Chile; [3]Laboratorio de Fisiología y Genética Marina (FIGEMA), Centro de Estudios Avanzados en Zonas Áridas (CEAZA), Coquimbo, Chile; [4]Facultad de Ciencias del Mar, Universidad Católica del Norte, Coquimbo, Chile; [5]Facultad de Ingeniería, Instituto de Ciencias Químicas Aplicadas, Universidad Autónoma de Chile, Santiago, Chile

Introduction

Bioprospecting is a source for finding new bioactive compounds, and today there are several sources to achieve this search. Collagen is one of the most abundant proteins in animal tissues, almost 30% of total protein [1], and in the case of salmon processing by-products, such as scales and skin, is the most abundant protein. Although about 30 types of collagens are reported, type I is the most abundant and the main one in the by-products of salmon processing [1,2].

Collagen is a target for applications in many fields such as the cosmetic industry, food additives, tissue regeneration, bioactive peptides, etc [3-8]. In this report, we work with the reported sequences of Atlantic salmon and rainbow trout collagen, doing an *in silico* hydrolysis with Alcalase (subtilisin) and characterizing the peptides obtained by a set of descriptors and physicochemical properties obtained with the Peptide package [5] implemented in Rstudio [6], and comparing them with other reported peptides of known activities. As a result, it is possible to classify the peptides from *Salmo salar* and *Onchorhynchus mykiss* collagen by including them in clusters of sequences related with specific activities. This methodology allows us to reduce the search space and to select sequences with potential activity that could be synthesized and tested. Additionally, this approach can be used as a way to add value to the by-products from the salmon industry [11,12].

Results and Discussion

In this work we chose proteins from collagen type I, which is the main type of collagen present in the byproducts of fish processing (Table 1). These proteins were hydrolyzed in silico, through the BIOPEP server [13], by using the enzyme Alcalase, resulting in a total of 477 unique peptides.

Table 1. Salmo salar and Oncorhynchus mykiss collagen proteins used for this study.

Chain	Source	Uniprot ID	Length	# Unique peptides
Alpha 1	*Salmo salar*	A0A1S3RF89	544	125
	Oncorhynchus mykiss	Q910C0	1449	70
Alpha 2	*Salmo salar*	A0A1S3Q205	1356	132
	Oncorhynchus mykiss	O93484	1356	83
Alpha 3	*Oncorhynchus mykiss*	O93486	678	67

In parallel, peptides reported in databases with different activities were selected, as shown in Table 2.

Table 2. Number of peptides from databases with different activities, used in this study.

Activity	# Peptides
Antioxidant	230
Antifreezing	214
Cell Penetrating Peptides	228
Antiparasitic	403
Insecticidal	58
Collagen peptides	477
Total	2781

Peptide sequences were characterized in Rstudio [6], with the Peptides package [5], by initially using 71 descriptors listed below:

- aIndex: Aliphatic index defined as the relative volume occupied by the side chains of the aliphatic amino acids (Ala, Ile, Leu y Val).
- blosumIndices: Indices derived from the physicochemical properties contained in the BLOSUM62 matrices. It includes 10 indices from BLOSUM1 to BLOSUM10
- boman: Boman index, the potential for protein interaction
- Charge: Theoretical net charge at pH = 7 and using pKscale = EMBOSS.
- crucianiProperties: Use the scaled principal component scores that summarize a broad set of descriptors calculated based on the interaction of each amino acid residue with several chemical groups (or "probes"), such as charged ions, methyl, hydroxyl groups, and so forth; PP1: related to polarity; PP2: related to hydrophobicity; PP3: related to formation of hydrogen bonds
- fasgaiVectors: The FASGAI vectors (Factor Analysis Scales of Generalized Amino Acid Information) are a set of amino acid descriptors, that reflects hydrophobicity, alpha and turn propensities, bulky properties, compositional characteristics, local flexibility, and electronic properties, that can be utilized to represent the sequence structural features of peptides or protein motifs, F1 to F6
- Hydrophobicity: Calculates the GRAVY index or average hydrophobicity based on the Kidera scale.
- kideraFactors: The Kidera Factors were originally derived by applying multivariate analysis to 188 physical properties of the 20 amino acids and using dimension reduction techniques. This function calculates the average of the ten Kidera factors for a protein sequence. KF1 to KF10.
- mswhimScores: Molecular Surface-Weighted Holistic Invariant Molecular. MS-WHIM scores were derived from 36 electrostatic potential properties derived from the three dimensional structure of the 20 natural amino acids.
- pI: Isoelectric point with pKscale = EMBOSS
- protFP: The ProtFP descriptor set was constructed from a large initial selection of indices obtained from the AAindex database for all 20 naturally occurring amino acids. From ProtFP1 to ProtFP8
- stScales: ST-scales were proposed by Yang et al, taking 827 properties into account which are mainly constitutional, topological, geometrical, hydrophobic, electronic, and steric properties of a total set of 167

The 71 descriptors were transformed by using principal component analysis, selecting the first seven Principal Components (PC) to perform a Kmeans clustering analysis with pheatmap [14] implemented in Rstudio. As result we obtained the clusters showed in Figure 1.
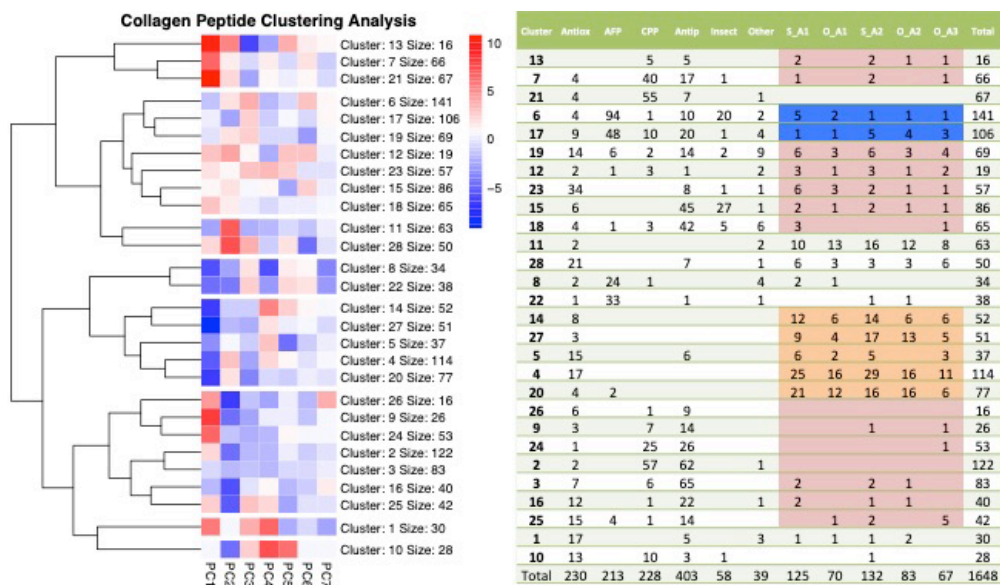
Collagen Peptide Clustering Analysis

Cluster	Antiox	AFP	CPP	Antip	Insect	Other	S_A1	O_A1	S_A2	O_A2	O_A3	Total
13			5	5			2		2	1	1	16
7	4		40	17	1		1		2		1	66
21	4		55	7		1						67
6	4	94	1	10	20	2	5	2	1	1	1	141
17	9	48	10	20	1	4	1	1	5	4	3	106
19	14	6	2	14	2	9	6	3	6	3	4	69
12	2	1	3	1		2	3	1	3	1	2	19
23	34			8	1	1	6	3	2	1	1	57
15	6			45	27	1	2	1	2	1	1	86
18	4	1	3	42	5	6	3					65
11	2					2	10	13	16	12	8	63
28	21			7		1	6	3	3	3	6	50
8	2	24	1			4	2	1				34
22	1	33		1		1			1	1		38
14	8						12	6	14	6	6	52
27	3						9	4	17	13	5	51
5	15			6			6	2	5		3	37
4	17						25	16	29	16	11	114
20	4	2					21	12	16	16	6	77
26	6		1	9								16
9	3		7	14					1		1	26
24	1		25	26							1	53
2	2		57	62		1						122
3	7		6	65			2		2	1		83
16	12		1	22		1	2		1	1		40
25	15	4	1	14					1	2	5	42
1	17			5			1	1	1	2		30
10	13		10	3	1				1			28
Total	230	213	228	403	58	39	125	70	132	83	67	1648

Fig. 1. Clustering analysis of the 2781 peptides characterized with seven PC. Left: dendrogram of the kmean clustering with 28 clusters. Rigth: clusters members according the activity, Antioxidant, Antifreezing (AFP), Cell penetrating peptides (CPP), Antiparasitic (Antip), Insecticidal (Insect), others, and the fish collagen peptides S_A1,O_A1 for alpha 1 chain, S_A2, O_A2 for alpha chain 2 for salmon and oncorhynchus, and O_A3 for oncorhynchus alpha 3 chain.

From these results it is possible to establish groups of similarity of the peptides obtained from the *in silico* collagen hydrolysis with the reported bioactive peptides. We found 24 peptides associated with antioxidant activity, clusters 6 and 17 (highlighted in blue in Figure 1). 278 peptides with potential antioxidant activity in clusters 14, 27, 5, 4 and 20 (highlighted in orange in Figure 1) and three different groups of clusters of peptides with potential antiparasitic activity, the first group of 10 peptides of clusters 13 and 7, the second of 56 peptides of clusters 19, 12, 23, 15 and 18, and the third with 20 peptides of the clusters 9, 24, 3, 16 and 25.

This procedure constitutes the first filter in the search for bioactive peptides, and the projection of the work will be the synthesis of these potentially active peptides to be tested in *in vitro* assays against the parasite *Caligus rogercresseyi*. Another projection is to use byproducts from fish processing to obtain hydrolysates, and be able to isolate fractions with bioactive peptides, having as background the results obtained here.

Acknowledgments

References

1. Silvipriya, K.S., et al. *J App Pharm Sci*. **5**, 123-127 (2015), https://doi.org/10.7324/JAPS.2015.50322
2. Al-Nimry, S., et al. *Mar Drugs* **19**,145, (2021), https://doi.org/10.3390/md19030145
3. Geahchan, S., Baharlouei, P., Rahman, A. *Mar Drugs* **20**(1), 61 (2022), https://doi.org/10.3390/md20010061
4. Jana, S., et al. *J Mater Chem B*. **10**(4), 489-505 (2022), https://doi.org/10.1039/d1tb02125g
5. Yamada, S., et al. *Dent Mater J*. **40**(6), 1295-1302(2021), https://doi.org/10.4012/dmj.2020-446
6. Wu, R., et al. *Food Chem*. **248**, 346-352 (2018), https://doi.org/10.1016/j.foodchem.2017.12.035
7. Derkach, S.R., et al. *Polymers (Basel)* **12**(12), 3051 (2020), https://doi.org/10.3390/polym12123051
8. Nuñez, S.M., et al. *Electron J Biotech*. **48**, 101-108 (2020), https://doi.org/10.1016/j.ejbt.2020.09.009

9. Osorio, D., Rondon-Villarreal, P., Torres, R. *The R Journal* **7**(1), 4-14, ISSN 2073-4859 (2015), https://journal.r-project.org/archive/2015/RJ-2015-001.pdf
10. RStudio Team (2015) *RStudio: Integrated Development for R. RStudio*, Inc., Boston, MA URL http://www.rstudio.com/
11. Coppola, D., et al. *Mar Drugs* **19**(2), 116 (2021), https://doi.org/10.3390/md19020116
12. Caruso, G., et al. *Mar Drugs* **18**(12), 622 (2020), https://doi.org/10.3390/md18120622
13. Minkiewicz, P., Iwaniak, A., and Darewicz, M. (2019) BIOPEP-UWM Database of Bioactive Peptides: Current Opportunities. *International journal of molecular sciences* **20**(23), 5978 (2020), https://doi.org/10.3390/ijms20235978. https://biochemia.uwm.edu.pl/biopep-uwm/
14. Kolde, R., *Pheatmap: pretty heatmaps. V1.0.12. R package*. (2012). https://cran.r-project.org/web/packages/pheatmap/index.html

Protein Structure Alignment and RMSD Calculations

Fatima I. Sapundzhi and Metodi S. Popstoilov

South-West University "Neofit Rilski", 2700 Blagoevgrad, Bulgaria

Introduction

In recent years, the alignment of protein structures is a fundamental problem for computational chemistry, computational structure biology and bioinformatics research. Alignment of protein structures can be performed as pairwise structure alignment (PSA) and multiple structure alignment (MSA). This task can be considered as an NP-hard problem. More information and reviews about this problem could be found in [1-5]. Initially, it is important to choose the way in which the protein structure will be represented - for example, it can be represented as a C-alpha-based distance map (C- map), secondary structure elements (SSEs) and other methods [6-7]. The next step is to consider the protein as rigid or flexible and choose a structure alignment method, which may consist of a scoring function to measure protein similarity and a search algorithm to optimize the function [8-9]. For more details of scoring function see Sapundzhi et al [10-11]. An important task for researchers is to evaluate the similarity of two protein structures. To compare the degree of similarity of two three-dimensional (3D) structures, the root means square deviation (RMSD) measure or the sum of squared "errors" (the squared distance between the corresponding points) is used. We use the RMSD function

$$RMSD = \sqrt{\frac{1}{n}\sum_{i=1}^{n}\delta_i^2} \quad (1)$$

where δ_i is the distance between atom *i* and either a reference structure or the mean position of the *n* equivalent atoms [12]. The purpose of this study is to present a simple procedure to calculate the RMSD between pairs of 3D structures and to find the minimum RMSD value. The implementation for the program is realized in the C# programming language.

Results and Discussion

In the current study, we present a program implemented in the C# programming language that can calculate the root mean square distance (RMSD) between two 3D structures [13,14]. The developed tool calculates minimal RMSD between two Cartesian coordinates in either. xyz or .pdb format (Protein Data Bank files). Both files (structures) must contain the same number of atoms in a similar order for the program to run correctly. The implementation of the program is based on the Kabsch algorithm [15,16] and Quaternion algorithm [17] for rotation. First, the structures are translated to the center of the coordinate system, then the covariance matrix and the optimal rotation matrix are calculated. The developed tool shows the RMSD calculated in three ways (Figure 1).

Fig.1. RMSD calculation between two structures. The tool accepts as arguments two files: .pdb and .xyz.

The results of the program implementation with the given example from https://github.com/ are shown as follows: Normal RMSD: 1.25, Translated RMSD: 1.24; Rotated RMSD: 1.245. The obtained results are compared with the similar tools developed in Python [18] and Perl [19] and show that for these implementations the algorithm gives almost identical results. The developed tool

has an easy-to-use graphical user interface that will be uploaded to a server and can be freely used by researchers in the field of bioinformatics research.

Acknowledgments

References

1. Eidhammer, I., Jonassen, I., Taylor, W.R. *Journal of Computational Biology: A Journal of Computational Molecular Cell Biology* **7(5)**, 685-716 (2000), https://doi.org/10.1089/106652701446152
2. Koehl, P. *Reviews in Computational Chemistry* **22**, 1 (2006), https://doi.org/10.1002/0471780367.ch1
3. Brylinski, M., Skolnick, J. *Proceedings of the National Academy of Sciences* **105**(1), 129-134 (2008)
4. Ilinkin, I., Ye, J., Janardan, R. *BMC Bioinformatics* **11**, 71 (2010), https://doi.org/10.1186/1471-2105-11-71
5. Irving, J.A., Whisstock, J.C., Lesk, A.M. *Proteins: Structure, Function, and Bioinformatics* **42(3)**, 378-382 (2001), https://doi.org/10.1017/S0033583503003901
6. Jianzhu, Ma, Wang, S. *Advances in Protein Chemistry and Structural Biology* **94**, 121-75 (2014), https://doi.org/10.1016/B978-0-12-800168-4.00005-6
7. Holm, L., Rosenstrom, P. *Nucleic Acids Research* **38** (Suppl. 2), W545-W549 (2010), https://doi.org/10.1093/nar/gkq366
8. Taylor, W.R. *Comparing Secondary Structure 'Stick' Models of Proteins Using Graph Matching with Double Dynamic Programming* (Mewes, H, Seidel, H., Weiss, B. Eds) Bioinformatics and Genome Analysis. Ernst Schering Research Foundation Workshop, **38**. Springer, Berlin, Heidelberg, 2002, https://doi.org/10.1007/978-3-662-04747-7_7
9. Hasegawa, H., Holm, L. *Current Opinion in Structural Biology* **19 (**3) 341-348 (2009), https://doi.org/10.1016/j.sbi.2009.04.003
10. Sapundzhi, F., Prodanova, K. and Lazarova, M., *AIP Conference Proceedings* **2172**, 1, 100008 (2019), https://doi.org/10.1063/1.5133601
11. Sapundzhi, F. *International Journal of Online and Biomedical Engineering (iJOE)* **15(11)**, 139-145 (2019), https://doi.org/10.3991/ijoe.v15i11.10893
12. Topalska, R., Sapundzhi, F. *Journal of Chemical Technology and Metallurgy* **55(4)**, 714-718 (2020)
13. Coutsias, E., Seok, C., Dill, K. *J Comput Chem*. **25** (15), 1849-1857, (2004)
14. Armougom, F., Moretti, S., Keduas, V., Notredame, C. *Bioinformatics* **22** (14) e35-39 (2006), https://doi.org/10.1093/bioinformatics/btl218
15. W. Kabsch, *Acta Crystallographica Section A* **32**(5), 922-923, (1976), https://doi.org/10.1107/S0567739476001873
16. W. Kabsch, *Acta Crystallographica Section A* **34** (5), 827-828, (1978), https://doi.org/10.1107/S0567739478001680
17. Walker, M., Shao, L., Volz, R., *CVGIP: Image Understanding* **54 (3)**, 358-367 (1991), https://doi.org/10.1016/1049-9660(91)90036-O
18. http://github.com/charnley/rmsd
19. Sapundzhi, F., Slavov, V. *Journal of Chemical Technology and Metallurgy* **55(4)**, 935-938 (2020)

Design and Synthesis of Pin1-PROTACs as Potential Therapeutic Tools for Cancer Treatment

Lorenzo Meneghelli[1], Lamia El Guermah[2], Maud Larregola[1], Sabrina Kellouche-Gaillard[2], Franck Carreiras[2], Julien Pytkowicz[1,] and Chiara Zanato[1]

[1]CY Cergy Paris Université, CNRS, BoCIS, 95000, Cergy Pontoise, France, Université Paris-Saclay, CNRS, BioCIS, 92290, Châtenay-Malabry, France; [2]CY Cergy Paris Université, Equipe de Recherche sur les Relations Matrice Extracellulaire-Cellules, ERRMECe, EA1391, Groupe Matrice Extracellulaire et physiopathologie MECuP, Institut des Materiaux, I-MAT, FD4122, France

Introduction

Peptidyl-prolyl isomerase NIMA-interacting-1 (Pin1) is a small two-domain protein member of the Peptidyl-Prolyl *cis-trans* Isomerases (PPIases) which catalyses the *cis-trans* isomerisation of Xaa-Proline amide ω-bonds in proteins [1]. Pin1 is structurally made up of two different domains, WW and PPIase, connected by a flexible linker loop region [2]. Pin1 differs from all others 30 PPIases through its unique substrate specificity for phosphorylated Serine/Threonine-Proline peptide bonds. Pin1 interacts with conformation-specific Pro-directed phosphatases and kinases to control common targets' stability, subcellular localization, and activity [3]. Pin1 is frequently overexpressed and/or overactivated in different types of cancer, and elevated Pin1 overexpression correlates with poor clinical prognosis [4]. Polymorphisms that under express Pin1 are linked with reduced tumour risk [5], and the depletion of Pin1 significantly inhibits tumorigenesis in mice models [6]. However, since Pin1 is not essential for cellular viability [7], its inhibition represents a potential strategy for cancer therapy.

Nevertheless, the development of Pin1 inhibitors remains challenging, despite decades of research, since Pin1 is considered "undruggable" [1]. Although many Pin1 inhibitors have been identified [8], most lack potency, specificity, cell permeability, and safety in clinical application [9]. To overcome this issue and, considering the rise of protein degradation as a promising therapeutic strategy [10], we decided to target the degradation of Pin1 as an alternative to inhibition. To reach our goal, we take advantage of PROTACs (PROteolysis TArgeting Chimeras) strategy. PROTACs [11] are bifunctional molecules made up of a ligand for the target protein of interest (POI) and a ligand for an E3 ubiquitin ligase (E3), joined by a flexible linker. Mechanistically, PROTACs promote the recruitment of the E3 ligase close to the POI, forming a ternary complex. This proximity enables E3 ligase-mediated ubiquitination of the POI, followed by its consecutive recognition and degradation by the Ubiquitin Proteasome System. Thanks to their unique catalytic mode of action, PROTACs present different advantages over small molecule-based inhibitors, including the capability to target "undruggable" protein [12]. In this work, we report the design, the synthesis, and the preliminary biological evaluation of the first series of Pin1-PROTACs. These degraders could have remarkable applications as potential therapeutic tools for cancer treatment. Pin1-PROTACs could also represent a helpful gear for investigating the complex biology of Pin1.

Results and Discussion

Designing and predicting the structure of a surely effective PROTAC is quite challenging, especially when the POI, as Pin1, has never been targeted for degradation using this technology before. Indeed, PROTAC's activity depends not only on the affinity of the ligand for the POI but, mainly, on its capability to form the ternary complex and, consequently, on its geometry. For this reason, we have synthesised four Pin1-PROTACs to maximise the probability of having an active degrader (Figure 1, **1a-4a**).

The scaffold of Pin1 ligands (**1b-4b**) was based on a versatile template that comprised the minimal peptide backbone length (three residues) and exploited the Pin1 preference for *C*-terminal aromatic amino acid and *N*-terminal aromatic moiety [13]. A terminal alkyne was incorporated at the *N*-terminal (**1b**, **2b**) or *C*-terminal (**3b**, **4b**) of the pseudopeptides, to allow the CuAAC (Copper-catalysed Alkyne-Azide Cycloaddition) with the flexible azide linker **5**. Both *N*-Fmoc protected (**1b-3b**) and the *N*-acetylated versions (**2b-4b**) of Pin1 ligands were synthesised in order to tune the solubility and affinity of the molecules. All the Pin1 ligands also bear a SATE (*S*-acyl-2-thioethyl) moiety, to mask

the anionic phosphoric group allowing the degraders to penetrate the cell membrane. Upon cell entry, SATE will be enzymatically removed, and the Pin1-PROTACs will be converted into their biologically active form. On the other side, a ligand of the E3 (**6**), accessorised with a terminal carboxylic acid, was synthesised. Between all the suitable E3 ligases, we decided to target Cereblon (CRBN) since it is present in the same type of cells where Pin1 is also expressed. CRBN ligand **6** was coupled with the amino PEG linker **5** *via* an amide bond formation reaction.

The synthetic pathway for the *N*-Fmoc protected Pin1 ligands (**1b** and **3b**) is reported in Scheme 1. The synthesis of **3b** started with the Fmoc-L-Ser(O*t*Bu)-OH (**7**), which reacted with NH$_2$-L-Pro-OBn under usual peptidic coupling conditions to obtain dipeptide **8** in excellent yield. After debenzylation with (Pd/C, H$_2$), the subsequent reaction with *O*-propargyl serotonin provided compound **9**. Deprotection of the *t*Bu group (TFA/DCM) and phosphorylation of the resulting alcohol gave the desired pseudopeptide **3b**. The synthesis of **1b** started with the benzyl deprotection (at *C*- terminal) of compound **8**. After that, the coupling with tryptamine, the Fmoc deprotection (at *N*- terminal), and the reaction with Fmoc-L-propargylglycine provided the pseudopeptide **10**. Deprotection of the *t*Bu group (TFA/DCM) and the subsequent phosphorylation gave Pin1 ligand **1b**. The acetylated version of **1b** and **3b** (**2b** and **4b**) were synthesised following a similar pathway, adding a deprotection (piperidine/DMF 20:80) and an acetylation (acetyl chloride/DCM) steps before the deprotection of *t*Bu group. The rest of the synthesis of Pin1-PROTAC **1a** is also reported in Scheme 1. After synthesising the E3 ligand scaffold starting from compound **11**, the carboxylic acid moiety was inserted to obtain the thalidomide analogue **12**. The reaction of **12** with the 11-azido-3,6,9-trioxaundecan-1-amine **5** in presence of HATU and DIPEA provided the azide **13**. Finally, copper catalysed click chemistry was employed to obtain Pin1-PROTAC **1a**. Pin1-PROTACs **2a**, **3a** and **4a** were synthesised following the same pattern of **1a** starting from the appropriate Pin1 ligands.

In order to check if the presence of the terminal alkyne on Pin1 ligands scaffold affected the binding affinity of the ligands for the protein, we evaluated their K$_d$. The affinity constants were calculated by NMR, using the CSP (Chemical Shift Perturbation) method. Pin1 was titrated with a ligand until saturation, and after each addition, a ^{1}H-^{15}N HSQC (500 MHz, 298 K) was recorded. Following the changes in the chemical shifts of Pin1 NMR spectrum, we were able to evaluate the K$_d$ of **1b** (37 ± 0.4 μM), **2b** (285 ± 8 μM) and **4b** (373 ± 31 μM) for Pin1 (WW domain). **3b** was not soluble in water and we were unable to perform the CSP NMR experiment and calculate its affinity constant. We compared the affinity constants of **1b**, **2b**, **4b** with the ones of Fmoc-pSer-Pro-Tryptamine (26 ± 6 μM) and Ac-pSer-Pro-Tryptamine (32 ± 6 μM), two Pin1 inhibitors previously developed in our laboratory. As a result, we were able to conclude that the insertion of the alkyne moiety at *C*-terminal of the pseudopeptide (**4b**) is detrimental for the affinity. At the same time, the scaffold modification at *N*-terminal is relatively well tolerated (**1b-2b**).
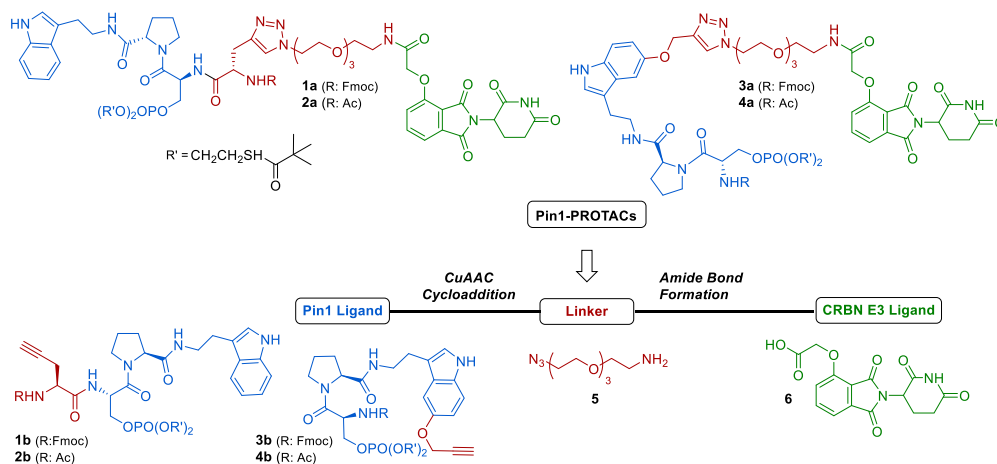
Fig. 1. Pin1-PROTACs scaffolds.
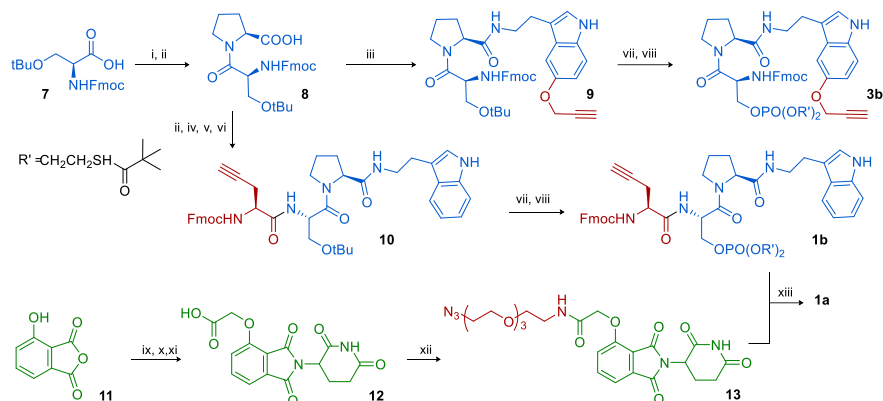
*Scheme 1. Synthesis of Pin1-PROTACs **1a**. Conditions: i) H-Pro-OBzl·HCl, DIPEA, EDC, HOBt; ii) H₂, Pd/C; iii) O-propargyl serotonin, DMAP, EDC, HOBt; iv) Tryptamine, DMAP, EDC, HOBt; v) DEA / DCM; vi) Fmoc-propargylglycine, DMAP, EDC, HOBt; vii) TFA / DCM; viii) (iPr₂N)P(OR'))₂ 5-ethylthio-H-tetrazole, tBuOOH; ix) 3-Aminopiperidine-2,6-dione·HCl, pyridine; x) Ethyl 2-bromoacetate, K₂CO₃; xi) TFA / DCM; xii) 11-azido-3,6,9-trioxaundecan-1-amine, HATU, DIPEA; xiii) **1b**, CuSO₄, Na-ascorbate.*

Finally, preliminary biological results were performed to confirm the presence and the localization of Pin1 and E3 CRBN inside the tumour cell lines that will be employed for the Pin1-PROTACs degradation assay (IGROV1 ovarian adenocarcinoma cell lines). Confocal microscopy analysis of IGROV1 shows the presence of both Pin1 and CRBN in the cytoplasm and nucleus.

Acknowledgments

References

1. Gestwicki, J.E., et al. *J. Med. Chem.* **59**, 9622-9644 (2016), https://doi.org/10.1021/acs.jmedchem.6b00411
2. Matena, A., et al. *Biol. Chem.* **399**, 101-125 (2018), https://doi.org/10.1515/hsz-2017-0137
3. Pawson, T., Scott, J. *Trends Biochem. Sci.* **30**, 286-290 (2005), https://doi.org/10.1016/j.tibs.2005.04.013
4. Liang, C., et al. *Cancer Res.* **79**, 133-145 (2019), https://doi.org/10.3389/fcell.2020.00168
5. Li, Q., et al. *PLoS ONE* **8**, e68148 (2013), https://doi.org/10.1371/journal.pone.0068148
6. Girardini, J. E., et al. *Cancer Cell.* **20**, 79-91 (2011), https://doi.org/10.1016/j.ccr.2011.06.004
7. Nabet, B., et al. *Nat. Chem. Biol.* **14**, 431-41 (2018), https://doi.org/10.1038/s41589-018-0021-8
8. Asano, T., et al. *Curr Med Chem* **27**, 3314-3329 (2020), https://doi.org/10.2174/0929867325666181105120911
9. Potter, A., et al. *Bioorg. Med. Chem.* **23**, 4283-4291 (2013), https://doi.org/10.1016/j.bmcl.2013.05.088
10. Sun, X., et al. *Sig Transduct Target Ther* **4**, 64 (2019) https://doi-org/10.1038/s41392-019-0101-6
11. Sakamoto, K.M., et al. *PNAS* **98**, 8554-8559 (2001) https://doi.org/10.1073/pnas.141230798
12. Xiao, X., et al. *Eur. J. Med. Chem.* **210**, 112993 (2021), https://doi.org/10.1016/j.ejmech.2020.112993
13. Xu, G.G., et al. *Biochemistry* **50**, 9545-9550 (2011), https://doi.org/10.1021/bi201055c

Beyond the Low Hanging Fruit: Rationally Designed Peptide as Regulators of Protein-Protein Interactions and Their Applications to Human Disease

Nir Qvit

The Azrieli Faculty of Medicine in the Galilee, Bar-Ilan University, Safed 1311502, Israel

Introduction

Protein-protein interactions (PPIs) play a fundamental role in all life events and cellular activities and represent a significant portion of functionally relevant biological interactions; therefore, they are well-established as a class of promising drug targets for their implications in a wide range of biological processes. Peptides and peptidomimetics (modified peptides) can serve as effective PPI inhibitors. Herein we describe the development of novel peptide-based PPI inhibitors for various therapeutic applications [1,2].

Results and Discussion

Based on rational approach we developed peptide PPI inhibitors. We previously found that peptides corresponding to specific regions in proteins, such as (i) docking sites, sites for PPI between a substrate and kinase that is outside of the active/catalytic site of the enzyme, or (ii) regions of homology of otherwise unrelated but interacting proteins, are effective inhibitors of PPIs. Initially using advanced bioinformatic algorithm we identified these regions in target proteins, next, we confirm that the amino acids in these regions are conserved in various species and unique to these proteins. Finally, based on these regions we developed peptides and evaluated their bioactivity in various biological assays [3,4].

Initially we used this approach to target protein kinases, a large and diverse multigene family that catalyze phosphorylation of proteins. Phosphorylation is the most widespread type of post-translational modification (PTM) used in signal transduction, and it is estimated that one-third of the total proteins in a cell may be phosphorylated on at least one residue at any one time. Phosphorylation also plays major roles in numerous cellular functions, including metabolism, proliferation, and survival. Importantly, protein kinases are the second most targeted group of drug targets, and the pharmaceutical industry has dedicated approximately one-third of new drug development programs over the last decade to the development of protein kinase modulators [5,6].

We hypothesized that in the inactive kinase conformation the substrate-specific docking site on the kinase may be masked by an intramolecular interaction, yet upon its activation a conformational change will reveal this docking site, which may be the kinase-binding site on the substrate, and therefore will have similar sequence. Based on this rational we developed novel peptide inhibitors of PPIs derived from the sequence homology of protein kinase C (PKC) and various substrates. Next we synthesized the peptides and evaluated their bioactivity *in vitro*, in cells and in various animal models, demonstrating their efficacy [7]. For example, based on a distal docking site on PKCδ and its substrate, pyruvate dehydrogenase kinase (PDK), a selective inhibitor of PDK docking to PKCδ was developed. The peptide demonstrated high binding to the target protein *in vitro* (K_D ~50 nM), and reduced cardiac injury induced by ischemic events in *ex vivo* and *in vivo* animal models (IC_{50} ~5 nM) [8]. Based on the same rational, peptides that target the PPI sites of PKCδ and other substrates were developed, including glyceraldehyde-3-phosphate dehydrogenase (GAPDH) [9], myristoylated alanine-rich C-kinase substrate (MARCKS), dynamin-related protein 1 (Drp1), insulin receptor substrate 1 (IRS1) [10], and Troponin I [11]. All these peptides demonstrated high specificity and bioactivity. The same exact approach was also used to protein kinase Cdc37 out of the PKC family, such as protein kinase Cdc37 and its binding partner the molecular chaperone Hsp90 [12].

Next, based on the idea that regions of homology of otherwise unrelated but interacting proteins are effective inhibitors of PPIs, we identified regions of homology between proteins that regulate mitochondrial homeostasis. Mitochondria are membrane-bound cell organelles that generate most of the chemical energy needed to power the cell's biochemical reactions. The major mechanisms by which mitochondria maintain their homeostasis are mitochondrial quality control mechanisms such as mitophagy and mitochondrial dynamics including both fission and fusion. Mitophagy, the degradation

and removal of selectively damaged or dysfunctional mitochondria via autophagy, is mediated mainly by the Parkin/PTEN-induced putative kinase 1 (Pink1) pathway. Fission and fusion are mediated by large guanosine triphosphatases (GTPases). Fission, controlled mainly by Dynamin related protein 1 (Drp1) and Fission 1 (Fis1), increases mitochondrial number and can separate damaged parts of the organelle from the functional ones for their selective removal. Fusion, however, is mediated by Optic atrophy 1 (Opa1) and Mitofusin 1/2 (Mfn1/2) and prevents mitochondrial damage by mixing the contents of partially damaged (compromised) mitochondria with healthy mitochondria and allow complementation of dysfunction components [13].

For example, we developed a selective peptide inhibitor of excessive mitochondrial fission, P110, which inhibits Drp1 enzyme activity and blocks Drp1/Fis1 PPI *in vitro* and in cultured neurons. Furthermore, P110 was found to be neuroprotective using a model of Parkinson's disease (PD) in culture by inhibiting mitochondrial fragmentation and reactive oxygen species (ROS) production and subsequently improving mitochondrial membrane potential and mitochondrial integrity. In addition, P110 increased neuronal cell viability by reducing apoptosis and autophagic cell death, and reduced neurite loss of primary dopaminergic neurons in PD cell culture model [14]. The same approach was used to target additional mitochondrial homeostasis proteins, such as Mfn1 [15], Mfn2 [16], transient receptor potential vanilloid 1 (TRPV1) [17], Fis1 [18] and Pink1 [19].

While the prominent role of peptides in controlling important physiological events and in influencing many pathological mechanisms is widely recognized, yet many peptides do not enter clinical trials because of inherent challenges, such as enzymatic susceptibility and membrane impermeability. Peptidomimetics are compounds whose essential elements (pharmacophore) mimic a natural peptide, they are peptide analogs able to mimic the structural elements and functionality of natural peptides retaining the capability to interact with the biological target and produce the same biological effect, while simultaneously addressing the associated undesirable pharmacological properties. In our studies we used several types of modifications to develop peptidomimetic compounds with improved pharmacological properties; these include local modifications, such as the incorporation of non-natural amino acids, as well as global modifications, such as, polypeptide chains that contain a circular sequence, or cyclization [20,21]. In addition, we also modified some peptides to optimize their bioactivity (*e.g.*, introduction of post-translational modifications) [22,23], attached various labels (*e.g.*, biotin or fluorescein isothiocyanate (FITC)) [19,24], and improved their stability (*e.g.*, incorporation of non-natural amino acids and/or cyclization) [25,26].

Peptides and peptidomimetics as drugs show unique characteristics and can be very effective, and their rational design have identified peptides that bind with exquisite specificity and affinity to their targets, therefore having relatively few off-target effects. In addition, they are highly bioactive, very specific, demonstrate low toxicity, and in many cases are developed from natural endogenous scaffolds with known biological activity, thereby making them particularly attractive therapeutic agents [27-29]. Over the years, peptides and peptidomimetics have been evolved as promising therapeutic agents in the treatment of different diseases [21,28,30,31] such as parasitic diseases [32-34], cancer [35,36], diabetes [37], and cardiovascular diseases [8,10,38-42]. There is an increased interest in regulation of PPIs to target intracellular signaling events. Herein we present a rational approach to develop effective pharmacological tools to inhibit PPIs. These peptides and peptidomimetics are useful pharmacological tools *in vitro*, in cell culture and in various animal models, and are promising candidates as therapeutics for various human diseases.

Acknowledgments

References

1. Churchill, E.N., Qvit, N., et al. *Trends Endocrinol. Metab.* **20**, 25-33 (2009), http://dx.doi.org/10.1016/j.tem.2008.10.002
2. Mochly-Rosen, D., Qvit, N. *Chimica Oggi / CHEMISTRY Today* **28**, 14-16 (2010)
3. Cunningham, A.D, Qvit, N. *Chimica Oggi/Chemistry Today* **34**, 22-25 (2016)
4. Cunningham, A.D., Qvit, N, et al. *Current Opinion in Structural Biology* **44**, 59-66 (2017), http://dx.doi.org/10.1016/j.sbi.2016.12.009

5. Attwood, M.M., Fabbro, D., et al. *Nat Rev Drug Discov* **20**, 839-861 (2021), http://dx.doi.org/10.1038/s41573-021-00252-y
6. Cohen, P., et al. *Nat Rev Drug Discov* **20**, 551-569 (2021), http://dx.doi.org/10.1038/s41573-021-00195-4
7. Qvit, N., Mochly-Rosen, D. *Biochem Soc Trans* **42**, 1529-1533 (2014), http://dx.doi.org/10.1042/bst20140189
8. Qvit, N., Disatnik, M.H., et al. *J Am Chem Soc* **138**, 7626-7635 (2016), http://dx.doi.org/10.1021/jacs.6b02724
9. Qvit, N., Joshi, A.U., et al. *J Biol Chem* **291**, 13608-13621 (2016), http://dx.doi.org/10.1074/jbc.M115.711630
10. Qvit, N., Kornfeld, O.S., et al. *Angew Chem Int Ed Engl* **55**, 15672-15679 (2016), http://dx.doi.org/10.1002/anie.201605429
11. Qvit, N., Lin, A.J., et al. *Pharmaceuticals* **15**, 271 (2022).
12. Lerner, Y., Sukumaran, S., et al. *JoVE*: e63495 (2022), http://dx.doi.org/doi:10.3791/63495
13. Youle, R.J., van der Bliek, A.M. *Science* **337**, 1062-1065 (2012), http://dx.doi.org/10.1126/science.1219855
14. Qi, X., Qvit, N., et al. *Journal of Cell Science* **126**, 789-802 (2013), http://dx.doi.org/10.1242/jcs.114439
15. Ferreira, J.C.B.,et al. *Nat Commun* **10**, 329 (2019), http://dx.doi.org/10.1038/s41467-018-08276-6
16. Franco, A., Kitsis, R.N., et al. *Nature* **540**, 74-79 (2016), http://dx.doi.org/10.1038/nature20156
17. Hurt, C.M., Lu, Y., et al. *J. of the American Heart Association* **5**, 1-13 (2016), http://dx.doi.org/10.1161/jaha.116.003774
18. Kornfeld, O.S., Qvit, N., et al. *Scientific Reports* **8**, 14034 (2018), http://dx.doi.org/10.1038/s41598-018-32228-1
19. Ben-Uliel, S.F., Zoabi, F.H., et al. *Intl. J. of Molecular Sciences* **23**, 6076 (2022).
20. Qvit, N., Reuveni, H., et al. *J Comb Chem* **10**, 256-266 (2008), http://dx.doi.org/10.1021/cc700113c
21. Rubin, S., Qvit, N. *Critical Reviews in Eukaryotic Gene Expression* **26**, 199-221 (2016).
22. Qvit, N. *Chemical Biology & Drug Design* **85**, 300-305 (2014), http://dx.doi.org/10.1111/cbdd.12388
23. Qvit, N., Hatzubai, A., et al. *Biopolymers* **91**, 157-168 (2009), http://dx.doi.org/10.1002/bip.21098
24. Qvit, N., Monderer-Rothkoff, G., et al. *Biopolymers* **90**, 526-536 (2008), http://dx.doi.org/10.1002/bip.21010
25. Rubin, S.J.S., Tal-Gan, Y., et al. *Current topics in Medicinal Chemistry* **18**, 556-565 (2018).
26. Rubin, S.J.S., Qvit, N. *Curr Top Med Chem* **18**, 526-555 (2018), http://dx.doi.org/10.2174/1568026618666180518092333
27. Qvit, N. *chimica Oggi / CHEMISTRY today* **29**, 4-7 (2011).
28. Qvit, Nir, Rubin, Samuel J. S., et al. *Drug Discovery Today* **22**, 454-462 (2017), http://dx.doi.org/10.1016/j.drudis.2016.11.003
29. Qvit, N. 2021. In *Encyclopedia of Molecular Pharmacology*, ed. S Offermanns, W Rosenthal: Springer
30. Zorzi, A., Deyle, K., et al. *Curr Opin Chem Biol* **38**, 24-29 (2017), http://dx.doi.org/10.1016/j.cbpa.2017.02.006
31. Lau, J.L., Dunn, M.K. *Bioorganic & Medicinal Chemistry* **26**, 2700-2707 (2018), http://dx.doi.org/https://doi.org/10.1016/j.bmc.2017.06.052
32. Qvit, N., Crapster, J.A., *Chimica Oggi / CHEMISTRY today* **32**, 62-66 (2014).
33. Qvit, N., Schechtman, D., et al. *International Journal for Parasitology: Drugs and Drug Resistance* **6**, 74-84 (2016), http://dx.doi.org/http://dx.doi.org/10.1016/j.ijpddr.2016.02.003
34. Qvit, N., Kornfeld, O.S. *Journal of Visualized Experiments*: e53589 (2016), http://dx.doi.org/doi:10.3791/53589
35. Marqus, S., Pirogova, E., et al. *Journal of Biomedical Science* **24**, 21 (2017), http://dx.doi.org/10.1186/s12929-017-0328-x
36. Rubin, S.J.S, Qvit, N. *Current Topics in Medicinal Chemistry* (2020).
37. Flatt, P.R., Conlon, J.M. *Peptides* **100**, 1-2 (2018), https://doi.org/10.1016/j.peptides.2018.01.004
38. Qvit, Nir, Mochly-Rosen, Daria. *Drug Discovery Today: Disease Mechanisms* **7**, e87-e93 (2010), http://dx.doi.org/10.1016/j.ddmec.2010.07.001
39. Kornfeld, O. S., Hwang, S., et al. *Circulation Research* **116**, 1783-1799 (2015), http://dx.doi.org/10.1161/circresaha.116.305432
40. Recio, C., Maione, F., et al. *Frontiers in Pharmacology* **7**, 526 (2016), http://dx.doi.org/10.3389/fphar.2016.00526
41. Heymann, H.M., Wu, Y., et al. *Br J Pharmacol* **24**, 4826-4835 (2017), http://dx.doi.org/10.1111/bph.14064
42. Lerner, Y., Hanout, W., et al. *Current Topics in Medicinal Chemistry* (2020).

A Novel Selection Technology Identifies Potent Inhibitor Peptides Against 3CL Protease of SARS-Cov-2 Coronavirus

Alexander Pisarchik and Edmund Nesti

1450 S. Rolling Rd., Suite 4.069, Halethorpe MD 21227, USA

Introduction

Modern day drug discovery has focused on the development of small molecule therapeutics. While small molecules offer many advantages, such as economical manufacturing, lower complexity and better bioavailability as compared to other drug modalities (e.g. antibodies and nucleic acid based therapeutics), they can only target 2-5% of the proteome [1,2]. Biologic-based drugs (e.g. antibodies) have a larger binding surface and therefore a higher target specificity, allowing them to access targets that are beyond the reach of small molecules and have fewer off-target effects. However, most biologics are large molecules that cannot cross cell membranes, which restricts their use to extracellular targets. Peptide drugs, on the other hand, have advantages of both small molecule therapeutics and biologic drugs, but do not have many of their disadvantages. Like biologic-based drugs, peptides have a large binding surface to target leading to their higher specificity and fewer off-target effects [3]. Similar to small molecules, they are smaller, have lower immunogenicity [4] and higher bioavailability. Recent advances in cell penetrating peptide technology have enabled peptide drugs to be designed to access intracellular targets [5]. Peptide drugs can therefore achieve the level of bioavailability comparable to that of small molecule therapeutics and activity and safety of biologic-based drugs which makes them prime candidates for "undruggable" targets.

The development of therapeutic peptides commonly starts with a combinatorial biology approach that involves the generation of chemical or biosynthetic peptide libraries. Chemical peptide synthesis is a well-established method for developing peptide libraries [6]; however, the biosynthetic approach offers many advantages. One key advantage is the library size. Biosynthetic libraries can easily contain as many as 10^9 peptides, while chemical synthesis is limited to approximately 10^4 peptides. The most commonly used biosynthetic selection methods are phage display [7], yeast display [8] and mRNA display [9]. All of these methods select peptides that bind to the target protein most tightly. However, a major limitation to these approaches is that the best binders may not be the best inhibitors of the target protein, because binding does not always occur in the active region of the protein.

One way to solve this problem is to establish a link between binding and function by screening peptides intracellularly for their ability to attenuate or inhibit cellular processes. None of the existing cell-based assays has taken full advantage of this approach. Currently, the most promising *in vivo* peptide selection method, called split-intein circular ligation of peptides and proteins (SICLOPPS), is based on protein trans-splicing. This involves self-excision of an internal protein segment (intein) resulting in a cyclized polypeptide [10]. Typically, such libraries are screened in *E.coli* cells using bacterial two-hybrid system. Selection relies on disruption of a targeted protein-protein interaction, detected through a reporter gene expression. False positive clones often result, due to fluctuations of gene expression, mutations in the regulatory sequences and mutations in the bacterial genome. Additionally, construct design for these peptide "processing" enzymes (inteins) is complex, generally restricted to a reduced environment [11], and are time consuming [12].

To solve this problem, we developed a new selection system based on direct inhibition of a cytotoxic protein (Figure 1). Peptides mimic cyclization by insertion into a protein loop, thus avoiding the need for any processing enzymes (like inteins). This gives the flexibility of screening constrained and linear peptides, which further increases the library size and improves the chances for identification of the optimal peptide inhibitor. As a proof-of-concept for this new approach, we performed the selections for a small pool of peptides (10^6 variants) that consisted of constrained and linear peptide inhibitors targeting main coronavirus protease (3CL). Within five weeks, we identified an inhibitor with an IC$_{50}$ of 33 µM, validating this screening approach.
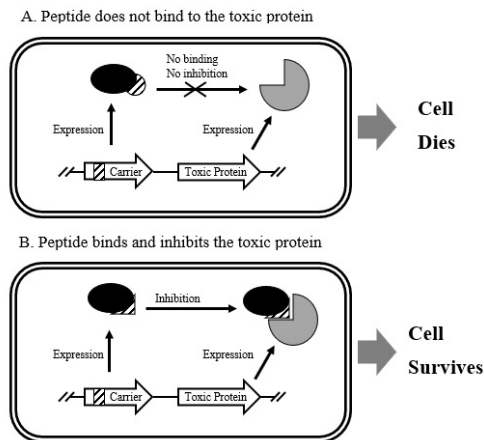
Fig. 1. Selection System. Toxic protein is co-expressed with a library of peptides. Peptide variants are inserted into a carrier protein. A) When a peptide does not inhibit the toxic protein, host cell dies. B) If a candidate peptide binds to and inhibits the target protein, its cytotoxicity is neutralized and host cells survives.

Results and Discussion

Selection. A significant disadvantage of current display technologies (eg. Phage display, RNA display, yeast display) is the lack of a connection between binding and function. That means that a peptide binding to the target protein may not necessarily inhibit its enzymatic activity or disrupt a protein-protein interaction. We addressed this problem by developing a selection based on the cytotoxicity of the target protein. Other *in vivo* selection methods have relied on the toxicity of an enzyme's (target protein) substrate [13], products of the enzymatic reaction [14], a particular intermediate [15], or resistance to inhibitors [16]. Our selection approach is the first to capitalize on the cytotoxicity of the target protein itself. It involves co-expression of the cytotoxic target protein and a library of peptide variants. Host cells survive only when a particular peptide variant inhibits the cytotoxic protein (Figure 1). Main protease (3CL) of SARS-CoV2 virus was chosen as a model protein because it plays a central role in the virus life cycle. It processes viral polyproteins and controls the replicase complex activity [17], which makes it very attractive target for drug development.

Cytotoxicity of 3CL protease was confirmed by expressing it in *E.coli*. We've built the p3CL plasmid where 3CL gene was cloned under the control of arabinose-inducible promoter of pBAD-HisA vector (Figure 2). This plasmid was transformed in 10G strain of *E.coli* and streaked on the plates with 0.4% arabinose. Strain harboring p3CL plasmid did not grow under these conditions while strains containing empty vector or mutant 3CL proteases did which confirmed our hypothesis that toxicity of this protease was caused by its enzymatic activity.

Libraries. We inserted our peptide libraries into the first loop of ubiquitin. We selected ubiquitin because of its small size (8.6kD), stability in *Ecoli*, and history of used to expressing proteins and peptides [18]. The first loop was selected for library insertion because loops are generally tolerant to insertions and deletions and this particular loop was previously used for insertions [19]. Ubiquitin was co-expressed with 3CL from the same expression construct pUbi-3CL which is shown in Figure 2. In this construct ubiquitin and 3CL genes are arranged in an operon fashion under the control of the arabinose-inducible promoter. A Shine-Dalgarno sequence is inserted between 3CL and Ubiquitin to ensure the expression of both genes.

Fig. 2. Expression constructs. Expression of 3CL and Ubiquitin is controlled by the arabinose-inducible promoter in both constructs. 3CL is fused to GST for the expression purposes.

The library construction method is presented in Figure 3. The first peptide library was random, built with 14 degenerate codons, resulting in up to 1.6×10^{18} variants. The second library was based on published sequences [20] recognized by 3CL, and contained approximately 2×10^9 variants. Variant sequences with no stop codons or frame-shifts were fully integrated into the loop of the full-length ubiquitin protein and served as a model of cyclic peptides. Variants with stop codons were expected to produce linear peptides attached to the first beta strand of ubiquitin.
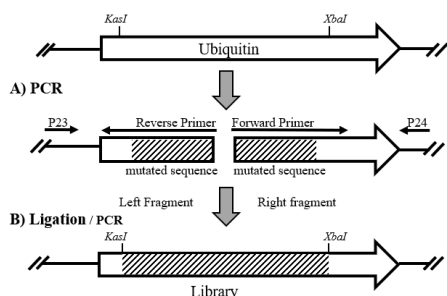
Fig. 3. Library Construction. Degenerate sequences are introduced by PCR: A) The sequences are amplified by degenerate oligos: B) Mutated fragments are phosphorylated by T4 polynucleotide kinase and ligated using T4 DNA ligase.

Selection. Both peptide libraries were cloned in the pUbi-3CL construct (Figure 2) and taken through five rounds of selection in *Ecoli*. Selection was done by inoculating libraries in liquid LB media with 0.4% arabinose and incubation overnight at 37°C with shaking. Every round of selection included 1 million clones for each library. To weed out false positives that may result from frame-shifts, deletions of 3CL and somatic mutations libraries were re-cloned into the original vector (pUbi-3CL) after each round of selection. The fifth round of selection generated several sequences that were significantly overrepresented in the population. We chose the most abundant peptides for further testing. They inhibited the 3CL protease with IC50 ranging from 100 µM to 1.2 mM. The two best peptides were M1 (RQGLDEDLHRW) and M5 (TANAFLS). Their IC_{50} was 249 and 101 µM, respectively (Table 1). Peptide M1 originated from the random library and peptide M5 originated from the library based on the published sequences that are recognized by 3CL. This observation demonstrates that this approach can identify inhibitors without prior knowledge of their ligands and can improve the inhibitory activity of known ligands.

Table 1. Peptide Inhibitors of 3CL Protease.

Peptide Name	Peptide Sequence		IC50 (µM) N=4, P<0.05
M1	GAR<u>QGLDEDLHRW</u>	linear	249±47
M5	GA<u>TANAFLS</u>GSGSRG	linear	101±17
M5c	WRRWWRRRR<u>TANAFLS</u>	cyclic	34±8

Selected peptide sequences are underlined

It is also important to note that peptide M5 was fully integrated in the first loop of the carrier protein (ubiquitin) which gives it a cyclic structure. To be consistent with the structure in the original screen, we also synthesized peptide M5 in a cyclic form (peptide M5c, Table 1) fused to a custom cell penetration sequence (WRRWWRRRR) to improve its stability and intracellular transport. Cyclization improved IC50 of M5 peptide significantly from 101 to 33 µM (Table 1). These data demonstrate the utility of this selection approach for screening both linear and cyclic peptides.

A weakness of this study is that we were able to screen only a small fraction of all available peptide variants (1 million clones at each stage of selection). We also do not know the exact mechanism of the inhibition yet. Despite these shortcomings, we were able to rapidly identify (in a few weeks) potent peptide inhibitors with low µM activity (Table 1), validating this approach.

References

1. Hopkins, A.L., Groom, C.R. *Nat. Rev. Drug Discov*. **1**, 727-730 (2002), http://dx.doi.org/10.1038/nrd892
2. Drews, J. *Science* **287**, 1960-1964 (2000), http://dx.doi.org/10.1126/science.287.5460.1960
3. Craik, D.J., Fairlie, D.P., Liras, S., Price, D. *Chem. Biol. Drug Des*. **81**, 136-147 (2013), http://dx.doi.org/10.1111/cbdd.12055
4. Van Regenmortel, M.H.V. *Biologicals. Academic Press* **29**, 209-213 (2001), http://dx.doi.org/10.1006/biol.2001.0308
5. Dougherty, P.G., et al. *Chem. Rev.* **119**, 10241-10287 (2019), http://dx.doi.org/10.1021/acs.chemrev.9b00008

6. Marasco, D., et al. *Curr. Protein Pept. Sci.* **9**, 447-467 (2008), http://dx.doi.org/10.2174/138920308785915209
7. Smith, G.P. *Science* **228**, 1315-1317 (1985), http://dx.doi.org/10.1126/science.4001944
8. Bowen, J., et al. *Int. J. Mol. Sci*. **22**, 1-20 (2021), http://dx.doi.org/10.3390/ijms22041634
9. Roberts, R.W., Szostak, J.W. *Proc. Natl. Acad. Sci. USA* **94**, 12297-12302 (1997), http://dx.doi.org/10.1073/pnas.94.23.12297
10. Tavassoli, A., Benkovic, S. *J. Nat. Protoc*. **2**, 1126-1133 (2007), http://dx.doi.org/10.1038/nprot.2007.152
11. Bhagawati, et al. *Proc. Natl. Acad. Sci. USA* **116**, 22164-22172 (2019), http://dx.doi.org/10.1073/pnas.1909825116
12. Aranko, et al. *Protein Eng. Des. Sel.* **27**, 263-271 (2017), http://dx.doi.org/10.1093/protein/gzu028
13. Jiang, P., et al. *Sci. Rep*. **5**, 8563 (2015), http://dx.doi.org/10.1038/srep08563
14. McLoughlin, S.Y., et al. *Protein Expr. Purif*. **41**, 433-440 (2015), http://dx.doi.org/10.1016/j.pep.2005.01.012
15. Boersma, Y.L., et al. *ChemBioChem* **9**, 1110-1115 (2008), http://dx.doi.org/10.1002/cbic.200700754
16. Dickinson, et al. *Nat. Commun*. **5**, 5352 (2014), http://dx.doi.org/10.1038/ncomms6352
17. Anand, K., et al. *Science* **300**, 1763-1767 (2003), http://dx.doi.org/10.1126/science.1085658
18. Baker, R.T. *Curr. Opin. Biotechnol*. **7**, 541-546 (1996), http://dx.doi.org/10.1016/s0958-1669(96)80059-0
19. Ferraro, D.M., et al. *J. Mol. Biol*. **352**, 575-584 (2005), https://doi.org/10.1016/j.jmb.2005.07.012
20. Muramatsu, T., et al. *Proc. Natl. Acad. Sci. USA* **113**, 12997-13002 (2016), http://dx.doi.org/10.1073/pnas.1601327113

Fluorinated Peptide Approach for the Inhibition of Rotamase

Guy Gouarin[1], Chiara Zanato[1], Soha Abou Ibrahim[2], Stephanie Davidson[2], Maud Larregola[1,2], Grégory Chaume[1], Nathalie Lensen[1], Ludovic Carlier[2], Bogdan Iorga[3], Emeric Miclet[2], and Thierry Brigaud[1]

[1]CY Cergy Paris Université, CNRS, BioCIS, 95000, Cergy Pontoise, France, Université Paris-Saclay, CNRS, BioCIS, 92290, Châtenay-Malabry, France; [2]Sorbonne Université, École Normale Supérieure, PSL University, CNRS, Laboratoire des Biomolécules, 4 place Jussieu, F-75005 Paris, France; [3]Institut de Chimie des Substances Naturelles, CNRS UPR 2301, Centre de Recherche de Gif-sur-Yvette, 91198 Gif-sur-Yvette, France

Introduction

Peptidyl-Prolyl isomerase NIMA-interacting-1 (Pin1) is a small two-domain protein member of the Peptidyl-Prolyl *cis-trans* Isomerases (PPIases) which catalyses the *cis-trans* isomerisation of Xaa-Proline amide ω-bonds in proteins [1]. Pin1 is structurally made up of two different domains, WW and the catalytic PPIase, connected by a flexible linker loop region [2]. Pin1 differs from all others 30 PPIases through its unique substrate specificity for phosphorylated Serine/Threonine-Proline (pSer/Thr-Pro) peptide bonds. Pin1 interacts with conformation-specific Pro-directed phosphatases and kinases to control common targets' stability, subcellular localization, and activity [3]. Pin1 is frequently overexpressed and/or overactivated in different types of cancer, and elevated Pin1 overexpression correlates with poor clinical prognosis [4]. Polymorphisms that under-express Pin1 are linked with reduced tumour risk [5], and the depletion of Pin1 significantly inhibits tumorigenesis in mice models [6]. However, Pin1 is not essential for cellular viability [7]. Therefore, the development of potent inhibitors of Pin1 is an attractive topic for cancer therapy. Both small molecules and peptides have shown Pin1's inhibition and cancer suppression ability in multiple studies [8]. Nevertheless, despite decades of research, developing selective and potent Pin1 inhibitors remains challenging. Compared to small-molecules, peptides display generally more selectivity towards the target but suffer of chemical and/or metabolic instability as well as poor cell-permeability [9]. The incorporation of fluorine into biomolecules has gained a considerable interest due to its ability to modulate properties of pharmaceutical compounds [10]. In this context, we decided to design and synthesize fluorinated peptidic Pin1 inhibitors. This way, we could access inhibitors with high selectivity, potency and enhanced biological profiles.

Our group is interested in the synthesis of enantiopure fluorinated amino acids and their incorporation into peptides in order to tune their properties. The aim of this project is to rationally design fluorinated peptide ligands to access Pin1 inhibitors with enhanced biological profile. Previously, we demonstrated that the introduction of CF_3-pseudoproline can lower the rotational barrier of the *cis-trans* peptide bond [11]. Moreover, the CF_2-phosphonate moiety is known to be a stable bioisostere of phosphate group [12]. Therefore, we decided to introduce these two moieties into a peptide scaffold to access potent Pin1 inhibitors, stabilizing the transition state conformation and/or improving their metabolic stability (Figure 1). Our peptide scaffold is based on previously reported Pin1 ligands that comprised the minimal peptide backbone length (three residues) and exploited the Pin1 preference for *C*-terminal aromatic amino acid and *N*-terminal aromatic moiety [13].
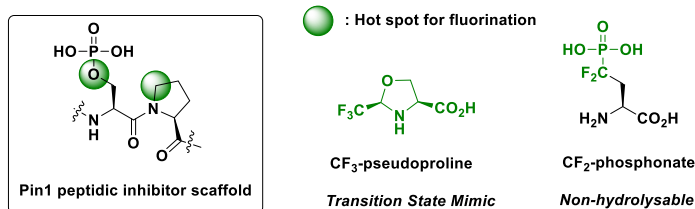
Fig. 1. Modification of the Pin1 inhibitor's scaffolds.

Results and Discussion

Synthesis of Pin1 ligands

Two "transition state mimic" Pin1 ligands **P1** and **P2** have been synthesized in solution (Scheme 1). The first step involves the coupling reaction between the Fmoc-L-Ser(O*t*Bu)-OH **1** and Ser($\Psi^{CF3,H}$Pro)-OBn **2**. Because of the lack of nucleophilicity of the amino group and the steric bulkiness of the vicinal CF$_3$-group of the pseudoproline, the usual coupling reagent are not effective.

Therefore, the *N*-coupling reaction has been achieved using the most electrophilic Fmoc-protected serine acyl chloride to give the dipeptide **3** in very good yield. Then, debenzylation under hydrogen atmosphere in the presence of Pd/C catalyst, and the subsequent reaction with tryptamine under standard conditions provided compound **4**. Deprotection of the *t*Bu group (TFA/DCM) and phosphorylation of the resulting alcohol gave the desired peptide **P1**. The acetylated analogue **P2** were synthesized from compound **4**. The sequence Fmoc-deprotection/acetylation afforded compound **5** in good yield. Finally, peptide **P2** was obtained following the similar *t*Bu deprotection/phosphorylation sequence used for **P1**.

In order to assess the effect of the trifluoromethylated pseudoproline in terms of affinity for Pin1, we synthesized the non-fluorinated analogues replacing the pseudoproline by the proline residue. Peptides **P3** and **P4** were prepared started from Fmoc-L-Ser(O*t*Bu) **1** and L-Pro-OBn **6** following the same pathway than **P1** and **P2** with the exception of the conditions of the first step (HOBt, EDC, DIPEA, DMF) (Scheme 1, intermediates **7**, **8**, and **9**).

i) SOCl$_2$, DCM; ii) H-Ser($\Psi^{H,CF3}$Pro)-OBzl **2**, DCM (89%); iii) (a) H$_2$, Pd/C, MeOH (b) Tryptamine, DMAP, EDC, HOBt, DMF (94%); iv) 20% TFA/DCM (48% NHfmoc, 60% NHAc); v) (a) P(OtBu)$_2$N(iPr)$_2$, 5-ethylthio-1H-tetrazole (b) tBuOOH (50% NHfmoc, 50% NHAc); vi) 20% TFA/DCM (68% NHfmoc, 70% NHAc); vii) 20% Pip/DMF (98%); viii) Ac$_2$O, DCM (93%).

i) H-Pro-OBzl·HCl **6**, DIPEA, EDC, HOBt, DMF (97%); ii) H$_2$, Pd/C, MeOH; iii) Tryptamine, DMAP, EDC, HOBt, DMF (93%); iv) 20% TFA/DCM (50% NHfmoc, 60% NHAc); v) (a) P(OtBu)$_2$N(iPr)$_2$, 5-ethylthio-1H-tetrazole (b) tBuOOH (45% NHfmoc, 50% NHAc); vi) 20% TFA/DCM (62% NHfmoc, 60% NHAc); vii) 20% Pip/DMF (70%); viii) Ac$_2$O, DCM (96%).

i) H-Pro-OBzl·HCl **6**, EDC, HOBt, DMAP, DMF (72%); ii) TFA, TIPS H2O; iii) Ac$_2$O, DIPEA, DCM; iv) H$_2$, Pd/C, MeOH (35% in 3 steps); v) TMSI, ACN then H$_2$O; vi) Tryptamine, DIPEA, HBTU, DMF (31% in 2 steps).

*Scheme. 1. Synthesis of **P1-P5** Pin1 Ligands.*

Table 1. Pin1 ligands Kd values and trans/cis ratio of the pSer-Pro amide bond.

Peptide	$Kd_{WW}(\mu M)$	$Kd_{PPIase}(\mu M)$	trans/cis ratio[a] (D_2O - 298 K)
P1	7 ± 4	41 ± 9	0:100
P2	> 1 mM	490 ± 50	0:100
P3	26 ± 6	438 ± 80	82:18
P4	32 ± 6	> 1 mM	70:30
P5	275 ± 55	430 ± 123	73:27

A "non-hydrolysable" Pin1 ligand **P5** has also been prepared (Scheme 1). The synthesis of the phospho-serine bioisostere **10**, namely the Boc-protected L-2-amino-4-(phosphono)-4,4-difluoro-butanoic acid, was performed by adapting a procedure reported in the literature [14]. Coupling reaction between compound **10** and proline benzyl ester **6** gave the corresponding dipeptide **11** in good yield. Removal of the Boc protecting group (TFA/TIPS/H_2O) followed by acetylation (Ac_2O, DIPEA, DMC) and benzyl deprotection (H_2, Pd/C) provided carboxylic acid **12**. Finally, deprotection of the ethyl groups of the difluorophosphonate moiety and the coupling with tryptamine (HBTU, DIPEA, DMF) gave peptide **P5**.

NMR affinity constant (Kd) evaluation

The affinity constants were calculated by NMR, using the experimental CSP (Chemical Shift Perturbation) upon ligand addition. Pin1 titrations were performed for each ligand by recording a series of ^{1}H-^{15}N HSQC (500 MHz, 298 K). The *Kd* values of **P1-P5** for each Pin1 domain (WW/PPIase) were determined by fitting the shape of the titration curve (CSP vs. concentration of ligand) (Table 1) [15]. The binding preference of our peptides towards Pin1 domains is correlated to the *trans/cis* conformation of the pSer-Pro amide bond, in agreement with the literature [16]. In most of the cases, *cis* amide bond shows a preference for the catalytic domain (PPiase) while *trans* amide bond targets the WW domain. The incorporation of the trifluoromethylated pseudoproline into the peptide scaffold (**P1** and **P2**) strongly favors the *cis* amide bond while the use of the difluorophosphonate **P5** does not affect the *trans/cis* ratio compared to the non-fluorinated phosphate analogue **P4**. The *trans/cis* conformations of Pin1 ligands **P1-P5** were determined by NMR (Table 1). 2D ^{1}H NMR NOESY experiments allowed the assignment of the pSer-Pro amide bond conformation while the *trans/cis* ratio was determined by ^{1}H, ^{31}P and ^{19}F NMR experiments.

Acknowledgments

References

1. Gestwicki, J.E., et al. *J. Med. Chem.* **59**, 9622-9644 (2016), https://doi.org/10.1021/acs.jmedchem.6b00411
2. Matena, A., et al. *Biol. Chem.* **399**, 101-125 (2018), https://doi.org/10.1515/hsz-2017-0137
3. Pawson, T., Scott, J. *Trends Biochem. Sci.* **30**, 286-290 (2005), https://doi.org/10.1016/j.tibs.2005.04.013
4. Pu, W., Zheng, Y., Peng, Y. *Front. Cell Dev. Biol.* **8**, 168 (2020), https://doi.org/10.3389/fcell.2020.00168
5. Li, Q., et al. *PLoS ONE* **8**, e68148 (2013), https://doi.org/10.1371/journal.pone.0068148
6. Girardini, J.E., et al. *Cancer Cell.* **20**, 79-91 (2011), https://doi.org/10.1016/j.ccr.2011.06.004
7. Nabet, B., et al. *Nat. Chem. Biol.* **14**, 431-441 (2018), https://doi.org/10.1038/s41589-018-0021-8
8. Asano T., et al. *Curr Med Chem* **27**, 3314-3329 (2020), https://doi.org/10.2174/0929867325666181105120911
9. Potter, A., et al. *Bioorg. Med. Chem.* **23**, 4283-4291 (2013), https://doi.org/10.1016/j.bmcl.2013.05.088
10. Inoue, M., et al. *ACS Omega* **5**, 10633-10640 (2020), https://doi.org/10.1021/acsomega.0c00830
11. Feytens, D., et al. *J. Phys. Chem. B.* **116**, 4069-4079 (2012), https://doi.org/10.1021/jp300284u
12. Elliott, T.S., et al. *Med. Chem. Commun.* **3**, 735-751(2012), https://doi.org/10.1039/C2MD20079A
13. Xu, G.G., et al. *Biochemistry* **50**, 9545-9550 (2011), https://doi.org/10.1021/bi201055c
14. Berkowitz, D.B., et al. *J. Org. Chem.* **61**, 4666-4675 (1996), https://doi.org/10.1021/jo9604752
15. Williamson, M.P. *Prog. Nucl. Magn. Reson. Spectrosc.* **73**, 1-16 (2013), doi.org/10.1016/j.pnmrs.2013.02.001
16. Wang, X. *Structure* **23**, 2224-2233 (2015), https://doi.org/10.1016/j.str.2015.08.019

Control, Quantification and Assignment of Screw-Sense Preference in Helical Aib Foldamers by Introducing the Chiral Constrained α-Trifluoromethylalanine

Lizeth Bodero,[1] Grégory Chaume,[1] Nathalie Lensen,[1] Karine Guitot,[1] Sandrine Ongeri,[2] Olivier Lequin,[3] and Thierry Brigaud[1]

[1]CY Cergy Paris Université, CNRS, BioCIS, 5 mail Gay Lussac, 95000, Cergy Pontoise, France; [2]BioCIS, CNRS, Paris Saclay Université, Bat. Henri Moissan, 17 av. des Sciences, 91400 Orsay, France; [3]Laboratoire des Biomolécules, Sorbonne Université, École normale supérieure, PSL University, CNRS, 4 place Jussieu, 75005 Paris, France

Introduction

Foldamers are oligomers with a strong tendency to fold into a defined conformation [1]. Among the different types of foldamers, the oligomers of α-aminoisobutyric acid (Aib) have been widely investigated for their ability to form stable 3_{10}-helices, and their similitude with natural antimicrobial peptides. Because of the achiral nature of Aib, these hydrophobic foldamers do not exhibit axial chirality and present equal population of left- and right-handed conformers. Yet, the equilibrium between the two forms may be altered by incorporating a single chiral residue at *N*- or *C*- terminus, inducing a screw-sense preference on the helical chain [2].

The use of fluorine-containing amino acids is becoming a very promising tool for the design of new bioactive molecules [3,4]. However, their use for the design of fluorinated peptide-based foldamers remains in its infancy with only a few examples reported so far [5-10].

As α-trifluoromethyl-α-amino acids (Tfm-AAs) are interesting to promote the helical secondary structures of peptides [10-12], we propose to investigate the ability of a single fluorinated chiral residue, namely the (*R*)- and (*S*)-α-trifluoromethylalanine (TfmAla) to stabilize the 3_{10}-helical conformation and to act as chiral controller to induce a screw-sense preference when incorporated at the *N*-terminus of short Aib oligomers (Figure 1). We also aim to demonstrate that (*R*)- and (*S*)-TfmAla can serve as efficient ^{19}F NMR probe to reliably determine both the magnitude of the screw-sense preference and its sign assignment. The first series of fluorinated Aib foldamers is based on the introduction of a *C*-terminal ester groups while in the second series, a glycinamide ^{1}H NMR reporter was added at the *C*-terminal position to quantify the induced screw-sense preference of the helix.

Results and Discussion

Synthesis of fluorinated Aib-oligomers
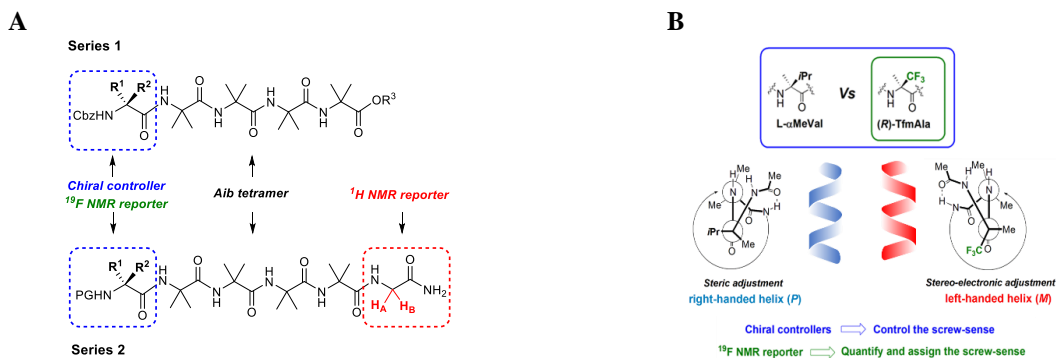
Fig. 1. A: Chemical structure of Aib-foldamers and their non-fluorinated analogues; B: Influence of the stereoelectronic properties of chiral TfmAla in the control of screw-sense preference.
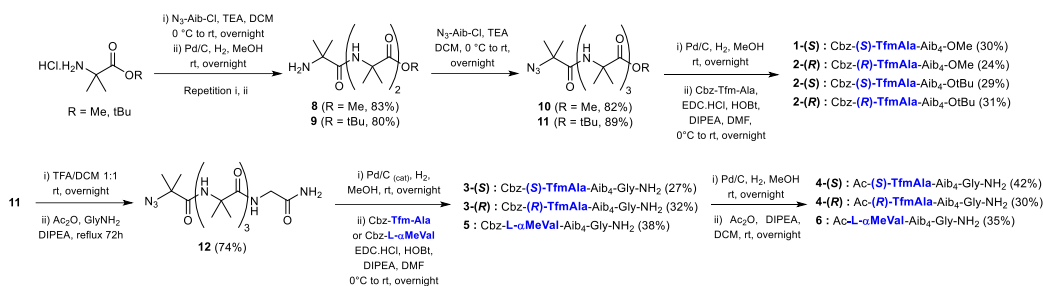
*Scheme. 1. Synthesis of Aib foldamers **1-6**.*

The synthesis of oligomers **1–6** started with the preparation of the Aib tetramers precursors **10** and **11**, bearing respectively a methyl or a *tert*-butyl ester at the *C*-terminus, via iterative coupling of N$_3$-Aib-Cl and reduction of the *N*-terminal azide functional group (Scheme 1) [13]. After the azide reduction of **10** and **11**, the incorporation of the Cbz-protected (*S*)- and (*R*)-TfmAla [14,15] at the *N*-terminal position was carried out under typical EDC/HOBt coupling conditions in solution to afford the final compounds **1–2**. Oligomers **3** and **4**, containing a *C*-terminal glycinamide residue, were prepared upon removal of the *tert*-butyl group of **11**, activation with acetic anhydride and reaction with glycinamide hydrochloride. Azide reduction followed by coupling with Cbz-protected (*S*)- and (*R*)-TfmAla afforded the peptides **3**. The substitution of the Cbz group of **3** provided the peptides **4**. Reference compounds **5** and **6**, containing the L-α-methylvaline residue (L-α-MeVal) as chiral controller were also prepared to study the conformations obtained with fluorinated oligomers compared to non-fluorinated ones.

Conformational studies of fluorinated Aib-oligomers

Intramolecular (i → i+3) H-bonding pattern of 3$_{10}$ helix structure has been confirmed by temperature coefficients (Δδ/ΔT) of NH protons for compounds **1-4**. The presence of the Schellman motif at the *C*-terminus of oligomers **1** and **2** did not perturb the intramolecular hydrogen-bonding contacts, even when using the more sterically demanding *tert*-butyl ester. Sequential NH(i)/NH(i+1) ROE correlations and the absence of NH(i)/NH(i+2) cross-peaks support the 3$_{10}$-helix conformation.

The CD spectra of foldamers **1-4** displayed a major band near 205 nm similar to the spectra of the reference compounds **5–6** and consistent with a 3$_{10}$-helix structure [16]. (*R*)-enantiomers of the fluorinated foldamers **1-4** induce a left-handed helicity (*M*), the mirror image of that induced by their non-fluorinated analogs **5** and **6**.

Finally, X-ray crystallography of **4-(S)** showed 2 conformers **4-(S)**$_M$ and **4-(S)**$_P$ in equal population exhibiting a 3$_{10}$-helix. The CF$_3$ group in **4-(S)**$_P$ is eclipsed to the C=O group leading to an alignment of their dipoles.

Quantification of screw-sense preference

The helical excess (h.e.) was calculated by measuring the ratio of anisochronicity of the Gly diastereotopic protons at fast and slow exchange regime in methanol (h.e. = Δδ_{fast}/Δδ_{slow}) [17] (Figure 2A). Fluorinated foldamers **3-4** display slightly lower helical excess (ca. 10%) compared to their non-fluorinated analogues **5-6** (Table 1).

The CF$_3$ group can also be used as highly sensitive probe for ^{19}F NMR spectroscopy to assess the degree of control exerted by the chiral TfmAla controller itself and the variation of the conformational preference along the

Table 1. Anisochronicity of the Gly diastereotopic protons at slow and fast exchange regime.

Compound	Δδ_{fast}^{293K} (ppb)[a]	Δδ_{slow} ^{193K} (ppb)[b]	^{1}H NMR reporter h.e.$_{obs}$[c], h.e.$_0$[d] (%)	^{19}F NMR reporter h.e.$_{obs}$[e] (%)
3-(S)	261	417	+62, +81	+80
3-(R)	264	419	−63, −83	−80
5	275	382	+72, +95 (+52, +68)[f]	
4-(S)	198	417	+47, +62	+66
4-(R)	198	417	−47, −62	−68
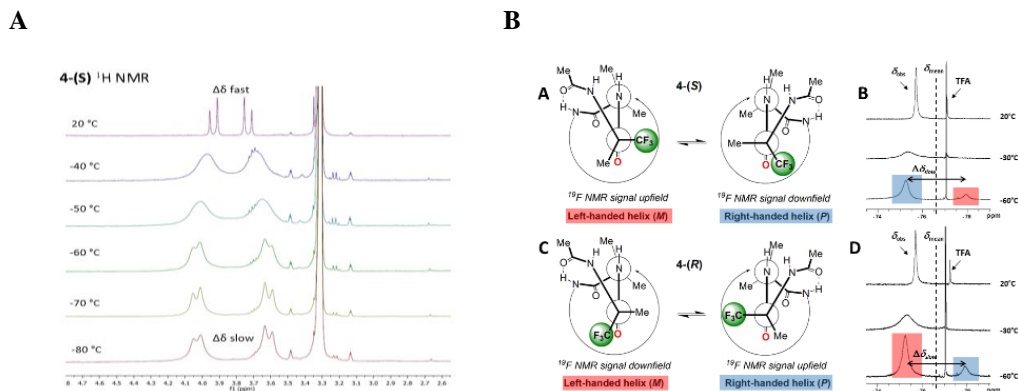
Fig. 2. A: NMR spectra of peptides 4-(S) showing Gly CH₂ signals and chemical shifts from -80°C to 20°C; B: Newman projections of the N-terminal turn of 4-(S) and 4-(R) in left-handed and right-handed helices and ¹⁹F NMR spectra of 4-(S) and 4-(R) in CD₃OD. TFA: trifluoroacetic acid.

peptide chain. Two distinct peaks corresponding to the CF₃ resonances of the (*M*)- and (*P*)-helices were observed when slow regime exchange was reached (Figure 2B). The helical excess (h.e.$_{obs}$) of the fluorinated peptides **3** and **4**, obtained by integrating the isolated resonances, were found to be ca. 80% and 67% respectively, in good agreement with the inferred helical excess values (h.e.$_0$). We were also able to assign the screw-sense preference by observing whether the predominant CF₃ signal appears upfield or downfield to that of the minor one.

To conclude, we report the synthesis of two series of Aib-based short fluorinated foldamers containing the (*S*)- or (*R*)-α-TfmAla as chiral controller at the *N*-terminus and an ester or glycinamide unit at the C-terminus. NMR conformational studies, circular dichroism and X-ray crystallography were consistent with a 3$_{10}$-helix type for fluorinated Aib oligomers, indicating a right-handed screw-sense preference for the (*S*)-enantiomers and left-handed screw-sense preference for the (*R*)-enantiomers. The selectivity of the screw-sense preference is reversed compared to that induced by the non-fluorinated L-α-MeVal chiral inducer due to the electronic properties of the CF₃ group. The CF₃ group can also be used as ¹⁹F NMR probe allowing the easy determination of both the magnitude of the screw-sense preference and the assignment of its sign.

Acknowledgments

References

1. Gellman, S.H. *Acc. Chem. Res.* **31**, 173-180 (1998), https://doi.org/10.1021/ar960298r
2. Clayden, J., et al. *J. Am. Chem. Soc.* **132**, 4548-4549 (2010), https://doi.org/10.1021/ja100662d
3. Soloshonok, V.A., et al. *Eur. J. Med. Chem.* **186**, 111826 (2020), https://doi.org/10.1016/j.ejmech.2019.111826
4. Koksch, B., et al. *Chem. Rev.* **119**, 10718-10801 (2019), https://doi.org/10.1021/acs.chemrev.9b00024
5. Cobb, S.L., et al. *Angew. Chem. Int. Ed.* **57**, 10549-10553 (2018), https://doi.org/10.1002/anie.201804488
6. Ishida, Y., et al. *Chem. Commun.* **50**, 9855-98578 (2014), https://doi.org/10.1039/C4CC02136C
7. Aitken, D.J., et al. *New J. Chem.* **39**, 3270-3279 (2015), https://doi.org/10.1039/C4NJ01929F
8. Li, Z.-T., et al. *Angew. Chem. Int. Ed.* **44**, 5725-5729 (2005), https://doi.org/10.1002/anie.200500982
9. Li, Z.-T., et al. *Chem. Eur. J.* **20**, 1418-1426 (2014), https://doi.org/10.1002/chem.201304161.
10. Tanaka, M., et al. *ChemistrySelect* **5**, 10882-10886 (2020), https://doi.org/10.1002/slct.202002888
11. Ulrich, A.S., et al. *Chem. Eur. J.* **24**, 4328-4335 (2018), https://doi.org/10.1002/chem.201704307
12. Ulrich, A.S., et al. *J. Am. Chem. Soc.* **131**, 15596-15597 (2009), https://doi.org/10.1021/ja9067595
13. Chaume, G., et al. *Chem. Eur. J.* e202103887 (2022), doi.org/10.1002/chem.202103887
14. Brigaud, T., et al. *Amino Acids* **48**, 1457-1468 (2016), https://doi.org/10.1007/s00726-016-2200-9
15. Chaume, G., *Eur. J. Org. Chem.* 5717-5724 (2009), https://doi.org/10.1002/ejoc.200900768
16. Toniolo, C., et al. *J. Am. Chem. Soc.* **118**, 2744-2745 (1996), https://doi.org/10.1021/ja9537383
17. Clayden, J., et al. *J. Org. Chem.* **78**, 2248-2255 (2013), https://doi.org/10.1021/jo302705k

ELISA Based Quantification of Chicken Specific Troponin-T Peptide in Skeletal Muscle TCA Extracts

Ioannis Sarrigeorgiou[1], Gerasimina Tsinti[1], Evgenia Fotou[2], Vasiliki Moulasioti[2], Dimitra Kyriakou[2], Constantinos Tellis[2], Vassilios Moussis[2], Apostolos Patsias[3], Theodora Stivarou[1], Vassilios Tsikaris[2], Vasileios Tsiouris[3,4], Demokritos Tsoukatos[2], and Peggy Lymberi[1]

[1]*Laboratory of Immunology, Immunology Department, Hellenic Pasteur Institute, Athens, Greece;* [2]*Department of Chemistry, Section of Organic Chemistry & Biochemistry, University of Ioannina, Ioannina, Greece;* [3]*Microbiology & Chemical Laboratory, Pindos APSI, Ioannina, Greece;* [4]*Unit of Avian Medicine, Faculty of Veterinary Medicine, School of Health Sciences, Aristotle University of Thessaloniki, Thessaloniki, Greece*

Introduction

Skeletal muscle troponin consists of the TnC (the sensor), TnI (the regulator), and TnT (the link to the muscle thin filament). Troponin T (TnT) represents the tropomyosin (Tm)-binding subunit of the troponin (Tn) complex whose role resides in the Ca^{2+}-dependent regulation of vertebrate striated muscle contraction. TnT interacts with its other counterparts and may be considered as an organizer molecule [1]. Moreover, due to the complex splicing of the NH_2-terminal variable region, a large number of fast skeletal muscle TnT isoforms are expressed in contrast to cardiac and slow skeletal muscle TnTs, and all of them are differentially expressed during myogenesis and development in a tissue specific manner [2]. In postmortem muscle, after rigor mortis, actin and myosin do not present enhanced degradation [3]. Several key myofibrillar proteins, however, have been shown to be degraded at differing rates [4]. TnT degradation and the detection of fragmentation products, represent a widely reported and well-established marker of skeletal muscle aging also in several animal products intended for commercial distribution in the food industry [4-7]. TnT fragments have been detected in various animal species such as beef, rabbit, lamb, fish, camel and poultry and have been positively associated with increased meat tenderness during aging [8-13]. The effect of aging on the chicken meat quality has been reported in a study by Wei *et al*., who observed in muscle extracts a significant increase in two specific peptides, which were later identified as products of chicken fast skeletal muscle TnT degradation [8].

Based on our previously developed competitive ELISA for the detection and quantification of TnT (16-31) fragment in trichloracetic acid (TCA) soluble beef skeletal muscle extracts [6, 14], as a marker of meat tenderness, an ELISA was similarly/respectively developed for the detection of the 21 aa TnT fragment EPAPPPEEKPRIKLTAPKIPE, which was reported to be present, in chicken skeletal muscle extracts [8].

Results and Discussion

In silico analysis of the reported peptide sequence in NCBI database led to the identification of the 21aa fragment as part of the fast skeletal muscle TnT isoforms (*TNNT3* gene) present in *Gallus gallus* and conserved in many other bird species. The fragment spans from aa position 61 to 81 of the 287 total aa protein (NP_990253.1) (Figure 1). This fragment will further be referred as TnT-21.

High affinity polyclonal anti-TnT-21 antibodies were generated in New Zealand white rabbits through a 3-dose immunization protocol with KLH as carrier, according to established methods. Immunization led to highly reactive antisera against TnT-21 (Figure 2a).

Isolation and purification of specific anti-TnT antibodies through protein A column (1st step) and TnT-

troponin T, fast skeletal muscle isoforms [Gallus gallus]
Sequence ID: NP_990253.1 Length: **287** Number of Matches: **1**

See 1 more title(s) ▼ See all Identical Proteins(IPG)

Range 1: 61 to 81 GenPept Graphics   ▼ Next Matc

Score	Expect	Identities	Positives	Gaps
70.6 bits(159)	2e-12	21/21(100%)	21/21(100%)	0/21(0%)

```
Query  1   EPAPPPEEKPRIKLTAPKIPE  21
           EPAPPPEEKPRIKLTAPKIPE
Sbjct  61  EPAPPPEEKPRIKLTAPKIPE  81
```

Fig. 1. In silico analysis of EPAPPPEEKPRIKLTAPKIPE peptide.

21 immunoadsorbent (2nd step) resulted in purification of highly specific anti-TnT-21 polyclonal antibodies as confirmed by indirect ELISA against TnT-21 (Figure 2b).

a.

b.
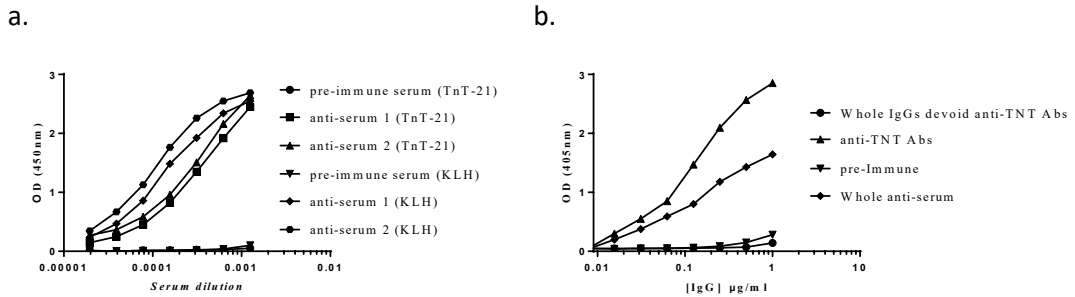
Fig. 2. a. Indirect ELISA against TnT-21 (2µg/ml) and KLH (1µg/ml) immobilized on the microplates, for the evaluation of rabbit immunization effectiveness. Antiserum 1 & 2 correspond to the samples after two consecutive booster immunizations in-between 1-month period. b. Indirect ELISA against TnT-21 (2µg/ml) for the evaluation of anti-TnT-21 Abs purification and reactivity.

To develop the competitive ELISA procedure, affinity-purified anti-TnT-21 Abs were conjugated to biotin using glutaraldehyde, and then commercial peroxidase-labelled streptavidin was used as detection system. The ELISA is based on the binding inhibition of anti-TnT-21 Abs to immobilized TnT-21 by soluble TnT-21. For the measurement of chicken TnT degradation in muscle tissue and potential delivery of the respective TnT-21 peptide as catabolic product, the conjugate anti-TnT-21 affinity purified Ab-biotin was co-incubated (v/v) with soluble peptide at serial dilutions for the standard curve formation. After optimization, biotin labelled anti-TnT-21 Abs were co-incubated at a final concentration of 200ng/ml and the respective standard curve had useful range 15pmol to 500pmol TnT-21/well (100µl/well). The results were expressed as inhibition percent (%) plotted

Fig. 3. Standard curve of competitive ELISA. The working volume per well is 100µl. The useful range for TNT quantitation is 15pmol to 500pmol TnT-21/well.

versus the concentration of inhibitor TnT fragment in pmol/well (Figure 3).

For TnT-fragments tissue analysis, thirty (30) TCA muscle extracts were produced based on previously described methods [7] from conventional chickens (C), free range chickens (FR) and FR chickens in which aromatic herbal extracts had been added to their diet (FRp) (Table 1). All chickens were raised under industrial conditions for commercial food consumption. Chicken thigh muscles were excised at slaughter, just before product processing, and muscle samples were immediately stored at -80°C until use. For the aging procedure thigh muscle pieces, prior to the experiment, were vacuum packed in plastic sealed bags, after removing visible fat and connective tissues and afterwards thawed at 4°C for 0, 24, 72 hours and 7 days [8-13]. Measurement results for different time points of *post mortem* aging are shown at Figure 4.

Table 1. Chicken*/ tissue specifications.

Genotype	Type	Raise Conditions/ Diet	Skeletal muscle tissue	
			N	Weight/pc (mean ±SD)
Ross 508	Fast Growth	Conventional (C)	10	7±2.3 gr
Sasso	Slow Growth	Free range (FR)	10	6±3.1 gr
		Free range + Aromatic herbals (FRp)	10	6±4.4 gr
Total			30	19±3.7 gr

*all chickens were raised under industrial scale production for food/meat consumption
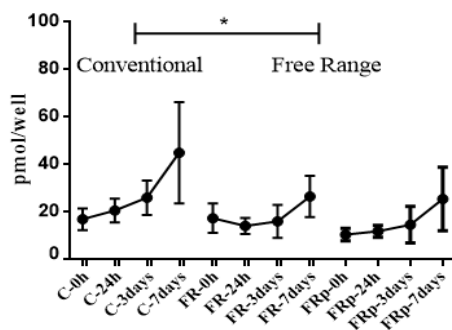
Fig. 4. Measurements of soluble TnT-21 in chicken's skeletal muscle 5%TCA extracts. Post-mortem aging process of skeletal muscle tissue was held at 4^oC in 4 distinct time points (0, 24, 72 and 168 hours).

A Troponin-T fragment, a protein degradation product, was detected in chicken skeletal muscle TCA extracts and was identified as a potential marker of *post mortem* aging. Our quantitative competitive ELISA for specific TnT-21 fragment in free range poultry will be further used for the correlation analysis between TnT-21 concentration and qualitative characteristics of the meat during *post mortem* aging. This quantitative ELISA may be proved advantageous for future use at the research and industrial level.

Acknowledgments

References

1. Vinogradova, M.V., Stone, D.B., Malanina, G.G., Karatzaferi, C., Cooke, R., Mendelson, R.A., et al. *Proc Natl Acad Sci*. **102**, 5038-5043 (2005), https://doi.org/10.1073/pnas.0408882102
2. Jozaki, M., Hosoda, K., Miyazaki, J.I. *J Muscle Res Cell Motil*. **23**, 235-243 (2002), https://doi.org/10.1023/a:1020956216423
3. Li, S., Xu, X., Zhou, G. *Poult Sci*. **91**, 150-160 (2012), https://doi.org/10.3382/ps.2011-01484
4. Iwasaki, T., Taniguchi, H., Hasegawa, Y., Maeda, N., Yamamoto, K. *J Sci Food Agric*. **96**, 3944-3949 (2016), https://doi.org/10.1002/jsfa.7558

5. Huang, M., Huang, F., Xu, X., Zhou, G. *Food Chem*. **115**, 181-186 (2009), https://doi.org/10.1016/j.foodchem.2008.11.095
6. Zhang, Y., Zhang, D., Huang, Y., Chen, L., Bao, P., Fang, H., et al. *Food Chem*. **318**, 126516 (2020), https://doi.org/10.1016/j.foodchem.2020.126516
7. Tsitsilonis, O.E., Stoeva, S., Echner, H., Balafas, A., Margomenou, L., Katsoulas, H.L., et al. *J. Immunol. Methods* **268**, 141-148 (2002), https://doi.org/10.1016/S0022-1759(02)00186-2
8. Wei, Z., Muraoka, J., Tanabe, S., Nishimura, T. Changes in taste components of japanese native fowl hybrid during postmortem conditioning. 48" ICoMST-Rome, 25-30 August 2002 - Vol.1.
9. Zhao, L., Xing, T., Huang, J., Qiao, Y., Chen, Y., Huang, M. *Anim. Sci. J*. **89**, 423-431 (2018), https://doi.org/10.1111/asj.12921
10. Wang, J., Zhou, J., Chen, Y., Zhang, X., Jin, Y., Cui, X., et al. *J. Anim. Sci. Biotechnol.* **10**, 1-10 (2019), https://doi.org/10.1186/s40104-019-0389-7
11. Zhang, X., Gao, T., Song, L., Zhang, L., Jiang, Y., Li, J.L., et al. *Int J Food Sci Technol*. **52**, 2097-2105 (2017), https://doi.org/10.5713/ajas.16.0435
12. Husak, R.L., Sebranek, J. G., Bregendahl, K. *Poult Sci*. **87**, 2367-2376 (2008), https://doi.org/10.3382/ps.2007-00294
13. Lin, C.-Y., Kuo, H.-Y., Wan, T.-C. *Asian-Australasian J Anim Sci.* **27**, 880 (2014), https://doi.org/10.5713/ajas.2013.13646
14. Voelter, W., et al. *J. Prakt. Chem*. **342**, 179-191 (2000), https://doi.org/10.1002/(SICI)1521-3897(200002)342:2<179::AID-PRAC179>3.0.CO;2-2

Author Index